EPRI | ELECTRIC POWER RESEARCH INSTITUTE

EPRI Yucca Mountain Total System Performance Assessment Code (IMARC) Version 10

Model Description and Analyses

EPRI Yucca Mountain Total System Performance Assessment Code (IMARC) Version 10

Model Description and Analyses

1018712

Final Report, June 2009

EPRI Project Manager
A. Sowder

ELECTRIC POWER RESEARCH INSTITUTE
3420 Hillview Avenue, Palo Alto, California 94304-1338 • PO Box 10412, Palo Alto, California 94303-0813 • USA
800.313.3774 • 650.855.2121 • askepri@epri.com • www.epri.com

DISCLAIMER OF WARRANTIES AND LIMITATION OF LIABILITIES

ORGANIZATION(S) THAT PREPARED THIS DOCUMENT

Monitor Scientific, LLC

Electric Power Research Institute

NOTE

For further information about EPRI, call the EPRI Customer Assistance Center at 800.313.3774 or e-mail askepri@epri.com.

CITATIONS

This report was prepared by

Monitor Scientific, LLC
3900 South Wadsworth Blvd.
Denver, CO 80235

Principal Investigator
M. Kozak

Electric Power Research Institute (EPRI)
1300 West W.T. Harris Blvd.
Charlotte NC 28262

Principal Investigators
A. Sowder
J. Kessler

This report describes research sponsored by EPRI.

The report is a corporate document that should be cited in the literature in the following manner:

EPRI Yucca Mountain Total System Performance Assessment Code (IMARC) Version 10: Model Description and Analyses. EPRI, Palo Alto, CA: 2009. 1018712.

REPORT SUMMARY

Since 1989, EPRI has been conducting independent assessments of the proposed deep geologic repository for the disposal of spent nuclear fuel (SNF) and high level radioactive waste (HLW) at Yucca Mountain, Nevada. EPRI pioneered application of the total system performance assessment (TSPA) approach for evaluating performance of geologic repository systems on a probabilistic basis. Along the way, EPRI developed the Integrated Multiple Assumptions and Release Code (IMARC) as its primary analytical tool for TSPA-based evaluations. Over this two-decade time period, IMARC has been periodically revised to reflect the evolving state of knowledge and the changing programmatic and regulatory environment.

Background

The governing U.S. Environmental Protection Agency (EPA) standards and Nuclear Regulatory Commission (NRC) regulations for the proposed Yucca Mountain repository are probability-based. This probabilistic nature and the long time frames associated with geologic disposal led to development of the TSPA methodology for demonstrating repository performance and regulatory compliance. As part of its preparation for a license application for repository construction, the U.S. Department of Energy (DOE), the licensee, has developed a comprehensive and highly complex TSPA program. The NRC, the designated regulator for this facility, has done likewise in support of its license review. As an independent third party, EPRI developed IMARC, not to duplicate the DOE and NRC efforts in rigor and depth, but rather to provide technical insights into important repository system features, events, and processes (FEPs) with respect to repository performance and estimates of future radiation doses to the public, specifically a hypothetical "reasonably maximally exposed individual" (RMEI). Implementation of IMARC is intended to reflect a best-estimate philosophy, consistent with the EPA standard codified in 40 CFR 197.14, as opposed to pessimistic or worst-case approaches.

Objectives

- To document development of the EPRI TSPA code, IMARC.
- To address comments and recommendations from an EPRI-commissioned independent peer-review of IMARC Version 9, published in their entirety as a separate EPRI report: *International Review Team Report: A Peer Review of the Yucca Mountain IMARC Total System Performance Assessment EPRI Model* (EPRI 1018711, 2009).
- To provide a comprehensive, updated description of the latest version of the EPRI TSPA code, IMARC 10.

Approach

IMARC treats many conceptual models and individual model parameters by including uncertainty distributions via either a Monte Carlo approach (continuous uncertainty distribution) or a logic tree (discrete uncertainty values). Several scenarios are addressed by the code. The "nominal release" scenario is the behavior of the repository in the absence of disruptive events. Seismic events are expected to occur at the site during the period of performance; the implications of potential seismic events are explored as deviations from the nominal scenario. EPRI has developed additional analyses associated with alternative potentially disruptive natural scenarios to address low-probability igneous events, which theoretically could intrude into or erupt through the proposed repository footprint. The conceptual model in IMARC can be directly applied to the igneous intrusion scenario, with changes to the input parameters; consequently, the discussions in this report on IMARC model structure apply to both the nominal and igneous intrusive scenarios. Evaluation of the igneous eruption scenario is performed outside of the IMARC framework.

Results

This report summarizes IMARC, Version 10, beginning with an overview of the code, followed by detailed descriptions of individual IMARC components, including linkages, testing, and benchmarking. Major IMARC FEPs are also described, with emphasis on climate change; net infiltration; focusing of unsaturated zone groundwater flow; groundwater percolation into repository drifts; degradation of drip shields, cladding, and waste packages; waste form dissolution; radionuclide transport through the drifts, unsaturated zone, and saturated zone; and multiple exposure pathways in the biosphere. The report also describes how combinations of embedded numerical submodels are coupled with stand-alone analyses and lookup tables to evaluate annual radiological doses to the RMEI. Results from selected IMARC 10 analyses and sensitivity studies are presented.

EPRI Perspective

This report provides a comprehensive overview and documentation of EPRI's TSPA code, IMARC, to clarify and enhance the technical basis for analyses conducted using this code and to facilitate understanding of the code itself in terms of development, structure, and implementation. EPRI analyses continue to indicate that the Yucca Mountain repository system will maintain doses to the public well below governing regulatory limits. While IMARC has been developed for evaluation of the Yucca Mountain system, the code or its components may also prove of value for the evaluation of other repository systems and waste management aspects of alternative fuel cycles.

Keywords

Yucca Mountain
High Level Radioactive Waste (HLW)
Spent Nuclear Fuel (SNF)
Total System Performance Assessment (TSPA)
Integrated Multiple Assumptions and Release Code (IMARC)

CONTENTS

LIST OF FIGURES

LIST OF TABLES

1
INTRODUCTION

The federal regulations applicable to the proposed spent nuclear fuel (SNF) and high-level nuclear waste (HLW) repository at Yucca Mountain, Nevada (primarily 10 CFR Part 63 and 40 CFR Part 197) are risk-informed and probability-based, necessitating a quantitative assessment of total performance. Within the Department of Energy's (DOE's) Yucca Mountain Project (YMP), this assessment is known as the Total System Performance Assessment (TSPA). TSPA is a key component in the license application submitted by the DOE to the Nuclear Regulatory Commission (NRC) as it provides the required regulatory assessment of the suitability of the Yucca Mountain site. A major focus of EPRI's high-level waste program has been to provide independent, third-party assessments of the performance of the proposed repository.

Since 1990, EPRI has published a series of reports documenting the development of its own total system performance assessment code, IMARC (Integrated Multiple Assumptions and Release Code) and the evolution of that code over the past fifteen years. Prior reports on IMARC have provided extensive and detailed information regarding the code and its underlying basis and philosophy (EPRI, 1990; 1992; 1996; 1998; 2000; 2002a; 2002b; 2003; 2004a,b; 2005a,c,d; 2006a,b,c). These reports and the incremental changes made to IMARC through this process are described more fully in Appendix A.

1.1 Purpose of the Report

Generally, previous IMARC code descriptions have focused on incremental changes or new developments in EPRI's TSPA methodology and the IMARC computer code; as a result, the complete technical basis for the code is scattered among several reports. A primary purpose of this report is to provide a description of the latest version of the IMARC code in a single report to an adequate level of detail such that the underlying conceptual approaches, how IMARC fits into the overall EPRI effort on TSPA for Yucca Mountain, the code structure, and necessary inputs and outputs for the code can be readily understood. As part of this documentation, a consolidated review of the IMARC code development history is presented in Appendix A to illustrate how and why the current IMARC conceptual model has reached its current form. Many alternative conceptual models have been evaluated and incorporated in earlier IMARC versions, and these models have been progressively modified or replaced as better understanding of the key phenomena were developed, so that the current model represents a culmination of understanding developed using the many previously evaluated models.

A second purpose of this report is to incorporate new information from ongoing scientific and engineering studies to reflect the most current state of knowledge related to the YM repository system, including revised model conceptualizations and parameter values provided by DOE in 2008 with the publication of the License Application (LA) and supporting documentation for the

latest DOE TSPA version: TSPA-LA (DOE/OCRWM, 2008b). The changes made to IMARC 9 were judged to be significant enough to warrant the generation of a new version, IMARC 10, as described in this report.

A third purpose of this report is to address comments made by an independent International Review Team (IRT) following its peer review of interim version, IMARC 9, which represented the status of the code as of early 2008 (EPRI, 2009). This review was commissioned by EPRI in 2007 to build confidence in the IMARC code and its underlying approach and methods. As a result of this peer review, changes to IMARC and an effort to consolidate and enhance code documentation were made.

1.2 Scope of the IMARC Methodology

As discussed in Appendix A, the IMARC methodology and software has tracked the evolution of Yucca Mountain regulations, disposal system design, and conceptual understanding of the proposed repository over the years. Current regulatory emphasis is on three primary scenario variants:

- a nominal scenario, which is the primary focus of this report;
- an igneous intrusive scenario; and
- an igneous extrusive scenario.[1]

Of these three scenarios, the nominal and igneous intrusive scenarios are explicitly addressed using IMARC (EPRI, 2005a).

The features, events, and processes (FEPs) associated with the igneous extrusive scenario are very different than those implemented in IMARC, and as a result this scenario is evaluated using a different modeling approach using a probabilistic framework separate from the IMARC code (EPRI, 2004a,b). The resulting event analysis evaluated the sequence of FEPs that could occur in an extrusive igneous event, including:

- probability of a future igneous event (basaltic dike) below Yucca Mountain,
- ascent and propagation of dike near the proposed site of the repository,
- magma-drift interaction,
- magma-waste package interaction,
- dispersal of erupted contaminated magma, and
- biosphere pathway analysis.

[1] While EPRI believes the probability of igneous activity within the repository footprint is less than 10^{-8} per year (EPRI, 2008b,c), EPRI has included its analyses of igneous events since igneous event consequences are being estimated by others; however, the results of these analyses are not reported as contributors to RMEI dose (Chapter 10, Table 10 – 6).

The inadvertent human intrusion scenario established in 10 CFR Part 63 is not addressed in IMARC or in other EPRI analyses (EPRI, 2005c).

The nominal scenario includes normal processes expected to occur for the repository as it evolves into the future, with the design behaving as designed. The nominal scenario includes cases in which the drifts remain open, and cases in which rockfall occurs throughout the analysis. The reason for this is that EPRI analyses of rockfall indicate that the drifts will remain open and intact for extended periods of time. The analyses also do not include the contribution of the rock support structures, which are quite robust, and which may reduce the amount of rockfall expected in the drifts for extended periods of time. However, it is recognized that some rockfall will likely occur over 1,000,000 years. As a result, the nominal scenario results from IMARC are generally presented as both "nominal" results, which do not contain rockfall, and "nominal plus seismic," which include the effects of rockfall and seismicity.

The set of FEPs involving seismicity and rockfall, which are a subset of the nominal scenario, is focused on the potential effects of rock fall on the engineered barrier system. This set of FEPs is the subject of several investigations by EPRI (2005d, 2006c), which conclude that rockfall does not lead to dramatically different performance than the situation in which the drifts remain open indefinitely. In IMARC, effects of seismicity and rockfall are expressed as modified input parameters for the engineered barrier system component failure rates. Therefore, the only differences between the nominal case and cases considering rockfall effects are in the input parameters. These considerations are summarized in Chapter 4.

Colloid-aided transport FEPs are potentially applicable to the nominal and igneous intrusion scenarios. EPRI has conducted an examination of colloid-aided transport and concludes that it is a negligible contributor to system behavior, and that it does not need to be included in the IMARC conceptual model (EPRI, 2006a). The conclusion that colloid-aided transport is of negligible importance is consistent with the conclusions of equivalent DOE reports on colloid-aided transport, although the DOE TSPA includes colloids for the sake of completeness, even though they are acknowledged to have negligible effect on system performance (BSC, 2003).

It should be noted that 40 CFR 197 and 10 CFR 63 call for the performance of analyses that are consistent with a "reasonable expectation" philosophy as opposed to a "most conservative" philosophy. EPRI's analytical efforts to date and the implementation of the IMARC code are generally consistent with the "reasonable expectation" philosophy and the applicable regulations, although some conservatisms in the IMARC models remain. This is in contrast to the much more conservative approach taken by the DOE (DOE/OCRWM, 2008b).

In line with EPRI's focus on the commercial electric power industry, IMARC analyses have examined the consequences of the commercial SNF inventory, which comprises the majority of the full legal capacity for the proposed repository at Yucca Mountain. EPRI analyses have not included the inventories associated with defense-related activities that make up the remainder of the inventory. Accordingly, the current IMARC inventory considers nuclides only from commercial spent nuclear fuel (CSNF). This is not an intrinsic limitation of the code, but rather reflects EPRI's research focus. In the current statuary limit of waste capacity 70,000 MTHM for the Yucca Mountain repository, 63,000 MTHM is from CSNF, comprising 7,796 waste packages (TSPA-LA Table 6.3.7-1) including PWR and BWR spent-fuel with various burnups. The activity contained in co-disposal waste packages is about two orders of magnitude less than the

activity in CSNF waste packages, so the focus on CSNF does not significantly limit the analysis. In DOE TSPA analyses (DOE/OCRWM, 2008b) the co-disposal waste packages tend to fail earlier than CSNF waste packages. As a result, inclusion of the co-disposal waste packages in IMARC would change the shape of the curve of dose to the RMEI, but it would not significantly alter the peak dose.

A set of radionuclides, shown in Table 1-1, has been chosen for analysis in IMARC, based on risk importance. The selection has taken account of past IMARC analyses, and reviews of contemporary analyses of DOE and NRC that identify the key radionuclides of concern for CSNF. A full discussion of the basis for the inventory, its historical development, and the radionuclides included in IMARC is provided in Appendix A. The numerical activity values for these radionuclides in CSNF have been adopted from the TSPA-LA.

Table 1-1
Radionuclides included in the IMARC inventory.

Nuclide	Half Life [yrs]
Ac-227	21.773
Am-241*	432.2
Cl-36	3.01×10^{5}
Cm-245*	8,500
I-129	1.59×10^{7}
Np-237	2.14×10^{6}
Pu-239	2.44×10^{4}
Pu-241*	14.35
Pu-242**	3.73×10^{5}
Ra-226	1,600
Se-79	2.95×10^{5}
Tc-99	2.15×10^{5}
Th-229	7,340
Th-230	7.7×10^{4}
U-233	1.59×10^{5}
U-234	2.47×10^{5}
U-235	7.1×10^{8}
U-238	4.51×10^{9}

* Radionuclide included by adding the inventory to the inventory of Np-237, which results in an overestimate of Np-237 inventory of about a factor of 3 for waste packages that fail at very early times. However, the ingrowth of Np-237 from Am-241 occurs in the first few thousand years, so the effect of this assumption on peak dose is negligible.

** Pu-242 decays to produce U-238. However, the contribution of Pu-242 to U-238 is negligible, and Pu-242 is a radionuclide of interest as a potential dose contributor. Therefore Pu-242 is modeled in IMARC as a simple decaying radionuclide and not as a U-238 parent.

IMARC comprises a set of models for the behavior of these radionuclides in various parts of the disposal system, and the parameters needed for those models. This report provides the description and justification for both models and parameters. Chapters of this report present descriptions and justifications for the models in IMARC, as well as values and justification for values of a few parameters. However, in most cases the discussions of parameter values have been placed in appendices, to assist in clarity of presentation for the main text.

2
SUMMARY OF IMARC CONCEPTUAL MODEL AND CODE COUPLING

2.1 Overview to IMARC 10 Chain of Models

The IMARC 10 total system performance assessment (TSPA) code consists of a modular implementation of individual models representing the processes affecting the long-term containment and isolation of spent nuclear fuel and defense high-level waste within a repository located at Yucca Mountain, Nevada (DOE/OCRWM, 2008b). The intent of the code is to evaluate the most risk-significant FEPs leading to the potential exposure of a Reasonably Maximally Exposed Individual (RMEI) at Yucca Mountain (40 CFR 191; 10 CFR 63). The code takes account of uncertainty in key parameters via a logic-tree format, conducting and combining a series of deterministic calculations for each "branch" of the logic-tree to produce probabilistic estimates of RMEI dose rates that are suitable for comparison with established safety standards and regulations for Yucca Mountain (40 CFR 197; 10 CFR 63).

IMARC 10 was developed by EPRI to provide an independent TSPA capacity for evaluation of performance- and safety-related issues associated with the Yucca Mountain repository (EPRI, 1990; 1992; 1996; 1998; 2000; 2002a,b; 2004a; 2005c; 2006b). EPRI's technical experts, working independently of the Yucca Mountain program, formulated separate TSPA sub-models that were combined into the overall IMARC 10 code. Because the Yucca Mountain repository concept has evolved over time with respect to site data, engineered barrier designs, applicable regulations, and other programmatic factors, the IMARC code has evolved as well. An overview of this evolution is presented in Appendix A. The current IMARC 10 implementation described in this report reflects changes to the Yucca Mountain repository system design and understanding of the repository system based on EPRI's review of DOE's June 2008 license application (DOE/OCRWM, 2008b).

The IMARC 10 code and associated TSPA calculations are intended to reveal and evaluate risk-important aspects affecting repository performance, providing risk –informed insights into the system behavior. To this end, IMARC 10 implements abstracted sub-models of the behavior of the repository, including the key FEPs that influence performance of the repository in a manner that permits assessment of regulatory compliance with mean-annual dose rates, as well as permitting exploration of sensitivity of key FEPs on dose rate. As an independent third party, EPRI developed the IMARC code primarily to provide technical insights into the most risk-important features, events, and processes affecting overall repository performance and regulatory compliance. The code also provides a credible, independent, technically defensible TSPA capability to evaluate DOE and NRC models and parameters. Implementation of IMARC is intended to reflect a reasonable or best-estimate philosophy, consistent with the EPA standard

codified in 40 CFR 197.14, as opposed to bounding or worst-case approaches. IMARC is not intended to duplicate the DOE and NRC codes in rigor and depth.

EPRI's abstraction process applied in the development and evolution of IMARC combined generalized knowledge about science with site-specific knowledge and understanding of the Yucca Mountain repository. This knowledge base was then combined with the expertise, judgment, and experience of EPRI's team of independent experts to develop technically credible and defensible alternative TSPA sub-models of processes affecting performance of a Yucca Mountain repository (see Appendix A). As discussed in Section 1.1 and Appendix A, understanding which sub-models of the repository system are important to performance has evolved over the past 20 years. This evolution has been made even more complex because of changes in barrier designs and regulatory standards during this period. A full review of the co-evolution of US regulations, engineered barrier designs, Yucca Mountain site characterization and TSPA studies by EPRI is, however, beyond the scope and intent of this report.

IMARC 10 is implemented as a chain of linked sub-models of key processes affecting containment, isolation and potential dose uptake, as shown in Figure 2-1 (EPRI, 1990; 1992; 1996; 1998; 2000; 2004a; 2005c; 2006b). Key aspects and attributes of each sub-model are briefly summarized here, while subsequent sections in this chapter provide more detailed information on the conceptualization, implementation, verification and application of each IMARC 10 sub-model.

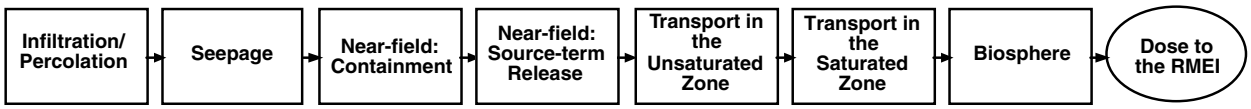

Figure 2-1
Chain of Models Implemented in IMARC 10.

2.1.1 Infiltration and Percolation

The beginning point for EPRI's TSPA analysis with IMARC 10 is the infiltration and percolation rate at the repository horizon. The percolation rate at the repository horizon is treated as an input parameter, and conceptually may be considered a boundary condition for the remainder of the code. Physical processes that play a role in determining the range in percolation rate values include: climate/ climate changes, moisture redistribution at the surface, evapo-transpiration, infiltration of water through the soil horizon, and moisture redistribution within the fractured unsaturated tuff that represents the upper natural barrier of the Yucca Mountain repository system above the engineered barrier system (DOE/OCRWM, 2008b). The net result of these processes is the percolation rate at the repository horizon.

In previous versions of IMARC, sequential time intervals have been set to represent changes in climate. In IMARC 10, this approach has been reduced to a single time interval that remains constant over the entire million year performance period. IMARC 10 adopts percolation rates from the range of percolation rates specified in the USNRC's 10 CFR 63. Since the period after 10,000 years is the by far the most important to performance, it was found that using climate variations in the period before 10,000 years does not meaningfully change the TSPA results as

compared to applying the NRC values for all times. Spatial variability of the percolation is taken into account using a flow-focusing factor, so that part of the repository experiences flow rates higher than average, and part of the repository experiences no flow.

2.1.2 Seepage

Within IMARC 10, the percolation rate is used to calculate the seepage rate into repository drifts using a function that determines the seepage rate and the fraction of the repository experiencing seepage as a function of percolation rate. Spatial variability in the percolation rate is modeled as a fraction of the repository experiencing focused flow, which leads to portions of the repository that experience higher seepage than others. The seepage rate and seepage fraction are used to establish the advective velocity in the near-field model for radionuclide transport. A full discussion of the treatment of seepage is presented n Chapter 3.

2.1.3 Near-field: Containment and Source term

The near-field model is composed of modules for determining the:

1. degradation and failure rates of *containment* components of the engineered barrier system (EBS),
2. *source-term release* of radionuclides from nuclear waste forms, involving dissolution of nuclear waste forms, application of radioelements solubility limits as appropriate, and transport of radionuclides through the EBS of the near field into the lower natural barrier.

The containment-degradation analyses take account of various corrosion processes for containment-related barriers (titanium (Ti) drip shield, alloy-22 outer barrier of waste packages, zircaloy cladding), and when necessary, contributing processes associated with seismicity, rockfall and igneous events. Corrosion modeling performed for IMARC TSPA calculations provide distributions of failures (defined as penetration through, or physical collapse, of the barrier) over time for each of the containment-related barriers. For the seismic scenario, the corrosion modeling is augmented by analyses of waste package collisions during a seismic event, the impacts of dynamic impacts of rocks, and the static load from rocks that have previously fallen. Similarly, for the igneous intrusion scenario, the corrosion modeling is altered to take into account the temperature history of the metal, its contact with corrosive materials in the magma, and its likelihood of early failure during the eruptive event.

To assess the performance impact of the possible emplacement of waste packages and drip shields with undetected fabrication defects, one waste package - drip shield combination is assumed to be emplaced in a failed state. This failed state is modeled as providing no barrier functionality at time zero. The “initial-defect” approach to containment allows for easy bounding analyses that have, in turn, shown that initial fabrication defects are not a risk significant issue. This is, in fact, a very conservative assumption, because manufacturing defects, if they exist at all, would most likely be represented by poorly completed welds or a misaligned drip shield. In addition, DOE’s detailed analysis of the probability of undetected manufacturing defects shows the expected value of initially defective waste packages and drip shields to be less than one of each. With these considerations, combined with the high-temperature operating mode (HTOM), which prevents seepage of water for several 1000’s of years after repository closure, the

containment barriers would be expected to continue to provide a substantial benefit in terms of waste isolation.

The source-term release of radionuclides from the commercial spent nuclear fuel (CSNF) waste form considers two types of initial release processes for commercial spent nuclear fuel (CSNF):

1. an instant release fraction (IRF) of volatile radioelements located along the gap between the fuel UO_2 matrix and the cladding and in grain boundaries, and
2. the remaining radioelements located in the fuel matrix that are released congruently with the dissolution rate (also referred to as "alteration rate") of the UO_2 matrix[2].

At each time step in the analysis, the fraction of newly failed waste packages is calculated, and the instant release fraction associated with those waste packages is included in the overall release rate. For IMARC 10, an external physicochemical model for the long-term dissolution rate of CSNF was developed to provide input into the IMARC source-term model.

Source-term transport of radionuclides in the near field is calculated using a compartment-based model for key components of the near field, taking account of the processes of solubility limitation, advection, dispersion, diffusion, and sorption. The result of the near-field model is the overall release rates of radionuclides from the boundary of the near field into the lower natural barrier (unsaturated zone) as a function of time.

2.1.4 Transport in the Unsaturated Zone (UZ)

The release rate of radionuclides from the near-field is assumed to occur uniformly across the contacting horizon of the underlying unsaturated zone. This radionuclide release rate is then used as concentration boundary condition for a one-dimensional model for vertical transport through the unsaturated zone. Alternative approaches that included spatially variable release rates have been explored in past versions of IMARC, and this added level of complexity has been found to have an insignificant impact on performance assessments. The concentration boundary condition is determined by applying a mixing cell at the base of the repository, homogenizing the releases across the repository to produce a single output concentration. The unsaturated zone model takes account of flow and transport in fractured tuff, with fracture-matrix interaction parameters that can varied to evaluate the sensitivity of this factor. The unsaturated zone is vertically subdivided into four geological units, which represent the average properties of a number of units of the more complex Yucca Mountain stratigraphy, as implemented by DOE/OCRWM (2008b).

[2] IMARC does not explicitly address the non-CSNF inventory proposed for Yucca Mountain. However, IMARC 10 can be used to calculate the performance for defense high-level waste, simply by including different initial radionuclide inventories and glass-matrix dissolution rate relative to CSNF.

2.1.5 Transport in the Saturated Zone

The release rate of radionuclides from the bottom of the unsaturated zone is used as input to a two-dimensional model of the saturated zone. The saturated zone is represented as two geological units. The first unit is represented as a fractured rock unit 15-km in length, represented mathematically as a dual continuum, with advective transport through the fractures modified by diffusion into the matrix ("matrix diffusion"), and sorption in both fractures and matrix. The second rock unit, composed of 3-km of alluvium, is represented mathematically as a single continuum. A uniform infiltration rate is applied across the top of the entire modeling domain.

2.1.6 Biosphere Mode and Reasonably Maximally Exposed Individual (RMEI) Dose

The interface between the geosphere and the biosphere is calculated using the method established in 10 CFR 63, which defines the manner in which the groundwater plume is calculated to interact with a hypothetical well at the point of compliance. Indeed, it is this regulatory-defined concept (10 CFR Part 63.302 and 63.312) of a "well-capture zone" aggregating the plume of radionuclides crossing the 18-km boundary from the repository that justifies a number of the abstractions and simplifications adopted in the UZ and SZ models of IMARC 10.

The stylized well-capture approach defined in 10 CFR Part 63 provides the basis in IMARC 10 for deriving a concentration in well water used by the Reasonably Maximally Exposed Individual (RMEI). This concentration is then used as an input to a stand-alone biosphere model. The biosphere model uses assumptions about RMEI behavior, and calculates the dose to the RMEI for a unit input concentration of each radionuclide. Some assumptions are established in regulations, while other assumptions need to be made in implementing the biosphere model. The dose per unit concentration, known as a Biosphere Dose Conversion Factor (BDCF) is used as an input parameter to IMARC 10. When multiplied by the well concentrations and summed over all radionuclides, the dose to the RMEI is calculated.

The analysis described in this section represents the calculation approach for a single set of input parameters. IMARC 10 conducts this calculation for 108 combinations of input parameters. The values of the input parameters and their associated probabilities are established using discrete probability density functions. This allows the uncertainty in parameters to be propagated using an event tree approach.

2.1.7 IMARC as an Independent Assessment Code

Programmatically, the EPRI team comprises experts from a wide variety of disciplines. The software for several parts of the code have been developed independently by members of the EPRI team with appropriate background and expertise, and have then been coupled in the code to provide an overall systems-level analysis. Over the years, the EPRI project team has approached its independent model development by a multi-step process:

Team members monitor and review information, primarily publications and presentations, from DOE, NRC, USGS, and other entities involved in the investigation of the Yucca Mountain repository. These reviews focus on the implementation or screening of FEPs, on the scientific and technical credibility of the work, and on the risk importance of the implementation of specific FEPs.

Team members develop independent views on which FEPs should be included or excluded, which are likely to result in over-conservatism or under-conservatism of the TSPA, and whether a technically superior approach is possible given the state of the science and state of understanding of the repository. The foundation for these independent views is both in the understanding of the repository system and in the expert's broader scientific understanding.

As appropriate, team members develop independent models, technical approaches to specific issues, and independent assessments of model parameters needed for TSPA. These independent models are tested and verified to ensure that the results are correct and understandable in an independent context before they are integrated into the TSPA in IMARC.

When those models reach an appropriate stage of development, as appropriate they are incorporated into IMARC, and become the technical foundation for the next phase of IMARC development. The incorporation may involve recoding parts of IMARC, or may only require updating input parameters for IMARC. Numerous specific examples of the way IMARC has evolved through this process are described in Appendix A. The modular nature of IMARC minimizes the overall impact on the entire IMARC code, and concomitant testing required, of code changes and modifications.

Approaches and concepts in IMARC are therefore seen to be derived in part from approaches and concepts developed by DOE and other interested parties. Similarly, over the years, a number of EPRI concepts and approaches have been adopted by DOE and other interested parties as the basis for their further understanding and development. Therefore, many concepts and technical approaches first published in EPRI reports later found expression in the approaches and products used by DOE, NRC, and EPA. Consequently, while EPRI analyses have remained independent and EPRI has carefully chosen which concepts and developments to incorporate into IMARC, there has been a general convergence of understanding among the interested parties on TSPA of the repository.

This description shows that, while the EPRI analyses are independent of other interested parties associated with the repository development, they are also dependent on information from other parties. In particular, the EPRI TSPA effort is heavily reliant on DOE-sponsored data collection to provide the foundation of understanding about the repository system. EPRI's understanding of the key FEPs to be included in TSPA has evolved as improved data and scientific understanding of the repository has been developed by all interested parties.

The overall conceptual approach of the IMARC code and the elements it contains are shown in Figure 2-1. The basic elements of the analysis method are the same as in the most recently available version of DOE's TSPA (DOE/OCRWM, 2008a). Differences arise mainly in the manner in which the two codes are implemented along with the specific assumptions, models, parameters, and couplings used.

This section has provided an overview of IMARC 10 and how the parts of IMARC are coupled. In the remainder of Chapter 2, overviews are presented of each part of the IMARC chain of models, with full details of the models presented in Chapters 3 through 7.

2.2 Climate, Net Infiltration, Percolation, and Seepage

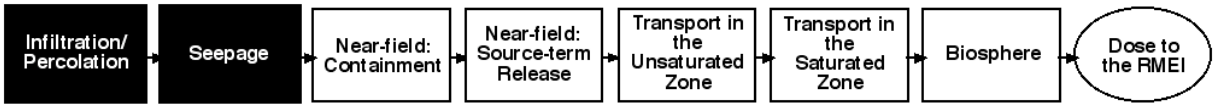

Figure 2-2
Implementation of Infiltration, Percolation, and Seepage Models in IMARC 10.

EPRI has developed a technical basis for the understanding of percolation to the repository horizon. In its proposed regulation for Yucca Mountain (NRC, 2005), NRC proposed a distribution of percolation rates to be used for the purposes of TSPA. These values are updated and increased somewhat by NRC (2008). EPRI believes the values incorporated in the NRC regulation are very conservative (Kessler, 2005). Therefore, while IMARC 10 uses parameter values to implement the NRC infiltration distribution, EPRI has continued to maintain its own positions on climate, infiltration, and percolation, which are documented in Chapter 3 of this report.

IMARC 10 analyses are based on an assumption that the post-10,000 year percolation flow rates specified by NRC apply beginning from time zero, so the percolation flow at the repository horizon is assumed to be the same at all times. This approximation does not have a significant effect on the model results, because experience has shown that before 10,000 years there are negligible releases from the repository. Similarly, the thermal period of repository performance is not taken into account in the flow and transport analyses in IMARC, because by the time significant releases from the repository begin, temperatures are low enough that the effect of temperature on repository performance is negligible. As a result, IMARC temperature only influences the degradation rates of components of the engineered barrier system (EBS).

The flow model in IMARC is based on an assumption of long-term steady percolation flow through the mountain. This assumption is based on observations made by DOE showing that the PTn unit above the repository has an ability to attenuate episodic signals from propagating through the subsurface. DOE has provided a substantial basis for this assumption in the license application:

> "The net surface infiltration at the bedrock surface (on top of the TCw unit) is conceptualized as episodic, with significant pulses occurring only once every few years … Spatially and temporally variable pulses of moisture percolate rapidly through the highly fractured tuffs of the TCw. However, at the TCw-PTn interface—where welded tuffs grade sharply into nonwelded tuffs—flow behavior changes from fracture dominated to matrix dominated flow. The highly porous PTn unit attenuates the episodic infiltration flux significantly such that the net episodic surface infiltration, once crossing the PTn, can be approximated as steady state …" (DOE/OCRWM, 2008b, Section 2.3.2.4.2.1.2).

EPRI concurs with this view of the function of this unit, and concurs that it is appropriate to eliminate the FEP for episodic deep percolation below the PTn from further consideration.

IMARC addresses water seepage into the repository drifts considering the possibility of "focused flow" due to heterogeneous fracture flow and have as their output a lookup table. The lookup table provides the fraction of the repository that will experience active seepage flow (rather than simply humid air conditions), as well as the seepage in the areas of active groundwater flow. For the igneous intrusion scenario, a separate lookup table is generated that takes into account the potential hydrologic properties of the solidified magma that is assumed to enter the drifts either partially or fully encapsulating the waste packages (EPRI, 2005a).

Detailed descriptions of the EPRI technical position on infiltration and percolation, and the IMARC 10 approach to seepage are presented in Chapter 3.

2.3 Engineered Barrier System Degradation

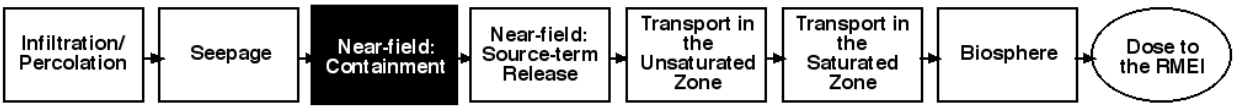

Figure 2-3
Implementation of Near-Field Containment Model in IMARC 10.

A large number of potential degradation mechanisms affecting drip shields, waste packages, and cladding are considered in the IMARC models. Uncertainty distributions are assigned to many of the individual model parameters based on their influence on degradation rates, and a set of Monte Carlo simulations are run using these distributions, and a *failure distribution curve* is generated for each of the tphree main engineered barrier system components. In IMARC 10, the input parameters for the engineered barrier system degradation analysis have been updated to reflect the most recent waste package design, as described by DOE/OCRWM (2008b).

A full description of the approach to evaluation of engineered barrier degradation used in IMARC 10 is presented in Chapter 4.

2.4 Near-Field Model and Coupling

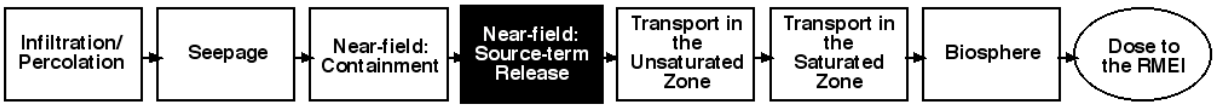

Figure 2-4
Implementation of Near-Field Source Term Release Model in IMARC 10.

The "near-field" in the IMARC model comprises all the components inside the drifts (*e.g.*, drip shield, waste package, cladding, waste form, pedestal, invert), along with the drifts themselves and a few meters[3] of the host rock surrounding the drifts. Releases from the repository are only assumed to occur after the period of significant thermal transient behavior based on the premise that there will be little to no liquid water present to facilitate radionuclide mobilization and movement until temperatures have decreased to near the local boiling point of water. As a result, thermal effects are omitted from flow and transport aspects of the model for the nominal release scenario.[4] The effects of temperature on the performance of the facility are therefore limited to effects on the degradation of components of the engineered barrier system.

The hydrologic behavior of the near field is represented by two zones: one in which water drips from fractures into the drifts, and one without dripping. Once simultaneous failure of the drip shield, waste package, and cladding is assumed to occur, these two zones are evaluated as two separate calculations using the COMPASS code, the first of the three numerical sub-models within IMARC. The zone in which dripping occurs releases radionuclides by both advection and diffusion, whereas the no-drip zone releases only by diffusion. Releases from both zones are summed to provide the total release from the repository level as a function of time. This release rate is then used as a boundary condition (release rate as a function of time) for the unsaturated zone code. The importance of this assumption is that all releases from the repository horizon are assumed to be laterally well mixed as they enter the unsaturated zone. This assumption is not significant in the overall TSPA, because of the regulatory requirement to normalize concentrations at the RMEI location to 3,000 acre-feet/y.

Inputs to the near-field model reflect several summary inputs, as follows:

- Seepage rate into the drift, for those drifts in which seepage occurs;
- The seepage rate according to a single projection of future climate; alternative climate projections are not currently considered in the uncertainty analysis;
- A variety of parameters intrinsic to the near-field analysis, including dimensions, sorption coefficients and solubility limits, densities, and porosities in the near field materials;
- Time-dependent probability of failure curves for waste packages and drip shields for dripping and non-dripping conditions, as described in Chapter 4;
- Time-dependent probability of failure curves for cladding (following EBS failure), for wet and dry conditions, as described in Chapter 4; and
- Diffusion/advection distance to the nearest flowing fracture. This captures the likelihood that radionuclides released from the drifts will travel slowly through the rock matrix immediately surrounding the drifts prior to encountering faster groundwater flow in nearby fractures.

[3] The amount of rock considered to be "near field" is an arbitrary distinction, since its properties are identical to the surroundings. As a practical matter, 4 m of rock is used in IMARC analyses as the distance into the surroundings included in COMPASS calculations.

[4] Thermal effects on drip shield, waste package, cladding, and in-drift groundwater flow behavior are considered for the igneous intrusion scenario.

It is useful to note that these input parameters represent the mean result of considering the probabilistic behavior of the system, so that the lumped parameters included in IMARC are derived from full representations of the uncertainty associated with the process under consideration.

A full description of the approaches used in IMARC 10 for near-field modeling is presented in Chapter 5.

2.5 Lower Unsaturated Zone Model and Coupling

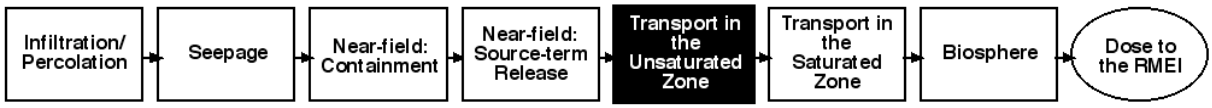

Figure 2-5
Unsaturated Zone Transport Model Implementation in IMARC 10.

The second numerical sub-model embedded within the IMARC code addresses flow and transport through the unsaturated zone beneath the repository horizon. Flow and transport through the unsaturated zone is treated as one-dimensional in the downward vertical direction. This model is arguably conservative compared to multidimensional models that allow for lateral flow and transport and therefore would predict longer radionuclide travel times and greater dispersion relative to a 1-D model representation. However, the dimensionality of the unsaturated zone does not strongly affect model results, given the model application for evaluating repository performance against regulatory criteria. Features and processes that lead to dispersion of contaminants play a small role in the Yucca Mountain TSPA because the well pumping rate is specified and the entire plume is calculated to be captured by the well. As a result, multidimensional effects in the unsaturated zone do not have a significant influence on TSPA results.

The unsaturated zone is subdivided into five segments:

- The first segment consists of only the first finite difference cell, which is used to apply the boundary condition of concentration from the near field, and
- The remaining four segments are used to represent different unsaturated horizons below the repository: TSw-3C, TSv-5, CHnv-5, and CHnz-6.

At the base of the unsaturated zone, the flux of radionuclides exiting the unsaturated zone is used as a time series input to the saturated-zone code.

A full description of the unsaturated zone model used in IMARC 10 is presented in Chapter 6.

2.6 Saturated Zone Model and Coupling

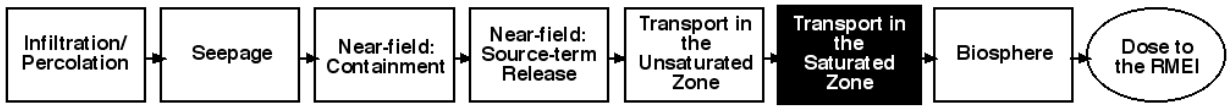

Figure 2-6
Saturated Zone Transport Model Implementation in IMARC 10.

The third numerical sub-model embedded within the IMARC code addresses flow and transport through the saturated zone. The saturated zone code has a specified upstream flow rate, and a uniform infiltration rate is added to the upper surface of the computation region, such that the groundwater flow velocity increases along the transport path length.

The saturated-zone model is composed of two segments:

1. a fractured tuff segment extending from beneath the repository to 15 km down-gradient, and
2. an alluvial segment extending from 15 km down-gradient to the location of the Reasonably Maximally Exposed Individual (RMEI) 18 km down-gradient, the "compliance point."

The unsaturated and saturated zone models communicate with the remainder of IMARC by the transfer of radionuclides from the near field and to the biosphere. All other parameters needed for the unsaturated and saturated zone models are unique to this part of the code, making them, to a large extent, stand-alone calculations.

IMARC 10 and all IMARC analyses after 2003 have implemented a 2-dimensional saturated zone representation. Previously, a full 3-dimensional saturated-zone model was implemented in IMARC was implemented, though without spatial variation of parameters in each segment of the model domain except at the downstream location where the saturated zone transitions from fractured tuff to alluvium. This approach resulted in very long run times. At the end of 2003, benchmark analyses conducted using the saturated zone code in a stand-alone analysis demonstrated that a two-dimensional representation produced essentially identical results as the 3-dimensional analysis, with significantly reduced run times. Reasonable agreement was also demonstrated for a one-dimensional representation of the saturated zone, but with only marginal further reductions in computation time. As a result, 2-dimensional representation was deemed adequate for IMARC.

Some regulatory requirements have profound consequences on the methodology used to conduct the overall analysis. Radionuclides exiting the saturated zone are, according to the requirements of 40 CFR 197, normalized to reflect a residential water usage of 3,000 acre-feet per year (3.7×10^6 m^3/y) – the so-called representative volume. Dispersion, therefore, has a minimal effect on analyses conducted for 40 CFR 197. Similarly, other phenomena that may affect the distribution of concentration in space (*e.g.,* the downward movement of the plume by infiltration from the surface) are of reduced importance following re-normalization and averaging of the concentrations. This outcome indicates that the potential to model the essential features of the groundwater transport analysis using a more simplified conceptual model.

A full description of the saturated zone model used in IMARC 10 is presented in Chapter 6.

2.7 Biosphere Model and Coupling

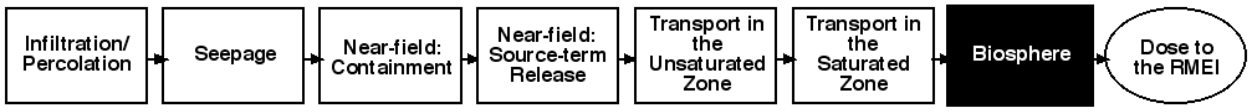

Figure 2-7
Biosphere Model Implementation in IMARC 10.

Any radionuclides released from the repository and transported 18 kilometers downstream in the saturated zone are assumed to enter the biosphere via groundwater used by the local community, including the Reasonably Maximally Exposed Individual (RMEI), for drinking, agriculture, and other purposes. Radionuclide fluxes in the groundwater at 18 km are adjusted to concentrations by use of the representative volume per 40 CFR 197. These concentrations are then multiplied by the radionuclide specific biosphere dose conversion factor (BDCF) for the RMEI to produce the dose to the RMEI for individual radionuclides at a given time of output concentration. The BDCFs are calculated independently to reflect steady-state conditions in the biosphere (see, *e.g.,* EPRI, 2002a). These individual radionuclide doses are then summed to produce the total dose to the RMEI at each time of output.

The biosphere model is entirely self-contained, and there are no common parameters between the biosphere model and the remainder of IMARC. Consequently, there are no issues of coupling between parts of the code that need to be evaluated. Values for the BDCFs have been periodically reviewed and updated, but from the perspective of the IMARC code, they are simply a set of radionuclide-specific parameters that are read in and used in the analysis.

In IMARC 10, for the first time, the effect of uncertainty in input parameters on the BDCFs has been incorporated for key radionuclides. Probabilistic analyses are carried out on selected radionuclides to determine the conservatism of the deterministic BDCFs used for the analysis. The probabilistic analyses are reported in Appendix C.

A full description of the biosphere model is presented in Chapter 7.

2.8 Treatment of Uncertainty

Uncertainty in input parameters for IMARC is propagated using two different methods. The primary method of uncertainty propagation uses the logic tree approach described in past IMARC publications (EPRI, 1992; 1996; 1998; 2000; 2002a,b; 2005c). In this approach, parameters are specified as high, moderate, and low values with probabilities associated with each. For instance, the moderate value of the parameter may be assigned a probability value of 0.9, with the high and low ends of the parameter range each assigned a probability of 0.05. The probabilities of values for a particular parameter necessarily sum to unity. In some cases, this triangular distribution is replaced by a high-low value set, with only two values of associated probabilities. The event tree approach identifies each permutation of the parameters, propagates

the associated probability of the combination of branches, and assigns probabilities to each branch end member. Monte Carlo methods are used to generate individual radionuclide BDCF distributions and time-dependent failure curves for key EBS components: drip shields, waste packages and fuel cladding. The reason for the use of these two methods has been entirely pragmatic. The event tree approach has advantages associated with transparency of the results, while the BDCF and failure curve analyses are carried out using stand-alone codes with built-n capabilities for Monte Carlo sampling.

In the current implementation of IMARC, the following uncertain parameters are included in the logic tree (See Figure 2-2):

- Infiltration rate, 3 branches reflecting high/moderate/low cases,
- Saturated Zone Retardation values, 3 branches reflecting high/moderate/low cases,
- Radionuclide Solubility/Waste Form Alteration Time, 3 branches reflecting high/moderate/low cases,
- Flow focus factor, 2 branches reflecting no focusing and strong focusing, and
- Seepage fraction/Flow rate, 2 branches reflecting a base case and a high value.

From combinations of this set of uncertainty parameters, IMARC derives the 3x3x3x2x2 = 108 calculation cases and associated probabilities that have formed the basis for IMARC analyses since the Phase 7 IMARC report (EPRI, 2002b). All other parameters in IMARC take single values. However, as noted above, a number of the parameters used as input to IMARC are mean values of full Monte-Carlo based probabilistic calculations. As a result, the single values used in IMARC embody the mean outcome of a more elaborate analysis conducted outside the framework of the code.

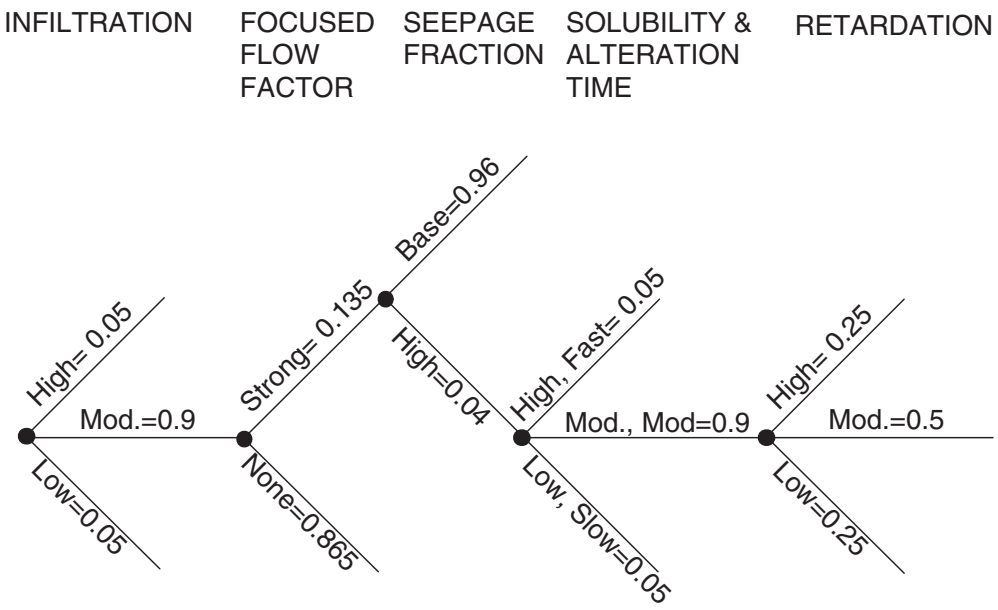

Figure 2-8
Logic tree of uncertain parameters currently in IMARC Version 10

3
CLIMATE, INFILTRATION, AND SEEPAGE

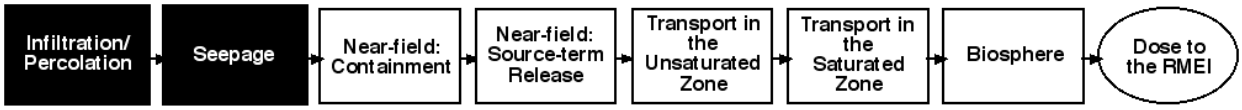

NRC (2005, 2008) has established, as part of 10 CFR Part 63, the rate of deep infiltration through Yucca Mountain that should be used for the TSPA analyses for the time period greater than 10,000 years. The intent of establishing these values in the regulation is to reduce speculation about future climate states and the implications of changes in infiltration on the TSPA. The IMARC code, beginning with version 9, implemented these values for the post-10,000 year period.

While EPRI supports this conceptual approach, the distribution of values for infiltration proposed by NRC (2005, 2008) are considerably higher (*i.e.,* more conservative) than are considered reasonable based on the results of EPRI's independent analysis (EPRI, 1998). Furthermore, NRC (2008) has recently increased the conservatism of infiltration rates. Therefore, in this chapter, EPRI's technical approach is described as a reasonable assurance basis for TSPA calculations, even though it is not currently implemented in IMARC 10. With the exception of the specific values for infiltration, EPRI's (2005b) approach and NRC's (2005, 2008) approach are consistent. The NRC (2005) values were implemented in IMARC 9 (Kessler *et al*., 2006) and the NRC (2008) values are implemented in IMARC 10.

The IMARC code contains process models only for phenomena occurring at and below the repository horizon. However, these phenomena are affected by processes occurring above the repository associated with climate, its influence on infiltration into the mountain, and the subsequent seepage to the repository horizon and its interaction with the drifts. All processes above the repository horizon are treated in IMARC as lumped parameters applied as boundary conditions for the subsequent analyses. Consequently, even though the EPRI project team has invested considerable effort over the years into developing independent evaluations for climate, infiltration, and seepage, these technical bases have been reduced to several rather straightforward parameters. These parameters are:

- Time history of infiltration rate (mm/y)
- Fraction of the repository that is wet (unitless)
- Flow focusing factor (unitless)

The time history of infiltration rate has now been set to the values proposed by NRC (2008) for all times greater than 2,000 years following repository closure, consistent with the EPRI technical position on climate (see Section 3.1). These constant infiltration rates range from 10

mm/y to 100 mm/y, with a mean value of 37 mm/y. Since waste package failure before 10,000 years is a low probability event, the difference between the use of these values after 2,000 years and after 10,000 years is negligible. Since the engineered barrier system provides substantial containment at early times, the post-10,000 year values are the most important infiltration rates to system performance. In IMARC, these values are implemented as a triangular distribution with upper and lower bounds set by the range, with each assigned a 0.05 probability. The mean is set to 37 mm/y with a probability of 0.9.

3.1 Climate

The basic climate types adopted in past IMARC analyses (EPRI, 2000; 2002a) continue to be used in IMARC 10 (EPRI, 2002b) for the first 2000 years after repository closure. The greenhouse climate is assumed to exist for the first 1,000 years beyond permanent closure after which the interglacial climate is assumed to exist for the next 1,000 years (EPRI, 2002b). Following this initial 2,000 year period, a full glacial maximum climate is assumed to persist for the remainder of the million years after present (EPRI, 2005b). At 1,000 years and at 2,000 years beyond permanent closure, therefore, there are step changes in infiltration rates associated with these different climates. EPRI (2005b) describes the uncertainties associated with projecting future climates, and concludes that a stylized approach to treatment of climate is appropriate.

3.2 Infiltration

EPRI's net infiltration modeling has not changed since Phase 4 (EPRI, 1998). The model considers evapo-transpiration, run-on and run-off, variable precipitation (treated stochastically), and other factors for each climate state. EPRI's ongoing review of this topic suggests that recent estimates of infiltration published by DOE and NRC appear to be based on excessively conservative assumptions; accordingly, the EPRI team has chosen not to update its analyses with respect to these revised infiltration estimates.

Each climate state is assigned a net infiltration rate, which is considered to be an uncertain parameter in the current IMARC event tree (EPRI, 2002a). Values for the low, moderate, and high branches of the infiltration rate currently used in IMARC are shown in Table 3-1, along with the "best estimate" value for Full Glacial Maximum determined from EPRI's independent research. The values for full glacial maximum used in IMARC 10 are based on the NRC (2008) recommendations, and are higher than EPRI's analyses show are appropriate. The values of net infiltration represent averages across the entire repository. The low infiltration rate is assigned a branch probability of 0.05, the moderate 0.9, and the high 0.05.

Table 3-1
Net infiltration rates (mm/y) used in the IMARC 10 event tree branches for infiltration

Climate	Low	Moderate	High
Greenhouse (1,000 y)	1.1	11	19
Interglacial (1,000 y)	1.1	7.2	9.6
Full Glacial Maximum – values adopted in IMARC 10 (NRC, 2008)	10	37	100
Full Glacial Maximum – EPRI "best estimate" values (EPRI, 2005c)	6.8	20	35

3.3 Focused Flow Factors

While the net infiltration rates in Table 3-1 describe area-averaged values, the fact that the unsaturated zone is fractured, porous tuff means there is a possibility that the average net infiltration may be distributed spatially as it approaches the repository horizon. Some of the groundwater flow may therefore undergo "focusing" by the fractured tuff into some areas and away from other areas. EPRI (2002a) describes the focused flow factors as an approach to capture a combination of spatial variability in the upper geological system, and uncertainty in the effect of localization of flow that approaches the repository drifts. IMARC represents this factor as an uncertain node in the event tree. When the flow is focused, the infiltration rate is increased by a factor of 4 compared to the values in Table 3-1 over 25 percent of the area of the repository; the seepage rate for the remaining 75% of the drifts is set to zero to maintain the groundwater flux balance for the focused flow case. The current logic tree in IMARC assigns a branch probability of 0.865 to the flow being unfocused (*i.e.*, no lateral redistribution of the area-average net infiltration values in Table 3-1), and 0.135 to flow focusing. These values are derived from a prior DOE analysis of the probability of flowing fractures, as documented in EPRI (2002a). The technical basis remains unchanged, and so the flow focus factor remains unchanged in IMARC 10 as well.

3.4 Seepage

EPRI (2002a) describes the approach to seepage used in IMARC. Under various flow conditions, a fraction of the repository may experience flowing water, while the remaining fraction remains dry. For the drip shields that are assumed to have failed in those areas assumed to have seepage into the drifts, the volumetric flow into the drift is assumed to drip directly onto the waste packages located under the failed drip shield, and the corresponding volumetric flow rate is used as a direct input to COMPASS, the numerical submodel within IMARC that calculates radionuclide release from the engineered barrier system. To evaluate the seepage fraction and the seepage flow rate, the EPRI team has relied on more complex DOE analyses, which led to estimates of both parameters shown in Table 3-2 as a function of infiltration rate. In IMARC, seepage fraction and flow rate are estimated by linearly interpolating between the values found in Table 3-2. Two conditions are included as branches in the IMARC event tree: a base-case

seepage and a high seepage case. The base-case seepage is assigned a branch probability of 0.96, and the high seepage case is assigned 0.04. These values are derived from prior DOE analyses of seepage and adapted for use in IMARC (EPRI, 2002b). The seepage analyses used in IMARC have not been updated to correspond directly to the updated seepage model used for the TSPA-LA (DOE/OCRWM, 2008a,b). Upon review and evaluation, the newer DOE analyses were judged to have introduced new conservatisms that were not deemed appropriate for the reasonable expectation goals of IMARC.

Table 3-2
Seepage fraction and flow rate as a function of infiltration rate (after EPRI, 2002a). ("q" is the infiltration rate immediately above the repository horizon.)

	Base-Seepage Case		High-Seepage Case	
q (mm/y)	Fraction	Flow Rate (m^3/y)	Fraction	Flow Rate (m^3/y)
2.4	0	0	0	0
5	0	0	0.083	0.086
14.6	0	0	0.083	0.401
60	0	0	0.310	0.701
73.2	.054	.365	.376	.788
213	.054	4.24	.452	4.24

Hence, for a given infiltration rate branch associated with a climate state, combined with the branch determining whether the flow is focused or not and the branch determining if the seepage is high or base-case, the rate of flow into the drift is determined along with the fraction of the repository that is assumed to experience seepage. These two parameters are then provided to COMPASS to establish input conditions to the source-term model. For example, for the Full Glacial Maximum climate state, there is a (0.05 x 0.135=) 0.68% probability that the seepage rate into 25% of the drifts would be (4 x 37mm/yr =) 148 mm/yr.

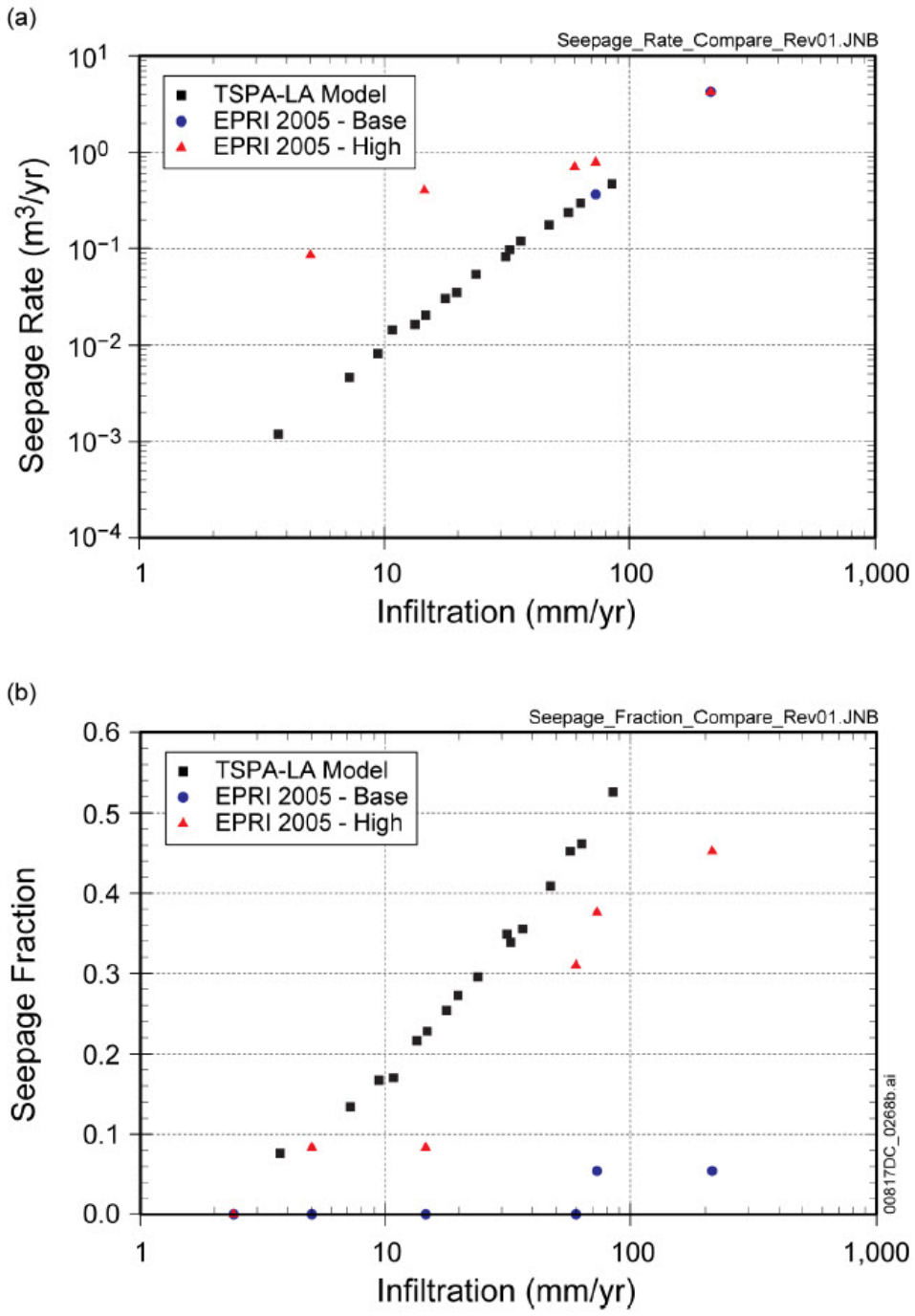

Figure 3-1
Comparison of seepage function used by the DOE's TSPA-LA and IMARC. (a) Seepage flow rate, (b) seepage fraction. Figure from DOE/OCRWM (2008a), Figure 7.7.3-1.

DOE/OCRWM (2008a) conducted a review of IMARC 8 (EPRI, 2005a) and noted that the seepage model is a primary difference between IMARC and the TSPA-LA. Their comparison of the two approaches is shown in Figure 3-1. The base IMARC seepage rates at low infiltration rates are lower than the TSPA-LA rates, with better agreement at higher infiltration values. The IMARC seepage fractions are lower than the TSPA-LA model at all values of infiltration. EPRI believes that the model in the TSPA-LA is overly conservative, and is inconsistent with observations of present day seepage in the Exploratory Studies Facility, and inconsistent with estimations of infiltration in paleoclimates (Marshall et al., 2003; Xu et al., 2003).

3.5 Saturated Zone Infiltration

Once seepage water leaves the repository, it passes through the remainder of the UZ and into the SZ where it may travel the 18 km to the compliance point. The rate of infiltration through the remainder of the UZ and throughout the SZ is also considered over the entire transport path length. There is no direct coupling between infiltration analyses through the mountain to the repository, and those analyses considering infiltration in the far field. There are several computational constraints that require the net infiltration to be fixed to a constant value over the entire period. Consequently, groundwater inflow at the upstream face, just upstream of the repository footprint, and the net infiltration rate over the water table of the saturated zone, is fixed at a steady-state value throughout the analysis, thus defining steady-state flow and constant water table depth. Additional discussion of flow and transport in the geosphere is presented in Chapter 6.

4
PERFORMANCE OF THE ENGINEERED BARRIER SYSTEM

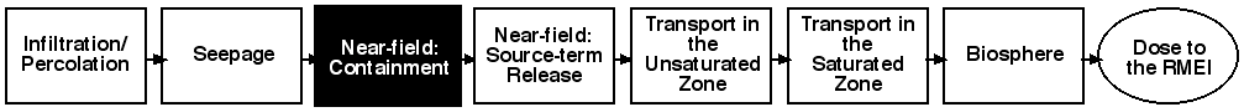

4.1 Introduction

A key input into IMARC is the rate of failure of the components of the engineered barrier system, in particular the titanium drip shield (DS) and the alloy C-22 waste package (WP). Calculations of the rates of corrosion processes affecting the DS and WP are performed by EPRI using a stand-alone probabilistic model. This section describes the development of the latest version of the engineered barrier system (EBS) failure model, the Engineered Barrier System Corrosion Model (EBSCOM). This is the first version of IMARC to used EBSCOM for conducting EBS failure analyses.

The two main purposes EBSCOM as implemented in IMARC are to determine:

- the total period of protection of the waste form from the time the waste is emplaced in the repository to the time when it may be exposed to groundwater and release of radionuclides can commence; and
- the rate of release of radionuclides from the waste form into the unsaturated zone once the waste form may be exposed via breach of the waste package and cladding.

The results of the probabilistic analysis are integrated into an IMARC calculation as a set of mean failure rates in time for each component of the engineered barrier system. Therefore, output from EBSCOM is used to generate time-dependent input parameters for IMARC.

EBSCOM builds on and retains many of the features and processes included in the previous EBS performance model (EPRI, 2002a). The previous model was used to predict the rate of EBS failure for the nominal scenario and, in an amended form, the effect of an intrusive igneous event (EPRI, 2005a). In addition, EBSCOM incorporates new processes and modifications to manner in which the older analyses addressed other important processes.

There were a number of drivers for the development of a revised version of the EBS failure model, including the need to:

- update the treatment of some of the corrosion processes based on newly available information from the literature, including DOE-funded research on corrosion and open peer-reviewed literature,
- update the treatment of certain corrosion processes in light of WP and DS design changes for the DOE Yucca Mountain license application,
- take into account the variability in environmental conditions within the drifts,
- address processes of importance beyond 10^4 years when considering a peak dose compliance criterion, and
- extend the model to predict the consequence of the igneous and seismic disruptive events.

There are three versions of the revised EBS code:

1. EBSCOM-nominal deals with the nominal scenario, including the effect, if any, of drift stability due to thermal stresses,
2. EBSCOM-seismic addresses the effects of time-dependent seismic disruptive event(s), and
3. EBSCOM-igneous addresses the effects of time-dependent igneous intrusion disruptive event(s).

The version of the code described here is EBSCOM-nominal Version 1.0, and the primary focus of this section is the nominal scenario, although mention is also made of the impact of both seismic and igneous disruptive events.

Failure rates of the engineered barrier system are based on current information about the waste package. The proposed waste package design, which was substantially revised for the 2008 DOE license application, now relies on the universal use of Transportation, Aging, and Disposal (TAD) canisters for commercial spent nuclear fuel. The approaches described in this report have been developed for earlier Yucca Mountain project waste package designs, but are applicable, with minor modifications, to the TAD canister, as described in Section 4.5.

4.2 Overview of the EBSCOM Nominal Model

4.2.1 Approach to Modeling the EBS

Like its predecessor, the EBSPA model, the EBSCOM code uses Monte Carlo techniques to account for uncertainty and variability in the prediction of DS and WP lifetimes. Uncertainty arises from the use of abstracted conceptual corrosion models, which are necessarily simplifications of the actual complex corrosion processes, and from uncertainty in the values of various input parameters. Variability results from variation in, for example, material properties, environmental conditions (both spatial and temporal variation), and the quality of the manufactured WP and DS.

A single run of the EBSCOM code typically comprises 1,000,000 individual realizations, representing ~100 realizations for each of the 7,796 WPs in the proposed repository. In a given realization, an individual DS is coupled to an individual WP and the computation is performed until such time that all components of the engineered barrier system have failed.

Again, as with the EBSPA model, the EBSCOM model is largely a thermally driven code. Thus, temperature, and how it evolves over time, is the principal environmental parameter determining the rate of various corrosion processes. However, environmental variability is also included in the EBSCOM model, primarily based on the different seepage water geochemistry "bins" defined by the DOE (BSC 2004a; also see EPRI, 2006b) and their effect on various corrosion processes (principally localized corrosion (LC) and stress corrosion cracking (SCC)).

EBSCOM is designed to be flexible so that the results of new experimental studies and material testing can be readily incorporated. Therefore, it includes mathematical treatment of some processes that have not yet been shown to be of concern, *e.g.*, localized corrosion (LC) of alloy C-22 due to microbial activity. These expressions are included in case future tests should indicate the possibility that this process is of importance and to allow sensitivity analyses.

4.2.2 Capabilities and Predictions

The EBSCOM code predicts the performance of various engineered barrier components; namely (Figure 4-1):

- the drip shield,
- the waste package shell,
- the waste package outer closure lid weld, and
- the waste package middle closure lid weld.

The WP shell is defined as the entire surface of the WP outer barrier excluding those areas of the outer and middle closure lids that are subject to thermal ageing during the final closure welding or subsequent stress-relief treatment. Thus, the WP shell comprises the cylindrical body, the non-closure lid, and the central portions of the outer and middle lids away from the circumferential closure welds.

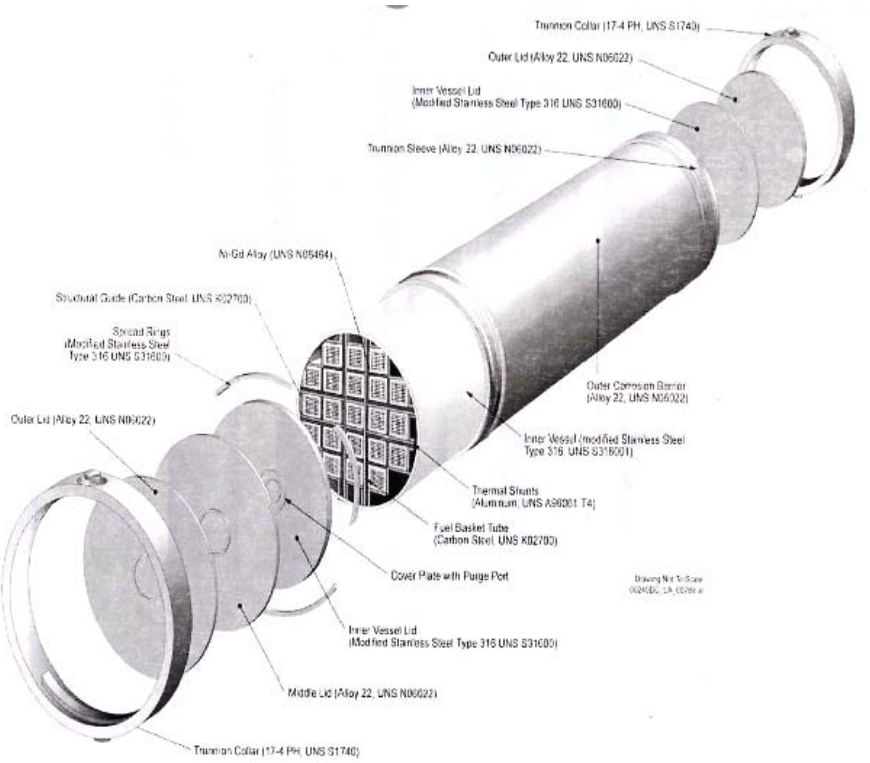

(a) Design Details of the 21 PWR waste package configuration (DOE/OCRWM, 2008b).

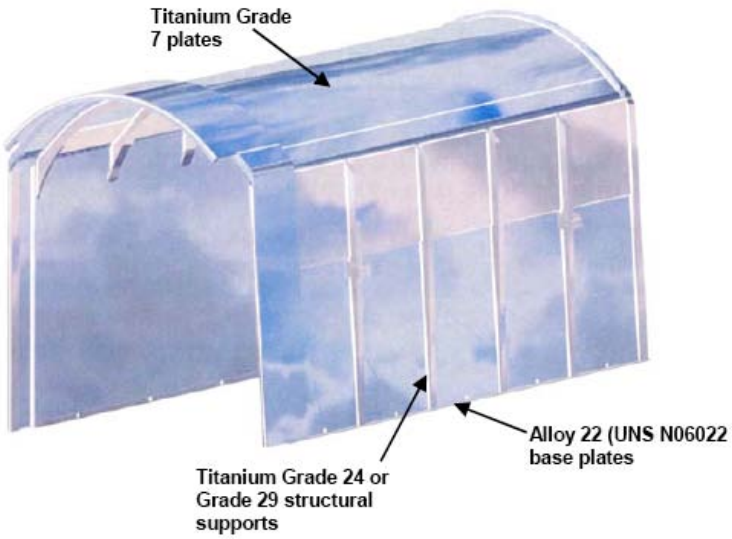

(b) Design details of the drip shield (DOE/OCRWM, 2008b).

Figure 4-1
Details of the designs of the engineered barrier system for the DOE license application (LA). (Note: Some of the actual details of the design of the middle and inner closure lids as presented in the LA differ slightly from those Shown in Figure 4-1(a)).

There are different possible failure mechanisms for each of the EBS components. The possible failure mechanisms for the DS in the nominal scenario are:

- initial failure due to an undetected manufacturing defect or emplacement error,
- general corrosion (GC), or
- hydrogen-induced cracking (HIC).

The possible failure mechanisms for the alloy C-22 outer shell of the WP in the nominal scenario are:

- initial failure due to an undetected manufacturing defect,
- general corrosion,
- localized corrosion (LC), or
- microbiologically influenced corrosion (MIC).

The possible failure mechanisms for the outer and middle WP closure lid welds in the nominal scenario are:

- initial failure due to an undetected manufacturing defect,
- general corrosion,
- localized corrosion,
- microbiologically influenced corrosion, or
- stress corrosion cracking (SCC).

Additional failure mechanisms are possible for one or more of the EBS components in the case of the seismic and igneous disruptive events, but they are not considered further here.

The basic output of the code is the failure time and mode for each of the EBS components. The failure time is generally expressed as the cumulative fraction of failed components as a function of time. The fraction of failures is defined for:

- the DS,
- the WP shell,
- the WP outer lid weld,
- the WP inner lid weld,
- the WP closure lid system (failure of both lids in a given realization),
- the WP as a whole (the earlier of the WP shell or the closure lid system), and
- the EBS as a whole (failure of both the DS and WP in a single realization).

Various criteria have been defined for failure for each failure mode (see Section 4.3). The process resulting in failure is defined as that corrosion mechanism that results in the ultimate loss of the containment or barrier function. However, in most cases, more than one corrosion process can lead to the degradation of the DS or WP. For example, although the WP shell may ultimately fail because of MIC-enhanced GC, much of the wall loss may have resulted from prior LC during the thermal pulse. Nevertheless, for the purposes of defining a single failure mode, the WP would, in this particular example, be defined as having failed from MIC-enhanced GC.

4.2.3 Environmental Variability

4.2.3.1 Evolution of the Drift Environment

There are two mechanisms by which an aqueous phase can form on the WP and/or DS surface; seepage and deliquescence (BSC, 2004a). Figure 4-2 illustrates the conceptual model for seepage and deliquescence.

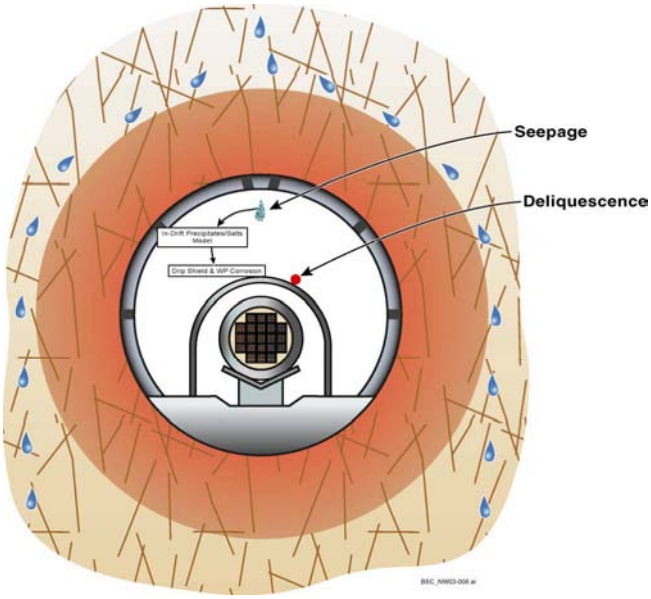

Figure 4-2
Schematic cross-section through the drift illustrating the Engineered Barrier System and the conceptual model for seepage and deliquescence (from DOE/OCRWM, 2008b).

The evolution of the repository environment is typically divided into three phases, based primarily on the evolution of the in-drift temperature (Figure 4-3(a)).

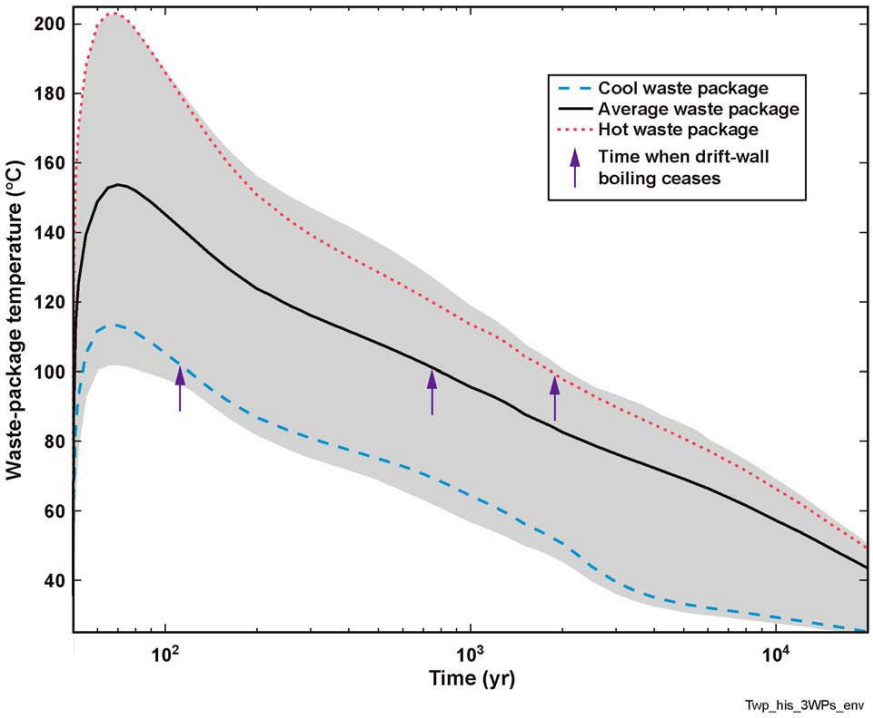

Figure 4-3(a) Range of temperature histories for all waste packages.

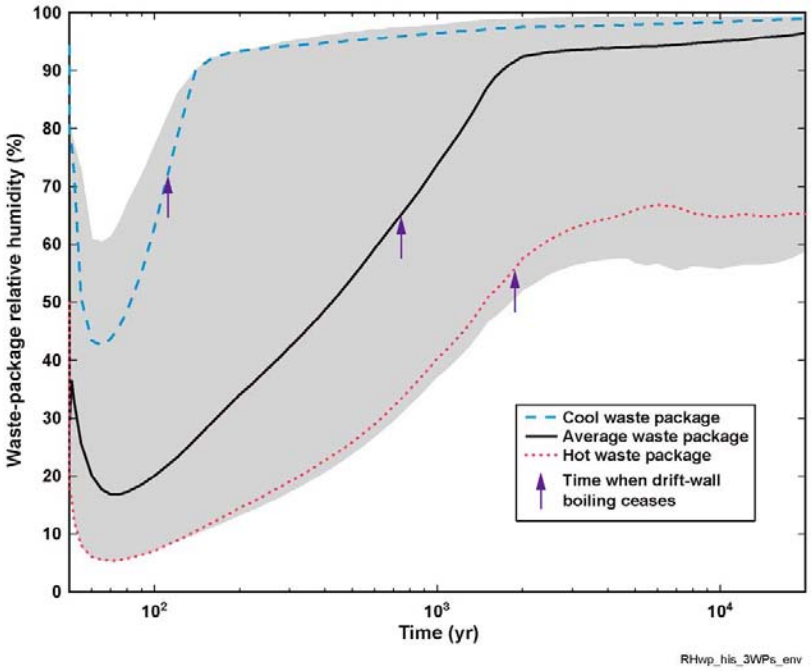

Figure 4-3(b) Range of relative humidity histories for all waste packages.

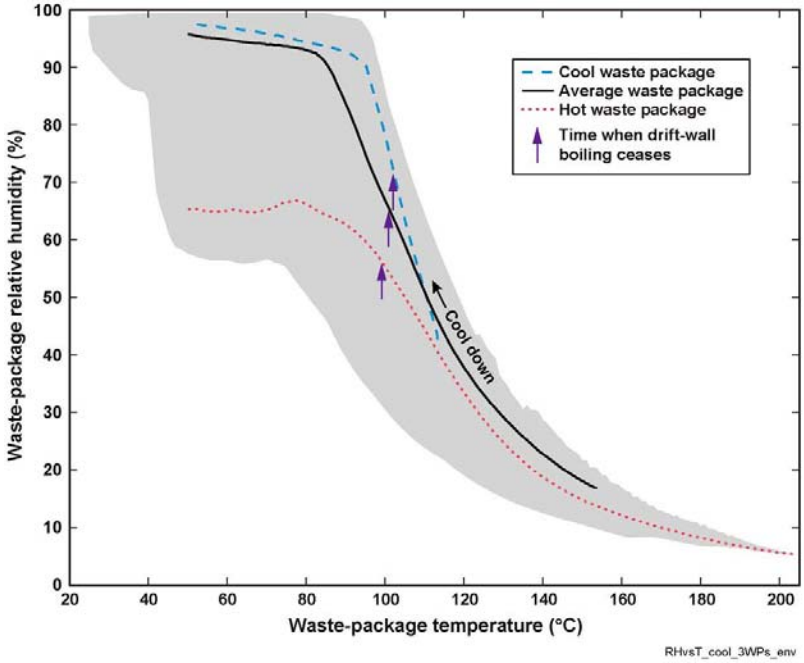

Figure 4-3(c) Range of temperature vs. relative humidity trajectories during cool down.

Figure 4-3
Ranges of temperature and relative humidity histories and of temperature vs. relative humidity trajectories during cool down for all waste packages, accounting for uncertainty of host-rock thermal conductivity and percolation flux (from BSC, 2004b).

4.2.3.1.1 Dry-out phase

During the dry-out phase following permanent closure, the EBS is protected from seepage by a capillary barrier, or boiling front, surrounding the drift (denoted by the orange-colored band around the drift opening in Figure 4-2). However, an aqueous phase can form on the surface of the EBS through the deliquescence of suitable minerals in dust accumulated on the surfaces of the DS or WP. Based on the range of WP temperatures expected in the repository (Figure 4-3(a)), the dry-out phase (defined here as the time during which the temperature at the drift wall is above boiling) persists for ~100 yr for the coolest WP to ~2,000 yr for the hottest WP.[5]

4.2.3.1.2 Transition Phase

As the temperature within the drift continues to cool, seepage water may enter the drift from the unsaturated zone (UZ). Seepage will not necessarily occur at all locations in all drifts, and the extent of seepage will depend on local hydrologic conditions. As defined here, the transition period lasts from the end of the dry-out phase (100-2,000 yrs) to the time at which evaporative concentration of seepage waters no longer poses the threat of LC of the WP. This latter time

[5] It is noted here that the cooler WPs tend to be those containing defense HLW, which have not been addressed by EPRI.

corresponds to a temperature of 80-120°C (depending on the metallurgical condition of the material and the composition of the solution), or a time of 7,000-8,000 years after permanent closure for the hottest WP (Figure 4-3(a)).

Deliquescence of minerals, either present in dust or as precipitated salt films from evaporated seepage drips, is also possible during the transition phase. However, EPRI has shown that deliquescence is a very unlikely phenomenon to occur, and that it is not significant to risk if it does occur (EPRI, 2006b).

4.2.3.1.3 Low-temperature Phase

The low-temperature period starts at the end of the transition phase and continues indefinitely. Both seepage and deliquescence are possible during this period, but again depend on the local hydrologic conditions and the presence of suitable deliquescent minerals, respectively.

In summary, therefore, the potential sources for an aqueous phase during the three phases of the repository evolution are:

1. Dry-out phase – no seepage, deliquescence possible
2. Transition phase – both seepage and deliquescence possible
3. Low-temperature phase - both seepage and deliquescence possible

4.2.3.2 Composition of the Aqueous Phase

Because the Yucca Mountain repository is located in the UZ above the water table, the composition of the aqueous phase on the surfaces of the EBS components is as much determined by the time dependence of the temperature and relative humidity in the drift as it is by the (initial) composition of the fluid. In general, evaporation of aqueous phases will generate concentrated solutions during the early high-temperature, low %RH period in the evolution of the repository environment. Later on, dilution arising from the increase in %RH during cool down (Figure 4-3(c)) and/or incoming seepage water will create more benign, dilute environments. Coupled with the decrease in temperature with time, the corrosiveness of the environment will diminish as the repository cools.

The DOE has developed a number of categories of seepage waters that are assumed to have the potential to enter the drift and contact the EBS (BSC, 2004a). To determine the composition of possible seepage waters, the DOE has mathematically simulated the interaction of ambient UZ pore waters with rock minerals during the thermal pulse using the coupled thermal-hydrological-chemical code TOUGHREACT. Various "bins" of water of common chemical characteristics are then developed from the resulting thousands of possible seepage-water compositions. A total of 11 bins are defined (Table 4-1), along with the respective frequency of occurrence. These 11 bins are then "numerically evaporated" using the EQ3/6 code and the resultant end-point brines determined. The corrosive environments corresponding to these end-point brines that have been used in corrosion testing by DOE are also defined in Table 4-1.

EPRI (2006b) reviews the binning methodology used by DOE to bound plausible ranges in the chemistry of seepage entering drifts at Yucca Mountain, and evaluates several alternatives to this approach. DOE's binning methodology is intended to provide a defensible basis for minimizing the number of distinct types of seepage waters that need to be considered in TSPA. Based on this study, EPRI concurs that the methodology proposed by DOE is based on reasonable and defensible conceptual and numerical models of processes that are likely to control the chemical evolution of seepage in host rocks at Yucca Mountain, and the subsequent evaporative evolution of any seepage that enters the drifts. EPRI (2006b) concludes that brines that may form in repository conditions will not support localized corrosion.

Most of the concentrated brines defined in Table 4-1 are alkaline and relatively innocuous. In particular, the only waters that may cause LC are the relatively infrequent Bins 1-3. Even for these compositions, however, the waters may contain significant quantities of nitrate (and sulfate and carbonate) ions, which serve to inhibit localized corrosion by countering the aggressive action of the calcium chloride solutions.

As noted above, seepage waters can only enter the drift once the drift wall temperature has dropped below the boiling point. At this time, seepage water could contact the DS and WP (if the DS has failed) and be concentrated by evaporation. The extent of evaporation of the seepage water is dependent on the temperature and %RH at the surface of the respective EBS components at that time.

An aqueous phase may also form on the DS or WP surface as the result of the absorption of moisture by deliquescent salts in dust deposits. Both the DOE (BSC, 2004a) and EPRI (EPRI, 2004a) have considered the generation of aggressive environments from the deliquescence of dust deposits. Using a process similar to that used for classifying the possible seepage waters, the DOE has defined six bins of possible deliquescent waters (Peters, 2003a). These waters tend to be generally nitrate- or carbonate-rich brines, similar to the Bin 4 to Bin 11 seepage waters (Table 4-1). None of the evaporated deliquescent solutions would support LC of the WP.

Table 4-1
DOE Classification of seepage waters by type, frequency of occurrence and representative laboratory test solution (from BSC, 2004a)

Bin	Time Integrated Relative Frequency for Crown Waters	Average End-Point RH	98% RH Bin	End Point Brine	Representative Corrosion Test Solution*
1	~0%	20%	Ca-Cl	Ca-Cl	5-8 M $CaCl_2$ + Nitrate
2	~0%	24%	Na-Cl	Ca-Cl	5-8 M $CaCl_2$ + Nitrate
3	~1%	40%	Na-Cl	K-Ca-Cl-NO_3	5-8 M $CaCl_2$ + Nitrate
4	~15%	50%	Na-Cl	Na-K-Cl-NO_3	SSW, SAW
5	~10%	60%	Na-Cl	Na-K-Cl	SSW, SAW
6	~1%	60%	Na-Cl	Na-K-Cl-NO_3	SSW, SAW
7	~1%	60%	Na-Cl	Na-K-Cl-NO_3	SSW, SAW
8	~1%	60%	Na-CO_3	Na-K-Cl	SDW, SCW, BSW
9	~20%	60%	Na-CO_3	Na-K-NO_3-Cl	SDW, SCW, BSW
10	~1%	60%	Na-CO_3	Na-K-CO_3-Cl	SDW, SCW, BSW
11	~50%	60%	Na-CO_3-Cl	Na-K-CO_3-Cl	SDW, SCW, BSW

* SSW = Simulated Saturated Water, SAW = Simulated Acidified Water, SDW = Simulated Dilute Water, SCW = Simulated Concentrated Water, BSW = Basic Saturated Water.

EPRI also considers the development of deliquescent solutions from various sources of dust, including dust from the YM Exploratory Studies Facility (ESF) and wind-blown dust (EPRI, 2004a). The major anionic constituents of the soluble salts in these dusts are nitrate and sulfate, both of which inhibit LC of alloy C-22. Furthermore, any $CaCl_2$ solution formed by deliquescence would be unstable and decompose upon evaporation. There is also an excess of insoluble mineral phases in the dust that would neutralize HCl formed by the decomposition of the brine solution forming on WP surfaces. Therefore, EPRI concludes that any deliquescent solution would not support LC of the WP (EPRI, 2004a). As a result, enhanced corrosion associated with deliquescence is not considered by EPRI to be a credible phenomenon at Yucca Mountain, and it is not included in the current failure functions used in IMARC.

4.2.3.3 Treatment of Environmental Variability in EBSCOM

4.2.3.3.1 Waste Package and Drip Shield Temperature

The temperature-time profiles used in the EBSCOM model are based on those provided by BSC (2004b). Although the temperature on the surface of the DS will be slightly lower than that of the WP because of the air gap between the two EBS components, the same profile is used to represent the temperature of the two components in EBSCOM.

The time dependence of the temperature of the average waste package shown in Figure 4-3(a) is simulated in EBSCOM by a series of polynomials covering different time periods following permanent closure of the repository. These various expressions and their respective time periods are given by:

for $50 \leq t < 60$ yrs

$$T = -0.2295t^2 + 30.205t - 836.5 \quad \textbf{Eq. 4-1a}$$

for $60 \leq t < 74$ yrs

$$T = -0.029t^2 + 4.14t + 5.6 \quad \textbf{Eq. 4-1b}$$

for $74 \leq t < 7830$ yrs

$$T = 2.480514\log t^4 - 35.686098\log t^3 + 189.220273\log t^2 - 477.349592\log t + 587.168405 \quad \textbf{Eq. 4-1c}$$

for $7830 \leq t < 10^5$ yrs

$$T = 20.439235 + 57.449779 \cdot \exp(-4.629365 \times 10^{-5} t) \quad \textbf{Eq. 4-1d}$$

for $t \geq 10^5$ yrs

$$T = 21^{\circ}C \quad \textbf{Eq. 4-1e}$$

where T is the temperature in $^{\circ}C$ and t is the time in years (since emplacement of the WP).

A different temperature profile is selected for each realization, so that the full range of WP temperatures is simulated in a given EBSCOM run. In a given realization, the temperature profile is based on the time-dependent temperature for the average WP (Equation 4-1) multiplied by a time dependent factor $f_T(t)$. The maximum value of f_{Tm} is sampled from an asymmetric triangular distribution with a lower bound of 0.67, an upper bound of 1.26, and a peak value of 1.00 (corresponding to the average WP). The value of $f_T(t)$ at different times is then given by:

for $50 \leq t < 1.25 \times 10^4$ yrs

$$f_T(t) = f_{Tm} \qquad \textbf{Eq. 4-2a}$$

for 1.25×10^4 yrs $\leq t < 10^5$ yrs

$$f_T(t) = f_{Tm} (D+C \exp(-2.5 \times 10^{-5})) \qquad \textbf{Eq. 4-2b}$$

where the values of C and D are determined so that the conditions given by Equations 4-2(a) and 4-2(c) are satisfied:

for $t \geq 10^5$ yrs

$$f_T(t) = 1 \qquad \textbf{Eq. 4-2c}$$

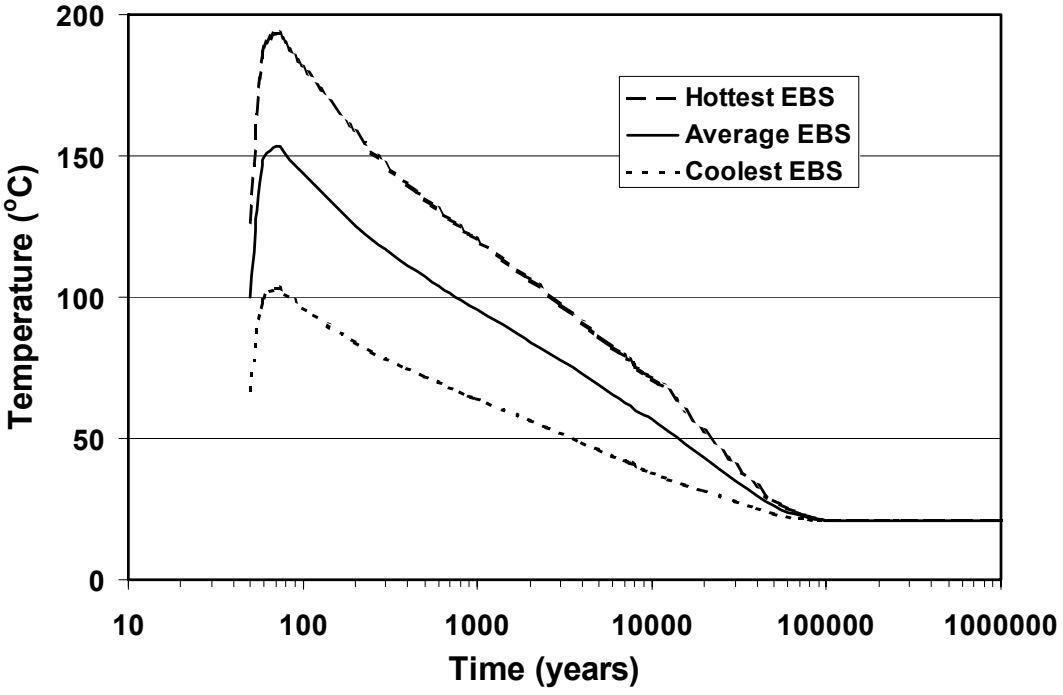

Figure 4-4
Temperature profiles for the average, hottest, and coolest engineered barrier components considered in the EBSCOM Code.

Figure 4-4 shows the temperature profiles for the average, hottest, and coolest EBS components considered in the EBSCOM code. These profiles are similar to those shown in Figure 4-3(a) and encompass the range of possible WP/DS temperatures. As the value of f_{Tm} is sampled from a triangular distribution, the majority of WP temperatures in the 10^6 realizations will be close to that for the average temperature, with correspondingly fewer for the hottest and coolest profiles.

4.2.3.3.2 Composition of the Aqueous Phase

As discussed above, the volume and composition of the aqueous phase on the EBS component surfaces varies as the repository environment evolves with time. Potentially aggressive environments are possible during the transition phase as a result of evaporative concentration, although the WP and DS have been designed to withstand these conditions.

Neither the time dependence of the composition of the aqueous phase nor its volume is explicitly modeled in EBSCOM. A single aqueous phase is selected for each realization and the composition of the solution is assumed to remain constant throughout the period of simulation. Furthermore, all DS and WP are deemed to be wetted at all times (although the WP is only contacted by seepage drips if the DS has failed), provided the temperature is equal to or less than that at which an aqueous phase can exist on the surface of the EBS.

The aqueous solutions included in the EBSCOM code represent the range of concentrated evaporated waters that could form from the various bins of seepage and deliquescent solutions described by the DOE (BSC, 2004a). A smaller number of environments are used in the EBSCOM code. The eleven bins of crown waters and the range of deliquescent solution compositions defined by the DOE are reduced to five environments that represent the eleven bins (Table 4-2). Note that the range of deliquescent solution compositions and their associated evaporates are similar to the distribution of seepage waters and their associated evaporates (BSC, 2004a). For simplicity and transparency, the reduced list of five waters is referred to by the same bin designation as the primary crown water in Table 4-1. Thus, the “new” Bin 3 water represents Bins 1, 2, and 3 from Table 4-1, the new Bin 4 water in Table 4-2 represents Bins 4, 6, and 7, Bin 5 represents Bins 5 and 8, Bin 9 in Table 4-2 is identical to Bin 9 in Table 4-1, and Bin 11 represents Bins 10 and 11 in the original list. This combination of aqueous compositions for the EPRI model is chosen on the basis of the chemical similarity and similarity in corrosiveness of the various compositions within one of the 5 bins of water in EBSCOM.

In the EBSCOM code, the different water composition for a particular realization is selected based on the relative frequencies in Table4-2. The relative frequency is used to represent the variability and uncertainty in the spatial distributions of waters within the repository, rather than the temporal variability of the water composition (as the water composition is assumed to be constant throughout the simulation period).

The impact of the aqueous solution composition on the rate or probability of general or localized corrosion, MIC, or SCC is discussed under the respective section below.

Table 4-2
Categories and properties of seepage waters used in EBSCOM.

Bin	Relative Frequency	Average End-Point RH	98% RH Bin	End Point Brine	Representative Corrosion Test Solution*
3	1%	40%	Na-Cl	K-Ca-Cl-NO_3	5-8 M $CaCl_2$ + Nitrate
4	17%	50%	Na-Cl	Na-K-Cl-NO_3	SSW, SAW
5	11%	60%	Na-Cl	Na-K-Cl	SSW, SAW
9	20%	60%	Na-CO_3	Na-K-NO_3-Cl	SDW, SCW, BSW
11	51%	60%	Na-CO_3-Cl	Na-K-CO_3-Cl	SDW, SCW, BSW

* SSW = Simulated Saturated Water, SAW = Simulated Acidified Water, SDW = Simulated Dilute Water, SCW = Simulated Concentrated Water, BSW = Basic Saturated Water.

4.2.4 Comparison with EBSPA

Significant changes have been introduced into the new EBSCOM code compared with the previous EPRI EBS model.

4.2.4.1 Spatial Variability in the EBS Temperature

A different temperature-time profile is selected for the EBS in each realization of EBSCOM. The WP and DS temperatures are assumed to be the same. In the earlier EBSPA code, all WP are assumed to have the same temperature profile, with a slightly lower temperature defined for the DS. The range of temperatures in a given EBSCOM run of 10^6 realizations represents the spatial variability of EBS temperatures in the repository, as well as the variability associated with different waste loadings and WP designs.

4.2.4.2 Spatial Variability in the Nature of the Aqueous Environment

A different aqueous environment is selected from one of five "bins" of possible waters in each EBSCOM realization. These bins represent the possible ranges of evaporated seepage and deliquescent solutions that could form on the EBS surfaces. The frequency of occurrence of each of the five bins is determined by the frequency at which each type of water has been predicted to occur at the YM repository by the DOE (BSC, 2004a). The nature of the water in each bin affects the corrosion behavior of the WP. While all bins of water are assumed to support GC and hydrogen-induced cracking (HIC) of the DS, and GC or MIC of the WP, only certain waters will support LC or SCC (see Sections 4.3.2.2 and 4.3.2.3 respectively). In contrast, there is no environment-specific information in EBSPA, and all forms of corrosion of the WP and DS are assumed to be possible in all realizations.

4.3 Corrosion Processes Included in EBSCOM

4.3.1 Drip Shield

As in the EBSPA code (Qin and Shoesmith, 2003), the corrosion processes considered to lead to failure of the DS in EBSCOM are general corrosion (GC) and hydrogen-induced cracking (HIC). The treatment of these processes in EBSCOM is similar to that used in the earlier model except for the following changes:

- inclusion of factor f_{O_2} to account for the fraction of GC of the DS supported by the cathodic reduction of O_2, which does not result in hydrogen absorption,
- the assumption that a fraction of the absorbed hydrogen is lost upon the continued corrosion of the DS by GC,
- corrosion of both the top- and under-sides of the DS is explicitly taken into account, and
- a modified distribution of rates of GC is used.

In comparison to the EBSPA code, these changes result in a lower probability of DS failure by HIC in the EBSCOM model.

4.3.1.1 General Corrosion

The general corrosion rate of the Ti-7 drip shield is given by an Arrhenius expression:

$$R_{GC}^{DS}(T) = 2f_F R_{GC}^{DS}(T_{ref}) \exp\left[\frac{\Delta E_{GC}^{DS}}{R}\left[\frac{1}{T_{ref}} - \frac{1}{T}\right]\right] \qquad \textbf{Eq. 4-3}$$

where $R_{GC}^{DS}(T)$ is the rate of general corrosion at temperature T (in K), ΔE_{GC}^{DS} is the activation energy, R is the gas constant (8.314 $J \cdot K^{-1} \cdot mol^{-1}$), T_{ref} is the reference temperature for the experimental values of the corrosion rate (348.15°K, 75°C), f_F is an enhancement factor due to the presence of fluoride ions, and the value of 2 accounts for the fact that corrosion can occur on both the top- and under-sides of the DS. The value of the corrosion rate at the reference temperature ($R_{GC}^{DS}(T_{ref})$) is chosen for each realization from a cumulative distribution function based on experimental measurements (see Section 4.7). The corrosion rate is independent of the environment.

The distribution of experimental corrosion rates used to derive the value of $R_{GC}^{DS}(T_{ref})$ is shown in Figure 4-5. These data were obtained with weight-loss samples exposed to various concentrated solutions for a period of 5 years (BSC, 2004c). These data have been fitted to a Weibull distribution (Section 4.7) from which a value is selected for each realization to account for the variability in the measured corrosion rate. Although salt deposits from the evaporation of seepage drips or deliquescent dust solutions may form on the top of the DS, the corrosion rate is assumed to be the same on both the top and under sides of the DS. No enhancement of the corrosion rate is expected under the precipitated salt deposits, as it is believed that such deposits

will be too porous to permit the creation of aggressive localized chemistries (Apted *et al.,* 2005; EPRI, 2004a). A factor of 2 is included in Equation (4-3) to account for the simultaneous corrosion of the top and under sides of the DS. Corrosion of the top-side of the DS could occur as a result of seepage or deliquescence of dust deposits, while corrosion of the under-side could be caused by the formation of a thin liquid moisture film.

Under very specific conditions, fluoride ions have been shown to accelerate the general corrosion of Ti alloys (Hua *et al*., 2004). However, these aggressive low-pH concentrated F^-/Cl^- environments cannot form in most seepage and deliquescent solutions because of the presence of Ca^{2+} (which will lead to the precipitation of F^- ions) and HCO_3^-/CO_3^{2-} (which will buffer the pH in the alkaline range). Accelerated corrosion is particularly unlikely for oxide-covered Ti surfaces, as is anticipated to be present on DS exposed to the drift environment for several hundreds or thousands of years prior to the onset of seepage. Nevertheless, a fluoride ion enhancement factor is included in Equation (4-3) for the purposes of sensitivity analyses.

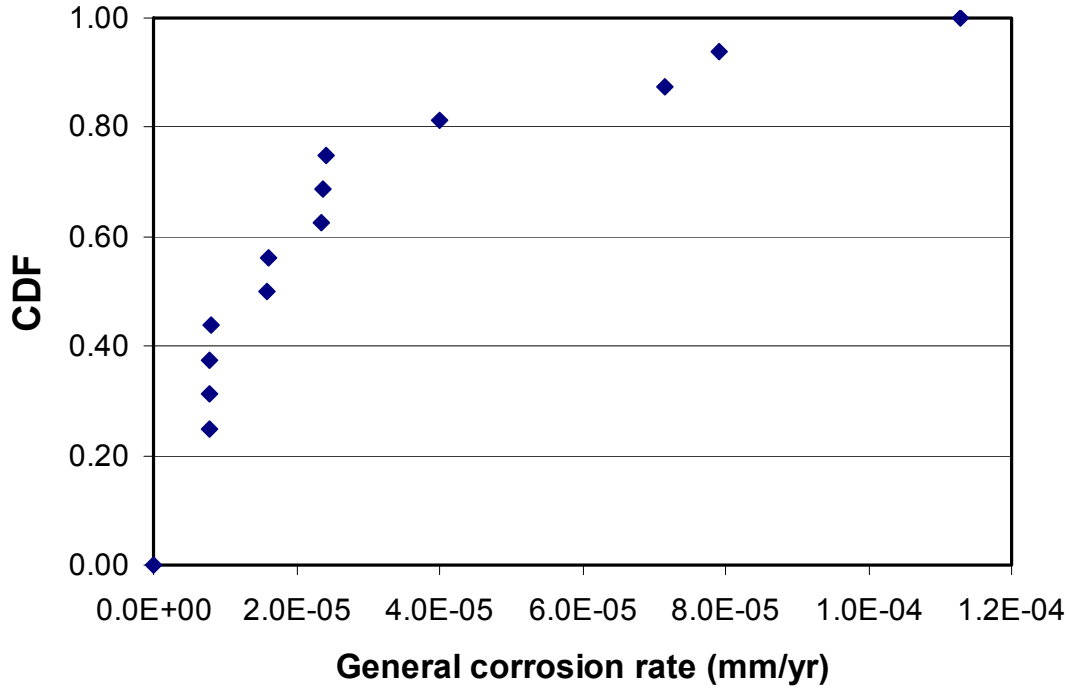

Figure 4-5
Cumulative distribution function for the general corrosion of titanium weight-loss samples after five years exposure in the Long Term Corrosion Test Facility (from BSC, 2004c).

Failure of the DS by general corrosion is assumed to occur when the total thickness of the DS has been consumed by corrosion occurring on both the top and under side of the DS.

4.3.1.2 Hydrogen Induced Cracking (HIC)

The general corrosion of Ti is supported by the reduction of O_2 or H_2O:

$$Ti + O_2 + H_2O \rightarrow TiO_2 + H_2O \qquad \textbf{Eq. 4-4a}$$

or

$$Ti + 2H_2O \rightarrow TiO_2 + 4H \qquad \textbf{Eq. 4-4b}$$

Only the corrosion of Ti by H_2O produces hydrogen atoms that can be absorbed by the DS and lead to hydrogen-induced cracking. Failure of the DS by HIC is deemed to occur once the absorbed hydrogen concentration [H_{ABS}] reaches a critical value H_{CRIT}. The value of H_{CRIT} is treated in the same way as in the EBSPA code (Section 4.7).

The rate of H absorption depends on a number of factors (Qin and Shoesmith 2003), including:

- the rate of general corrosion,
- the fraction of corrosion supported by the reduction of H_2O,
- the fraction of H produced by Reaction (4-4b) that is absorbed by the oxide-covered metal (fH), and
- the amount of absorbed H released from the matrix as corrosion proceeds.

As described above, the rate of general corrosion of Ti is given by Equation (4-3). Of this total rate of corrosion, a fraction f_{O_2} is assumed to be supported by the reduction of O_2 (Reaction 4-4a) and a fraction $(1-f_{O_2})$ by the reduction of H_2O (Reaction (4-4b)). The fraction of the total corrosion supported by O_2 reduction will be a function of the drift environment. At elevated temperatures, the solubility of dissolved O_2 will diminish, an effect that may be enhanced by the salting-out of O_2 in concentrated evaporates. At lower temperatures, the solubility of dissolved O_2 is higher, and a larger fraction of the overall corrosion may be supported by Reaction (4-4a). For simplicity, the value of f_{O_2} is assumed to be independent of temperature and the nature of the solution in the current version of EBSCOM. It should be noted that the Long-Term Corrosion Test Facility (LTCTF) tests from which the data in Figure 4-5 are taken were conducted under naturally aerated conditions at temperatures of 60°C and 90°C. Therefore, the observed corrosion is a result of the cathodic reduction of both O_2 and H_2O. No significant dependence on temperature was found in these tests, although more-recent data have shown a temperature dependence equivalent to an activation energy of ~23 kJ/mol (Hua *et al*., 2002).

As in earlier versions of the EPRI EBS model, the hydrogen uptake efficiency f_H is taken to be temperature dependent (EPRI, 2002; Qin and Shoesmith, 2003) (see Section 4.7).

The absorbed H is assumed to be uniformly distributed throughout the DS. Preferential precipitation of H (as Ti hydrides) is observed during localized corrosion of Ti alloys in regions that are corroding relatively rapidly and for which the protective oxide film is thin or absent due

to the low pH in the pit or crevice. However, for the general corrosion of the DS, the assumption of a uniform concentration throughout the structure is reasonable given the relatively slow rate of H absorption compared with the rate of diffusion of H in the Ti matrix.

As discussed elsewhere (EPRI, 2002; Qin and Shoesmith, 2003), the assumption made in the EBSPA code that all the H previously absorbed remains in the Ti matrix as corrosion of the DS continues is now believed to be unreasonable. The conversion of the Ti matrix to TiO_2 can be reasonably expected to release the absorbed H, which is then free to escape into the drift environment. In the EBSCOM code, therefore, it is assumed that H already absorbed is lost as the Ti matrix is converted into TiO_2. Thus, at each time step in the realization, a fraction of the previously absorbed H is lost and a fraction of the freshly generated H is absorbed. The amount of absorbed H lost in each time step is assumed to be equal to the total in that amount of Ti metal corroded during the time increment.

4.3.1.3 Stress Corrosion Cracking

Stress corrosion cracking (SCC) of the DS is not considered in EBSCOM-nominal Version 1.0. The introduction of dynamic or static loads due to seismic-induced rockfall may induce residual stress in the DS that could then render it susceptible to SCC (BSC, 2004d). Rockfall due to thermal stresses is considered as part of the nominal scenario, but has been shown to have no detrimental effects on the DS (BSC, 2004d; EPRI, 2005d) and as a result is not included in EBSCOM-nominal Version 1.0.

4.3.1.4 Comparison of Stress Corrosion Cracking in EBSCOM and EBSPA

As noted above, the EBSCOM code contains the following changes to the treatment of the DS compared with the EBSPA model:

- inclusion of factor f_{O2} to account for the fraction of the GC of the DS supported by the cathodic reduction of O_2, which does not result in hydrogen absorption,
- the assumption that a fraction of the absorbed hydrogen is lost upon the continued corrosion of the DS by GC,
- corrosion of both the top- and under-sides of the DS is explicitly taken into account, and
- a modified distribution of rates of GC is used.

The net effect of these changes is to lower the probability of HIC failure of the DS. The first two changes specifically reduce the concentration of absorbed H. Although the explicit inclusion of the corrosion of both sides of the DS would be expected to lead to faster GC failure of the DS in the EBSCOM code, the modified distribution of GC rates used in EBSCOM predicts lower corrosion rates than those used in the EBSPA model. These two effects effectively cancel out, so that the net rate of general corrosion is similar for the two models.

4.3.2 Waste Package

In the EBSCOM code, corrosion of the WP is assumed to take the form of general corrosion (GC), localized corrosion (LC), stress corrosion cracking (SCC), and microbially influenced corrosion (MIC). In EBSCOM, GC, LC, and SCC are treated in a manner similar to that used in the EBSPA code, except that LC and SCC are assumed to only occur in certain environments. The EBSPA model did not consider MIC.

4.3.2.1 General Corrosion

The rate of general corrosion of the WP ($R_{GC}^{WP}(T)$) is given by an Arrhenius relationship of the form:

$$R_{GC}^{WP}(T) = f_{MIC} R_{GC}^{WP}(T_{ref}) \exp\left[\frac{\Delta E_{GC}^{WP}}{R}\left[\frac{1}{T_{ref}} - \frac{1}{T}\right]\right] \quad \text{Eq. 4-5}$$

where ΔE_{GC}^{WP} is the activation energy, $R_{GC}^{WP}(T_{ref})$ is the rate of general corrosion at the reference temperature of 75°C, and f_{MIC} is an enhancement factor for the occurrence of MIC (see below). The value of the corrosion rate at the reference temperature ($R_{GC}^{WP}(T_{ref})$) is chosen for each realization from a Weibull distribution derived from experimental data in various repository-representative test solutions (Section 4.7). The corrosion rate is assumed to be independent of the environment as no such dependence was observed in the LTCTF tests (BSC, 2004e). The GC data used for EBSCOM-nominal Version 1.0 are from 5-year exposure test reports (BSC, 2003; BSC, 2004c,e).

There is contradictory evidence in the literature regarding the effect of thermal ageing on the rate of GC of alloy C-22. Rebak *et al*. (2000a,b) report enhanced corrosion rates of thermally aged material in a highly aggressive industry standard test environment (ASTM G28A, boiling 50% H_2SO_4 + 42 g/L $Fe_2(SO_4)_3$). However, tests in environments more relevant to those expected in the repository indicate no such enhancement (BSC, 2003; 2004e). Therefore, no enhancement factor is included in EBSCOM for the effect of thermal ageing.

4.3.2.2 Localized Corrosion

Localized corrosion (LC) of the alloy C-22 WP can occur in some environments, but only if seepage water can contact the waste package and concentrate by evaporation. A pre-requisite for LC of the WP, therefore, is that the DS has failed. EPRI has shown that deliquescent solutions that might form due to dust deposits cannot sustain localized corrosion (EPRI, 2004a). Localized corrosion of alloy C-22 has been observed in the laboratory in divalent cation (Ca^{2+}, Mg^{2+}) chloride solutions at elevated temperature (BSC, 2003; BSC, 2004e; Cragnolino, 2003; Cragnolino *et al*., 2004; Dunn *et al*., 2003; Farmer *et al*., 2000; Hua and Gordon, 2004). The addition of nitrate, sulfate, and/or carbonate ions to the solution inhibits the initiation of LC. The majority of seepage and deliquescent solutions that might form on the surface of the WP at Yucca Mountain do not contain the necessary ions to support LC. In fact, of the various bins of possible seepage waters sampled in EBSCOM, only Bin 3 water will support initiation of LC of

the WP. This water accounts for only 1% of all of the possible waters at YM so that, on average, LC is only possible in 1 out of every 100 EBSCOM realizations. The EBSCOM code addresses both the initiation and propagation of LC. Initiation is treated using a threshold temperature for LC. Once initiated, LC is assumed to continue to propagate at a rate that decreases with time, with the exception of Waste Packages for which localized corrosion initiates during the initial temperature increase (*i.e.*, for times between 50 years and ~100 years following emplacement of the WP (Figure 4-4)). If LC initiates during the initial heat-up phase, it is assumed that LC propagation ceases during the subsequent thermal peak until such time that the temperature falls into the range for LC. The rationale for excluding LC propagation during the thermal peak is that no continuous water phase can be present on the WP surface during this period so that even if water is trapped within an initiated occluded region, anodic dissolution inside the crevice cannot electrochemically couple to the cathodic reduction of O_2 on external surfaces. The duration of this period of zero LC propagation is defined by the time for which the WP temperature exceeds the threshold temperature for the formation of an aqueous solution T_{AQ}.

In a Ca^{2+}-Cl^--NO_3^- solution that could support LC, the probability of initiation of localized attack is a complex function of the chloride concentration [Cl^-], the ratio of chloride to nitrate in solution [Cl^-]:[NO_3^-], electrochemical potential, and temperature. As the solution composition changes with time because of the evolution of the temperature and %RH in the drift, the conditions for LC will also change. In order to encompass the complex interdependence of these parameters while maintaining a level of simplicity in the EBSCOM code, the threshold condition for the initiation of LC is reduced to a critical temperature (T_{LC}). Localized attack will not initiate below T_{LC} regardless of the composition of the solution on the WP surface (provided the selected water belongs to Bin 3) and regardless of the value of E_{CORR}. This is the same approach employed in the EBSPA code (EPRI, 2002a).

There is a large body of experimental evidence to support the use of a threshold temperature approach, in general, and for alloy C-22 in particular (ASM, 2003). The relevant data for the LC of alloy C-22 are summarized by BSC (2004e). Microstructural changes introduced during welding increase the susceptibility of alloy C-22 to LC initiation, so separate T_{LC} are defined in EBSCOM for the waste package outer barrier ($T_{LCshell}$) and for the outer and middle closure lid welds (T_{LCweld}).

In summary, therefore, the prerequisites for LC of the WP are:

- the temperature must be ≤ TAQ, the temperature at which a stable aqueous phase can form (this is a pre-requisite for all forms of corrosion of the WP and DS),
- the selected environment must support LC (*i.e.*, Bin 3 water),
- the drip shield must have failed, and
- the temperature must be ≥ TLC.

If LC initiates, it is assumed to continue to propagate indefinitely (with the one exception noted above). However, the rate of propagation is assumed to decrease with time, essentially stifling LC growth after a certain period of time. The rate of LC propagation R_{LC} is given by (EPRI, 2002a):

$$R_{LC} = Bnt^{n-1} \qquad \textbf{Eq. 4-6}$$

where n is the time exponent for LC and the temperature-dependent growth constant B is given by:

$$B(T) = B(T_{ref}) \exp\left[\frac{\Delta E_B}{R}\left(\frac{1}{T_{ref}} - \frac{1}{T}\right)\right] \qquad \textbf{Eq. 4-7}$$

where ΔE_B is the activation energy describing the temperature dependence of B and the value of B at the reference temperature of 75°C ($B(T_{ref})$) is selected for each realization from a Weibull distribution (see Section 4.7).

In the absence of information to the contrary, the LC kinetics of the WP shell and closure lid welds are assumed to be the same. That is, there is assumed to be no metallurgical difference between the two welds.

4.3.2.3 Stress Corrosion Cracking

In the nominal scenario, SCC only affects the WP closure lid welds. The WP shell (including the non-closure lid) is heat treated to relieve manufacturing stresses prior to loading of the spent nuclear fuel. Once filled with the waste form and sealed, the WP cannot be stress relieved through heat treatment, although the surface of the outer closure lid weld is stress relieved by laser peening or low-plasticity burnishing (Peters, 2003b).

Various approaches have been proposed for predicting the occurrence of SCC. Traditionally, SCC was described as the result of the conjoint action of a tensile stress on a susceptible material in a corrosive environment (Jones and Ricker, 1992). Staehle (2005) has suggested a more-extensive list of seven primary variables that determine the SCC behavior, namely: potential, pH, temperature, appropriate chemical species, alloy composition, strength of the material, and stress. Regardless, it is clear that for any material, SCC only occurs under certain environmental and mechanical loading conditions. Work reported by the DOE (Andresen *et al*., 2001; 2003; BSC, 2004f; Young *et al*., 2003) and CNWRA (Cragnolino *et al*., 2003; 2004; Dunn *et al*., 2002) has shown that alloy C-22 is highly resistant to crack initiation and growth. The DOE have only observed cracking under certain, very specific, environmental conditions (BSC, 2004f), while the CNWRA studies show no indications of crack initiation or growth at all. Nevertheless, the possibility of SCC is included in the EBSCOM code and, along with the treatment of other corrosion processes, is based on EPRI's best estimate of the likely SCC behavior of the WP derived primarily from the data presented by the DOE (BSC, 2004f).

In EBSCOM, there are a number of pre-requisites for SCC of the closure lid welds:

- the environment must support SCC,
- the value of the corrosion potential ECORR must be equal to or exceed the threshold potential for SCC, and
- the surface tensile stress in the weld (σ) must exceed the threshold stress for crack initiation (σINIT).

A fourth criterion for the SCC of the middle closure lid weld is that the outer closure lid must have previously failed, thus permitting an aqueous environment to form on the middle lid weld.

Crack propagation is assumed to be rapid compared with the periods under consideration, so the EBSCOM SCC sub-model is based on a threshold stress initiation criterion. A second initiation criterion will be considered in future versions of the model based on the threshold stress intensity factor for SCC K_{ISCC}. This criterion applies to pre-existing crack-like defects in the weld that act as stress intensifiers for crack propagation.

Information regarding the three SCC prerequisites listed above is derived from experimental data developed by the DOE (Andresen *et al*., 2001; 2003; BSC, 2004f; Young *et al*., 2003). Figure 4-6 shows a summary of the DOE slow strain rate test (SSRT) results in a range of environments as a function of the electrochemical potential. The results are expressed as the % reduction-in-area (%RA) of the round tensile specimen after the sample had been strained to failure. The smaller the %RA, the more brittle the sample, and vice versa. High %RA values indicate the sample is ductile and not susceptible to cracking. In the figure, tests in which SCC is observed are indicated by the full symbols, whereas the absence of SCC is indicated by the open symbols and horizontal lines. Figure 4-7 shows the results of the same tests, but as the time-to-failure (t_F) where, obviously, the shorter the value of $t_{F,}$ the more brittle and the more prone to cracking the sample.

The results in Figures 4-6 and 4-7 show that the susceptibility of alloy C-22 to SCC is a function of both the nature of the aqueous environment and of the electrochemical potential. (The tests shown in the two figures are performed at temperatures ranging from 22°C to 105°C, but no systematic effect of temperature is apparent from the results). Cracking is only observed in Simulated Concentrated Water (SCW) and then only at relatively positive potentials. Cracking is not observed in Simulated Acidified Water (SAW) with and without the addition of $Pb(NO_3)_2$, Basic Saturated Water (BSW) (including BSW modified by the removal of sulfate and/or nitrate ions), or Simulated Saturated Water (SSW). These test solutions represent concentrated solutions that might form on the surface of Waste Packages exposed to seepage or deliquescent solutions and that are subsequently concentrated by evaporation. EBSCOM takes into account the variability in the nature of the seepage and deliquescent waters and selects a particular water composition for each realization. Solutions that might evolve into a concentrated water similar to SCW (*i.e.*, Bins 9 and 11) constitute 71% of the waters simulated by the EBSCOM code (Table 4-2).

Even if the appropriate environment forms on the WP closure lid welds, SCC is only possible if E_{CORR} is sufficiently positive. SCC was only observed experimentally at potentials ≥200 mV_{SSC}, a potential that is typically 340-620 mV more positive than E_{CORR} (BSC, 2004f). In SCW solutions, E_{CORR} varied between –241 mV_{SSC} and –76 mV_{SSC} in the DOE tests. The shaded triangle in Figures 4-6 and 4-7 represent the range of potentials for which SCC is considered possible in EBSCOM. This region extends to a minimum potential of 0 mV_{SSC}, 200 mV below the minimum potential for SCC reported to date and, hence, retains a significant degree of conservatism. An asymmetrical triangular distribution is used for the threshold potential for SCC, with upper and lower bounds of +400 mV_{SSC} and 0 mV_{SSC}, respectively, and a maximum probability of SCC at +400 mV_{SSC}. In the model, SCC is only considered possible in the 71% of susceptible sampled waters if the calculated value of E_{CORR} exceeds the threshold potential.

DOE has developed an empirical expression for predicting the value of E_{CORR} based on fitting a range of data to various functional relationships (BSC, 2004e). The function found to best describe the observed dependence of E_{CORR} on temperature (T in °C), pH, and the $[Cl^-]$ and $[NO_3^-]$ (in $mol \cdot kg^{-1}$) is:

$$E_{CORR} = c_0 + c_1 T + c_2 pH + c_3 [Cl^-] + c_4 \log\left(\frac{[NO_3^-]}{[Cl^-]}\right) \qquad \textbf{Eq. 4-8}$$

In general, the value of E_{CORR} increases with temperature by 0.677 mV/°C, decreases with pH by 65.338 mV/pH unit, decreases modestly with increasing $[Cl^-]$ (c_3 = -7.6 $mV \cdot kg \cdot mol^{-1}$), and shifts to more positive potentials with increasing $[NO_3^-]$:$[Cl^-]$ ratio (c_4 = 37.1 mV). There is some variability in each of the fitting parameters, but in EBSCOM only the variability in c_0 (c_0 = 558.283 ± 36.156 mV_{SSC}) is taken into account as it has by far the largest influence on E_{CORR}.

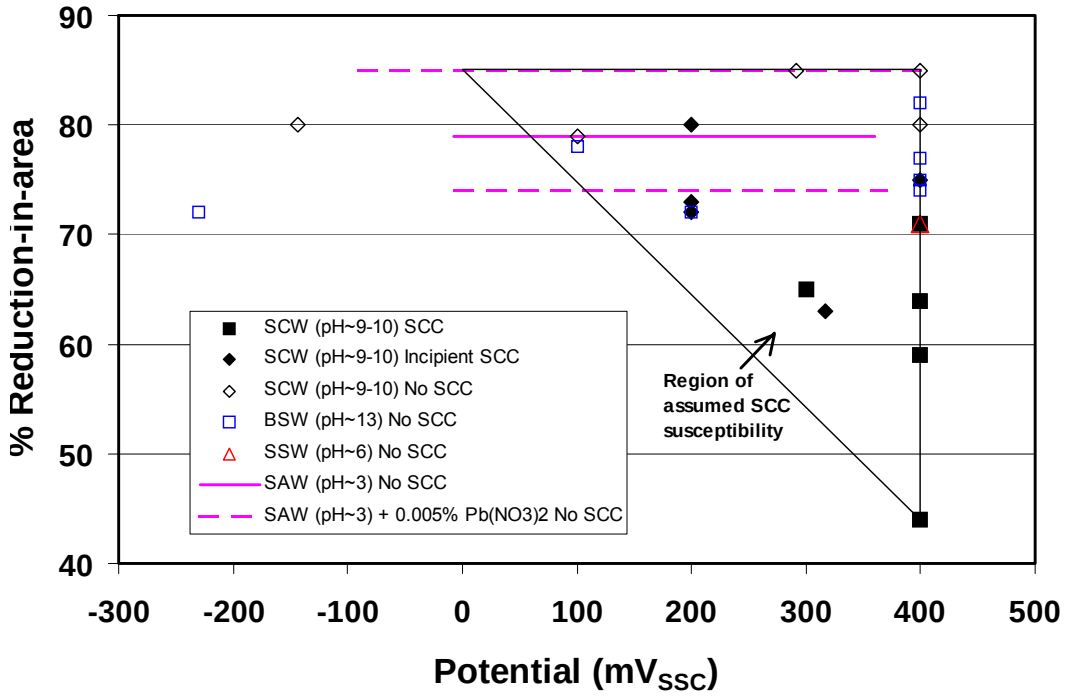

Figure 4-6
Summary of the DOE slow strain rate SCC Tests as a function of electrochemical potential expressed as the percent reduction-in-area.

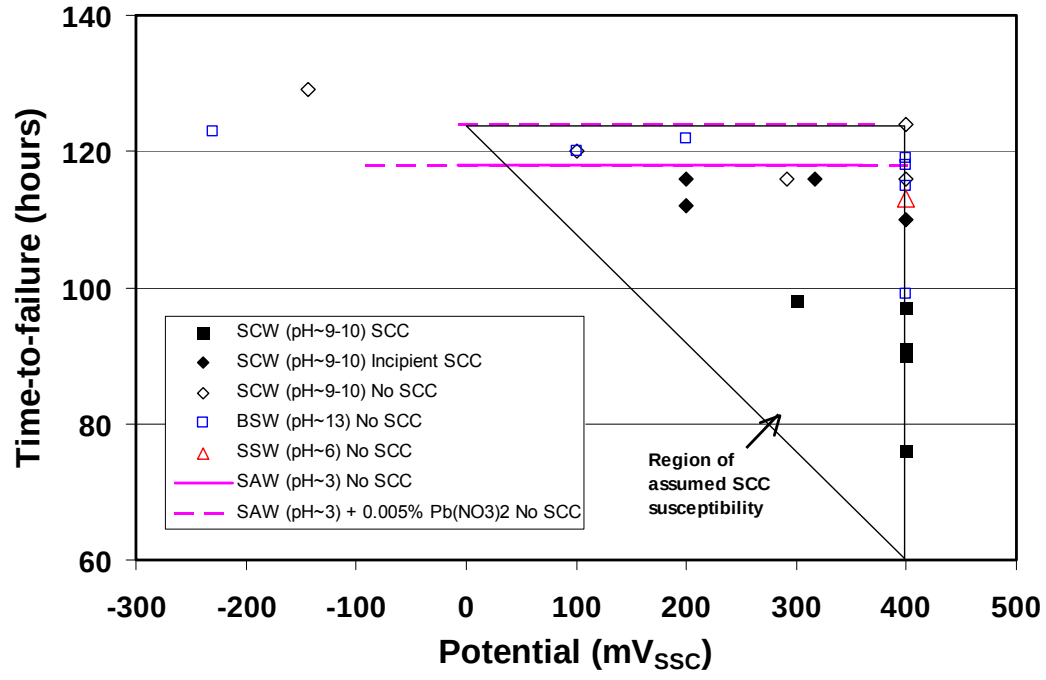

Figure 4-7
Summary of the DOE slow strain rate SCC tests as a function of electrochemical potential expressed as the time-to-failure.

The value of E_{CORR} will be different for each of the five bins of solution sampled in EBSCOM because of the different composition and pH. The corrosion potential will also vary with time because of the time-dependence of the temperature in the drift and because the composition evolves as the seepage waters evaporate on contact with a hot WP. The concentrated solutions used in the LTCTF tests represent the composition of a number of the different bins of seepage and deliquescence waters following evaporation (Table 4-2). In addition, the DOE has "numerically" evaporated each of the bins of water using the EQ3/6 software package and predicted the dependence of the composition on the % RH (BSC, 2004a; Peters, 2003a). Using the mean composition for relative humidities between 90% RH and dry-out as representative of the composition of the evaporated bin water, the temperature dependence of E_{CORR} for the different concentrated test solutions and evaporated bin waters is estimated from Equation (4-8).

Figure 4-8 shows the estimated temperature dependence of the E_{CORR} values for a range of solutions. The value of E_{CORR} is most positive in the SCW, primarily because of the lower pH of this solution (pH 9.5) compared with that for BSW, and Simulated Dilute Water (SDW). The Bin 9 water has a similar E_{CORR} value to SDW. In EBSCOM, the E_{CORR} for solutions that can support SCC (Bins 9 and 11) is assumed to be given by the expression:

$$E_{CORR} = -101.82 + 0.677T \text{ mV}_{SSC} \qquad \textbf{Eq. 4-9}$$

based on a composition of $[Cl^-] = 1 \text{ mol}\cdot\text{kg}^{-1}$, $[NO_3^-]:[Cl^-] = 1.057$, and pH = 10 (Peters, 2003a). The value -101.82 mV_{SSC} is assumed to be normally distributed with a standard deviation of 36.156 mV (as for the coefficient c_0 in Equation (4-8)).

The third criterion for SCC is that the surface stress exceeds the value of σ_{INIT}. Crack initiation generally requires some degree of plastic deformation, suggesting a threshold stress in the region of the yield stress (YS). This conclusion is confirmed by the results of DOE constant-load tests that showed no crack initiation for loads of up to 2.1YS (BSC, 2004f). Furthermore, plastically deformed alloy C-22 U-bend specimens have not shown crack initiation after exposure to various concentrated test waters in the LTCTF for periods of up to 5 years. The slow strain-rate testing (SSRT) described above in which some crack initiation is observed under specific environmental and electrochemical conditions are severe tests in which the sample is tested to failure. Initiation may have occurred at any time during the test but, based on the DOE constant-load and U-bend tests, it is likely to have occurred only after yielding of the sample has commenced (BSC, 2004f. Based on this evidence, the threshold stress for crack initiation in the EBSCOM model is assumed to be given by a uniform distribution with upper and lower bounds of 1.0YS and 0.9YS, respectively.

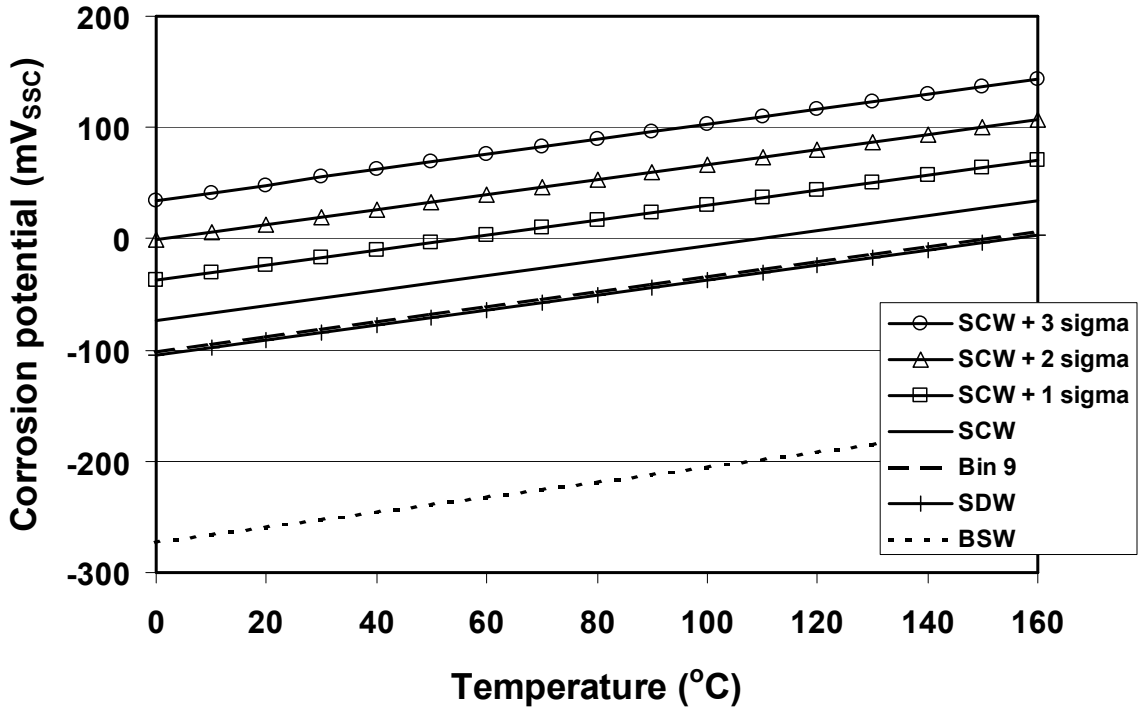

Figure 4-8
Predicted temperature dependence of the corrosion potential of Alloy C-22 in representative test waters and evaporated seepage waters. For Saturated Concentrated Water (SCW), curves are shown for the mean value of the C_0 fitting parameters and for values of C_0 plus 1, 2, and 3 standard deviations.

The distribution of residual stresses in the closure welds is required to determine whether the surface stress exceeds the value of σ_{INIT}. For the nominal scenario, the residual stresses in the hoop and radial directions for the outer and middle closure lid welds have been provided (BSC, 2004f). Figure 4-9 shows the distribution of residual stress as a function of depth through the weld. For both the outer and middle closure lid welds, the residual stress in the hoop direction is higher than the radial residual stress. Crack initiation and growth, therefore, is most likely to occur axially along the WP rather than circumferentially. Only the hoop stress component is considered in EBSCOM.

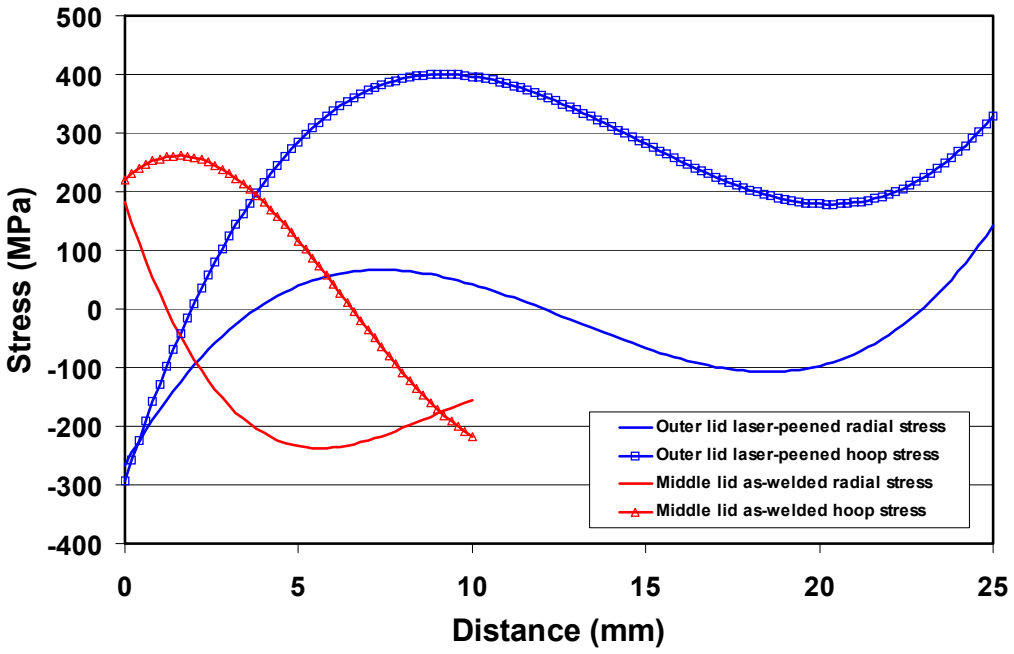

Figure 4-9
Depth dependence of the residual stress in the hoop and radial directions for the laser-peened outer closure lLid and the middle closure lid welds (BSC, 2004f)

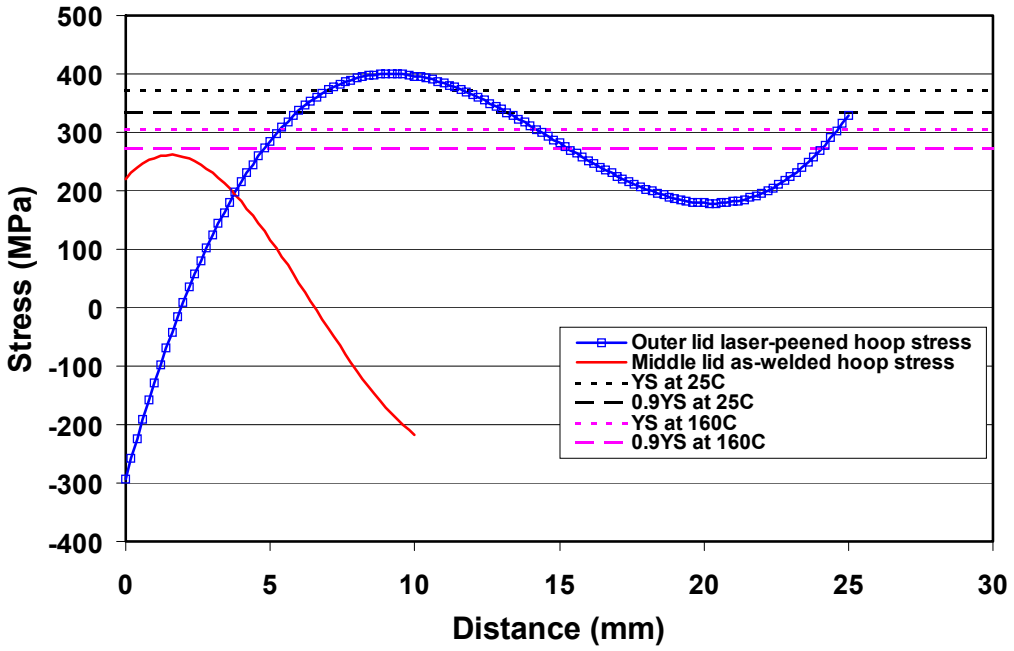

Figure 4-10
Comparison of the depth dependence of the residual hoop stress for the laser-peened outer closure lid and the middle closure lid welds and EBSCOM criteria for the threshold stress for crack initiation.

Figure 4-10 compares the residual hoop stresses with the criterion for the initiation of SCC established above. The figure shows thresholds based on 0.9YS and 1.0YS for temperatures of 25°C and 160°C. As the YS increases with decreasing temperature, the probability of crack initiation decreases with increasing time as the repository cools. The temperature dependence of the YS (σ_{YS}) for alloy C-22 is given (BSC, 2004f) by:

$$\sigma_{YS} = 382.21 - 0.48466\ T \quad \text{MPa} \qquad \textbf{Eq. 4-10}$$

where T is in °C.

It is apparent from Figure 4-10 that the outer closure lid weld is not susceptible to crack initiation in its pristine state because of the surface compressive stress produced by the laser-peening process. However, as the surface of the weld is corroded by a combination of general and localized corrosion, the sub-surface tensile region may be exposed to the environment. In EBSCOM, it is assumed that the residual stress distribution shown in Figure 4-10 remains unchanged as the surface of the weld is corroded. Thus, once the outer 2-3 mm of the outer closure lid weld has been corroded, the surface residual stress changes from compressive to tensile. Once 5-10 mm of the weld has been removed by corrosion, the surface tensile stress may be sufficiently high for crack initiation. This is a conservative assumption as, in reality, the residual stresses will re-distribute as the compressive surface layers are removed and the peak tensile stress would be expected to decrease.

4.3.2.4 Microbially Influenced Corrosion [MIC]

Microbially influenced corrosion of the WP is potentially important in the long term once environmental conditions in the drift have ameliorated sufficiently to allow microbial activity. One of the major stressors for microbial activity in the repository is the general lack of water, characterized by the low %RH in the drift. The RH is numerically equal to the thermodynamic water activity a_W, a parameter that has been linked to the viability of different types of microbes (Brown, 1990; King *et al*., 2004; Meike and Stroes-Gascoyne, 2000; Stroes-Gascoyne and King, 2002). Most microbial species are not active at $a_W < 96\%$, and this water activity has been proposed as a threshold value for the modeling of microbial activity in nuclear waste repositories (King *et al*., 2004). The time dependence of the %RH (or a_W) in the drifts is not explicitly included in EBSCOM but, as RH and temperature are closely linked, the conditions for the onset of microbial activity in the repository following the thermal pulse can be defined by a threshold temperature for MIC, T_{MIC}.

In the EBSCOM code, MIC can take two forms: MIC-enhanced general corrosion and MIC-induced LC. The DOE has reported an increase in the rate of general corrosion of alloy C-22 when exposed to microbial cultures and include this corrosion mechanism in WP degradation models (BSC, 2004c; Farmer *et al*., 2000; Horn *et al*., 1998). Localized corrosion of alloy C-22 due to microbial activity has never been reported in the literature, but is a common form of MIC for other, less-corrosion-resistant, passive alloys (Little *et al*., 1991). Although the possibility for MIC-induced LC is included in EBSCOM, it has not been implemented by EPRI in the default version of the code and, at present, EPRI does not believe that it should be implemented until such time that there is reliable experimental evidence to indicate that microbes can induce the localized corrosion of alloy C-22.

MIC-enhanced GC is treated in EBSCOM using a relatively simple approach. For each realization, a value of the critical temperature for MIC, T_{MIC}. and the MIC GC enhancement factor f_{MIC} are defined or selected from a distribution. This value of f_{MIC} applies to the WP shell and the outer and middle closure lid welds.

The temperature at which the %RH at the WP surface equals 96% (equivalent to the critical water activity of 0.96) depends on the temperature profile of the WP. Thus, cooler waste packages attain this RH at a higher temperature than hotter waste packages. Based on the temperature-%RH data in Figure 4-3(c), the critical temperature for MIC of alloy C-22 is given by:

$$T_{MIC} = (50/f_{Tm})\ ^{o}C \qquad \textbf{Eq. 4-11}$$

where f_{Tm} is the maximum value of the multiplying factor for the temperature profiles of the WP (Equation (4-2)). Thus, for the average (f_{Tm} = 1.0), coolest (f_{Tm} = 0.67), and hottest (f_{Tm} = 1.26) WP, the value of T_{MIC} is 50°C, 75°C and 40°C, respectively (see Figure 4-3(c)). For the expected evolution of the repository environment, there is no minimum temperature for microbial activity.

When the temperature is equal to or below T_{MIC}, the rate of GC is enhanced by the factor of f_{MIC} (Equation (4-5)). Following the treatment developed by the DOE (BSC, 2004c), the value of f_{MIC} in each realization is selected from a uniform distribution with lower and upper bounds of 1.0 (no enhancement) and 2.0, respectively. Alternatively, the value of f_{MIC} can be defined as a specific value for all realizations in an EBSCOM run (for example, to determine the effect of no microbial enhancement).

The treatment of MIC-induced LC is equally simple, at least in the current version of the EBSCOM code. For each realization, a probability of MIC LC (P_{MICLC}) is either defined or selected from a distribution. Since MIC-induced LC can lead to preferential attack at welds (ASM, 2003), a different value of P_{MICLC} is defined for the WP shell ($P_{MICLCshell}$) and for the outer and middle closure lid welds ($P_{MICLCweld}$). At this time, there is no evidence of MIC-induced LC of alloy C-22, so all values of P_{MICLC} are set to zero for the default input parameters. Therefore, there is no treatment of the kinetics of MIC LC in EBSCOM.

4.3.2.5 Comparison with EBSPA

The treatment of WP corrosion in the EBSCOM code differs from that in the EBSPA model in a number of ways, including:

General corrosion

- a term for the reduction in the rate of GC of the laser-peened closure weld on the outer lid, and
- an updated Weibull distribution of GC rates based on 5-year LTCTF data.

Localized corrosion

- the assumption that LC is only possible in certain environments, in particular the Bin 3 water representing only 1% of all the environments considered in the EBSCOM code,
- the possibility of initiation and propagation of LC during the initial repository heat-up phase,
- the inclusion of distributions for both TAQ and TLC, and
- the use of different TLC for the WP shell and closure lid welds in a given realization.

Stress corrosion cracking

- the assumption that SCC is only possible in certain waters (Bins 9 and 11), representing 71% of all possible environments,
- the inclusion of a potential threshold criterion for SCC initiation and the calculation of a temperature-dependent ECORR value,
- the explicit modeling of the depth-dependence of the stress in the closure-lid welds,
- the use of a distributed temperature-dependent threshold stress criterion for crack initiation, and
- the exclusion from EBSCOM-nominal Version 1.0 of effects due to crack-like weld defects based on a threshold stress intensity factor criterion.

Microbiologically influenced corrosion

- the inclusion of effects due to MIC, including MIC-enhanced GC and the possibility of MIC-induced LC.

The net effect of these changes is to reduce the probability of WP failure by LC or SCC compared to the probability calculated with the previous EBSPA code. In the case of LC, the lower failure probability is primarily a consequence of the inclusion of environmental variability in the EBSCOM code and the fact that very few of the possible YM environments will support LC. For SCC, the lower probability of failure is a consequence of the inclusion of the threshold potential criterion for SCC initiation and, to a lesser extent, the limitation of cracking to only two of the five possible environmental bins sampled in the EBSCOM code. These changes to the treatment of LC and SCC better reflect the results of laboratory studies that show that these forms of corrosion are unlikely for alloy C-22 WP in the YM repository.

4.4 Structure of the Model

The structure of the EBSCOM code is presented here in the form of a number of flow charts describing the treatment of the various corrosion processes for the WP and DS. These flow charts show the structure of a single run of the EBSCOM code, which typically comprises 1,000,000 individual realizations. Each realization describes the performance of a single WP and the corresponding DS. There is a certain probability that the WP shell, outer closure lid weld, inner closure lid weld, and/or DS may contain an undetected manufacturing defect or be emplaced incorrectly so as to cause failure of that particular component soon after permanent

repository closure. In EBSCOM, a mean initial failure fraction of 10^{-4} is used for all EBS components. See the previous sections for justification of the assumptions and parameter values cited below.

Each realization within a single run of the EBSCOM code is characterized by:

- one of five possible environments (denoted Bins 3, 4, 5, 9, and 11),
- a particular temperature-time profile,
- the temperature at which an aqueous phase is stable on the WP and/or DS surface,
- the temperature at which microbial activity is possible,
- the GC characteristics of the DS (including the rate of GC of the DS at the reference temperature of 75°C, the activation energy, factors for the effect of fluoride ions and the fraction of GC supported by O2 reduction),
- the HIC characteristics of the DS (including the temperature-dependent hydrogen uptake efficiency and the critical hydrogen concentration),
- the GC characteristics of the WP outer shell (including the rate of GC of the WP at the reference temperature of 75°C and the activation energy),
- the LC characteristics of the WP outer shell (including the threshold temperature for LC, the LC growth constant, activation energy, and time exponent),
- the MIC characteristics of the WP outer shell (including the MIC GC enhancement factor and the probability of MIC LC), and
- the specific corrosion characteristics of the closure lid welds (including the reduction factor for GC of the laser-peened weld (outer closure lid only), the probability of MIC LC, the threshold temperature for LC, and the threshold stress for SCC initiation).

Other characteristics of the EBS are the same for all realizations in a given run, including:

- the dimensions of the WP and DS, and
- the residual stress profile through the thickness of the outer and middle closure lid cuts.

4.4.1 Overall Model Structure

Figure 4-11 shows the overall structure of the various sub-components of the EBSCOM code. The primary flow chart (the EBSCOM Flow Chart, Figure 4-12) describes the selection of the environmental parameters common to all EBS components for a particular realization. The Drip Shield Flow Chart predicts the failure time and mode of the DS as a result of GC or HIC. The Waste Package Flow Chart performs a similar function for the WP, although in this case the corrosion behavior of the shell and outer and middle closure lid welds are assessed separately. In addition, separate flow charts are defined for the WP components depending upon whether LC is possible or not (LC does not occur if the DS is intact or, for a failed DS, if the temperature is below the threshold for the initiation of LC). The WP components are also assumed to be susceptible to MIC if the temperature is below the threshold for microbial activity. Finally, SCC can lead to failure of the outer closure lid weld if certain criteria are met. (For the nominal

scenario, the level of residual stress for the middle closure lid is insufficient to cause failure by SCC).

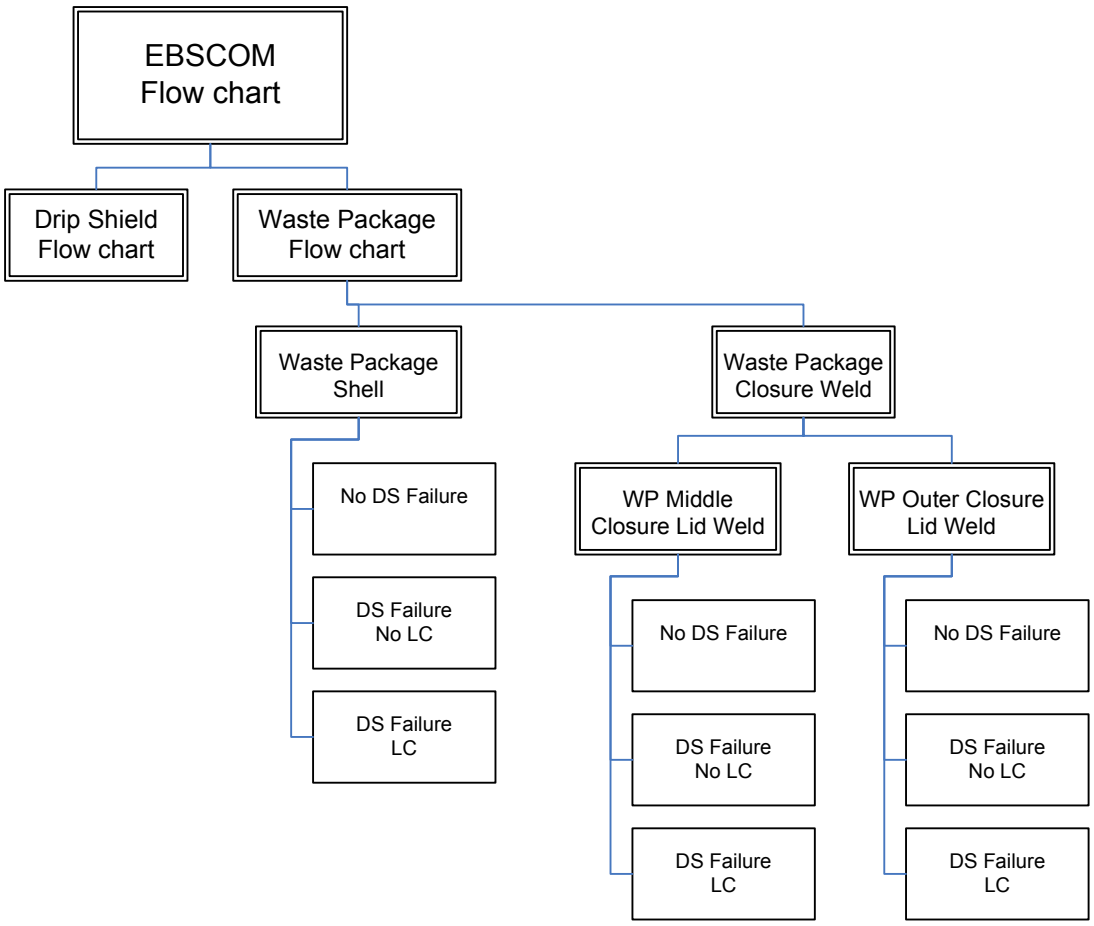

Figure 4-11
Hierarchy of flow charts for EBSCOM code.

Figure 4-12 shows the primary flow chart for the EBSCOM code that controls the execution of each realization. At the start of each realization, the value of the temperature for the formation of an aqueous phase (T_{AQ}), the temperature-time profile, and the nature of the environment are either defined or selected from the appropriate distribution. Next, the initial state of each EBS component considered (*i.e.*, drip shield, waste package outer shell, waste package outer and middle closure lid welds) is determined and the identity of any failed components (selected based on the defined initial failure frequency) recorded. The time is then incremented and the temperature (re-)calculated. Once $T \leq T_{AQ}$, the code proceeds to the DS and WP flow charts and the extent of corrosion damage is estimated for that time increment. Unless all of the EBS components have failed, the time is then incremented, the temperature re-calculated, and the extent of corrosion in the next time step estimated. This process is repeated until all EBS components of concern have failed, at which time the realization is stopped and the next realization is started. Once a particular EBS component has failed (*e.g.,* the DS fails by HIC), no further calculations are performed to determine the failure time by GC. Similarly, if the WP fails due to failure of the outer and middle closure lid welds, the calculation is terminated and the

lifetime of the WP shell is not computed. Furthermore, no credit is taken for the WP 316NG stainless steel inner shell.

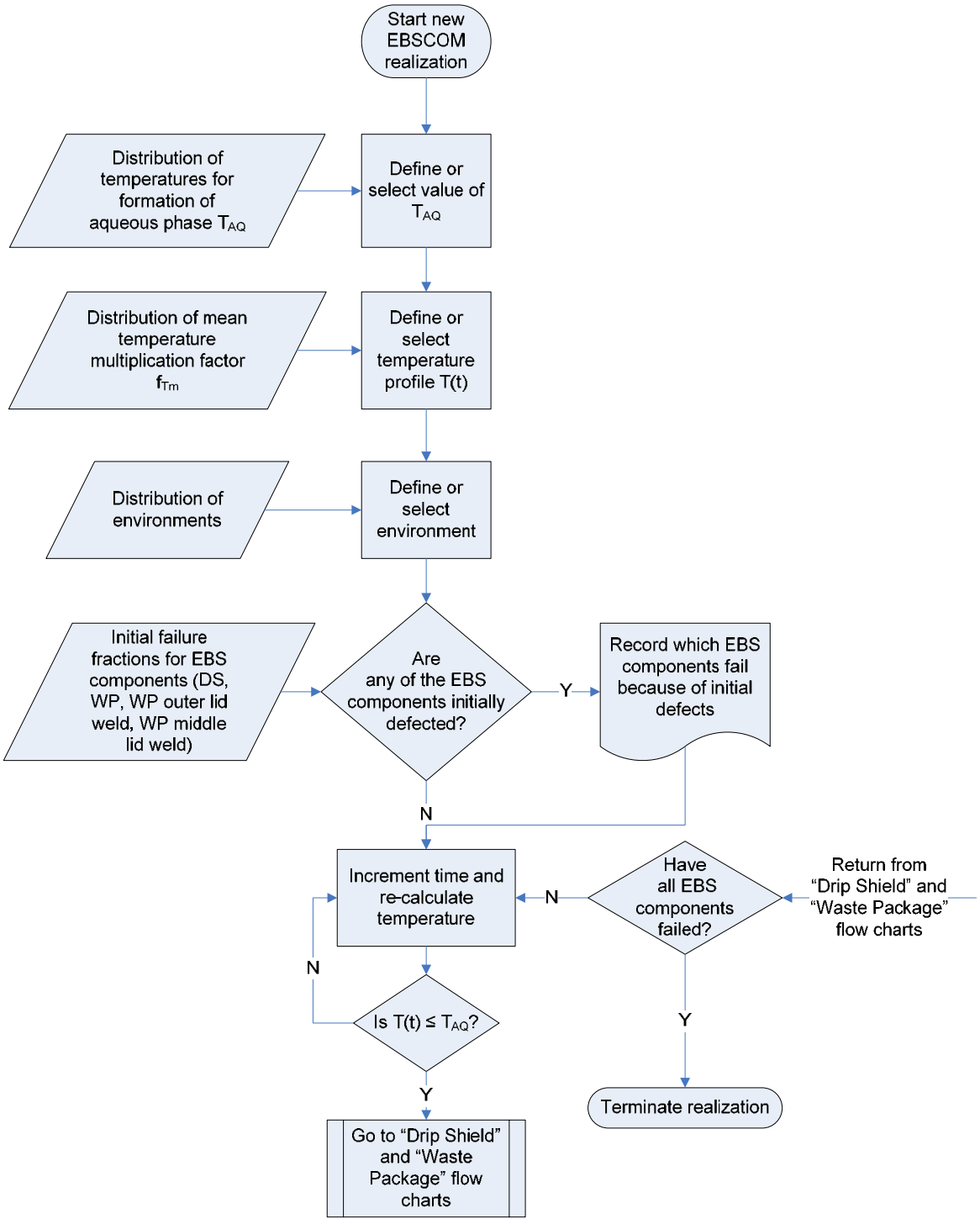

Figure 4-12
Overall EBSCOM flow chart.

4.4.2 Drip Shield

Figure 4-13 shows the overall flow chart for calculating the time-to-failure of the DS in a given realization. At the beginning of each realization, the values of five parameters are defined and remain fixed for all time increments. These parameters are: the value of the rate of GC at the reference temperature, the activation energy for GC, the critical hydrogen concentration for HIC, the temperature-dependent H uptake efficiency, and the fraction of Ti corrosion supported by O_2 reduction. Each of the parameters is either defined or a value is selected from a pre-defined distribution.

At each time step (determined by the Overall EBSCOM Flow Chart, Figure 4-12), the incremental depth of GC and the incremental increase in the absorbed hydrogen concentration H_{ABS} is determined. As noted in Section 4.3.1.2, the latter is determined by the extent of GC, the fraction of corrosion supported by the reduction of H_2O, the H uptake efficiency, and the amount of H lost by corrosion of the Ti matrix. The increment in GC is compared with the remaining wall thickness and the new H_{ABS} is compared with the value of H_{CRIT} defined for the realization. If either criterion results in DS failure, then the cause of failure is recorded and the code increments the time (if the WP has not yet failed). If neither failure criterion results in DS failure, then the code similarly increments the time and recalculates the depth of GC and the new H_{ABS}. If both failure criteria are satisfied in a single time step, then failure of the DS by GC is recorded (on the rationale that GC must occur before any H can be absorbed) and the realization continues with the calculation of the corrosion of the WP alone.

4.4.3 Waste Package

Figures 4-14 through 4-27 describe the EBSCOM structure for the calculation of the failure times of the WP. As noted in Figure 4-11, separate calculations are performed for the WP shell, and the outer and middle closure lid welds, with the latter being addressed only after the outer weld has failed and moisture enters the WP.

A number of parameters are common to all WP components, and these are identified in the Overall Waste Package Flow Chart in Figure 4-14. Within a given realization, a single value for the GC rate (at the reference temperature) and corresponding activation energy are used, as well as a single set of parameters describing the propagation of LC (*i.e.*, the growth constant B, activation energy ΔE_{LC}, and time exponent n). In addition, the same threshold temperature for MIC and MIC enhancement factor for GC are used for the WP shell and closure welds.

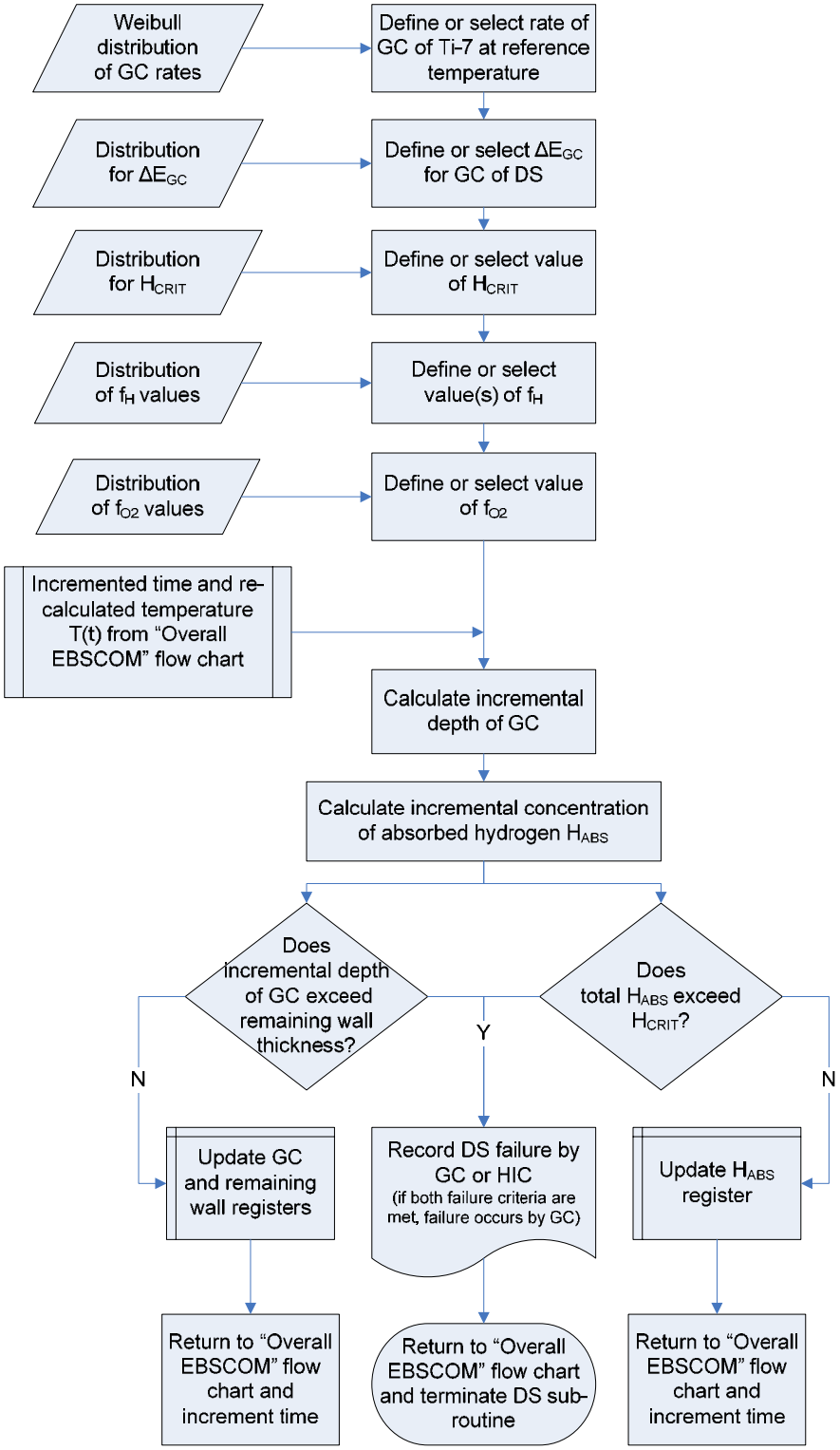

Figure 4-13
Drip shield flow chart.

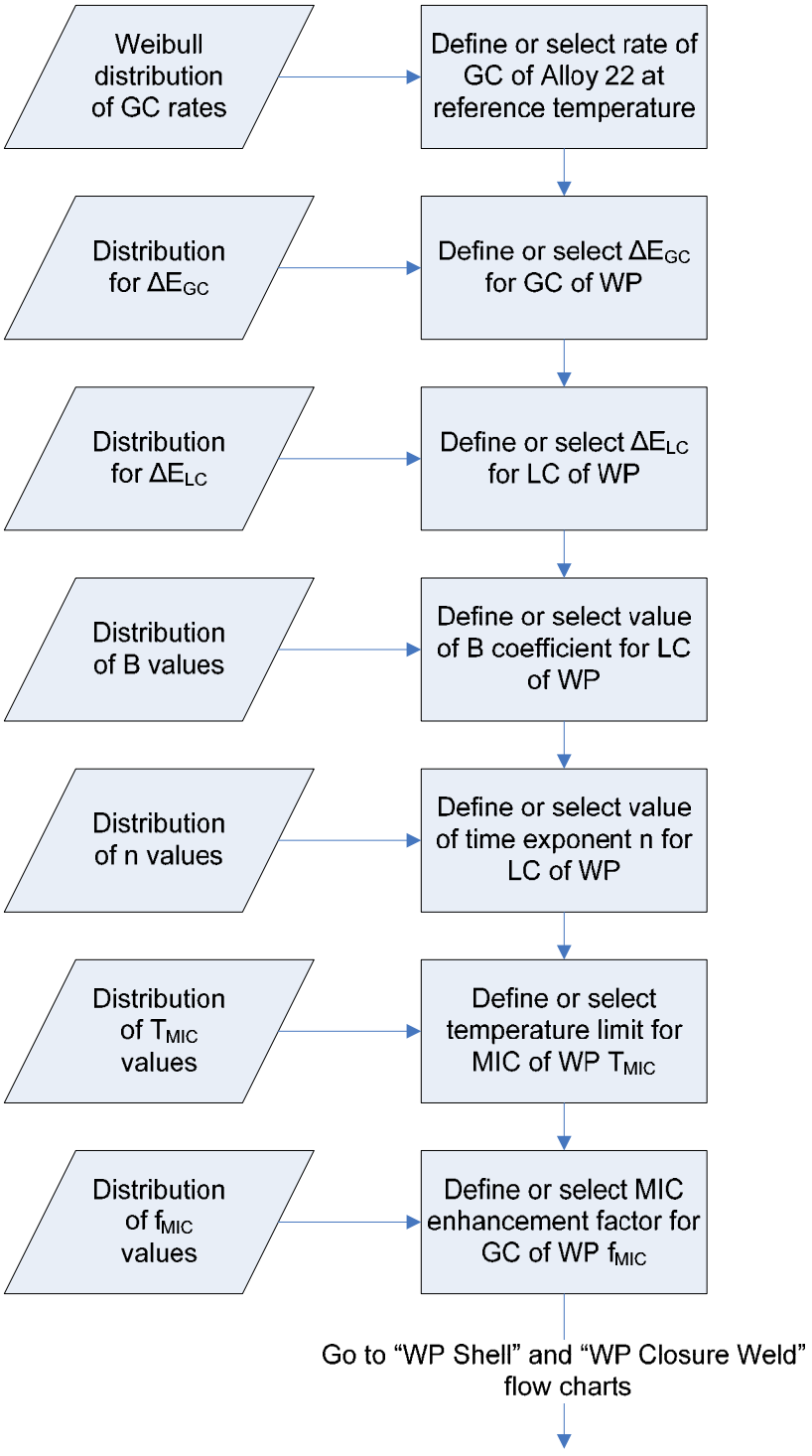

Figure 4-14
Overall waste package flow chart.

4.4.3.1 WP Outer Shell

Two parameters are specifically defined for the WP outer shell (Figure 4-15): the critical temperature below which LC cannot initiate ($T_{LCshell}$) and the probability of microbially influenced localized corrosion ($P_{MICLCshell}$).

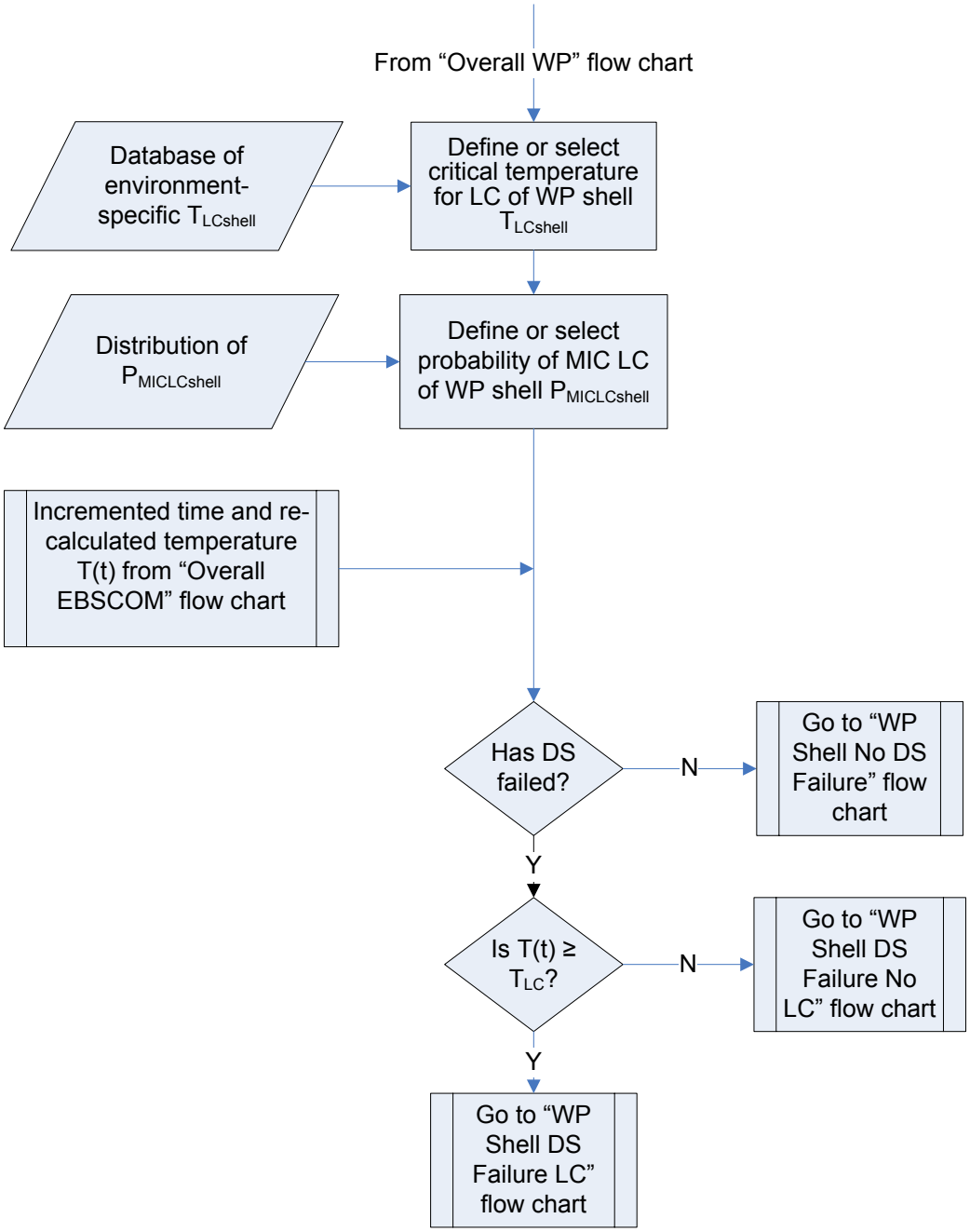

Figure 4-15
Waste package outer shell flow chart.

The nature of the corrosion processes for the WP shell, and hence the flow chart used to describe these processes, depends on the integrity of the DS and the temperature of the WP. If the DS is intact and is capable of diverting seepage drips away from the WP, then abiotic LC is not possible and the Waste Package Shell - No Drip Shield Failure flow chart (Figure 4-16) is followed. If the DS has failed but the WP temperature is less than $T_{LCshell}$,, then again abiotic LC is not possible and the corresponding flow chart (Waste Package Shell - Drip Shield Failure No Localized Corrosion) is shown in Figure 4-17. Finally, if the DS has failed but the WP temperature is equal to or greater than $T_{LCshell}$, then abiotic LC is possible and the Waste Package Shell - Drip Shield Failure Localized Corrosion flow chart (Figure 4-18) must be followed.

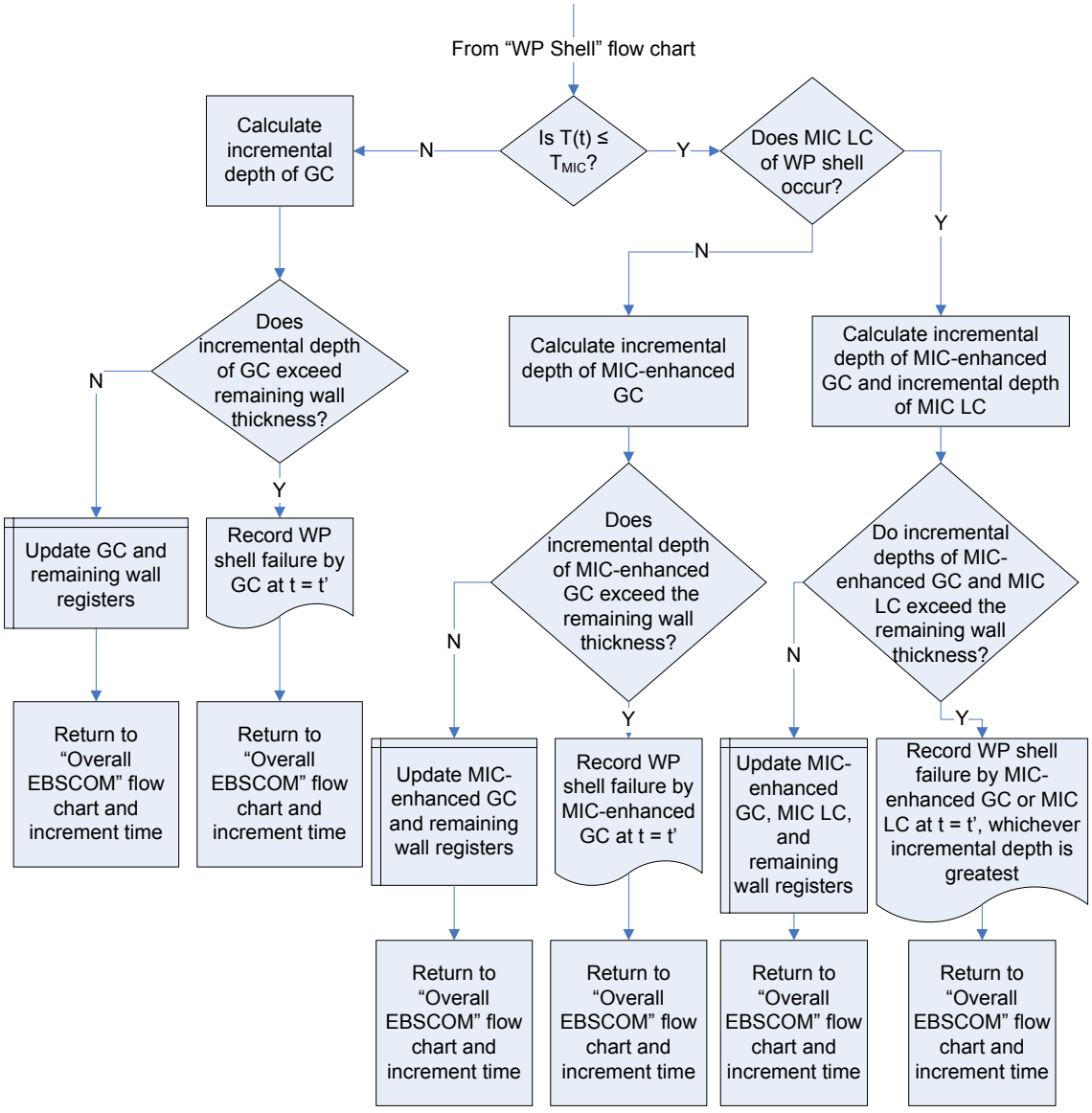

Figure 4-16
Waste package outer shell - no drip shield failure flow chart.

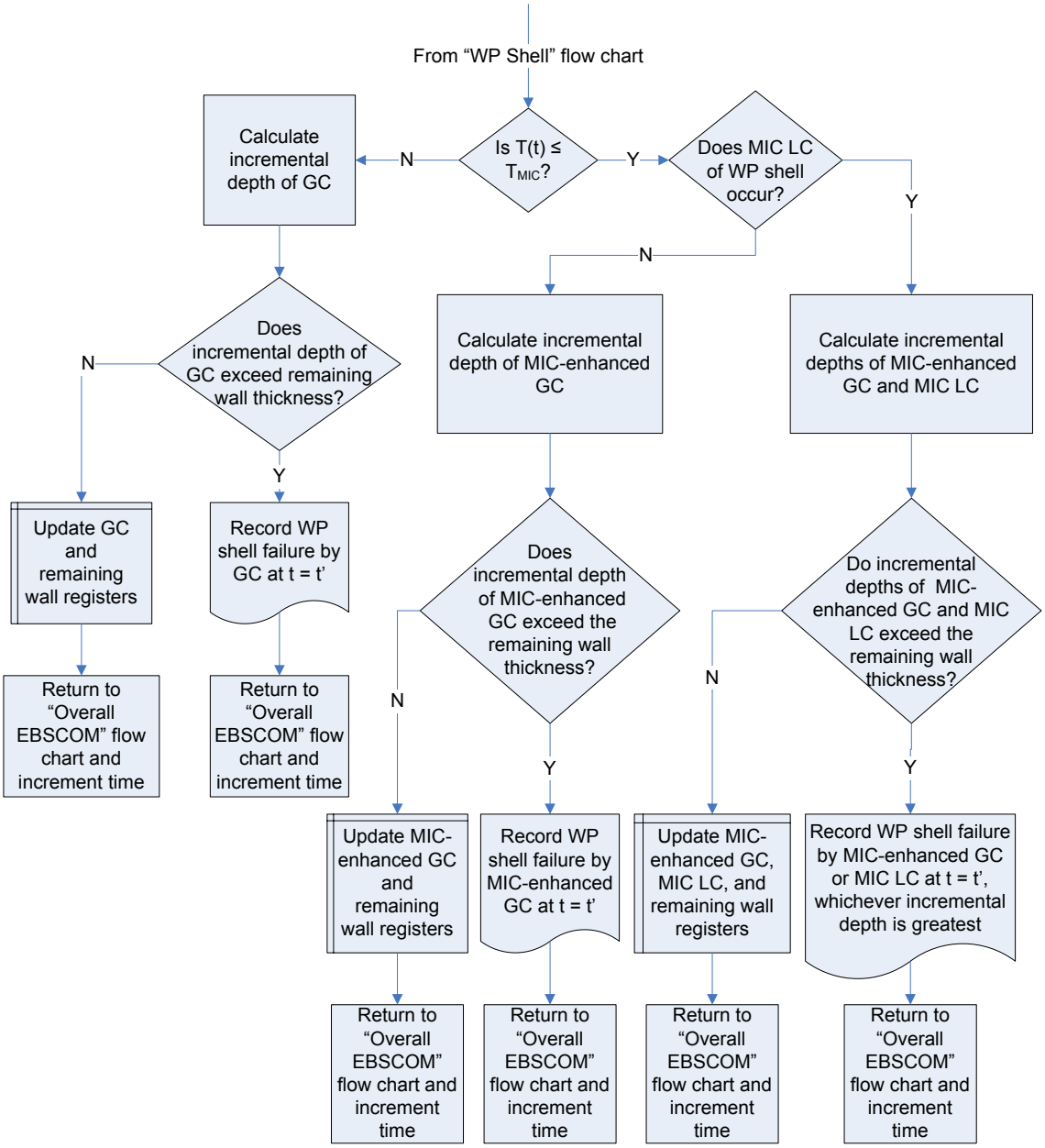

Figure 4-17
Waste package outer shell - drip shield failure no localized corrosion flow chart

The corrosion processes in the absence of LC are the same regardless of whether the DS is intact or the DS has failed but the WP temperature is below the threshold for LC. Therefore, the flow charts in Figures 4-16 and 4-17 are identical. For temperatures greater than the threshold temperature for microbial activity, the only corrosion process affecting the WP is GC. General corrosion is assumed to be possible at temperatures less than or equal to T_{AQ} because of the deliquescence of salts in dust deposits accumulated on the surface of the WP (no DS failure) or due to seepage (DS failure). No credit, however, is taken for the limited amounts of water expected in the drift and it is effectively assumed that the entire WP surface is wetted by an aqueous solution.

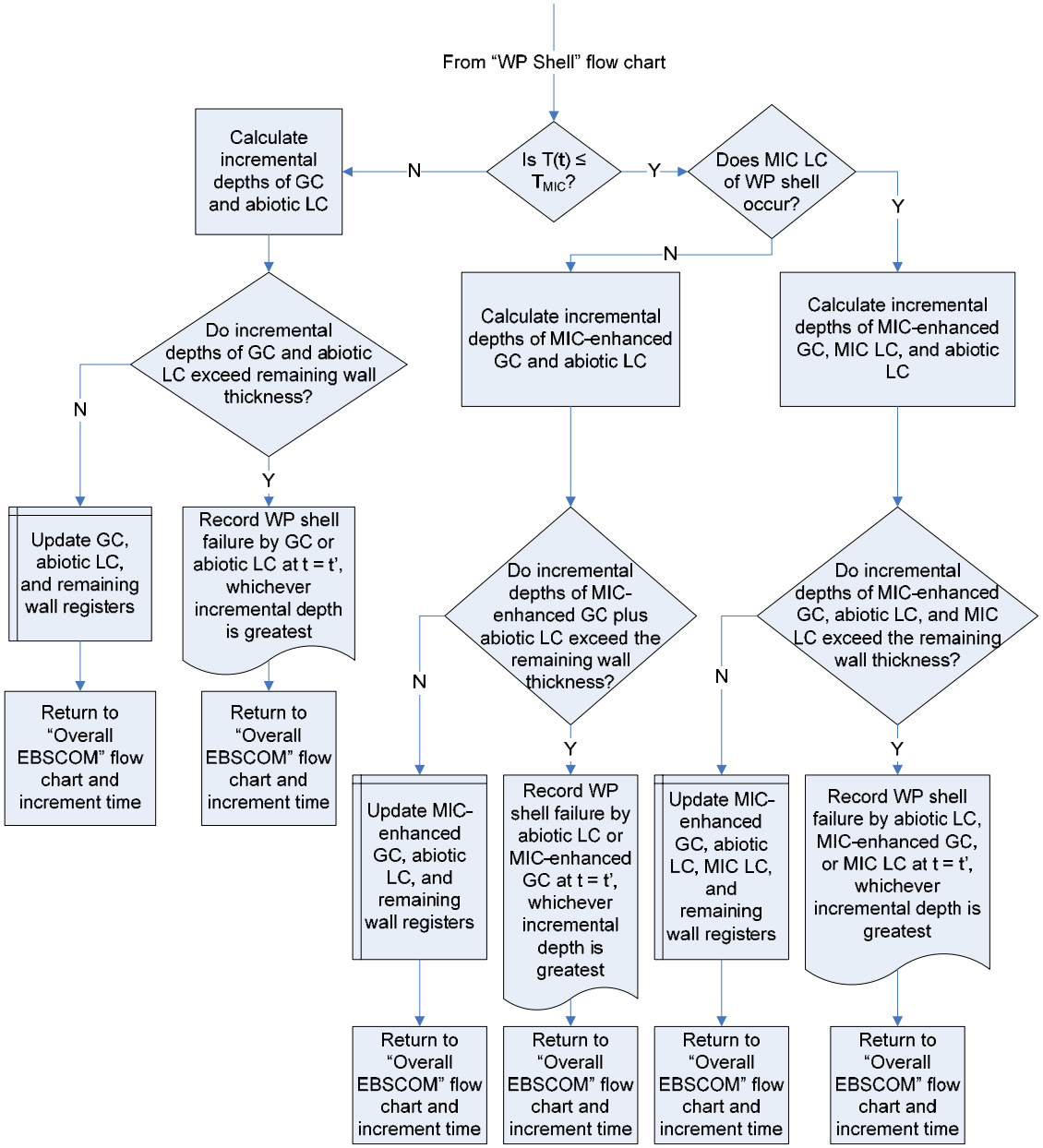

Figure 4-18
Waste package outer shell - drip shield failure localized corrosion flow chart

If the temperature is below the assumed threshold temperature for microbial activity, the WP is also susceptible to MIC. Microbially influenced corrosion can take the form of enhanced GC or, if shown by future testing to be important, LC. (The possibility of microbially supported localized corrosion is only included in EBSCOM because many forms of MIC tend to result in localized attack. However, it must be emphasized that currently there is no evidence of localized MIC of alloy C-22)

As noted above, abiotic LC of the WP is only possible if the DS has failed and the WP temperature is less than or equal to T_{AQ} but greater than or equal to $T_{LCshell}$ (Figure 4-18). A further criterion for LC is that the environment must support this form of corrosion, a condition that is only met for Bin 3 waters that represent only 1% of all waters sampled in EBSCOM (see Section 4.2.3.3.2).

In the unlikely event that LC does initiate, propagation is assumed to continue indefinitely. However, because of the use of a time-dependent LC penetration rate, the propagating crevice effectively stifles after a limited depth of corrosion. Failure of the WP outer shell by LC is unlikely to occur and the changes made to the treatment of LC in the EBSCOM code are chosen to reflect the unlikelihood of this form of corrosion for the design of EBS and the expected drift environment in the YM repository.

The possible failure modes for the WP outer shell are general corrosion, localized corrosion, microbially-enhanced GC, and, possibly, microbially-enhanced LC. The EBSCOM code records the failure mode of the WP outer shell, which is defined as that process that ultimately results in penetration of the wall. If there is more than one active mode of corrosion at the time of failure (for instance, both GC and LC can occur simultaneously in the model), the failure mode is defined as the process that results in the deepest penetration in the time increment preceding WP failure. However, corrosion processes other than that resulting in ultimate failure may have resulted in significant prior wall loss.

4.4.3.2 WP Outer Closure Lid Weld

The corrosion behavior of the outer and middle closure lid welds is calculated separately from that of the WP shell. A number of parameters common to both closure lid welds are defined by the Waste Package Closure Weld flow chart (Figure 4-19). In a given realization, both closure lid welds are assumed to exhibit the same critical temperature for LC (T_{LCweld}), the probability of MIC LC ($P_{MICLCweld}$), and threshold stress for crack initiation (defined as a fraction of the temperature-dependent yield stress between 0.9 YS and 1.0 YS). Lastly, the nature of the environment determines whether SCC will occur or not, with only Bins 9 and 11 (representing 71% of the total waters sampled, Table 4-2) supporting SCC.

If the outer closure lid is intact, the code assesses the corrosion of the outer closure lid weld (Figures 4-20 through 4-23). If the outer closure lid has failed, water can enter the WP and corrode the middle closure lid weld (Figures 4-24 through 4-27).

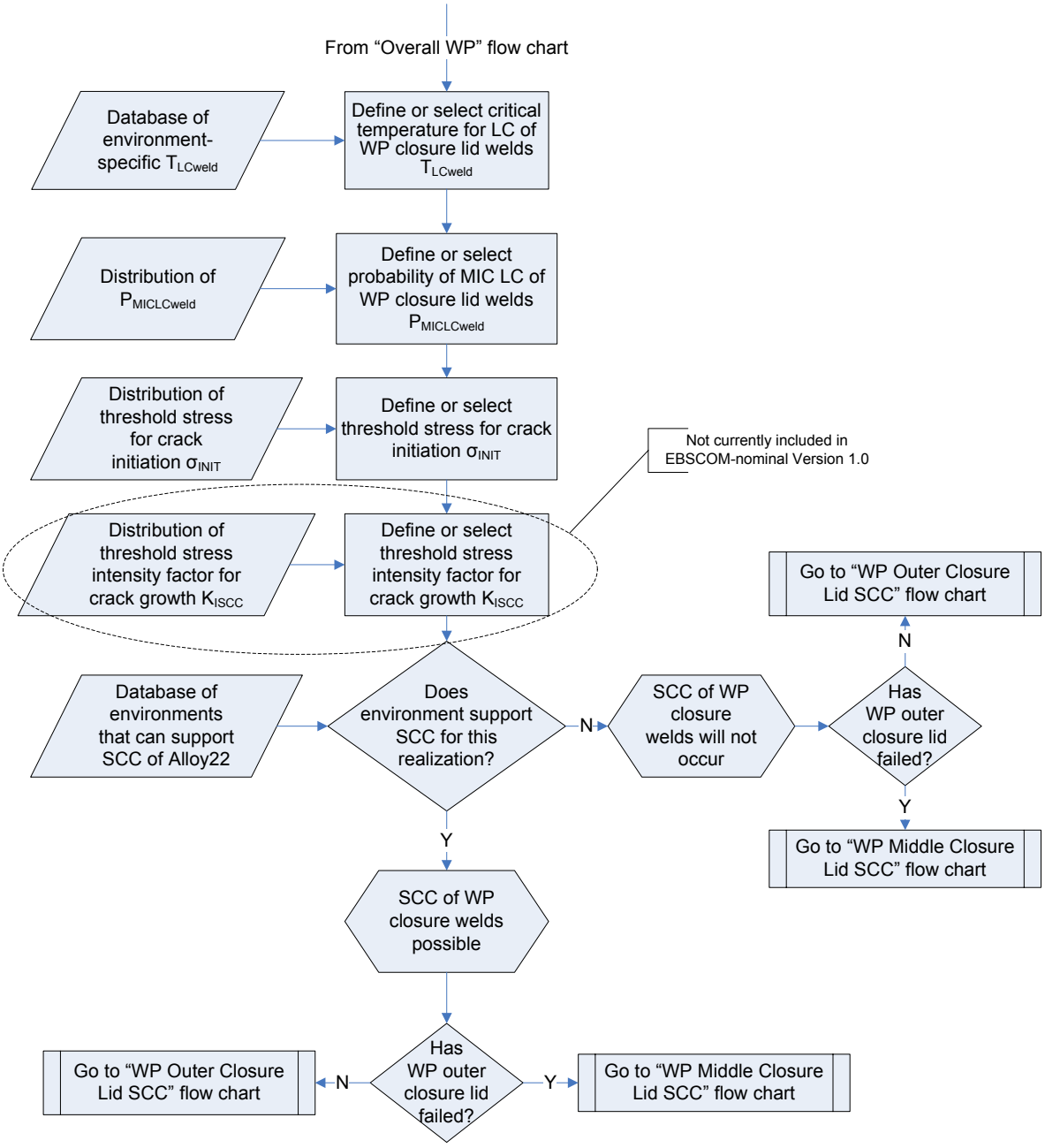

Figure 4-19
Waste package closure weld flow chart

If the outer closure lid weld is intact, the first flow chart determining the corrosion behavior is the WP Outer Closure Lid Weld chart (Figure 4-20). Two parameters specifically related to the outer closure lid weld are first defined; namely, the depth-dependence of the residual stress in the weld and the GC reduction factor of the laser-peened material (f_{GCLP}). At this stage in the flow chart, the second criterion for SCC is assessed by comparing the predicted corrosion potential E_{CORR} with the threshold potential for SCC. This comparison is made in each time increment because the predicted E_{CORR} is a function of temperature (Figure 4-8). If the predicted E_{CORR} value is equal to or exceeds the threshold potential for SCC, cracking is possible if the stress exceeds

the threshold for crack initiation. Regardless of whether SCC is possible or not, execution of the EBSCOM code proceeds to one of three flow charts, depending upon whether the DS has failed or not and upon whether LC is possible.

If the DS is intact, then the calculation follows the logic defined in Figure 4-21. If the stress at the surface of the weld is tensile, then the GC rate is reduced by the factor f_{GCLP} for both abiotic and MIC-enhanced corrosion. If the temperature is too high for microbial activity, failure of the outer lid closure lid weld can only occur by GC or SCC, and in the latter case only if the environment, potential, and stress meet the defined criteria. In EBSCOM, it is assumed that the environment necessary for SCC can be formed from the deliquescence of salts in dust deposits, as well as from seepage waters. Therefore, cracking is possible in the absence of DS failure. If the temperature is low enough that microbial activity is possible, then corrosion may result from MIC-enhanced GC, MIC LC, or SCC (Figure 4-21).

If the DS has failed but the WP temperature is below that for the initiation of LC, the corrosion processes to which the outer closure lid weld are susceptible are exactly the same as for the intact DS. These processes are described in the flow chart in Figure 4-22, which is exactly the same as that in Figure 4-21.

If, on the other hand, the DS has failed and the WP temperature is greater than or equal to T_{LCweld}, then the outer closure lid weld is also potentially susceptible to LC (Figure 4-23). As for the WP shell, LC of the closure welds is only considered possible in Bin 3 water, representing just 1% of all of the sampled waters. The flow chart in Figure 4-23, therefore, includes a calculation of the extent of LC, in addition to the estimates for GC, SCC, MIC-enhanced GC, and (possibly) MIC LC.

4.4.3.3 WP Middle Closure Lid Weld

Assessment of the corrosion behavior of the middle closure lid weld is very similar to that for the outer closure lid weld. As the middle closure lid weld does not receive a post-weld stress relief, however, the GC reduction factor f_{GCLP} is not applied in the estimation of the rate of GC. Therefore, the only input parameter specific to the middle closure lid weld is the stress distribution as a function of depth (Figure 4-24). The outer and middle closure lid welds are assumed to exhibit the same temperature-dependent E_{CORR} value.

With the exception of the reduction in the rate of GC due to the laser peening process, the flow charts describing the corrosion of the middle closure lid weld for (a) no DS failure (Figure 4-25), (b) DS failure, temperature below the threshold for LC (Figure 4-26), and (c) DS failure, temperature exceeds the threshold for LC (Figure 4-27) are identical to those for the outer closure lid weld. Thus, the middle closure lid weld is susceptible to GC, SCC, MIC-enhanced GC, (possibly) MIC LC, and abiotic LC (under the appropriate environmental and thermal conditions).

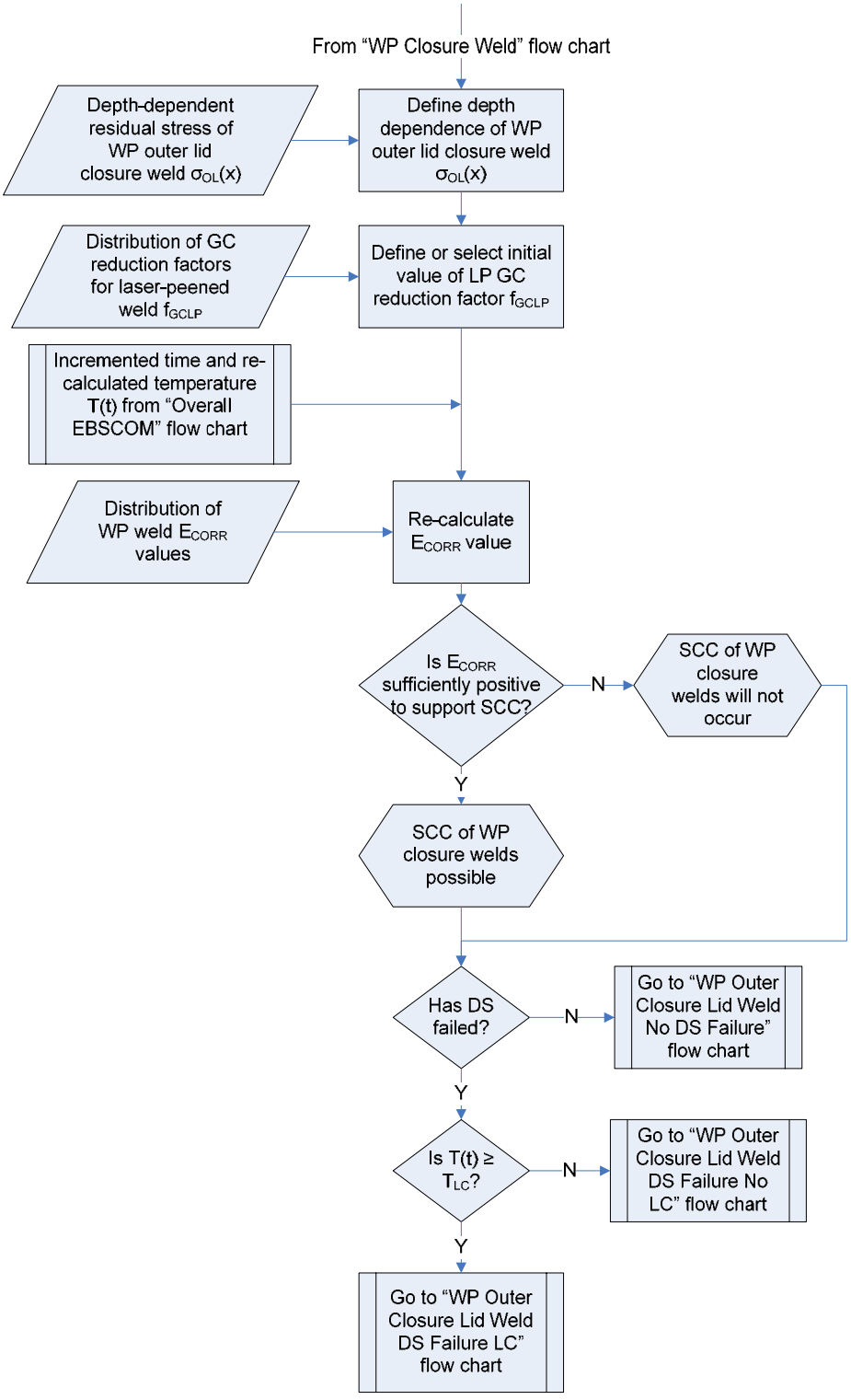

Figure 4-20
Waste package outer closure lid weld flow chart.

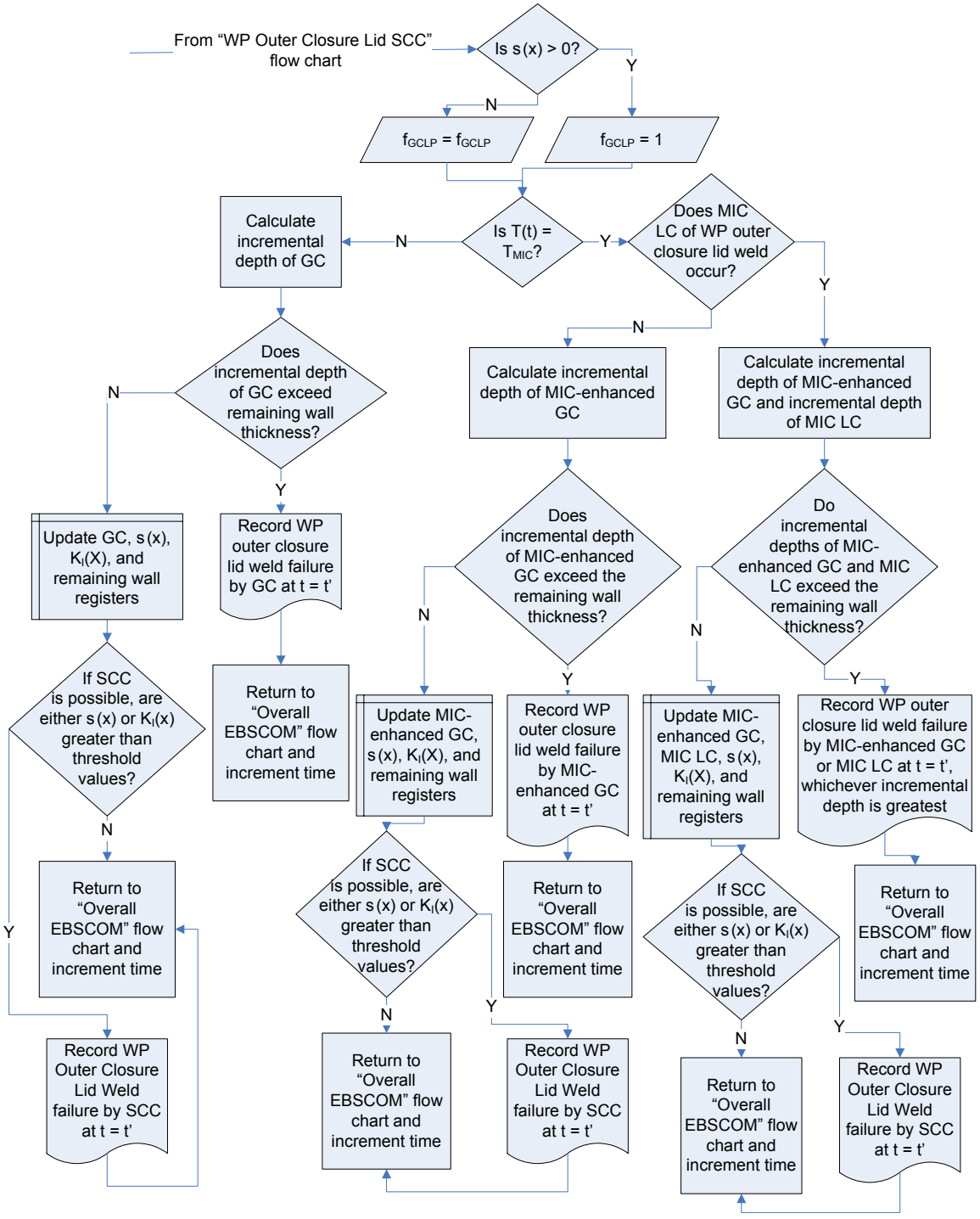

Figure 4-21
Waste package outer closure lid weld - no drip shield failure flow chart

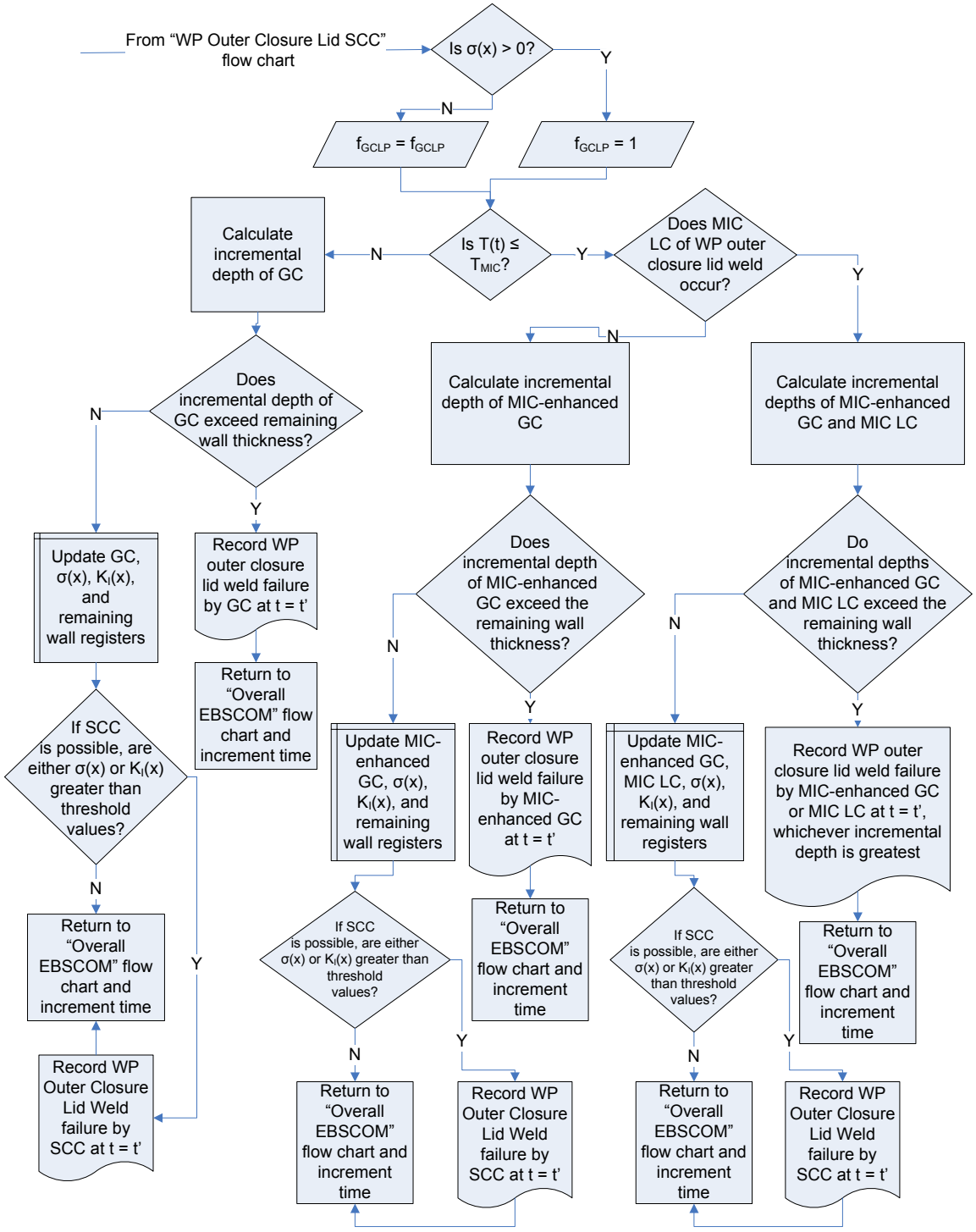

Figure 4-22
Waste package outer closure lid weld - drip shield failure - no localized corrosion flow chart.

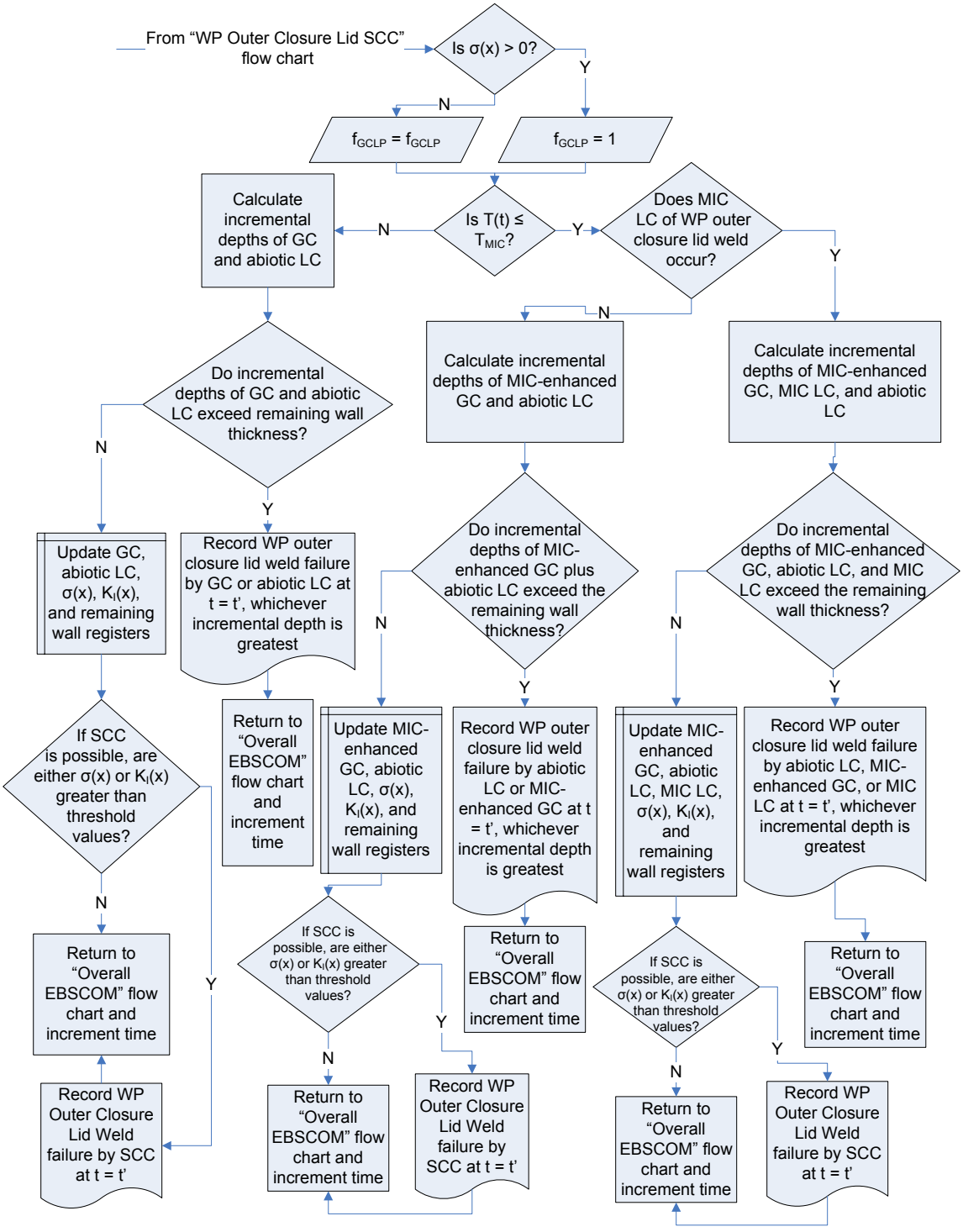

Figure 4-23
Waste package outer closure lid weld - drip shield failure - localized corrosion flow chart.

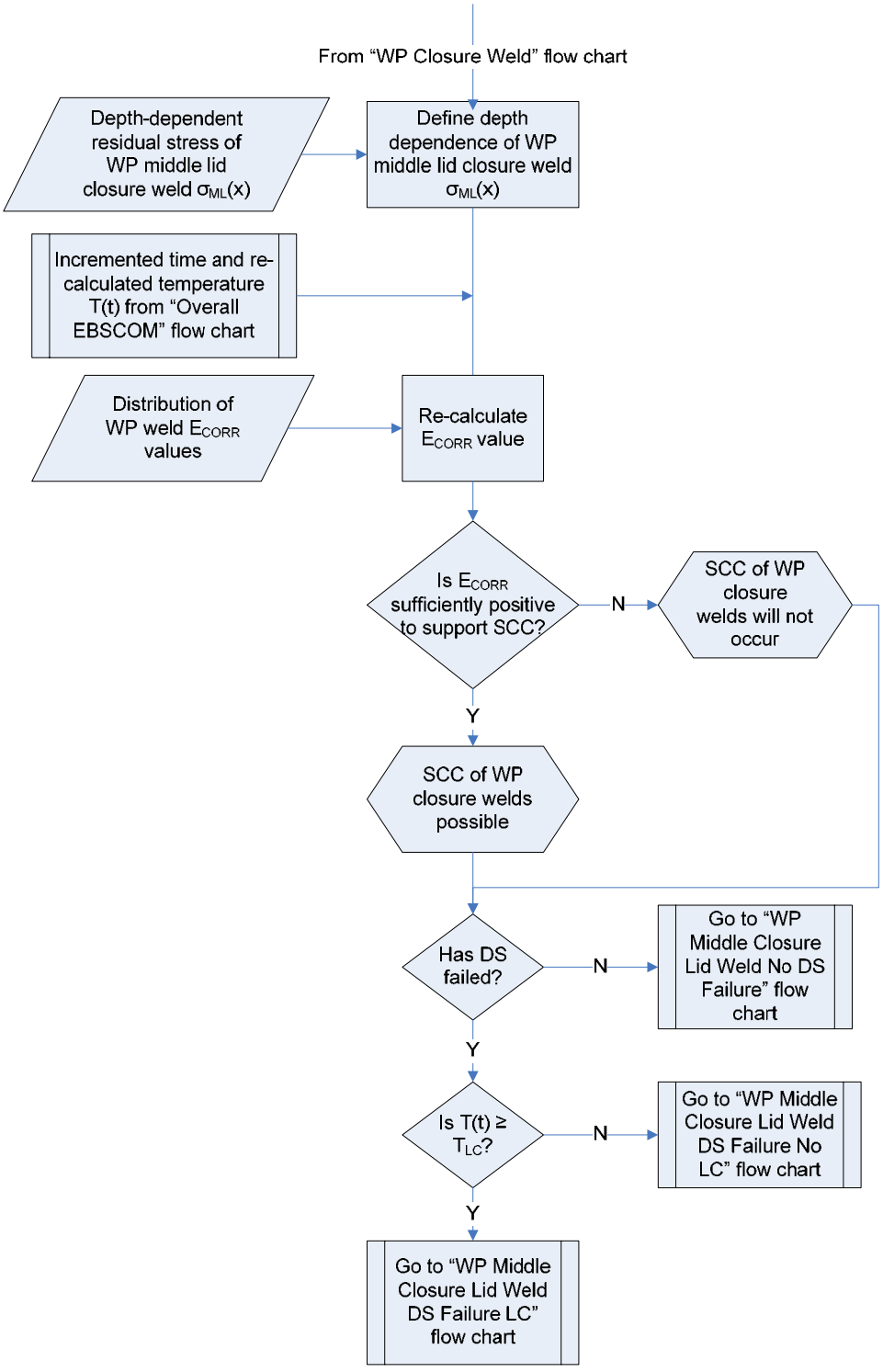

Figure 4-24
Waste package middle closure lid weld flow chart.

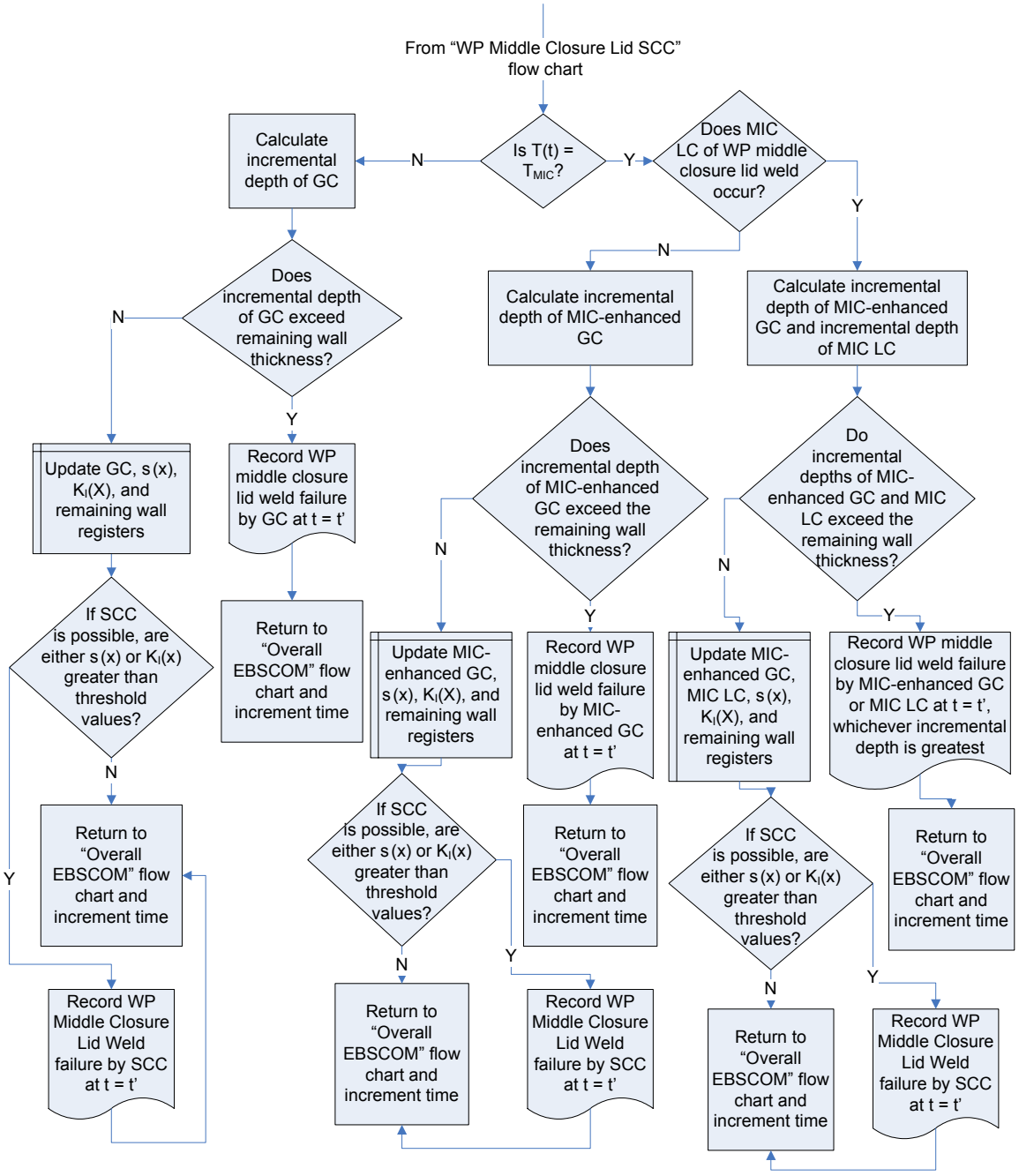

Figure 4-25
Waste package middle closure lid weld - no drip shield failure flow chart.

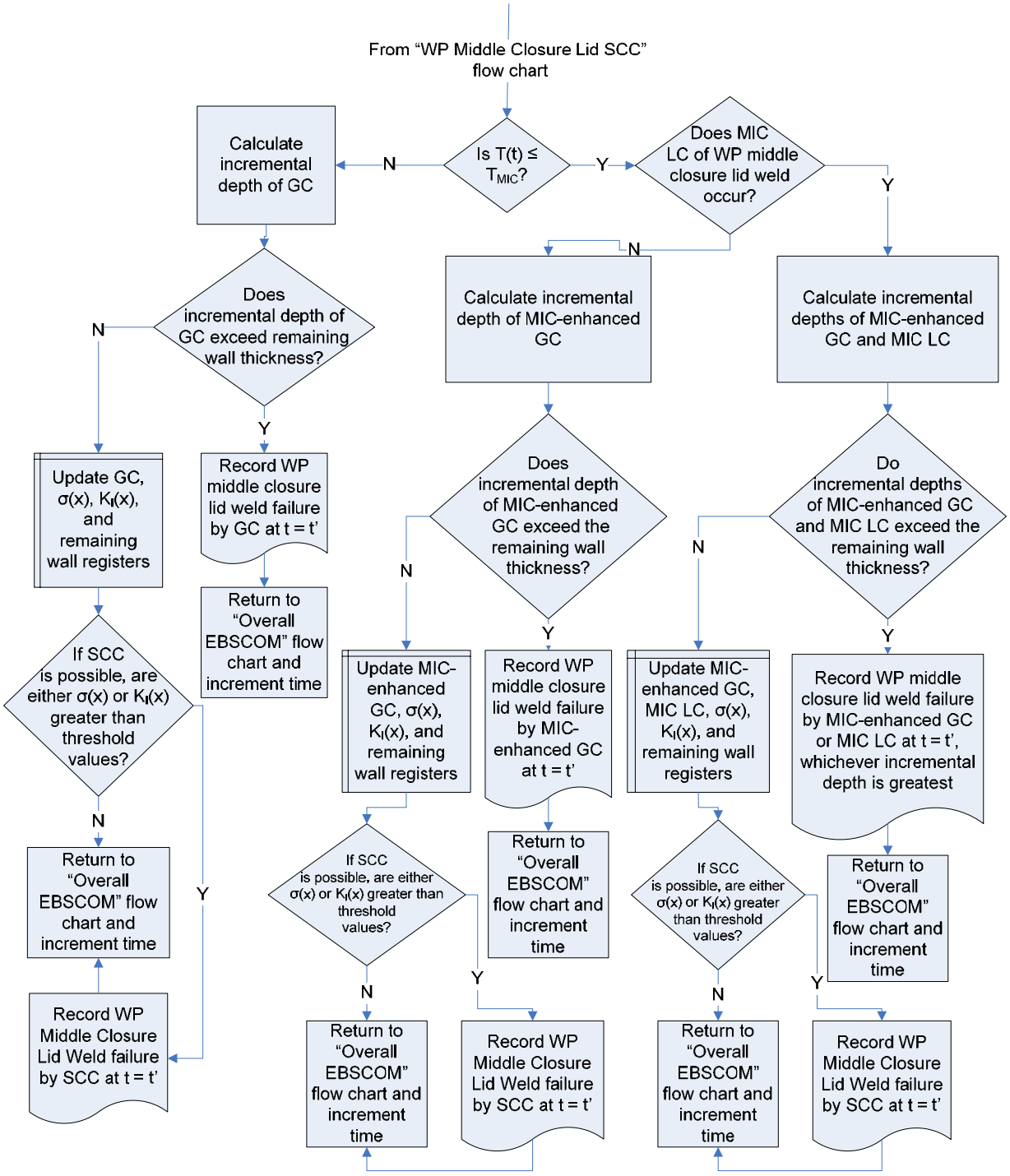

Figure 4-26
Waste package middle closure lid weld - drip shield failure - no localized corrosion flow chart.

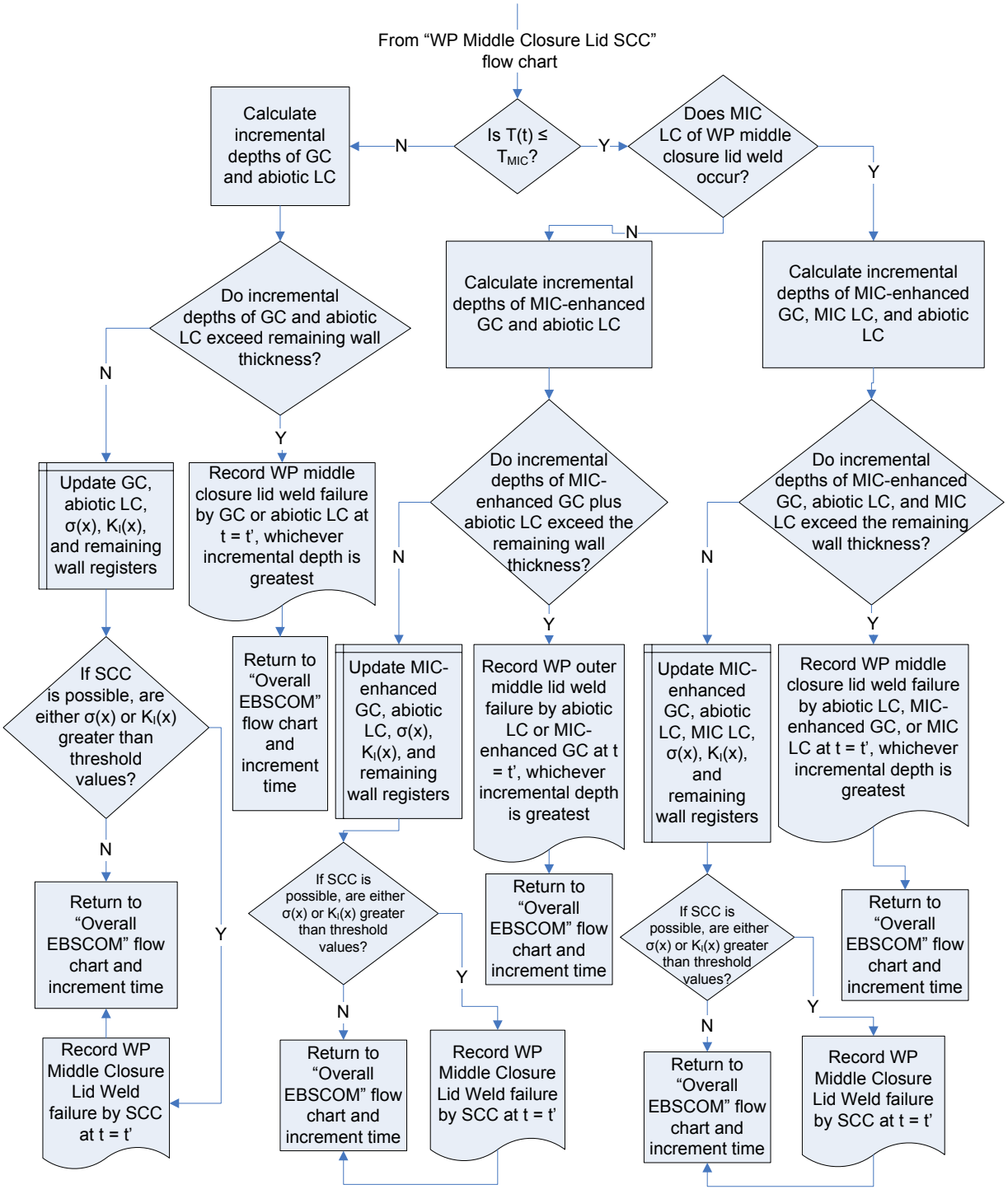

Figure 4-27
Waste package middle closure lid weld - drip shield failure - localized corrosion flow chart.

4.4.4 Assumptions

There are a number of assumptions inherent in the EBSCOM code, the most important being:

- Wall loss due to various corrosion processes is cumulative. This assumption is deemed to be either reasonable or conservative. There is only one wall-loss mechanism for the DS, *i.e.*, general corrosion. For the WP, the extent of LC is likely to be small because, on average, it will only occur in a maximum of 1% of the realizations in which Bin 3 water is selected. Therefore, the most likely failure mechanism is general corrosion, possibly microbially enhanced, for which the assumption of cumulative wall loss is appropriate.
- SCC crack growth is rapid. There is no attempt in EBSCOM to predict the growth rate of a propagating crack. If crack initiation occurs (or, for subsequent versions of the EBSCOM-nominal code, if the threshold stress intensity factor for a crack-like weld flaw is exceeded), it is assumed that the closure lid weld fails instantly. As the principal stress is in the hoop direction, the crack will tend to align axially along the WP. Thus, the lid will remain in place and provide some barrier function, although it will no longer act as an absolute containment barrier. Measured crack growth rates (BSC, 2004f) are of the order of 10^{-9} to 10^{-11} mm/s, which would result in a 10-mm through-wall crack in 300-30,000 years. Although the lower period is short in comparison to the timescales of interest, the potential additional credit for the slower crack growth rate is significant. Therefore, the assumption of instant failure following crack initiation is deemed to be reasonable/conservative.
- Rockfall due to thermal stress has no effect on the EBS performance. Rockfall resulting from drift degradation and thermal stresses are considered as part of the nominal scenario. Both EPRI and DOE analyses (EPRI, 2005d; BSC, 2004d; EPRI, 2006b) have shown that damage due to drift degradation under the nominal scenario is minimal and has little effect on the EBS lifetimes. Even during a seismic event, during which larger rock blocks can be ejected from the drift walls, the effect of their impact on the DS and WP is minimal (EPRI, 2005d; BSC 2004d), and the cumulative effect of multiple events is similarly small (EPRI, 2006b). Thus, even for the seismic disruptive event (not explicitly considered here), the only consequences for the EBS are those resulting from WP-WP interactions due to the ground motion, there being no significant effects of rockfall.
- The DS is immune to LC and HIC. These are considered to be reasonable assumptions, and the evidence has been extensively documented elsewhere (Hua et al., 2004). Briefly, however, for the expected YM environments, the pitting potential for Ti Grade-7 and Grade-24 are too positive to be achieved on the DS. Furthermore, these two alloys are highly resistant to crevice corrosion as a consequence of the addition of Pd. Titanium alloys are amongst the few alloys for which no instance of microbially assisted corrosion has been reported (Little et al., 1991).

Other assumptions are discussed in each of the sections dealing with specific corrosion issues.

4.5 Results for the Nominal Scenario and Sensitivity Analyses

A number of runs have been performed by EPRI for the nominal scenario and to determine the sensitivity of the predicted results to various parameters. The default input parameters for the nominal scenario are defined in Section 4.7.

4.5.1 Results for the Nominal Scenario

EBS components of interest (*i.e.*, drip shield and waste package) are evaluated as a function of time up to 10^6 years for the nominal scenario. The analyses have been updated to reflect the current TAD design (DOE, 2008). After 1,000,000 years, ~66% of the drip shields are predicted to have failed, but only ~6% of the waste packages. Failure of co-located DS and WP is predicted to occur in only ~4% of the realizations. The times for the first corrosion failures are 40,000 years, 420,000 years, and 450,000 years for the DS, WP, and DS/WP combination respectively. Figure 4-28 shows the mean of the realizations for the predicted cumulative fraction of failed EBS components of interest (*i.e.*, drip shield and waste package) as a function of time up to 10^6 years for the nominal scenario.

Virtually all WP failures are the result of general corrosion of the shell. Because microbial activity in the repository becomes possible as the temperature cools, the actual failure mode is predicted to be microbiologically-enhanced GC. After 1,000,000 years, there may be one failure of the lid system, most likely resulting from either (i) SCC of the outer closure lid weld combined with an initially failed middle lid or (ii) microbially enhanced GC of the middle lid combined with an initially failed outer lid.

The relative lack of importance of SCC and LC as failure modes for the WP compared with earlier EBSPA predictions (EPRI, 2002a) is a consequence of the changes made for the EBSCOM code. In particular, the probability of failure by LC is significantly reduced by the introduction of environmental variability in the new model and the fact that LC is now considered to be only possible for 1% of the realizations (corresponding to the frequency of the Bin 3 water). This change is made to properly reflect the low probability that waters that can sustain LC will be found in the YM repository. The low probability of SCC is the result of (i) the introduction of a threshold potential criterion for crack initiation, (ii) the use of a realistic threshold stress, and (iii) the reduced rate of GC of the laser-peened outer closure lid weld (which extends the time until a sufficient tensile stress develops on the surface of the WP). These changes are made to the model to reflect the current understanding of the SCC behavior of alloy C-22.

Both LC and SCC failure of the WP are possible under some circumstances. For example, a single realization is performed for an initially failed DS in Bin 3 water (which supports LC). Waste package failure due to LC of the outer shell is not predicted to occur until after 1,000,000 years. Failure by SCC can occur, as described above, and is most likely for combinations of (i) a small reduction in the rate of GC of the laser-peened weld material, (ii) a low threshold stress for crack initiation, and (iii) a threshold potential for SCC close to the lower bound of 0 mV_{SSC}. As a consequence of these numerous requirements, failure by SCC is predicted to be relatively uncommon, consistent with the results of recent experimental studies.

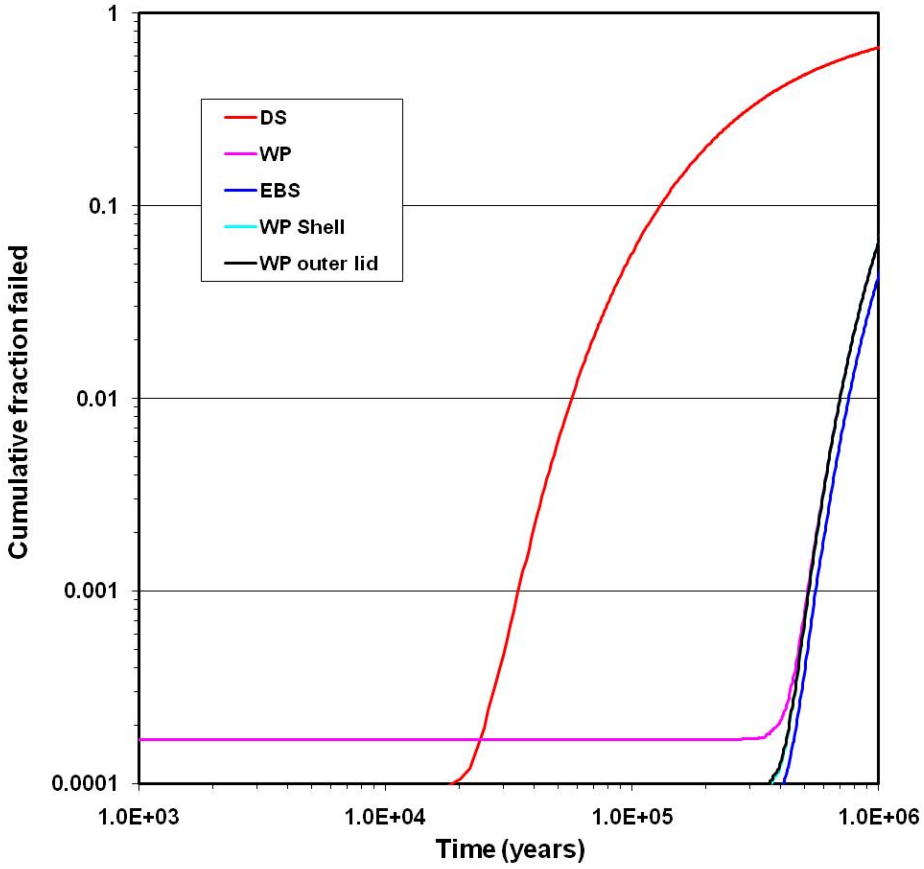

Figure 4-28
Time dependence of the cumulative fraction of failed EBS components based on EBSCOM predictions with the nominal input parameters.

The major corrosion failure mode for the DS is GC (Figure 4-29). Apart from a few HIC failures up to ~100,000 yrs, more than 99% of DS failures are due to GC. The reduction in the number of HIC failures for the EBSCOM code compared with the predictions from the earlier EBSPA model (EPRI, 2002a) is a consequence of the changes that have been made to the treatment of GC and hydrogen absorption in the new model. In particular, the assumptions that a fraction of the GC is supported by O_2 reduction and that previously absorbed H can be released as corrosion of the Ti matrix proceeds makes HIC failure less likely in the new model.

As the major failure mode is GC, neither the DS nor the WP can be considered to maintain their functionality (either as a barrier to drips or to radionuclide release) once they have failed. Table 4-3 lists the times for various values of the cumulative failure fraction (CFF) of the DS, WP, and failure of both the DS and WP in a single realization) For the DS and WP, the time for a fractional failure value of 0.0001 reflects the initially failed barriers. A CFF of 0.001 corresponds to ~11 failures. Thus, the vast majority of WP will remain intact for many hundreds of thousands of years.

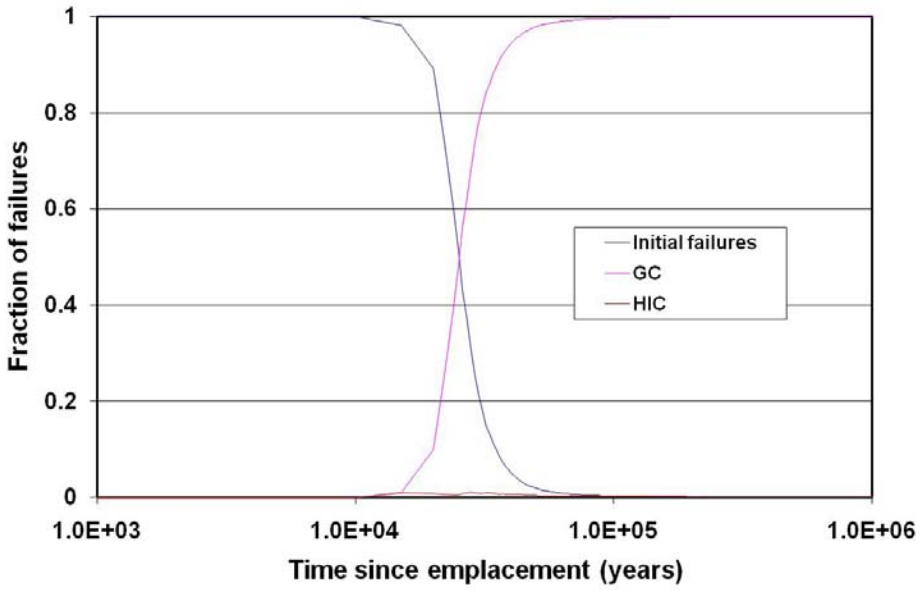

Figure 4-29
Time dependence of the fractional failure mode for the drip shields in the nominal corrosion scenario.

Table 4-3
Times for various fractional failures of the EBS components based on EBSCOM predictions for the nominal scenario

Cumulative fraction failed	DS	WP	EBS
0.0001	50 yrs	50	420,000
0.001	35,000	514,000	555,000
0.01	57,000	695,000	756,000
0.1	129,000	$>10^6$	$>10^6$
1	$>10^6$	$>10^6$	$>10^6$

4.5.2 Results for Seismic Effects

The IMARC EBSCOM model that includes seismic effects was presented in EPRI (2005d, 2006c). These results are reiterated here. Since the waste package design has become more robust since the publication of those analyses through the use of a thicker Allow 22 overpack, these results can be said to be conservative compared to a fully updated analysis. The new results therefore reflect corrosion failures for the thicker alloy C-22 shell added to the seismic failures from the older, thinner alloy C-22 shell.

A number of runs are performed to determine the effect on the repository of a single seismic event based on the seismic analysis developed by EPRI (EPRI, 2005d). In this analysis, the only effect of the seismic event results from WP-WP impacts due to the ground motion. Two types of impact are considered, involving flat end-on WP-WP impacts and a WP-WP impact at an oblique angle. As described in EPRI, 2005d, these impacts result in a modification of the residual stress distribution for the outer and middle closure lid welds. The change in stress distribution for the outer closure lid weld affects the SCC behavior, while the effect on the middle closure lid weld is sufficiently severe (due to the impact from the unconfined inner vessel containing the fuel assembly inside the WP) that it is conservatively assumed here that it results in failure of all of the middle lids at the time of the seismic event. There are considered to be no other adverse consequences of the WP-WP interactions on the subsequent corrosion behavior of the WP (EPRI, 2005d).

A single seismic event with a peak ground velocity of 4 m/s is assumed to occur[6] at one of three times: (i) 5,000 years following permanent closure of the repository (*i.e.*, after the thermal pulse), (ii) 250,000 years following permanent closure (corresponding to the time to corrode the WP shell by a thickness of 2 mm for the mean GC rate for alloy C-22), and (iii) 800,000 years following permanent closure.[7] These times are referred to below as early, mid, and late seismic events.

The results of the seismic analysis are compared to that for the nominal scenario in Table 4-4. As can be seen, a single seismic event of this magnitude has no effect on the fraction of DS, WP, or DS-WP combinations that have failed after 1,000,000 years. (The observed variation of ±0.001 is considered to be that expected for identical runs comprising 1,000,000 random realizations). The absence of any effect of the seismic event is due to the relatively small number of outer closure lid weld failures. If the outer lid does not fail within 1,000,000 years, it does not matter whether the middle closure lid (the failure of which is the major consequence of the seismic event) has failed or not.

[6] EPRI (2005d) erroneously indicated that a peak ground velocity (PGV) of 2 m/s was modeled in the WP-WP collision. In fact, a PGV of 4 m/s was modeled.

[7] The EPRI model conservatively assumed that adjacent WPs were moving toward each other, each with a velocity of 4 m/s. (EPRI, 2005d)

Table 4-4
Comparison of the fraction of failed drip shields, waste packages, and WP-DS after a period of one million years for the nominal and seismic scenarios

Scenario	DS	WP	WP-DS
Nominal	0.662	0.148	0.098
Early seismic – flat WP-WP interaction	0.662	0.148	0.098
Early seismic – oblique WP-WP interaction	0.662	0.147	0.098
Mid seismic – flat WP-WP interaction	0.662	0.148	0.098
Mid seismic – oblique WP-WP interaction	0.662	0.148	0.098
Late seismic – flat WP-WP interaction	0.663	0.147	0.098
Late seismic – oblique WP-WP interaction	0.662	0.148	0.098

4.6 Summary

A revised EBS model has been developed by EPRI to predict the time dependence of the failure of the drip shield and waste package. The revised model is based on the most recent EBS designs and on new information on various corrosion processes developed by the DOE and others. As with earlier EPRI corrosion models and in keeping with the EPRI approach, the EBSCOM code is intended to provide reasonable estimates of the failure times of the various barriers, while also maintaining a small degree of conservatism.

The most significant changes in and/or results of the new model include:

- The selection of a different environment for each of the 1,000,000 realizations in a run. The range and frequency distribution of the environments is based on the DOE "bins" of evaporated seepage and deliquescent waters of common chemical characteristics. Only one of the bins, representing 1% of the environments, can support LC of the WP. Approximately 70% of the waters can support SCC;
- As a consequence of the low probability of a suitable environment for LC, there are no WP failures due to LC;
- In addition to the revised environment for SCC, cracking is only possible at very positive potentials and for a sufficient tensile stress. These limitations result in, at most, one SCC failure of a waste package outer closure lid weld, and none prior to ~10^6 years;
- MIC of the WP is assumed to be possible at a sufficiently low temperature (high %RH) and to cause enhanced GC. The predominant failure mode for the WP is (microbially enhanced) GC;
- The use of a distribution of temperatures results in a number of hotter packages than previously assumed. However, overall WP lifetimes are longer than calculated in the previous EPRI model because of the use of a lower rate of GC based on 5-year LTCTF data; and

- There is a reduced probability of HIC of the DS because of several changes to the code, including the loss of absorbed H due to corrosion of the DS and O_2 reduction on the DS, which does not result in hydrogen absorption. Therefore, virtually all DS failures are due to GC, which means that the DS offers no barrier to seepage once failed.

For the nominal scenario for the current TAD design, ~66% of DS and only ~4% of WP are predicted to fail within the first 1,000,000 years. Failure of a co-located DS and WP combination is predicted to occur in only ~6% of the realizations. The times for the first corrosion failures are 40,000 years, 420,000 years, and 450,000 years for the DS, WP, and DS/WP combination, respectively. Analyses of the effect of a seismic event with a peak ground velocity of 4 m/s suggests that no additional EBS failures will result from the effects of ground motion and rockfall (EPRI, 2005d; 2006c).

4.7 Input Data for the EBSCOM Nominal Scenario

4.7.1 General

4.7.1.1 Environment

Table 4-5
Chemical Environment for the Corrosion Model.

Bin	Relative Frequency	Is localized corrosion possible?	Is SCC possible?
3	1%	Y	N
4	17%	N	N
5	11%	N	N
9	20%	N	Y
11	51%	N	Y

4.7.1.2 Maximum Temperature for Aqueous Corrosion (T_{AQ})

T_{AQ} is given by a specific value or can be selected for each realization from a uniform distribution.

The default is a specific value of $T_{AQ} = 130^{o}C$

The default uniform distribution is defined by lower and upper bound values of $120^{o}C$ and $140^{o}C$, respectively. For the results shown here, the default uniform distribution is used.

4.7.1.3 Temperature

A different temperature profile is selected for each realization. The temperature profile is based on the time-dependent temperature for the average WP multiplied by a factor f_T sampled from an asymmetric triangular distribution with a lower bound of 0.67, and upper bound of 1.26, and a peak value of 1.00 (corresponding to the average WP).

4.7.2 Drip Shield

4.7.2.1 General Corrosion Rate at Reference Temperature ($R_{GC}^{DS}(T_{ref})$)

The GC rate at the reference temperature of 75°C is given by the following CDF (BSC, 2004c).

Table 4-6
Cumulative distribution function for the general corrosion rate.

Corrosion rate (mm/yr)	Cumulative distribution function
0	0
7.905401E-06	0.2500
7.908996E-06	0.3125
7.917336E-06	0.3750
7.992055E-06	0.4375
1.596796E-05	0.5000
1.607404E-05	0.5625
2.356582E-05	0.6250
2.373022E-05	0.6875
2.403291E-05	0.7500
3.999769E-05	0.8125
7.149611E-05	0.8750
7.916412E-05	0.9375
1.127882E-04	1.0000

These data can be fitted to a Weibull distribution characterized by the following parameters:

- scale factor 21.52 x 10^{-6} mm/yr
- shape factor 0.841
- location factor 0 mm/yr

Several additional parameters are needed:

- Activation Energy for General Corrosion of Drip Shield (ΔE_{GC}^{DS})= 0 J·mol-1
- General Corrosion Enhancement Factor for Fluoride (f_F)= 1
- Fraction of General Corrosion Supported by O_2 Reduction (f_{O2})= 0.5

A uniform distribution is used to describe the uptake efficiency in each of four temperature ranges (Table 4-7).

Table 4-7
Uptake efficiency as a function of temperature.

Temperature range (°C)	Distribution type	Lower bound	Upper bound
≤100	Uniform	10^{-9}	0.02
100 <T ≤120	Uniform	0.02	0.04
120 <T ≤140	Uniform	0.04	0.06
140 <T ≤160	Uniform	0.06	0.08

The Critical Hydrogen Concentration for HIC (H_{CRIT}) is given by a uniform distribution between 800 and 1200 ppmw (parts per million by mass).

Parameters needed for the initial failure fraction of the drip shields are as follows:

- IFFDS = 10^{-4}, *i.e.*, 1 in 10,000 DS is emplaced in a state sufficiently defected (displaced, misaligned, missing, etc.) to constitute instantaneous failure
- Thickness of DS (dDS)= 15 mm
- Density of Ti-7/Ti-24 (ρTi)= 4.54 g·cm^{-3}
- Atomic mass of Ti (MTi)= 47.88 g·mol^{-1}

4.7.3 Waste Package General Inputs

4.7.3.1 General Corrosion Rate at Reference Temperature ($R_{GC}^{WP}(T_{ref})$)

The value of $R_{GC}^{WP}(T_{ref})$ is selected from a Weibull distribution described by the following parameters (BSC 2004e):

- scale factor 8.88 x 10^{-6} mm/yr
- shape factor 1.62
- location factor 0 mm/yr

4.7.3.2 Activation Energy for General Corrosion of WP (ΔE_{GC}^{WP})

The value of the activation energy for the general corrosion rate of the WP is given by a normal distribution with a mean value of 25.91 kJ/mol and a standard deviation of 2.46 kJ/mol.

4.7.3.3 Localized Growth Constant ($B(T_{ref})$)

The value of $B(T_{ref})$ is selected from a Weibull distribution described by the following parameters:

- scale factor 54.085 x 10^{-6} mm/yr
- shape factor 1.28
- location factor 0 mm/yr

4.7.3.4 Activation Energy for the LC Growth Constant (ΔE_B)

The value of the activation energy for the LC growth constant B is 55 kJ/mol.

4.7.3.5 Time Exponent for LC of Alloy C-22 (n)

The value for the time exponent for the propagation of LC of alloy C-22 is selected from a uniform distribution characterized by minimum and maximum values of 0.1 and 0.5, respectively.

4.7.3.6 Critical Temperature for MIC (T_{MIC})

The temperature at which the %RH at the WP surface equals 96% (equivalent to the critical water activity of 0.96) depends on the heat output of the WP. Thus, cooler waste packages attain this RH at a higher temperature than hotter waste packages. The critical temperature for MIC of alloy C-22 is given by:

$$T_{MIC} = (50/f_{Tm})\ ^{o}C \qquad \textbf{Eq. 4-12}$$

where f_{Tm} is the multiplying factor for the temperature profiles of the WP.

Thus, for the average WP, the value of T_{MIC} is 50°C (see Figure 4-3(c)) and for the coolest (f_{Tm} = 0.67) and hottest (f_{Tm} = 1.26) T_{MIC} equals 75°C and 40°C, respectively.

4.7.3.7 MIC Enhancement Factor for GC (f_{MIC})

The value of the enhancement factor for MIC GC (f_{MIC}) is given by a uniform distribution with minimum and maximum values of 1 and 2, respectively.

4.7.4 Waste Package Outer Shell

Parameters needed for the waste package outer shell are as follows:

- Thickness of WP outer shell (dWPOB) = 20 mm
- The minimum temperature for the initiation of LC of the WP outer shell is selected from a uniform distribution with minimum and maximum values of 90oC and 100oC, respectively.
- The probability of MIC-induced LC of the WP outer shell is given by PMICLCshell = 0.

4.7.5 Waste Package Outer Closure Lid Weld

Parameters needed for the waste package outer closure lid weld are as follows:

- Thickness of WP Outer Closure Lid Weld (dWPOL) = 25 mm

The minimum temperature for the initiation of LC of the WP closure lid welds is selected from a uniform distribution with minimum and maximum values of 60°C and 80°C, respectively.

The probability of MIC-induced LC of the WP closure lid welds is given by $P_{MICLCweld} = 0$.

4.7.6 Reduction Factor for GC of Laser-peened Outer Closure Lid Weld (f_{GCLP})

The reduction factor for the GC of the laser-peened region of the outer closure lid weld f_{GCLP} is given by a uniform distribution with minimum and maximum values of 0.43 and 0.54, respectively. These values are based on preliminary corrosion rate measurements on laser-peened material presented by Peters (2003a). This enhancement factor is only applied to the rate of GC of the outer closure lid weld when the surface stress is not tensile (*i.e.*, $\sigma \leq 0$).

4.7.7 Waste Package Middle Closure Lid Weld

Parameters needed for the waste package middle closure lid weld are as follows:

- Thickness of WP Middle Closure Lid Weld (d_{WPML}) = 10 mm
- The minimum temperature for the initiation of LC of the WP closure lid welds is selected from a uniform distribution with minimum and maximum values of 60°C and 80°C, respectively.
- The probability of MIC-induced LC of the WP closure lid welds is given by $P_{MICLCweld} = 0$.

4.8 Cladding

IMARC has included cladding as a component of the engineered barrier system since Phase 5 for the purpose of implementing a conceptual model with sufficient fidelity to produce reasonable estimates of performance. Recent EPRI sensitivity analyses (Section 5.8 below) indicate that, on the whole, the impact of cladding on repository performance is relatively minor, and the

exclusion of cladding credit introduces a minimal amount of conservatism in the TSPA analysis. Therefore, while IMARC results include the contribution of cladding, the dose estimates are not strongly dependent on the presence of cladding. In its most recent TSPA, DOE/OCRWM (2008b) has chosen not to include credit for cladding as a barrier to the release of radionuclides.

Prior to being sealed within the waste package and emplacement in the repository, prospective failure modes for the spent fuel cladding include failures occurring during reactor operation and subsequent failures caused by creep and iodine-induced SCC during dry storage and shipping to the repository, when temperatures of 350°C may be achievable (CRWMS M&O, 2000b; 2000c). As free-iodine concentrations within fuel rods are expected to be negligible, creep failure is the dominant failure mode anticipated during storage and transport. In addition, there is the possibility that fuel rod failures will occur by creep within sealed waste packages prior to closure of the repository. The combination of these effects means that there is the potential for some of the cladding to be failed inside the waste package before the initiation of failure of the waste package outer barriers.

Whether or not such in-package failures can occur can be directly related to the waste package surface temperature achieved in the repository, which itself is indicative of the maximum cladding temperature achievable within the waste packages. The adopted criterion is that the cladding temperature must not exceed 350°C if the fuel rod creep strain is not to exceed the creep failure strain criterion. The analysis in CRWMS M&O (2000b) shows that in-package creep failures will be negligible if the waste package surface temperature does not exceed 250°C after emplacement in the repository (CRWMS M&O, 2000b, Figure 8). As such temperatures will not be achieved (CRWMS M&O, 2000b) at any time, it is assumed that the possibility of creep failures after waste package sealing can be ignored.

Thus, on first failure of a waste package in the repository, the number of fuel rods already failed and, hence, in a state to allow fuel wetting and the immediate commencement of radionuclide release from the waste form will be the sum of the fuel rods having been previously failed in the reactors prior to shipment to the repository and those failed during subsequent dry storage and transport to the repository. In the cladding model in IMARC, only a best estimate value of 2.44 percent of stored fuel rods is used, with no uncertainty distribution. This value is based on DOE estimates of initial cladding failure, as documented by EPRI (2000).

Any subsequent fuel clad failures will depend on cladding corrosion once the waste package is breached and water enters. The IMARC model is predicated on the common and reasonable assumption that the fraction of rods failed by corrosion as a function of time will be linearly dependent on the rate of water ingress into a failed waste package.

The cladding failure model used in IMARC acknowledges the susceptibility of zirconium and its alloys to localized corrosion processes, such as pitting in oxidizing saline conditions. A wealth of evidence exists to show that the critical potentials for film breakdown on zirconium alloys are low, in the range 0.1 to 0.3 V (vs SCE), a potential possibly achievable in the presence of relatively small concentrations of oxidants such as Fe^{3+}. This is acknowledged in a number of literature articles (Maguire, 1984; Yau and Maguire, 1990; Hornkjol, 1988; Greene *et al*., 2000).

Given the iron content of the internal structure of the waste package, and the fact that the fuel bundles remain forever a heat source with respect to their surroundings, it becomes a difficult argument to claim that seepage drips, evaporative processes and the accumulation of dissolved oxidizing metal ion species from steel corrosion processes can never lead to the formation of a sufficiently aggressive environment to initiate pitting of cladding. However, it is reasonable to assume that the development of such sites will be confined to those failed waste packages that experience drips. Within these waste packages, it is possible that a trickle down/evaporative process of seepage water will occur during which the accumulation of dissolved metal cations (Fe^{3+}), the concentration of groundwater anions (*e.g.*, Cl^-), and the formation of an acidified environment, could occur. This could lead to the establishment of a small number of localized corrosion sites on the cladding. While such sites could lead to the rapid failure of the cladding, the consequences of such failures are not expected to be significant. The aperture produced in the cladding will be small, and at least partially blocked by corrosion products, and should not, therefore, lead to a major exposure of fuel for dissolution.

Presently, only very limited information on the development of such environments within a failed waste package exists. Consequently, the IMARC model assumes that corrosion of the Zircaloy cladding will be general in nature, but not specifically driven by contact with fluoride. In the absence of specific low temperature values for general corrosion rates for zirconium and its alloys, it has been assumed that the corrosion rates will be similar to those measured for titanium alloys in the LTCTF at LLNL (CRWMS M&O, 2000d). This assumption is based on the similar properties of the oxides on these two materials, both metal cations being in the +4 oxidation state and both oxides exhibiting negligible solubility over a wide pH range. Thus, to calculate cladding corrosion rates for dripping conditions, the distribution of rates plotted in Figure 4-1 are used. In the absence of drips, a corrosion rate of 10 ± 5 nm/year with a normal distribution is used. These rates are used with a distribution of initial cladding thicknesses based on the 1999 historical and projected waste stream numbers of various PWR and BWR assembly types (CRWMS M&O, 1999, Tables 4-1 and 4-2) and information on the cladding thickness for each assembly type. These thicknesses are then reduced by 57% of the existing oxide thickness produced in-reactor, as discussed by EPRI (2000). The thickness of the oxide layer is taken to be normally distributed with a mean of 54 μm and a standard deviation of 29 μm (CRWMS M&O 2000c, p. 30). The distribution of resulting cladding thickness is shown in Table 4-8. Figure 4-5 shows the resulting cladding failure distribution for both dry and dripping conditions, with the mean initial failure fraction discussed above.

Table 4-8
Distribution of initial fuel rod cladding thickness

Initial Cladding Thickness (mm)	Probability of Thinner Cladding
0.569	0
0.572	0.310
0.615	0.380
0.635	0.455
0.660	0.457
0.673	0.513
0.711	0.562
0.749	0.589
0.762	0.596
0.813	0.960
0.864	0.979
0.902	0.983
0.914	0.985
0.940	0.997
1.016	0.998
1.168	1.000

In IMARC, this cumulative distribution is represented by a discrete distribution in time, shown in Figure 4-30. The discrete distribution is developed by fitting a discrete distribution to the cumulative distribution in Figure 4-31. This fitting procedure led to the minor binning fluctuations seen in Figure 4-30. The curves show the assumed initial 2.4 percent failure as a spike at time zero. Furthermore, the dry failure curve is truncated at 150,000 years when 98 percent of the cladding is calculated to have failed. At that stage, the remaining cladding is assumed to fail, leading to the spike in the dry failure curve at that time.

Hydride reorientation is another potential cladding failure mechanism for higher burnup spent fuel during storage and transportation. The NRC currently limits cladding temperatures for higher burnup spent fuels during drying operations (prior to transfer from pool to dry storage) to 400°C to avoid this phenomenon (NRC, 2003). Assuming this limit is maintained, little to no hydride reorientation should occur in spent fuel destined for Yucca Mountain. Hence, hydride reorientation as a potential failure mechanism during post-closure at Yucca Mountain has been neglected in IMARC.

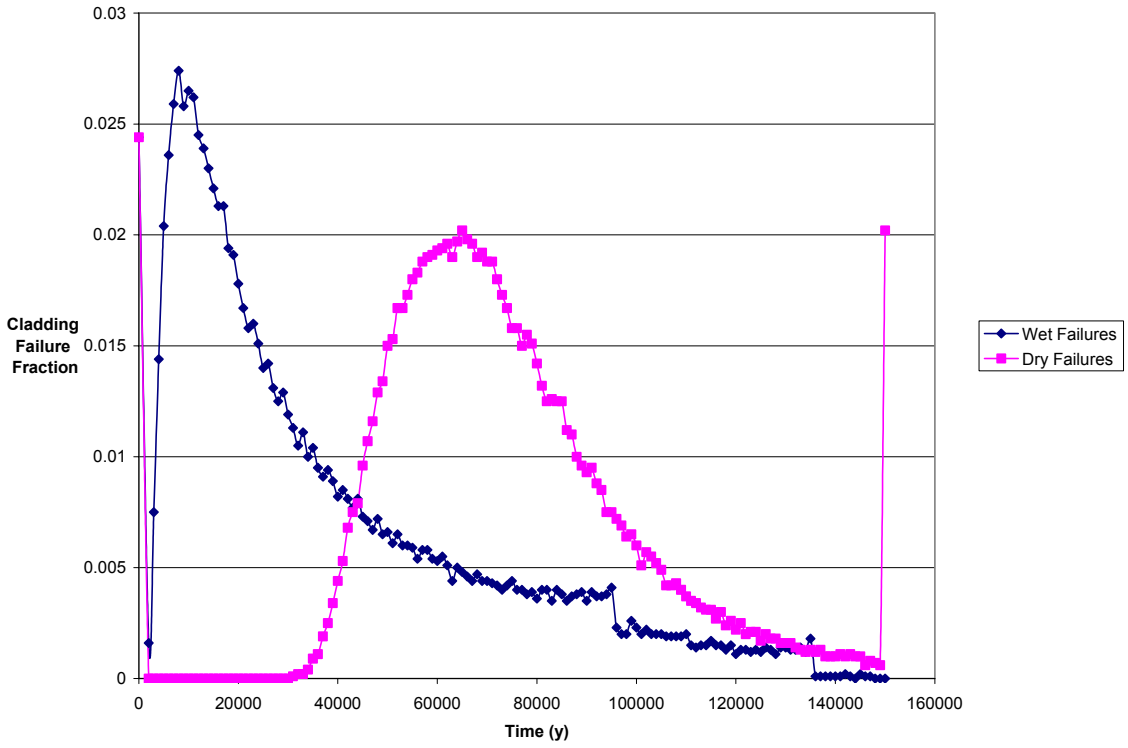

Figure 4-30
Cladding failure probability as a function of time after waste package failure used in IMARC. The high value at early times for dry failure represents early failure. The analysis is truncated at 150,000 years, and the cladding that remains unfailed at that time is assumed to fail at 150,000 years, leading to the peak at that time.

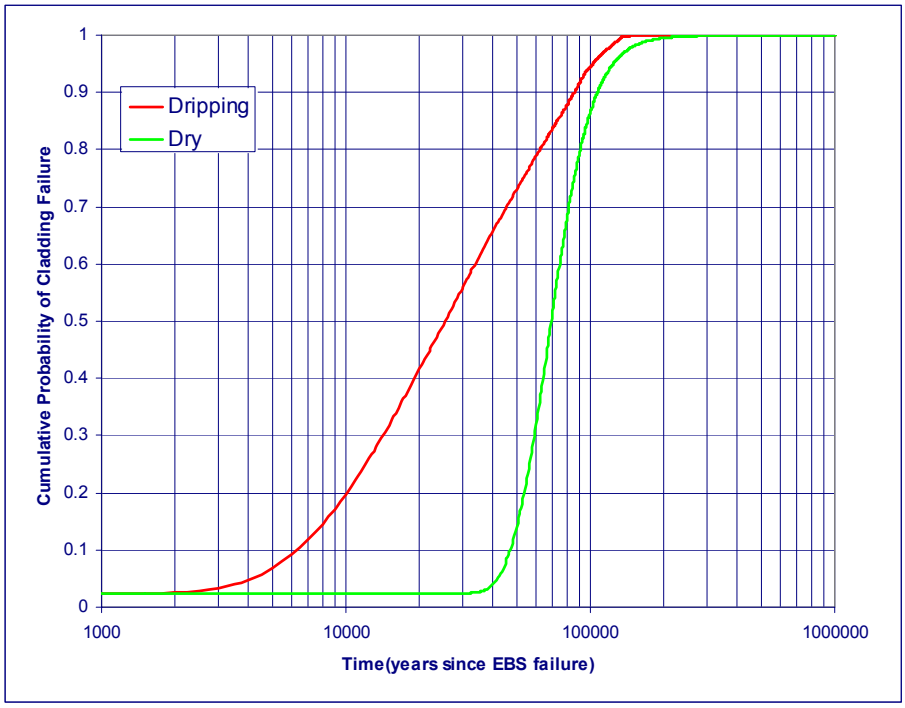

Figure 4-31
Fuel rod cladding failure distribution

4.9 Interface with IMARC

To produce the failure curve in the format used in IMARC in WPF.DAT, the following procedure is carried out. First, the 2008 corrosion curves and 2006 seismic effect curves are added in Excel. A cubic spline routine in Matlab™ Version 7.1 is used to transpose the output of EBSCOM, which is given as time vs. failure for the EBS components, into a table of failure vs. time used in IMARC. The cubic spline approach produces oscillations in the curves at low probability values where the curve undergoes instantaneous changes. These oscillations are manually corrected to be consistent with the EBSCOM analysis.

4.10 Summary

Models of the performance of containment barriers have been developed over many years by the EPRI team, and represent a sound understanding of the corrosion and degradation processes that are expected to occur at Yucca Mountain. Model calculations are carried out independently from the IMARC code, as Monte Carlo analyses that take into account uncertainty and variability in the key parameters. The mean results of these calculations are introduced as simple time-dependent parameters in the IMARC code. Consequently, while they are not directly treated as uncertain variables, they have a full treatment of uncertainty embedded in the mean. As such, they represent the central, expected tendency of the behavior of the containment barriers for conditions at Yucca Mountain.

5
NEAR-FIELD MODELING

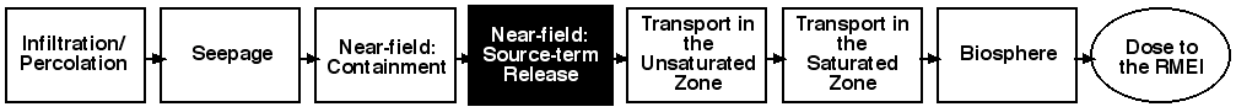

5.1 Introduction

In IMARC, the Near-Field Model is accomplished with COMPASS. COMPASS stands for "COMpartment model for PArtially Saturated repository Source term." COMPASS was first developed in 1996 for IMARC Phase 3 source-term and near-field assessment (EPRI, 1996). The purpose of the development is to provide a comprehensive code that simulates all significant processes of concern in the near field. The conceptual model for contact between water and the waste includes:

- a "bath-tub" model -- the canister is assumed to fail at the top leading to water flowing into the otherwise intact canister and subsequent release of radionuclides when overflow occurs);[8]
- a "flow-through" model -- advective release with canister failure at both the top and bottom; and
- a "diffusion release" model-- a release scenario with a backfill in the emplacement drift that isolates seepage flow from waste package, as envisioned in DOE/OCRWM (1995).

The EBS design has been changed since the original development of COMPASS, primarily by changes in the waste package design, and by the introduction of a titanium drip shield and a crushed tuff gravel invert. Over the years since the development of COMPASS, understanding of the key processes has also improved, which has also led to evolution of the COMPASS model over time to incorporate the new information and understanding. The fundamental modeling approach and underlying solution method, however, remain unchanged. In this section, the COMPASS code is described, including the modeling approach, conceptualization, mathematical equations, solution method, and verification. The required input parameters and the interface with IMARC are also described.

[8] The "bathtub" model was not used in IMARC 10 as EPRI considers significant filling of a failed WP with water highly unlikely.

5.2 Modeling Approach

COMPASS is intended to capture key FEPs in the source-term and near-field, and also to provide reasonable computational speed in order to accommodate probabilistic assessments. The approach is adopted from SCALIBRE, the compartment-model version of CALIBRE, a comprehensive finite-difference code used in support of the Swedish assessment of hypothetical SNF repository sites known as the SITE-94 program (SKI, 1996).

The compartment method is similar to the finite-difference method, but provides additional flexibility for adjusting spatial resolution. The method is equivalent to a coarse integral volume finite-difference model. As the number of compartments increases, the solution from the compartment model approaches the equivalent fine-resolution finite-difference model solution.

Because of the flexibility in handling geometry, the compartment method is able to capture important features and to model complicated processes in the system with a reasonable computational demands. In performance assessment calculations, uncertainties arising from limited knowledge of data and future conditions of the system overwhelm the demand for spatial resolution. Hence, the flexible geometry and fast computation offered by the compartment model are desirable features for probabilistic assessment, providing flexibility in comparing alternative conceptual models and facility designs, as well as ensuring the capability for robust sensitivity analysis.

In a compartment model, each EBS and near-field component is treated as one or more mixing cells where concentration is assumed to be uniform. In this way, an actual three-dimensional system is represented by a group of cells connected by mass transfer relationships that are explained in the next section.

5.3 Conceptualization

The Yucca Mountain repository is in unsaturated tuff. After an initial thermal transient period, the temperature at the repository horizon drops to below the boiling point and the repository emplacement drift is filled with humid air. Some drifts would be subject to seepage. The contact of liquid water and humid air with the drip shield and waste canister eventually leads to corrosion of these barriers. After the canister fails, the humid air and/or seepage water enter the canister and contact the waste, initiating dissolution of the waste form and release of radionuclides. Figure 5-1 schematically illustrates the release and transport of radionuclides from the repository when seepage is present.

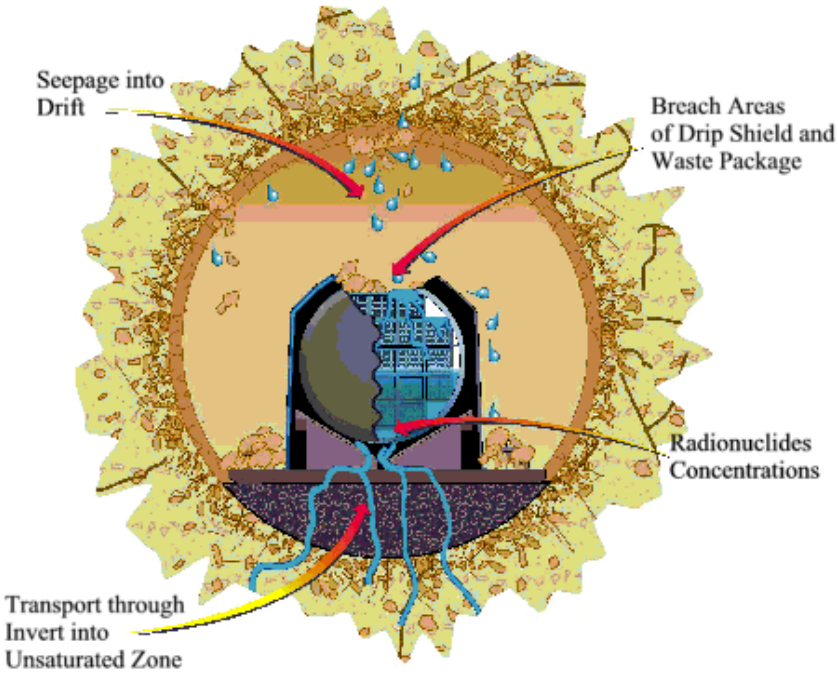

Figure 5-1
Schematic illustration of radionuclide release and transport with seepage from Yucca Mountain repository (from DOE/OCRWM, 2002).

Within the waste package, the spent-fuel rods are initially supported and surrounded by structural elements. After waste canister failure, the internal steel oxidizes to form a voluminous high-surface iron oxide corrosion product. This leaves spent-fuel assemblies unsupported and may lead to their rearrangement as shown in Figure 5-2(b). The highly reactive corrosion products are expected to remain in place and to act as a transport barrier. The stainless steel canister inner layer is also expected to corrode fast relative to the alloy C-22 outer barrier. The outer canister is expected to fail primarily by general corrosion, and to gradually lose its mechanical properties. Hence, eventually the entire waste package loses its original configuration.

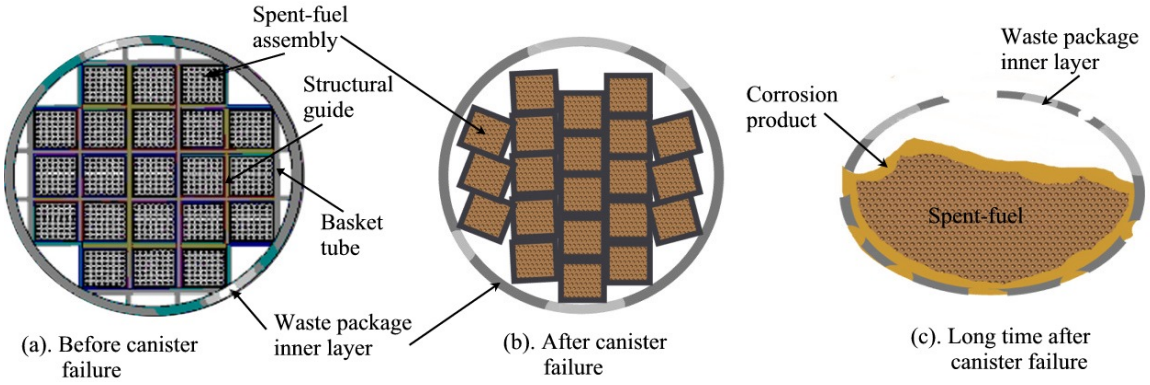

Figure 5-2
Schematic description of long-term spent-fuel waste package degradation (DOE/OCRWM, 2008b).

Upon contact of the water with the waste, those spent-fuel rods with failed claddings at the time of canister failure will start releasing radionuclides into the water. The intact cladding will gradually "unzip" (open along axial direction – a form of cladding failure) thereby increasing the spent fuel inventory exposed to water and increasing the release of radionuclides with time. Radionuclides within gaps between the spent-fuel matrix and cladding, within fuel pellet fractures, and within spent-fuel grain boundaries will dissolve quickly. Meanwhile, the spent-fuel matrix itself will begin oxidation and alteration in a well-documented corrosion process that will lead to a more gradual release of radionuclides, depending on the rate of alteration and the solubility limit of the radionuclides in the water contacting the spent fuel.

Because the steel surrounding the spent-fuel rods alters to a corrosion product, the released radionuclides must pass through the corrosion product before reaching the invert below the waste package. The dry conditions in Yucca Mountain and associated low moisture content result in an extremely low effective diffusion coefficient in the corrosion product, which will reduce release rates. Furthermore, some radionuclides may be sorbed onto corrosion products.

The failure mode of the canister is primarily general corrosion. Based on the heterogeneous temporal conditions in the repository, waste package failures are distributed in time. When a particular container is corroded, the interface area between the degraded waste package and the invert, potentially important to diffusive transport of radionuclides, will evolve with time. This contact area may be small initially, but will expand as the outer canister continues to degrade via general corrosion. The area is limited by the top area of the invert (Figure 5-1).

Once radionuclides are released from the waste canister, they migrate through the invert to the unsaturated zone below the waste package. The invert is composed of crushed tuff gravel that has the same geochemical characteristics as tuff. The dominant migration pathway of radionuclides is along a thin film of water on gravel surfaces under partially saturated conditions.

Immediately below the emplacement drift, there is a zone of relatively dry host rock due to diversion of water around the drift: the so-called the "drift shadow" effect (DOE/OCRWM, 2002). The drift shadow effect is the result of the capillary discontinuity between the cavity and the surrounding unsaturated medium, which diverts water from flowing into the cavity (Zhou and Zheng, 1994). As a result of the reduced flow below the cavity, water saturation is reduced, as shown in Figure 5-3. Therefore, radionuclides are transported by diffusion and advection at the reduced flow rate until reaching the host rock outside the shadow zone, where ambient saturations and infiltration rates prevail.

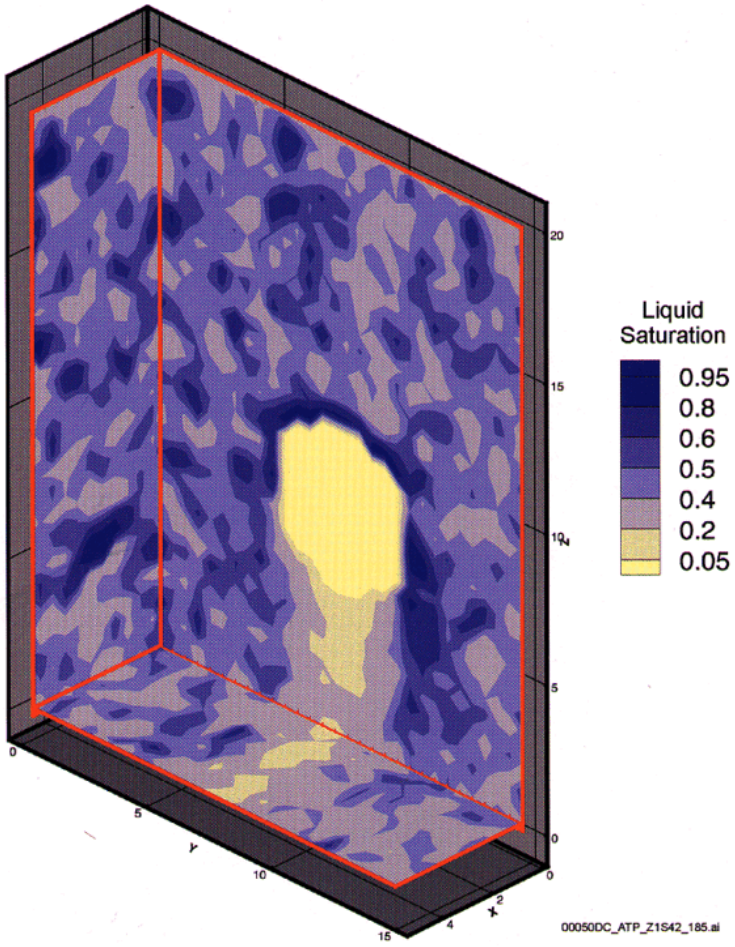

Figure 5-3
An example of illustrating reduced water saturation in host rock below an emplacement drift (from DOE/OCRWM, 2002).

The COMPASS code addresses these key FEPs relevant to the source-term, EBS, and near field after canister failure:

- water contact with the waste package due to seepage or condensation of water vapor;
- time-dependent seepage rate for the dripped drifts;
- distributed cladding failure over time;
- dissolution of radionuclides from spent-fuel;
- shared elemental solubility;
- sorption;
- radioactive decay/ingrowth; and
- diffusion and advection transport from waste form to the geosphere via corrosion product, invert, and near-field rock matrix and fracture.

To model the above FEPs, the following assumptions are made:

1. Upon failure of the container, water immediately contacts the waste package and forms a continuous liquid water pathway from the waste form to the EBS and near field outside the waste canister.
2. The steel guides and basket tubes that support spent-fuel rods are assumed to corrode and reduce to corrosion product immediately after water contact.
3. The corrosion product is assumed to be a porous material that is in close contact with spent-fuel rods.
4. Intact cladding is assumed to protect spent-fuel from contacting water.
5. The fraction of inventory exposed to water at a given time is assumed to be equal to the fraction of failed cladding.
6. The exposed spent fuel is assumed to fill with water in its void space where radionuclides dissolve.
7. Radionuclides residing in the gap between spent-fuel matrix and cladding as well as in the grain boundary of spent fuel are assumed to instantly dissolve upon contact with water.
8. Radionuclides bound with the spent-fuel matrix are assumed to dissolve into water congruently with spent-fuel alteration.
9. A constant spent-fuel alteration rate is assumed and is equal to the reciprocal of the time for completely altering the spent-fuel matrix.
10. The waste form, corrosion product, invert, near-field rock matrix, and near-field rock fracture are each treated as a single compartment, in which instant mixing of radionuclides is assumed.
11. Mass transfer between compartments occurs by diffusion and advection, if present, and may be retarded by sorption.
12. The time-dependent seepage rate is treated as a piecewise smooth step function.
13. The distributed cladding failure is treated as a piecewise smooth step function.
14. Sorption is treated using a linear equilibrium sorption model.
15. The nearest flow fracture is assigned a zero-concentration boundary condition.
16. Water flowing into the drift can be diverted, in which case only a portion of seepage water flows into the waste package while the rest flows to the invert and may dilute radionuclide concentrations there.

Assumptions (1) through (5) are related to the treatment of FEPs within the failed waste canister and can be illustrated in Figure 5-4. The compartment model representation of the system is depicted in Figure 5-5.

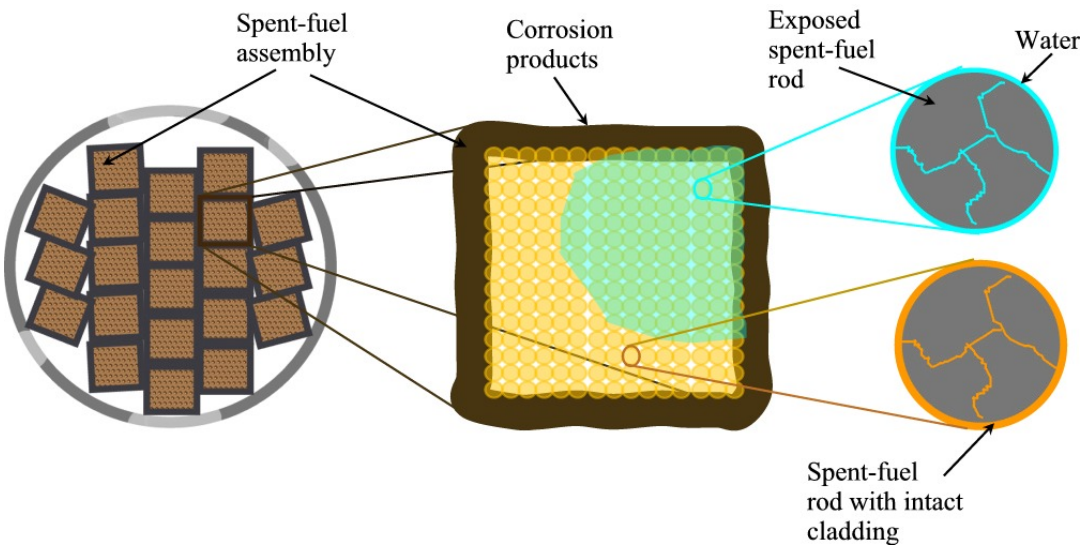

Figure 5-4
Conceptualization of a failed waste package consisting of spent-fuel rods, cladding, corrosion product, and water.

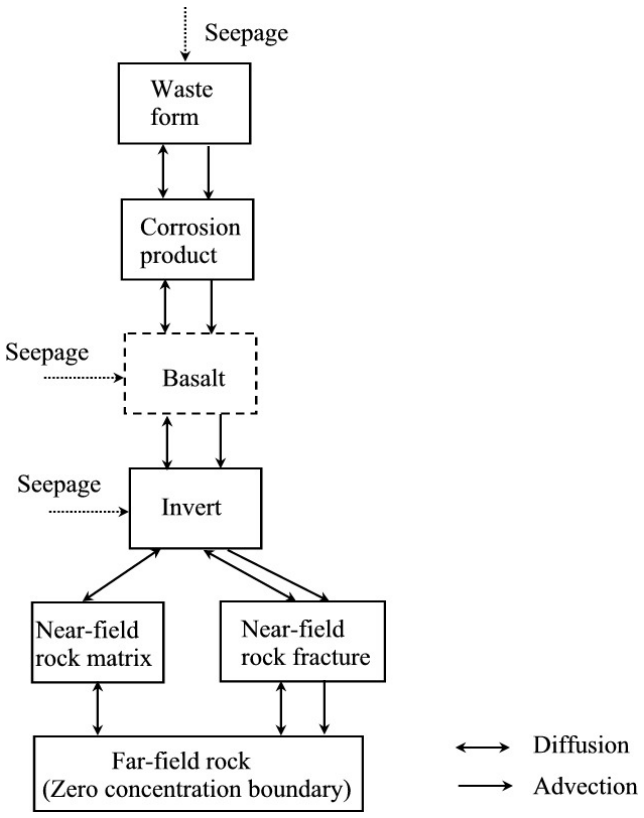

Figure 5-5
Compartment model for COMPASS.

In Figure 5-5, the "Basalt" compartment between corrosion product and invert is only used for the igneous-intrusion scenario, in which basaltic magma is postulated to flow into the emplacement drift, fill up the empty space, and form basaltic rock after cooling down. In this igneous-intrusion case, there may be diversion of seepage flow around the basalt, and preventing water contact with waste packages. This feature is only used for the low-probability igneous event scenario, and only as a sensitivity parameter, since information on the hydraulic properties of basalt formed from magma solidification within the drift have not been specifically evaluated.

5.4 Mathematical Equations

Mathematical equations for the system shown in Figure 5-5 follow mass conservation constitutive equations in a control volume. In the waste-form compartment, there are terms associated with the different release mechanisms. Thus, the following equation holds:

$$\frac{d\left(V_w A_{w,i}\right)}{dt} = -\lambda_i A_{w,i} + \lambda_{i-1} A_{w,i-1} + f_{g,i} f_c(t) M_i(t) \delta(t_f) + \frac{1}{t_a} f_{m,i} f_c(t) M_i(t) \times u(t_f + t_a - t) - T_{w,cp}\left(C_{w,i} - C_{cp,i}\right) - \dot{Q} C_{w,i}, \quad i = 1,2,...n, \quad t \geq t_f \,. \qquad \text{Eq. 5-1}$$

where:

A is the total concentration [mol/m^3],

V is volume [m^3],

t is time [yr],

λ is half life [yr],

f_g is the fraction of inventory for a given nuclide in the gap and grain boundary [unitless],

f_m is the fraction of inventory for a given nuclide in the spent-fuel matrix [unitless],

f_c is the cumulative fraction of failed cladding [unitless],

$M(t)$ is inventory of a given nuclide [mol],

$\delta(t)$ is a Delta function [1/yr],

t_f is the canister failure time [yr],

t_a is the spent-fuel alteration time [yr],

$u(t)$ is the unit function ($u(x) = 0$ if $x \bullet 0$; $u(x) = 1$ if $x > 0$) [unitless],

T is the mass transfer coefficient between two neighboring compartments [m^3/yr],

C is the aqueous concentration of a given radionuclide [mol/m^3],

$\dot{Q}$ is the seepage water flow rate [m^3/yr],

subscript "w" and "cp" denote the waste-form and corrosion-product compartments, respectively,

subscript "i" is the nuclide index in a decay chain, and

n is the total number of nuclides in a decay chain.

The inventory for the *i*th nuclide is determined by:

$$\frac{dM_i(t)}{dt} = -\lambda_i M_i(t) + \lambda_{i-1} M_{i-1}(t), \qquad i = 1,2,...n, \quad t \geq 0. \qquad \textbf{Eq. 5-2}$$

If the inventory starting time is $t = 0$, the initial condition for Equation 5-2 is:

$$M_i(0) = M_{i,0}, \qquad i = 1,2,...n. \qquad \textbf{Eq. 5-3}$$

The total concentration and aqueous concentration are related according to the following equation:

$$A_i = \theta C_i + (1-\phi) S_i + P_i, \qquad i = 1,2,...n. \qquad \textbf{Eq. 5-4}$$

where

θ is the moisture content [unitless] of the compartment and is equal to porosity multiplied by water saturation,

ϕ is the porosity of the compartment [unitless],

S is the amount of sorbed radionuclides per unit volume [mol/m^3] of the solid in the compartment, and

P is the amount of precipitated radionuclides per unit volume of the compartment [mol/m^3].

In other compartments, the mass balance equations are similar to Equation 5-1 except that no source term is present. Hence, the mass balance equation can be generally expressed as:

$$\begin{aligned} \frac{d\left(V_j A_{j,i}\right)}{dt} &= -\lambda_i A_{j,i} + \lambda_{i-1} A_{j,i-1} - \sum_{k \neq j} \left[T_{jk}\left(C_{j,i} - C_{k,i}\right)\right] - \dot{Q} C_{j,i} \\ &\quad + \sum_{l \neq j} \left[T_{lj}\left(C_{l,i} - C_{j,i}\right)\right] + \dot{Q} C_{l,i}, \qquad i = 1,2,...n, \quad j = 1,2,...m, \qquad t \geq t_f. \end{aligned} \qquad \textbf{Eq. 5-5}$$

where the third and fourth terms on the right hand side (RHS) of Equation 5-5 represent the total incoming fluxes from the contacting compartments, and the fifth and sixth terms represent the total outgoing fluxes to the contacting compartments if there are "*m*" number of compartments contacting the *j*th compartment.

The initial condition (*i.e.*, $t = t_f$) in all the compartments is zero concentration, expressed as follows using the subscript "*j*" as the compartment index:

$$A_{j,i}(t_f) = 0, \qquad j = 1,2,...m, \quad i = 1,2,...n. \qquad \textbf{Eq. 5-6}$$

If "*k*" is the element index, the capacity factor for the *k*th element in the *j*th compartment can be defined as:

$$\alpha_{j,k} = \theta_j + (1-\phi_j)\rho_j K_{d\,j,k}, \qquad j = 1,2,...m, \quad k = 1,2,...L. \qquad \textbf{Eq. 5-7}$$

where

ρ is the bulk density [kg/m^3] of the compartment,

K_d is the sorption coefficient [m^3/kg], and

L is the total number of elements in the problem.

Assuming that the *i*th nuclide is an isotope of the *k*th element, the total and aqueous concentrations can be related using the capacity factor defined in (Equation 5-7):

$$A_{j,i} = \alpha_{j,k} C_{j,i} + P_{j,i}, \qquad j = 1,2,...m, \quad i = 1,2,...n. \qquad \textbf{Eq. 5-8}$$

To determine the aqueous concentration of radionuclide with solubility limit consideration, the following equation is used:

$$C_{j,i} = \begin{cases} S_k \dfrac{A_{j,i}}{\sum_k A_{j,k}}, & \text{if} \quad \dfrac{\sum_k A_{j,k}}{\alpha_{j,k}} \geq S_k \\ \dfrac{A_{j,i}}{\alpha_{j,k}}, & \text{if} \quad \dfrac{\sum_k A_{j,k}}{\alpha_{j,k}} < S_k. \end{cases} \qquad \textbf{Eq. 5-9}$$

where

S_k is the solubility for the *k*th element [mol/m^3], and

$\sum_k A_{j,k}$ is the summation of total concentrations of all isotopes of the *k*th element considered in the problem.

Equation 5-9 means that if the summation of *aqueous* concentrations of *all* the isotopes belonging to the same element exceeds the solubility of the element, the aqueous concentration for the *i*th nuclide is determined as a fraction of the solubility. This fraction is equal to its total concentration over the summation of the total concentrations of all isotopes (top part of Equation 5-9). In this case, precipitation is present and can be determined from Equation 5-8. Otherwise, the aqueous concentration is simply the total concentration reduced by the capacity factor to take into account of sorbed radionuclides (bottom part of Equation 5-9).

The boundary condition is zero concentration in the last compartment:

$$A_{ff,i} = 0. \qquad \textbf{Eq. 5-10}$$

where the subscript "*ff*" denotes "far-field" rock.

The mass transfer coefficient between two compartments associated with diffusional transport is assumed to be proportional to the interface area and harmonic mean of diffusivities between the two compartments, *i.e.*:

$$T_{jk} = A_{jk}\left(\frac{1}{\frac{d_j}{D_j} + \frac{d_k}{D_k}}\right) \qquad \textbf{Eq. 5-11}$$

where:

A_{jk} is the interface area [m^2] of the two compartments,

d is the diffusive length [m] of the compartment, and

D is the effective diffusion coefficient [m^2/yr] of the compartment.

The radionuclide release rate from the near field to the far field takes into account diffusive release from both near-field fractures and the matrix, as well as advective releases from the fractures (see Figure 5.5):

$$\dot{m}_i = \left(\dot{Q} + T_{f,ff}\right)C_{f,i} + T_{m,ff}C_{m,i} \qquad \textbf{Eq. 5-12}$$

where:

$T_{f,ff}$ is the mass transfer coefficient between the near-field rock fracture and the far-field rock,

$T_{m,ff}$ is the mass transfer coefficient between the near-field matrix and the far-field rock, and

the subscript "*f*" and "*m*" denote fracture and matrix, respectively.

5.5 Solution Method

The compartment mass-balance equations for all the compartments shown in Section 5.4 form a group of first order differential equations with respect to time that are solved numerically in COMPASS. At each time step, the radionuclide decay and in-growth are solved analytically. In this manner, the equations reduce to linear differential equations that can be solved using typical linear equation solvers.

To solve the linear equation system, a fully-implicit method is used for treating temporal and spatial discretization in which radionuclide concentrations in all compartments are solved at $t + \Delta t$. This method is unconditionally stable for all time-step sizes, thus it is suitable for performance assessment calculations involving long time periods. Furthermore, this method allows fast computation times, which is desirable for probabilistic assessment calculations.

The resulting set of linear equations is solved using a banded matrix solution method. In this method, all elements in the matrix farther than the "bandwidth" (*i.e.*, one or two non-zero elements immediately adjacent to the diagonal elements) are zero and make no contribution to the solution. Hence, a banded matrix solver can be built that avoids operations over zero elements.

At each time step, COMPASS first calculates radionuclide decay / ingrowth and checks elemental shared solubility and determines aqueous concentrations according to Equation (5.9). The modified concentrations are then fed to the linear equation solver to obtain the concentrations due to transport.

The time-stepping scheme is controlled by considering the solutions obtained at $t + \Delta t$ by taking a whole step of length Δt to those obtained from taking two steps of length $\Delta t/2$. The next step is chosen such that the next step will be set to a factor times the current step. This factor is given by:

$$\eta = 0.9\sqrt{\frac{\beta}{E_{\max}}} \qquad \textbf{Eq. 5-13}$$

where β is a user given (or default) tolerance and $E_{\max}$ is the maximum error found. This error is defined as:

$$E_{\max} = \max_{\substack{i=1\ldots n \\ j=1\ldots m}} \frac{\left|A^1_{j,i}(t+\Delta t) - A^2_{j,i}(t+\Delta t)\right|}{\left|A^1_{j,i}(t+\Delta t) + A^2_{j,i}(t+\Delta t)\right| + \varepsilon} \qquad \textbf{Eq. 5-14}$$

where:

ε is a small number close to machine precision,

$A^1_{j,i}$ and $A^2_{j,i}$ represent the total concentrations for the ith nuclide in the jth compartment at the end of the time-step, obtained by the full and two half-step routes, respectively.

Clearly,

$$\eta < 1 \quad \text{if} \quad E_{\max} > \beta, \quad \text{and} \quad \eta > 1 \quad \text{if} \quad E_{\max} < \beta \qquad \textbf{Eq. 5-15}$$

The factor of 0.9 is inserted in Equation 5-13 to be cautious. Furthermore, the η values are "capped" above and below by minimum and maximum factors of 0.5 and 1.5. Such a time-stepping is similar to a second order Runge-Kutta or modified midpoint rule. On the two half-steps route, the radionuclide decay / in-growth and capacity factors need to be computed for each half of the route. The maximum time step is capped by 10% of the minimum half-life of the nuclides considered.

The solution scheme is also designed to take advantage of situations where the solutions have settled to a nearly constant value. At such times a decision is taken as to whether the two half steps are needed, thus increasing the computational efficiency. This feature is especially advantageous to a condition with a high infiltration rate in the near field. In this case, the radionuclides may be released from the near field soon after completion of waste dissolution such that the near field transport modeling may be terminated. As a practical matter, this situation does not occur in typical TSPA calculations associated with Yucca Mountain, owing to the low flow rates and long retention times in the near field.

COMPASS includes reports on system mass balance at any given time *t*. This includes:

- Inventory [mol] at t,
- Total nuclides [mol] at t remaining in the waste-form, corrosion-product, invert, and near-field rock compartments, and
- Cumulative output amount [mol] up to t to the far-field rock compartment (*i.e.*, leaving the near field).

The nuclide masses at a given time must satisfy the following relationship:

$$M_i(t) = \sum_{j=1,...m} A_{j,i}(t) V_j + \int_{t_f}^{t} \dot{m}_i(\tau) d\tau, \qquad i = 1,2,...n. \qquad \textbf{Eq. 5-16}$$

where the near-field release rate $\dot{m}_i(t)$ is obtained from Equation 5-12.

System mass balance reports provide two useful functions. First, a system mass balance report checks the correctness of physical and mathematical models as well as programming errors, if any, during code development.

Secondly, a system mass balance calculation can be used to evaluate the capabilities of various system components in containing radionuclides. For different disposal designs or designs with different properties, mass balance reports will show different amounts of radionuclides retained within the near field or released into the far field, thereby providing a quantitative basis for comparing designs and properties.

COMPASS outputs incremental cumulative release rates to the far-field models of IMARC. For a given nuclide, this is calculated according to:

$$\dot{R}_i(t_n) = \int_{t_{n-1}}^{t_n} \dot{m}(\tau) d\tau \qquad \text{Eq. 5-17}$$

where:

$\dot{R}_i(t_n)$ is the release rate [mol/yr] for the *i*th nuclide during the output time interval Δt,

$\dot{m}_i(t)$ is the instantaneous release rate [mol/yr] for the *i*th nuclide at time *t* given by Equation 5-12, and

$d\tau$ is the simulation time-step.

The output time interval is also the IMARC time-step and is normally greater than the COMPASS simulation time-step. This is determined by the two output (or IMARC) times t_n and t_{n-1} and hence $\Delta t = t_n - t_{n-1}$.

Equation 5-17 means that numerical integration of instantaneous release rate with respect to the simulation time-step is carried out for every output time interval, or IMARC time-step. In this way, the detailed evolution of the near-field system is incorporated into the output release rates to the far-field and no peak release rates during the interval will be missed.

5.6 Verification

Three test cases are conducted to verify the COMPASS code. The test cases are described below. The input files for these test cases are provided in Appendix D.

Case 1 tests the COMPASS capability to simulate transient diffusion transport with constant-concentration boundary conditions in a finite medium. For this purpose, a stable and conservative contaminant is assumed to have a large initial inventory (10^5 moles) and very low solubility (10^{-6} mol/m^3). Assuming instant dissolution of the inventory, the waste compartment concentration is kept constant and equal to its solubility at all times. In addition, all the compartments are assumed to have a unit volume, area, length, porosity, and saturation. The diffusion coefficient is assumed to be 0.0316 m^2/yr for all compartments. Transport into the near-field rock matrix is suppressed by assigning an extremely small value to the matrix diffusivity. The zero-concentration boundary is assumed to be held at approximately 5 m from the center of the "waste" compartment. The solubility-normalized concentration in the "fracture" compartment, approximately 4 m from the waste-package compartment, is plotted as a function of time in Figure 5-6.

This case is equivalent to a one-dimensional transient diffusion problem with a zero initial concentration, a constant concentration (C_0) at $x = 0$, and zero concentration at $x = L$. The analytical solution for the problem can be found from Carslaw and Jaeger (1986, p.103):

$$\frac{C(x,t)}{C_0} = 1 - \frac{x}{L} - \frac{2}{\pi}\sum_{1}^{\infty}\frac{1}{n}\sin\left(\frac{n\pi x}{L}\right)\left(1 - e^{-Dn^2\pi^2 t/L^2}\right) \qquad \text{Eq. 5-18}$$

By choosing L = 5 m, the normalized concentration at x = 4 m as a function of time is compared with its COMPASS counterpart in Figure 5-6. The constant boundary conditions in a finite region eventually lead to a steady state (*i.e.*, the third term in Equation 5-18 disappears), shown in Figure 5-6 as the horizontal line at later times. Figure 5-6 demonstrates that COMPASS is in excellent agreement with the analytical solutions for both the transient and steady-state cases.

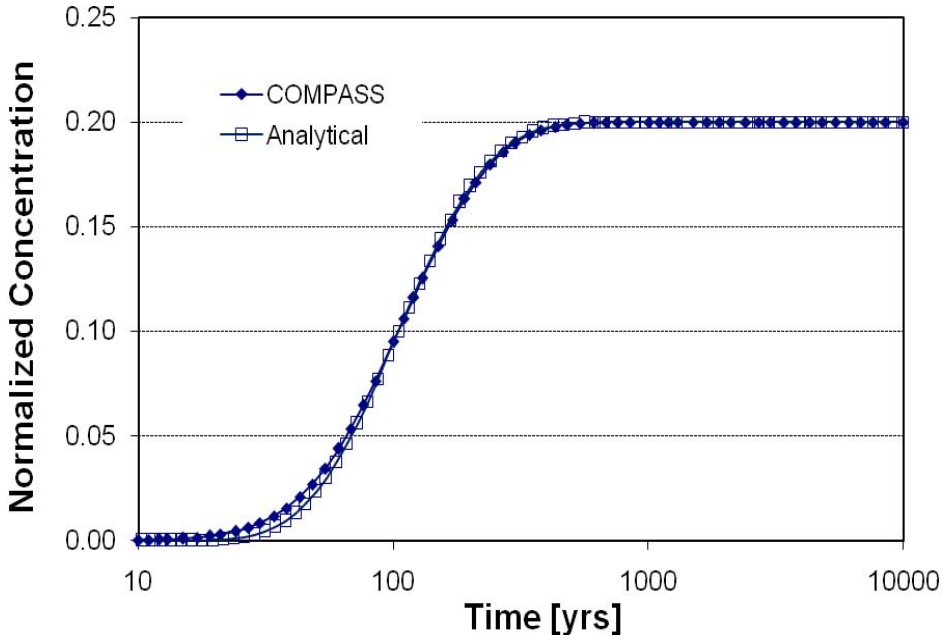

Figure 5-6
Comparison of COMPASS with analytical solution for one-dimensional transient diffusion transport of a conservative "nuclide" with constant concentration boundary conditions.

Case 2 tests the COMPASS capability for simulating advection transport of a radioactive decay chain. In this problem, a three-member decay chain is assumed to be instantly dissolved into water within the waste package and subsequently released at a given flow rate $\dot{Q}$. Such a problem can be described by the following differential equations for mass balance of the three nuclides:

$$\begin{aligned}
\frac{dM_1}{dt} &= -\left(\lambda_1 + \dot{Q}\right)M_1, \\
\frac{dM_2}{dt} &= -\left(\lambda_2 + \dot{Q}\right)M_2 + \lambda_1 M_1, \qquad t > 0. \\
\frac{dM_2}{dt} &= -\left(\lambda_3 + \dot{Q}\right)M_3 + \lambda_2 M_2.
\end{aligned} \qquad \textbf{Eq. 5-19}$$

where M_i is the mass of the ith nuclide [mol].

The initial conditions are:

$$M_i(0) = M_i^0, \qquad i = 1,2,3. \qquad \textbf{Eq. 5-20}$$

Assuming the unit volume, the analytical solutions for the release rates of the three nuclides are:

$$\begin{aligned}
\dot{m}_1(t) &= \dot{Q} M_1^0 e^{-(\lambda_1+\dot{Q})t}, \\
\dot{m}_2(t) &= \dot{Q} M_2^0 e^{-(\lambda_2+\dot{Q})t} + \frac{\dot{Q}\lambda_1 M_1^0}{\lambda_2-\lambda_1}\left[e^{-(\lambda_1+\dot{Q})t} - e^{-(\lambda_2+\dot{Q})t}\right], \\
\dot{m}_3(t) &= \dot{Q} M_3^0 e^{-(\lambda_3+\dot{Q})t} + \frac{\dot{Q}\lambda_2 M_2^0}{\lambda_3-\lambda_2}\left[e^{-(\lambda_2+\dot{Q})t} - e^{-(\lambda_3+\dot{Q})t}\right] \qquad t \geq 0. \\
&\quad + \frac{\dot{Q}\lambda_1\lambda_2 M_1^0}{(\lambda_2-\lambda_1)(\lambda_3-\lambda_1)}\left[e^{-(\lambda_1+\dot{Q})t} - e^{-(\lambda_3+\dot{Q})t}\right] - \frac{\dot{Q}\lambda_1\lambda_2 M_1^0}{(\lambda_2-\lambda_1)(\lambda_3-\lambda_2)}\left[e^{-(\lambda_2+\dot{Q})t} - e^{-(\lambda_3+\dot{Q})t}\right]
\end{aligned} \qquad \textbf{Eq. 5-21}$$

To simulate this case with COMPASS, the release of the decay chain $^{237}\text{Np} \rightarrow {}^{233}\text{U} \rightarrow {}^{229}\text{Th}$ is calculated for an advective water flow rate of 0.1 m^3/yr. The initial inventories for the three nuclides are 1,000, 100, and 10 moles, respectively, and are assumed to be instantly dissolved. The three nuclides are also assumed to be readily soluble. All compartments are assumed to have 0.4 porosity, 0.8 saturation, and unit interface area. The volumes of all compartments, except for the fracture compartments (see Figure 5-5), are assumed to be extremely small. (Note that the porosity and saturation together gives a moisture content of 0.32 and effective flow rate of 0.1/0.32 = 0.3125 m^3/yr.)

Furthermore, diffusion lengths as well as diffusion coefficients in all compartments are set to extremely small values. In this way, all compartments, except for those representing fractures, are eliminated from consideration along the radionuclide migration pathway in the near field, and the calculated release rates from the fracture compartment are equivalent to the waste package releases described in Equation 5-21. Figure 5-7 compares the release rates for the three nuclides calculated by COMPASS and the analytical solution using the same parameter values. The two solutions match each other to several significant figures.

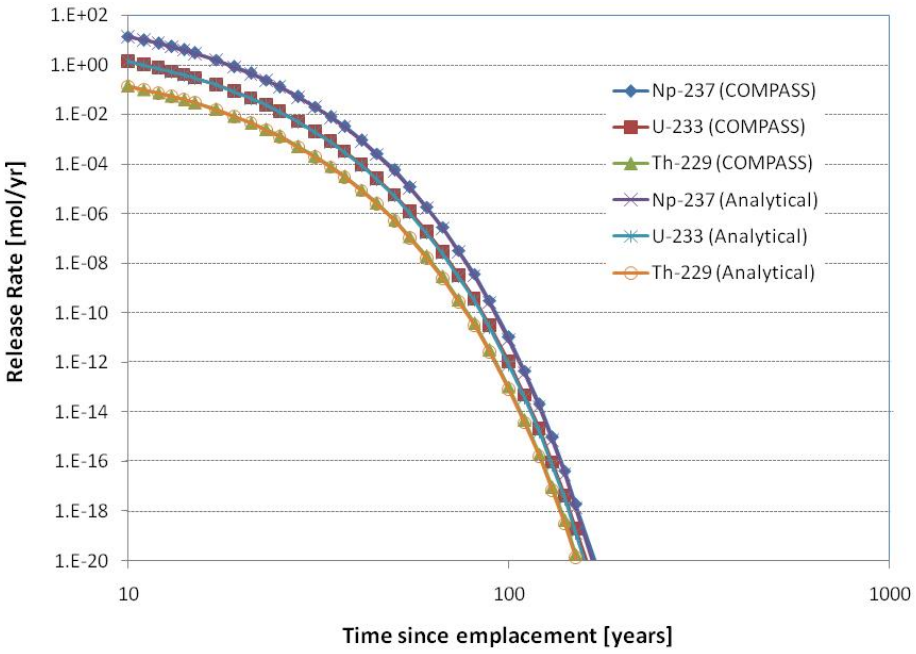

Figure 5-7
Comparison of advective release rates of the three-member decay chain calculated by COMPASS and the analytical solutions.

Case 3 tests COMPASS's capability for simulating advective release with sorption. The problem is defined as the advective release of a radionuclide with a given initial inventory M_i^0 from a domain that has the length *d* along the transport direction and a moisture content θ. The Darcy velocity is *v* and the retardation coefficient of the nuclide in the domain is *R*. This can be described by the study in Kozak et al. (1993) and the analytical solution is:

$$\dot{m}_i(t) = \frac{M_i^0}{\tau} e^{-(1/\tau+\lambda_i)t}, \quad \text{with} \quad \tau = \frac{d\theta R}{v}. \qquad \text{Eq. 5-22}$$

To simulate this case in COMPASS, a radionuclide with the half life of Np-237 and an initial inventory of 1,000 mol is assumed to be soluble and instantly dissolved upon contacting with water. All the compartments are assumed to have unit interface area and extremely small values for diffusion coefficients and distances. The corrosion-product compartment (Figure 5.5) is assumed to have a volume of 5 m^3. The volume of all other compartments is assumed to be extremely small so there is no delay time associated with these compartments. In this way, the release rate output from COMPASS is equivalent to that from the domain defined in the problem of Equation (5-22). The Darcy velocity is assumed to be 0.1 m/yr. Given a porosity of 0.4, a saturation of 0.8, a solid density of 2250 kg/m^3, and a sorption coefficient of 1.0 m^3/kg, the moisture content is equal to 0.32, the pore flow rate is 0.3125 m^3/yr, and the retardation factor is equal to 4,220 (unitless).

In Figure 5-8, the calculated COMPASS release rate is compared with that calculated by Equation 5-22 using the same parameter values. It can be seen that for ^{237}Np, the release rate is reduced due to sorption, as compared with Case 2 that has the same inventory and flow rate (Figure 5-7). In contrast, in Case 2 all the radionuclides are released earlier than 1,000 years. In this case, sorption greatly delays the release such that the inventory is not completely depleted until after 10,000 years. This process is captured by COMPASS and the comparison with analytical solution is exact to several significant figures.

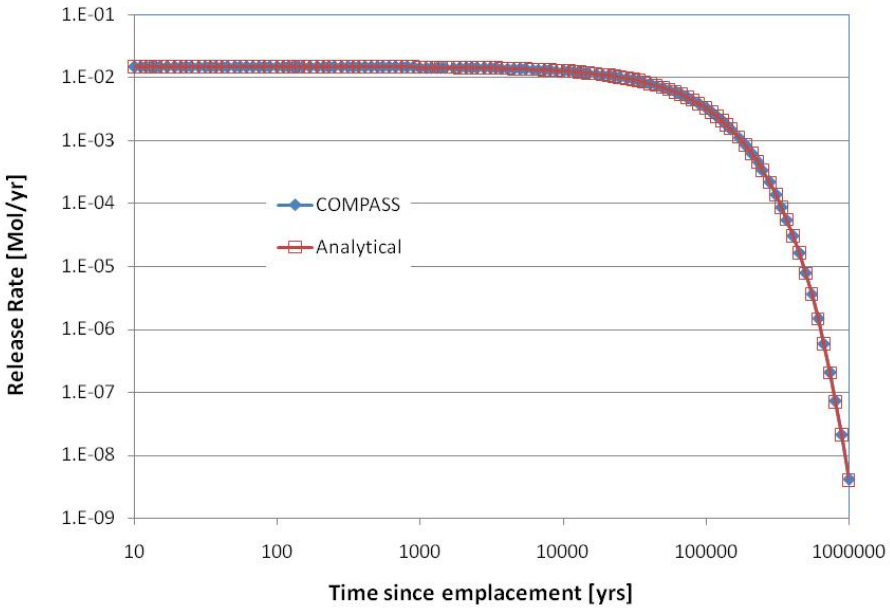

Figure 5-8
Comparison of COMPASS and the analytical solution with advective release of radionuclide retarded by sorption.

The results of these verification exercises demonstrate that COMPASS is able to accurately reproduce analytical solutions for the near field.

5.7 Interface with IMARC

As one component of the larger IMARC TSPA code, COMPASS is required to provide input to the unsaturated zone code, which is implemented with a concentration boundary condition at the upper edge of the unsaturated zone solution domain. Consequently, the output from COMPASS is translated into a concentration boundary condition using the average advective flow into the unsaturated zone:

$$C_i = R_i / vA, \qquad \text{Eq. 5-23}$$

where R_i is the release rate from COMPASS (mol/y), v is the infiltration rate outside of the shadow zone of the drift (m/y), and A is the cross sectional area of the repository (m^2). This simple approach will tend to understate concentrations at the interface between the near field and

the unsaturated zone; however, in terms of overall system performance the approach is appropriate. As discussed in the far-field model/code, the geosphere codes in IMARC are used to calculate the discharge rate (mol/y) at the accessible environment, using a standard 3000 acre-feet/year dilution factor. Consequently, alternative approaches for calculating concentrations at intermediate points in the geosphere do not affect the concentrations at the accessible environment.

An additional complication in the use of COMPASS arises from the multiple release mechanisms for the CSNF. At each interval in time in the performance period, IMARC evaluates the fraction of waste packages that have failed in the dripping and non-dripping parts of the repository, and conducts a COMPASS analysis for both of those conditions. Radionuclides contained in the gap fraction are released immediately upon waste package failure, so COMPASS must be run at each time step (in the distributed canister failure curve), to evaluate the releases from waste packages that have failed during that time increment. Therefore, at each time step, COMPASS is run for dripping and non-dripping conditions, and the resulting releases are added to releases occurring at that time from waste packages that failed at all previous time steps. The result is the cumulative release from a set of waste packages that have failed distributed in time, which have releases by different mechanisms over different time scales. Therefore, at any time, the summed releases represent the total release (mol/y) from all waste packages that have failed prior to that time.

The overall relationship between COMPASS and IMARC is illustrated in Figure 5-9.

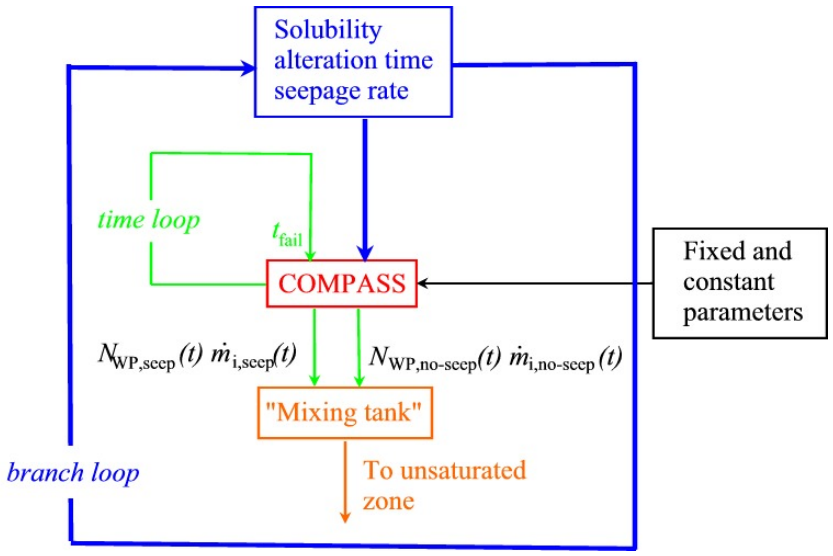

Figure 5-9
Illustration of integration of COMPASS in IMARC. $N_{WP,seep}(t)$ is the number of waste packages failed under seepage conditions. $N_{WP,no\text{-}seep}(t)$ is the number of waste packages failed under no-seep conditions. $m_{i,seep}(t)$ and $m_{i,no\text{-}seep}(t)$ and are the near-field release rates calculated by COMPASS under seeping and non-seeping conditions.

5.8 Sensitivity Analysis

There are unavoidable uncertainties in some of the COMPASS parameters. This section presents sensitivity analysis of some parameters, especially those that are considered potentially important and have greater uncertainties. In all the cases, the parameter values described in "Required Input Parameters" have been used. The canister failure time is assumed to be 1,000 years for the purpose of clarity for observing the impact on near-field release rates ("source term"). The seepage rate for the cases with seepage is assumed to be 0.4 m^3/yr. When varying other parameters, values for sorption in Appendix E and a rapid alteration time of 3,000 yrs (characteristic of the mean value used in IMARC 9) are used.

5.8.1 Cladding Credit

Four cases are set up for calculating near-field release rates by COMPASS. These cases test the sensitivity of distributed cladding failure under seeping and non-seeping conditions:

- Seeping conditions: waste packages without cladding credit (i.e., 100 percent of the cladding is assumed failed when the waste package fails),
- Seeping conditions: waste packages with cladding credit (i.e, distributed cladding failure per Figure 4-30),
- Non-seeping conditions: waste packages without cladding credit, and
- Non-seeping conditions: waste packages with cladding credit.

The total release rates in Bq/yr are shown in Figure 5-10. Note that the total release rates are dominated by ^{99}Tc and ^{129}I at early times.

For non-seeping conditions, the two cases are shown in Figure 5-10: without cladding credit at all ("no-seeping & no cladding") and with distributed cladding failure ("no-seeping & with cladding"). It can be seen that the two cases have the same peak release rates except that the distributed cladding failure delays the peak release rate by about 135,000 years, the approximate time period for complete cladding degradation (see Figure 5-10).

For the seeping case without cladding, the release of ^{99}Tc and ^{129}I is controlled by the alteration time. After the spent-fuel matrix is completely altered, the two more soluble and non/low sorbing nuclides are quickly removed from the near field due to the high seepage rate, leaving a tail in the release curve that is dominated by the less soluble and higher sorbing actinide nuclides. With cladding credit, the number of spent-fuel rods exposed to water contact is distributed over time, thereby reducing the early (up to 3,000 yrs) release rate but raising the later (from 3,000 to 135,000 yrs) release rates. When all the cladding has failed (at about 150,000 yrs), the release curve joins the release curve for waste packages under seeping conditions without cladding credit.

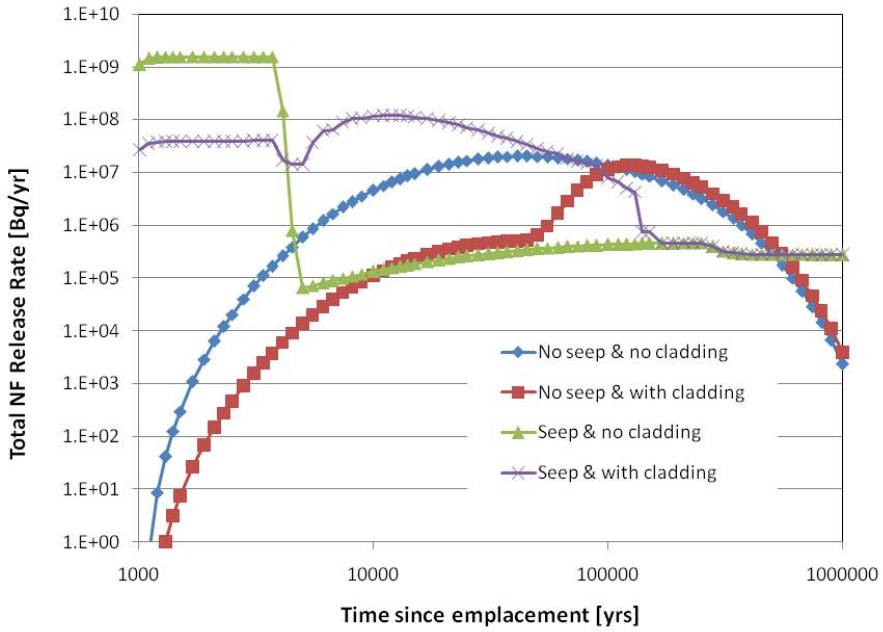

Figure 5-10
Sensitivity analysis on cladding credit: total release rates with and without cladding credit under seeping and non-seeping conditions. NF: Near Field.

5.8.2 Sorption by the Corrosion Products

It has been shown in the parameter section that corrosion products may be a significant diffusion transport barrier in waste packages that are not dripped on. The role of radionuclide sorption by corrosion products is investigated in this sensitivity analysis.

Four cases are set up for this purpose:

1. Seeping conditions: waste package with sorption by the corrosion products,
2. Seeping conditions: waste package without sorption by the corrosion products,
3. Non-seeping conditions: waste package with sorption by the corrosion products, and
4. Non-seeping conditions: waste package without sorption by the corrosion products.

The release rates of the actinides (the sum of the release rates from all actinides) and ^{237}Np (the primary dose contributor) in Bq/yr are shown in Figure 5-11. Note that the results exclude ^{129}I and ^{99}Tc because these nuclides are assumed to be non-sorbing, and thus there is no difference in their release rates when sorption by the corrosion products is assumed to be greater than zero and when sorption by the corrosion products is assumed to be zero.

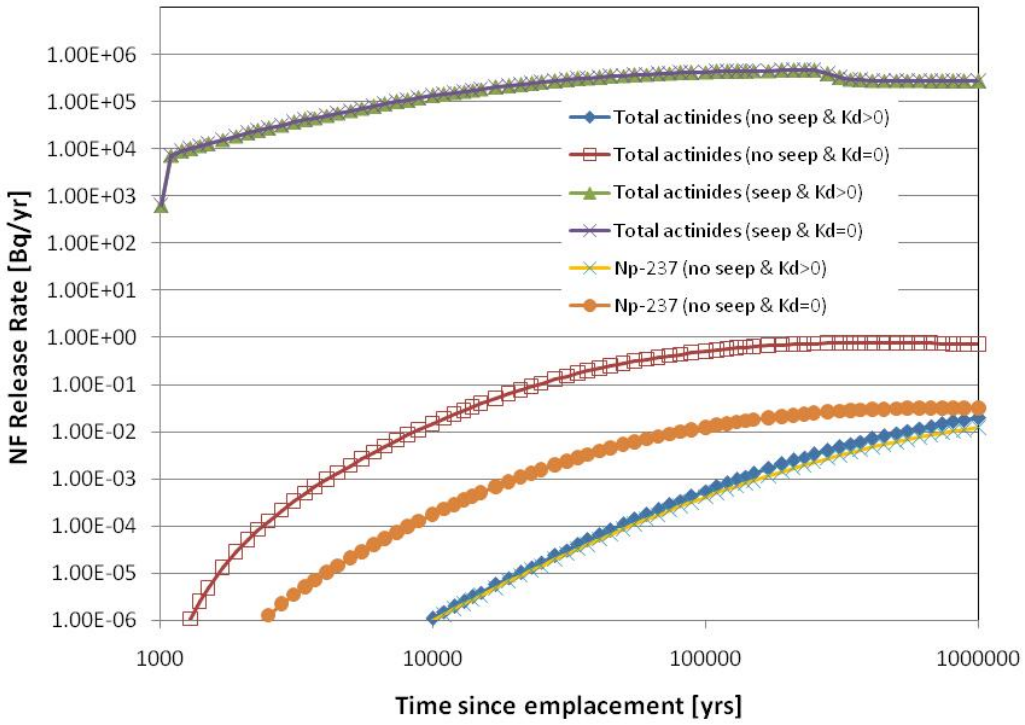

Figure 5-11
Sensitivity analysis on sorption by corrosion products: total actinide and ^{237}Np release rates with and without seepage.

The top two curves in Figure 5-11 are actinide release rates with and without sorption by the corrosion products under seepage conditions. It can be seen that seepage makes the release insensitive to sorption by corrosion products. Because the sorption is assumed to be reversible, the sorbed nuclides in the corrosion products can be released effectively when the seepage rate is sufficiently high.

The lower four curves are release rates from waste packages under non-seeping conditions. Comparing total actinide release rates, it can be seen that without sorption by the corrosion products, the release rate can be two (at 10^6 yrs) to many orders of magnitude (< 10^6 yrs) higher than that with sorption by the corrosion products. For ^{237}Np, the sorption effect is less significant because of the isotope's extremely long half-life (2.1 x 10^6 years) and lower retardation by corrosion products and higher mobility relative to other actinides (Appendix E). As a result, ^{237}Np dominates the total actinide release rate.

5.8.3 Alteration Time

To investigate the sensitivity of alteration time on radionuclide release, four cases are evaluated:

1. Seeping conditions: waste packages with alteration times of 3,000 yrs,
2. Seeping conditions: waste packages with alteration times of 30,000 yrs,
3. Non-seeping conditions: waste packages with alteration times of 3,000 yrs, and
4. Non-seeping conditions: waste packages with alteration times of 30,000 yrs.

The total radionuclide release and ^{129}I release rates under seepage conditions are shown in Figure 5-12. It can be seen that for slow diffusion transport of radionuclides from waste packages under non-seeping conditions, the release rates are not sensitive to alteration time.

Alteration time, however, can be relatively important for advective release from waste packages that experience seepage. The top two curves in Figure 5-12 are total release rates from waste packages under seepage conditions for alteration times of 3,000 and 30,000 years respectively. Because the total activity released from the waste package is dominated by ^{99}Tc and the release of this nuclide is controlled by the spent-fuel alteration rate, the early peak release rate is shown to decrease as alteration time increases. For ^{129}I, its instant-release fraction is not affected by the alteration rate, but its matrix fraction release rate decreases as alteration time increases. After the more mobile radionuclides ^{99}Tc and ^{129}I are removed from the near-field system, the near-field release rate ("source term") is dominated by the release rates of the less mobile actinides, which are not sensitive to alteration time.

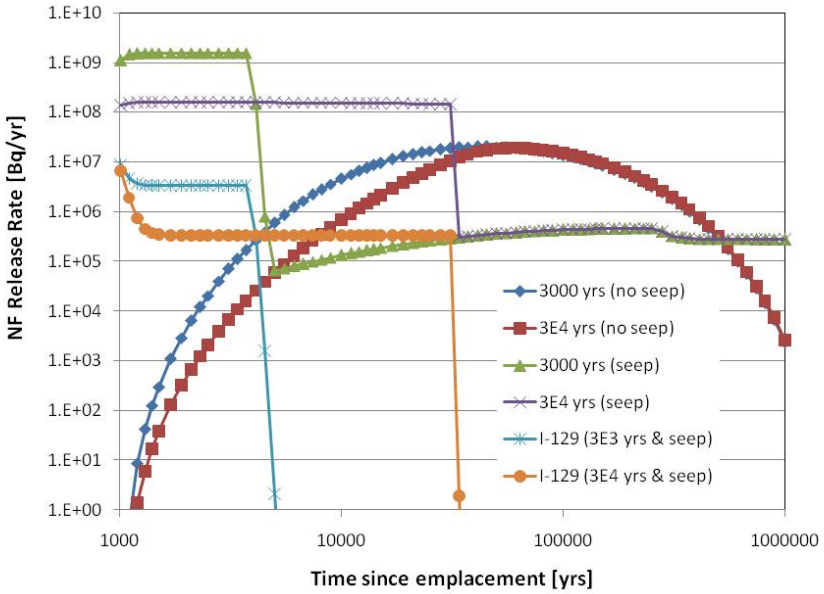

Figure 5-12
Sensitivity analysis of spent-fuel alteration time: total and ^{129}I release rates with different alteration times and seepage conditions.

5.9 Summary

The observations from the sensitivity analyses are summarized in Table 5-9.

The sensitivity of sorption and containment parameters depends on transport conditions in the near field; *i.e*., whether diffusive or advective transport is dominant. Advective release is not sensitive to sorption by the corrosion products while slow diffusive release is sensitive to sorption by the corrosion products.

On the other hand, containment parameters are more important to advective release than to diffusive release. Containment parameters are also more important to non-sorbing and soluble nuclides than sorbing and solubility-limited nuclides. Consideration of distributed cladding failure results in a lower peak release rates compared to the release rates without cladding credit. Similarly, longer alteration time helps lower the release rates of ^{99}Tc and ^{129}I in the spent-fuel matrix but not the release rates of ^{99}Tc and ^{129}I in the gap and grain boundary that are assumed to be released instantly.

Table 5-1
Summary of Sensitivity Analysis for Waste Packages Subjected to Advection (Active Seeping Conditions) and Diffusion (Non-Seeping Conditions)

	Advection	Diffusion
Sorption in corrosion-product	Not sensitive	Sensitive to actinide release
Cladding credit	Sensitive to ^{99}Tc and ^{129}I	Not sensitive
Alteration time	Sensitive to ^{99}Tc and ^{129}I	Not sensitive

It is worthwhile noting that the above observations are based on a single waste package. In the total system that involves other factors such as distributed waste canister failure, far-field retardation, and dilution, these near-field parameters may not play a significant role in the calculated peak dose release rates to the biosphere.

6
GEOSPHERE MODELS

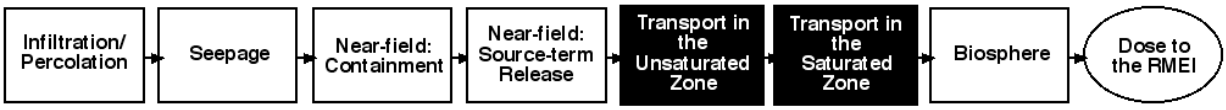

Models for describing the transport of radionuclides away from the repository near-field through the geosphere are described in a number of previous EPRI reports on the IMARC methodology (EPRI, 1996; EPRI, 1998). The underlying models have not changed since Version 6 (EPRI, 2002a, although the dimensionality of the saturated zone model was revised in Version 8 (EPRI, 2005c), and implementation and parameterization of the models has continued to evolve with the state of knowledge of the Yucca Mountain system. This section describes the current implementation of these models in IMARC 10.

IMARC 10 accounts for transient variably saturated flow and advective dispersive transport of a decay chain, in a coupled dual porosity, dual permeability context, from the base of the repository to the water table. The dual porosity, dual permeability approach allows for the coupling of fluid and solute interactions between the fractures and the porous rock matrix. Radionuclide sorption can occur both in the fractures and in the rock matrix. Upon reaching the saturated zone portion of the calculation at the water table, IMARC considers two-dimensional advective dispersive transport of the radionuclides during their migration to the RMEI location down gradient. The saturated zone module also accounts for matrix diffusion of radionuclides into immobile porewaters contained in the rock blocks below the water table, as well as radionuclide sorption and daughter-product in growth.

Radionuclides leached from the waste facility are advected and dispersed downward through the unsaturated zone. The unsaturated zone is modeled as a one dimensional column represented as a double porosity, double permeability continuum to represent coupled fracture/matrix interactions. The unsaturated zone is comprised of vertical fractures which are relatively permeable, and an intervening porous rock matrix which is much less permeable. A multiphase (air and water) approach is used to solve for the pressures, water saturations and water fluxes in both porosity zones and between the matrix and fracture regions, although the air phase is assumed to be passive in the context of Richards' equation describing transient unsaturated flow.

The radionuclides can decay into daughter species and form linear decay chains. The model can accommodate any number of decay chains, and each decay chain can be of any specified length. As well as being advected, dispersed and subject to radioactive decay, the radionuclides can adsorb onto fracture walls and the matrix solids.

Once the radionuclides reach the water table, they can advect, disperse and decay within the two dimensional saturated aquifer. Groundwater flow in the saturated zone is assumed to be

representative of long term steady state conditions with the bulk hydraulic conductivity of the fractured rock mass being assumed to be representative of an equivalent porous medium which may be anisotropic. The assumption of steady state flow was necessary to achieve the high level of computational efficiency needed for a risk assessment involving hundreds to thousands of scenarios. While the model currently assumes homogeneity of the rock mass in the saturated zone, the saturated zone flow and transport properties could be allowed to vary spatially in the future because the equations are solved numerically, meaning that the properties could be defined differently for each finite element in the mesh. Transient radionuclide transport in the saturated zone can be represented either in the context of a single or a double porosity medium. In both cases, the porosity of the mobile zone through which the groundwater is flowing is represented by the value of the input fracture porosity. For the double porosity transport situation, although the rock matrix (represented as spherical blocks) is assumed to contain immobile groundwater, radionuclides can diffuse into or out of the matrix which leads to a physical retardation effect. Dispersive mixing in the flowing groundwater is fully three dimensional and is represented in the classical Fickian context. The radionuclides can sorb onto the solid material of both porosity zones. The three dimensional velocity field can either be specified to be uniform by inputting the three components of the water velocity vector, or the velocity field can be obtained by solving the saturated groundwater flow equation. If the flow field is solved for, the model currently allows for one pumping well (which is assumed to be pumped at a constant rate) to be located within the aquifer.

6.1 Unsaturated Zone

The code used for analysis of transport in the unsaturated zone (UZ) has no formal name, and is referred to simply as the "UZ code." A multi phase approach is used to solve the unsaturated flow problem in which the water is mobile but the air phase is assumed to be passive, which is consistent with the use of Richards' equation. The model uses a control volume spatial discretization scheme, and includes the following features:

Relative permeability and capillary pressure data are input separately (via tables) for each rock strata for both the rock matrix and the fractures.

The unsaturated zone is modeled as a double porosity, double permeability (matrix fractures) system.

6.1.1 Unsaturated Zone Flow

Beginning with the usual form for the variably-saturated flow equation:

$$\frac{\partial (\theta S_w)}{\partial t} = -\nabla \cdot (V_w) \pm q_w' \qquad \textbf{Eq. 6-1}$$

where the Darcy flux of the water phase is

$$V_w = -K \cdot \lambda_w (\nabla P_w - \rho_w g \nabla D) \qquad \textbf{Eq. 6-2}$$

and where:

S_W is the water saturation

θ is the porosity

P_W is the water pressure

K is the absolute permeability tensor

$\lambda_w = k_{rw} / \mu_w \mu_w$ is the viscosity of water

ρ_w is the density of water

K_{rw} is the relative permeability of water

D is the depth

G is the gravitational acceleration and

q_w' is a source/sink term representing fluid exchange between the fractures and the rock matrix.

The basic form of Equations 6-1 and 6-2 are assumed to hold for both the fractures and the rock matrix. The values of parameters such as porosity and permeability (matrix versus fracture), the form of the constitutive relations, as well as the pressures and saturations are, however, different between the fracture and the rock matrix.

The water pressure is related to the air pressure by the capillary pressure P_{caw} according to

$$P_a = P_w + P_{caw}(S_w) \qquad \textbf{Eq. 6-3}$$

The porosity is given by

$$\theta = \theta_o(1 + c_m(P_w - P_{wo})) \qquad \textbf{Eq. 6-4}$$

where:

c_m is the compressibility of the medium, and

θ_o is the porosity at $P_w = P_{wo}$.

Equation 6-1 is discretized using a mass conservative, monotone, fully implicit, finite volume method. The discretized equations have the same form for both matrix and fractures. If N is the time level, then the discretized equation for either the fractures or the matrix is of the form:

$$\{ [\ \theta\ S_w\ ]_i^{N+1} - [\ \theta\ S_w\ ]_i^N \} \frac{V_i}{\Delta t} = \sum_{j \in \eta_i} (\ \lambda_w\ )_{ij+1/2}^{N+1} \gamma_{ij} (\ \psi_{wj}^{N+1} - \psi_{wi}^{N+1}\ ) \pm (\ q_w\ )_i^{N+1} \qquad \textbf{Eq. 6-5}$$

where

$\psi_{wi} = P_{wi} - \rho_{wi} g D_i$,

V_i is the volume of node i, and

η_i are the neighbor nodes for node i.

Upstream weighting is used for $(\rho_w \lambda_w)_{(ij+1/2)}$:

$$(\rho_w \lambda_w)_{ups(i,j)} = (\rho_w \lambda_w)_i^{N+1} \text{ if } \gamma_{ij}(\psi_{lj}^{N+1} - \psi_{li}^{N+1}) < 0$$
$$= (\rho_w \lambda_w)_j^{N+1} \text{ if } \gamma_{ij}(\psi_{lj}^{N+1} - \psi_{li}^{N+1}) > 0 \qquad \textbf{Eq. 6-6}$$

Equation (6-5) is valid for both the matrix and fractures. If i and j are both matrix nodes, or both fracture nodes, then

$$\gamma_{ij} = K_{ij+1/2} \frac{A_{ij}}{\Delta z_{ij}} \qquad \textbf{Eq. 6-7}$$

where:

A_{ij} the interfacial area between node i and node j,

$K_{ij+1/2}$ is the absolute permeability, and

Δz_{ij} is the distance between node i and node j.

If node i is a fracture node, and node j is a matrix node, then

$$\gamma_{ij} = 4 K_{matrix} V_i \left(\frac{1}{L_x^2} + \frac{1}{L_y^2} + \frac{1}{L_z^2}\right) \qquad \textbf{Eq. 6-8}$$

where L_x, L_y and L_z are the fracture spacings in the x-, y- and z-directions.

Equation 6-5 is solved using full Newton iteration, with variable substitution, using either P_{wi} or S_{wi} as the primary variable. This method has proved to be very reliable for dual-porosity, dual-permeability systems. For the case of fracture-matrix coupling, there exist two unknowns at each node (pressures or saturations in both fractures and matrix) which are solved for simultaneously in a fully-coupled fashion.

6.1.2 Unsaturated Zone Transport

The transient, unsaturated zone, advective-dispersive transport equations are solved using the same finite volume technique used to solve the unsaturated zone flow equations. Mass transfer between the fractures and the rock matrix is accommodated by including an advective-dispersive flux between matrix nodes and the adjacent fracture nodes. Equilibrium radionuclide sorption is modeled using a linear isotherm. The time varying source concentrations for each species at the repository level is passed to the unsaturated transport model and used as the top boundary condition. The concentrations are set to zero for the initial condition. The model outputs either the solute flux history at the water table for each species.

Summarizing, the unsaturated zone transport model includes the following features as implemented in the current version of IMARC:

- Initial concentrations are set to zero for each species.
- Source concentration histories for each species can vary with time.
- Each species is allowed to have a different decay parameter, and ingrowth of daughter products via chain decay is accounted for.
- The sorption parameter K_d for each species varies with depth through the unsaturated zone and between matrix and fracture nodes.

With this conceptual model, the conservation of species α is expressed by the following mass balance equation:

$$\frac{\partial}{\partial t}\{(\theta S_w + \rho_b K_d^{\alpha}) C_{\alpha}\} = -\nabla \cdot \{V_w C_{\alpha} - \theta S_w D_{\alpha} \nabla C_{\alpha}\}$$
$$+ \theta S_w \{R_{p(\alpha)} \lambda_{p(\alpha)} P_{\alpha} - R_{\alpha} \lambda_{\alpha} C_{\alpha}\} \pm q^{ext} C_{\alpha}^{*} \pm G_{\alpha} \qquad \text{Eq. 6-9}$$
$$\alpha = 1,2,...,N_s$$

and where:

C_α is the concentration of species α

P_α is the concentration of parent of species α

D_α is the dispersion/diffusion tensor of species α

λ_α is the decay constant for species α

$\lambda_{p(\alpha)}$ is the decay constant for parent of species α

ρ_b is the bulk density of matrix or fracture surface density of fractures

K_d^{α} is the linear sorption coefficient for species α

$$R_\alpha = 1 + \frac{\rho_b K_d^\alpha}{\theta S_w}$$

q^{ext} is the Darcy flux crossing an external boundary

$C_\alpha^* = C_\alpha$ if q^{ext} is exiting the unsaturated zone

$C_\alpha^* = C_\alpha^0$ if q^{ext} is entering the unsaturated zone

G_α is the mass flux between the fractures and the rock matrix

C_α^0 is the time varying source concentration in the repository.

As was the case for the flow equation, a transport equation analogous to Equation (6-9) is written for both the fractures and the rock matrix in which fracture-matrix coupling is assumed in the context of a dual-porosity, dual-permeability medium.

The governing equations are discretized using a finite volume method. For the case of a double-porosity, double-permeability system, the unsaturated zone is discretized as a two-dimensional grid for both flow and transport, with two horizontally linked control volumes at each depth to represent the matrix and fracture nodes. The mass transfer between the two zones is determined by calculating the advective-dispersive flux between the two adjacent control volumes at each elevation and each time step. If N is the current time step and i is the control volume under consideration, then the discretized form of the solute conservation equation for any particular species (*i.e.* dropping the α subscripts) for either the fractures or the matrix is:

$$\begin{aligned}
&\{[\theta S_w R C]_i^{N+1} - [\theta S_w R C]_i^N\} \frac{V_i}{\Delta t} \\
&= \sum_{j \in \eta_i} C_{ij+1/2}^{N+1/2} (\lambda_w)_{ij+1/2}^{N+1} \gamma_{ij} (\psi_{wj}^{N+1} - \psi_{wi}^{N+1}) \\
&+ \sum_{j \in \eta_i} (\alpha^{disp} |V_w| + \theta D^{diff})_{ij+1/2}^{N+1} (S_w)_{ij+1/2}^{N+1} \gamma'_{ij} [(C)_j^{N+1/2} - (C)_i^{N+1/2}] \\
&+ (\theta S_w)_i^{N+1} \{(R_p)_i^{N+1} \lambda_p P_i^{N+1/2} - R_i^{N+1} \lambda C_i^{N+1/2}\} V_i + (C^*)_i^{N+1/2} q_i
\end{aligned} \qquad \textbf{Eq. 6-10}$$

The external source term q_i is given by , $q_i = (q^{ext})_i^{N+1}$, α^{disp} the dispersivity of either the fractures or rock matrix, and D^{diff} is the diffusion coefficient. Note that the transport equations can be solved sequentially for each species in turn, with the parent species concentrations being known quantities. In Equation (6-10),

$$\gamma'_{ij} = \frac{A_{ij}}{\Delta z_{ij}} \qquad \textbf{Eq. 6-11}$$

if i and j are both matrix or fracture nodes. If node i is a fracture node, and node j is a matrix node, or *vice versa*, then:

$$\gamma'_{ij} = 4\, V_i \left(\frac{1}{L_x^2} + \frac{1}{L_y^2} + \frac{1}{L_z^2} \right) \qquad \textbf{Eq. 6-12}$$

The velocity used in the dispersion term in Equation (6-10) is given by:

$$\left(|V_w| \right)_{ij+1/2} = \gamma_{ij} \left(\lambda_w \right)_{ij+1/2}^{N+1} \left| \psi_{wj}^{N+1} - \psi_{wi}^{N+1} \right| / A_{ij+1/2} \qquad \textbf{Eq. 6-13}$$

where $A_{ij+1/2}$ is the usual interfacial area for matrix-matrix or fracture-fracture flow. For matrix-fracture flow, then:

$$A_{ij+1/2} = 2\, V_i \left(\frac{1}{L_x} + \frac{1}{L_y} + \frac{1}{L_z} \right) \qquad \textbf{Eq. 6-14}$$

The concentration used in the source/sink term is:

$$\begin{aligned} \left(C^* \right)_i^{N+1/2} &= \left(C \right)_i^{N+1/2} \quad \text{if } q_i < 0 \\ &= \left(C \right)_{source}^{N+1/2} \quad \text{if } q_i > 0 \end{aligned} \qquad \textbf{Eq. 6-15}$$

In order to maintain monotonicity, upstream spatial weighting and fully implicit temporal weighting is used. An adaptive time-stepping procedure is used for the transient unsaturated flow and transport problems whereby the value of the time step is increased as the response of the system slows with time.

The stratification of the unsaturated zone is represented as six overlying segments:

- The first segment consists of one finite difference cell only, which is used to specify the boundary conditions for the water in-flow and radionuclide fluxes from the near field;
- The next four segments are used to represent different unsaturated horizons below the repository: TSw-3C, TSv-5, CHnv-5, and CHnz-6; and
- The last segment consists of one cell only situated below the water table and used as a boundary condition to fix pressure.

In each of the segments, irregular discretization, which is finer at the top and the bottom of each layer and coarser within, is used. The grid has been chosen to ensure an accurate spatial solution of the differential equations. The unsaturated zone is discretized spatially as shown in Figure 6-1.

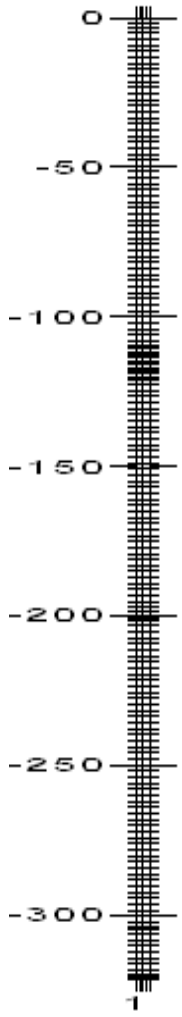

Figure 6-1
Discretization of the Unsaturated Zone

6.2 Saturated Zone Flow and Transport

The steady-state velocity field in the saturated zone is specified by solving the steady-state saturated groundwater flow equation. The domain is spatially discretized using the finite element method, but a modified influence coefficient approach (Therrien and Sudicky, 1996) has been implemented to mimic a 7-point finite difference operator to conserve memory and decrease execution time. An automated grid generator ensures that the finite element grid, consisting of hexahedral brick elements, is sufficiently resolved to ensure good convergence of the flow solution. Flow is assumed to occur only in the mobile fracture zone.

The bottom ($z = 0$) and side ($y = 0$ and $y = YL$) boundaries of the aquifer are no flow boundaries. The downstream boundary ($x = XL$) is a prescribed head boundary. The upstream boundary ($x = 0$) is a specified water flux boundary representing a background lateral inflow to the saturated zone. Finally, the top boundary ($z = ZL$) assumes a known water flux enters across the water table. The net infiltration of water entering across the water table below the repository is

computed by the unsaturated zone flow module as the total time-integrated volume of water which leaves each unsaturated zone column representing the areal extent of each repository sub-region divided by the total simulation time. The result is a time averaged infiltration rate across the water table for each unsaturated zone column which underlies the repository. The recharge of water entering across the portion of the water table outside of the repository is specified as a constant given by the space-time average of the infiltration in each unsaturated-zone column.

The steady-state, saturated groundwater flow equation is given by:

$$\nabla \cdot (\mathbf{K} \nabla h) \pm Q = 0 \qquad \textbf{Eq. 6-16}$$

where:

- Q is the source/sink term for water entering or leaving the domain via the well,
- h is the total hydraulic head and
- $\boldsymbol{K}$ is the bulk hydraulic conductivity tensor of the saturated zone rock mass.

The three-dimensional form of the transient saturated-zone transport equations for the mobile (*i.e.,* fracture) and immobile (*i.e.,* rock matrix) zones are solved using the finite element method to spatially discretize the aquifer. As is the case for the flow problem, a modified influence coefficient is, however, used to mimic a 7-point finite difference operator. The grid generator ensures that the mesh is sufficiently resolved under and near the repository at the water table to ensure good convergence of the transport solution. Solute mass transfer between the fractures and rock matrix zones is modeled using a first-order mass transfer approach which accounts for a diffusive mass exchange between the two regions (Sudicky, 1990). Because water is assumed not to flow in the immobile zone in the interior of the rock matrix blocks, this region acts as a contaminant source or sink (depending whether the concentration in the mobile zone is less than or greater than the concentration in the immobile zone). Solute sorption is again modeled using a linear isotherm approach. The same contaminant decay rates from the unsaturated zone transport simulation are used for the saturated zone. The transport equation for each radionuclide is solved using the Laplace Transform Galerkin (LTG) technique.

The bottom (z=0), side (y=0 and y=YL), and downstream (x=XL) boundaries of the aquifer are all zero dispersive flux boundaries. The concentrations of all nodes on the upstream (x=0) boundary are set to zero. The portion of the top (z = ZL) water table boundary which is not directly beneath the waste repository is assumed to be a type III (or Cauchy) boundary, where solute-free water enters at the prescribed recharge rate.

The boundary conditions for the portion of the water table which lies underneath the repository is a type III boundary condition, in which the unsaturated zone transport module computes the solute flux history at the water table for each unsaturated zone column and passes this information to the saturated zone transport module. With this boundary condition, the continuity in the solute mass flux is preserved at the water table between the unsaturated and saturated zones

The model computes two breakthrough/flux-history curves; one for the fractures and one for the matrix. The breakthrough data from both the fractures and the rock matrix is incorporated into a composite breakthrough/flux-history curve which is then used as the input into the saturated zone transport module. The composite flux-history curve is calculated from:

$$q_{WT}^{c}(t) = q_{f}^{ext} C_f + q_{m}^{ext} C_m \qquad \textbf{Eq. 6-17}$$

where q_{WT}^{c} is the total solute flux crossing the water table from the unsaturated zone.

The saturated zone transport model outputs maximum and areally-averaged concentrations and advective fluxes at the downstream compliance boundary.

The conservation of species α in the mobile zone is expressed by the following mass balance equation:

Mobile Zone:

$$\frac{\partial}{\partial t}\{\theta_m R_{\alpha m} C_\alpha\} = -\nabla \cdot \{\overline{q_m} C_\alpha - \theta_m \overline{\overline{D_{\alpha m}}} \nabla C_\alpha\}$$

$$+\theta_m \{R_{p(\alpha)m} \lambda_{p(\alpha)} P_\alpha - R_{\alpha m} \lambda_\alpha C_\alpha\} - \Gamma_\alpha (C_\alpha - C_\alpha') \qquad \textbf{Eq. 6-18}$$

$$\alpha = 1, 2, ..., N_s$$

where:

the subscript *m* denotes the mobile (*i.e.*, fracture) zone,

$\overline{q_m}$ is the Darcy flux in the saturated zone,

$\overline{\overline{D_{\alpha m}}}$ is the hydrodynamic dispersion coefficient, and

C_α' represents the concentration in the rock matrix containing the immobile porewater.

The term containing Γ_α accounts for the transfer of mass between the mobile and immobile zones. Assuming that the rock matrix blocks are comprised of spheres, then the diffusive mass transfer coefficient Γ_α is given by:

$$\Gamma_\alpha = \frac{15 \theta_{im} D_{\alpha im}^{*}}{r_b^2} \qquad \textbf{Eq. 6-19}$$

where

$D^{*}_{\alpha im}$ is the effective diffusion coefficient of the rock matrix and
r_b is the radius of a spherical matrix block.

The remaining symbols correspond to those used in the unsaturated zone transport section. A similar equation, but without the advective and dispersive flux terms, describes mass conservation in the immobile zone which is given below.

Immobile Zone:

$$\frac{\partial}{\partial t}\{\theta_{im} R_{\alpha im} C_{\alpha}'\} =$$
$$\theta_{im}\{R_{p(\alpha)im}\lambda_{p(\alpha)} P_{\alpha}' - R_{\alpha im}\lambda_{\alpha} C_{\alpha}'\} + \Gamma_{\alpha}(C_{\alpha} - C_{\alpha}') \qquad \text{Eq. 6-20}$$
$$\alpha = 1, 2, ..., N_s$$

where the subscript *im* refers to the immobile *(i.e.,* rock matrix) zone.

As mentioned earlier, the transient transport equation is solved by the LTG procedure. In this procedure the Laplace transform of the spatially-discretized nodal concentrations is obtained. When the values are inverted numerically, the result yields the time domain concentration values at specified output times.

The discretized form of the transport equations are presented elsewhere (see *e.g*., Sudicky, 1989; Therrien and Sudicky, 1996; Lacombe *et al*., 1995) and therefore need not be presented here. The discretized equations for both flow and transport are solved using an efficient implementation of the ORTHOMIN-accelerated iterative sparse-matrix solver which only stores and operates on the nonzero entries in the matrices.

EPRI (1996; 1998; 2000) describes the conceptual model for flow in the SZ and its implications for mass transport. That discussion is summarized here. In particular, as the flow becomes more channelized, the size of rock blocks increases. This increase in size of the rock blocks in a fractured medium reduces the potential for matrix diffusion and, accordingly, the travel time for contaminant migration. DOE has adopted this idea of channelized flow or *flowing intervals.*

A flowing interval, shown schematically in Figure 6-2, is defined as a fractured zone that facilitates flow in the SZ. It is defined on the basis of borehole flow meter surveys. The flowing interval is characterized in terms of interval spacing, which is not the same as the fracture spacing. Figure 6-2 shows the difference between the flowing interval spacing and the fracture spacing. The flowing interval spacing is taken as the distance from the mid-point of the flowing interval to the midpoint of the next flowing interval. As the figure suggests, the flowing interval spacing is greater than the fracture spacing. This conceptualization for flow in the SZ is deemed to be more realistic than simply taking the fracture spacings in the SZ (EPRI, 2000).

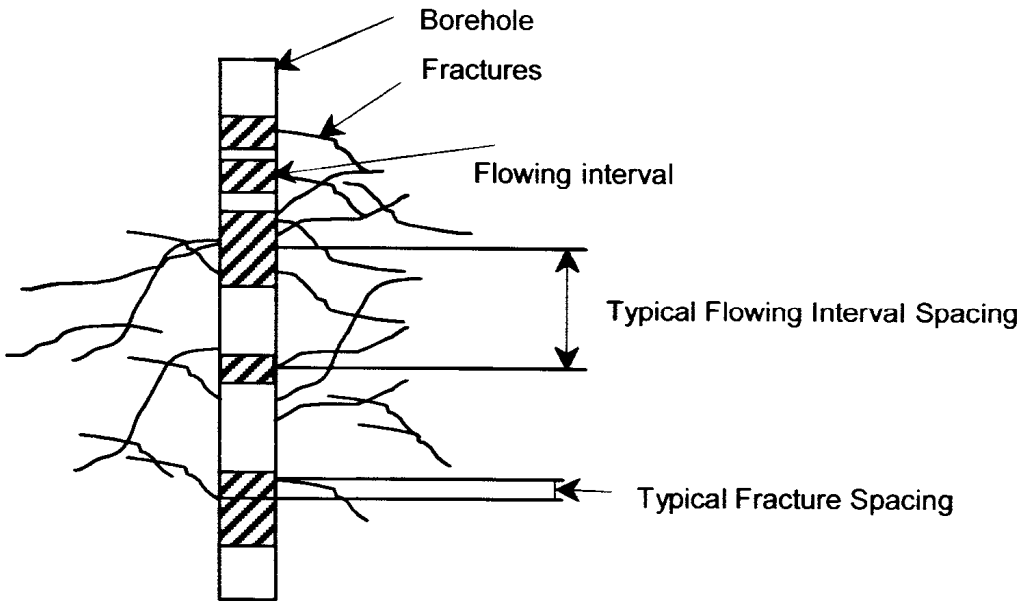

Figure 6-2
Conceptualization of flowing intervals (The flowing interval spacing is defined as the distance from the midpoint of one flowing interval to the midpoint of the next. The typical spacings between the flowing intervals are much greater than the fracture spacings (after EPRI, 2000).

The mean flowing interval spacing for the SZ is estimated to be 19.5 m (Figure 6-3). This value is significantly larger than the mean fracture spacing, which is a fraction of a meter (Figure 6-3). With large blocks, diffusion into the matrix is likely less effective in attenuating the rate of spread of contaminants than would be the case with smaller blocks. Figure 6-4 illustrates features of the flowing intervals defined in wells at Yucca Mountain for which flow-meter surveys were available. The flowing intervals represent a relatively small proportion of the total vertical section in each borehole (EPRI, 2000).

EPRI (2000) noted that ground-water flow in the uppermost 200 m of the SZ is being carried in one-quarter of the vertical section. With the flowing intervals developed in this manner, linear flow velocities within the flowing intervals are four times higher than would be the case if flow were assumed uniform across the entire vertical section. EPRI (2000) further assumed that within the flowing interval, the fracture spacings and resulting block sizes will be much smaller than flowing-interval spacings and in keeping with fracture spacing measurements made from the SZ (Figure 6-2).

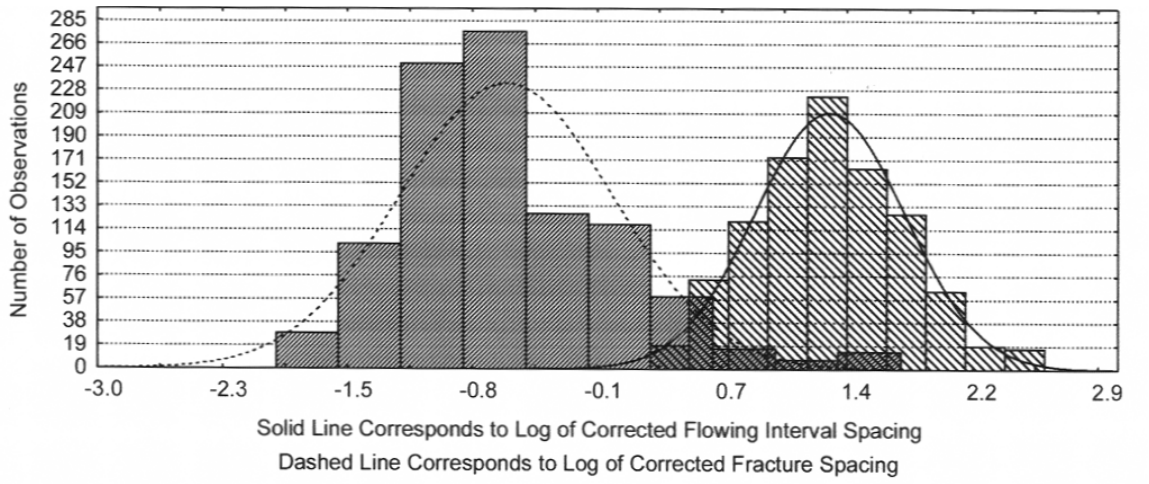

Figure 6-3
Comparison of the probability distributions of the log of corrected flowing interval spacing and corrected fracture spacing (after EPRI, 2000)

EPRI (2000) postulated that representing the flowing zone as a fracture removes credit for matrix diffusion into the blocks along the flowing interval. This conceptualization remains the basis for flow and transport in the saturated zone in IMARC 10. In addition, the definition of the flowing interval spacing is made in such a way that the actual thickness of the intact rock block is exaggerated. Conceptualizing the SZ in terms of flowing intervals with rock blocks determined by the fracture spacings makes matrix diffusion more viable as a mechanism to attenuate the rate of contaminant migration.

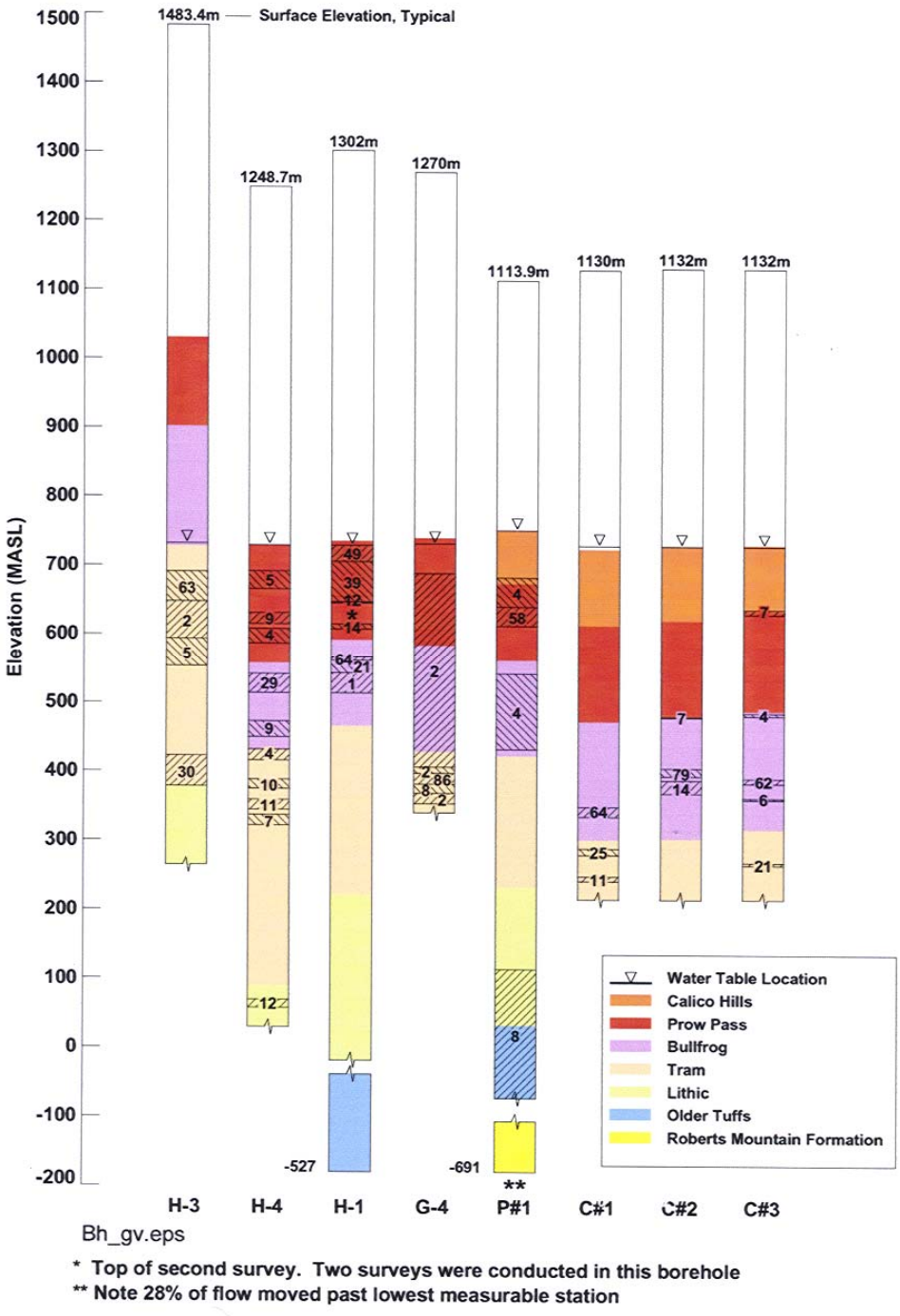

Figure 6-4
Comparison of the flow meter survey Information among various boreholes (the cross-hatched areas indicate the flowing intervals and the number within the flowing interval represents the percentage of total flow in that interval) (CRWMS, M&O, 2000e).

The saturated-zone transport zone conceptual model has two segments:

- A fractured tuff segment extending from beneath the repository to 15 km down gradient, and
- A subsequent alluvial segment extending over the next 5 km down gradient to the location of the Reasonably Maximally Exposed Individual (RMEI), the "compliance point."

The three-dimensional spatial discretization of the saturated zone is shown in Figure 6-5 and Figure 6-6.

The SZ code offers a number of capabilities for using alternative calculation approaches. The code provides two approaches to solve the transport equations for each radionuclide – either the Laplace Transform-Galerkin (LTG) method or a standard time-stepping integration method. The LTG technique for solving the linear mass transport equation in a steady-state flow field has been developed by Sudicky and coworkers; the the approach is described in detail by Sudicky (1989), Sudicky and McLaren (1992), and EPRI (1996). The application of the Laplace transformation of a finite-difference advection-dispersion equation eliminates the temporal derivative term and, thus, avoids the time-step integration, which for TSPA analyses over long times is a very heavy computational burden. The transformed equation in the Laplace *p*-space is then solved using conventional methods. The SZ code employs the Galerkin technique, and then the nodal *p*-space solutions for the radionuclide concentrations are inverted to the primary temporal domain. The method of de Hoog *et al.* (1982) is used for the numerical inversion the Laplace *p*-space solutions.

The boundary conditions for the transport equation are specified as follows:

- initial concentrations at all nodes of the SZ computational domain are set to zero;
- there is no other dispersive boundary flux except one from the repository footprint, where the fluxes from the fractures and from the matrix for every one of the vertical columns are incorporated as one
- A uniform recharge rate is applied over the entire simulation domain; and
- boundary condition type III (Cauchy condition) is always used over the entire water table surface (Bear and Verruijt, 1987).

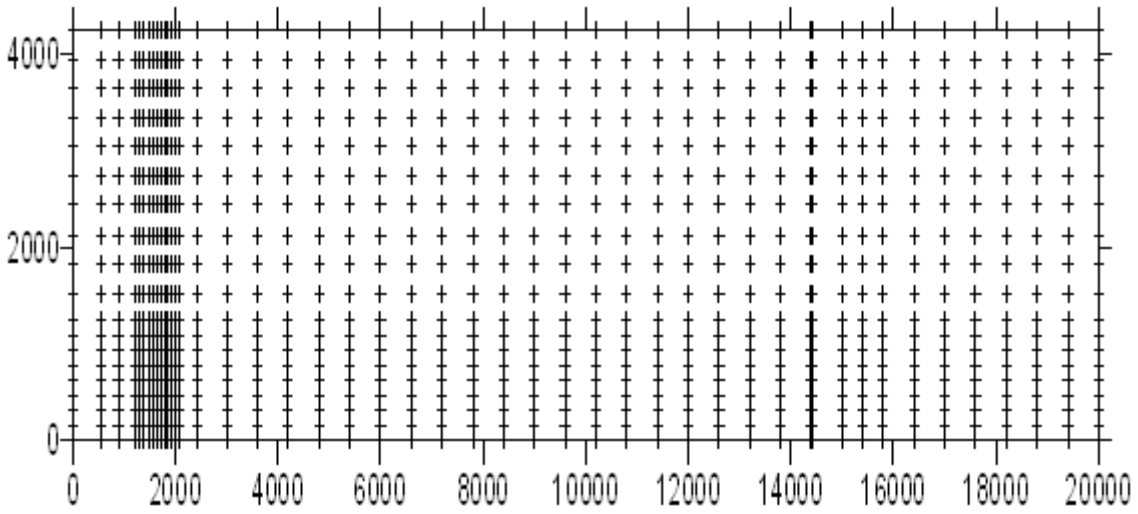

Figure 6-5
Three-dimensional discretization of the saturated zone in plan view

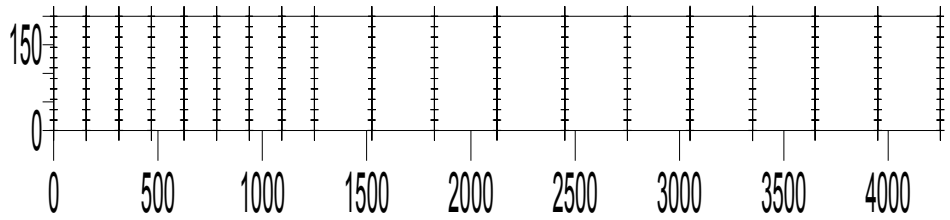

Figure 6-6
Three-dimensional discretization of the saturated zone in profile view

The LTG method provides the flexibility to have different resolving time steps in periods of special interest. This is achieved by specifying several Laplace spaces with an equal number of nodal *p*-space solutions, with each one extending over different time scales. This is of practical interest for high release rates concentrated in short time periods. It is also important for improving resolution of the arrival time and the peak values of the maximum concentrations crossing the downstream face of the SZ.

6.3 Verification and Testing

6.3.1 Unsaturated Zone Transport

The transport code was verified using the analytical model CMM (Wu, 1991). Table 6-1 displays the simulation parameters for a verification example in which a non-retarded parent decays into a retarded non-decaying daughter. Figure 6-7 shows profiles through the unsaturated zone for this simulation. Results are given in Figure 6-7 at 25 and 75 *days*, and it can be seen that there is excellent agreement between the numerical and analytical results.

Table 6-1
Unsaturated zone parameters for verification example involving transport of a two-member decay chain a single-porosity column.

Parameter	Value
Darcy flux (m/day)	1.0
Water content (θSw)	0.35
Parent decay constant (day-1)	1.139×10^{-2}
Daughter decay constant (day-1)	0.0
Parent diffusion coefficient (m2/day)	10^{-4}
Daughter diffusion coefficient (m2/day)	10^{-4}
Longitudinal dispersivity (m)	0.5
Parent retardation factor	1.0
Daughter retardation factor	2.0

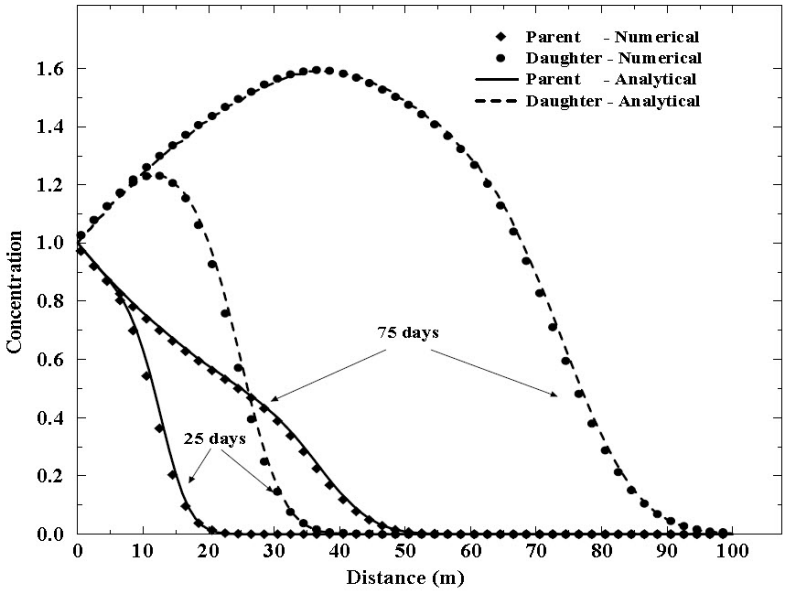

Figure 6-7
Concentration profiles for the unsaturated zone verification problems

6.3.2 Saturated Zone Transport

The saturated zone transport model was verified against two analytical models, CMM which was mentioned above, and a double-porosity solution for a set of parallel fractures developed by Sudicky and Frind (1982).

The CMM verification example involved the transport of a two-species decay chain along a one-dimensional single porosity column. This example was selected to ensure the saturated zone transport code was correctly handling the decay of the parent species and the ingrowth of its daughter. The relevant simulation parameters are given in Table 6-2. The results of the CMM verification simulation are displayed in Figure 6-8. The results indicate that the numerical model is capable of faithfully reproducing analytical results.

The next example consists of transporting a decaying, non-sorbing solute through a one-dimensional, double-porosity column. This example was chosen to verify that the code was correctly transferring mass between the mobile and immobile zones. The relevant simulation parameters are given in Table 6-3. The results of the double porosity verification simulation are displayed in Figure 6-9. The results again indicate that the numerical model is reproducing analytical results.

Table 6-2
Saturated zone parameters for verification example involving transport of a two-member decay chain and a single-porosity column.

Parameter	Value
Darcy flux (m/day)	10^{-4}
Longitudinal dispersivity (m)	1.0
Mobile zone porosity	10^{-4}
Parent decay constant (day^{-1})	$1.54x10^{-4}$
Daughter decay constant (day^{-1})	0.0
Parent diffusion coefficient (m^2/day)	$1.38x10^{-4}$
Daughter diffusion coefficient (m^2/day)	$1.38x10^{-4}$
Parent retardation factor	1.0
Daughter retardation factor	1.0

Table 6-3
Saturated zone parameters for double-porosity verification example.

Parameter	Value
Darcy flux (m/day)	10^{-4}
longitudinal dispersivity (m)	0.1
mobile zone porosity	10^{-3}
immobile zone porosity	10^{-2}
decay constant (day^{-1})	$1.54x10^{-4}$
mobile zone diffusion coeff. (m^2/day)	$1.38x10^{-4}$
immobile zone diffusion coeff. (m^2/day)	$1.38x10^{-5}$
mobile zone retardation factor	1.0
immobile zone retardation factor	1.0

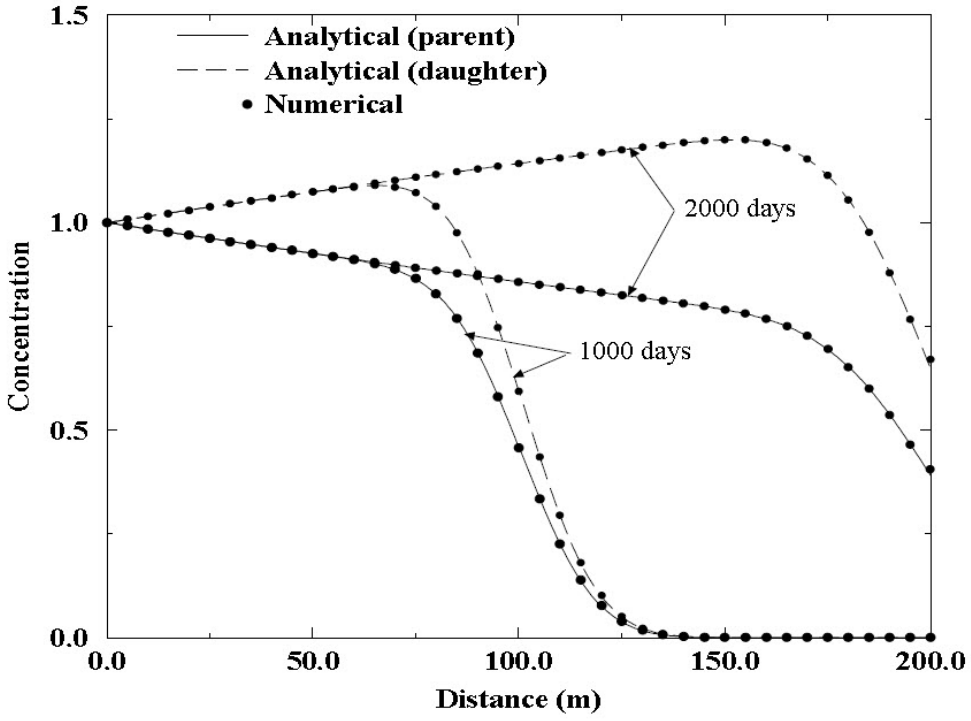

Figure 6-8
CMM saturated zone verification results

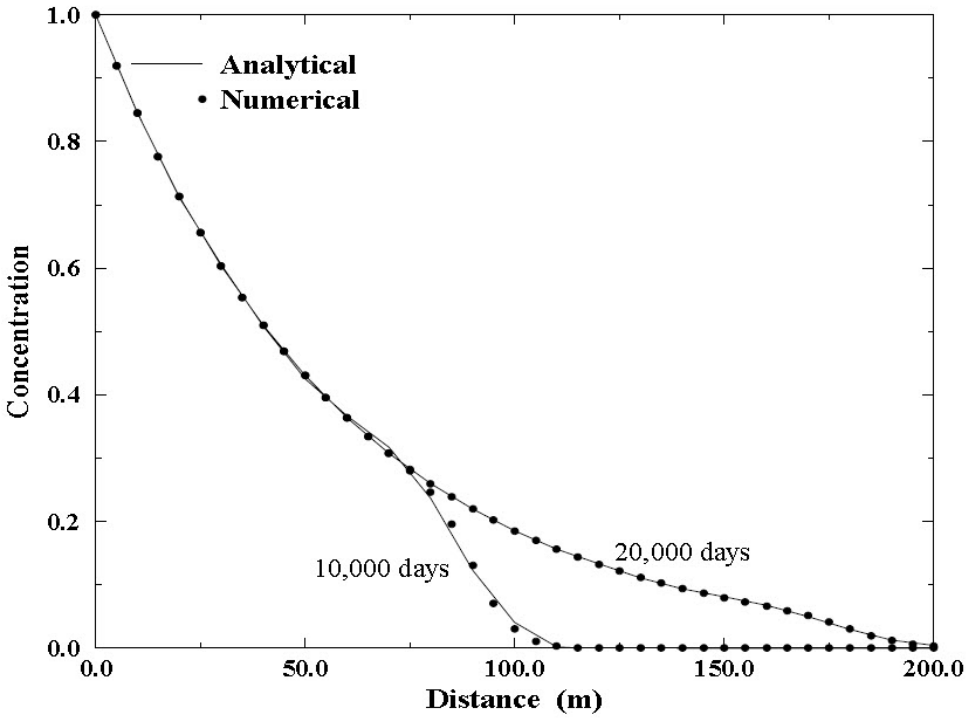

Figure 6-9
Double porosity saturated zone verification results

Another verification test reported by EPRI (2000) involved the SZ module in the IMARC code and the numerical model FRAC3DVS (Therrien and Sudicky, 1996). FRAC3DVS has been verified against many different analytical solutions for a wide range of problems. The simulation domain for this test was 1000 m in the x-direction, 5000 m in the y-direction and 1000 m in the z-direction. The input data for this test are not related to Yucca Mountain. A uniform darcy flux of 3.3 m/yr parallel to the x-axis was imposed. For the first trial, the longitudinal dispersivity was 20 m, while transverse horizontal and transverse vertical dispersivities were each 5 m. For the second trial, the longitudinal and transverse horizontal dispersivity values were held at 20 m and 5 m, respectively, while the transverse vertical dispersivity was reduced to 0.05 m. This latter trial was designed to test the ability of the SZ flow and transport module to handle a second component of transverse dispersivity. The source for both of these trials was a 100 m by 100 m patch, which was oriented perpendicular to flow with a specified concentration of 1.0.

Figure 6-10 compares the results of these verification tests with FRAC3DVS and the SZ module in IMARC. The breakthrough curves for the two models at a hypothetical observation point 500 m down gradient are nearly identical, for the set of parameters used in the analysis.

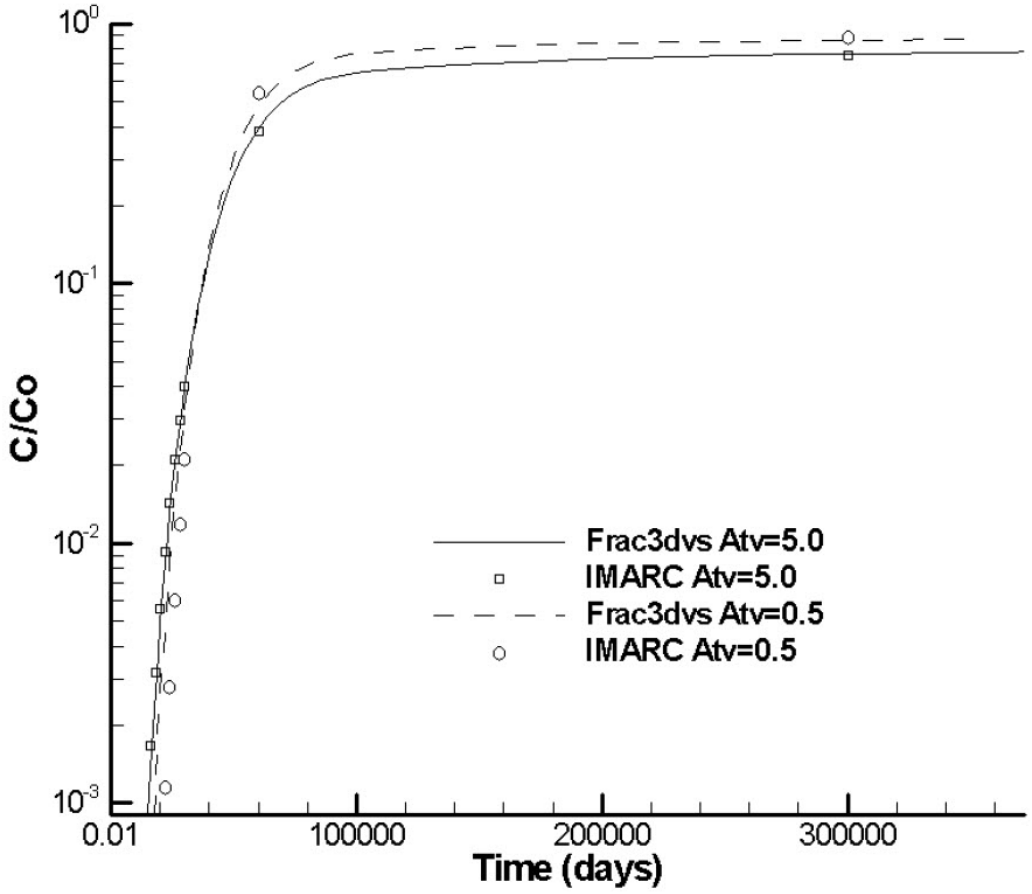

Figure 6-10
Comparison of concentration vs time at a point 500 m downgradient from the source for a transverse-dispersivity verification example.

The results for the concentrations at the downstream face from three-dimensional and two-dimensional representation of the saturated zone have been compared. These tests result in very close agreement. This is the result of minimal vertical variation in concentrations, as shown in Figure 6-11. The good agreement is due to the very low lateral dispersivity of the SZ media and practically vertical isolines for the concentrations at the downstream face outside of the repository footprint as shown in Figures 6-11a and 6-11b. These findings are corroborated by the three-dimensional view displayed in Figure 6-12.

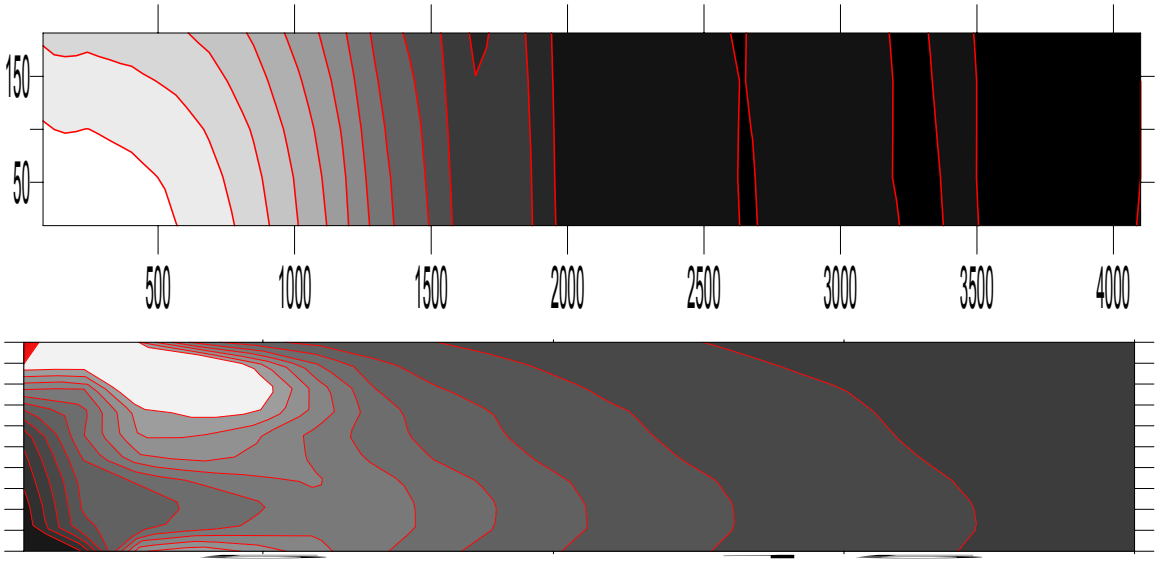

Figure 6-11
(a, top): Concentrations at downstream face for ^{99}Tc at year 500,000 obtained from 3D model formulation;
(b, bottom): relative concentrations along the central line of the computational domain for ^{99}Tc at year 500,000 obtained from the 3D model formulation.

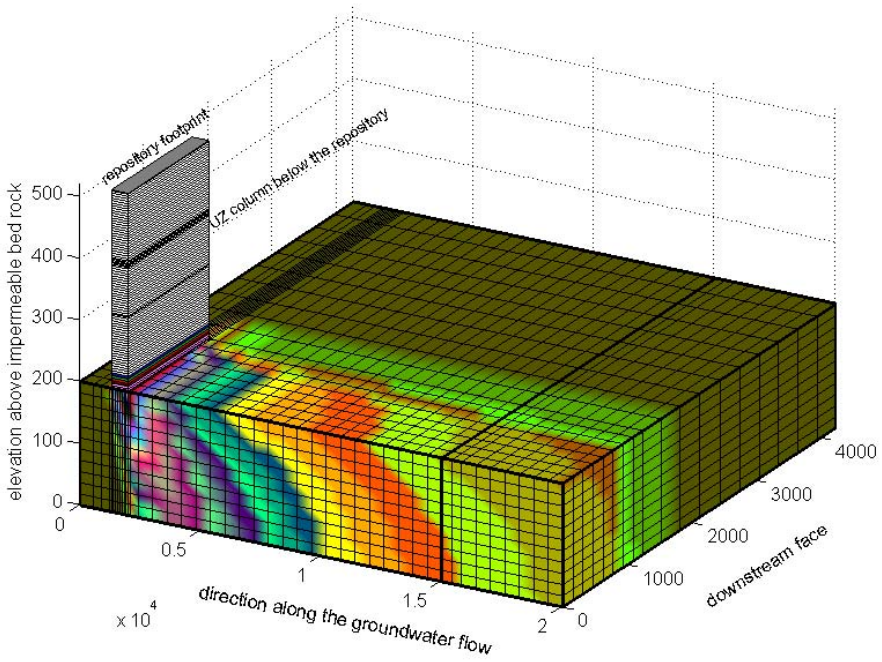

Figure 6-12
Concentration profile at 1,000,000 years for the best-estimate set of input parameters.

The SZ code has been heavily tested over the years, and is considered highly reliable. However, the combination of the Laplace transform method and Galerkin finite elements leads to a lack of continuity between portions of the solution domain at low and intermediate concentrations and under some other conditions. Examples of this lack of continuity are shown in Figure 6-13, which shows the effect of subdividing the time domain into differing numbers of Laplace *p*-spaces. Here the introduction of more Laplace *p*-spaces partially avoids the step-wise form of the maximum concentrations at the downstream face and approaches a smooth curve. It is necessary to point out that the subdivision of the temporal domain in more Laplace spaces does not affect either the arrival of the maximum concentration or its value. The numerical instabilities occur for the low concentration range, which by definition are not risk significant. This numerical artifact was addressed in detail to provide improved understanding of the shape of the curves under various conditions. These numerical issues do not affect TSPA calculations carried out to the time of peak dose.

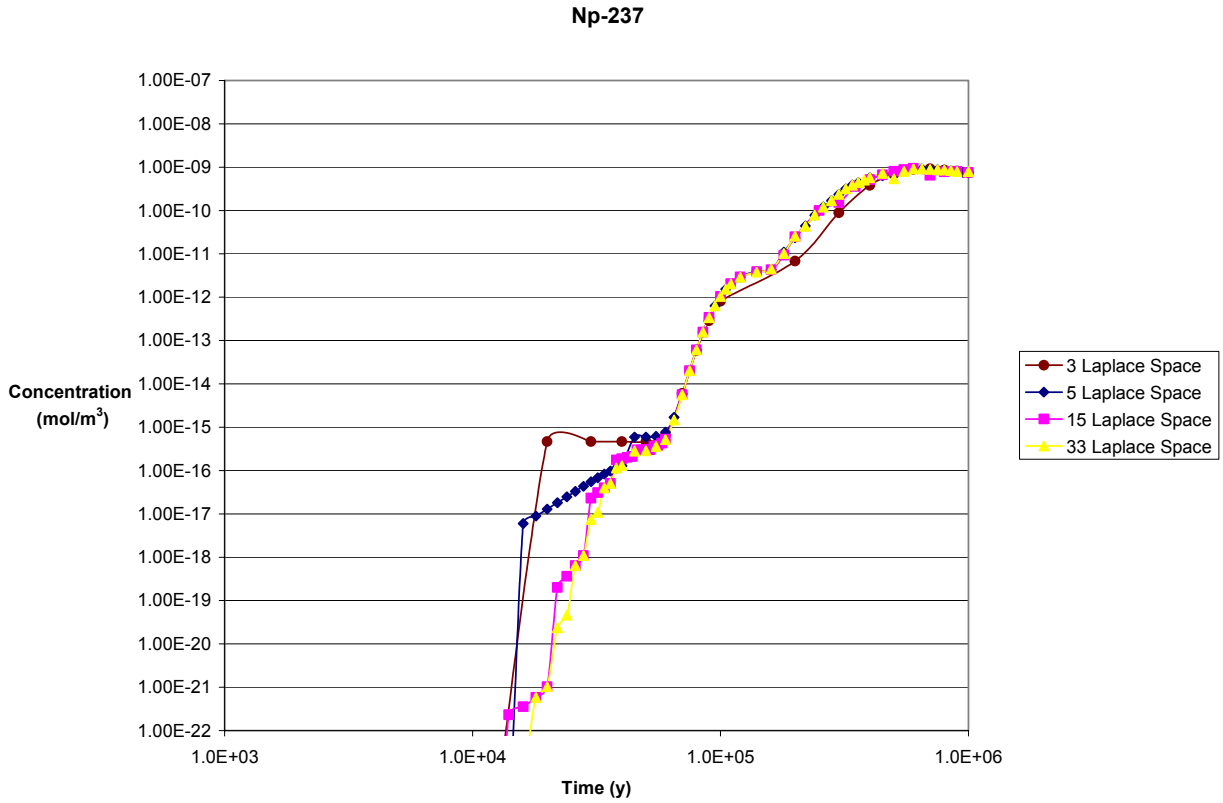

Figure 6-13
Discontinuities at the interfaces of the Laplace p-spaces

An attempt has been made to overcome the discontinuities in the numerical inversion procedure of the Laplace *p*-spaces by applying quadruple precision arithmetic.[9] However, this effort did not resolve the issue of discontinuities of the inversion method. This set of tests illustrates that the problem of discontinuities does not arise from the numerical inversion method itself, but is a complex feature of the LTG solution method.

Several key features of the discontinuities are noted:

- They occur at low concentrations; the peak concentrations produced in the code are not affected by these artifacts;
- They occur at times when the boundary condition of the flux input to the solution are changing at the same time that the boundary of a Laplace p-space is encountered;
- There is no general method for eliminating the discontinuities for all combinations of input parameters; when discontinuities have been encountered, the numerical method has been tuned to eliminate them for that particular set of conditions; and
- As the number of p-spaces increases, an exact solution is approached, but at the cost of slightly increased computation time.

The effect of the number of p-spaces on computation time is shown in Table 6-4.

Table 6-4
CPU time for varying numbers of Laplace p-spaces in the time domain. The columns show the amount of computation time used by the submodels in IMARC. As the number of Laplace spaces increases, the proportion of the overall CPU time resulting from the

Case	Output times	COMPASS [min]	UZ Model [min]	SZ Flow Model [min]	SZ Transport Model [min]	Total CPU Time [min]
3 Laplace spaces 2D	27	0.60	0.39	4.667E-03	0.44	1.44
5 Laplace spaces 2D	65	1.50	0.38	4.683E-03	0.76	2.64
15 Laplace spaces 2D	60	1.45	0.38	4.683E-03	1.85	3.69
33 Laplace spaces 2D	66	1.54	0.38	4.500E-03	4.41	6.34
3 Laplace spaces 3D	27	0.62	0.38	7.578E-02	11.50	12.58

Despite these issues with the numerical solution at low concentrations, the code provides satisfactory results at higher concentrations, where doses are higher and the results are more important for making decisions about the acceptability of the analysis. Consequently, EPRI has concluded that the SZ code is fit for purpose.

[9] The Allan Miller package for quadruple real and complex arithmetic has been downloaded from his quadruple precision (home page http://users.bigpond.net.au/amiller/quad.html) and the recommendations at the "High-Precision Software Directory" of Bailey *et al*. (2003) from Lawrence Berkeley National Laboratory used.

6.4 Conversion to a Standard Dilution

Regulatory requirements in 40 CFR 197 and 10 CFR 63 require a basic assumption of the use of 3,000 acre-feet per year (3.7×10^6 m^3/y) by the RMEI. This value is called the "representative volume." Specific approaches are described in the regulations for carrying out the conversion from TSPA analyses to the standardized groundwater usage.

10 CFR 63.332 provides the acceptable alternatives for performing the conversion:

> "DOE must use one of two alternative methods for determining the dimensions of the representative volume. The DOE must propose its chosen method, and any underlying assumptions, to NRC for approval.
>
> (1) DOE may calculate the dimensions as a well-capture zone. If DOE uses this approach, it must assume that the:
>
> (i) Water supply well(s) has (have) characteristics consistent with public water supply wells in the Town of Amargosa Valley, Nevada, for example, well-bore size and length of the screened intervals;
>
> (ii) Screened interval(s) include(s) the highest concentration in the plume of contamination in the accessible environment; and
>
> (iii) Pumping rates and the placement of the well(s) must be set to produce an annual withdrawal equal to the representative volume and to tap the highest concentration within the plume of contamination.
>
> (2) DOE may calculate the dimensions as a slice of the plume. If DOE uses this approach, it must:
>
> (i) Propose, for approval, where the location of the edge of the plume of contamination occurs. For example, the place where the concentration of radionuclides reaches 0.1% of the level of the highest concentration in the accessible environment;
>
> (ii) Assume that the slice of the plume is perpendicular to the prevalent direction of flow of the aquifer; and
>
> (iii) Assume that the volume of ground water contained within the slice of the plume equals the representative volume."

In IMARC, the approach in paragraph (2) has been implemented. Nodes at the end of the saturated zone are identified where the concentrations equal 0.1 percent of the peak concentration; this delineates the extent of the plume according to provision 10 CFR 63.332 (2)(i). The orientation of the model grid ensures that provision 10 CFR 63 (2)(ii) is met. Water flow associated with this plume is calculated and compared to the representative volume. Experience in evaluating IMARC outputs has shown that the use of a low transverse dispersivity leads to narrow plumes, so that the volumetric water flow associated with the plume is below the representative volume. Consequently, for IMARC with the current sets of input parameters, it is acceptable to calculate the total discharge in the plume (mol/y), and to divide that value by the

representative volume (m^3/y) to produce concentrations (mol/m^3) as output from the saturated zone. IMARC contains the algorithms the convert to concentrations if the flow in the plume are to exceed the representative volume, but the algorithms have been unnecessary in any calculations to date owing to the low values of transverse dispersivity used.

Concentrations calculated in this manner are used as input to the biosphere analysis. Biosphere considerations are described in Chapter 7 and Appendix B of this report.

6.5 Input Parameters

Analysis in the geosphere requires input of an extensive set of parameters. Among the most important parameters for the unsaturated zone are the characteristic curves, expressed in IMARC as saturation versus air entry pressure and saturation versus relative conductivity. Characteristic curves represent the constitutive relationship between saturation of water and pressure head on the one hand, and saturation and relative hydraulic conductivity on the other. These characteristic curves are input in tabular form as sets of 400 sets of values for each of the four geological units in the unsaturated zone, and for fracture and matrix properties. These tabulated curves are presented in graphical form in Figures 6-14 to 6-17.

Values for the sorption coefficient K_d used in IMARC 10 geosphere are presented in Tables 6-5 through 6-7. The values for Kd are treated as uncertain in the IMARC event tree, with the low and high values assigned a 5% probability, and the mean value assigned a 90% probability. The values in these tables are based on the values used by DOE in the TSPA-LA (DOE/OCRWM, 2008, 2008a), with professional judgment used to adapt the values to the fewer number of geological units represented in the IMARC conceptual model. Additional parameters needed to evaluate the unsaturated and saturated zone model in IMARC are presented in Appendix A.

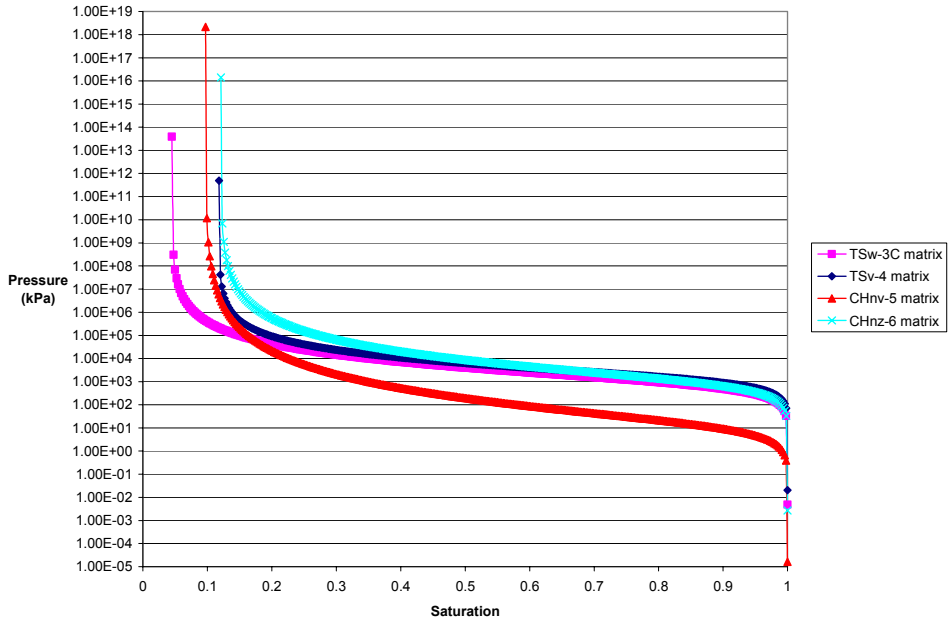

Figure 6-14
Pressure-saturation curves for the matrix of each geological unit in the IMARC Unsaturated Zone (EPRI, 2005c).

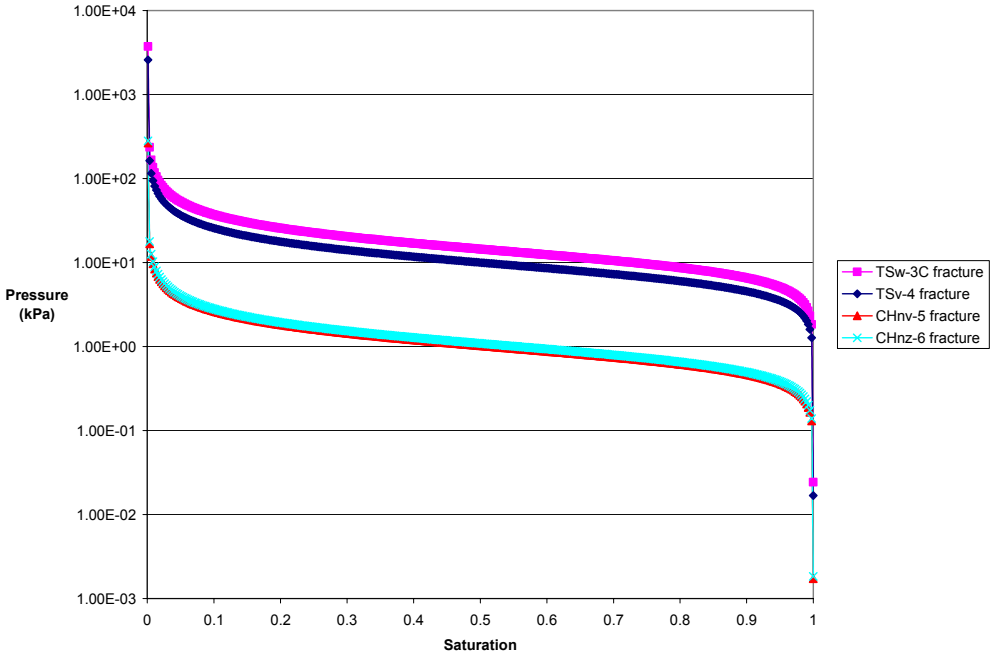

Figure 6-15
Pressure-saturation curves for the fractures of each geological unit in the IMARC Unsaturated Zone (EPRI, 2005c).

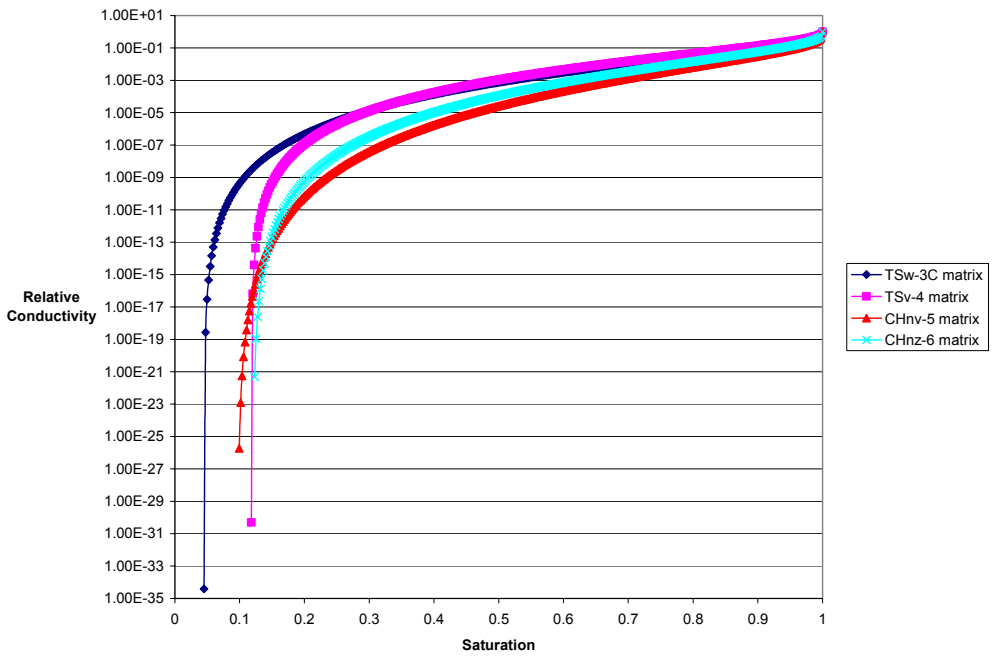

Figure 6-16
Relative conductivity – saturation curve for the matrix of each geological unit in the IMARC Unsaturated Zone (EPRI, 2005c).

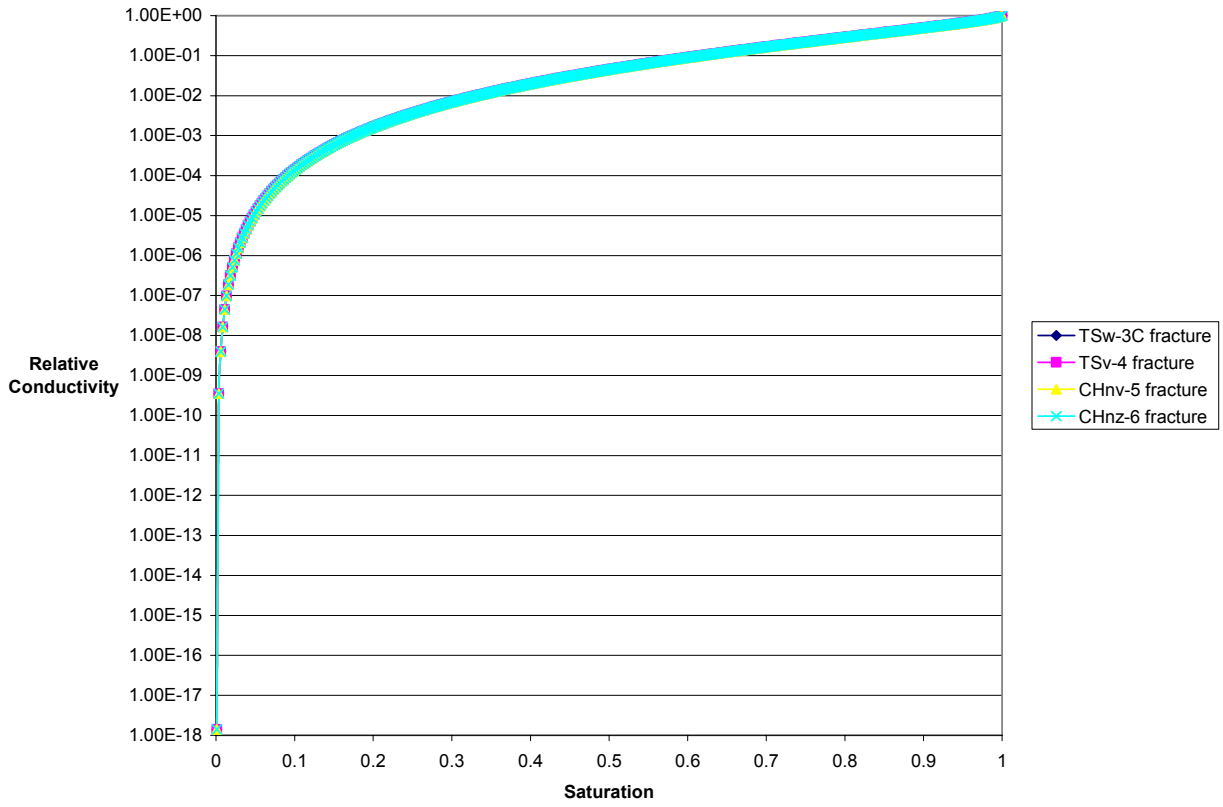

Figure 6-17
Relative conductivity – saturation curve for the fractures of each geological unit in the IMARC Unsaturated Zone (EPRI, 2005c).

Table 6-5
Values for K_d (m^3/kg) for the unsaturated TSw2-3 and TSv 4 units.

Unit	TSw2-3			TSv 4		
	Low	Mean	High	Low	Mean	High
Cl	0.00E+00	0.00E+00	0.00E+00	0.00E+00	0.00E+00	0.00E+00
I	0.00E+00	0.00E+00	0.00E+00	0.00E+00	0.00E+00	0.00E+00
Np	3.00E-04	5.00E-04	3.00E-03	5.00E-04	1.00E-03	2.00E-03
Pu	4.00E-02	7.00E-02	1.50E-01	5.00E-02	1.00E-01	1.50E-01
Ra	0.00E+00	3.00E-02	5.00E-01	3.00E-01	5.00E-01	8.00E-01
Se	0.00E+00	3.00E-02	2.00E-01	8.00E-03	1.40E-02	2.00E-02
Tc	0.00E+00	0.00E+00	0.00E+00	0.00E+00	0.00E+00	0.00E+00
Th	3.00E+00	5.00E+00	8.00E+00	3.00E+00	5.00E+00	8.00E+00
U	1.00E-04	2.00E-04	2.00E-03	1.00E-04	2.00E-04	1.50E-03

Table 6-6
Values for K_d (m^3/kg) for the unsaturated CHnv and CHnZ units.

Unit	CHnv			CHnZ		
	Low	Mean	High	Low	Mean	High
Cl	0.00E+00	0.00E+00	0.00E+00	0.00E+00	0.00E+00	0.00E+00
I	0.00E+00	0.00E+00	0.00E+00	0.00E+00	0.00E+00	0.00E+00
Np	5.00E-04	1.00E-03	2.00E-03	3.00E-04	5.00E-04	3.00E-03
Pu	5.00E-02	1.00E-01	1.50E-01	5.00E-02	1.00E-01	1.50E-01
Ra	2.00E-01	3.00E-01	5.00E-01	2.00E+00	3.00E+00	4.00E+00
Se	3.00E-03	9.00E-03	1.50E-02	8.00E-03	1.40E-02	2.00E-02
Tc	0.00E+00	0.00E+00	0.00E+00	0.00E+00	0.00E+00	0.00E+00
Th	3.00E+00	5.00E+00	8.00E+00	8.00E+00	1.50E+01	2.00E+01
U	1.00E-04	2.00E-04	1.50E-03	2.50E-04	5.00E-04	1.50E-02

Table 6-7
Values for K_d (m^3/kg) for the saturated units.

Unit	Fractured SZ			Alluvial SZ		
	Low	Mean	High	Low	Mean	High
Cl	0.00E+00	0.00E+00	0.00E+00	0.00E+00	0.00E+00	0.00E+00
I	0.00E+00	0.00E+00	0.00E+00	0.00E+00	0.00E+00	0.00E+00
Np	1.00E-03	1.50E-03	2.00E-03	5.00E-03	6.00E-03	7.00E-03
Pu	9.00E-02	1.00E-01	1.10E-01	8.00E-02	1.00E-01	2.00E-01
Ra	3.00E-01	5.00E-01	8.00E-01	3.00E-01	5.00E-01	8.00E-01
Se	8.00E-03	1.40E-02	2.00E-02	8.00E-03	1.40E-02	2.00E-02
Tc	0.00E+00	0.00E+00	0.00E+00	0.00E+00	0.00E+00	0.00E+00
Th	3.00E+00	5.00E+00	8.00E+00	3.00E+00	5.00E+00	8.00E+00
U	5.00E-03	6.00E-03	7.00E-03	3.00E-03	4.00E-03	5.00E-03

6.6 Geosphere Summary

IMARC 10 contains models for flow and transport in the unsaturated and saturated zones at Yucca Mountain. These models are abstractions of the real conditions in the vicinity of the repository, and are simplifications of comparable models implemented by DOE for their TSPA. The current models are the end result of many years of incremental updates, which have developed in response to improved understanding of the geosphere.

The current unsaturated flow model is founded on a one-dimensional representation of the unsaturated zone, in which four hydrological units are specified. The model for transport of radionuclides takes the output from the near field model, and calculates the discharge to the saturated zone as a function of time. The saturated zone module calculates transport to the location of the RMEI using a two-dimensional representation of the aquifer. Two zones with different properties are incorporated in the conceptual model: a fractured zone and an alluvial zone. Both the unsaturated and saturated zone models have been subjected to extensive testing and verification to ensure that the models have been correctly implemented in IMARC.

7
BIOSPHERE MODEL

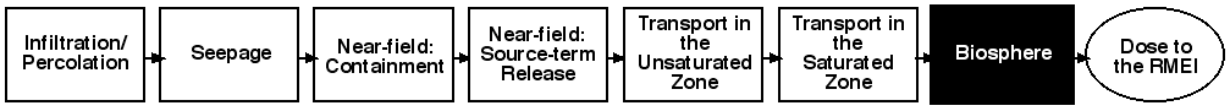

7.1 Background, Objectives and Scope

This chapter describes the approach used to develop and implement Biosphere Dose Conversion Factors (BDCFs) that can be used to convert assessed concentrations of repository derived radionuclides in groundwater at Amargosa Valley into radiation doses to the Reasonably Maximally Exposed Individual (RMEI), as prescribed by regulation. Deterministic evaluations of such BDCFs were first developed within the EPRI program in 1996 (EPRI, 1996). The justification and explanations for updated calculations were then reported in EPRI's Phase 6 TSPA published in February 2002 (EPRI, 2002). Those reports and other interim work considered alternative conceptual assumptions and data assumptions, as well as the sensitivity of results to those assumptions.

The biosphere model is implemented in IMARC as a radionuclide-specific set of Biosphere Dose Conversion Factors (BDCFs). As implemented in IMARC 10, a BDCF is a single-valued conversion factor that has concentration in groundwater as an input, takes into account the potential exposure pathways to the RMEI, and converts the groundwater concentration to a dose to the RMEI. Groundwater concentrations are calculated in IMARC per 10 CFR 63 and 40 CFR 197 with regard to the use by the RMEI of 3,000 acre-feet per year (3.7×10^6 m^3/y).

Use of the BDCF is predicated on the assumption that the dynamic response of the biosphere to changes in groundwater concentration are rapid compared to the changes themselves, such that the biosphere is in equilibrium with the groundwater concentration. For the exposure pathways in the biosphere analysis, this assumption is more closely associated with the dynamics of the surface soil layer. The BDCF for an individual radionuclide is taken to be the equilibrium annual dose to the RMEI derived assuming indefinite unit concentration of that radionuclide in abstracted groundwater.

In IMARC, the BDCFs are solely an input parameter, which is read by the code and multiplied by groundwater concentrations to produce dose. The BDCFs are calculated externally to IMARC using the computer code AMBER, Version 4.5. A description of AMBER can be found in Enviros and Quintessa (2003), and Enviros (2003). The steady-state BDCF is calculated using a transient calculation assuming a steady-state unit concentration input. In the interests of completeness, the remainder of this chapter is dedicated to a more thorough description of the

conceptual model implemented in AMBER. This discussion is an update from earlier descriptions of the treatment of the biosphere (EPRI, 1996; 1998; 2002a).

The main changes made to IMARC since Phase 8, the last published IMARC version, are:

- Assumption of a lower average irrigation rate, more consistent with the range of agricultural and gardening produce practice in Amargosa Valley;
- Updated assumptions for RMEI consumption of locally produced (*i.e.* contaminated) foodstuffs;
- Revision of the enhancement factor applied to the level of contamination assumed present in airborne dust, compared with the soil from which it arises; and
- Changes to a variety of element dependent parameter values based on review the BIOPROTA[10] database and other sources.

In exposure assessment, the features correspond to a particular contaminated medium, rather than a physical location. Thus, for example, exposure to contaminated soil might arise from material that has been transferred on clothing from the land into the domestic environment. The following media were identified as sources of radiation exposure:

- Water (for domestic use, animal watering and irrigation),
- Atmosphere (indoor and outdoor),
- Arable Crops (in field and storage),
- Animals (in field or barn),
- Cultivated Soil, and
- Farm Products in the Storage, Distribution and Processing System.

The exposure pathways shown in Table 7-1 are carried forward for consideration in the mathematical model. The relative significance of the pathways has been assigned by a combination of professional judgment and experience, and a critical evaluation of the screening of pathways conducted by DOE in their biosphere assessment.

[10] BIOPROTA is an international program set up to address the key uncertainties in long term assessments of contaminant releases into the environment arising from radioactive waste disposal, which EPRI has participated in as part of the Yucca Mountain project.

Table 7-1
Exposure Pathways

Source	Pathway
Domestic Water	Ingestion– included Spray Inhalation– omitted, low significance Immersion (bathing) - included External (exposure to storage/distribution system) – omitted, low significance
Irrigation Water	Spray Inhalation – included
Atmosphere	Suspended soil and other dust – included vapor/gas – omitted, low significance
Cultivated Soil	Ingestion, with food product, and direct ingestion – included External exposure – included
Crops in Field and Storage	External exposure– omitted, low significance
Animal in Field/Barn	External exposure– omitted, low significance
Food Products	External (*e.g.*, silage clamp) – omitted, low significance Ingestion – included

As in previous EPRI work (2002a), uptake via dermal contact has not been considered as this is not believed to be a significant exposure pathway from groundwater contamination (IAEA, 2003).

The main additional feature of the new results is that key parametric uncertainties are identified, specifically those for which there is some useful basis for adopting a probability distribution function, and the dose results are presented as distributions for each radionuclide based on Monte Carlo sampling of parameter values for those parameters. Also presented are the means, confidence in the means and the 5^{th} and 95^{th} percentiles of the overall distributions. At the same time, deterministic calculations have been made according to the procedure used in previous assessments (EPRI; 1996, 2002a) but using updated best estimate values of parameters. The purpose was to determine if there was a systematic difference between the best estimate BDCFs and the means of the probabilistic results.

7.2 Conceptual Model Basis

The methodology for the biosphere assessment is based on the BIOMASS methodology (IAEA, 2003). This methodological approach was previously used in draft form during work for EPRI (1996) and EPRI (2002a), and is now updated accordingly. Ideally in the BIOMASS approach, all the elements of the Interaction Matrix for radionuclide transfer and RMEI exposure should be cross-referenced to the System Description output and to the list of FEPs. Accordingly, the Interaction should contain all the FEPs identified as being relevant to a model description of radionuclide transfer, while a list of excluded FEPs, with the rationale for exclusion, is also

retained. That process is only summarized here, but the outcome is the same as if a more formal interaction matrix approach was used.

7.2.1 Water Supply

A variety of FEPs have been identified in the conceptual model that could potentially change the concentration of radionuclides in the water supply, compared with that in the abstracted well water. These include evaporation of the water, sorption onto sediments or other surfaces, sedimentation, precipitation and dissolution.

Evaporation of water during storage and distribution might give rise to a small increase in concentration of those radionuclides remaining in solution. However, total water losses via this route are considered unlikely to be significant, in an arid environment (Walter, 1985), and the process is not included in the model.

Although suspended sediment may be present within the water supply, the total sediment load must be low enough for the water to remain potable (since no deliberate water treatment is assumed to take place). Sorption onto suspended sediment, and subsequent sedimentation, may occur over time; however, the overall effect of this will only be to reduce radionuclide concentrations in bulk water supplied at the point of delivery. The periodic removal of accumulated sediments from cisterns and other parts of the storage and distribution system could potentially give rise to a transient "spike" in water concentration resulting from the remobilization of radionuclides. This might possibly be relevant if the focus of interest were the dose from exposure with a specific year; over a longer period, however, the average concentration in the water supply will not exceed that delivered at the well head. Furthermore, any transfer of radionuclides associated with the possible removal to soil of accumulated sediment from within the water distribution system is unlikely to be significant, since the volumes involved will be comparatively small. Moreover, if the material is suitable for spreading on the land, sorption coefficients are unlikely to be significantly different from those for the irrigated soil itself. The effects of sorption and sedimentation in modeling radionuclide transfer within the water distribution system can therefore be ignored.

Precipitation and/or dissolution of radionuclides associated with changes to water chemistry (*e.g.* redox conditions or microbial action) may possibly affect concentrations in bulk water. Again, however, their net effect can only be to reduce radionuclide concentrations in bulk water compared with that delivered at the well head. Therefore, provided that the radionuclide concentration in bulk water (*i.e.* including suspended solids) is specified at the geosphere-biosphere interface (*i.e.* in the part of the geosphere from which water is directly abstracted), it will be cautious (*i.e.*, "conservative") to ignore the effects of precipitation and dissolution in the water supply.

Potential exposures linked to contact with contaminated sediments and other surfaces within the water supply system are considered negligible compared with those associated with other media. This might be less easy to justify for an 'industrial' or 'commercial' biosphere system, in which maintenance of water storage, distribution and supply systems could potentially constitute a specialized job. However, the present assessment context excludes consideration of large-scale commercial/industrial activities. Hence, sorption and sedimentation within the water storage and

distribution system can also be ignored in the context of evaluating radiological exposures. Decay and in-growth of radionuclides would also be negligible compared with geosphere processes and processes occurring at the well head. For modeling purposes, it is assumed that the water supply to other parts of the biosphere system is provided at the same bulk concentration as that delivered at the well head, as calculated in the geosphere model within the TSPA.

7.2.2 Atmosphere

Concentrations of dust or trace materials in the atmosphere can vary rapidly over a considerable range according to local meteorological conditions (atmospheric pressure, wind speed, precipitation etc) as well as factors such as artificial disturbance (*e.g.* dusts generated by plowing). The processes involved are complex; however, a significant proportion of the locally-generated transfer of aerosol and vapor will typically remain within a near-surface atmospheric boundary layer and not travel very far before being deposited again. Nevertheless, over time, such transport can lead to losses of radionuclides from the biosphere system; at the same time, other material will be brought into the system from outside by atmospheric processes. Because such transfers are expected to be small compared with, for example, irrigation and percolation in groundwater, it is considered appropriately cautious, without being excessively so, to make the simplifying modeling assumption that their effect can be ignored.

Such simplifications mean that there is no need for an explicit representation of atmospheric transfer processes, and no atmosphere compartment is therefore incorporated in the assessment model. However, radioactive vapor, gas or aerosol within the atmosphere can represent a potentially important exposure pathway for some radionuclides leading to a dose via inhalation. It is therefore appropriate to evaluate radionuclide concentrations in the near-surface atmospheric boundary layer, or in indoor atmospheres that may receive releases of gas or vapor. Standard practice is to represent the long-term equilibrium relationship between average atmospheric concentrations and those in soils, plants and other environmental media using empirical correlations.

7.2.3 Arable Crops

Crops will become contaminated due to direct deposition of irrigation water. A fraction can be retained on the plant surface and another fraction can be transferred within the plant, particularly to edible parts. Weathering of plant surfaces results in transfer of radionuclides that have fallen onto crops down to the soil. Crops may then become contaminated by root uptake. Soil splash may result in further crop contamination. Although seasonal factors can substantially influence details of what could happen within any one year, given the nature of the time frames of interest as discussed above, all the above processes can be modeled on the basis of equilibrium between the concentration in the irrigation water and the concentration in crops, or between the soil and crops. Models, for this set of processes with the same type of context, commonly use this approach (BIOMOVS II, 1996).

EPRI (1996) identified fruit consumption as an important pathway for some radionuclides. BIOMASS (IAEA, 2003) included a special working group to consider this process. While the

IAEA work has some implications for model parameter values, no changes to the EPRI (1996) model structure are suggested.

7.2.4 Animals

The same equilibrium approach is adopted for animal product contamination, with concentrations being directly related to concentrations in the irrigation water (for consumption of water but also contribution via crop contamination) or in soil (for contribution via crop contamination or direct ingestion).

7.2.5 Cultivated Soil

Cultivated soil is assumed to be plowed or dug over, if not every year then every few years. Given the time frames under consideration this means that detailed soil structure is not to be modeled. A "well mixed" layer is assumed associated with typical plowing depths and to the dominant region in the profile for root uptake by crops and other biotic activity. Processes within the soil result in downward movement, primarily due to infiltration of water. Loss from soil due to erosion is identified in the interaction matrix; however, noting the sensitivity studies in IAEA (2003), this process is ignored due to low significance compared with infiltration. Cropping is assumed to effectively remove activity from soil though this may also be of low significance for most radionuclides.

7.2.6 Farm Products in Storage, Distribution and Processing Systems

Radionuclide behavior in stores is not considered to be of great interest only producing a minor decay effect. However these assumptions for storage etc can affect how food is distributed (diluted) before consumption. Processing may result in changed concentrations in the foods/fodder.

7.2.7 Radiation Exposure Pathways

It should be noted that, in the case of exposure assessment, the items of interest correspond to a particular contaminated medium, rather than a physical location. Thus, for example, exposure to contaminated soil might arise from material that has been transferred on clothing from the land into the domestic environment. Based on the Radionuclide Transfer Interaction Matrix, and the corresponding definitions for each leading diagonal elements, the following media can be identified as qualitatively distinct sources of radiation exposure:

- Water (for domestic use, animal watering and irrigation)
- Atmosphere (indoor and outdoor)
- Arable Crops (in field and storage)
- Animals (in field or barn)
- Cultivated Soil

- Farm Products in the Storage, Distribution and Processing System

The following exposure pathways are carried forward for consideration in the mathematical model.

As in previous EPRI work (2002a), uptake via dermal contact has not been considered since this is not believed to be a significant exposure pathway from groundwater contamination (IAEA, 2003).

7.3 Mathematical Model for Radionuclide Behavior and Radiation Dose Assessment

7.3.1 Introduction

The model used to represent the dynamic transfers in the biosphere arising from the application of contaminated well-water is represented in Figure 7-1. Mathematical representations of the transfers are described in subsection 7.3.2. The equations used to represent the doses arising from the identified exposure pathways are described in subsection 7.3.3.

The AMBER computer program, Version 5, was used to evaluate appropriate BDCFs for the exposure pathways (see Table 7-1) arising from the agricultural and domestic use of the contaminated well water. A description of AMBER can be found in Enviros and Quintessa (2006).

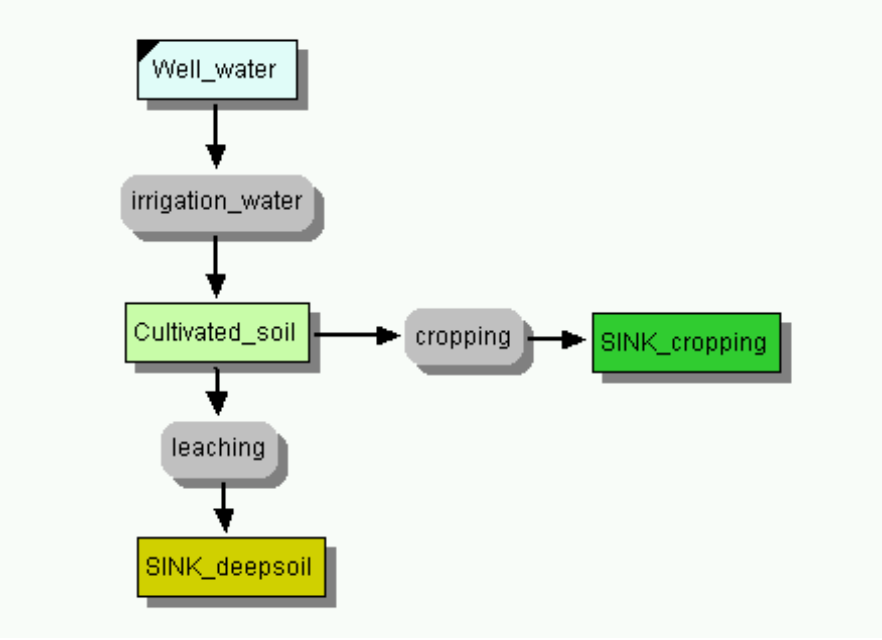

Figure 7-1
Representation of the transfers between compartments of the biosphere

7.3.2 Mathematical Model

7.3.2.1 Inter-compartmental Transfer Processes

The mathematical representation of the inter-compartment transfer processes takes the form of a matrix of transfer coefficients that allow the compartmental inventories to be represented as a set of first-order, linear differential equations. Generally, for the *i*th compartment, the rate at which the compartment inventory changes with time is given by:

$$\frac{dN_i}{dt} = \left(\sum_{j \neq i} \lambda_{ji} N_j + \lambda_N M_i + S_i(t) \right) - \left(\sum_{j \neq i} \lambda_{ij} N_i + \lambda_N N_i \right) \qquad \textbf{Eq. 7-1}$$

where:

- N_i is the activity of radionuclide N in biosphere compartment i, Bq,
- N_j is the activity of radionuclide N in biosphere compartment j, Bq,
- M_i is the amount of radionuclide M in biosphere compartment i (M is the precursor radionuclide of N in a decay chain), Bq,
- $Si_{(t)}$ is an external source term of radionuclide N to compartment i, Bq y-1,
- λ_N is the decay constant for radionuclide N, y-1,
- λ_{ji} is a set of transfer coefficients inputs to compartment i from the other j ($\neq$ i) compartments in the system, y-1,
- λ_{ij} is the set of transfer coefficients representing the loss terms of N from compartment i to the other j ($\neq$ i) compartments of the system and to sinks.

The inter-compartment transfer rate coefficients (λ_{ij}) are the mathematical representation of the transfer processes identified in the conceptual model.

The processes included dynamically in the conceptual model are shown in Figure 7.1. The calculations are made on the basis of irrigation of unit area (1 m^2), avoiding the need to quantify the areas irrigated on the assumption that enough water is available to irrigate sufficient land to support the needs of the candidate critical groups. A single soil compartment is considered, even though soil concentrations may vary with crop type, because some rotation of crops is assumed in the long term. There are a number of loss mechanisms from this soil, as well as radioactive decay and in-growth, to calculate.

7.3.2.1.1 Irrigation source term

Irrigation water, extracted from a contaminated well, is assumed to be applied to cultivated soil. Although a fraction of irrigation water is intercepted by crops, all the activity in the water is assumed to enter the soil immediately (concentrations of radionuclides in crops due to interception of irrigation water are assessed assuming equilibrium with concentrations in the irrigation water). The relatively short delay before weathering removes intercepted activity to the

soil is ignored (so far as the concentration in soil calculation is concerned). Similarly, the proportion of intercepted activity which is absorbed by the crop is also ignored (so far as calculation of this concentration is concerned). It is assumed that plant material, excluding the cropped fraction, is recycled and incorporated into the soil. Changes in irrigation water concentrations from the well head to the soil surface are also ignored. Thus, the source term to the soil due to irrigation, S, mol $m^{-2}y^{-1}$, is given by:

$$S = V_{irr}C_w \qquad \textbf{Eq. 7-2}$$

where,

V_{irr} is the rate of irrigation water applied to the soil, $m^3m^{-2}y^{-1}$,

C_w is the radionuclide concentration in the well water, mol m^{-3}.

7.3.2.1.2 Leaching (and other downward losses) from cultivated soil

The rate coefficient for the transfer of radionuclides out of cultivated soil due to leaching, λ_{1I}, y^{-1}, is given by:

$$\lambda_{1I} = \frac{I}{R\ \theta_w\ d} \qquad \textbf{Eq. 7-3}$$

where:

I is the net annual infiltration/recharge rate, m y^{-1},

R is the retardation coefficient for contaminants within the cultivated soil compartment,

θ_w is the water-filled porosity of the cultivated soil compartment,

d is the thickness of the cultivated soil compartment, m.

The R term is calculated using the following equation:

$$R = 1 + \frac{(1-\theta_t)\rho}{\theta_w} K_d \qquad \textbf{Eq. 7-4}$$

where:

θ_t is the total porosity of the cultivated soil compartment,

ρ is the grain density of the cultivated soil compartment, kg m^{-3}, and

K_d is the linear, reversible sorption coefficient of the cultivated soil compartment, m^3kg^{-1}.

Sorption-derived values obtained from column experiments are considered more relevant than batch experiments, where available, being more likely to represent fully the effect of water moving through the soil.

As discussed in Section 7.2.1, the use of Equation 7-4 neglects a number of chemical effects that may occur in surface soil, such as precipitation. Water extracted from a borehole will reflect the chemistry of the geological conditions deep in the borehole. As that water contacts the surface soil, the potential exists for it to experience significantly different chemical conditions, which may lead to reductions in the water concentrations of some radionuclides. Since the radionuclides are dissolved in borehole water as they contact the new chemical regime, the only potential effects would be to decrease the concentration, for instance by precipitation or co-precipitation of the radionuclide. There are no chemical processes that would tend to concentrate the aqueous concentration of a contaminant during these processes. As a result, the use of Equation 7-4 is appropriate, and if additional processes exist it will tend to err on the side of high concentrations, leading to high doses.

7.3.2.1.3 Cropping

In circumstances of high uptake of radionuclides from soils into growing plants the concentration in soils would be modified. The activity in that proportion of plants not returned to soil through plant decay, *i.e.* the proportion removed in cropping, would be lost from the system. It is recognized that this process is only significant for those radionuclides that are significantly taken up into crops. The crops are assumed to be grown in rotation on the unit area of land, and so the loss rate is taken to be the average associated with the five crops considered. The rate constant for removal from the soil, λ_{1C}, y^{-1}, is given by:

$$\lambda_{1C} = \frac{\sum_{crop} \frac{1}{5}(CF_{crop} + S_{crop})Y_{crop}}{(1-\theta_t)\rho d} \qquad \textbf{Eq. 7-5}$$

where:

CF_{crop} is the concentration factor from root uptake for the crop, $Bq \cdot kg^{-1}$ (fresh weight of crop)/$Bq \cdot kg^{-1}$ (dry weight of soil),

S_{crop} is the soil contamination on the crop, kg (dry weight soil) kg^{-1} (fresh weight of crop),

Y_{crop} is the wet weight biomass of the crop, kg $m^{-2} \cdot y^{-1}$, obtained at harvest from the unit area irrigated.

In Equation 7-5, the 1/5 term comes from an assumption that all 5 crops are grown in equal proportion.

The equation for the radionuclide concentration in the bulk cultivated soil compartment, C_s, for radionuclide N, mol m^{-3}, is:

$$\frac{dC_s}{dt} = -(\lambda_N + \lambda_{1C} + \lambda_{1I})C_s + \frac{V_{irr}C_w}{d} \qquad \textbf{Eq. 7-6}$$

Losses due to wind and water erosion are ignored on the basis that either they are not significant compared with the other transfers or they are so slow as to require the consideration of biosphere change before it would have a significant effect on the radionuclide concentration of the soil compartment.

7.3.2.2 Dose Equations

Doses have been assessed for each of the pathways indicated in Table 7-1.

7.3.2.2.1 Consumption of Drinking Water

The annual individual dose from the consumption of unfiltered drinking water from the well is given by:

$$D_w = ING_w \; DC_{ing} \; C_w \qquad \textbf{Eq. 7-7}$$

where:

D_w is the individual dose from consumption of well water, mrem y^{-1},

ING_w is the individual ingestion rate of well water, $m^3 y^{-1}$,

DC_{ing} is the dose coefficient for ingestion, mrem mol^{-1}.

7.3.2.2.2 Consumption of Agricultural Crops

The annual individual dose from the consumption of agricultural crops is given by:

$$D_{crop} = ING_{crop} \; DC_{ing} \; C_{crop} \qquad \textbf{Eq. 7-8}$$

where:

D_{crop} is the individual dose from consumption of the crop, mrem y^{-1},

ING_{crop} is the individual ingestion rate of the crop, kg y^{-1}, and

C_{crop} is the radionuclide concentration in the edible part of the crop, mol kg^{-1} (fresh weight of crop).

The C_{crop} term is calculated using the following equation:

$$C_{crop} = \frac{(F_{p2} CF_{crop} + F_{p1} S_{crop}) C_s}{(1-\theta_t)\rho} + I_{crop} V_{irr} C_w \left(\frac{(1-F_{abs}) e^{-WT} F_{p3}}{Y} + \frac{F_{abs} F_{p2} F_{trans}}{Y} \right) \qquad \textbf{Eq. 7-9}$$

where:

I_{crop} is the fraction of radionuclide in spray irrigation water that is initially deposited on standing biomass,

F_{trans} is the fraction of absorbed activity that is translocated to the edible portion of the plant by the time of harvest (translocation fraction),

F_{abs} is the fraction of intercepted radionuclide initially deposited onto the plant surface that is absorbed from external surfaces into plant tissues,

F_{p1} is the fraction of external soil contamination on the edible part of the crop retained after food processing,

F_{p2} is the fraction of the internal contamination associated with the edible part of the plant at harvest that is retained after food processing has occurred,

F_{p3} is the fraction of external contamination from interception that is retained on the edible part of the crop after food processing,

W is the removal rate of radionuclide deposited on plant surface by irrigation by weathering processes (weathering rate) including mechanical weathering, wash-off and leaf fall, y^{-1},

T is the interval between irrigation and harvest, y.

It should be noted that it is assumed that the crop can be contaminated due to:

- internal uptake of contaminants from the cultivated soil compartment into the crop via the roots (represented by the $\frac{CF_{crop}C_s}{(1-\theta_t)\rho}$ term),
- external contamination of the crop due to deposition of re-suspended sediment from the surface soil compartment (represented by the $\frac{S_{crop}C_s}{(1-\theta_t)\rho}$ term),
- irrigation (represented by the $I_{crop}V_{irr}C_w$ term).

It is assumed that contamination can be lost due to:

- food preparation (represented by F_{p1}, F_{p2} and F_{p3} terms),
- weathering of the external contamination to the soil (represented by the e^{-WT} term).

An alternative to the e^{-WT} formulation is applied for pasture, see Equation 7-14. This averages out processes on-going through the year, and is more appropriate in the case of pasture since cropping by cows or sheep would be continuous. Using e^{-WT} allows the investigation of alternative assumptions for T, potentially more significant for crops directly consumed by humans.

7.3.2.2.3 Consumption of Animal Products

The annual individual dose from the consumption of animal products is given by:

$$D_{prod} = ING_{prod}\ DC_{ing}\ C_{prod} \qquad \textbf{Eq. 7-10}$$

where:

D_{prod} is the individual dose from consumption of the animal product, mrem y^{-1},

ING_{prod} is the individual consumption rate of the animal product, kg y^{-1},,

C_{prod} is the radionuclide concentration in the animal product, mol y^{-1}

The C_{prod} term is calculated using the following equation:

$$C_{prod} = TF_{proding}\left(C_{fodd} ING_{fodd} + C_w ING_{wa} + \frac{C_s\ \ ING_{sa}}{(1-\theta_t)\rho + \theta\rho_w} \right) + \\ + (BR_a O_{an} C_{airs}) TF_{prodinh} \qquad \textbf{Eq. 7-11}$$

where:

$TF_{proding}$ is the transfer factor for ingestion for the animal product, d kg^{-1} (fresh weight of product),

C_{fodd} is the radionuclide concentration in the animal fodder, mol kg^{-1} (fresh weight of fodder),

$TF_{prodinh}$ is the transfer factor for inhalation for the animal product, d kg^{-1} (fresh weight of product),

ING_{fodd} is the consumption rate of fodder by the animal, kg (fresh weight) d^{-1},

C_w is the radionuclide concentration in the well water, mol m^{-3},

ING_{wa} is the consumption rate of water by the animal, $m^3 d^{-1}$,

ING_{sa} is the consumption rate of soil from the cultivated soil compartment by the animal, kg (wet weight of soil) d^{-1},

ρ_w is the density of water, kg m^{-3},

BR_a is the breathing rate of the animal, $m^3 h^{-1}$,

O_{an} is the occupancy time of the animal in the cultivated soil compartment, h d^{-1},

C_{airs} is the radionuclide concentration in the air above the cultivated soil compartment, mol m^{-3}

The C_{airs} term is calculated using the following equation:

$$C_{airs} = \frac{E_f C_s}{(1-\theta_t)\rho} \cdot \frac{(R-1)}{R} dust_s \qquad \textbf{Eq. 7-12}$$

where:

$dust_s$ is the soil derived dust level in the air above the cultivated soil compartment, kg m^{-3}.

E_f is an enhancement factor to account for the higher activity concentration on the dust particles compared with the average soil component particles from which the dust is derived.

The $TF_{prodinh}$ term is calculated using the following equation:

$$TF_{prodinh} = TF_{proding} \frac{f_L + f_C\, f_1(inh)}{f_1(ing)} \qquad \textbf{Eq. 7-13}$$

where:

f_L is the fraction of inhaled activity reaching the systemic circulation following transfer across the lung lining.

f_C is the fraction of inhaled activity that is cleared to the gastrointestinal tract.

$f_{1(inh)}$ is the fraction of inhaled activity, cleared to the gastrointestinal tract, that is transferred to the systemic circulation.

$f_{1(ing)}$ is the fraction of ingested activity reaching the body fluids in man.

The nature of the fodder consumed by the animal depends on the type of animal. In this example, one animal type is considered, cows. It is assumed that the cows consume fodder grown on irrigated land. The C_{fodd} term, Bq m^{-3}, is calculated using the following equation:

$$C_{fodd} = \frac{(CF_{past} + S_{past})C_s}{(1-\theta_t)\rho} + \frac{I_{past} V_{irr} C_w}{SB_{past} W_{past} + 365\, ING_{fodd} SD} \qquad \textbf{Eq. 7-14}$$

where:

CF_{past} is the concentration factor for pasture, Bq kg^{-1} (fresh weight of pasture)/Bq kg^{-1} (dry weight of soil)

S_{past} is the soil contamination on pasture, kg (dry weight soil)/kg (fresh weight of pasture),

I_{past} is the interception fraction for irrigation water on pasture,

SB_{past} is the standing yield of pasture, kg,

W_{past} is the removal rate of irrigation water from pasture by weathering (weathering rate), y^{-1},

SD is the number of animals per unit area, m^{-2},

ING_{Fodd} here, CF (Equation 7-11), has to be multiplied by 365 to convert to intake as kg fw y^{-1}.

Mechanistically, it is assumed that the animal can be contaminated due to:

- consumption of contaminated fodder (represented by the C_{fodd} ING_{fodd} term in Equation 7-11);
- consumption of contaminated water (represented by the C_w ING_{wa} term in Equation 7-11);
- consumption of contaminated soil (represented by the $\frac{C_s ING_{sa}}{(1-\theta_t)\rho + \theta\rho_w}$ term in Equation -7-11);
- inhalation of contaminated soil (represented by the BR_a O_{an} C_{airs} term in Equation 7-11).

7.3.2.2.4 Consumption of Soil

Apart from inadvertent consumption due to soil contamination of crops, soil can be consumed by humans both inadvertently and deliberately. The annual individual dose to humans from this type of soil consumption is given by:

$$D_{soil} = ING_{soil} DC_{ing} \frac{C_s}{(1-\theta_t)\rho + \theta_w \rho_w} \quad \textbf{Eq. 7-15}$$

where:

D_{soil} is the individual dose from consumption of the soil, mrem y^{-1},

ING_{soil} is the individual consumption rate of the soil, kg y^{-1}, wet weight.

7.3.2.2.5 External Irradiation from Soil

The annual individual dose to humans from external irradiation from soil/sediment, during occupancy of the soil compartment, is given by:

$$D_{exsoil} = \frac{O_s DC_{exts} C_s}{(1-\theta_t)\rho + \theta_w \rho_w} \quad \textbf{Eq. 7-16}$$

where:

D_{exsoil} is the individual dose from external irradiation from the soil, mrem y^{-1},

O_s is the individual occupancy in the soil compartment, h y^{-1},

DC_{exts} is the dose factor for external irradiation from soil, mrem h^{-1}/mol kg^{-1}.

7.3.2.2.6 External Irradiation from Immersion in Water

The annual individual dose to humans from external irradiation from immersion in water is given by:

$$D_{imwat} = O_{wat}\ DC_{imw}\ C_w \qquad \textbf{Eq. 7-17}$$

where:

D_{imwat} is the individual dose from external irradiation from immersion in the water, mrem y^{-1},

O_{wat} is the individual occupancy in the water, h y^{-1},

DC_{imw} is the dose coefficient for external irradiation from immersion in water, mrem h^{-1} / mol m^{-3}.

7.3.2.2.7 Inhalation of Dust

The annual individual dose to humans from the inhalation of dust, during occupancy of the soil compartment, is given by:

$$D_{dust} = DC_{inh}(C_{airs}^{norm} BR\ O_{inh} + C_{airs}^{phy} BR_{phy} O_{inh/p}) \qquad \textbf{Eq. 7-18}$$

where:

D_{dust} is the individual dose from the inhalation of dust, mrem y^{-1},

DC_{inh} is the dose coefficient for inhalation, mrem mol^{-1},

BR is the normal breathing rate of the human, $m^3 \cdot h^{-1}$,

BR_{phy} is the breathing rate for physical working in dry soil conditions, $m^3 \cdot h^{-1}$,

O_{inh} is the inhalation occupancy for normal activity, h y^{-1},

$O_{\text{inh/p}}$ is the inhalation occupancy during hard physical activity in dry soil conditions, h y^{-1},

C_{airs} is as defined by Equation 7-12 with appropriate substitution for dusts under normal dust loading conditions (norm) and under physical working conditions (phy) as defined in Table C-2, Appendix C, mol m^{-3}.

7.3.2.2.8 Inhalation of Aerosols/Spray in Irrigation Activities

The annual individual dose to humans from the inhalation of aerosols in water spray is given by:

$$D_{aero} = DC_{inh} BR\ AIR_{aero} O_{aero} C_w \qquad \textbf{Eq. 7-19}$$

where:

D_{aero} is the individual dose from the inhalation of aerosols, mrem y^{-1},

Air_{aero} is the aerosol level in the air in the area affected by aerosols/spray, $m^3 \cdot m^{-3}$,

O_{aero} is the individual occupancy in the area affected by aerosols, h y^{-1}.

Biosphere Dose Conversion Factors (BDCFs) used in IMARC 10 are listed in Table 7-2. Sensitivity and uncertainty analyses have been carried out for the BDCFs implemented in IMARC 10, and are presented in Appendix C. The purpose of these analyses is to provide a foundation for understanding the variability of the biosphere model output on variability and uncertainty in the model input parameters. These analyses demonstrate that the deterministic BDCFs used in the model are moderately conservative compared to values that would represent the mean value of an output distribution. The deterministic value for ^{129}I (the dominant TSPA radionuclide) is higher than the mean by about a factor of 4, but other key radionuclides (e.g. ^{99}Tc, ^{237}Np) are higher by less than a factor of 2.

Table 7-2
BDCF values used in IMARC 10, derived from the parameters presented in Appendix C.

Radionuclide	BDCF (mrem/y per mol/m^3)
Tc-99	8.0E6
I-129	3.9E7
Np-237	4.5E8
U-233	1.2E9
Th-229	2.8E12
Pu-239	1.3E11
U-235	2.5E5
U-238	3.8E4
U-234	7.6E8
Th-230	1.3E11
Pu-242	4.5E9
Cl-36	3.1E7
Se-79	2.9E7

7.4 Model Comparisons and Verification

Since 2002, the EPRI conceptual model has been compared with other models designed for similar long-term performance assessment purposes within a series of model comparison exercises carried out as part of the international BIOPROTA program www.bioprota.com. These comparisons addressed: accumulation of radionuclides in soil; inhalation exposure due to dust suspension; and the direct food chain contamination effects of spray irrigation (BIOPROTA, 2005a; b; c). The radionuclides considered in each case include those pertinent to the EPRI TSPA. The program of comparison exercises effectively constituted a major peer review process among radio-ecology and dose assessment experts from around the world. No substantive errors or omissions were found in the EPRI approach.

8
DESCRIPTION OF IMARC CODE STRUCTURE

In this chapter, the structure of the IMARC software is outlined. These details are included to provide a clear concept of the organization of the software.

8.1 Context for the Current IMARC Structure

The IMARC code, version 7 was placed under a configuration management system in 2003. IMARC 7.0 has since undergone restructuring first as IMARC 8.0 in 2005 and subsequently IMARC 9.0 in 2007 and IMARC 10 in 2008. The code structure for Versions 8 - 10 is described in this chapter.

IMARC 7.0 was a set of more than 40 FORTRAN source code files, each one of which contained multiple subroutines. These files were developed at different times for different purposes and under different Fortran compilers: Microsoft Power Station 4.x, Compaq 6.x Salford, Watcom and AIX Fortran (UNIX). Currently, IMARC is compiled under Compaq Visual Fortran version 6.6. In addition, IMARC 7.0 contained features intended to be run on different computing platforms: from PC to VAX, DEC and IBM UNIX workstations.

Given the complexity of the history of the component codes, IMARC was restructured to provide greater traceability and clarity in the FORTRAN coding. In addition, it was found that several variables had the same name, but different interpretations in different subroutines making it difficult to follow the code logic, the sequence of computations, and data transfers. As a result, an extensive revision of the code was undertaken, with the result denoted as IMARC 8. It is noteworthy that the changes resulting in IMARC 8 were predominantly those associated with code restructuring, testing, and maintenance. There were few substantive changes in the TSPA methodology from Phase 7 to Phase 8.

8.2 Development of IMARC 8 through 10

The programmatic structure of the EPRI team led to a modular development of IMARC 8 (carried forward into the current IMARC 10). The modular structure is intended to allow independent research providers to modify parts of the code as new information becomes available. The current structure of IMARC is an aggregation of four “stand-alone” programs, with the data transfer between them carried out by COMMON blocks with subsequent re-assignment of the variables and arrays in each individual subroutine. IMARC 10 represents updated parameters and improved estimations. The four main programs in IMARC 10 are:

- IMARC, which is an executive program used to establish the event tree, propagate uncertainty through the models, and control execution of the process model software;
- COMPASS, which is a process model code for evaluating transport of radionuclides from the repository. The processes considered in the model include considerations of flow, chemistry, radioactive decay and ingrowths, and the effects of the waste package on limiting transport;
- the unsaturated-zone (UZ) code (unnamed) is a process model code accounting for flow and transport below the repository horizon to the water table. This code carries out a solution of the transport equations using a finite difference representation for the spatial variable and an implicit time-stepping method for the time domain; and
- the saturated-zone (SZ) code (unnamed) is a process model code accounting for flow and transport in the saturated zone. This solves the transport equation using the Galerkin finite-element method in the spatial domain and a Laplace transform solution for the time domain.

As discussed in Chapter 4, failure distributions for the drip shield, waste package, and cladding were generated in a separate, Monte Carlo program. The mean of each of these failure distributions was translated into a lookup table used in the IMARC program. Mathematically, the flow and transport solutions for both UZ and SZ are carried out using different methods, and are conceptually considered distinct codes. However, functionally, the flow and transport codes are quite intertwined, using common input and output files, from a software perspective the UZ and SZ codes represent a single code.

Changes in the code between Versions 7 through 10 are documented using extensive comments and remarks in the FORTRAN source code. In the code, they are indicated by *, *gm, or *mwk rather than “c” in the first column of the comment lines, which indicated comments from older versions of IMARC. Wherever possible, comments have been added describing the module purpose, input/output files, associated INCLUDE files, called subroutines, main variables, their dimensions, and unit conversions. More significant changes to the structure and organization of the code include:

- The call from TREEU/TREEU2 to external routine END_ROUTINE is replaced with one explicit call to subroutine TERMU;
- In the IMARC Version 7.0 source code the “event tree path sampling” processing is organized in an implicit manner by internal recursive calls between the two identical subroutines TREEU and TREEU2 until the entire event tree is processed. This organization is replaced by one explicit do-while loop located in the main IMARC program. In general, this loop incorporates the same algorithm from the TREEU/TREEU2 with minor changes concerning the termination of the processing along the individual and along the main paths of the logic tree. When all paths of the logic tree are processed, there is an exit from this do-while loop calling subroutine TERMU to perform an end-branch analysis for the given combination of the input parameters. In this way the code and the algorithm of IMARC was made more clear and easy to understand;
- During the phased development of IMARC, several parameters were assigned different names when passing them from one subroutine to another mainly as formal arguments in the call operators. A change has been made to unify parameter names throughout the code; and

- All real scalars and arrays have been set to REAL*8, as it has been found that throughout the code several of them are transferred with changing precision between the routines. This is particularly important since the concentrations produced in IMARC have very low values.
- In the IMARC 7.0 source code there was an option specifying the flow velocities in the SZ either to be computed or to be introduced from external files. For large numbers of computations this could lead to the use of improper velocity fields. To prevent this from occurring, the flow velocity fields have been set to be computed on every run. This does not cause a significant increase in computation time, as one run of the module FLOW3D takes about 10 seconds.

In the subroutine NUMSZT, the Laplace Transform Galerkin method is applied to compute the transport in the saturated zone. The previous IMARC versions assumed the Laplace inverse transformation of the nuclide's concentrations on selected set of nodes including those at the downstream and top stream faces and the nodes in close vicinity of the observational wells only. For the purpose of investigating the temporal-spatial distribution of the radionuclides in the water table (saturated zone) the modified code now assumes Laplace inverse transformation of the nuclide's concentrations in the entire saturated domain. The tests do not show any significant change in computation time.

8.3 Input Structure

In IMARC, there are two approaches for character recognition during reading and processing input data. The first one is used in COMPASS. These data are read from the input file *ST.dat*, which provides repository and the container parameters, corrosion parameters, radionuclides and their decay chains, *etc*. The character recognition is used to define which block of the input data is currently processed according to set of "key words" previously defined in the code. The subroutines used for this character recognition have been placed in the file *Imarc_input.f*. The key words are situated at the beginning of the first line of each data block in the file *ST.dat*. These key words control the calls to subroutines for reading and processing the input parameters. This organization of the input is very flexible and it does not require any previously defined sequence of the data blocks in the file *ST.dat*.

The second approach is used in the input of hydrological data from the file *HT.dat*. The code uses character recognition only to identify which lines in the input file contain comments, which contain data, and which represent the end of a data block. At the beginning of every line in *HT.dat*, a text character string is read. It is then written to an internal buffer defined in *Imarc_IO_buf.fi*. If the first character in the text string is "c" (denoting "comment") or "e" ("end" used to define the end of the data block) this line is skipped and the next line is processed. This approach is applied to skip the numerous and useful comment lines in the file *HT.dat*, so as to overcome the problems caused by differences between early versions of DOS/Windows and UNIX in coding the "end of line" (line feed or carriage return). The sequence of the input data is strictly defined in subroutines READinit, READst and INRES called during the first runs of the modules calculating the flow and the transport in the unsaturated and saturated zones.

All input files are placed in a subfolder called .\INPUT. These input files are:

LOGICTREE.IM3,
LAPLACE.DAT,
ST.DAT,
WPF.DAT,
THERMOHYD.INP,
NUCLID.PAR,
HT.DAT, and
SATRAP.DAT.

All output files are placed in a subfolder called .*RES*. These output files are:

IMARC.OUT,
DOSE.OUT,
ST.OUT,
IMARC_WPF.OUT,
PROFMF.OUT,
IMARC_NUC.OUT,
HT.OUT,
SATRAP.OUT,
BTC.OUT,
BTC_NC.OUT, and
FLUX.OUT.

The grid generation module for the SZ flow and transport computations allows the possibility to generate either 3D or 2D computational domains based on hexahedral (or brick) elements with varying dimensions. The 2D representation of the SZ is carried out with one hexahedral element in the vertical direction. The tests comparing the results from the 2D and the 3D cases (EPRI, 2004a) indicate that precision is not lost in the arrival time and in the values of the maximum concentrations at the downstream face but that significant reduction in computer time is achieved.

The present 2D version of the transport in the SZ is found to be relatively fast and computational constraints could be loosened, increasing the number of the output times, allowing for improved output resolution. It is necessary to evaluate the relationship between the number of output times and the Laplace spaces. This evaluation illustrates the desirability of the use of a new input file to define the output times and the number of the Laplace spaces. This file is named *LAPLACE.DAT*; it is opened in the main IMARC routine, as the output times are needed for the formation of the final output tables. The tests with more detailed temporal discretization show that unexplained peaks or depressions in the concentrations at the downstream face, observed in older versions of IMARC, are associated with the relationship between the number of Laplace spaces and the output discretization. The basic principle for the number of Laplace spaces is that the number of the output times has to be equal and evenly spaced in each one of the Laplace spaces (Sudicky, 1989; Sudicky and McLaren, 1992).

9
CONFIGURATION MANAGEMENT AND QUALITY ASSURANCE

All IMARC activities are carried out under an appropriate quality assurance program. This program has several main elements:

- Testing, verification, and benchmarking of components of IMARC,
- Ensuring traceability of results,
- Documentation of each stage of development of IMARC, and
- Comparison of IMARC with DOE and NRC TSPA analyses of Yucca Mountain.
- Publication of IMARC results in peer-review literature, at conferences, and to oversight committees such as the Nuclear Waste Technical Review Board (NWTRB) and the NRC's Advisory Committee on Nuclear Waste and Materials (ACNW&M).

In this chapter, a summary is presented of activities in each of these elements of the configuration management and quality assurance program.

9.1 Component Testing, Verification, and Benchmarking

Individual chapters of this report have presented details of specific testing activities that have been conducted for component models in IMARC. These activities are summarized in Table 9.1.

Table 9-1
Summary of Testing Activities for Component Models in IMARC

Component Model	Testing Activities
Climate, Infiltration, and Percolation	Comparisons conducted between FEPS and results from analyses conducted by DOE, NRC, USGS, and others.
Seepage	Model is derived from DOE's analysis of seepage. Comparisons conducted of FEPs and results with DOE analyses.
Near Field	Benchmarking analyses conducted for analytical solutions for near-field transport.
Corrosion	Benchmarking analyses conducted with prior analyses of corrosion by the EPRI team. Comparisons conducted of FEPs included in DOE analyses. Comparisons conducted of results from DOE analyses.
Unsaturated Zone	Benchmarking analyses conducted with analytical solutions and alternative numerical methods. Comparison with FEPs implemented in DOE and NRC conceptualizations. Alternative conceptual models implemented outside the IMARC framework to evaluate the response of the hydrological system.
Saturated Zone	Benchmarking analyses conducted with analytical solutions and alternative numerical methods. Evaluation of the numerical implementation of the Laplace Transform inversion method to ensure its convergence. Comparison with FEPs implemented in DOE and NRC conceptualizations. Alternative conceptual models implemented outside the IMARC framework to evaluate the response of the hydrological system.
Biosphere	International peer review through participation in BIOMASS. Intercomparison of the biosphere model with alternative models for the same processes. Comparisons conducted of FEPs and results with DOE's biosphere model.

9.2 Ensuring Traceability of Results

9.2.1 Introduction

Information technologies have advanced in parallel with the development of IMARC, and approaches to establishing traceabilty of calculations and input data that were appropriate in early phases of IMARC no longer represent best practice. As a result, an information management system has been implemented to improve the approaches to documenting and tracing IMARC analyses. The intention of this information management system is to provide the ability to trace inputs and outputs associated with an IMARC analysis.

An IMARC analysis contains the detailed input and output of a number of subsystems that directly or indirectly interact with the repository over a long period of time. These subsystems include climate/infiltration, seepage, near field (NF), engineered barrier system (EBS), unsaturated zone (UZ), saturated zone (SZ), and biosphere. The important aspects of "proper management" of the TSPA calculation are transparency, traceability, and consistency. Traceability and transparency are intended to allow any individual to trace the TSPA results to the conceptual models and parameter values used in the calculation. The individual would also be able to trace the parameter values to their original sources. Consistency is intended to ensure that information used in more than one place in the analysis is conceptually consistent. For example, water chemistry affects two subsystem models: the near field and the unsaturated zone. If new information is introduced reading water chemistry, the corresponding input parameters in both subsystems should be changed accordingly.

To serve the above purposes of information management for IMARC, the ACCESS IMARC Information Management System (temporarily named as AIMS) has been developed. The system uses Microsoft ACCESS, which makes it easily available and easy to use. The other advantage is that ACCESS can interchange spreadsheets with Excel, which allows importation of IMARC results into AIMS.

9.2.2 AIMS Structure

AIMS consists of the information container and user interface shell. The procedures, a series of Visual Basic program commands, serve as links and communications between the information and the user interface at the user's discretion, as shown in Figure 9-1.

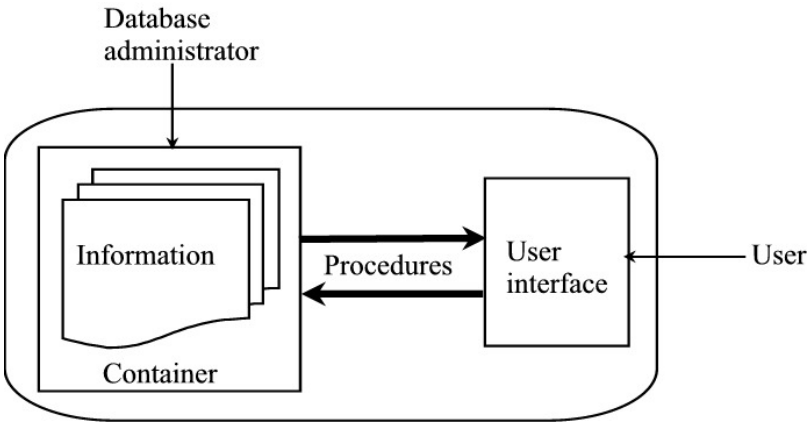

Figure 9-1
AIMS structure.

The Information Container contains all the information necessary to IMARC including value, unit, subsystem, sources, date (of entering the system), person (who entered the information), and IMARC number. The IMARC number is a unique IMARC run number that links the parameters to a specific IMARC calculation, as well as input files used in and output files from the calculation.

The information includes input parameters, output results, and conceptual model description. The type of information can be fixed single-value or tabulated tables, uncertain parameter with low, mean, and high values and their corresponding probabilities, files, words, and graphics. The information will be grouped into tables. These tables look similar to spreadsheets in Excel but have a lot of functions for linking, tracing, and querying data. A few examples will be given below.

Table 9-2 gives an example of uncertain parameters, which, in this case, is alteration time. Note that the "Source" information shown in the following tables are abbreviated reference. The actual reference in the actual database is complete. For example, "EPRI (1998) TR-1011813" shown in Table 1 is actually "EPRI (1998) Alternative Approaches to Assessing the Performance and Suitability of Yucca Mountain for Spent Fuel Disposal: Phase 4, TR-108732" in the database.

Table 9-3 is an example of information of tabulated data with graphics that are stored in Excel files. The "value" of "Filename" column is the hyperlink to the file in the disk. Table 9-4 is an example of information of tabulated table, which, in this case, is the climate information containing sequence, climate description, and duration. Table 9-5 is an example of fixed parameters.

Table 9-2
Alteration Times

Unit	Low	P_{low}*	Medium	P_{med}*	High	P_{high}*	Subsysten	IMARC Number	Note	Source	Date	Person
years	3000	0.05	1000	0.9	5000	0.05	NF	1		EPRI(1998) TR-108732	7/24/07	W. Zhou

*"P_{low}", "P_{med}", and "P_{high}" denote probabilities for low, medium, and high values.

Table 9-3
Characteristic Curves

Material	Filename	Sub-system	IMARC Number	Note	Source	Date	Person
Ch1VI	CHnv_Curve.xls	UZ	1		EPRI (2005) TR-1011813	7/24/07	W. Zhou
Ch2 Ze	CHnz_Curve.xls	UZ	1		EPRI (2005) TR-1011813	7/24/07	W. Zhou
TSw35	TSw_Curve.xls	UZ	1		EPRI (2005) TR-1011813	7/24/07	W. Zhou
TSw38	TSv_Curve.xls	UZ	1		EPRI (2005) TR-1011813	7/24/07	W. Zhou

Table 9-4
Climate Parameters

Sequence	Climate	Duration [y]	Sub-system	IMARC Number	Note	Source	Date	Person
1	Greenhouse	1000	climate	1		EPRI (2005) TR-1011813	7/24/07	W. Zhou
2	Interglacial	1000	climate	1		EPRI (2005) TR-1011813	7/24/07	W. Zhou
3	Full glacial maximum	998000	climate	1		EPRI (2005) TR-1011813	7/24/07	W. Zhou

Table 9-5
Density Parameters

Material	Unit	Value	Sub-system	IMARC Number	Note	Source	Date	Person
Alluvium	kg/m^3	1910	SZ	1		EPRI (2002) TR-1003031	7/24/07	W. Zhou
Bf	kg/m^3	2040	SZ	1		EPRI (2002) TR-1003031	7/24/07	W. Zhou
Ch1 VI	kg/m^3	1737	UZ	1		EPRI (1998) TR-108732	7/24/07	W. Zhou
Ch2 Ze	kg/m^3	1746	UZ	1		EPRI (1998) TR-108732	7/24/07	W. Zhou
Corrosion product	kg/m^3	5240	NF	1	assume Fe_2O_3	DOE (2001) TDR-MGR-MG-000007	7/24/07	W. Zhou
Invert	kg/m^3	2250	NF	1		EPRI (2002) TR-1003031	7/24/07	W. Zhou
NF rock	kg/m^3	2250	NF	1		EPRI (2002) TR-1003031	7/24/07	W. Zhou
TSw35	kg/m^3	2247	UZ	1		EPRI (1998) TR-108732	7/24/07	W. Zhou
TSw38	kg/m^3	2308	UZ	1		EPRI (1998) TR-108732	7/24/07	W. Zhou
Waste	kg/m^3	5240	NF	1	compart ment model	EPRI (2002) TR-1003031	7/24/07	W. Zhou

Each column represents a unique property of the information. The combination of these properties defines a unique record of the information. These properties are the basis for building functions such as querying, tracking, relating, etc.

On the other hand, categorizing information in the way shown in above table examples help ensure the consistency of the information. For example, the "NF rock" and "TSw35" densities are used in different subsystem models but their values should be, at least, similar. Any differences that cannot be comprehended would indicate potential errors and deem a scrutiny.

Figure 9-2 displays all the primary tables in the database. Each box represents a table. Each line of word(s) in a table represents a column that is a property of the information contained in the table. It can be seen that there are common properties in all tables: "IMARC_No" (*i.e.*, IMARC Run Number), "Subsystem", "Note", "Source", "Date", and "Person". These are properties for quality assurance purposes. There are also common properties such as "Nuclide", "Element", and "Subsystem", etc that link the different tables so that the information is traceable and consistent.

An important table "IMARC Runs" shown in Figure 9-2 records each IMARC calculation that is defined by the "Phase" (*i.e.*, the phase number: *e.g.*, "Phase 9" or "Phase 9a". The latter denotes a small deviation from "Phase 9"), the "Purpose" (*e.g.*, sensitivity analysis, new parameters, …), the "Scenario" (*e.g.*, nominal), etc. This table is linked with another two tables through the IMARC Number: "IMARC Input" and "IMARC Output". The latter two tables link the input files used in, and the output files generated from, the given IMARC calculation to the database. All the parameter values used in the given IMARC calculation are also linked through the IMARC Number. Furthermore, the table "IMARC Runs" also links with the "Model" table that contains conceptual model description for each subsystem.

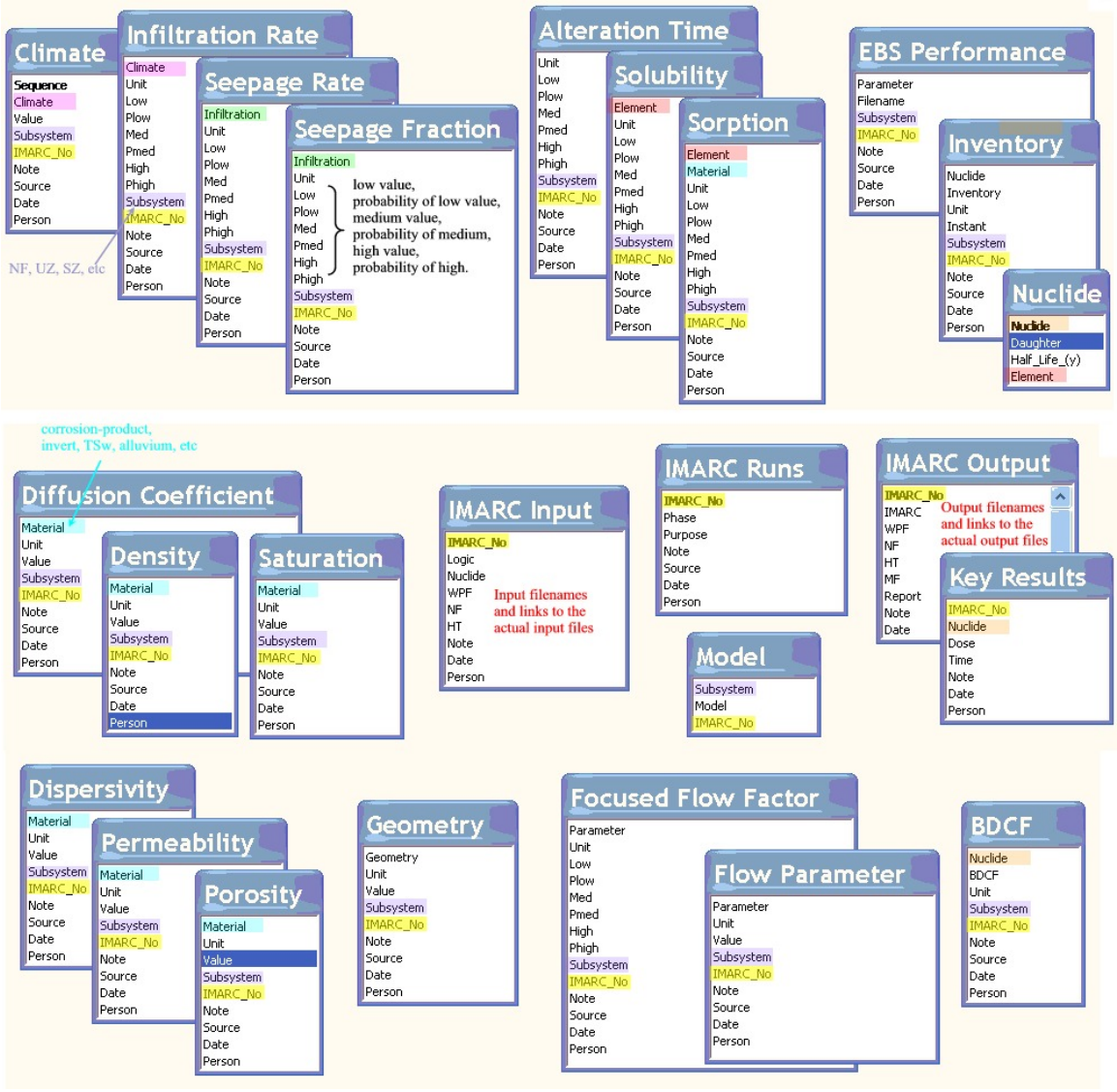

Figure 9-2
Primary information tables in AIMS. The colored properties are common properties that link information in different tables.

9.2.3 AIMS Functions

The structure described above is the basis for the database functionality. When opening AIMS, the main window shows up (Figure 9.3). This window displays the two main functions provided by AIMS. These functions reflect the user requirements that have been identified up to date. The users may be EPRI IMARC team members or independent reviewers. Two major functionalities in the current version of AIMS are:

- Review of previous IMARC calculations and
- Launch new IMARC calculations.

The first function requires traceability from the results to the models and parameter values. The second function provides a QA guidance to the user who wish to launch a new IMARC calculation, thereby reducing human errors. Both functions will be described below in details.

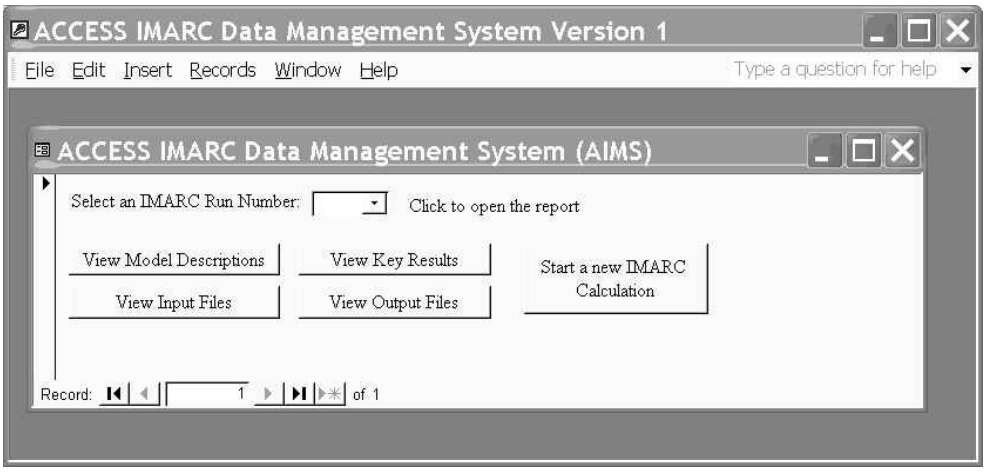

Figure 9-3
The main window shown after AIMS is launched.

9.2.3.1 Review of Previous IMARC Calculations

This function is designed to fulfill requirements by users who wish to inspect previous IMARC calculations. The information includes

- Key results
- Conceptual models (descriptions and major assumptions)
- Parameter values

The information trail provided by the current version of AIMS is illustrated in Figure 9-4. As shown in Figure. 9-4, once the user select a previous IMARC run, the user has four trails to review the information that has been related to the calculation:

- Check the input and main output files;
- Read the detailed report;
- Follow the trail of a given subsystem: conceptual model and the parameters used;
- Follow the trail of a given nuclide: the peak dose and time as well as all the parameters related to the given nuclide/ radio-element.

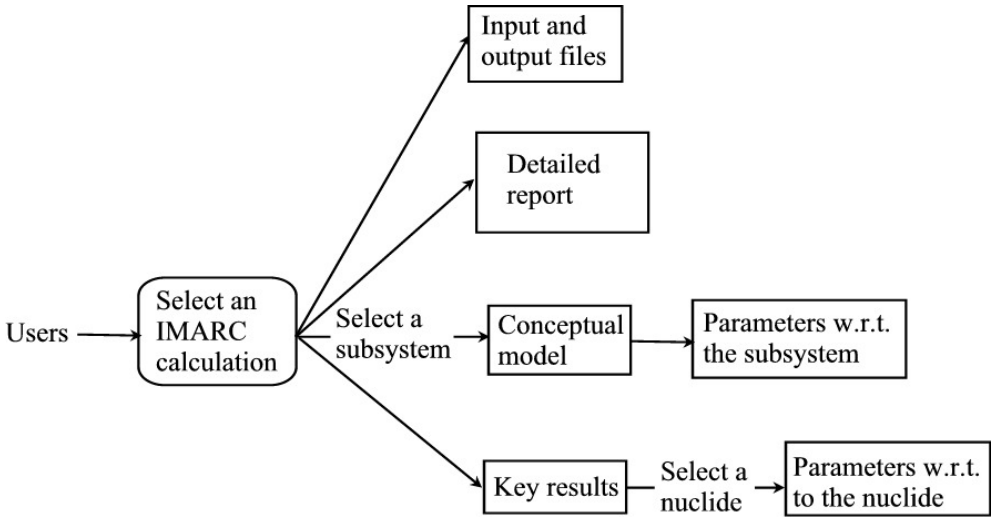

Figure 9-4
The four information trails provided by the current version of AIMS.

To use this function, the user must first select an IMARC run from the list box shown in Figure 9-3. The selection prompts a summary report for the given calculation as shown in Figure 9-5. Meanwhile, the hyperlink to the detailed report shows up in the main window (Figure 9-5). Clicking the hyperlink, the user can open the detailed report in either Word or PDF format.

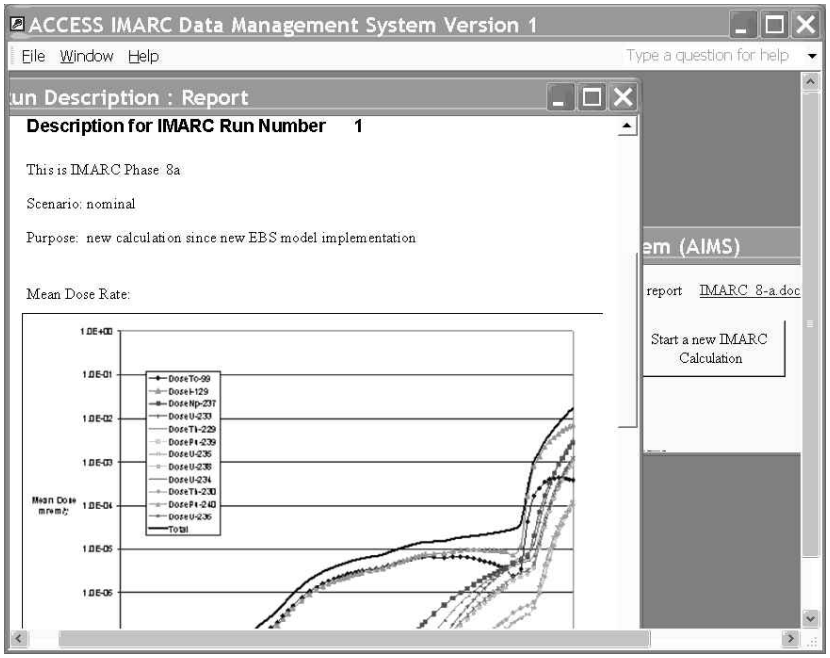

Figure 9-5
Summary report of a previous IMARC run prompted after selecting a run number from the list box. The hyperlink to the detailed report is also shown.

To view the input or output files directly, the user simply clicks "View Input Files" or "View Output Files" buttons shown in the main window (Figure 9-3).

To follow the subsystem model and parameter trail, the user clicks "View Model Description" button in the main window (Figure 9-3). This opens a window shown in Figure 9-6(a) where the subsystem and a brief conceptual model description are displayed. If clicking "View Parameters" button, all the parameter values related to the given subsystem are displayed in a new window shown in Figure 9-6(b). By navigating records at the left bottom of the "Models" window shown in Figure 9-6(a), the user can obtain the similar information for other subsystems. The subsystem example in Figure 9-6 is the Climate/Infiltration.

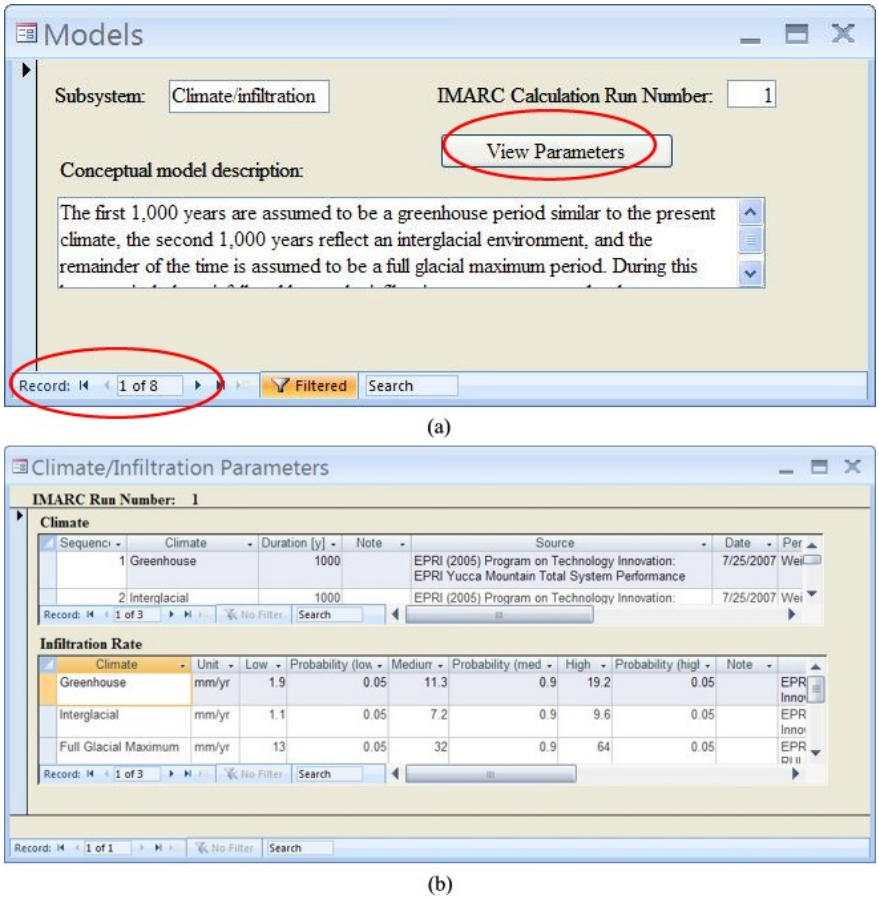

Figure 9-6
(a) The "Models" window displays the subsystem model assumptions.
(b) The subsystem parameter window displays all the parameter values related to the selected subsystem. AIMS These parameters are read-only.

To follow the key result to nuclide parameter information trail, the user must click the "View Key Results" button in the main window shown in Figure 9-3. Then, AIMS opens a window shown in Figure 9-7(a) that displays the peak dose and peak time for all nuclides. Below the dose results, there is a list box containing nuclides. By selecting a nuclide and then click "View Nuclide Parameters", AIMS opens a another window that displays all parameter values relevant to the selected nuclide shown in Figure 9-7(b). The example in Figure 9-7(b) is Np-237.

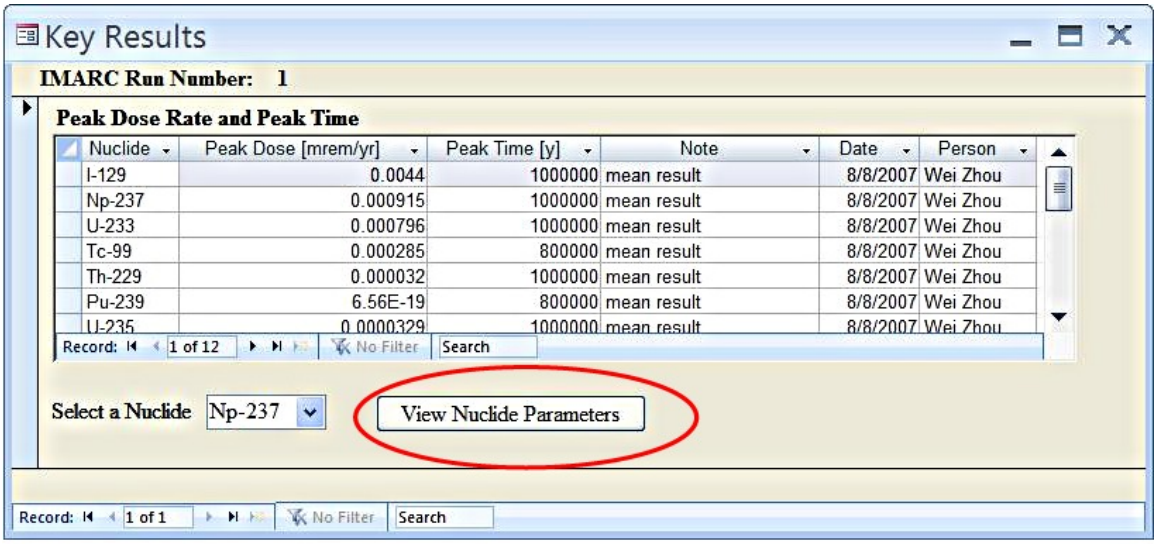

(a)

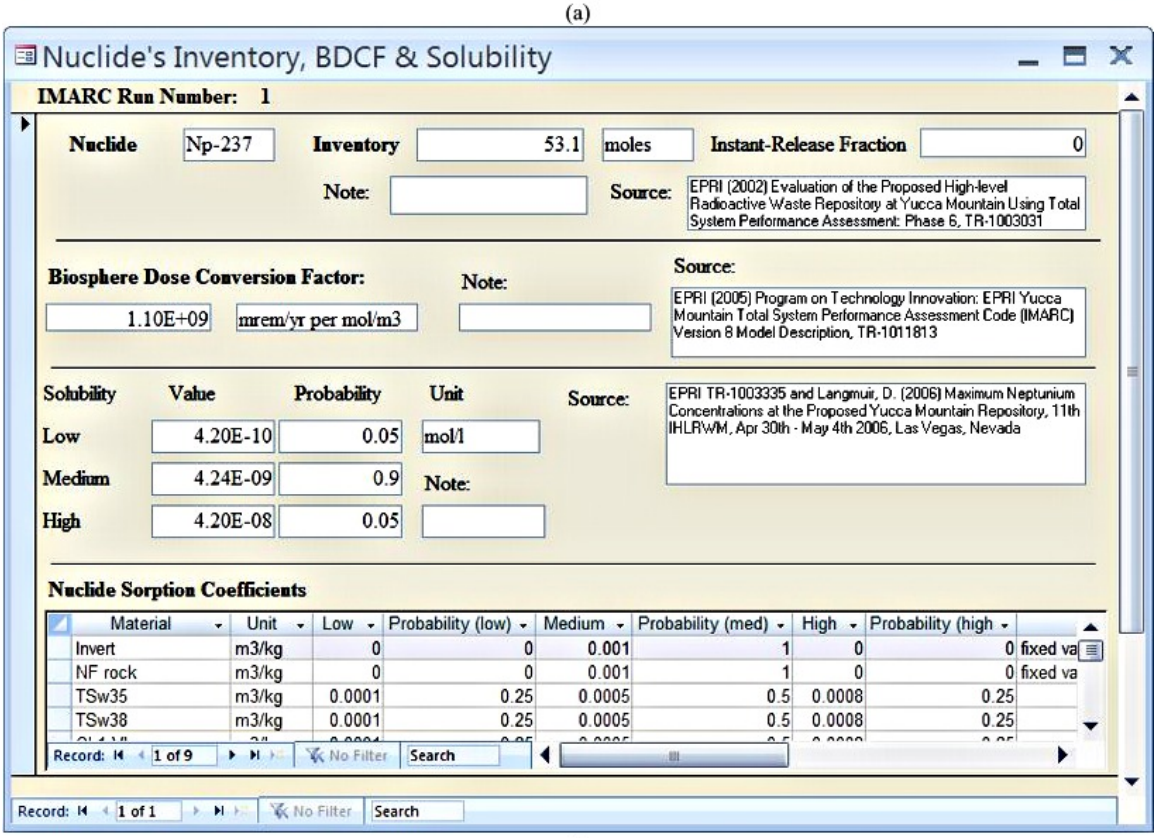

(b)

Figure 9-7
(a) The "Key Results" window displays peak doses and times for all nuclides.
(b) The nuclide information window displays all the necessary information related to the selected nuclide (Np-237 as an example).

9.2.3.2 Start a New IMARC Calculation

The second major function is designed for IMARC team members. The purpose is to minimize human errors while the user is conducting a new IMARC calculation. The built-in procedures guide the user with automated steps and document the process. Once the user chooses to generate a new calculation, AIMS automatically assigns a new IMARC run number. Afterwards, an interface will be prompted to guide the user going through eight steps as shown Figure 9-8. Each step, except for the first step, relies on the completion of the previous steps. The completed steps are documented such that the user may interrupt and then resume the process anytime. Each step will be explained as follows.

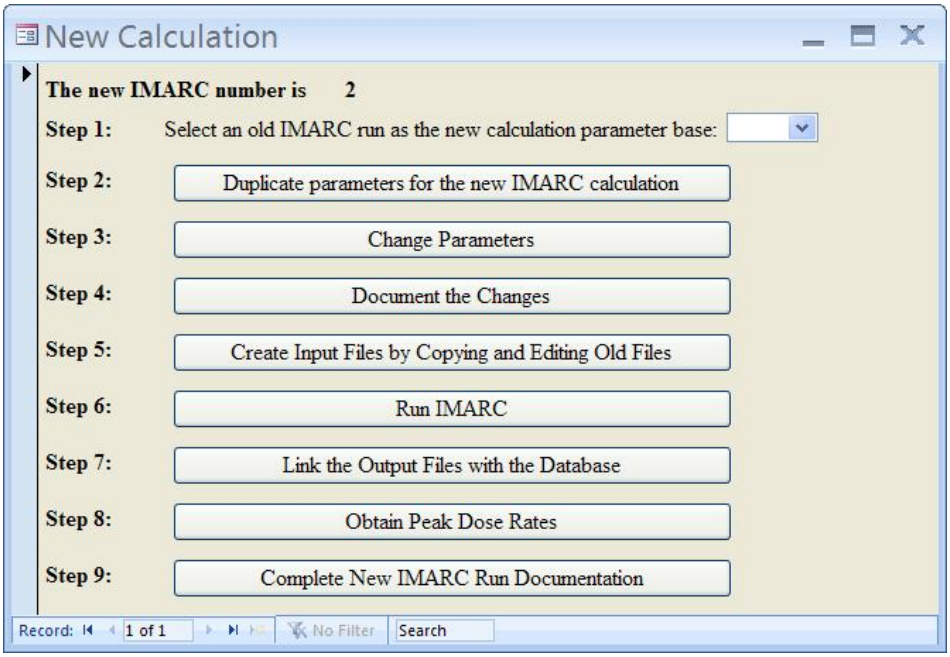

Figure 9-8
The "New Calculation" menu guides the user to conduct a new IMARC calculation.

Step 1: Select an old IMARC run number on which the new IMARC calculation will be based. Assuming most parameter values and conceptual models remain the same as one of the previous IMARC calculations, the user would wish to change one or more parameters for various purposes such as sensitivity analysis, implement new information, etc. Without selecting an old IMARC run, the user will not be allowed to go to the next step.

Step 2: Duplicate the information (*i.e.*, parameters and model descriptions) in the database and assign the new IMARC number for each piece of information. In this way, all the parameters for the new calculation have been registered in the database. The user will be informed when the duplication is completed.

Step 3: Enter the new parameter values and/or information by modifying the duplicated parameters. The user has choices to modify one or all the information relevant to the new IMARC calculation. By clicking this button, AIMS opens a new window that allows the user to

modify one or all parameters/information by clicking a button shown in the window (Figure 9-9(a)). Figure 9-9(b) shows an example of modifying alteration time. Before these modification windows open, AIMS will ask for the user's name and register the date of the change. After modification of parameters, AIMS will remind the user to provide the source for the new information. AIMS will also automatically put the user's name and the date to the new information record. Note that it is the user's responsibility to enter the valid name and source.

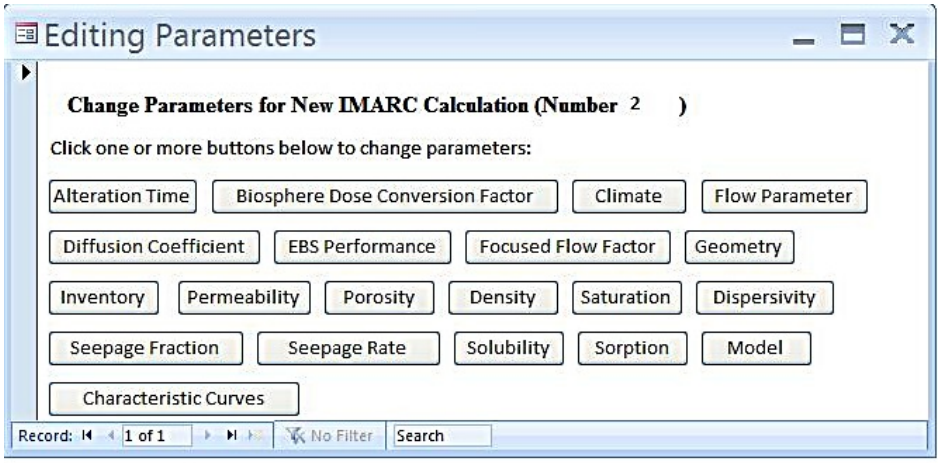

(a)

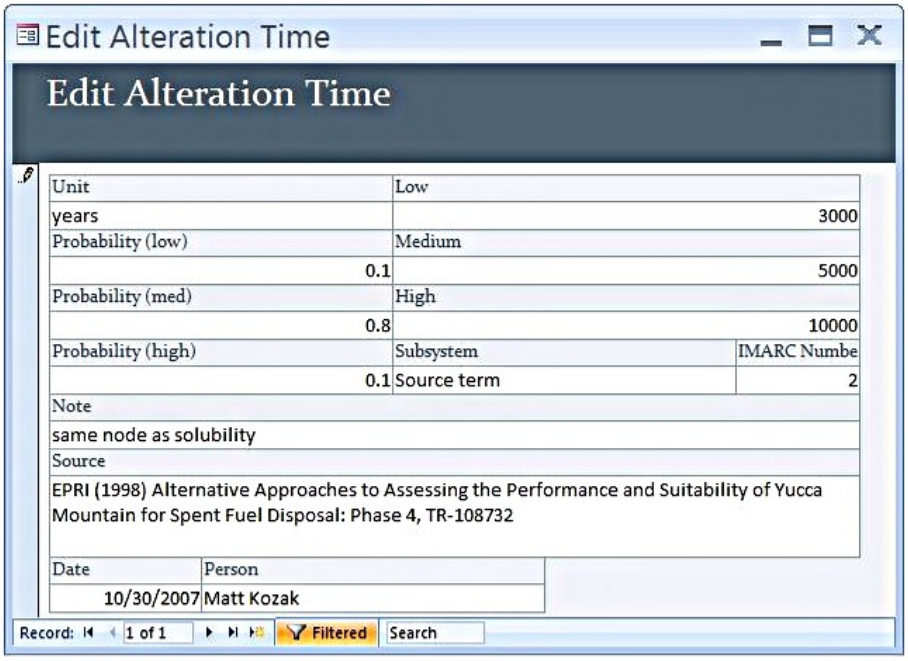

(b)

Figure 9-9
Step 3: (a) The menu allows the user to modify any parameters. (b) A parameter modification example: modifying alteration time.

Step 4: After completing parameter/information modification, the user must document the changes by clicking the Step 4 button. AIMS will then scan the changes by comparing the data for the new IMARC run with the previous run that the new run is based on and document the changes in a text file. AIMS will show a hyperlink of the file as shown in Figure 9-10. By clicking the hyperlink, the file will be open and can be used to guide the modification of the input files.

Figure 9-10
The hyperlink of the file documenting the changes the user made for the new IMARC calculation (Step 4).

Step 5: After documenting the information modification, the user is ready to create the input files for the new IMARC calculation. The current version of AIMS does not provide the user interface for creating new input files. Instead, AIMS guides the user to create input files by copying and modifying the input files of the old IMARC run that the new run is based on. By clicking the button for Step 5, AIMS creates a subdirectory for the new IMARC calculation. Then, AIMS copies the old input files to the new subdirectory and rename the files with the new IMARC run number. To understand this process and also to maintain the database subdirectory, an example is shown in Figure 9-11.

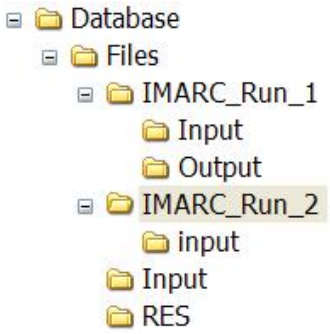

Figure 9-11
The layout of AIMS directory and subdirectories.

In Figure 9-11, the "\Database" directory is where AIMS resides. The "\Files" subdirectory contains the following directories and files:

- "IMARC_Run_1" is a directory storing an old IMARC calculation designated as the Run No.1. The "Input" and "Output" subdirectories store the input and output files, respectively, related to IMARC Run No.1.
- "IMARC_Run_2", in this example, is a new directory created for the new IMARC calculation designated to Run No.2. Its input files are copied from an old IMARC run (No.1 in this example) and are stored in the "Input" subdirectory. Because the Run No.2 has not completed in the example, there is no "Output" subdirectory.
- IMARC.exe is the executable code of IMARC.
- "\Input" is the directory storing IMARC input files that will be accessed by IMARC.exe during execution.
- "\RES" is the directory storing IMARC output files during IMARC.exe execution.

Note that all the files and directories should not be removed nor renamed.

After the input files are copied, AIMS opens a table that contains the hyperlinks to the files as shown in Figure 9-12. The user can then open these files and make changes as necessary.

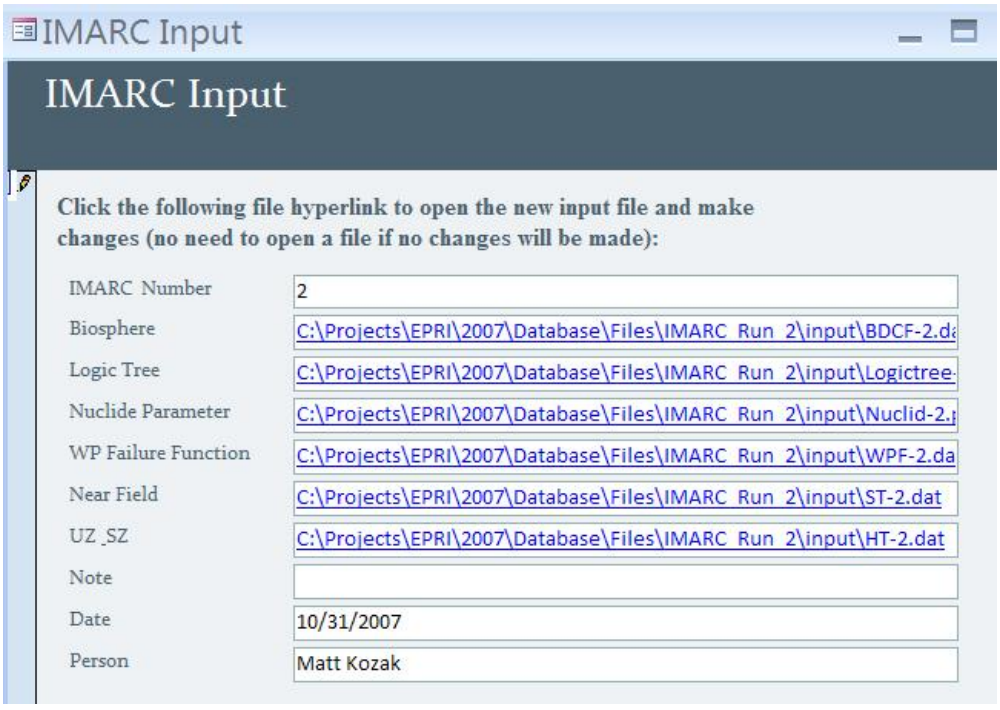

Figure 9-12
The AIMS window shows the hyperlinks to the input files. By clicking a link, the input file will be open and ready for modifications (Step 5).

Figure 9-12 shows that six input files are specific for a given IMARC calculations:

- BDCF.dat: biosphere dose conversion factors
- LogicTree.IM3: logic tree information
- Nuclid.Par: sorption and solubility data
- WPF.dat: distributed waste canister failure
- St.dat: source-term data
- Ht.dat: UZ and SA flow and transport data.

Note that the filenames shown in Figure 9-12 all have the Run Number attached for QA purposes. It is user's responsibility to ensure the modified files are valid input files of IMARC. Other files that are read by IMARC are actually invariant to most IMARC runs and thus are saved in the "\Files\Input" all the time.

Step 6: Clicking this button, the user is first asked if ready for making IMARC calculation. By answering "yes", AIMS first copies all the input files from, for example, "…\Files\IMARC_RUN_2\Input" to "…\Files\Input" and rename them to those that IMARC can recognize (*i.e.*, without the Run Number). Then AIMS launches the IMARC calculation. During the calculation, a console window is shown that displays the calculation progress (Figure 9-13).

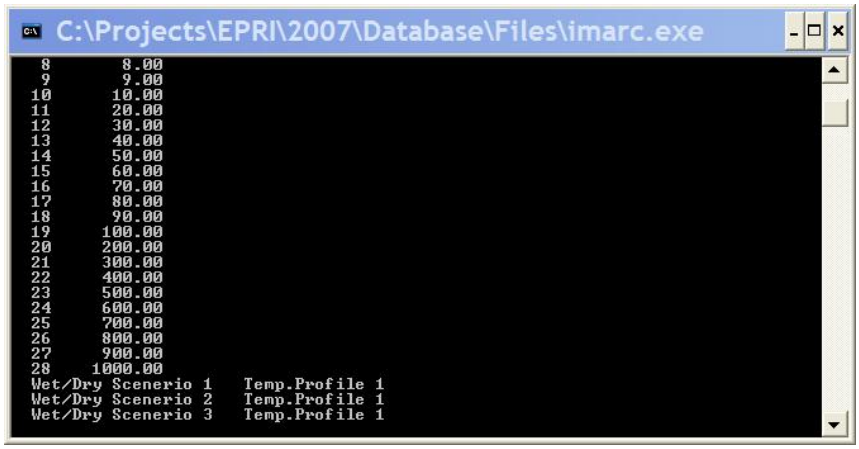

Figure 9-13
The PC console shows IMARC calculation progress (Step 6).

Step 7: After IMARC calculation is completed, the user must copy the major output files from "…\Files\RES" directory into the directory designated for this calculation (the "…\IMARC_Run_2\Output" directory in the example shown in Figure 9-11 and Figure 9-12) and link the files to the database by clicking Step 7 button. Afterwards, the output file hyperlinks are displayed as shown in Figure 9.14. The user can click the link to view the files. It can be seen that two major output files that are saved with the database are IMARC-2.out and Dose-2.out. Note that "IMARC-2.out" is the copy of "IMARC.out" and "Dose-2.out" is the copy of "IMARC_epadose.out" in the "…\Files\RES", respectively. Other output files will not be linked with the database due large volume with relatively less useful information and will be overwritten once a new IMARC calculation is launched. However, by preserving all the input files for this IMARC run, these output files can be recreated at anytime if necessary.

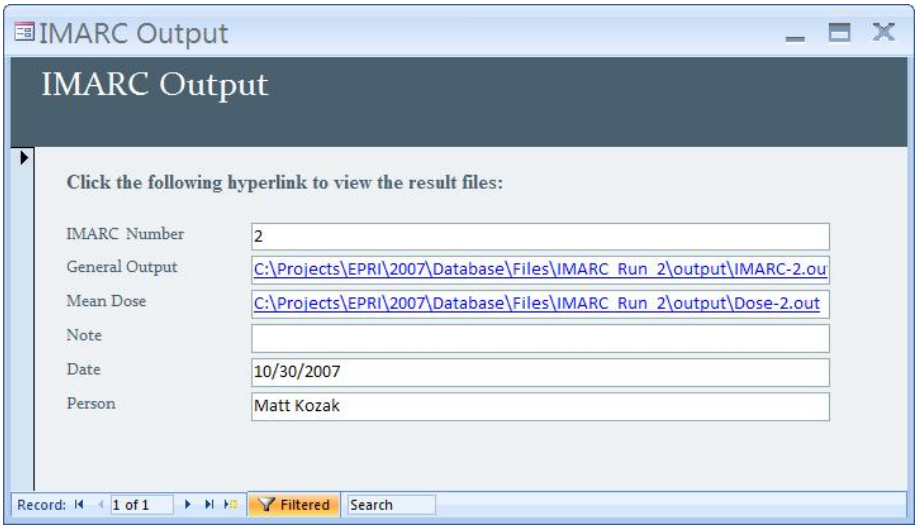

Figure 9-14
The AIMS window shows the IMARC output file hyperlinks for the IMARC calculation just completed.

Step 8: The key information from any IMARC calculations is the peak dose the time for each nuclide. This information can be obtained by clicking Step 8 button. AIMS will calculate the peak dose and time for each nuclide from the dose file and put the results into the database. At the end of the operation, AIMS will open the table containing the results as shown in Figure 9-15.

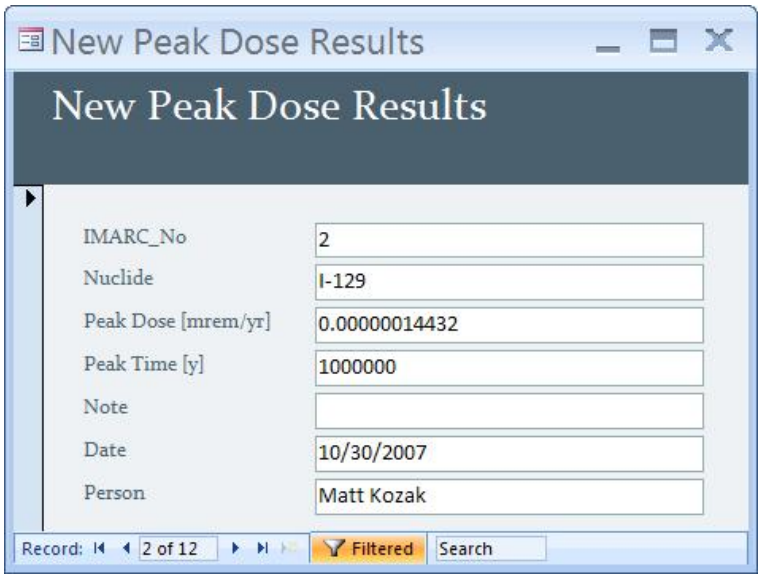

Figure 9-15
The AIMS window displays peak dose and time for a given nuclide (Step 8). The example shown in the figure is for I-129. The navigator at the bottom of the window allows the user to see the peak doses and times for other nuclides.

Step 9: This is the last step for completing the documentation of a new IMARC run. By clicking this button, a window shown in Figure 9-16 is open and allows the user to enter the necessary information. The user does not have to complete this form in one session and AIMS will remind the user about the unfinished tasks. After all the necessary information is entered, AIMS will regard the documentation completed, which means that this IMARC run can be available for inspection by any individuals and the new run will be allowed.

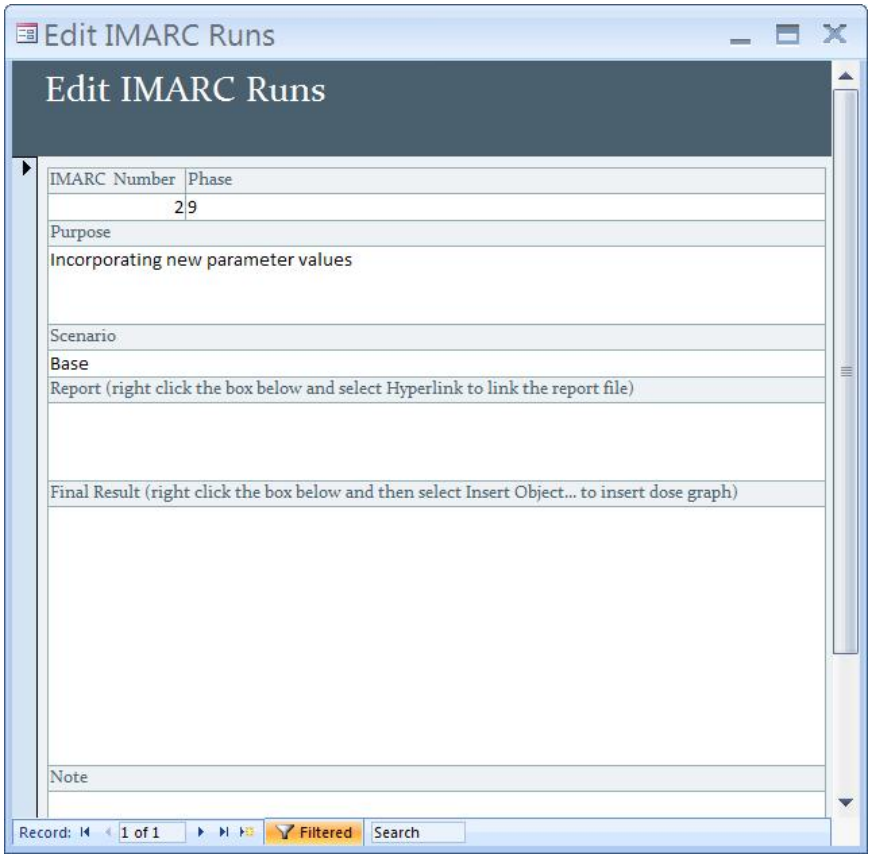

Figure 9-16
The final documentation window for the new IMARC calculation (Step 9).

9.2.4 Summary

AIMS is the information management system for IMARC modeling and calculation. AIMS currently provides two user functions: information inspection for previously completed IMARC calculations and QA documentation for a new IMARC calculation. The structure of AIMS is tailored to the current event-tree approach and the current IMARC code structure. Implementation of AIMS is intended to improve the tracebility, transparency, and consistency of IMARC analyses, and to ensure that future developments of IMARC are conducted according to these improved standards.

9.3 Documentation of IMARC Phases

The third element in quality assurance of IMARC has been complete documentation and version control of each phase of the development of the code, as well as reports of topical interest, publications in journals, and conference presentations that have drawn on IMARC for results. A complete description of the development of IMARC, as well as a summary of key elements of each phase of IMARC development as described in the various IMARC reports, is presented in Appendix A. It is necessary to consider each stage of IMARC development in the context of the time of its development, since over time understanding of the repository has changed, and the design has evolved.

In addition, IMARC has been used to support a number of EPRI reports of topical interest (see, *e.g.* EPRI, 2004a, 2005a,d, 2006b,c, 2008a). Within these reports lies additional support for the capabilities of IMARC. Furthermore, in these topical reports are additional comparisons between the consideration of FEPs in IMARC and those implemented by DOE and NRC. The complexity and diversity of the topics addressed in these reports makes it difficult to easily discuss, in a summary fashion, their impact on IMARC quality assurance. However, in all cases there has been a clear understanding by the EPRI project team of the IMARC analysis, and the alternative viewpoints held by DOE or NRC. In all cases the reasons for differences between the analyses were understood and justified, and those differences assisted in producing insight into the potential performance of the Yucca Mountain repository.

9.4 Independent Peer Review

An independent peer review of IMARC 9 was commissioned in 2007 by EPRI to help substantiate the quality of the software and its documentation. The peer review was conducted by an international review team of acknowledged subject matter experts (EPRI, 2009). The primary objective of the review team was to review and critically analyze the TSPA methodology and rationale used in the development of IMARC 9 including its sub-models, in view of current scientific knowledge and understanding. Additional objectives were:

- to comment on the adequacy of the IMARC 9 methodology for supporting *EPRI's* objective of developing an independent code for gaining risk-informed insight into major features, events and processes associated with the YM TSPA;
- to provide recommendations for specific improvements that would help IMARC's continued role in evaluating issues and sensitivities associated with the YM TSPA.

The review team concluded that IMARC is "fit for purpose" in the sense that it provides a risk-based methodology for integrating information from various disciplines affecting long-term repository performance and focuses on reasonable expectation of the dose consequence to the RMEI. He review team also concluded that "IMARC 9 is a very well integrated model which focuses on those processes which could affect the long-term performance of the repository."

The review team also provided a number of comments and suggestions for improvement of IMARC, its technical basis, and its documentation. Each of the comments made by the review team has been addressed in developing IMARC 10 and its documentation. A summary table describing how each comment has been addressed is presented in Appendix G.

In addition to the formal, comprehensive peer-review provided in the 2007 – 2008 IRT activity, IMARC analyses and approaches have been subjected to independent peer-review throughout the two decade period of development through internal reviews, publications in peer-reviewed journals, presentations at technical conferences, and invited presentations at meetings of the Nuclear Waste Technical Review Board (NWTRB) and Advisory Committee on Nuclear Waste and Materials (ACNW&M).

9.5 Comparison of IMARC with Other TSPA Analyses

The fourth element of quality assurance of IMARC has always been close consideration of the IMARC results with the results by other interested parties, most prominently DOE and NRC. As IMARC has evolved through the years (see Appendix A), developments have always been driven by the need to produce insights with respect to the current understanding of the repository and its design.

At all stages of the development of IMARC, there has been good qualitative agreement between DOE TSPA results and those of IMARC. That is, the analyses have shown that similar FEPs have driven the performance of the repository, the timing of peak doses and the dominant radionuclides have been consistent, and risk-informed insights have been similar. Differences between the analyses have been driven by differences in details of how FEPs have been represented. In particular, IMARC has long striven to embody the philosophy of reasonable expectation, as it is defined in 40 CFR 197. This has often led to a less conservative representation of FEPs than has been implemented by DOE. In all cases, when differences between EPRI and DOE TSPAs have existed over the years, there have been clear reasons for the differences.

The most direct and recent comparison between DOE and EPRI TSPAs was documented by DOE/OCRWM (2008a). In that report, DOE compared IMARC 8 (EPRI, 2005c) to a simplified TSPA approach that was used as a confidence-building measure for their own TSPA. The report noted that

> "The mean annual dose history curves for TSPA-LA Model and IMARC show a similar trend in the dose histories, with a significant increase in dose to the RMEI after about 100,000 years."

and

> "Overall, the EPRI TSPA Analysis accounts for the same model components and considers the same FEPs as the TSPA-LA Model. The EPRI model implementation is a more simplified abstraction of the relevant processes and uncertainty in model parameters."

With respect to IMARC, DOE/OCRWM (2008a) concluded that

> "In general, the main features of the dose release curves for the nominal scenario compare reasonably well with the TSPA-LA Model. The differences can be related mostly to differences in seepage and in different implementation of the inventory and EBS failure characteristics. This is primarily due to the fact that the EPRI TSPA did not use the most recent analysis and/or model report results."

As has been discussed in Appendix A, it has not been uncommon for IMARC parameters and inputs to be based on prior information compared to contemporary DOE analyses, since the EPRI team has to wait for the publication of DOE results before implementation in IMARC.

IMARC 10, however, benefits from the DOE submission of its Yucca Mountain license application and supporting documentation in 2008. Specific exceptions are identified in Chapter 10, where information from IMARC 9 analyses has been used in conjunction with IMARC 10 to conduct specific analyses. In particular, resource constraints precluded updating of failure functions associated with rockfall and seismic activity for the new TAD design, and as a result earlier results are used to augment the IMARC 10 technical basis.

9.6 Quality Assurance Summary

The quality assurance of IMARC rests on five main elements:

- Testing, verification, and benchmarking of components of IMARC,
- Ensuring traceability of results,
- Documentation of each stage of development of IMARC,
- Independent peer review, and
- Comparison of IMARC with other TSPA analyses of Yucca Mountain.

In this chapter, a summary has been provided of information available for each of these elements. As a result of this body of information, EPRI concludes that there is a high degree of confidence in IMARC, its results, and its credibility in assisting to develop insights into the performance of the Yucca Mountain repository.

10
IMARC 10 RESULTS AND ANALYSIS

10.1 Nominal Scenario

Results have been calculated using IMARC 10 for the "nominal scenario", which excludes all disruptive events such as volcanism and seismic activity and rockfall. The nominal scenario results presented in Figure 10-1a on a log-log scale and Figure 10-1b on a log-linear scale. IMARC analyses over the years have typically been presented on log-log plots, and Figure 10-1a facilitates comparisons with older versions of IMARC. DOE results in the license application have been presented on log-linear scales, and Figure 10-1b is presented to facilitate comparisons with those results. The input files associated with this analysis are documented in Appendix F. The assumption of a juvenile failure from manufacturing defects leads to an initial early (10,000 years to 100,000 years) dose, mainly associated with ^{99}Tc and ^{129}I. The peak dose occurs at 10^6 years, and the peak dose contributors are ^{129}I and the ^{237}Np chain.

The IMARC 10 results are similar to IMARC 9 results. The revised radionuclide inventory has not altered the key dose contributors as the re-introduced radionuclides (notably Pu-242 and Ra-226) are not significant for RMEI dose. In general, understanding of the Yucca Mountain disposal system appears to be converging, and any updates to the TSPA analysis are incremental.

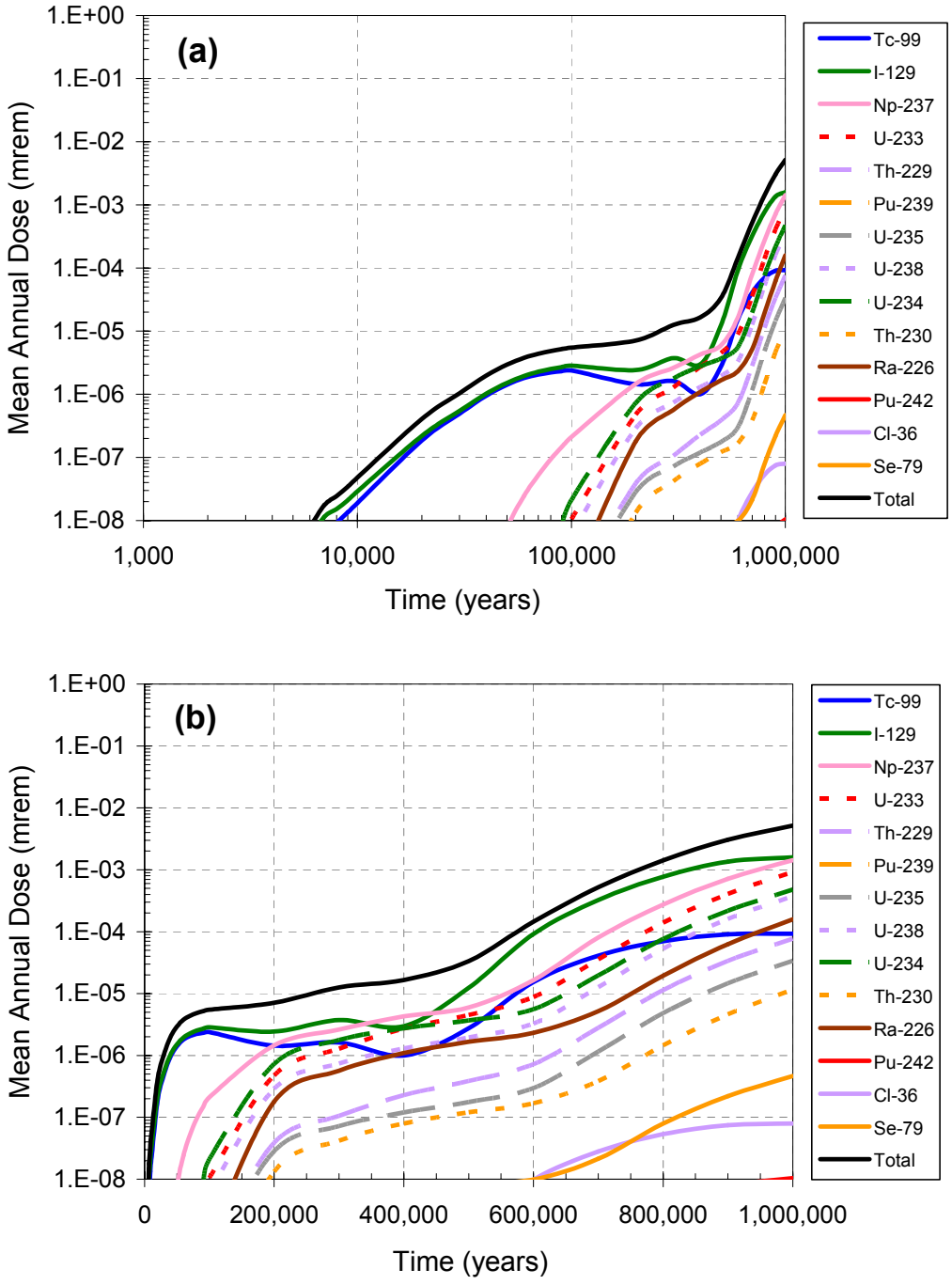

Figure 10-1
IMARC 10 results for the nominal scenario presented on (a) log-log and (b) log-linear scales.

10.2 Nominal plus Seismic Scenario

Results have been calculated using IMARC 10 for the nominal plus seismic scenario. As discussed in EPRI (2006c), a reasonable expectation case for this scenario is to represent the seismic behavior as a series of seismic events with peak ground velocity (PGV) of 0.75 m/s. The analysis presented in this section is therefore comparable to the results presented in EPRI (2006c). For the current analysis, an update to the seismic damage analysis is necessary, owing to the update in the TAD waste package design, and specifically to the increase in the alloy C-22 overpack thickness from 20 mm to 25 mm.

The analysis presented in EPRI (2006c) was based on a detailed analysis of the effect of dynamic and static rockfall on the thinner overpack design. It has not been possible to reproduce that exact analysis for the TAD design during 2008 due to limited resources. As a result, the following composite analysis is performed. The IMARC 10 corrosion failure (based on the new TAD design) has been superposed with the seismic effects on the old disposal-only waste package design to produce an effective failure curve for the combination of corrosion and seismic effects on the waste package. Since the seismic failure function is based on the earlier, less robust design, the overall failure function is conservative compared to a fully updated analysis. The results of this analysis are depicted in Figure 10-2. As noted by EPRI (2006c), this failure function represents conditions in which “A total of 64 waste packages are predicted to fail as a result of the repeated seismic events, 18 as a result of dynamic rock impacts and 46 as a result of seismic-induced SCC of the outer barrier due to a static load >10 m in height. All of these failures are predicted to occur during the first seven seismic events, with no further drift degradation predicted after 650,000 yrs.” EPRI (2006c) noted a number of conservatisms in this analysis, which led to the conclusion that the estimates of the number of failed waste packages produced by this analysis is conservative.

As seen in Figure 10-2, the cumulative probability of waste package failure in the first 1,000,000 years is approximately 15%. This value is contrasted with a mean cumulative failure rate of about 54% for the nominal scenario class in the TSPA-LA (contrast Figure 10-2 with Figure 7.7.3-2 of DOE/OCRWM, 2008a). However, the TSPA-LA failure curves include both CSNF and co-disposal waste packages, while the IMARC curves only include CSNF waste packages. Since the co-disposal waste packages fail at a more rapid rate than CSNF waste packages (DOE/OCRWM, 2008a, page 7.7.1-15 states that all co-disposal waste packages fail around 24,000 years), the two failure functions are more similar than they appear from a casual comparison. The co-disposal waste packages constitute 28% of the total number of waste packages, so the IMARC analysis represents a mean cumulative failure of CSNF waste packages at 1,000,000 years about 11% lower than the TSPA-LA.

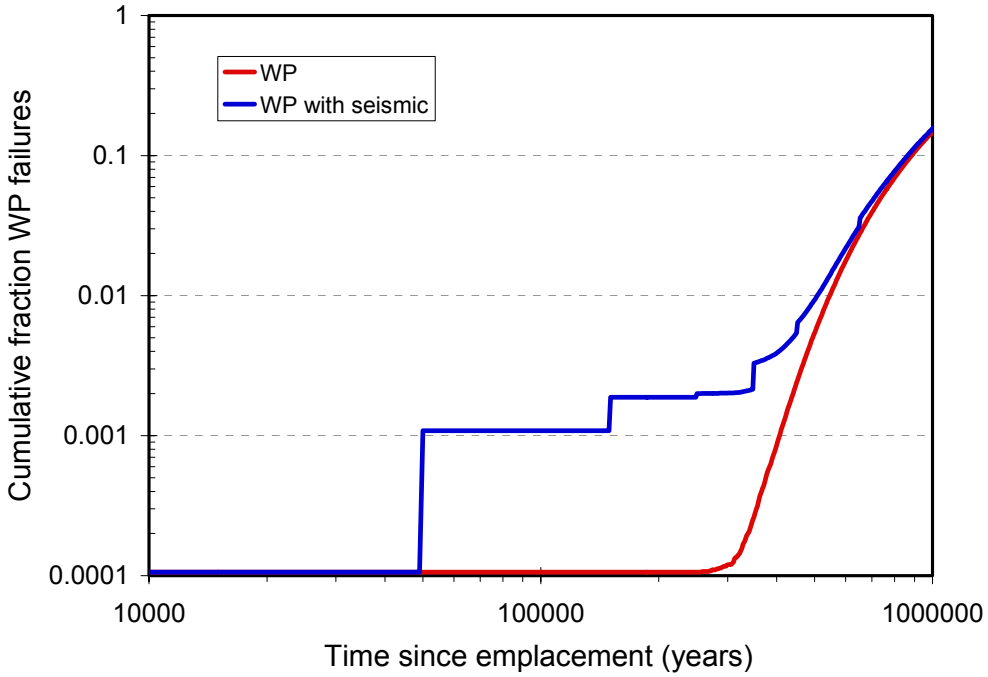

Figure 10-2
IMARC 10 nominal and nominal plus seismic waste package failure curves for the prior Yucca Mountain "disposal-only" waste package design.

IMARC 10 results from this analysis are shown in Figure 10-3a and 10-3b on log-log and log-linear scales, respectively. As in the case of the nominal scenario, the two graphs are intended to facilitate comparisons with past IMARC analyses and current DOE analyses.

The initial seismic event is assumed to occur at 50,000 years, consistent with the return period for the Solitario Canyon fault (EPRI, 2006c). During this event, all of the drip shields and approximately 0.001 of the waste packages are calculated to fail. Subsequent events produce progressively smaller fractional failures as more of the packages are buried under rockfall, which provides protection from waste package-to-waste package collisions. These additional early failures produce a higher dose for times less than 10^5 years than the nominal scenario, and produce a bump in the dose curve that peaks at about 10^5 years. These results are similar to and consistent with prior results using IMARC 10.

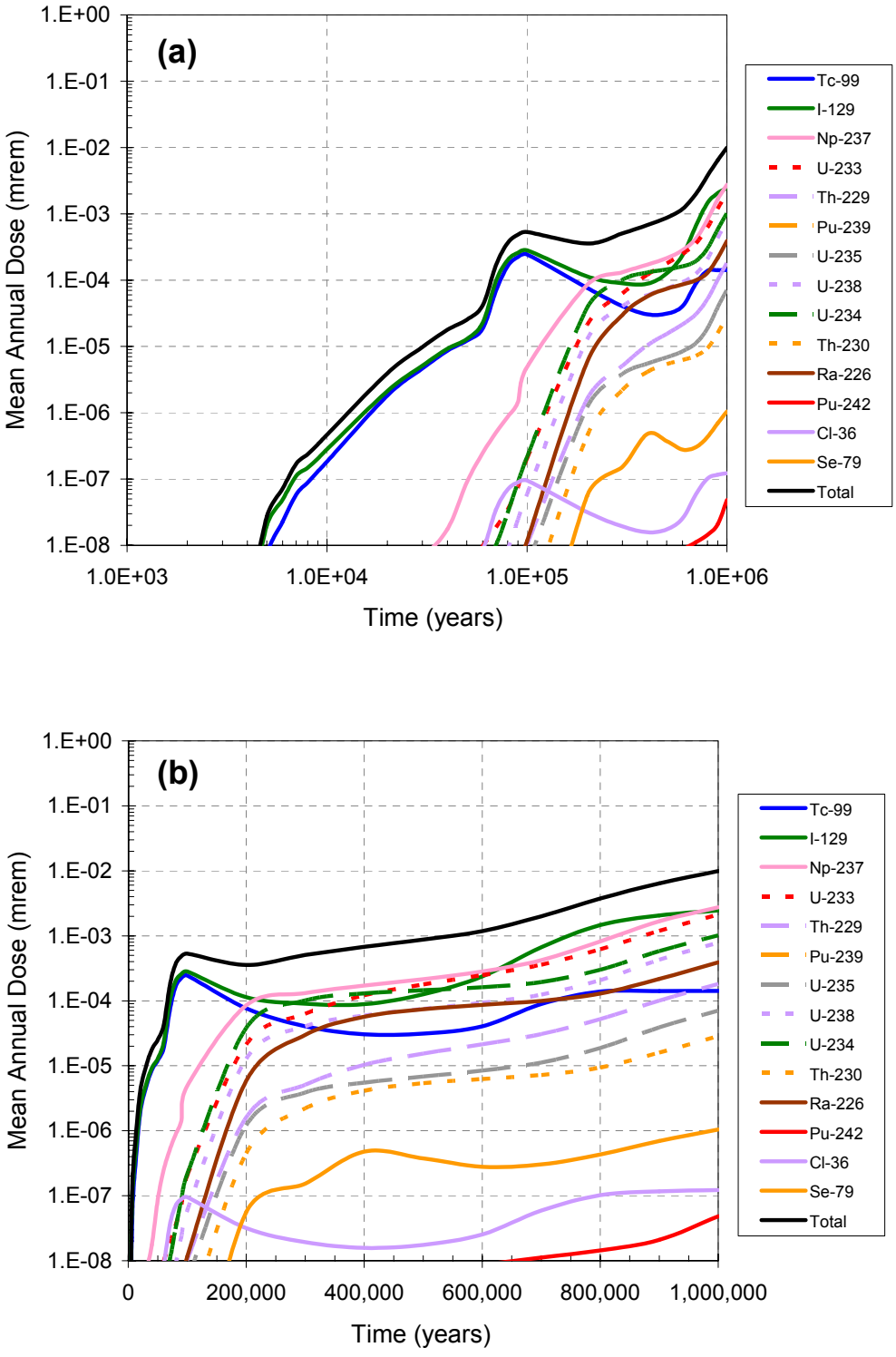

Figure 10-3
IMARC 10 results for the nominal plus seismic scenario presented on (a) log-log scale and (b) log-linear scales.

10.3 Sensitivity Calculations

10.3.1 Effect of Probability Distributions

One of the recommendations of the IRT peer-review (EPRI, 2009) was to explore how sensitive the IMARC results are to the selected probabilities of each branch. A set of sensitivity analyses has been conducted to examine the effect of the shape of the probability distributions used in IMARC. To conduct this analysis, different probabilities are assigned to the nodes of the IMARC event tree for each of the variables treated in the event tree. This analysis is equivalent to a one-parameter ("one off") sensitivity variation analysis.

The baseline probability values are presented in Table 10-1. Specific values for the parameters assigned these probability values are documented in the appropriate sections of this report.

The assignment of probabilities for the sensitivity analysis is shown in Table 10-1. The sensitivity analysis did not include infiltration rate, since the values and the shape of the distribution are established in 10 CFR 63. Results of this analysis are presented in Figure 10-4.

Table 10-1
IMARC 10 baseline values for the shape of the probabiity density function for each parameter.

Parameter	P(low)	P(mean)	P(high)
Infiltration Rate	0.05	0.90	0.05
Retardation	0.25	0.5	0.25
Seepage Fraction and Flow	0.0*	0.96	0.04
Focused Flow Factor	0.865	0.135	0.0
Alteration Rate and Solubility	0.05	0.90	0.05

*Set to zero as Seepage Fraction and Flow and Focused Flow Factor uncertainties are represented by just two branches.

Table 10-2
IMARC 10 sensitivity analysis runs for the effect of the shape of the probability density function.

Run	Parameter	P(low)	P(mean)	P(high)
1a	Retardation	0.90	0.05	0.05
1b	Retardation	0.05	0.05	0.90
2a	Seepage Fraction and Flow	0.0	0.90	0.10
2b	Seepage Fraction and Flow	0.0	0.99	0.01
3a	Focused Flow Factor	0.73	0.27	0.0
3b	Focused Flow Factor	0.9325	0.0675	0.0
4a	Alteration Rate and Solubility	0.90	0.05	0.05
4b	Alteration Rate and Solubility	0.05	0.05	0.90

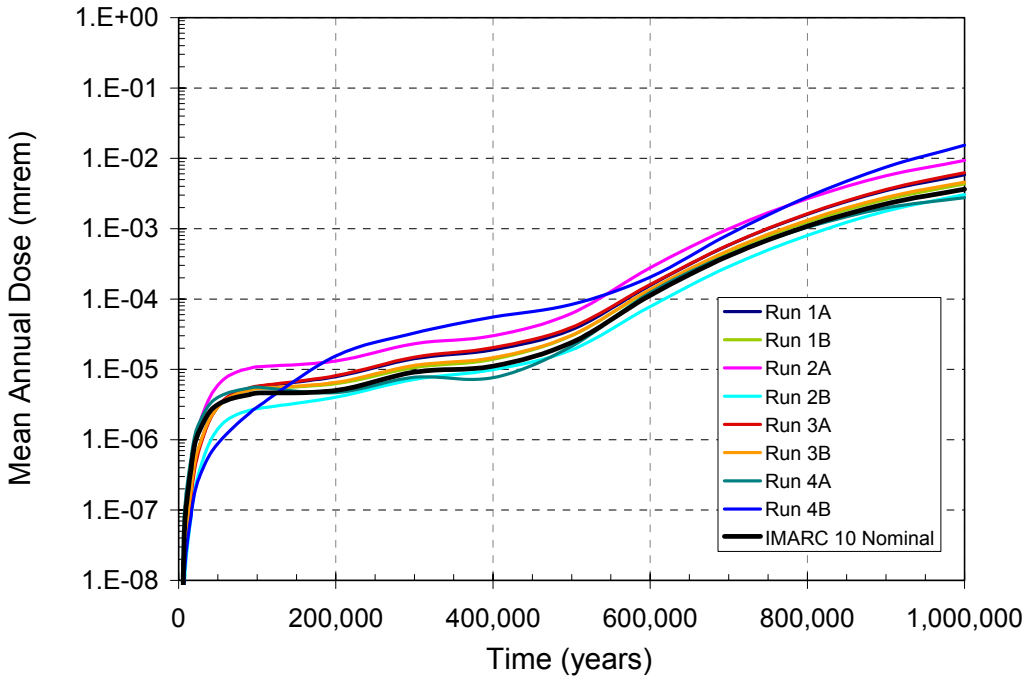

Figure 10-4
Results of the sensitivity analysis showing the effect of different probability weighting of the IMARC 10 event-tree branches.

The analyses that lead to the greatest increase in peak dose are runs 2a and 4b, corresponding to high seepage and to high alteration rate and solubility, respectively. Similarly, the greatest decrease in peak dose is the result of runs 2b and 4a, corresponding to low seepage and low

alteration rate and solubility. The variations in retardation and in flow focusing produced less variation in peak dose. These sensitivities are consistent with understanding and past experience in TSPAs of Yucca Mountain. Solubility and alteration rate have a significant influence on the peak doses associated with radionuclides in the Np decay chain, which is one of the main contributors to peak dose. Seepage rate is a nonlinear function, so that increases in the probability of high seepage results in disproportionate increases in seepage rate and seepage fraction, leading in turn to higher release rates from the repository. Similarly, the variation in retardation applies to retardation factors in the geosphere, which will delay but not decrease doses from long-lived radionuclides. Changes in the flow focusing factor only produce changes in the fraction of the repository that experience focused flow, and this effect would not be expected to produce the same magnitude of effects as the changes in seepage. Therefore, the variations in the output from IMARC 10 in this sensitivity analysis are consistent with understanding of the model.

10.3.2 Effect of Alternative Solubility Assumption

Another IRT peer-review recommendation (EPRI, 2009) called for EPRI to provide additional information regarding the effect of uncertainty in the nature of the solid precipitate and its effect on value of Np solubility on the overall dose results. Past versions of IMARC addressed this issue, particularly Kessler et al. (2006), in the development of IMARC 9. However, in IMARC 10 the alteration rate has been changed compared to IMARC 9, and alteration rate and solubility both have effects on the peak dose. As a result, to address this comment a sensitivity analysis was conducted to examine the effect of higher Np solubility on the peak dose. To carry out this sensitivity analysis, the Np solubility was changed to the higher solubility values used in IMARC 8 and previous versions. A comparison of the current and higher solubility distributions is shown in Table 10-3. In this sensitivity analysis, the values for alteration rate remain at their IMARC 10 values.

Table 10-3
Values for neptunium solubility distributions (mol/m^3) used in the IMARC 10 sensitivity analysis. In both cases the probability of the low and high values is 5 percent, and the probability of the mean is 90 percent.

Source for Solubility Parameters (Version)	Low	Mean	High
IMARC 10	4.20×10^{-7}	4.24×10^{-6}	4.20×10^{-5}
IMARC 8	4.2×10^{-3}	8.4×10^{-2}	8.4

The result of the calculation with the higher solubility is shown in Figure 10-5, and compared to the nominal result for IMARC 10. It is noteworthy that the increase in solubility values was about 4 orders of magnitude, but use of the older solubility values only results in about an order of magnitude increase in peak mean dose compared to the nominal values.

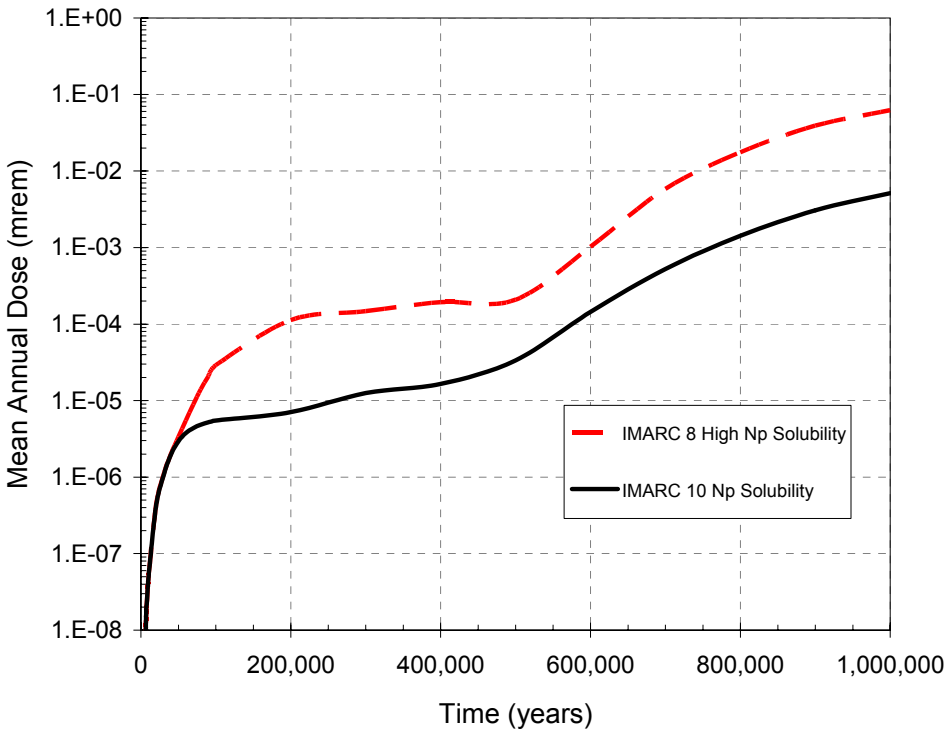

Figure 10-5
Effect of higher solubility on TSPA results. The solubility values previously used in IMARC 8 are compared to the current nominal case. All other parameters are set to IMARC 10 values.

10.3.3 Effect of Cladding

Among the recommendations of the IRT (EPRI 2009), one is to provide additional justification for the cladding credit taken in IMARC. In support of this objective, a sensitivity calculation has been undertaken to quantify the importance of cladding on the overall TSPA results. To this end, a set of calculations are performed for the nominal and nominal plus seismic scenarios with and without cladding. In the "without cladding" analysis, the failure function for cladding was set to 99.9 percent failure at time zero.

Results are presented in Figure 10-6. For the nominal scenario, cladding provides a limited benefit associated with doses from the juvenile failure waste packages, but has no consequence on peak dose. For the nominal plus seismic scenario, the cladding provides an additional moderate benefit of smoothing the peak that occurs when excess waste packages fail during early seismic events. The spike in the curve for nominal plus seismic at 100,000 years is associated with the waste packages that fail during a seismic event; the smoother and lower peak when cladding is included represents the additional benefit of the intact cladding. In both scenarios, the benefit associated with cladding credit is limited to about an order of magnitude decrease of the small doses at times less than about 100,000 years.

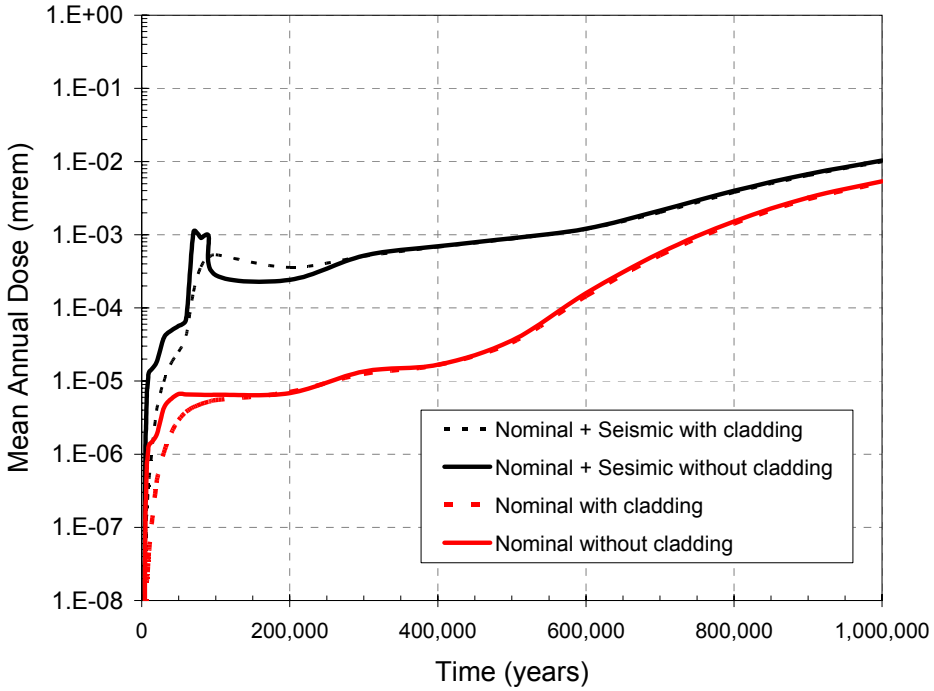

Figure 10-6
The effect of cladding credit on IMARC 10 TSPA results. The figure compares results when cladding is present and when it is absent for both the nominal and nominal plus seismic scenarios.

10.3.4 Effect of Drip Shields

EPRI (2008a) has published results using IMARC 9 showing that the drip shields have a minor positive benefit on the results of the TSPA. To confirm this observation, analyses were run using IMARC 10 for both the nominal and nominal plus seismic scenarios. The analysis was carried out by assigning a probability of 1.0 to the juvenile failures, effectively giving all the drip shields a life expectancy of zero years.

The results are presented in Figure 10-7. The results with and without drip shields are identical for the nominal plus seismic scenario. This result is expected, since the seismic failure analysis had all of the drip shields failing at 50,000 years. Because the waste packages last substantially longer than 50,000 years, there is no difference in performance whether the drip shields fail at zero years or at 50,000 years. The results are very close to results for cases with and without drip shields for the nominal scenario, with a very small performance benefit at early times and identical peak doses. The performance with and without drips shields is closer in this analysis than previously published by EPRI (2008a) using IMARC 9. The explanation of this change in the analysis is in the longer UO_2 alteration times in IMARC 10. As an illustration of this effect, an additional sensitivity analysis is run using IMARC 10, but with the faster IMARC 9 alteration rates. This analysis is also shown in Figure 10-7, and it demonstrates a similar behavior to that published by EPRI (2008a). Therefore, it is concluded that with the updated and improved

estimates of alteration rate, the net performance benefit of drip shields is even smaller than previous EPRI analyses indicated. DOE's own analysis (Figure 10-12) similarly indicates that repository performance is only marginally impacted by early drip shield failure.

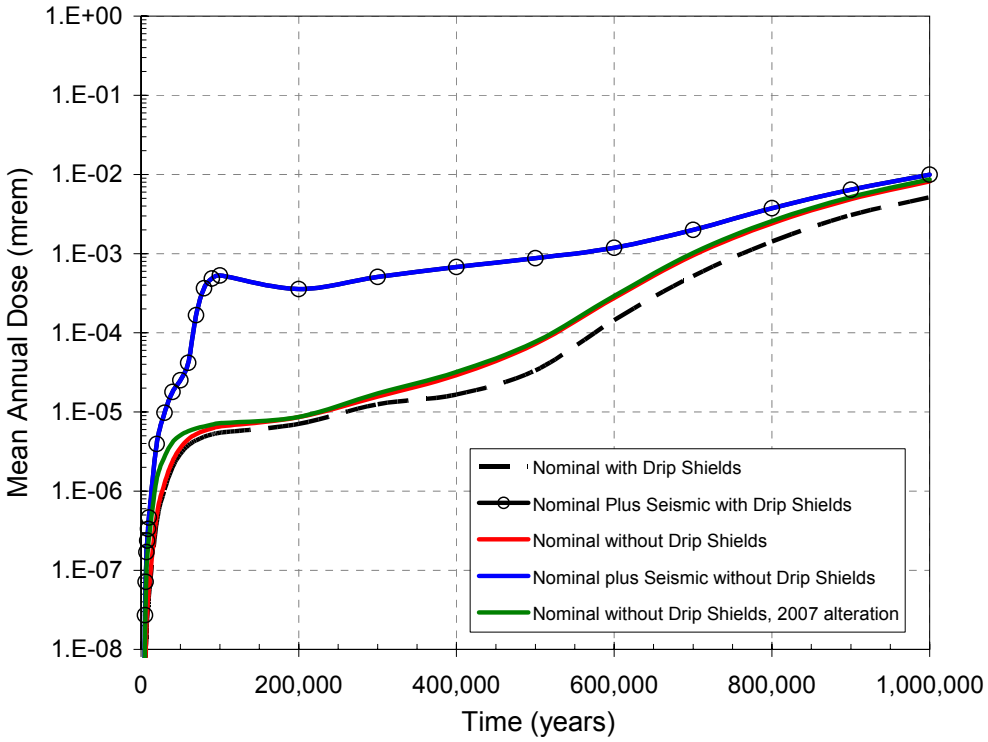

Figure 10-7
Comparison of repository performance with and without drip shields showing negligible performance benefit from the drip shields. Also shown on the figure is an IMARC 10 run using the older, more rapid alteration estimates, which explains the difference between IMARC 9 and IMARC 10 results.

10.3.5 Overall Effect of the Engineered Barrier System

Regulatory requirements in 10 CFR 63 state that several barrier components of the disposal system should contribute to the performance of the repository ("multiple barrier concept"). It is, therefore, desirable to quantify the relative contributions of the engineered barrier system (EBS) and the geosphere to the performance of the repository. To address this question, a sensitivity analysis was performed in which the EBS components (waste package, drip shield, and cladding) degrade rapidly and completely. That is, all of the waste packages in the repository are assumed to suffer juvenile failures, and the cladding is assumed to fail at time zero in the same way as in Section 10.3.2.

Results of this analysis are compared to the *nominal* and *nominal plus seismic* results in Figure 10-8. The peak doses rapidly increase to about 5 mrem/y, and remain at about that level for the entire duration of the analysis. The EBS is therefore seen to produce between 2 - 3 orders of

magnitude improvement in performance at 10^6 years. Also note that the geological setting by itself is sufficient to meet the performance objectives in 10 CFR 63.

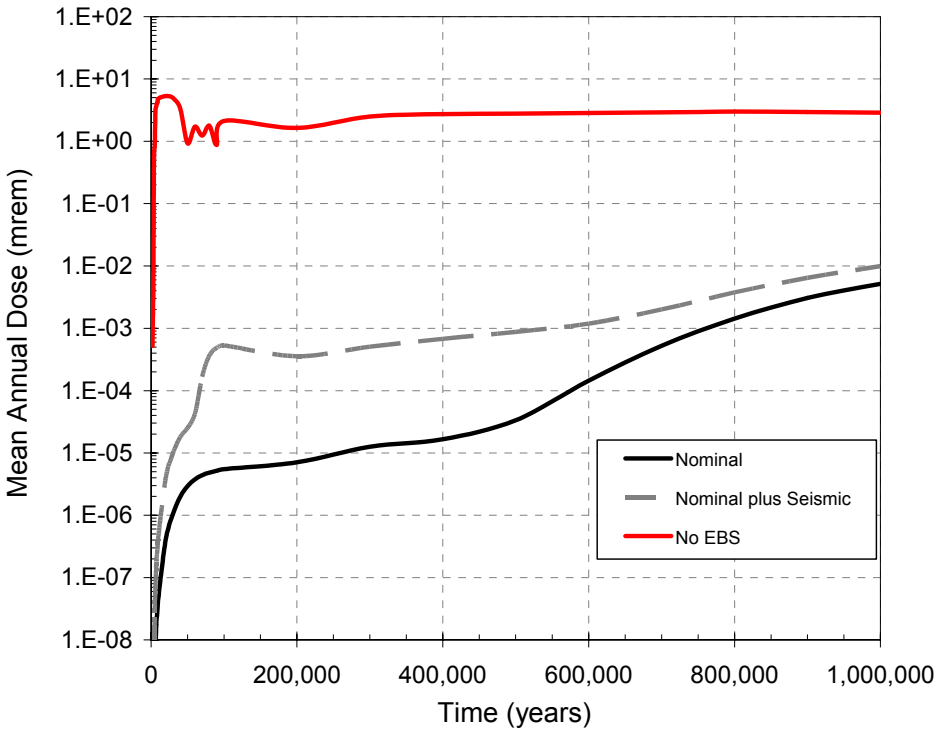

Figure 10-8
Results of IMARC 10 sensitivity analysis assuming complete EBS failure at t = 0.

10.3.6 Comparison of IMARC 10 and DOE TSPA-LA Results

This section provides a side-by-side comparison of several key results from the EPRI IMARC 10 and DOE TSPA-LA models. Direct comparison between the full DOE TSPA and IMARC results is difficult, because DOE results generally combine scenarios together to produce an overall performance result, whereas IMARC results are presented in a disaggregated form, in keeping with the different roles and purposes of the two programs.

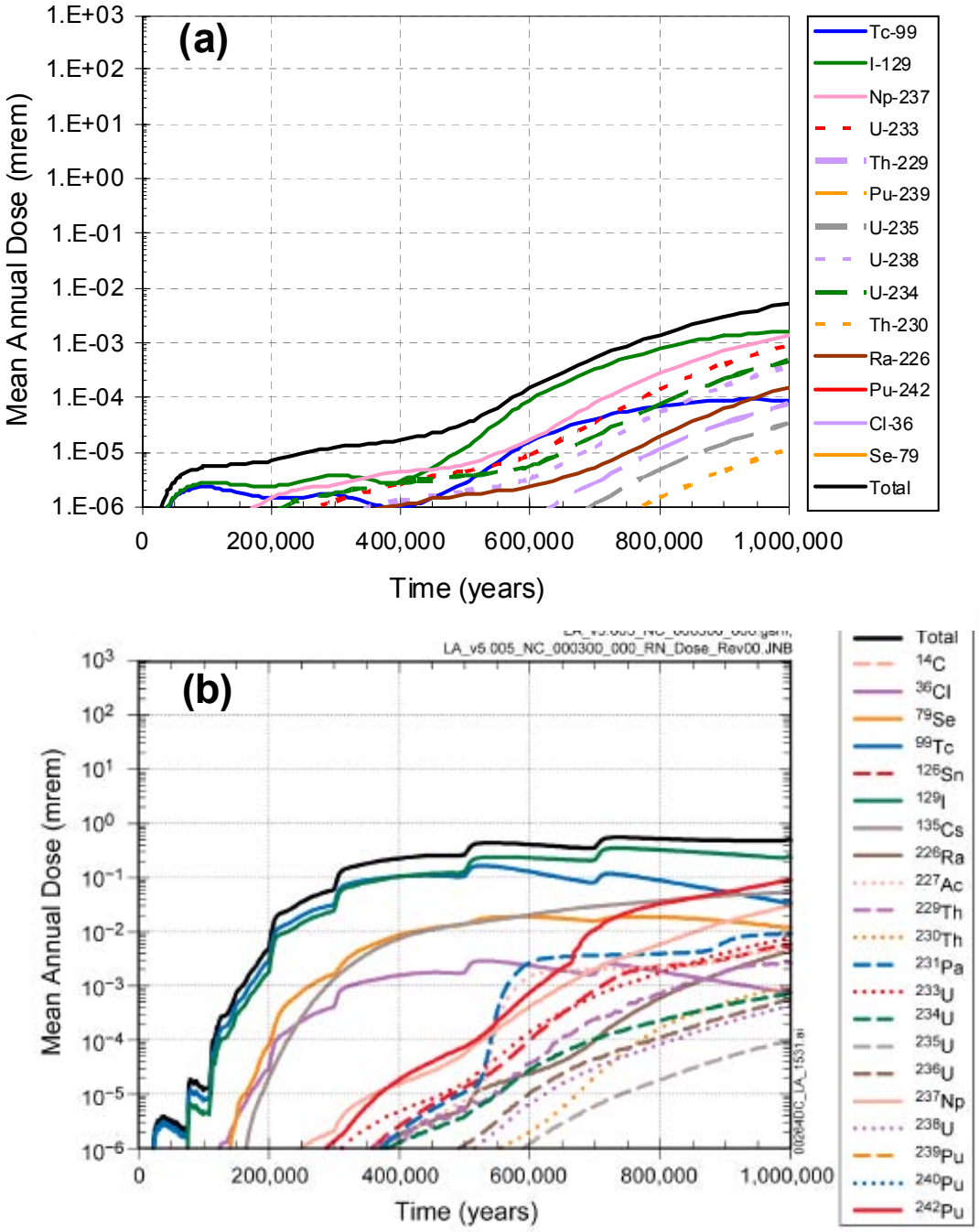

Figure 10-9
Comparison of (a) EPRI IMARC 10 and (b) DOE TSPA-LA annual RMEI dose estimates for the nominal scenario (Figure 10-9b adapted from DOE/OCRWM, 2008b; YM-LA Ch. 2, Figure 2.4-22b).

The FEPs included in the DOE's nominal scenario are comparable to the IMARC nominal scenario, so direct comparisons are possible and useful for this case. Figure 10-9 compares TSPA results for the "nominal" case, which does not include seismic or igneous events. The nominal scenario for both models shows the effects of long-term EBS degradation, radionuclide release and transport, and uptake by the RMEI assuming no seismic, rockfall, or igneous intrusion or eruption events occur. It should be noted that the IMARC 10 nominal case includes assumption of one early WP failure, whereas DOE's TSPA-LA treats early WP failure as a separate scenario. This difference should have little impact on the direct comparison of the two nominal cases, as the dose contribution from the TSPA-LA early WP failure case is minor relative to the nominal scenario, i.e., 2 – 3 orders of magnitude lower (see Figure 10-12). Figure 10-9a presents the IMARC 10 mean RMEI annual dose (mrem/yr) for the nominal case. IMARC 10 estimates dose assuming 100% of the repository is CSNF, i.e., no co-disposal waste packages are modeled in IMARC 10 (see Section 2.1). Figure 10-9b presents the DOE TSPA-LA mean annual RMEI dose for the nominal case. The DOE TSPA-LA model assumes 90% CSNF and 10% co-disposal waste (vitrified HLW and spent fuel from defense related activities) based on the equivalent metric tons of heavy metal.

The peak mean annual dose at 1 million years is approximately 0.005 and 0.5 mrem/yr for the EPRI and DOE models, respectively. There are many factors that contribute to the difference in these dose estimates and are described in EPRI (2008c) and DOE/OCRWM (2008a,b). Dominant radionuclides (those contributing the most to total mean annual RMEI dose) at later times in DOE's TSPA-LA for the nominal case are I-129, Pu-242, Cs-135, and Np-237; in EPRI's IMARC 10, the dominant radionuclides at later times are I-129; Np-237; and U-233. EPRI reintroduced Pu-242 and Ra-226 in its IMARC 10 analyses and found them to be minor contributors to RMEI mean annual dose.

Perhaps the most important contributor to the differences in dose estimates and dominant radionuclides are the different solubility values for U, Np, and Pu used in the two TSPA models. Pu solubility in the DOE TSPA-LA is 2 to 3 orders of magnitude higher than in IMARC 10; Np solubility in the DOE TSPA-LA is 3 to 4 orders of magnitude higher than in IMARC 10. Moreover, EPRI has determined the contribution from colloid-facilitated transport to be negligible for RMEI dose and does not include colloidal transport in IMARC (EPRI, 2006a). Biosphere Dose Conversion Factors (BDCFs) in IMARC 10 for the major actinides are 2 to 6 times larger than those in DOE's TSPA-LA. These two factors alone may explain much of the difference between the two models for total mean annual dose estimates late in the 1 million-year compliance period.

Table 10-4
Comparison of primary features, events, and processes in the DOE and EPRI TSPA models.

Feature, Event or Process	DOE TSPA-LA (DOE/OCRWM, 2008a,b)	EPRI IMARC 10
Infiltration	3 pre-10,000 yr climate states: present, monsoon, glacial transition prescribed post-10,000 yr climate	EPRI has adopted 1 climate state in 0 – 10,000 yr timeframe based on low risk importance of early climate states prescribed post-10,000 yr climate
Drift seepage	Low seepage rates High seepage fractions (nominal: 30 – 40% of repository)	Higher seepage rates Much lower seepage fractions (nominal: 1.25% of repository)
Inventory	CSNF and co-disposed HLW	CSNF only
Dominant Alloy 22 failure mechanism	SCC then GC	GC
Dominant radionuclides late in compliance period	Pu-242, I-129, Np-237	I-129, Np-237, U-233
Colloid-facilitated transport	included in TSPA-LA	negligible, not included in IMARC (EPRI, 2006a)
$\log_{10}$ solubility (mg/L)	Th: -2.1 to 1.1 U: 0.6 to 2.9 Pu: -1.2 to 1.1 Np (NpO2): -1.1 to 2.1	Th: -4.7 to -1.7 U: -1.0 to 1.7 Pu: -4.7 to -0.7 Np (NpO2): -4.0 to -2.0
UZ Kd's for Pu, Np (mL/g)	Th: 5500 to 15500 U: 0.2 to 0.5 Pu: 70 – 100 Np: 0.5 to 1.0	Th: 3000 to 20,000 U: 0.1 to 0.9 Pu: 40 to 150 Np: 0.3 to 3.0
BDCFs (Sv/y per Bq/m^3)	Th-229: 2.62×10^{-6} U:-233: 9.20×10^{-8} Np-237: 2.79×10^{-7} Pu-239: 9.74×10^{-7}	Th-229: 1.57×10^{-5} U:-233: 1.49×10^{-7} Np-237: 7.24×10^{-7} Pu-239: 2.37×10^{-6}

In spite of the differences in mean annual dose estimates at 1 million years obtained from IMARC and TSPA-LA models, the mean IMARC dose to the RMEI falls within the uncertainty band, i.e., around the 5th percentile, presented for the DOE TSPA-LA (DOE/OCRWM, 2008b) nominal scenario analysis (Figure 10-10).

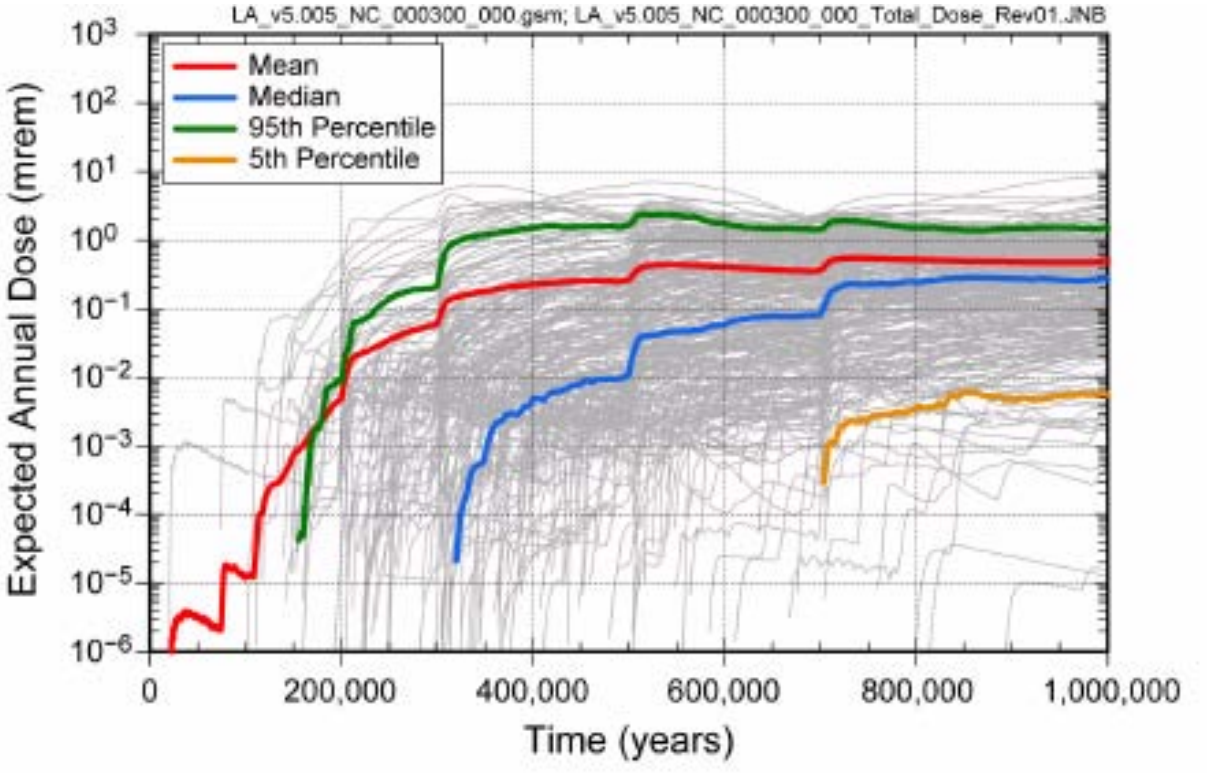

Figure 10-10
TSPA-LA results for the nominal scenario (excerpted from DOE/OCRWM, 2008b; YM-LA Ch. 2 Figure 2.4-22a). IMARC 10 nominal results fall around the 5th percentile for TSPA-LA expected annual doses, in spite of the different approaches and philosophies adopted by each program.

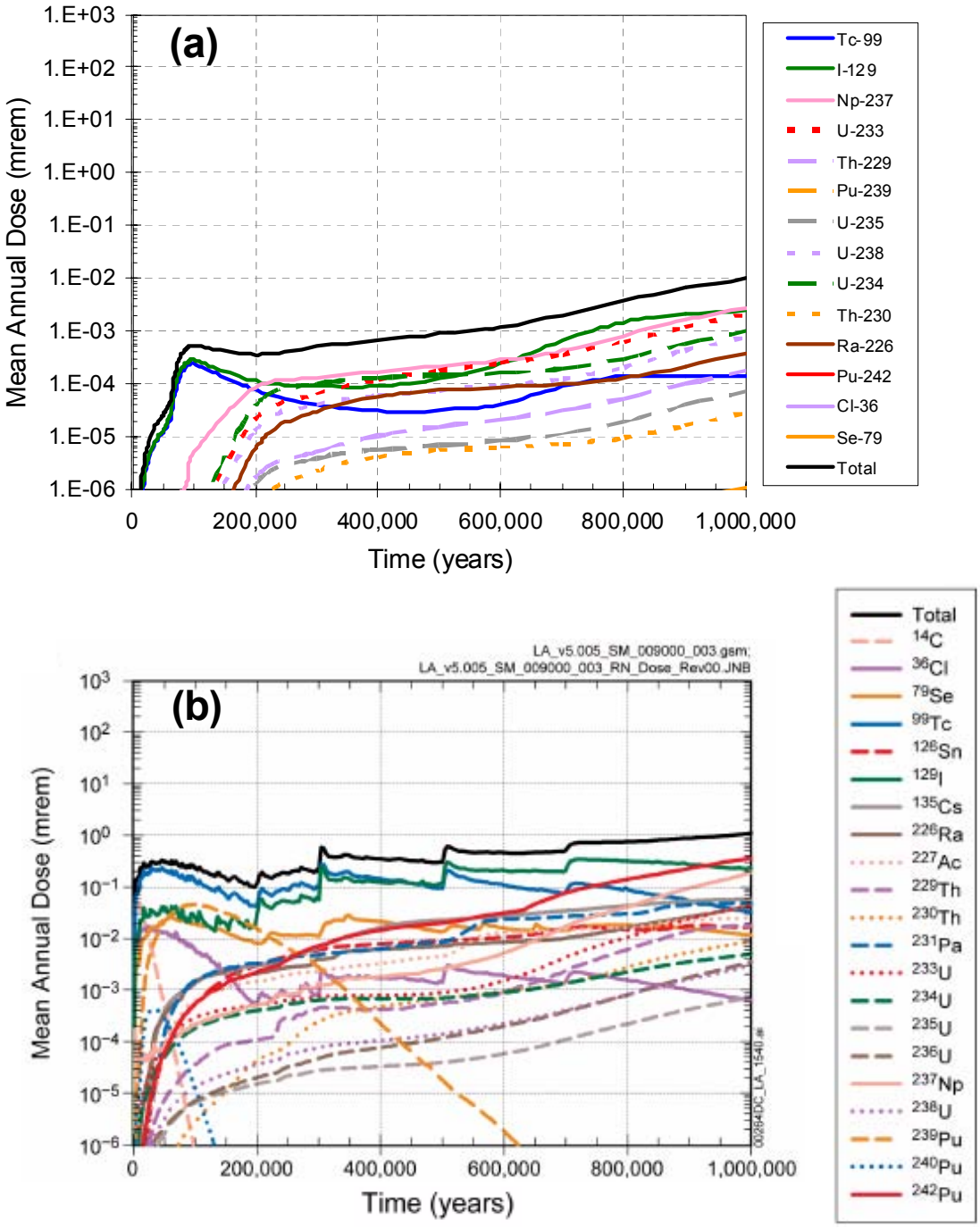

Figure 10-11
Comparison of (A) EPRI IMARC 10 and (B) DOE TSPA-LA annual RMEI dose estimates for the nominal + seismic scenario (Figure B adapted from DOE/OCRWM, 2008b; YM-LA Ch. 2, Figure 2.4-26b).

Figure 10-11 compares IMARC 10 and TSPA-LA results from dose calculations incorporating nominal processes and seismic events. Seismic ground motion contributes approximately 0.5 mrem/yr to the total dose estimate from the DOE TSPA-LA (DOE/OCRWM, 2008b) modeling (Figure 10-11b); this dose contribution is roughly the same as from nominal processes alone. Likewise, EPRI modeling (Figure 10-11a) shows an incremental increase in dose from seismic effects of 0.005 mrem/yr, which also represents the same dose contribution from nominal processes alone.

However, in terms of magnitude, the dose contribution from seismic ground motion in the IMARC model is two orders of magnitude smaller than the seismic contribution reported from DOE TSPA-LA analyses. Likely sources of this discrepancy between the two models are:

- The intensity of the peak ground motion for large seismic events. While the DOE model assumes peak ground velocities (PGVs) as high as 4 m/s, the EPRI model assumes a PGV for large seismic events in the range of 0.75 to 1 m/s.
- The predicted amount of damage sustained by waste packages due to seismic activity. Due to the lower PGV estimates in IMARC, EPRI finds that damage to the WPs in WP to WP collisions when the drip shields are intact is minimal, such that there is very little potential for subsequent SCC. Furthermore, the less severe damage to WP determined by EPRI modeling also results in part from the important role that drip shield failure and rockfall can play in limiting seismic damage to waste packages through restriction of WP motion. In the EPRI modeling, all drip shields are assumed to fail after the first seismic event (at 50,000 years). Consequently, rockfall caused by subsequent seismic motion serves to pin down waste packages, dampen WP motions, and limit severity of WP to WP collisions; these collisions are primary drivers for potential plastic deformation which, in turn, may initiate SCC. For the DOE TSPA-LA modeling, this beneficial effect of rockfall is less pronounced as drip shield failures do not occur at once but, instead, are distributed over time (DOE/OCRWM, 2008a,b).
- The EPRI model predicts that approximately 15% of the waste packages will be breached in one million years; only 0.7% of that 15% is due to seismic activity (Figure 10-2).

Table 10-5 summarizes the dominant failure mechanisms for the Alloy 22 outer waste package corrosion barrier in the DOE and EPRI TSPA models for the nominal + seismic scenario. The DOE and EPRI models differ with respect to the dominant Alloy 22 degradation mechanism in the 10^4- to 10^5-year time frame. The DOE model results indicate stress corrosion cracking (SCC) as the primary degradation mechanism during this time frame, whereas EPRI modeling finds general corrosion (GC) as the primary degradation mechanism. Therefore, according to EPRI model estimates, SCC is not expected to play a major role in waste package degradation.

Table 10-5
Dominant Alloy 22 waste package (WP) failure mechanisms in the DOE and EPRI TSPA models for nominal + seismic scenario.

Timeframe	DOE (Sandia, 2008; DOE/OCRWM, 2008a,b)	EPRI
Early (T_0 – 10^4 yr)	Seismic damage to co-disposal WPs Negligible for CSNF WPs	Negligible for CSNF WPs
Intermediate (10^4 – 10^5 yr)	SCC failure of CSNF	Limited GC failure of CSNF WPs
Late (10^5 – 10^6 yr)	GC failure of co-disposal and CSNF WPs	GC failure of CSNF WPs

SCC: stress corrosion cracking
GC: general corrosion

Table 10-6
Comparison of the DOE LA and EPRI TSPA estimated annual RMEI dose rate contributions from the major repository evolution scenarios at 1 million years.

Rank	DOE LA (DOE/OCRWM 2008a,b)	EPRI IMARC 10
1	igneous intrusion 0.9 mrem/yr	nominal 0.005 mrem/yr
2	seismic ground motion 0.5 mrem/yr	seismic 0.005 mrem/yr
3	nominal 0.5 mrem/yr	*Igneous intrusion and volcanic eruption scenarios are not considered in IMARC 10. Annual probability of igneous event intersecting repository below 10^{-8} yr^{-1} threshold per EPRI (2008b)*
4	volcanic eruption 0.0001 mrem/yr	

Thus, in addition to the difference in magnitude between dose estimates, the different approaches taken by DOE and EPRI in modeling repository performance lead to differences in the relative ranking of the various processes (nominal, seismic, etc.). Table 10-6 compares RMEI dose rate estimates and relative rankings in the DOE (e.g., Figure 10-12) and EPRI TSPA models for the four major scenario classes. The DOE estimate for igneous intrusion contribution contributes the most to peak RMEI dose rate. The significant dose contribution from igneous intrusion in DOE TSPA-LA analyses can be largely attributed to the conservative assumption made by DOE that 100% of waste packages are breached following the intersection of an igneous event with the repository footprint (EPRI, 2005a).

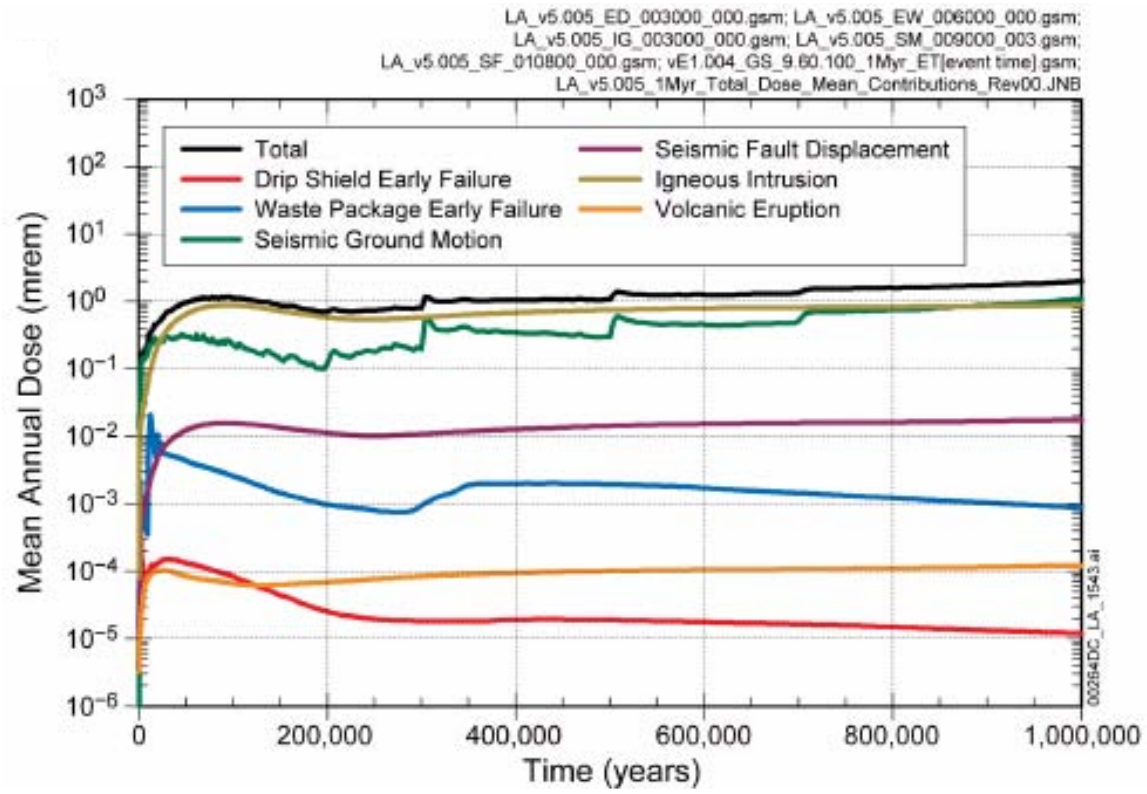

Figure 10-12
Contributions of DOE scenarios to total annual dose estimates versus time (adapted from DOE/OCRWM, 2008b; YM-LA Ch. 2, Figure 2.4-18b).

11
SUMMARY

This report provides a history of EPRI's IMARC TSPA code and a detailed discussion of the conceptual model implemented in IMARC Version 10. This discussion is intended to provide information about the code in a single report including some level of detail of the underlying conceptual model as well as input parameters used in the current implementation. IMARC is intended to reflect the "reasonable expectation" philosophy established in the applicable regulations promulgated by EPA and NRC, although some conservatisms remain in the IMARC model.

The FEPs included in IMARC have co-evolved along with the understanding of the Yucca Mountain repository, and along with design changes. The FEPs currently implemented in IMARC 10 are consistent with the EPRI team's understanding of the performance of the repository as described by DOE in the license application (DOE/OCRWM, 2008). It is difficult to directly compare the full DOE TSPA results to IMARC analyses, since DOE has convoluted the scenarios together while in IMARC the scenarios remain disaggregated. However, direct comparison is possible for the nominal scenario. Qualitatively, both analyses show similar behavior, with the peak dose occurring at 1,000,000 years, mainly associated with ^{129}I. Qualitative differences between the shapes of the curves are explicable by the DOE's inclusion of co-disposal waste packages, which lead to a more rapid rise in dose at intermediate time scales. Quantitatively, the IMARC peak mean dose is approximately 2 orders of magnitude lower than the DOE nominal scenario peak mean dose, which is within the band of uncertainty reported for the DOE TSPA-LA estimates. This difference primary results from the use of a less conservative best-estimate philosophy in IMARC analyses.

A number of parts of the code, and the code as a whole, have recently been subjected to review and/or validation activities by the EPRI team. An independent peer review was completed (EPRI, 2009), and the results of the peer review have been incorporated into this document. Considerable effort has gone into benchmarking each module against available comparable analytical and numerical solutions. These tests provide confidence that IMARC calculations are consistent with the intent of the conceptual model and that EPRI's TSPA modeling remains fit for purpose.

12
REFERENCES

Andresen, P.L., P.W. Emigh, L.M. Young, and G.M. Gordon, 2001. "Stress Corrosion Cracking of Annealed and Cold Worked Titanium grade 7 and Alloy 22 in 110°C Concentrated Salt Environments." *CORROSION/2001* (NACE International, Houston, TX), paper no. 01130.

Andresen, P.L., P.W. Emigh, L.M. Young, and G.M. Gordon, 2003. "Stress Corrosion Cracking Growth Rate Behavior of Alloy 22 (UNS N06022) in Concentrated Groundwater." *CORROSION/2003* (NACE International, Houston, TX), paper no. 03683.

Apted, M., F. King, D. Langmuir, R. Arthur, and J. Kessler, 2005. "The Unlikelihood of Localized Corrosion of Nuclear Waste Packages Arising from Deliquescent Brine Formation." *Journal of Materials* 57, 43-48.

ASM, 2003. Corrosion: Fundamentals, Testing, and Protection. *ASM Handbook*, Volume 13A, American Society of Metals, Metals Park, OH.

Bailey, D. H., Y. Hida, X. S. Li, and Br. Thompson, 2003. High-Precision Software Directory. LBNL, Berkley CA, *http://crd.lbl.gov/~dhbailey/mpdist/*, and *http://crd.lbl.gov/~xiaoye/*.

Bear, J., and A. Verruijt, 1987. *Modeling Groundwater Flow and Pollution*. D. Reidel Publising Company, Dordrecht-Boston-Lankaster-Tokyo.

BIOMOVS II, 1996. *Development of a Reference Biospheres Methodology for Radioactive Waste Disposal*, BIOMOVS II Technical Report No. 6, published on behalf of the BIOMOVS II Steering Committee. ISBN 91-972134-5-4, Swedish Radiation Protection Institute, Stockholm.

BIOPROTA, 2005a. *Model Intercomparison with Focus on Accumulation in Soil. A report prepared within the international collaborative project BIOPROTA: Key Issues in Biosphere Aspects of Assessment of the Long-term Impact of Contaminant Releases Associated with Radioactive Waste Management*, Main contributors: A. Albrecht, C. Damois, E. Kerrigan, R. Klos, G.M. Smith, M.C. Thorne, S.M. Willans and H. Yoshida. Published on behalf of the BIOPROTA Steering Committee by ANDRA (Agence nationale pour la gestion des dechets radioactifs), Chatenay-Malabry, France.

BIOPROTA,2005b. *Modelling the Inhalation Exposure Pathway. A report prepared within the international collaborative project BIOPROTA: Key Issues in Biosphere Aspects of Assessment of the Long-term Impact of Contaminant Releases Associated with Radioactive Waste Management*. Main Contributors: M. Wasiolek (Task Leader), A. Aguero, A. Albrecht, U. Bergstrom, H. Grogan, G.M. Smith, M.C. Thorne, S.M. Willans and H. Yoshida. Published on behalf of the BIOPROTA Steering Committee by Nexia Solutions Ltd, UK.

BIOPROTA, 2005c. *Model Review and Comparison for the Spray Irrigation Pathway. A report prepared within the international collaborative project BIOPROTA: Key Issues in Biosphere Aspects of Assessment of the Long-term Impact of Contaminant Releases Associated with Radioactive Waste Management*. Main Contributors: U. Bergstrom (Task Leader), A. Albrecht, B. Kanyar, G. Smith, M.C. Thorne, H. Yoshida and M. Wasiolek. Published on behalf of the BIOPROTA Steering Committee by the Swedish Nuclear Fuel and Waste Management Company, Stockholm.

Brown, A.D. 1990. *Microbial Water Stress Physiology*. John Wiley, Chichester, U.K.

BSC, 2003. Total System Performance Assessment- License Application Methods and Approach. TDR-WIS -PA-000006 REV 00 ICN 01.

BSC, 2004a. *Engineered Barrier System: Physical and Chemical Environment Model*. Bechtel SAIC Company report to DOE, ANL-EBS-MD-000033 Rev 02, February 2004.

BSC, 2004b. *Multiscale Thermohydrologic Model*. Bechtel SAIC Company report to DOE, ANL-EBS-MD-000049 Rev 02, October 2004.

BSC, 2004c. *WAPDEG Analysis of Waste Package and Drip Shield Degradation*. Bechtel SAIC Company report to DOE, ANL-EBS-PA-000001, REV 02, ICN 00.

BSC, 2004d. *Seismic Consequence Abstraction*. Bechtel SAIC Company report to DOE, MDL-WIS- PA-000003 Rev 01, October 2004.

BSC, 2004e. *General Corrosion and Localized Corrosion of Waste Package Outer Barrier*. Bechtel SAIC Company report to DOE, ANL-EBS-MD-000003 Rev 02, October 2004.

BSC, 2004f. Stress Corrosion Cracking of the Drip Shield, the Waste Package Outer Barrier, and the Stainless Steel Structural Material. Bechtel SAIC Company report to DOE, ANL-EBS-MD-000005 Rev 02, October 2004.

Carslaw, H. S. and J.C. Jaeger, 1986. *Conduction of Heat in Solids,* Oxford University Press; 2nd edition.

Cragnolino, G., 2003. *Corrosion Research at the Center for Nuclear Waste Regulatory Analyses*. Presentation to the Nuclear Waste Technical Review Board, Spring Meeting, May 2003.

Cragnolino, G.A., D.S. Dunn, and Y.M. Pan, 2003. "Effects of Potential and Environment on the Stress Corrosion Cracking Susceptibility of Nickel-Chromium-Molybdenum Alloys." In Proc. *CORROSION/2003* (National Association of Corrosion Engineers International, Houston, TX), paper no. 03541.

Cragnolino, G.A., D.S. Dunn, and Y.M. Pan, 2004. "Evaluation of Corrosion Processes Affecting the Performance of Alloy 22 as a Proposed Waste Package Material." In *Scientific*

Basis for Nuclear Waste Management XXVII, V.M. Oversby and L.O. Werme (eds.), Mat. Res. Soc. Symp. Proc. 807 (Materials Research Society, Warrendale, PA), pp. 435 440.

CRWMS M&O, 1999. Design Basis Waste Input Report for Commercial Spent Nuclear Fuel. B0000000-01717-5700-00041 REV 01.

CRWMS M&O, 2000a. Drift Scale Coupled Processes (DST and THC Seepage) Models, MDL-NBS-HS-000001 REV 00.

CRWMS M&O, 2000b. *Clad degradation – summary and abstraction*. ANL-WIS-MD-000007 REV 00.

CRWMS M&O, 2000c. *Initial cladding condition*. ANL-EBS-MD-000048 REV 00.

CRWMS M&O, 2000d. General corrosion and localized corrosion of the drip shield. ANL-EBS-MD-00000 4 REV 00.

CRWMS, M&O, 2000e. Probability Distribution for Flowing Interval Spacing. ANL-NBS-MD-000003. Las Vegas Nevada: CRWMS M&O.

de Hoog, F.R., J.H. Knight, and A.N. Stokes, 1982. "An Improved Method for Numerical Inversion of Laplace Transforms." *SIAM J. Sci. Stat. Comput*. 3, 357-399.

DOE/OCRWM, 1995. *Total System Performance Assessment-1995: An Evaluation of the Potential Yucca Mountain Repository*, B00000000-01717-2200-00136, REV 1, US Department of Energy, Office of Civilian Radioactive Waste Management, Washington, DC.

DOE/OCRWM, 2002. *Yucca Mountain Science and Engineering Report*, Technical Information Supporting Site Recommendation Consideration Revision 1, DOE/RW-0539-1, U.S. Department of Energy, Office of Civilian Radioactive Waste Management, February 2002.

DOE/OCRWM, 2008a. Total System Performance Assessment Model/Analysis for the License Application, MDL-WIS-PA-000005 Rev. 0 January 2008 Office of Civilian Radioactive Waste Management, Las Vegas, NV.

DOE/OCRWM, 2008b. Yucca Mountain Repository License Application Safety Analysis Report, DOE/RW-0573, Rev. 0 June 2008 Office of Civilian Radioactive Waste Management, Las Vegas, NV.

Dunn, D.S., Y.M. Pan, and G.A. Cragnolino, 2002. "Stress Corrosion Cracking of Nickel-Chromium-Molybdenum Alloys in Chloride Solutions." In Proc. *CORROSION/2002* (National Association of Corrosion Engineers International, Houston, TX), paper no. 02425.

Dunn, D.S., L. Yang, Y.-M. Pan, and G.A. Cragnolino, 2003. "Localized Corrosion Susceptibility of Alloy 22." *CORROSION/2003* (NACE International, Houston, TX), paper no. 03697.

Enviros and Quintessa, 2003. *AMBER Version 4.5 Release Note, Version 1.00*, May 2003, Enviros, Culham, UK.

Enviros, 2003. *AMBER – Contaminant Modelling*. see www.enviros.com/amber/.

EPRI, 1990. *Demonstration of a risk-based approach to high-level waste repository evaluation*. EPRI, Palo Alto, CA: 1990. NP-7057.

EPRI, 1992. *Demonstration of a Risk-Based Approach to High-Level Waste Repository Evaluation: Phase 2*. EPRI, Palo Alto, CA: 1992, TR-100384

EPRI, 1996. *Yucca Mountain Total System Performance Assessment, Phase 3*. EPRI, Palo Alto, CA: 1996. TR-107191.

EPRI, 1998. *Alternative Approaches to Assessing the Performance and Suitability of Yucca Mountain for Spent Fuel Disposal*, EPRI, Palo Alto CA: 1998. TR-108732.

EPRI, 2000. *Evaluation of the Candidate High-Level Radioactive Waste Repository at Yucca Mountain Using Total System Performance Assessment: Phase 5*. EPRI, Palo Alto, CA: 2000. 1000802.

EPRI, 2002a. *Evaluation of the Proposed High-Level Radioactive Waste Repository at Yucca Mountain Using Total System Performance Assessment: Phase 6*. EPRI, Palo Alto, CA: 2002. 1003031.

EPRI, 2002b. *Integrated Yucca Mountain Safety Case and Supporting Analysis: EPRI's Phase 7 Performance Assessment*. EPRI, Palo Alto, CA: 2002. 1003334.

EPRI, 2003. *Scientific and Technical Priorities at Yucca Mountain*. EPRI, Palo Alto, CA: 2003. 1003335.

EPRI, 2004a. *Evaluation of a Spent Fuel Repository at Yucca Mountain, Nevada: 2004 Progress Report*. EPRI, Palo Alto, CA: 2004. 1009705.

EPRI, 2004b. *Potential Igneous Processes Relevant to the Yucca Mountain Repository: Extrusive-Release Scenario Analysis and Implications.* EPRI, Palo Alto, CA: 2004. 1008169.

EPRI, 2005a. *Program on Technology Innovation: Potential Igneous Processes Relevant to the Yucca Mountain Repository: Intrusive-Release Scenario, Analysis and Implications*. EPRI, Palo Alto, CA: 2005. 1011165.

EPRI, 2005b. *Yucca Mountain Licensing Standard Options for Very Long Time Frames: Technical Bases for the Standard and Compliance Assessments*. EPRI, Palo Alto, CA: 2005. 1011754.

EPRI, 2005c. *EPRI Yucca Mountain Total System Performance Assessment Code (IMARC) Version 8*. EPRI, Palo Alto, CA: 2005. 1011813.

EPRI, 2005d. *Effects of Seismicity and Rockfall on Long-Term Performance of the Yucca Mountain Repository: 2005 Progress Report*. EPRI, Palo Alto, CA: 2005. 1011812.

EPRI, 2006a. *Treatment of Colloid-Facilitated Transport for Yucca Mountain Total System Performance Assessment*. EPRI, Palo Alto, CA: 2006. 1013440.

EPRI, 2006b. *Program on Technology Innovation: EPRI Yucca Mountain Spent Fuel Repository Evaluation, 2006 Progress Report*. EPRI, Palo Alto, CA: 2006. 1013445.

EPRI, 2006c. *Effects of Multiple Seismic Events and Rockfall on Long-Term Performance of the Yucca Mountain Repository*. EPRI, Palo Alto, CA: 2006. 1013444.

EPRI, 2008a. *Occupational Risk Consequences of the Department of Energy's Approach to Repository Design, Performance Assessment and Operation in the Yucca Mountain License Application*. EPRI, Palo Alto, CA: 2008. 1018058.

EPRI, 2008b. *Independent Probabilistic Volcanic Hazard Analysis for the Yucca Mountain Region*. EPRI, Palo Alto, CA: 2008. 1018059.

EPRI, 2008c. *Evaluation of a Spent Fuel Repository at Yucca Mountain, Nevada: 2008 Progress Report*. EPRI, Palo Alto, CA: 2008. 1016631.

EPRI, 2009. *International Review Team Report: A Peer Review of the Yucca Mountain IMARC Total System Performance Assessment EPRI Model*. EPRI, Palo Alto, CA: 2009. 1018711.

Farmer, J., D. McCright, G. Gdowski, F. Wang, T. Summers, P. Bedrossian, J. Horn, T. Lian, J. Estill, A. Lingenfelter, and W. Halsey, 2000. "General and Localized Corrosion of Outer Barrier of High-level Waste Container in Yucca Mountain." *Proc. Transportation, Storage, and Disposal of Radioactive Materials – 2000*, PVP-Vol. 408 (American Society of Mechanical Engineers, New York, NY), pp. 53 69.

Greene, C.A., C.S. Brossia, D.S. Dunn and G. Cragnolino, 2000. "Environmental and electrochemical factors on the localized corrosion of Zircaloy-4." Paper 210, *CORROSION 2000*, NACE International, Houston, TX.

Horn, J.A., A. Rivera, and T. Lian, 1998. In Proc. *CORROSION/98* (National Association of Corrosion Engineers International, Houston, TX), paper no. 98152.

Hornkjol, S., 1988. "Pitting corrosion of zirconium and hafnium." *Electrochimica Acta*, 33, 289 292.

Hua, F. and G. Gordon, 2004. "Corrosion Behavior of Alloy 22 and Ti Grade 7 in a Nuclear Waste Repository Environment." *Corrosion* 60, 764 777.

Hua, F., J. Sarver, J. Jevec, and G. Gordon, 2002. "General Corrosion Studies of Candidate Container Materials in Environments Relevant to Nuclear Waste Repository." In Proc.

CORROSION/2002 (National Association of Corrosion Engineers International, Houston, TX), paper no. 02530.

Hua, F., K. Mon, P. Pasupathi, G. Gordon, and D. Shoesmith, 2004. "Corrosion of Ti Grade 7 and Other Ti Alloys in Nuclear Waste Repository Environments – A Review." In Proc. *CORROSION/2004* (National Association of Corrosion Engineers International, Houston, TX), paper no. 04689.

IAEA, 2003. *"Reference Biospheres" for Solid Radioactive Waste Disposal*. Report of BIOMASS Theme 1 of the BIOSPHERE Modelling and Assessment (BIOMASS) Programme. IAEA-BIOMASS-6. International Atomic Energy Agency (IAEA), Vienna, July 2003.

Jones, R.H. and R.E. Ricker, 1992. *Mechanisms of Stress-corrosion Cracking. In Stress-corrosion Cracking*, R.H. Jones (ed.), Chap. 1, ASM International, Metals Park, OH.

Kessler, J. H., 2005. Letter to Mr. Rodney McCullum, "Comments related to future climates and net infiltration on NRC Proposed Amendments to 10 CFR Part 63, Implementation of a Dose Standard after 10,000 Years", dated September 8, 2005.

Kessler, J., M.W. Kozak, M. Apted, W. Zhou, and G. Mungov, 2006. "EPRI's Total System Performance Assessment of Yucca Mountain using IMARC 9," *Proc. International High-Level Waste Management Conference.* Las Vegas.

King, F., M. Kolar, S. Stroes Gascoyne, and P. Maak, 2004. "Model for the Microbiological Corrosion of Copper Containers in a Deep Geologic Repository." *Proc. Scientific Basis for Nuclear Waste Management XXVII*, Mat. Res. Soc. Symp. Proc. 807, V.M. Oversby and L.O. Werme (eds.), Materials Research Society, Warrendale, PA), 811-816.

Kozak, M.W., N.E. Olague, R.R. Rao, and J.T. McCord, 1993. *Evaluation of a Performance Assessment Methodology for Low-Level Radioactive Waste, Volume 1: Evaluation of Modeling Approaches*, NUREG/CR-5927 Vol. 1, SAND91-2802/1, Sandia National Laboratories.

Lacombe, S., E.A. Sudicky, S.K. Frape, and A.J.A. Unger. 1995. "Influence of Leaky Boreholes on Cross-Formational Groundwater Flow and Contaminant Transport." *Water Resour. Res.*, 31(8), 1871-1882.

Little, B., P. Wagner and F. Mansfeld, 1991. "Microbiologically Influenced Corrosion of Metals and Alloys." *Int. Mater. Rev*. 36, 253-272.

Maguire, M., 1984. The pitting susceptibility of zirconium in aqueous Cl-, Br-, and I- solutions. In *Industrial Applications of Titanium and Zirconium: Third Conference*; ASTM STP 830, R.T. Webster and C.S. Young (editors), American Society for Testing and Materials, 175 189.

Marshall, B.D., Neymark, L.A., and Peterman, Z.E. (2003) Estimation of past seepage volumes from calcite distribution in the Topopah Spring Tuff, Yucca Mountain, Nevada: Journal of Contaminant Hydrology, vol. 62-63, p. 237-247.

Meike, A. and S. Stroes Gascoyne, 2000. Review of Microbial Responses to Abiotic Environmental Factors in the Context of the Proposed Yucca Mountain Repository. Atomic Energy of Canada Limited Report, AECL 12101.

NRC, 2003. Cladding considerations for the transportation and storage of spent fuel. Interim staff guidance 11, revision 3, US Nuclear Regulatory Commission, available at http://www.nrc.gov/reading-rm/doc-collections/isg/ISG-11R3.pdf.

NRC, 2005. Nuclear Regulatory Commission, Rulemaking Issue Proposed Rule; 10 Cfr Part 63: "Implementation Of A Dose Standard After 10,000 Years," (RIN 3150-AH68) August 10, 2005 SECY-05-0144.

NRC, 2008. Nuclear Regulatory Commission, "Final Rule: 10 CFR Part 63, Implementation of a Dose Standard After 10,000 Years," (RIN 3150-AH68) November 4, 2008 SECY-08-0170.

Peters, M.T., 2003a. *The Character of the In-drift Environment*. Presentation to the US Nuclear Waste Technical Review Board, May 14, 2003.

Peters, M.T., 2003b. *Status of On-going Testing*. Presentation to the US Nuclear Waste Technical Review Board, May 14, 2003.

Qin, Z. and D.W. Shoesmith, 2003. "Lifetime Model for Ti-7 Drip Shields Within the Yucca Mountain Repository," in *Proc. NACE International Northern Region Eastern Conference*, Ottawa, ON, September 2003 (NACE International, Houston, TX.

Rebak, R.B., N.E. Koon, J.R. Dillman, P. Crook, and T.S.E. Summers, 2000a. "Influence of Aging on Microstructure, Mechanical Properties, and Corrosion Resistance of a Ni 22Cr 13Mo 3W Alloy." *CORROSION/2000* (NACE International, Houston, TX), paper no. 00181.

Rebak, R.B., T.S.E. Summers, and R.M. Carranz, 2000b. "Mechanical Properties, Microstructure and Corrosion Performance of C 22 Alloy Aged at 260°C to 800°C." *Mat. Res. Soc. Symp. Proc. (*Materials Research Society, Warrendale, PA), 608, 109 114.

Sandia, 2008. Total System Performance Assessment Results. Presented to: NRC/DOE Technical Exchange on Total System Performance Assessment for Yucca Mountain. Sandia National Laboratory. April 3, 2008, Las Vegas, NV.

SKI, 1996. SITE-94: Deep Repository Performance Assessment Project, Volume II, Swedish Nuclear Inspectorate, SKI Report 96:36.

Staehle, R.W., 2005. "Use of Sequential Microprocesses for Predicting New SCC Failures in Water-cooled Nuclear Plants." In *Proc. Second Int. Conf. on Environment-Induced Cracking of Metals EICM-2*, September 19 23, Banff, AB, in press.

Stroes Gascoyne, S. and F. King, 2002. "Microbially Influenced Corrosion Issues in High-level Nuclear Waste Repositories." In *Proc. CORROSION/02 Research Topical Symposia*, NACE International, Houston, TX.

Sudicky, E.A., and E.O. Frind, 1982. "Contaminant Transport in Fractured Porous Media: Analytical Solution for a System of Parallel Fractures." *Water Resour. Res.* 18(6), 1634-1642.

Sudicky, E.A., 1989. "The Laplace Transform Galerkin Technique: A Time-Continuous Finite Element Theory and Application to Mass Transport in Groundwater." *Water Resour. Res.*, 25, 1833-1858.

Sudicky, E.A., 1990. "The Laplace Transform Galerkin Technique for Efficient Time-Continuous Solution of Solute Transport in Double-Porosity Media." *Geoderma*, 46, 209-232.

Sudicky, E.A., and R.G. McLaren, 1992. "The Laplace Transform Galerkin Technique for Large-Scale Simulation of Mass Transport in Discretely Fractured Porous Formations." *Water Resour. Res.*, 28, 599-515.

Therrien, R., and S. A. Sudicky, 1996. "Three-dimensional Analysis of Variably-Saturated Flow and Solute Transport in Discretely-Fractured Porous Media." *J. Contam. Hydrol.*, 23, 1-55.

Walter H (1985). Vegetation of the Earth and Ecological Systems of the Geo-Biosphere. Springer-Verlag, New York, 318 pp.

Wu, Y. S., 1991. "CMM - A Semi-Analytical Computer Model for Simulating Ground Water Fate and Transport of Contaminants Subject to Chained-Decay Reaction," Prepared for the Office of Solid Waste of U.S. EPA, May 1991.

Xu, T., E. Sonnenthal, and G. Bodvarsson,A reaction-transport model for calcite precipitation and evaluation of infiltration-percolation fluxes in unsaturated fractured rock, Journal of Contaminant Hydrology, 64, 113 - 127, 2003.

Yau, T.L. and M. Maguire, 1990. "Control of localized corrosion of zirconium in oxidizing chloride media." In *Advances in Localized Corrosion*, H.S. Isaacs, U. Bertocci, J. Kruger and S. Smialowska (editors), 311-319, NACE International, Houston, TX.

Young, L.M., G.M. Catlin, P.L. Andresen, and G.M. Gordon, 2003. "Constant Load SCC Initiation Response of Alloy 22 (UNS N06022), Titanium Grade 7 and Stainless Steels at 105°C." *CORROSION/2003* (NACE International, Houston, TX), paper no. 03685.

Zhou, W. and C.M. Zheng, 1994. "Numerical Simulation of Unsaturated Seepage near a Cavity in Fractured Rock", in the Proceedings of 1994 Groundwater Modeling Conference in Fort Collins, Colorado, USA, Aug 10-12, 1994, pp.395 – 403.

A
APPENDIX A: HISTORY OF IMARC

A.1 Development of the IMARC Code

The development and evolution of the IMARC code, starting in 1989, is closely tied to the development and evolution of the proposed geological repository at Yucca Mountain. Increasing site characterization data, alternative conceptual models of repository processes, changes in engineered barrier system (EBS) designs, revised safety regulations, new congressional mandates, and court decisions have all affected the development and modification of IMARC to remain relevant to these changing factors. The IMARC code has evolved in distinct steps associated with so-called "Phase" reports by EPRI. To better understand the current version of the IMARC code, a history of its development and evolution in these "Phase" reports is summarized here. The focus is on development of code capabilities, identifying the specific structure and modeling capabilities that were sequentially added and modified since the inception of the IMARC code in 1990. Details on specific results can be found in each cited Phase report.

A.2 Phase 1 Report (EPRI, 1990)

In 1989, EPRI decided to develop a performance assessment methodology to independently evaluate the Yucca Mountain site in Nevada as a prospective site for the US CSNF and HLW geological repository[11]. EPRI selected a risk-based approach that was patterned after previous EPRI risk-based analyses of nuclear reactor safety. Key objectives in EPRI's project were to:

- demonstrate that a risk-based methodology was feasible and could be used by scientists and engineers familiar with issues surrounding long-term disposal of radioactive waste,
- provide a methodology for integrating information (including uncertainties in this information) from various disciplines affecting long-term repository performance, and
- illustrate potential insights resulting from application of a risk-based methodology (EPRI, 1990).

Initially, the EPRI (1990) project (later termed "Phase 1") was viewed as a demonstration of feasibility of applying a risk-based approach to geological disposal, and not as an assessment of HLW sites in general or any site in particular.

[11] The Yucca Mountain repository is intended to include the disposal of commercial spent nuclear fuel (CSNF), as well as naval reactors and reprocessed high-level waste (borosilicate glass) from US defense operations. In conformance with terminology by the International Atomic Energy Agency, "HLW" in this report will be used as a simple collective term for all of these types of wastes destined for Yucca Mountain, unless otherwise specifically modified (e.g., "HLW glass").

The specific example of the Yucca Mountain repository examined in EPRI (1990) did, however, coincide with similar safety analyses by the US Department of Energy (DOE) Office of Civilian Radioactive Waste Management (OCRWM) in the late 1980's and early 1990's (Dudley *et al.*, 1985; O'Connell and Drach, 1986; Apted *et al.*, 1991). A new DOE/OCRWM TSPA of Yucca Mountain appeared in 1993 (Wilson *et al.*, 1993), with regular updates thereafter (*e.g.,* DOE/OCRWM, 1995).

EPRI's (1990) risk-based approach was based on a logic-tree format, although equivalent techniques such as influence diagrams, event trees and faults trees also were considered. The logic tree format is a special application of a decision tree approach in which only uncertain events or states of a system are considered. Quoting from EPRI (1990, page 1-3):

> "Figure 1-1 [Figure A-1 in this report] shows an elementary logic tree representing two variables, A and B, whose values are uncertain. The values of variable A have been determined to be independent of B, so the left-hand node indicates the possible values of A and their assumed probabilities. The values of variable B have been determined to depend on A, so B is shown to the right of A with values and probabilities that depend on A. The combinations of A and B values are shown to the right of the logic tree, along with the probability of each combination; derivation can be made of a parameter X that is a function of A and B, and the probabilities calculated for combinations of A and B can be ascribed to the associated values of X."

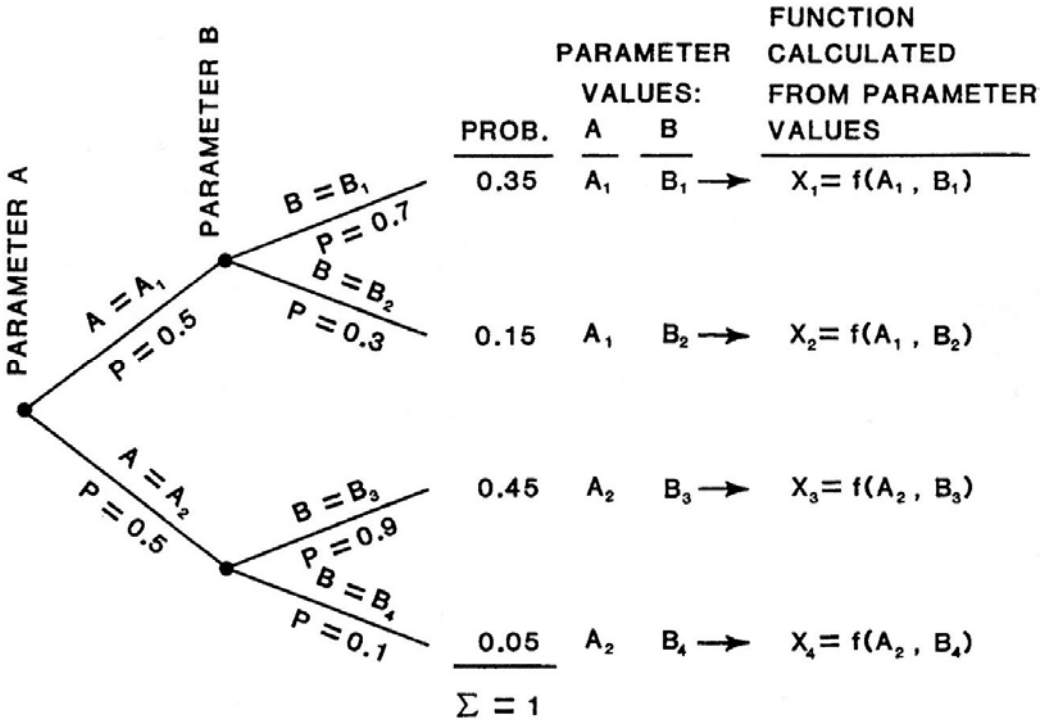

Figure A-1
General conceptualization of logic-tree format (Figure 1-1 from EPRI, 1990).

The value of the logic-tree approach, as stated by EPRI (1990), was that this approach structures and documents the interpretations made by the judgments of technical experts. Particularly when combining models, parameters, or assumptions among diverse technical disciplines, a common format for communicating the relevant variables and their uncertainties was considered desirable. The logic tree facilitated the derivation of subsequent effects (parameter *X* in the example cited from EPRI (1990), which could be taken as a dose or release rate of radionuclides from a repository) and the individual probabilities of each *X* value as a function of the selected values and probabilities of input parameters *A* and *B* (as well as *C, D, E, etc*.). Thus, each discipline (corresponding to each input parameter) could readily understand how it contributes to the overall system model. Furthermore, alternative input parameter values and uncertainties could be readily incorporated as alternative conceptualizations. The flexibility to incorporate alternative conceptual models, as well as expanding to incorporate entirely new models, was considered a key advantage in the logic-tree approach given the early stages of site characterization and repository design for the Yucca Mountain site in 1990.

EPRI's initial project team included experts in climatology, tectonics, volcanology, rock mechanics, hydrology, geochemistry, and waste package engineering (EPRI, 1990). Each expert developed a logic-tree representation of the values of key input parameters and uncertainties (expressed as expert judgment "probabilities" for each different value of a given input parameter).

A computer software package, called the Integrated Multiple Assumption and Release Calculations (IMARC) code, was developed (EPRI, 1990) to link the various logic-tree representations prepared by the EPRI team of experts. The overall performance model was based on the release of a solubility-limited radionuclide (^{237}Np was the single radionuclide adopted in the initial Phase 1 calculation of EPRI, 1990) from a single waste package in the engineered barrier system (EBS), followed by vertical downward transport through unsaturated formations of Yucca Mountain, then lateral flow and transport in saturated formations to the accessible boundary of the site (Figure A-2), as required in the Environmental Protection Agency (EPA) safety standard for a geological repository as drafted in 1990. The output from the initial IMARC code was the time-dependent cumulative release of radionuclides at the accessible boundary, defined by the prevailing regulations in 1990 as 5 km from the edge of the repository. To obtain a measure of the overall cumulative release for the repository, the calculated cumulative release was multiplied by the total number of waste packages in the repository. Calculations were made over a 100,000-year time post-closure period, although 10,000 years was the period of EPA regulatory compliance in 1990.

Based on the 11 nodes represented in the initial IMARC logic tree (Figure A-3), a total of 1022 separate realizations of cumulative release were calculated (EPRI, 1990). Each of these realizations had an associated probability. Thus, histograms were calculated of the probability of a given cumulative release at a given time after repository closure. These histograms were then converted into complementary cumulative distribution functions (CCDFs[12]) by summing release probabilities, starting at the highest release values.

[12] The CCDF format was part of the draft 1990 EPA 40 CFR Part 191 safety standard, but this metric has since been replaced by a probability-weighted dose rate as the EPA's draft 40 CFR Part 197 safety standard specific to Yucca Mountain. The output of the IMARC code has been modified in accordance with 40 CFR Part 197.

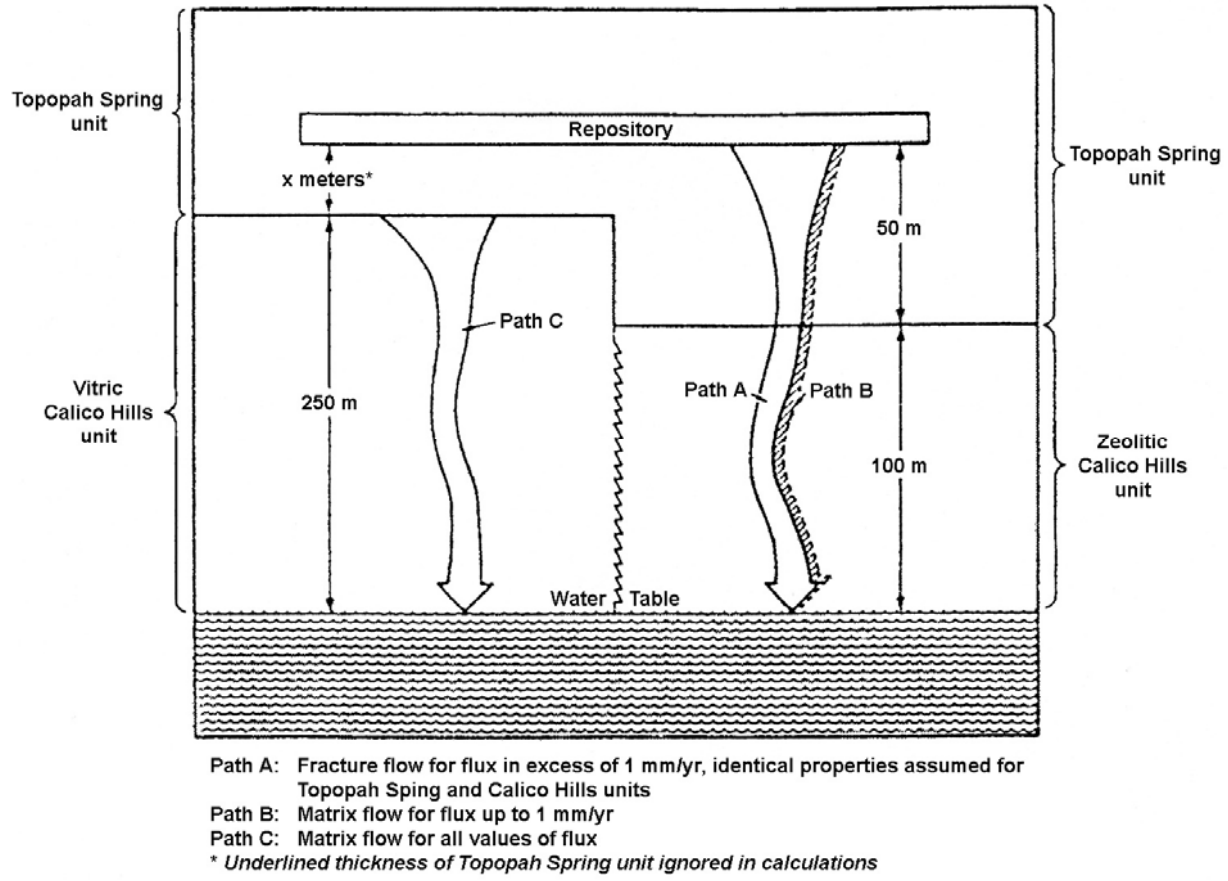

Figure A-2
Schematic of hydrological system considered in IMARC Phase 1 (EPRI, 1990).

The Phase 1 report confirmed the feasibility of a logic-tree approach to integrate various technical disciplines into a risk-based analysis of a geological repository for the disposal of HLW. Furthermore, the Phase 1 report (EPRI, 1990), using Yucca Mountain as an example, illustrated how the IMARC code could be used to gain insight into the type of research that would most efficiently reduce uncertainties in calculated performance of a geological repository at Yucca Mountain. Sensitivity studies further demonstrated ways in which risk-important inputs and assumptions could be identified to aid in future decisions regarding the acceptability of a given repository site and concept. Perhaps most importantly, EPRI's Phase 1 report represented a "proof-of-principle" that different engineering and scientific disciplines could be integrated into a total system performance assessment framework to assess not only regulatory safety compliance but also to give feedback as to key areas for further research. As noted earlier, EPRI's Phase 1 report was similar to the integrated total system performance assessment program conducted by DOE/ OCRWM that continues to this day.

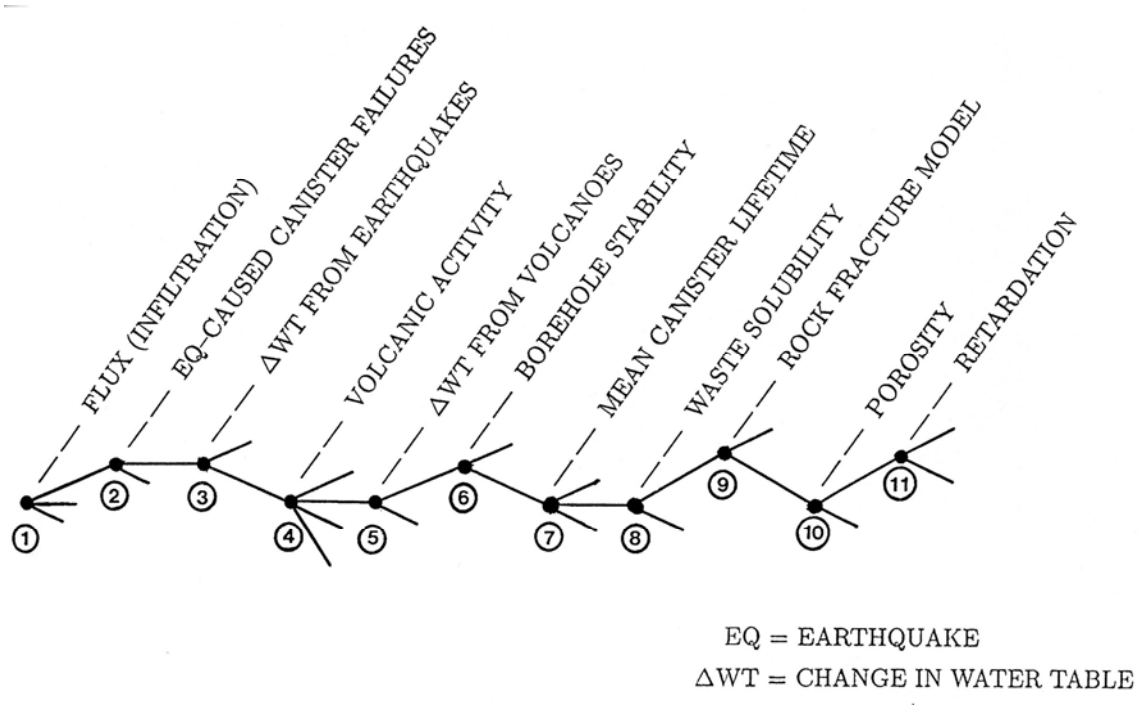

Figure A-3
Initial Logic-Tree Nodes for IMARC Phase 1 Analysis (EPRI, 1990).

A.3 Phase 2 Report (EPRI, 1992)

In 1992, EPRI decided to revise and upgrade its risk-based methodology and associated IMARC code in several ways, reflecting emerging issues relevant to a repository at Yucca Mountain. Specific objectives included:

- conversion of the Phase 1 illustrative IMARC model to a more realistic, technically defensible Phase 2 model,
- expansion from 1 radionuclide (^{237}Np) to a set of 13 key radionuclides (9 radioelements), and
- evaluation of specific new scenarios, including potential release of gaseous radionuclides (*e.g.,* ^{14}C), time-dependent changes in climate, net infiltration, seismic effects on the height of the water table, thermal impacts from radiogenic heating, and human intrusion (EPRI, 1992).

There were numerous IMARC modifications in EPRI's Phase 2 study that were subsequently found to have important implications in the safety assessment of a repository at Yucca Mountain. The event tree for IMARC Phase 2 was modified as shown in Figure A-6. These modifications and safety implications are summarized below.

A.3.1 Climate and Rainfall Model

The Phase 2 report initiated a nuanced consideration of the change in climate that might occur over time at the Yucca Mountain site, particularly with respect to rainfall that was considered an important factor in the net infiltration of water into the upper unsaturated formations at Yucca Mountain. The climate in the 10,000 year period following repository closure was sub-divided for the first time into possible "current," "greenhouse," "micropluvial" (later called "monsoon"), and "full glacial maximum" conditions, each with an associated rainfall and probability of occurrence over time. The rainfall inputs were based on statistical distributions of rainfall duration, intensity and seasonal timing based on current-day analogue sites. The possible impacts of large and more numerous storms, as well as cooler climate, on rainfall also were identified. In 1992, it was still considered that the net evaporation flux out of Yucca Mountain exceeded current precipitation. Hence, the Phase 2 consideration of a future wetter climate, greater precipitation, and the potential for net infiltration was a significant advancement in the understanding and modeling of the long-term performance of a repository at Yucca Mountain.

A.3.2 Net Infiltration Model

The sophistication of the infiltration model for the Phase 2 report was greatly increased. Areal and temporal factors potentially affecting net infiltration, such as plant community dynamics, spatial variability of soil properties, local topography runoff-infiltration relations in arid regions, evapo-transpiration, and local climate patterns, were introduced for the first time in building a model for net infiltration. By considering a range of credible conditions, some net infiltrations rates derived in Phase 2 were a factor of 10 higher than other 1993 estimates (e.g., Wilson *et al.*, 1993), although EPRI's Phase 2 values are now considered to be close to the representative values for the Yucca Mountain site (DOE/ OCRWM, 2002). The results of the revised net infiltration model were abstracted into Node 1 in Figure A-6.

A.3.3 Model of Changes in Water Table

Possible changes in the water table beneath a repository at Yucca Mountain resulting from either climate change or seismic events (so-called "seismic pumping") were considered in the EPRI Phase 2 study. Based on limited data at the time, increases in the height of the water table by up to several hundreds of meters were included in the Phase 2 analyses, albeit at appropriately low probabilities. A panel, specially convened by the US National Academy of Sciences and the National Research Council, later independently confirmed the possibility of such unlikely high rises in the water table (NAS, 1992). The results of the revised water table change model were abstracted into Node 2 in Figure A-6.

A.3.4 Volcanism and Seismic/ Earthquake Analyses

EPRI's Phase 2 report was the first to set out a systematic approach to evaluating the characteristics and probabilities of potential volcanic and seismic events in the Yucca Mountain region. The EPRI Phase methodology later became the basis for the DOE/ OCRWM's Probabilistic Volcanic Hazard Analysis (PVHA), and the first analysis was reported in 1996 (Geomatrix, 1996). A second iteration by the DOE/ OCRWM was released in 2008 (DOE, 2008). The key feature of EPRI's Phase 2 report was that it was the first examination of possible safety consequences arising from a low-probability volcanic event, as well as the consequences of earthquakes possibly leading to earlier-than-expected waste package failure.

A.3.5 Thermal Model

The Phase 2 report included an explicit treatment of both conduction and convection modes of heat transfer, and the implications of such heating on the timing and amount of eventual seepage of water into emplacement drifts of a repository at Yucca Mountain. Based on variability in rock properties and heat loading, as well as uncertainty in heat-transfer mechanisms, 3 separate "temperature cases" of temperature change over time were developed (see Figure A-4). The alpha (α) case ("hot case" in Phase 2 report) corresponded to limited heat-pipe and buoyant gas flow, and the temperature of the drift wall might reach a temperature approaching 200ûC. In the gamma (γ) case ("warm case" in Phase 2 report), a stronger heat-pipe effect was assumed, which acted to restrain temperature to the local 96ûC boiling point of water at the Yucca Mountain elevation. For the beta (β) case ("cool case" in Phase 2 report), a combination of low thermal loading and effective convective loss of heat acted to maintain drift temperature below the boiling point for all time. These three limiting cases were applied in subsequent analyses in the Phase 2 report, such as thermal spalling of rock faces and containment time for waste packages.

Subsequent site characterization and application of fully 3-dimensional coupled temperature-hydrology (TH) modeling supported the expectation of the alpha-like temperature profile for drifts at Yucca Mountain, although the peak temperature could be much lower in areas of low heat loads (*e.g.,* at the end of emplacement drifts), leading to profiles approaching the beta curve. These alpha and beta curves first derived and incorporated in EPRI's Phase 2 report also illustrated the difference between design concepts based on a high-temperature operating (HTOM, the current reference design for Yucca Mountain repository) versus a low-temperature operating mode (LTOM), these differences later received attention by some reviewers (*e.g.,* NWTRB, 2000).

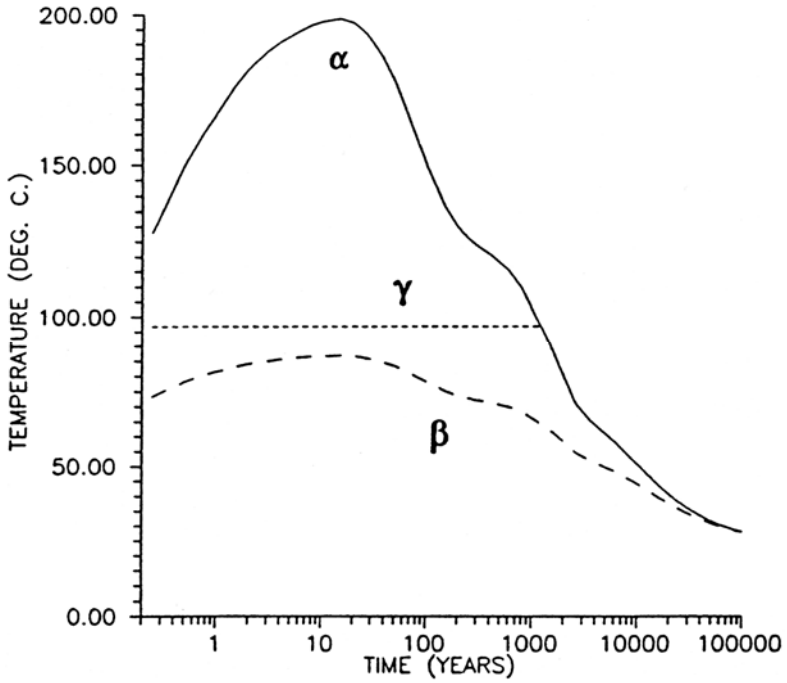

Figure A-4
Three alternative temperature-time curves calculated for the surface of the emplacement drift (EPRI, 1992).

A.3.6 Thermal Spalling Model

Excavation and heating from radiogenic decay from emplaced waste packages were anticipated to induce stresses at the rock surface of the emplacement drifts. The potential for thermal spalling of rock surfaces of vertical emplacement boreholes (DOE/OCRWM, 1988) was explicitly modeled in EPRI's Phase 2 report in 1992 (EPRI, 1992). Several different potential failure conditions were considered and a variety of representative rock properties were modeled using the UDEC discontinuum finite-element rock mechanics code (EPRI, 1992). Overall, the results indicated that the damage zone, if it occurred, would be limited to a thin zone around the borehole. The consequence of thermally induced rock spalling was that the air-gap between the vertical waste package and the wall of the emplacement borehole would be compromised, forming a continuous water pathway to form between the waste package and the surrounding tuff.

A.3.7 Containment Model

The reference waste package in 1992 was the same basic design as proposed in the 1988 Site Characterization Plan (SCP) for Yucca Mountain (DOE/OCRWM, 1988), which was composed of a single, thin-walled, 304-grade stainless steel container. A flexible Weibull-distribution approach was implemented in IMARC Phase 2 (EPRI, 1992) to evaluate cumulative containment failure times for such a container. This Weibull formulation allowed for broad consideration of (1) different corrosion failure modes for a given container metal, and (2) different container metals (304-grade stainless steel was the reference, but other metals such as alloy 825 were also

under consideration in 1992). The failure times derived from the container models were controlled primarily by the temperature-time profiles (*i.e.*, α, β and γ curves of Figure A-4).

A.3.8 Source-term Model

The proposed commercial spent nuclear fuel (CSNF) waste package design for the Yucca Mountain repository in 1992 was a thin-walled 304-grade stainless steel disposal container emplaced vertically into the floor of a backfilled drift (O'Connell and Drach, 1986). Three bounding source-term release models, or "modes," were envisioned:

- "dry" waste packages, in which only gaseous release could occur once the container failed,
- "wet-continuous" waste packages in which there was a continuous film of water that connected the waste packages (hence, CSNF when the container failed) to the hydrological setting of the unsaturated tuff and that could provide a conduit for aqueous radionuclide releases, and
- "wet-drip" waste packages in which dripping water could provide a conduit for aqueous radionuclide releases once the container of the CSNF waste packages failed (EPRI, 1992).

The proportion of waste packages in each of these "modes" was a user-defined parameter in IMARC. In 1992 there was significant debate on water movement in and around the EBS for a Yucca Mountain repository (*e.g.*, Apted *et al.*, 1991).

The CSNF was sub-divided into separate sources for radionuclides for the first time in the Phase 2 report:

- UO_2 matrix,
- zircaloy cladding and irradiated hardware, and
- instant release fraction of "gap" and "grain boundary" phases (EPRI, 1992).

For each of these "sources," reference Yucca Mountain sources were used to obtain the inventories for these nine safety-related radioelements: C, Se, I, Tc, Cs, Ra, U, Np, Pu (13 safety-related radionuclides). These representative radioelements were selected on the basis of previous safety analyses of long-term releases from CSNF repositories (EPRI, 1992).

Two basic constraints on the release of radionuclides from the UO_2 matrix and cladding were implemented into the Phase 2 IMARC code: (1) radioelement solubility limits, and (2) dissolution/ corrosion rates. Possible temperature dependencies on these values were not considered, based on the fact that containment times were calculated to be significantly longer than the initial several thousand year thermal period. Reference solubility and dissolution rate data as reported at that time by the Yucca Mountain Project were used (EPRI, 1992). A series of existing, well-verified analytical source-term models (Pigford and Chambré, 1988) were implemented into the IMARC code for calculating aqueous and gaseous steady-state release rates for all three source-term "modes."

In the final Phase 2 implementation of the IMARC code (EPRI, 1992), the near-field source-term model linked "low," "moderate" and "high" values for solubility and dissolution rate. This implied correlation in IMARC between solubility values and dissolution rates was based on the need for calculational efficiency. It was noted that if IMARC sensitivity analyses showed a strong impact of variations of solubility and dissolution rate values on overall repository performance, that a more detailed source-term model could be implemented at a later time, which indeed was done in later Phases.

A.3.9 Groundwater Flow and Transport Model

In the Phase 2 report (EPRI, 1992,), the groundwater system at Yucca Mountain was represented by a logic tree consisting of four nodes. The motivations and bases for considering these nodes were as described below.

The "Groundwater Flux at the Repository" node considered possible lateral diversion of water by the densely welded Paintbrush Tuff unit overlying the repository horizon at Yucca Mountain. In 1992, it was speculated that the net infiltration flux calculated at the surface of Yucca Mountain might be reduced because of such lateral diversion.

The second hydrological node, "Fracture/ Matrix Coupling," considered the radionuclide-bearing water moving vertically under gravitation in the unsaturated zone below the repository. Flow in a fractured porous medium was described mathematically in its most complete form by considering separate non-linear flow equations for the matrix and the fracture network. Terms in these equations accounted for the extent of coupling (*i.e.,* water movement) between these two systems. While it was possible to solve the pair of coupled equations, this approach was judged to be too computationally intensive for the purposes of IMARC analyses. A simplifying assumption was made that any difference in pressure head developed within a fracture would be instantaneously redistributed within the matrix, and vice versa (see Dudley *et al.,* 1985). This assumption yielded a single flow equation in which key hydrological parameters were presented as bulk or "composite" values. For example, hydraulic conductivity and capacitance terms were defined as the volume-weighted contributions from the matrix and the fractures. This "composite" relationship, illustrated in Figure A-5, showed the combined effects of fractures and matrix. As the unsaturated medium (*i.e.,* unsaturated tuff) became drier (higher negative pressure heads), the matrix conductivity controlled the "composite" conductivity, whereas when the unsaturated medium became wetter, the fracture conductivity became controlling.

In the same way that there was flow coupling between the fracture system and matrix, the Phase 2 report (EPRI, 1992) considered possible coupling between the diffusive mass flux of dissolved radionuclides between the fracture system and the pores within the matrix. Two limiting conditions for such diffusive-transfer coupling were implemented into the Phase 2 IMARC code; "strong" coupling in which the radionuclide mass was instantaneously redistributed between matrix pores and the fracture system, and "weak" coupling in which there was a reduced, finite rate of diffusive transfer between fractures and matrix (possibly arising from the precipitation of fracture-lining minerals, for example). The effect of "weak" coupling was most evident for relatively higher groundwater fluxes, leading to dissolved radionuclides moving downward along fractures significantly in front of dissolved radionuclides moving in the matrix.

A third node of "Matrix Sorption" was considered in the Phase 2 IMARC code (EPRI, 1992). "Low," "moderate" and "high" sorption coefficient values (K_d's) for the nine considered radioelements were identified for both Topopah Springs and Calico Hills tuff units that underlie the repository horizon at Yucca Mountain (see Figure A-2).

The fourth and final groundwater node for Yucca Mountain considered "Saturated Flow." Transport was assumed to be affected only by advection, and thus was characterized by an average groundwater velocity. Sorption effects were also considered in this saturated flow calculation, although there was no lateral or vertical dispersion considered.

A.3.10 Model for Transport of Gaseous Radionuclides

A simplified model for the release of gaseous ^{14}C from a Yucca Mountain repository to the ground surface[13] was also implemented into the Phase 2 IMARC code (EPRI, 1992). Travel times of ^{14}C from the repository upward to the ground surface were calculated and plotted as a histogram as a function of rock properties, repository temperature at the time of containment failure, and exchange of ^{14}C (retardation) between water and gas phases during this migration. These histograms provided "low," "moderate" and "high" estimates of ^{14}C release to the surface of Yucca Mountain that were implemented into the IMARC code.

[13] The possibility and consequences of release of gaseous radionuclides (notably ^{14}C) from the unsaturated Yucca Mountain site were significant issues in the US in 1992 (*e.g.,* Lu *et al.*, 1991). The EPA draft standard at that time, 40 CFR 191, was promulgated on the assumption of a deep geological repository located below the water table (*i.e.*, solely an aqueous release pathway). While calculated releases of ^{14}C from a Yucca Mountain repository were far below cosmogenic sources, calculated CCDFs for ^{14}C often indicated a technical violation of the 40 CFR 191 criterion for ^{14}C.

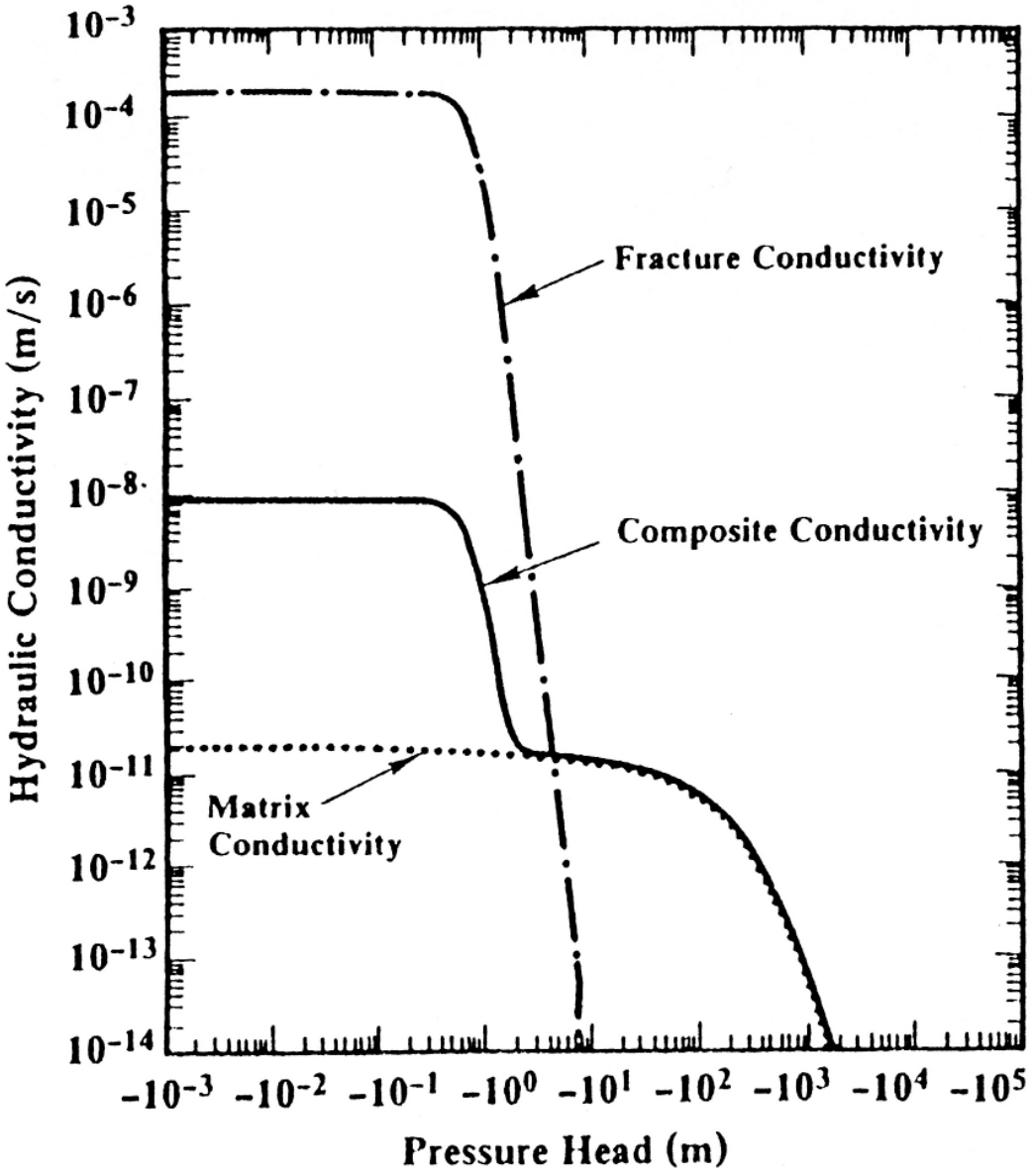

Figure A-5
Example of a composite Conductivity Curve Developed from Separate Fracture and Matrix Conductivity Curves (Dudley *et al.,* 1985; EPRI, 1992).

A.3.11 Human Intrusion Model

The Phase 2 report (EPRI, 1992) also examined a possible logic-tree approach to the human intrusion scenario. A general model estimating the likelihood of human intrusion was proposed consisting of five factors:

- status of society,
- knowledge of the site,
- value of potential site resources,
- activities at the site in the future, and
- intrusion given such activities.

With respect to the implications of human intrusion on the isolation performance of a repository at Yucca Mountain, the "intrusion given such activities" node of the human intrusion logic tree considered three basic types of impacts:

- waste packages directly hit by drilling,
- waste packages excavated to the surface, and
- waste packages impacted by increased water flow.

Further analysis of the human intrusion scenario for a repository at Yucca Mountain was obviated by US Congressional mandates to the EPA, including future recommendations to the EPA by the US National Academy of Sciences on a Yucca Mountain-specific standard.

A.3.12 Phase 2 Results

For the Phase 2 analyses, the IMARC code was extended to 14 nodes (Figure A-6). The technical aspects of each node have been reviewed above.

The key conclusions of EPRI's Phase 2 report (EPRI, 1992) were

> "Sensitivity studies for aqueous pathways indicate that critical factors affecting nuclide release include the amount of groundwater infiltration, solubilities of radioelements, dissolution rate of the waste matrix, lateral diversion of groundwater flow around the repository, characteristics of the engineered barrier system, and coupling between fracture and matrix flow."

IMARC Phase 2 results also provided EPRI with insights on policy issues of the day, including the release of gaseous ^{14}C and a human intrusion scenario, with respect to the prevailing regulatory framework of 1992.

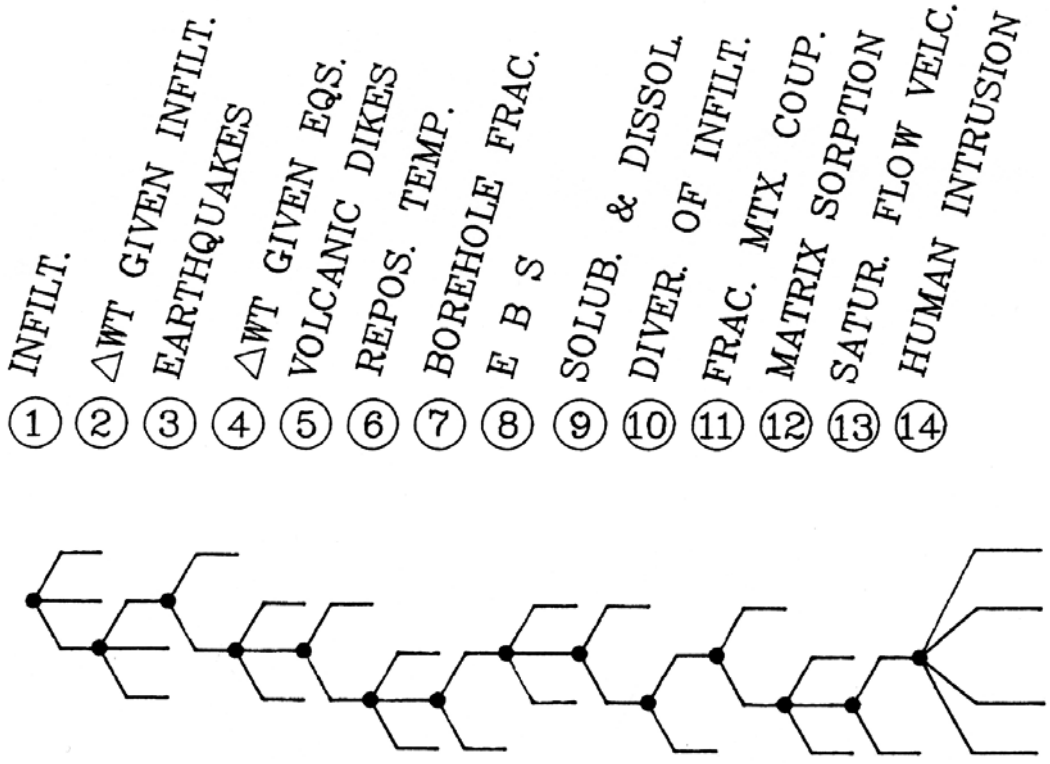

Figure A-6
Logic-tree nodes for IMARC Phase 2 analysis (EPRI, 1992).

A.4 Phase 3 Report (EPRI, 1996)

The purpose for EPRI's Phase 3 report (EPRI, 1996) using the IMARC code was to explore the various models, parameters, and assumptions affecting estimated performance of the 1996 Yucca Mountain repository concept, thus allowing inferences to be made about which of those models, parameters and assumptions were robust, which were relatively unimportant, and which had remaining uncertainties that substantially contribute to uncertainties in repository performance. A key aspect of EPRI's IMARC analysis was to make an independent assessment of the performance-related issues of the repository concept under consideration, in order that decision-makers in the utility industry could better judge the potential outcome of a future licensing process.

By 1996, the situation for HLW geological disposal in the US had greatly changed from the 1992 Phase 2 report (EPRI, 1992). The changes relevant to IMARC are listed here:

- the US National Academy of Sciences had published its "Technical Bases for Yucca Mountain Standards" ("TYMS Report") (NAS, 1995);
- the EPA was developing a new, Yucca Mountain specific safety standard, 40 CFR 197, although no decision had been reached on the time period of regulatory compliance (possibly either 10,000 years or one million years) and the acceptable level of exposure for compliance;

- there had been a fundamental change in the understanding of groundwater flow and dissolved contaminant transport for the unsaturated zone portion of Yucca Mountain;
- controversial measurements were reported of downward migration of bomb fall-out ^{36}Cl to several hundred meters depth at Yucca Mountain, suggesting that perhaps a small fraction of water moved rapidly in the unsaturated tuff;
- the areal density, hence thermal loading, of emplaced HLW waste packages had been significantly increased, leading to higher peak temperature and extended periods of above-boiling conditions;
- the original thin-walled, vertically emplaced waste package had been modified to the so-called "Advanced Conceptual Design" (ACD), which was a much larger waste package, composed of multiple layers of different kinds of steel, that was to be horizontally emplaced in open drifts (or only partially backfilled) drifts;
- the 1995 TSPA report by DOE/OCRWM (1995) was a significantly more detailed and comprehensive analyses than the previous TSPAs by the DOE, explicitly considering both a 10,000-year and a 1,000,000-year period of performance, as well as the comparative effects of different engineered barrier options (*e.g.,* inclusion of a capillary-breaking backfill in the repository drifts led to decreases in estimated peak doses of key radionuclides by up to eight orders of magnitude);
- debate had started on whether an alternative waste package design that would remain sub-boiling for all times after emplacement might avoid uncertain impacts from local hydrothermal processes; and
- on a programmatic/policy level, the Technical Site Suitability (TSS) analysis, originally required by the Nuclear Waste Policy Act of 1982, had been amended by Congress to a less formal "Viability Assessment."

In response to these changing factors, many of the IMARC sub-models were necessarily revised, updated, or in several areas, such as site hydrology, near-field source-term and biosphere pathway analysis, new calculational models were developed, verified and implemented into IMARC. Indeed, because many of these changed factors in 1996 were to become standard features of the current Yucca Mountain concept (*e.g.*, horizontal waste package, integrated unsaturated and saturated hydrological model, climate changes up to one million years, *etc.*), many of the current sub-models of IMARC date to the Phase 3 report (EPRI, 1996). The most significant of these sub-models are discussed below.

A.4.1 Climate Change Model

The possible need to evaluate repository performance out to one million years obviously entailed consideration of possible climate changes over this period. Following the work of Goodess and Palutikof (1993), the Phase 3 report identified three possible future climate sequences:

- Sequence 1: anthropomorphic activities (*i.e.*, greenhouse, GH) having no effect on the next glaciation,
- Sequence 2: anthropomorphic activities affecting the onset and magnitude of the next glaciation, and

- Sequence 3: "runaway"[14] impacts from anthropomorphic activities (EPRI, 1996).

For Sequence 2, judged to be the most likely for future conditions at Yucca Mountain, changes to current seasonal (winter *vs*. summer) temperature and precipitation were estimated and normalized to three climate regimes; interglacial (today's climate), greenhouse modified climate and full glacial maximum (Table A-1). These calculations provided estimates of the duration and pattern of occurrence of the climate regimes over the next one million years, which served as inputs to subsequent net infiltration calculation described below.

A.4.2 Net Infiltration Model

Basically the same modeling approach as conducted for Phases 1 and 2 was applied for modeling net infiltration in Phase 3 IMARC analyses. The inputs to these models, and the time frame over which they were applied, however, were considerably revised in Phase 3. Calculations were made for three soil/ hydrological units, and three basic possible sequences of climate regime, as discussed above. Model time-steps of 500 years were employed to calculate net infiltration changes over time.

The primary outputs of these calculations were (1) probability distributions of net infiltration for a given climate regime (Figure A-7), and (2) calculated relationships between net infiltration and annual precipitation (Figure A-8). The latter calculated relationships were verified by comparison with modern day sites with corresponding climate and topographic conditions (EPRI, 1996).

A.4.3 Thermal Model and Seepage Model

The timing and magnitude by which water may eventually seep into open emplacement drifts at Yucca Mountain has potentially important impacts on the (1) corrosion of water packages (hence, on containment time before release of radionuclides could be initiated), and (2) subsequent mobilization and release of radionuclides once the waste package container had failed. By 1996, DOE / OCRWM (1995) was considering the various ways that areal thermal loading and spacing between waste packages (as well as spacing between emplacement drifts) might be used to favorably reduce seepage.

[14] "Runaway" means future climates no longer include glaciation periods.

TableA-1
Phase 3 Climate Timeline for Sequence 22 at Yucca Mountain (from EPRI, 1996).

Years AD	Avge. Atm CO_2 level	Winter Δ temp	Summer Δ temp	Winter Δ precip	Summer Δ precip
2000 to 2100	500ppm (2xCO_2)	+1.2°C	+1.3°C	+4%	–2%
2100 to 2500	900ppm (peak>1000)	+4.0°C	+4.8°C	+14.8%	–7.4%
2500 to 5000	750ppm	+2.4°C	+2.6°C	+8.0%	–4.0%
5000 to 10,000	650ppm	+2.0°C	+2.2°C	+6.8%	–3.4%
10,000 to 25,000	270ppm, post GH	[10.7°C, mod.]*	[25.7°C, mod.]*	100mm "modern"*	57mm "modern"*
25,000 to 50,000	1/3 full glacial	–2.0°C	–2.5°C	+22%	–16%
50,000 to 65,000	2/3 full glacial	–4.0°C	–5.0°C	+44%	–32%
65,000 to 90,000	1/3 full glacial	–2.0°C	–2.5°C	+22%	–16%
90,000 to 100,000	interglacial	0.0°C	0.0°C	0%	0%
100,000 to 140,000	1/3 full glacial	–2.0°C	–2.5°C	+22%	–16%
140,000 to 155,000	2/3 full glacial	–4.0°C	–5.0°C	+44%	–32%
155,000 to 165,000	3/3 full glacial	–6.0°C	–7.5°C	+66%	–48%
165,000 to 190,000	2/3 full glacial	–4.0°C	–5.0°C	+44%	–32%
190,000 to 200,000	interglacial	0.0°C	0.0°C	0%	0%
⊥	⊥	⊥	⊥	⊥	⊥

* This time frame represents the post-greenhouse extended interglacial, considered to be the most likely scenario by Nirex[1]. Following French's (1985) division of months into winter (Oct, Nov, Dec, Jan, Feb, Mar, Apr) and summer (May, June, July, Aug., Sept.), and Diaz's (1993) summary of modern temperature data for extreme southern Nevada, today's average winter temperature is 10.7°C, and the average summer temperature is 25.7°C. French (1985) reports 100 mm/yr for the 7 months of winter precipitation, and 57 mm/yr for 5 summer months for the Nevada Test Site. This is lower than the 170 mm annual value Flint finds for the last two or three years. However, the most recent years may be anomalous due to an El Nino effect on precipitation and the current anthropogenic CO_2 effect on temperatures. *Note that other values shown in table are given with respect to these presumed modern values.*

In the Phase 3 IMARC modeling, various representative values of

- areal thermal (mass) loading (25 or 83 MTU/ acre),
- heat-transfer mechanisms ("conduction" dominated vs. "convection" dominated vs. "heat-pipe" dominated),
- water-flow regimes ("fracture only" in which water entered into matrix only until 100% saturation is reached vs. "strong focusing" in which water only flowed in major fracture zones spaced 100's or 1000's of meters apart and intervening rock was dry vs. "weak focusing" in which water flow was inhomogeneous, but zones of higher percolation flux,

involving fracture flow, were distributed widely and were not limited to major fracture zones), and

- temperature histories (see Figure A-4)

were combined in a coupled process model. This coupled process model was used in Phase 3 to estimate the percentage of waste packages that might experience one of four different types of "seepage" modes:

- "dry": the waste package was not contacted by liquid water, either because of capillary forces diverted water around that particular part of the emplacement drift or that the rock overlying the waste package remained dried out,
- "reflux": the waste package was contacted by water only during the time interval after the emplacement drift descended below the boiling point of water, and condensate water formed by reflux (cyclic boiling and condensation in the rock) dripped onto the waste package. (At all other times, the waste package was assumed to be dry),
- "wet-drip": once the emplacement drift descended below the boiling point of water, the waste package experienced a steady rate of dripping water onto its upper surface, and
- "episodic": the waste package was contacted only episodically and for limited durations by water flow in fractures, possibly arising from fluctuations in net filtration, seismic events, changes in fracture mineralization, *etc*.

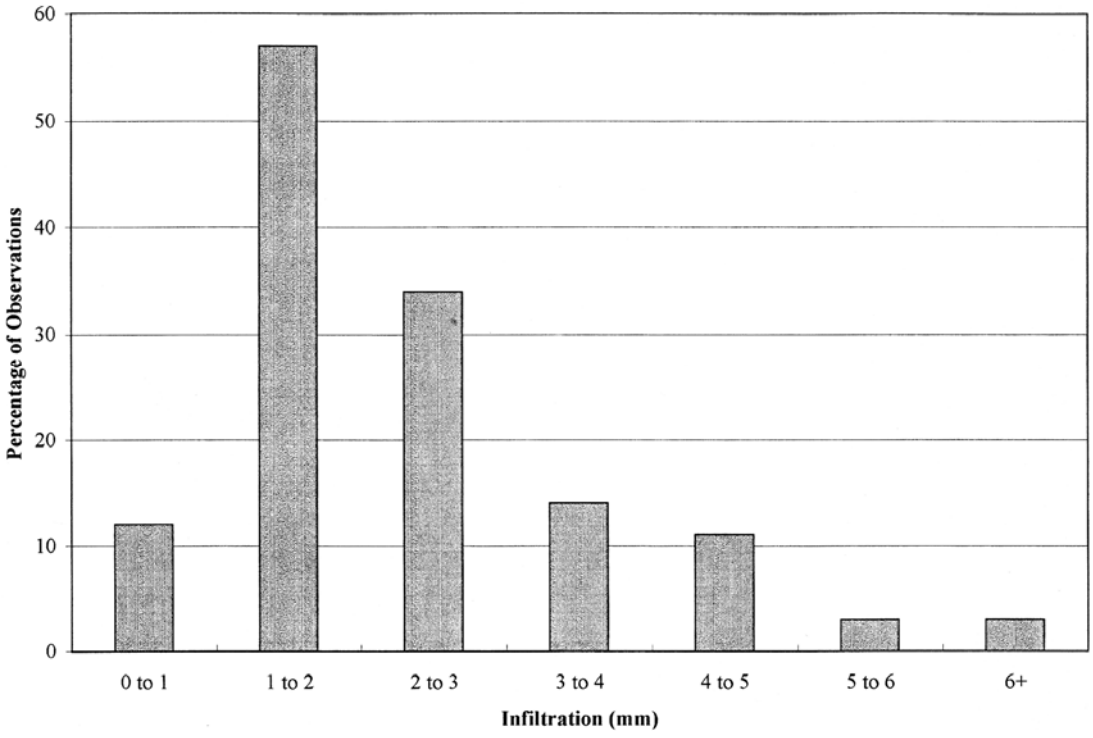

Figure A-7
Phase 3 Histogram of Net Infiltration Rates (EPRI, 1996)

The actual model description has been provided in EPRI (1996). A summary table of results from that Phase 3 couple-process analysis showing how IMARC Phase 3 estimated the percentages of waste packages experiencing the four various "seepage" modes for different sets of conditions is shown in Table A-2.

A.4.4 Containment Model

In 1996, a variety of new materials and designs for waste package containers were under consideration by DOE (DOE/OCRWM, 1995). Both single-wall and double-wall (*e.g.*, inner container of alloy 825 with an outer container of mild steel) container designs were being investigated. The original 304-grade stainless steel container material had been superseded by consideration of alloy 825, grade 16 titanium, high-nickel alloy C-22 (also called "alloy 22"), and a Pb-Bi alloy, and each of these materials had several possible corrosion failure modes to be evaluated. Also, because DOE / OCRWM was considering the possible containment performance from irradiated zircaloy cladding of disposed CSNF, the EPRI Phase 3 report also developed a containment failure model for such cladding. Finally, given a possible 1,000,000-year timescale for regulatory compliance, additional failure modes, such as microbially influenced corrosion (MIC) and mechanical failure from collapse of open drifts over long time periods, were also considered.

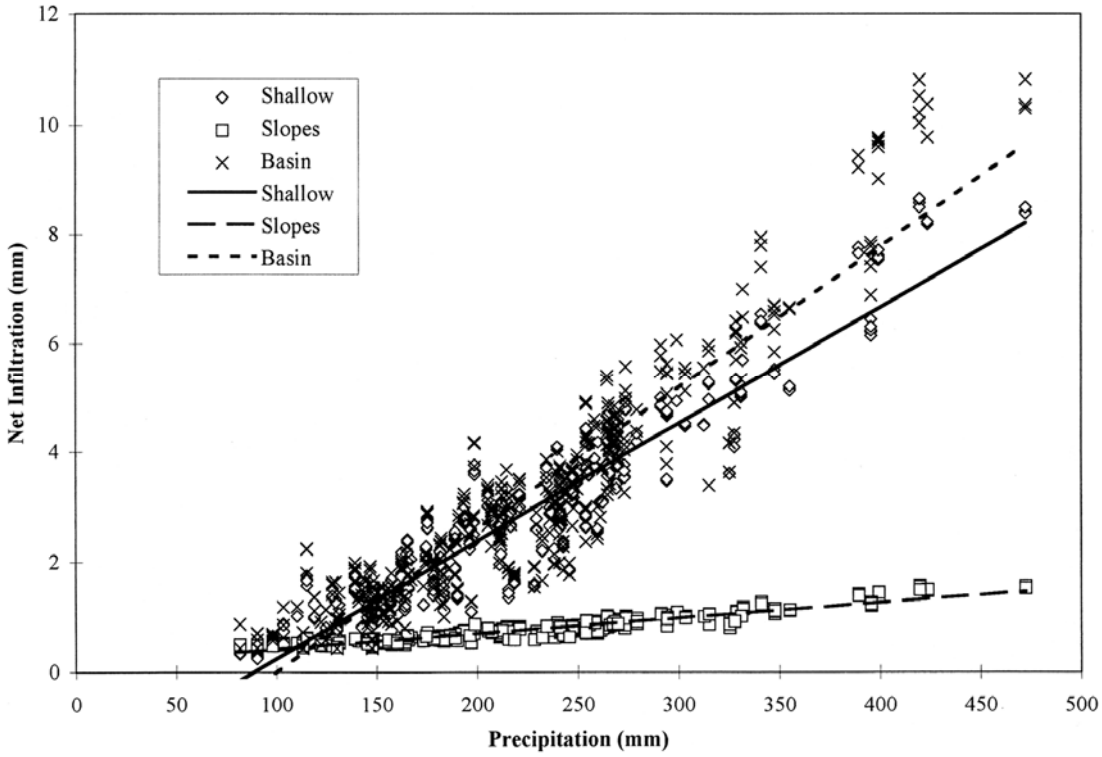

Figure A-8
Phase 3 relationships between precipitation and net infiltration (EPRI, 1996).

The Phase 3 approach (EPRI, 1996) for developing failure models for each type of container material and each applicable corrosion modes was essentially the same as for Phase 2 (EPRI, 1992). Each basic failure model employed multi-parameter Weibull equations to describe the containment failure rate as a function of time for a specific:

- container material (including cladding),
- type of corrosion mode for that container material
- set of temperature-time conditions (Figure A-4), and
- "seepage" mode (Table A-2).

For waste packages remaining "dry" (Table A-2), the humid environment of the repository was assumed to allow limited dry oxidation of various waste package materials, so appropriate models were developed in Phase 3 (EPRI, 1996) for this corrosion mode.

Table A-2
Summary table of fraction of waste packages experiencing various types of water contact modes (EPRI, 1996).

		Dry			Reflux*			Wet-Drip			Episodic		
		α	β	γ	α	β	γ	α	β	γ	α	β	γ
Fracture Only	Conduction, 25	0	0.18	0.75	0	0	0	0	0.01	0.04	0	0.01	0.01
	Conduction, 83	0.65	0.23	0	0	0	0	0.04	0.05	0	0.01	0.02	0
	Convection, 83	0.43	0.35	0.04	0.02	0	0	0	0.1	0.005	0	0.05	0.005
	Heat Pipe, 83	0.4	0.45	0	0	0	0	0	0.1	0	0	0.05	0
Weak Focusing	Conduction, 25	0	0.15	0.5	0	0.01	0	0	0.03	0.2	0	0.01	0.1
	Conduction, 83	0.6	0.12	0	0.1	0.02	0	0	0.1	0	0	0.06	0
	Convection, 83	0.15	0.3	0.06	0.02	0.09	0	0.02	0.12	0.07	0.01	0.09	0.07
	Heat Pipe, 83	0	0.2	0.04	0	0	0	0	0.5	0.05	0	0.2	0.01
Strong Focusing	Conduction, 25	0	0.16	0.7	0	0.02	0	0	0.01	0.05	0	0.01	0.05
	Conduction, 83	0.5	0.2	0	0.2	0.04	0	0	0.05	0	0	0.01	0
	Convection, 83	0.3	0.15	0.06	0.2	0.2	0	0	0.04	0.03	0	0.01	0.01

*Reflux mode operates for 2000 years following the descent of the repository below the boiling point. At other times, these packages are dry.

A.4.5 Source-term Model

One of the most significant changes in the Phase 3 IMARC code (EPRI, 1996) was replacement of numerous steady-state analytical equations by a general compartment model (akin to a simplified finite-element approach) for describing radionuclide source-term release from the EBS. Similar compartment model approaches had been successfully used in other national repository programs (*e.g.*, Romero *et al.*, 1991; Worgan and Robinson, 1992) for source-term modeling and overall repository assessment.

For the Phase 3 compartment model named COMPASS, different regions of the EBS and near-field rock were explicitly defined as spatial "compartments" with specific physical (length, surface area, volume, porosity, hydraulic conductivity, *etc*.) and chemical (solubility limits, sorption coefficients, *etc*.) characteristics. These separate compartments were then linked by mass-transfer relationships and appropriate boundary conditions. The complexity and computational efficiency of the COMPASS source-term model could be easily changed by changing the number of "compartments." Furthermore, by implementing this flexible COMPASS compartment model into IMARC, any future changes in types, dimensions, number, boundary conditions, or characteristics of engineered barriers could be readily analyzed by reconfiguring the "compartments."

Three different COMPASS source-term models (Figure A-9) were implemented into IMARC in Phase 3 (EPRI, 1996) to model three limiting modes of radionuclide release:

- An "over-flow" model in which dripping water was assumed to enter through a failure at the top of the waste package, to react with the waste form, and to cause the release of radionuclides into the internal water volume. The waste package would eventually fill with this water (so-called "bath tub"), then the radionuclide-bearing water would gravitationally flow out of a failure at the top the waste package, then flow into underlying gravel backfill, then the concrete invert, and eventually the radionuclide-bearing water would enter into the underlying unsaturated fractured tuff;
- A "through-flow" model in which dripping water was assumed to enter through a failure at the top the waste package, to react with the waste form, and to cause the release of radionuclides into the internal water volume. Then this radionuclide-bearing water would gravitationally flow out of a failure at the bottom the waste package (no "bath tub"), then flow into underlying gravel backfill, then the concrete invert, and eventually the radionuclide-bearing water would enter into the underlying unsaturated fractured tuff; and
- A "no-flow" model in which there would be no advective (no water dripping) onto a failed waste package. Formation of a continuous layer of condensate water, however, would allow release and diffusive migration of dissolved radionuclides from the waste form out through the failed waste package, then diffuse through the gravel backfill and subsequently diffuse through the cement invert, and eventually the radionuclide-bearing water would enter into the underlying unsaturated fractured tuff.

A fourth model for the highly unlikely occurrence of fully-saturated conditions within the EBS was also implemented into IMARC, but there never has been any credible evidence to support the speculation that such saturated-flow conditions could ever be obtained, even temporarily, for a repository at Yucca Mountain (NAS, 1992).

The implementation of the COMPASS compartment model in the IMARC Phase 3 code fundamentally changed and greatly enhanced the overall capabilities of the IMARC code. Given the inherent flexibility in revising such "compartments," it has been possible to readily apply the IMARC code in subsequent analyses of newer EBS designs, as well as in analyses of possible scenarios, such as rockfall/ drift collapse and formation of so-called "shadow zones" (regions of unsaturated fractured tuff in which water occurs only in matrix, thereby limiting migration of radionuclides to extremely slow diffusive transport through the matrix).

A.4.6 Groundwater Flow and Transport Model

Another important development in the Phase 3 report (EPRI, 1996) was the implementation of a new, combined unsaturated and saturated flow model. The conceptual model was based on work by Kool, *et al.* (1994), who presented a composite approach linking one-dimensional flow and transport through an unsaturated zone with a three-dimensional representation of flow and transport in an underlying saturated zone (Figure A-10).

With respect to the unsaturated zone, the new Phase 3 IMARC model for flow and transport allowed the EBS to be sub-divided into separate vertical-column sub-regions (sometimes referred to as "stove pipes"), and each columnar sub-region of the unsaturated fractured tuff could be assigned different properties and performance characteristics. Time varying infiltration/ seepage rates, water table depths, and source-term release rates could all be assigned different values for each columnar sub-region, with no lateral coupling assumed between different sub-regions. All physical properties controlling water flow and radionuclide transport could be varied with depth within each columnar sub-region, and between one column and the next.

Because isothermal conditions were assumed, given the expected extended containment of waste for several 1000's of years, the energy transport conditions were not coupled into the model, although the model could be modified to approximate non-isothermal conditions if that option became of interest.

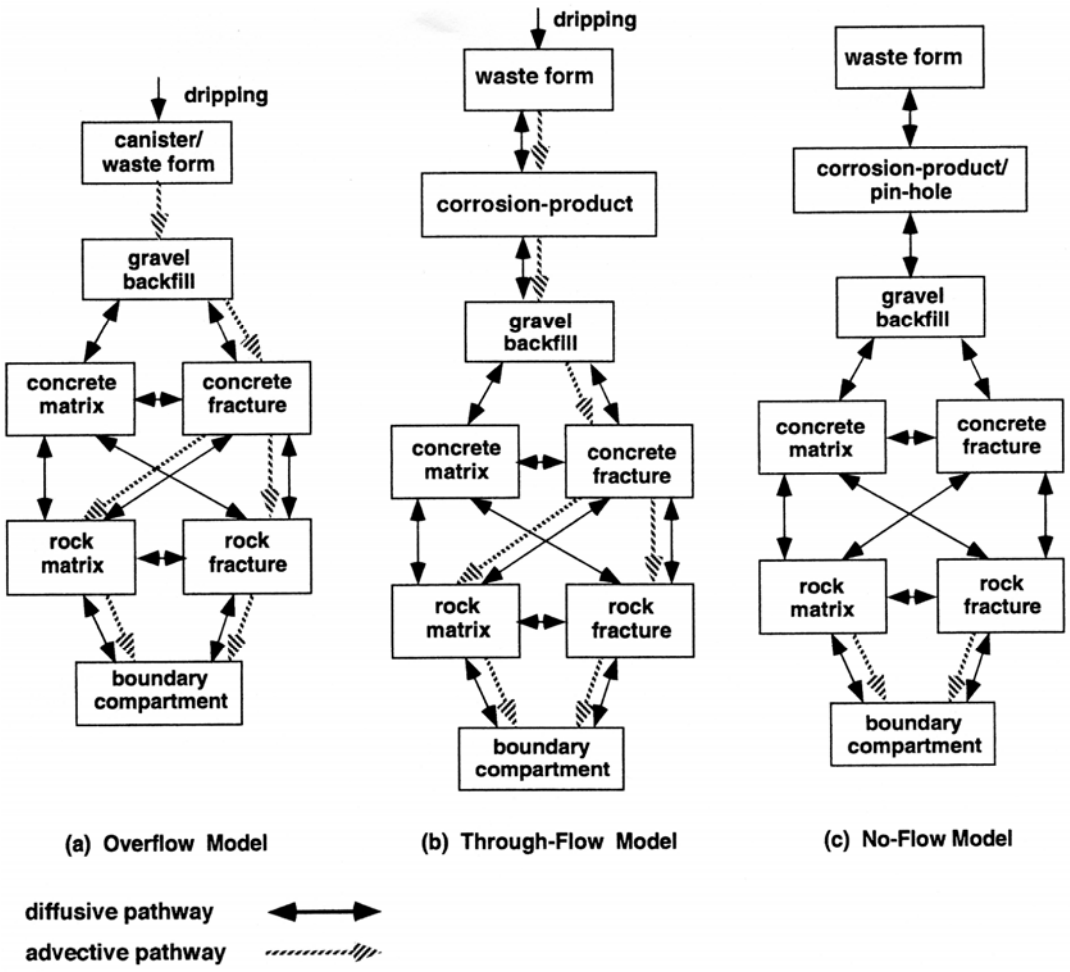

Figure A-9
Schematic representation of compartments for various source-term release modes (EPRI, 1996).

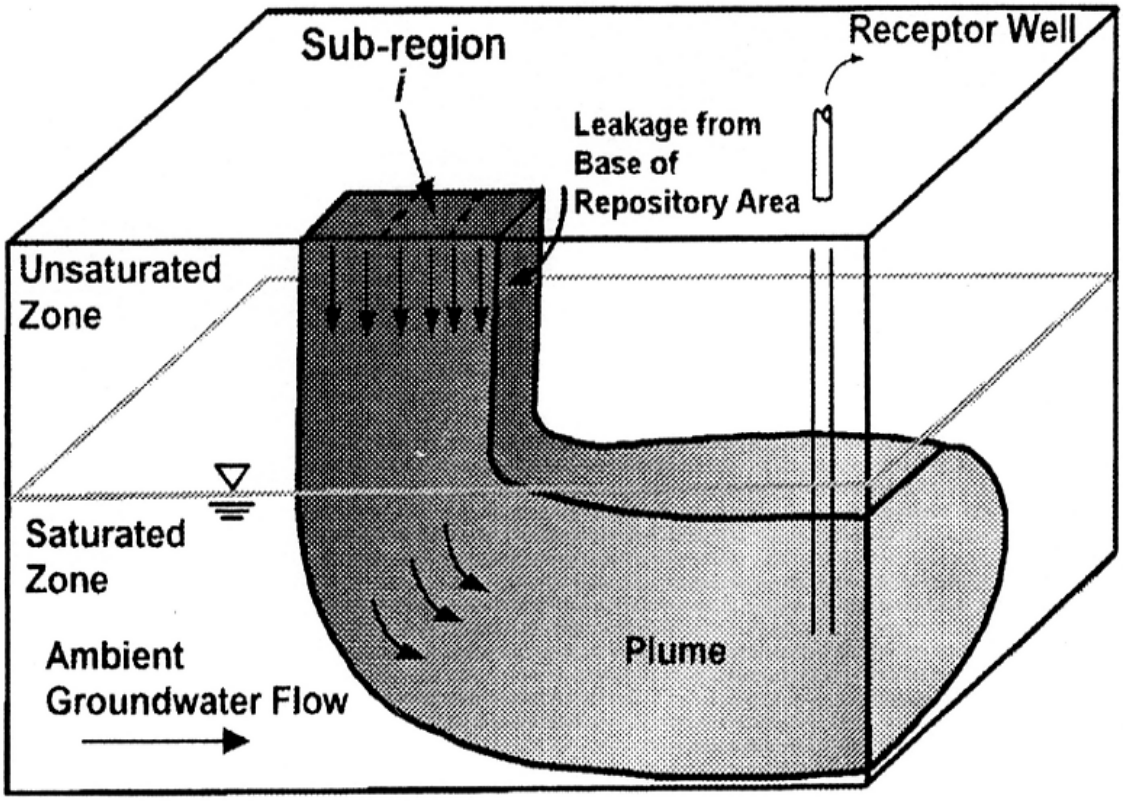

Figure A-10
Schematic of the flow and transport model implemented into IMARC 3 (EPRI, 1996).

Flow and transport in each columnar sub-region could be represented either as a single-porosity/single-permeability continuum or a double-porosity/double-permeability continuum to represent coupled fracture-matrix interactions. For a single-porosity simulation, the physical properties of the unsaturated tuff were taken to be representative of a system of discrete vertical fractures. For a double-porosity simulation, the unsaturated tuff was characterized by vertical fractures that were relatively permeable, with an intervening porous tuff matrix that was less permeable. The coupling of water pressures between matrix and fractures could be specified to occur rapidly or slowly, allowing simulation of "weak" or "strong" coupling as in the Phase 2 IMARC analysis (EPRI, 1992). Sorption and radioactive decay (including decay chains) were also explicitly incorporated into the Phase 3 unsaturated zone model.

With respect to the saturated zone flow and transport model for Phase 3, groundwater flow was assumed to be represented by long-term, steady-state conditions, with the bulk hydraulic conductivity of the fracture rock mass being assumed to be representative of an equivalent porous medium that may be anisotropic. The assumed steady-state condition was necessary to achieve the requisite computational efficiency within the multi-branched logic-tree structure of the IMARC code (EPRI, 1996). Transported radionuclides could advect, disperse, sorb, and decay within the three-dimensional saturated aquifer. The three-dimensional velocity field could either be specified to be uniform by inputting the three components of the water velocity vector, or the velocity field could be obtained by solving the saturated groundwater flow equation. If the

flow field was solved for, the Phase 3 saturated flow and transport model allowed for locating one pumping (extraction) well within the aquifer.

The Phase 3 report (EPRI, 1996) also combined the new flow and transport model for saturated flow with numerous field data measured in the area around the Yucca Mountain site to calculate the likely size and location of a radionuclide-bearing contaminant plume that might eventually arise from the HLW repository. This analysis was made, in part, to help inform discussions regarding the development of an appropriate Yucca Mountain-specific safety standard. Uncertainties in measured properties and regarding possible changes from future climate changes were evaluated. The conceptualized plume emanating from a Yucca Mountain repository (Figure A-11) was relatively narrow (about 3.5 km wide) because of focusing of flow along the eastern margin of the ground water basin in this region. Contaminants in the plume were conjectured to migrate southward, with possible interception by wells in Amargosa Valley (the nearest permanent population to Yucca Mountain, which was later adopted by the EPA as the "accessible environment boundary" in its Yucca Mountain specific safety standard 40 CFR 197) at a distance of 20-30 km from the repository site. It was estimated that dispersion during transport would result in dilution in radionuclide concentrations by about a factor of 15 assuming present day climate; greater dilution factors would occur for wetter pluvial conditions because the plume would move deeper during transport.

A.4.7 Biosphere Model

Another significant advancement to the Phase 3 IMARC code (EPRI, 1996) was the implementation of an independent biosphere model to support calculation of possible dose effects arising from a Yucca Mountain repository, per the recommendation of a health-risk standard made by the National Academy of Sciences review to the EPA (NAS, 1995). In particular, the Phase 3 biosphere model implemented into IMARC considered not just drinking water as the only exposure pathway, but also a variety of other possible exposure pathways, as also recommended by the NAS (1995) report. The biosphere pathway model added to Phase 3 IMARC is summarized in Figure A-12.

Combined with this pathway analyses, dose conversion factors of key dose-contributing radionuclides for a unit flux to an extraction well assumed as the "accessible environment" were derived for use in the Phase 3 IMARC code (EPRI, 1996).

A.4.8 Thermal Spalling (Rockfall) Model

The reference repository design (DOE/OCRWM, 1995) envisioned horizontal emplacement of waste packages into drifts that were only partly (or not at all) backfilled, a departure from the previous Site Characterization Plan concept of waste packages emplaced vertically in the floor of backfill access drifts (DOE/OCRWM, 1988). The induced stresses in the crown of the emplacement drift, in particular with no supporting backfill, could lead to possible rock loosening from the top of the drift and rock fall. Such potential rockfall raised concerns for operational safety during emplacement, as well as degraded post-closure performance, either due to rockfall damage of waste packages or to unfavorable alteration of the hydrological properties of tuff surrounding the drift (EPRI, 1996).

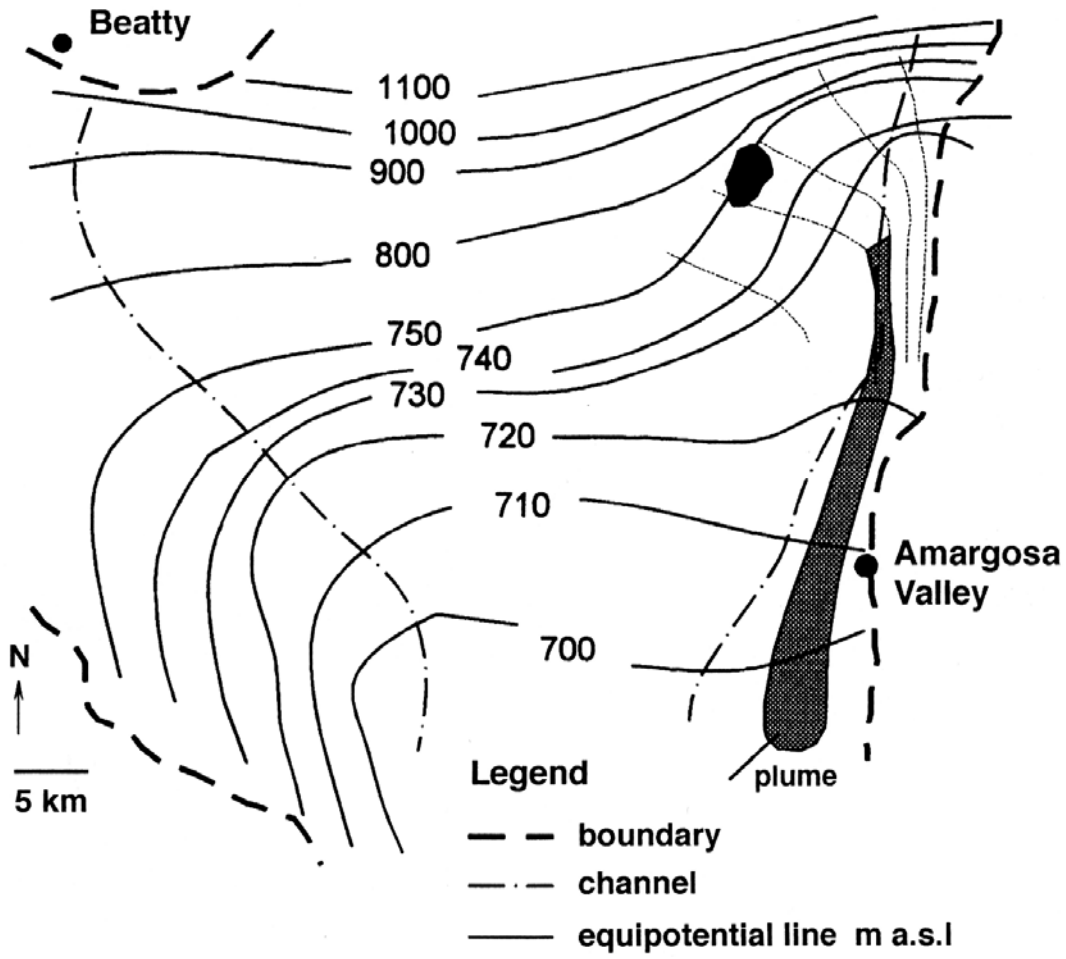

Figure A-11
Map illustrating the likely size and location of a contaminant plume moving south toward Amargosa Valley (EPRI, 1996).

To estimate the probability and magnitude of a possible rock block falling due to thermal spalling, a series of finite-element, discontinuum (*i.e.,* specific inclusion of fractures and joints in the tuff, and the properties of such discontinuities) calculations were made in the Phase 3 report (EPRI, 1996). Specific inputs to this modeling included:

- reference rock-mechanical property data collected by the DOE for four rock-strength categories of the Topopah Springs tuff unit ("strong," "medium," "weak," and "very weak"),
- reference data on the distribution and physical properties of joints that could slip as a function of resolved shear, normal stress and time (not included in the Phase 2 analysis), and
- three different thermal-loading constraints (alpha, beta and gamma temperature-time profiles, see Figure A-4).

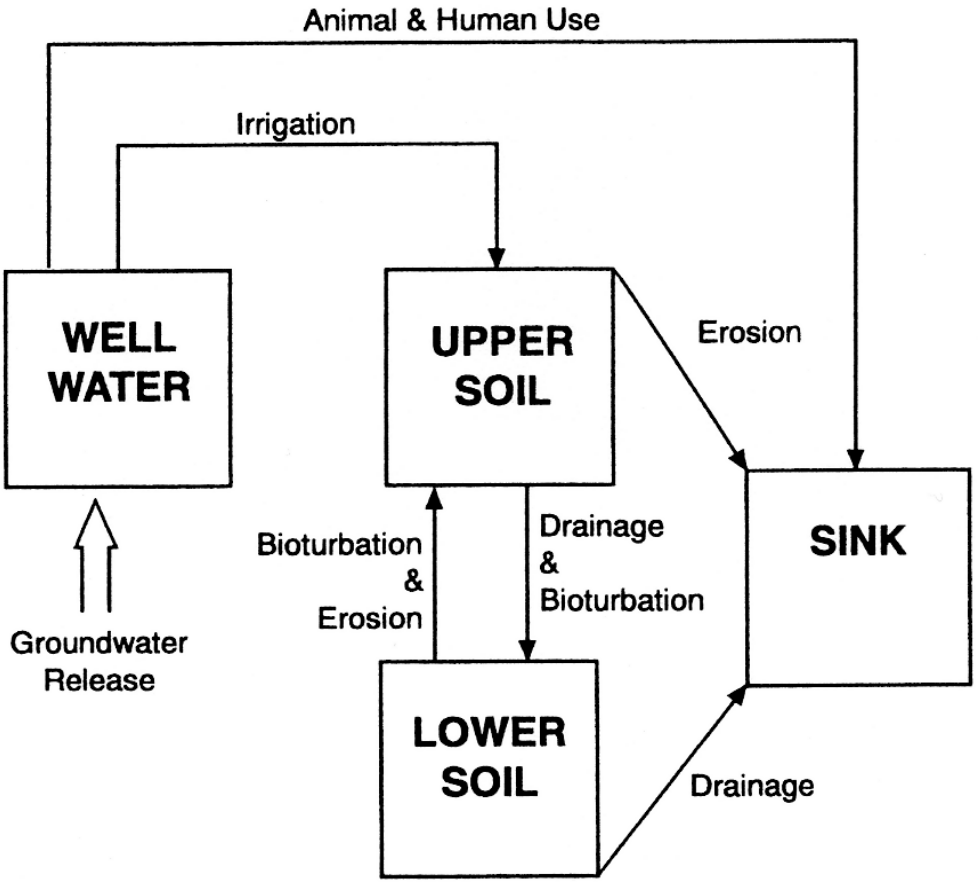

Figure A-12
Schematic of biosphere transfer processes considered in EPRI (1996).

From this range of thermal, mechanical and physical data inputs, multiple finite-element, discontinuum analyses were made to develop a statistical representation of possible thermal spalling. In particular, the following factors were evaluated:

- maximum size of a possible rock block that might fall,
- average size of a possible rock block that might fall,
- probability of rockfall in the first 1,000 years after repository closure (*i.e.*, thermal period), and
- probability of rockfall at time greater than 1,000 years after repository closure.

Table A-3 shows the "look-up" table derived from these analyses.

Based on the relatively low likelihood of rockfall, and the estimated small size of any rock block that might fall (Table A-3), the Phase 3 report concluded that the effects of rock spalling on repository performance appeared to be minor. Because of the minimal impact on performance, these rockfall effects were not included in the IMARC 3 code and the calculations reported in EPRI (1996).

Table A-3
Results of Phase 3 rockfall analyses (EPRI, 1996).

Properties		Rock Fall			
Thermal	Material	Max Size (meters)	Ave Size (meters)	Probability in the first 1000 years	Probability after the first 1000 years
Alpha	Strong	0.5	0.3	0.01	0
	Medium	0.2	0.15	0.14	0.07
	Weak	0.1	0.075	0.064	0.032
	Very Weak	0.075	0.04	0.032	0.032
	Probability of not falling			0.754	0.866
Beta	Strong	0.5	0.3	0	0
	Medium	0.2	0.15	0	0
	Weak	0.1	0.075	0.032	0.032
	Very Weak	0.075	0.04	0.032	0.032
	Probability of not falling			0.936	0.936
Gamma	Strong	0.5	0.3	0	0
	Medium	0.2	0.15	0	0
	Weak	0.1	0.075	0.016	0.032
	Very Weak	0.075	0.04	0.032	0.032
	Probability of not falling			0.952	0.936

A.4.9 Phase 3 Results

The logic-tree structure for the Phase 3 IMARC calculations is shown as Figure A-13. The full set of logic-tree branches was 162 for the full simulation "Base Case." The expanded number of branches and the increased complexity of some new sub-models within IMARC3, notably the flow and transport sub-model, greatly increased the computation time for analyses. Accordingly, certain simplifications were made in Phase 3 analyses (EPRI, 1996). A reduced set of 7 radionuclides (^{79}Se, ^{99}Tc, ^{129}I, ^{231}Pa, ^{237}Np, ^{233}U, and ^{229}Th) were considered, selected on the basis of biosphere pathway analysis and likelihood of being key contributors to total dose estimates. Infiltration and thermal/seepage models were narrowed to single representations, and "medium" values case for solubility, dissolution rate and sorption were omitted.

The calculation cases in the Phase 3 report (EPRI, 1996) were largely directed towards helping to develop an informed perspective on the many open technical issues and policy decisions in the US repository program in 1996. These included:

- implications of the recommendations in the NAS (1995) "Technical Bases for Yucca Mountain Standards" report,
- the time-scale and health-risk formulation for an eventual EPA standard specific to Yucca Mountain (EPA was still working on its first draft of its 40 CFR 197 standard in 1996),
- performance and safety implications of revised hydrological models of Yucca Mountain,
- selection of new container materials,
- alternative EBS designs,
- relative contributions to performance and safety among engineered and natural barriers,
- performance and safety impacts of "conservative" versus "reasonably assured" conditions and assumptions
- identifying key research priorities for the future, and
- the suitability of Yucca Mountain as a geological repository.

With respect to these last point objectives, the Phase 3 report concluded (EPRI, 1996):

> "Sensitivity studies indicate that the key technical components affecting total system performance are: the amount of water flowing through the repository; the assumed biosphere exposure pathways; flow and transport properties in both the unsaturated and saturated zones of the Yucca Mountain geology; container material; and elemental solubilities.
>
> Reasonable assurance of very low dose rates to hypothetical individuals living in the Yucca Mountain vicinity (due to operation and closure of the candidate spent fuel and HLW disposal facility) can be provided for several thousands years into the future-perhaps for a time period longer than the recorded history of human civilization. Furthermore, IMARC Phase 3 analyses suggest peak dose rates beyond several thousand years will likely be limited to natural background levels or lower. Thus, we find Yucca Mountain technically suitable for continued development as a permanent spent fuel and HLW disposal facility."

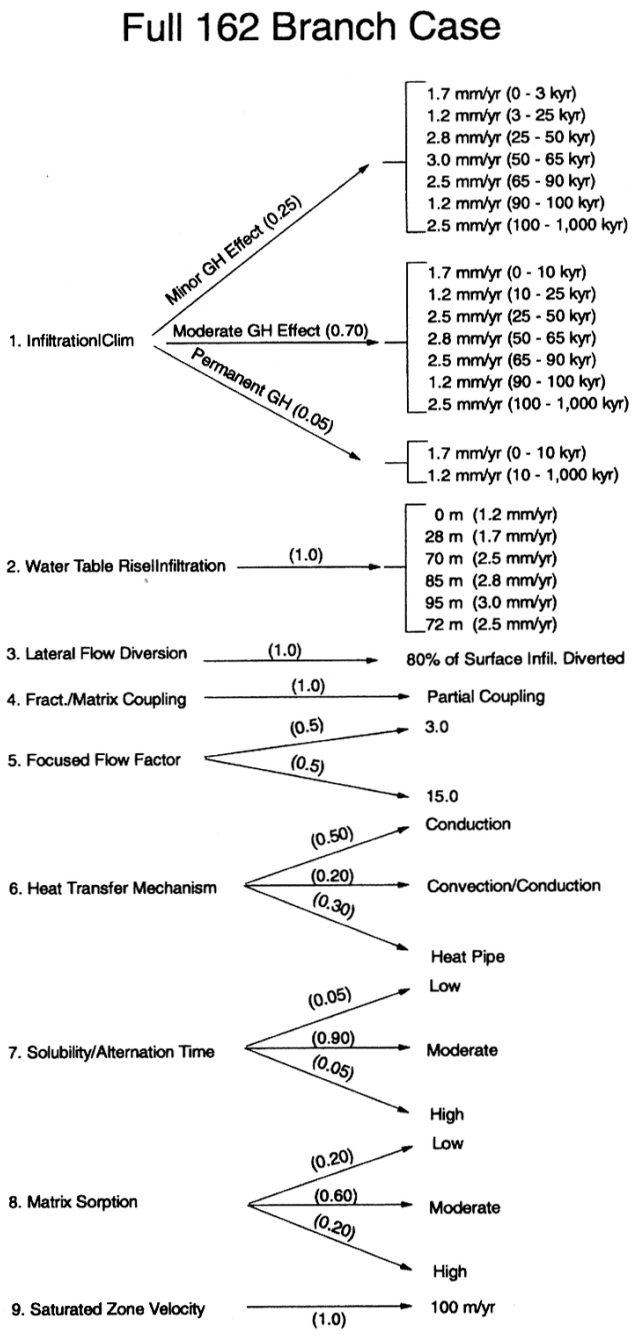

Figure A-13
Logic-tree structure for "Base Case" calculations using the Phase 3 IMARC code (EPRI, 1996).

With respect to the IMARC code itself, the Phase 3 study (EPRI, 1996) represented a significant advance in both capabilities and flexibility of sub-models. Sub-models developed during the Phase 3 study in the areas of flow and transport, source-term and biosphere still remain as core capabilities of the present day version of the IMARC code.

A.5 Phase 4 (EPRI, 1998)

The stated objectives for the Phase 4 study were to:

- update the IMARC code based on new information and recent regulatory developments,
- identify the key technical issues important to total system performance, and
- provide an assessment of whether protection of human health and the environment as a result of HLW disposal at the candidate Yucca Mountain facility can be adequately demonstrated (EPRI, 1998).

In 1998, the first draft of the EPA's site-specific safety standard for Yucca Mountain, 40 CFR 197, was about to be issued. DOE/OCRWM was preparing to publish a congressionally mandated "Viability Assessment" (VA) report on Yucca Mountain. The reference waste package design consisted of a dual-wall arrangement in which a 2 cm-thick alloy C-22 inner barrier was to be encapsulated within a 10 cm-thick mild steel outer barrier, and the entire waste package to be emplaced horizontally in an un-backfilled drift.

With respect to updating the Phase 3 IMARC code, most of the activities focused on compiling, critically reviewing and selecting revised input data. Particular areas of data updating included climate change, net infiltration, the number of waste packages possibly wetted over time, and radioelement solubilities and sorption coefficients. Most of the IMARC sub-models were not significantly revised in the Phase 4 study. Two IMARC sub-models, the Containment Model and the Biosphere Model, were modified, however, as discussed in sections below.

Several key technical issues were also directly evaluated in the Phase 4 study. These issues included:

- much higher precipitation (rainfall) values for the future at Yucca Mountain, proposed on the basis of certain ostracode fossils,
- alternative safety indicators to complement dose-rate calculations calculated out to one million years,
- use of influence diagrams and interaction matrices as a basis to audit and illustrate the completeness of safety analyses,
- appropriate timeframes for safety assessment based on international comparisons,
- uncertainties in future human habits as related to dose modeling, and
- the impact of corrosion products on source-term release of radionuclides.

Phase 4 activities for the various IMARC sub-models are summarized in the following sections.

A.5.1 Climate Change Model

Evidence from ostracode fossils from Washington and Minnesota were interpreted by some researchers as indicating that past (and hence, by inference, future) precipitation rates at Yucca Mountain would be many times higher than previous estimates (see DOE/OCRWM, 1995 and

EPRI, 1996 for relevant references). Phase 4 analyses based on multiple lines of other evidence, including specific plant taxa near Yucca Mountain and stable isotope data from deep sea cores and ice cores, indicated that the ostracode interpretation for much higher rainfall rates for pluvial conditions than previously estimated for Yucca Mountain were over-estimates.

A.5.2 Net Infiltration Model

Two adjustments were made to the net infiltration sub-model in IMARC in Phase 4. First, values for physical parameters in the surface soil layer for Yucca Mountain were updated based on new site data. Second, a more realistic model for the effects of runoff was implemented. In particular, the effect of capture of run-off of water moving along slopes from high elevations to lower-lying soil/hydrological basin units was added to the model, as well as possible run-off of water from this lower-lying basin. When no basin run-off occurred, net infiltration was higher. This effect was found to be small for present day climate conditions (0 to 17% increase) and somewhat higher (up to 60% higher) for full glacial conditions.

The calculated net infiltration rates derived in Phase 4 are shown in Table A-4, along with other reported infiltration values cited in EPRI (1998). The EPRI Phase 4 values were in reasonably good agreement with other independent researchers listed in Table A-4.

A.5.3 Seepage Model and Thermal Model

Revised estimates of the proportion of waste packages that might be contacted by seeping water, and the relative rates of such seeping water, were made in the Phase 4 report (EPRI, 1998). One new factor concerned possible focusing of water flow as infiltrating water approached the repository horizon. "Strong Focusing" was attributed to infiltrating water migrating dominantly in fractures (and not in equilibrium with the tuff matrix), whereas "Weak Focusing" was attributed to rock regions in which infiltrating water equilibrated and moved in both fractures and the tuff matrix.

An analytical solution (EPRI, 1998, Appendix D) was applied in Phase 4 to combine the following factors in order to estimate the local percolation rate of water in the region of tuff around the repository horizon:

- rock regions with "strong focusing" of infiltrating water in fractures versus rock regions with "weak focusing" of infiltrating water moving through both fractures and tuff matrix,
- regions of the repository that were relatively "hot" (termed "De-focused Flow Zones") versus regions of the repository that were relatively "cool" (termed "Focused Flow Zones"),
- net infiltration rates ("low," "base" and "high" values from the net infiltration logic-tree node for a given climatic condition), and
- repository lifetime ("Thermal" period representing 0 – 3,000 years after closure; "Current" representing the current climate from 3,000-25,000 years after closure; "Glacial" representing full glacial maximum conditions prevailing from 25,000 years after repository closure).

Table A-4
Comparison of estimated Phase 4 net infiltration rates with other contemporary sources ("This Study 1996 (Phase 4)" refers to EPRI, 1998).

Author/Date	Net Infiltration (mm/yr)	Comment
Flint & Flint, 1994	1.2	Matrix flow saturated conductivity is 0.02 mm/yr for 80% of site; 13.4 mm/yr maximum rate
Fabryka-Martin, 1996	0 - 5.4	Cl^{36} mass balance
Flint et al., 1996	6.7	Neutron logs from 90 bore holes, includes El Nino years
Bodvarsson, 1996	5.0	UZ5 Temperature profile matching
Geomatrix Consultants, Inc. and TRW, 1997	10 (0.5 - 50)	Expert elicitation
EPRI 1996 (Phase 3)	1.2	Interglacial climate (154.6 mm/yr)
	2.9	Full glacial climate (194.5 mm/yr)
This Study (Phase 4)	7.2	Interglacial climate (154.6 mm/yr)
	19.6	Full glacial climate (194.5 mm/yr)
Lichty & McKinley, 1995	11.4 - 32.5	Hydrologic/watershed estimates 336.3 mm precipitation zone
Gauthier, 1998	32.5	Full glacial climate (300 mm/yr) Flint et al. 1996 model

The derived percolation fluxes were, in turn, converted in the Phase 4 IMARC code into estimates of the fractions of waste packages being contacted by seeping water via use of the relationship curve shown in Figure A-14, which was derived from DOE/OCRWM data. The final tabulated values for fractions of waste packages that were contacted by seepage water from Phase 4 analyses (EPRI, 1998) are shown in Table A-5 for the various rock (strong vs. weak focusing) and repository (hot vs. cool) regions of the repository horizon. The average seepage rate (assumed equal to the estimated percolation rate) for any one of the fractions shown in Table A-5 was derived in IMARC Phase 4 by application of the relationship illustrated in Figure A-14.

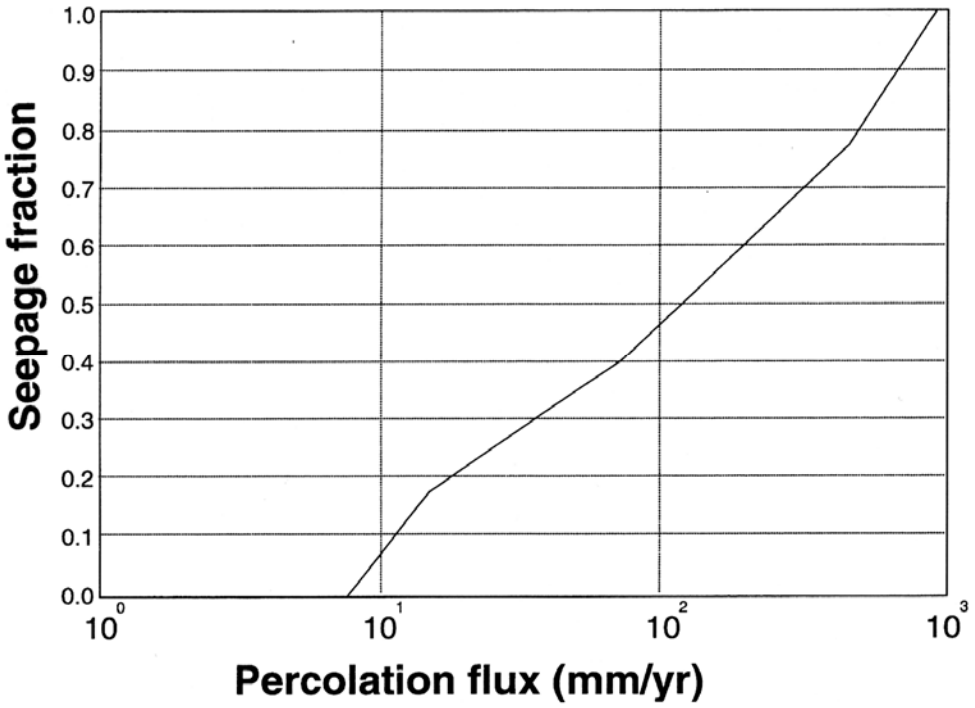

Figure A-14
Fraction of waste packages that will be wetted, as a function of local percolation rate (EPRI, 1998).

In addition, the temperature-time curves originally derived in Phase 2 (Figure A-4) were updated to support the revised thermohydraulic analysis. The revised temperature-time curves are shown in Figure A-15. The "δ" curve in Figure A-15 was added to reflect a second repository design with natural ventilation under consideration by DOE during the Phase 4 analyses.

A.5.4 Containment Model

In the Phase 3 Containment Model of IMARC, uncertainties in corrosion rates of different materials exposed to different environments were expressed in a series of Weibull distributions. This approach required the establishment of numerous (in some cases, more than 100) fitting parameters that controlled the shape of the derived distribution of container failures, and especially the threshold time to failure (*i.e.,* the lower estimate of container lifetime). In Phase 4, the uncertainties incorporated into the new Containment Model expressed those uncertainties inherent in the corrosion data used to the extent that such uncertainties were known, as well as uncertainties derived from expert judgment. The new Phase 4 Containment Model was believed to more closely represent then-current knowledge and opinion on corrosion rates than the previous Phase 3 Containment Model.

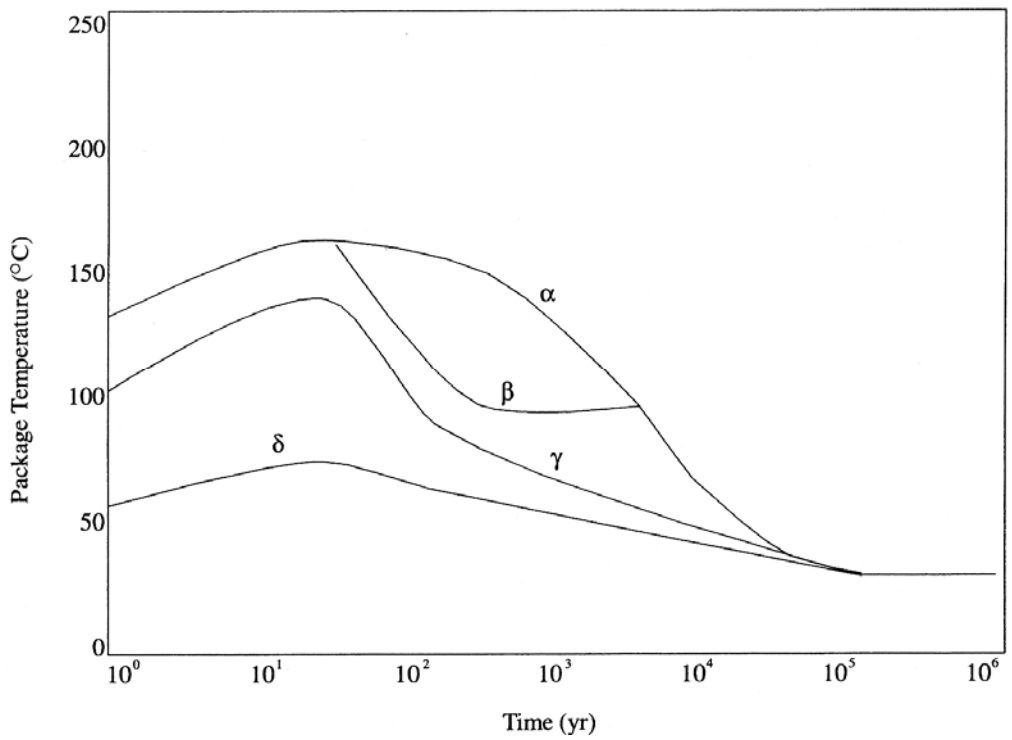

Figure A-15
Temperature-time curves used in calculations: α-T, "hot" packages, strongly focused water flow; β-T, "hot" packages, weakly focused water flow; γ-T, "cold" packages; δ-T, relationship expected if the repository is naturally ventilated (EPRI, 1998).

Phenomenalogically, the Phase 4 Containment Model advanced several important concepts that have since become standard features not only of the EPRI approach to assessing containment but also of the independent modeling by the OCRWM/DOE and the Nuclear Regulatory Commission (NRC). An example of the evolution of relative humidity (RH) at the surface of waste packages as a function of time is shown in Figure A-16. Experimentally, the necessary RH values for the onset of humid air corrosion (HAC) and aqueous corrosion (AQC) could be well established. In turn, the RH versus time curve of Figure A-16 could be combined with a representative temperature versus time curve, as shown in Figure A-17. Thus, the RH, temperature and duration for HAC and AQC corrosion modes could be derived, as well as an initial period of dry-air oxidation.

A further enhancement to the Phase 4 IMARC Containment Model was in identifying temperature thresholds below which crevice corrosion (CC) cannot occur for a given material (*e.g.,* alloy C-22). As shown in Figure A-18, by combining the onset time for possible AQC (represented in Figure A-18 by the TAQC line, the assumed 100ûC boiling point line) and the lower threshold temperature for *CC* (represented in Figure A-18 by the *TCC* line, assumed to be 80ûC for alloy C-22), a finite period for possible corrosion failure by CC (shaded region of Figure A-18) was derived. For the lower temperature-time curve, the estimated duration of conditions for the occurrence of *CC* was about 100 years and an approximately 3,000 year duration was estimated for the higher temperature-time curve. Below the *TCC* condition of Figure A-18, only general corrosion (and MIC) of the alloy C-22 could occur.

Table A-5
Fraction of waste packages wetted used in IMARC 4 (EPRI, 1998).

		Strong Focusing			Weak Focusing		
		Low	Base	High	Low	Base	High
De-Focused Flow Zone ('hot')	Thermal	0	0	0	0.2	0.2	0.2
	Current	0	0	0	0	0	0
	Glacial	0	0	0	0	0.1	0.2
Focused Flow Zone ('cool')	Thermal	0.4	0.4	0.4	0.4	0.4	0.4
	Current	0	0.35	0.35	0	0.2	0.2
	Glacial	0.3	0.5	0.6	0.1	0.35	0.4

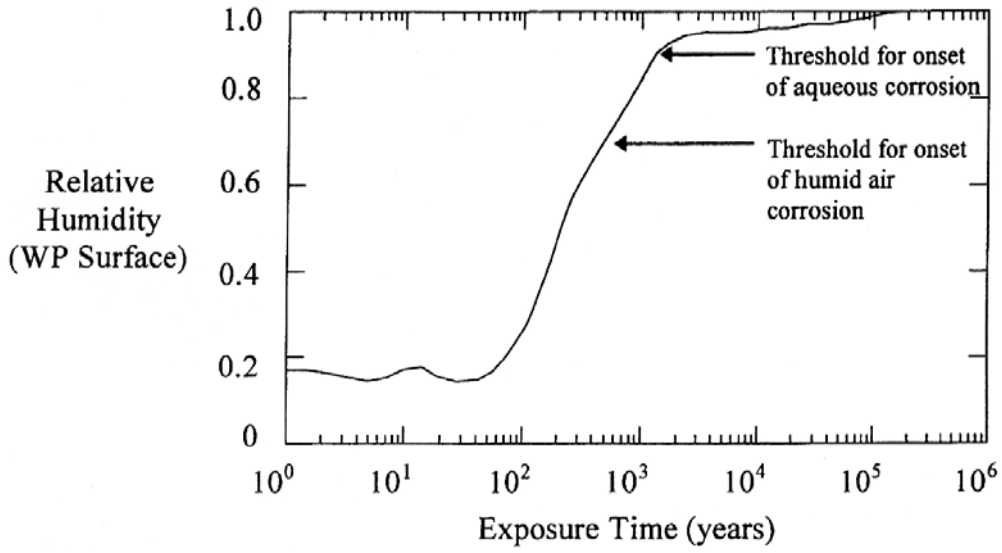

Figure A-16
An example of calculated relative humidity (RH) at the waste package surface as a function of time after exposure (EPRI, 1998).

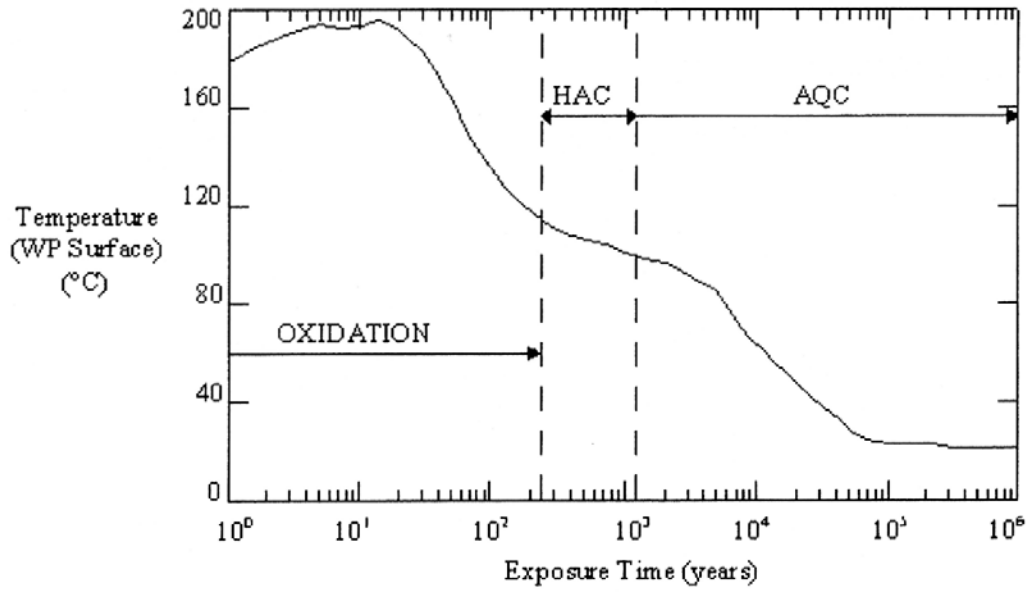

Figure A-17
An example of a calculated temperature at the waste package surface as a function of time after exposure (EPRI, 1998).

Based on these physicochemical constraints, a new Containment Model approach was implemented in the Phase 4 IMARC code (Figure A-19). Numerous analyses were provided in the Phase 4 report (EPRI, 1996) to derive the time for first waste package containment failure and the cumulative failure rate of containers for various temperatures, water contact times and groundwater compositions. An example of such a derived cumulative failure function plot is given in Figure A-20 for a specific seepage rate and for various temperature-time profiles (the "α", "β", "γ" and "δ" designations represent Phase 4 modifications to the Phase 2 temperature-time curves as shown in Figure A-15).

A.5.5 Source-term Model

The primary activity in the Phase 4 report (EPRI, 1998) with respect to source-term modeling was an extensive review of input data on the dissolution behavior of CSNF, radioelement solubilities, and radioelement sorption coefficients for components (including metal corrosion products) of the EBS. The Phase 4 report cautioned that interpretations on experimental data of waste-form performance could be non-unique. Specific recommendations were made regarding future data needs and appropriate experimental techniques to obtain data to confirm alternative conceptual models regarding the release and migration behavior of radionuclides within a Yucca Mountain repository. The potential for co-precipitation of radionuclides, such as the inclusion of actinides into uranium-dominated alteration phases from dissolution of the UO_2 of CSNF, was specifically discussed.

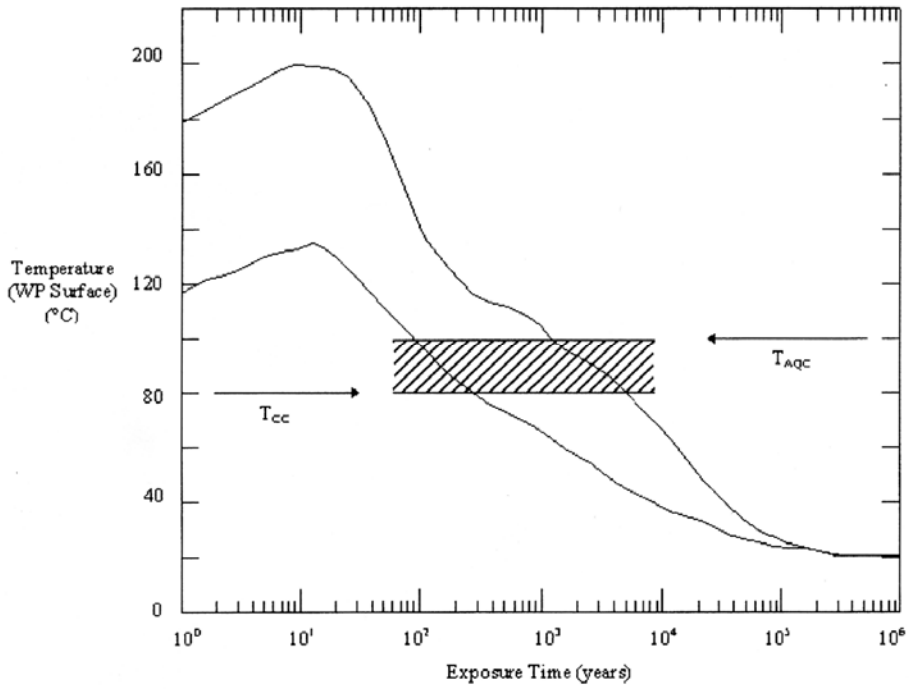

Figure A-18
Anticipated range of temperature-exposure time curves for the surface of the waste package. T_{CC} is the threshold temperature below which crevice corrosion cannot occur; T_{ACQ} is the temperature for the onset of aqueous corrosion (EPRI, 1998).

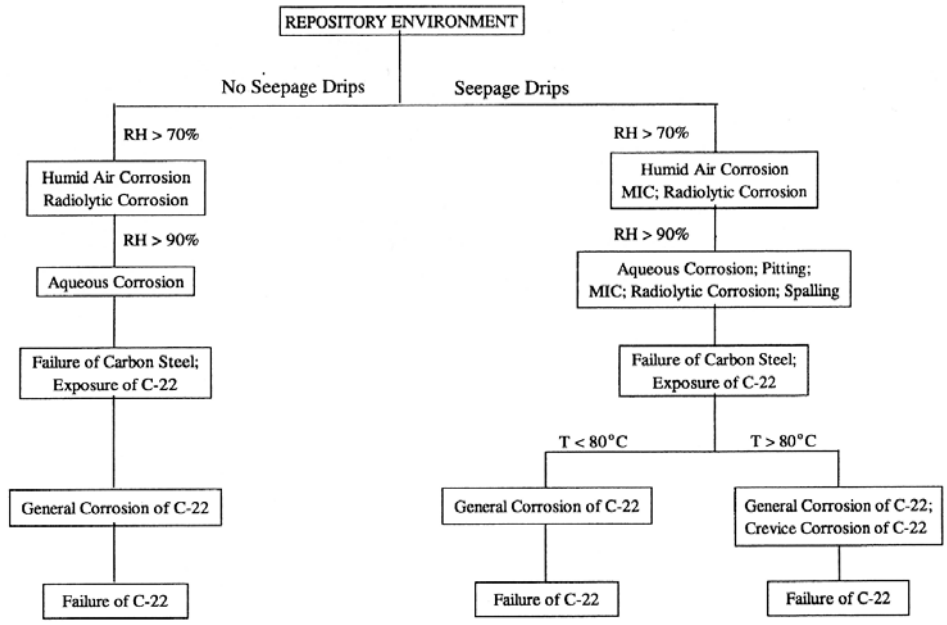

Figure A-19
IMARC Phase 4 flowchart for waste package corrosion degradation for Yucca Mountain conditions (EPRI, 1998).

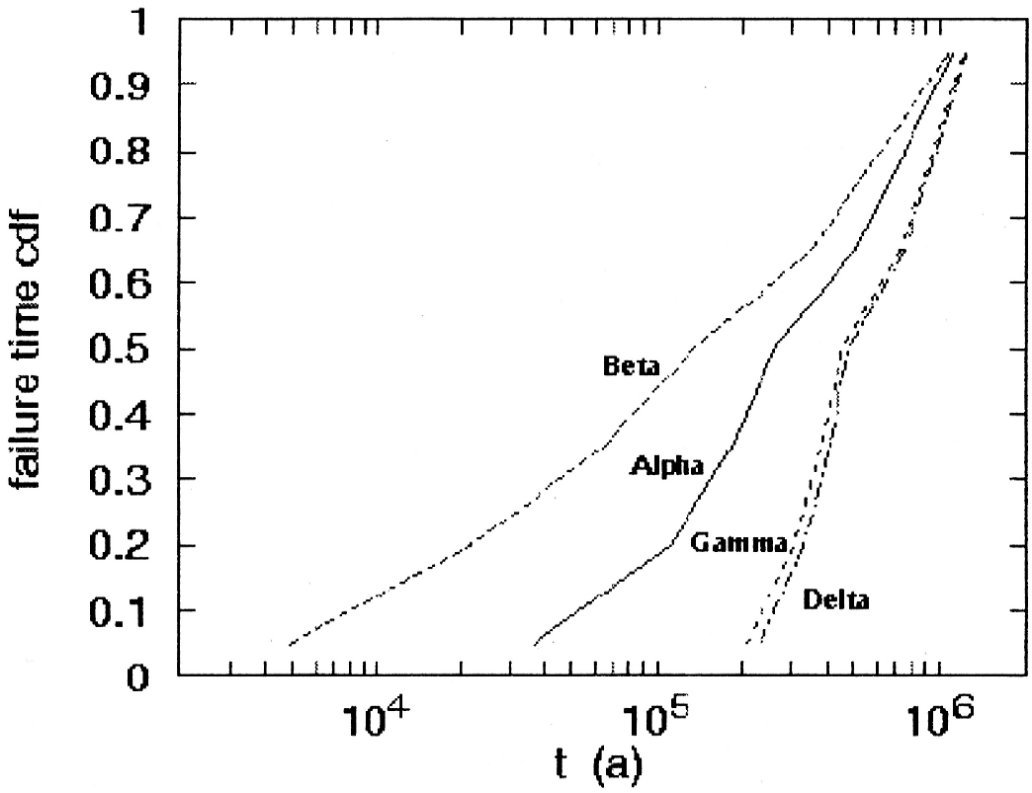

Figure A-20
Predicted cumulative distribution functions for C-22, seepage drips, (EPRI, 1998)

A.5.6 Flow and Transport Model

The flow and transport model used in IMARC Phase 4 report (EPRI, 1998) was the same as used in the Phase 3 report (EPRI, 1996). Considerable new data had been obtained between 1996 and 1998, however, so that the input parameters for both the unsaturated zone and saturated zone were updated.

A.5.7 Biosphere Model

In the absence of a draft EPA safety standard for Yucca Mountain, the Phase 4 report (EPRI, 1998) for biosphere modeling explored a number of possible approaches for a quantitative measure of compliance. Factors affecting a biosphere release pathway were identified, and discussed within the context of various national and international perspectives. No significant modifications to the Phase 3 biosphere model or model inputs were made, however, in IMARC Phase 4.

A.5.8 Phase 4 Results

The Phase 4 IMARC report (EPRI, 1998) contained numerous sensitivity calculations intended to explore and evaluate the "defense-in-depth" of the various barriers and processes by which HLW would be safely isolated in a repository at Yucca Mountain for time periods up to one million years after repository closure. While many barriers and processes were found to provide significant contributions to isolation, no single barrier or process was found to be the sole driver of repository performance.

Most of the IMARC Phase 4 sub-models were essentially the same as those for IMARC Phase 3, although extensive data reviews and updates were made for all sub-models. An important exception was the Containment Model, which was significantly modified to conform to published corrosion test data on the various containment materials under consideration. While the IMARC Containment Model has been revised several times since the Phase 4 report (EPRI, 1996), the basic approach first introduced in the Phase 4 report has been maintained.

A.6 Phase 5 Report (EPRI, 2000)

By 2000, the draft EPA safety standard for Yucca Mountain, 40 CFR Part 197 had been issued setting 10,000 years as the period for a probability-weighted peak dose-rate criterion of 15 mrem/yr. The accessible environment had been defined in the draft 40 CFR Part 197 as a reasonably maximally exposed individual (RMEI) located 18-km from the edge of the Yucca Mountain repository. A fixed water well-extraction pathway and exposure scenario was also established in the regulation. The Nuclear Regulatory Commission (NRC) had followed the draft 40 CFR 197 with their own Yucca Mountain specific regulation, 10 CFR Part 63, which adopted the same criteria.

A major development in the Yucca Mountain Project (YMP) during this period was the establishment of a modified repository design, called the Site Recommendation Characterization Report (SRCR) design. The SRCR design was new in several important ways; (1) implementation of a "line loading" thermal management strategy, (2) waste packages composed of an outer alloy C-22 corrosion barrier with an inner stainless steel container for added strength, and (3) the inclusion of a titanium (grade-7) drip shield. The 1998 IMARC Phase 4 report (EPRI, 1998) had been based on a waste package with an outer mild steel container and an inner alloy C-22 container.

The SRCR "line-loading" thermal management strategy entailed placing waste packages within an emplacement drift so closely together (within 0.10 meters) that they acted as essentially a single heater-line, prolonging the period of above boiling conditions along the length of each emplacement drift. At the same time, the spacing between emplacement drifts was increased from 29-meters to 81-meters in order to ensure that a sub-boiling "pillar" of tuff rock would always be preserved between emplacement drifts (Figure A-21). In this manner, there would be an extended dry-out period preventing any early contact of water with waste packages, while at the same time allowing ample drainage of any condensate water that may be formed by development of above-boiling conditions around emplacement drifts.

The combination of these "line-loading" features led to an expected thermal evolution history as illustrated in Figure A-22. Three basic periods of post-closure performance can be envisioned in Figure A-22. First, an initial "dry-out" period from 0 to many 100's of years after waste emplacement, in which conditions within open emplacement drifts were at above boiling conditions, while any condensate water would drain gravitationally downward around the drifts in sub-boiling pillars. The second intermediate period was characterized as between the time when at-boiling conditions would be reached within a drift to the time that temperature dropped below the critical threshold for crevice corrosion (line "*TCC"* in Figure A-18). The duration of this second period was on the order of several 1,000's of years. The third long-term period, in which further corrosion of waste packages would be limited to only general corrosion, was envisioned to extend thereafter.

Uncertainty regarding the potential for crevice corrosion of waste package alloy C-22 material during the second period was the motivation for the second new feature of the SRCR design, inclusion of a titanium "drip shield." This drip shield was an inverted "U-shaped" structure that would run the entire length of all emplacement drifts (on the order of 50 km) to prevent the dripping of water on to the waste package during the second period (Figure A-23). The functional life expectancy for the drip shield estimated by DOE/OCRWM was only several 1,000's of years of the second period, although longer performance was considered to be possible.

Thus, regulatory compliance analyses in 2000 addressed a 10,000-year post-closure period. The containment performance of three metal barriers (titanium drip shield, alloy C-22 waste package and zircaloy cladding of disposed CSNF) of the SRCR design was expected to contain HLW in a Yucca Mountain repository for this 10,000-year period, minimizing the impact of remaining uncertainties on site performance.

Based on these developments, the IMARC Phase 5 study (EPRI, 2000) was conducted to explore sub-system and total system performance (and uncertainties in that performance) of the new SRCR design concept. A review by EPRI-sponsored technical experts was made of YMP's revised performance models for the SRCR design. Modifications were made for the Phase 5 IMARC code as described in the following sub-sections, in particular, a new model for the effect of "line-loading" and wide (81m) drift spacing on water seepage and a model for cladding corrosion were also introduced into IMARC 5. A series of calculations using the revised IMARC 5 code were also made (EPRI, 2000) to identify key factors, uncertainties and conservatisms affecting the performance of a repository at Yucca Mountain.

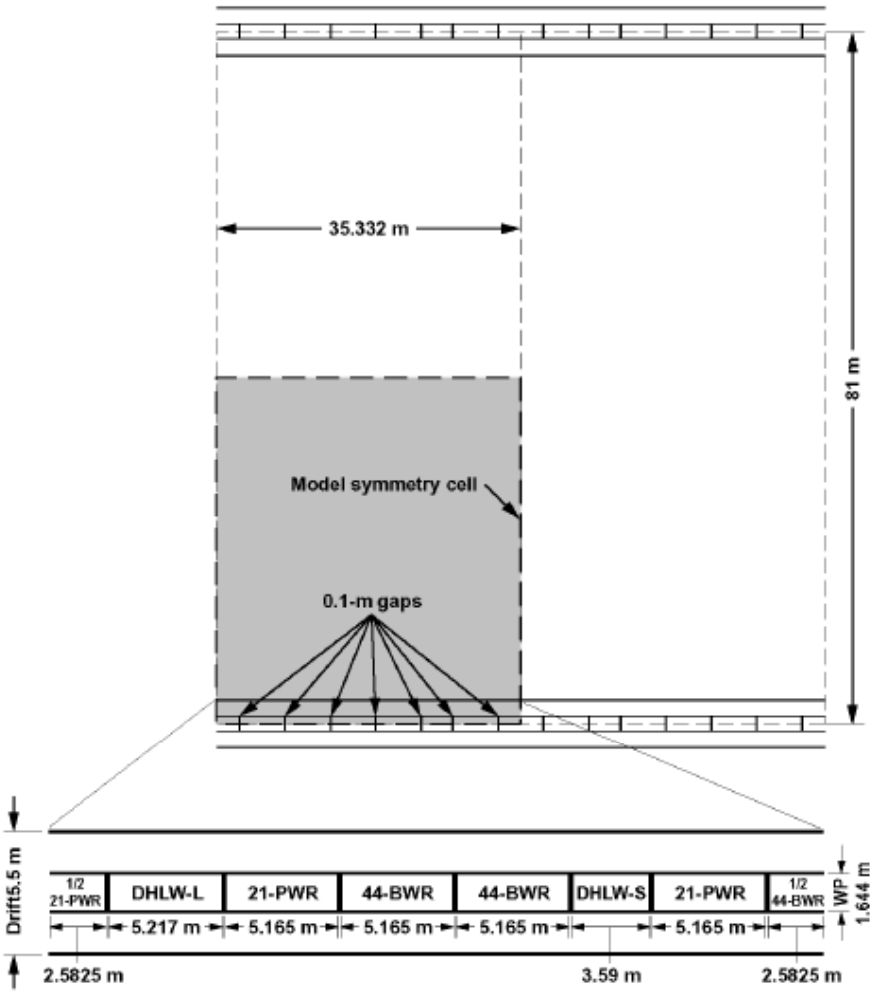

Figure A-21
Schematic plan view of reference SRCR concept for a repository at Yucca Mountain (CRWMS M&O, 1994).

A.6.1 Net Infiltration Model

The derived infiltration values from the Phase 4 study (EPRI, 1998) were compared to the range of reported values by independent sources as of 2000 (Table A-6). EPRI's Phase 4 values were found to be consistent with these other sources for similar sets of assumptions. Accordingly, there was no change in the IMARC Phase 5 net infiltration modeling from that used in Phase 4.

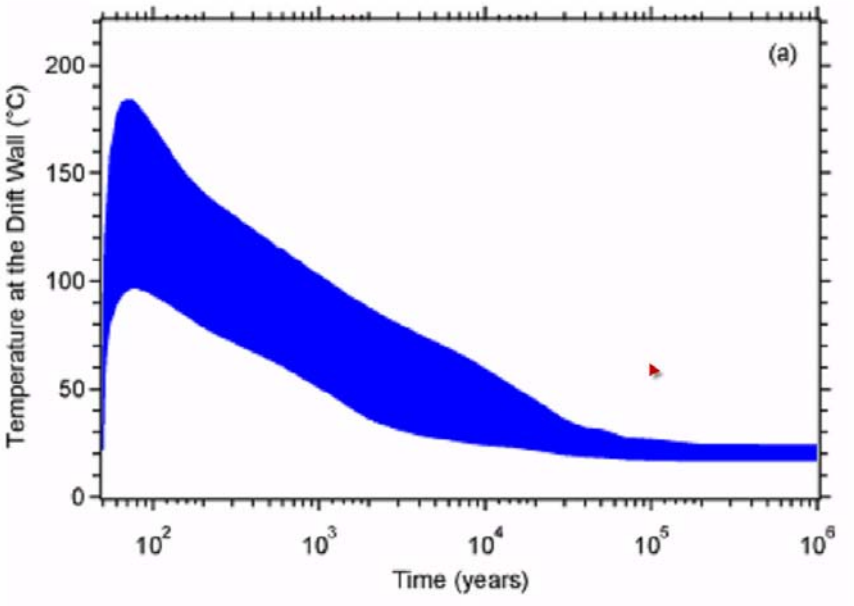

Figure A-22
Temperature-time history for the drift wall at Yucca Mountain (DOE, 2008b, Figure 2.3.5-33).

A.6.2 Thermal and Seepage Models

Estimates for the fraction of waste packages wetted by seepage and the rate of seepage (see Figure A-14 and Table A-5) were updated for IMARC Phase 5, based on site data collected by the YMP (CRWMS M&O, 2000a; 2000b). The Phase 5 report (EPRI, 2000) also presented for the first time, EPRI's review of potential coupled thermal-hydrological-chemical (THC) effects. These included the potential for changes in fracture flow from either mineral dissolution/ precipitation arising from imposition of elevated temperature and temperature gradients during the initial thermal period. Also, the EPRI Phase 5 report reviewed possible changes in composition of groundwater due to a reflux process of boiling and condensation. However, explicit consideration of such THC effects on seepage flow or groundwater composition were not included in IMARC 5 analyses.

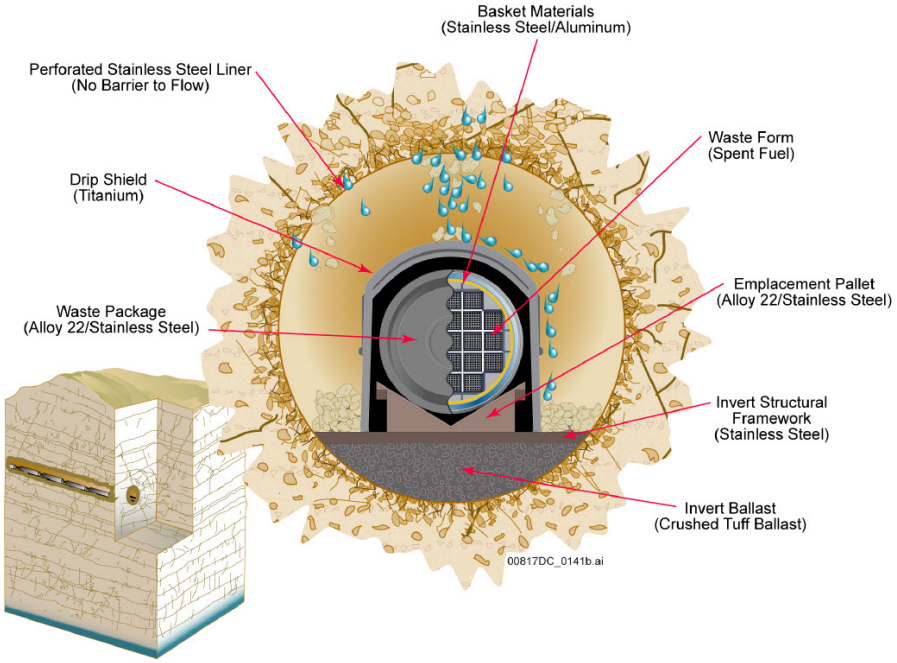

Figure A-23
Cross Section of Typical Emplacement Drift (DOE, 2008a, Figure 6.3.6-3).

A.6.3 Containment Models

The Phase 5 study (EPRI, 2000) evaluated new data on the corrosion modes and rates for titanium drip shield, alloy C-22 outer waste package barrier, and zircaloy cladding. Containment models from Phase 4 (EPRI, 1998) were revised for alloy C-22, and new containment models for titanium and zircaloy were added to the IMARC Phase 5 code. The results of these Phase 5 analyses are summarized here.

The failure of the titanium grade-7 (Ti-7) drip shield was assumed to possibly occur by two corrosion modes: (1) general corrosion, or 2) hydrogen-induced cracking (HIC). Based on the data available at that time, four cumulative failure curves of Ti-7 as a function of time (Figure A-24) were derived for a matrix of conditions of (a) dripping (AGC) and non-dripping (HAC) conditions and (b) with or without HIC. Note that the Phase 5 estimated time for 50% cumulative failure of a Ti-7 drip shield was on the order of 100,000 years (or longer), as shown in Figure A-24; only 0.03% (or less) of drip shields were anticipated to be penetrated in the first 10,000 years.

Table A-6
Comparison of reported net infiltration values for Yucca Mountain (from EPRI, 2000).

DATE	Net Infiltration (mm/year)	Precipitation (mm/year)	Author	Comment
		Modern Climate		
1950	0	<203	Maxey and Eakin	Death Valley groundwater recharge estimate
1992	0.9	150.3	EPRI Phase 2	Initial numerical model
1994	1.2		Flint and Flint	Saturated hydraulic conductivity of matrix
1996	0 – 5.4		Fabryka-Martin	Cl^{36} mass balance
1996	6.7		Flint et al.	Neutron logs from 90 borings
1996	5.0		Bodvarsson, Ed.	UZ5 temperature profile matching
1996	1.2	154.6	EPRI Phase 3	Improved climate model
1997	10 mean (range: 0.5 – 50)		Geomatrix and TRW	Expert elicitation
1998	7.2	154.6	EPRI Phase 4	Improved runoff model
2000	2.2 – 5.1	188	USGS 2000a	Model calibration for 123.7 Km^2 area
2000	7 – 14	170	CRWMS M&O 2000c	Saturated zone chloride data
2000	5	170	CRWMS M&O 2000b	Unsaturated zone chloride data
		Glacial / Wetter Climates		
1950	21 – 27	305 – 380	Maxey and Eakin	Death Valley groundwater recharge estimate
1995	11.4 – 32.5	336.3	Lichty and McKinley	Hydrologic/watershed estimates
1996	2.9	194.5	EPRI Phase 3	Improved climate model for Full glacial climate
1998	19.6	194.5	EPRI Phase 4	Improved runoff model for full glacial climate
1998	32.5	300	CRWMS M&O, 1998	Flint et al. 1996 model for Full glacial climate
2000	14	342.8	USGS 2000a	Model calibration for 123.7 Km^2 area

Three corrosion processes leading to penetration of the alloy C-22 were considered in the Phase 5 study (EPRI, 2000):

- general corrosion,
- crevice corrosion arising from a creviced contact between the waste package and support pedestal, and
- stress corrosion cracking (SCC) arising from the presence of a critical flaw in the alloy C-22.

The sequential organization of environmental conditions necessary for these various models to arise is graphically shown in Figure A-25. Based on data available in 2000, the derived cumulative failures of the waste package outer cylinder of alloy C-22 over time is shown in Figure A-26 for general corrosion and combined general corrosion + localized corrosion. Note that no waste package penetrations were anticipated at 10,000 years after emplacement, and only about 1.5% of the waste packages were anticipated to be penetrated at 100,000 years after emplacement.

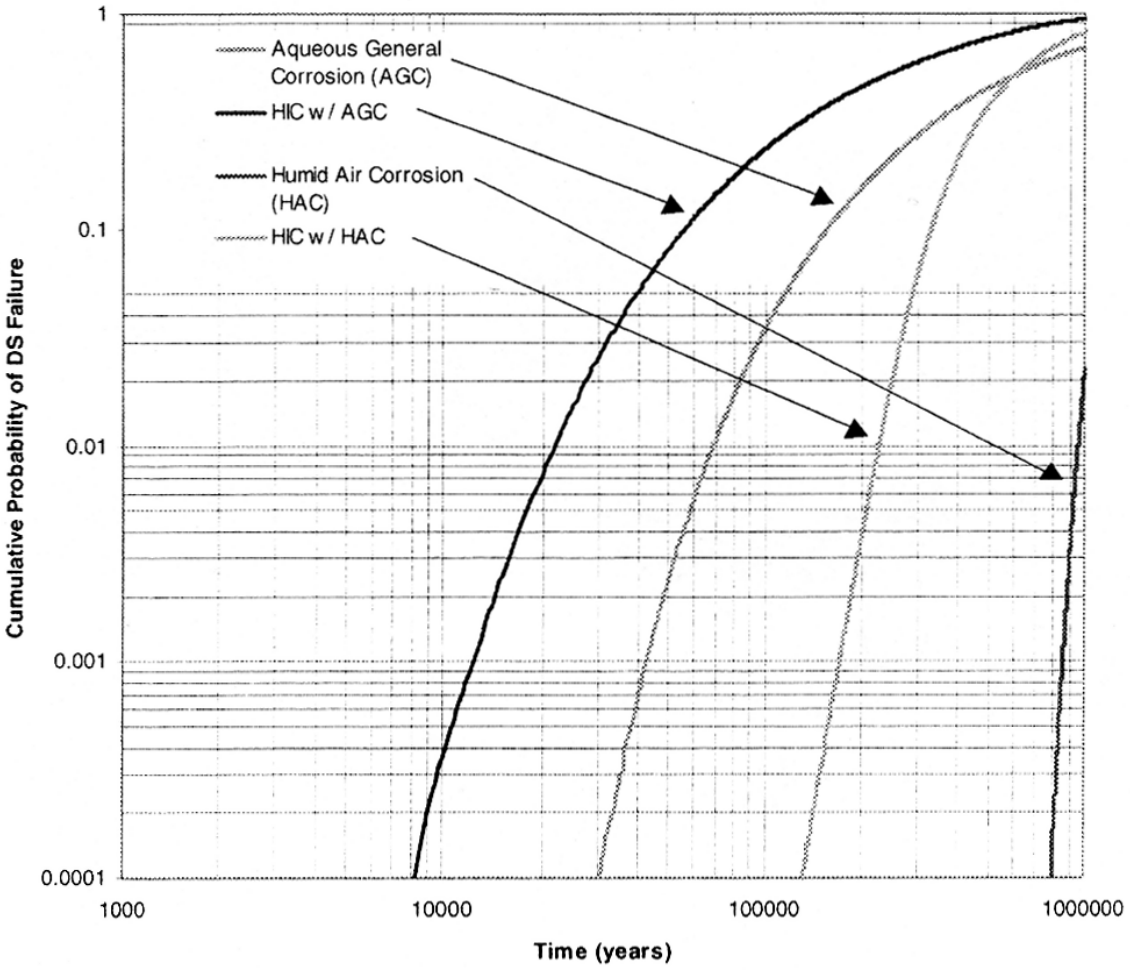

Figure A-24
Alternative failure curves for titanium grade-7 drip shields (EPRI, 2000).

Finally, available data on the corrosion of zircaloy cladding were also evaluated to derive an estimated cumulative failure curve as a function of time (Figure A-27). It was assumed that approximately 2% of the cladding had failed prior to emplacement in a repository. After eventual failure of the waste package/EBS, two corrosion modes for the cladding were considered: (1) general corrosion under dry (moist air) conditions, and (2) general corrosion under dripping conditions. At 10,000 years after EBS failure, about 20% of cladding was projected to have failed under dripping conditions and no additional cladding failures were predicted to occur under dry conditions.

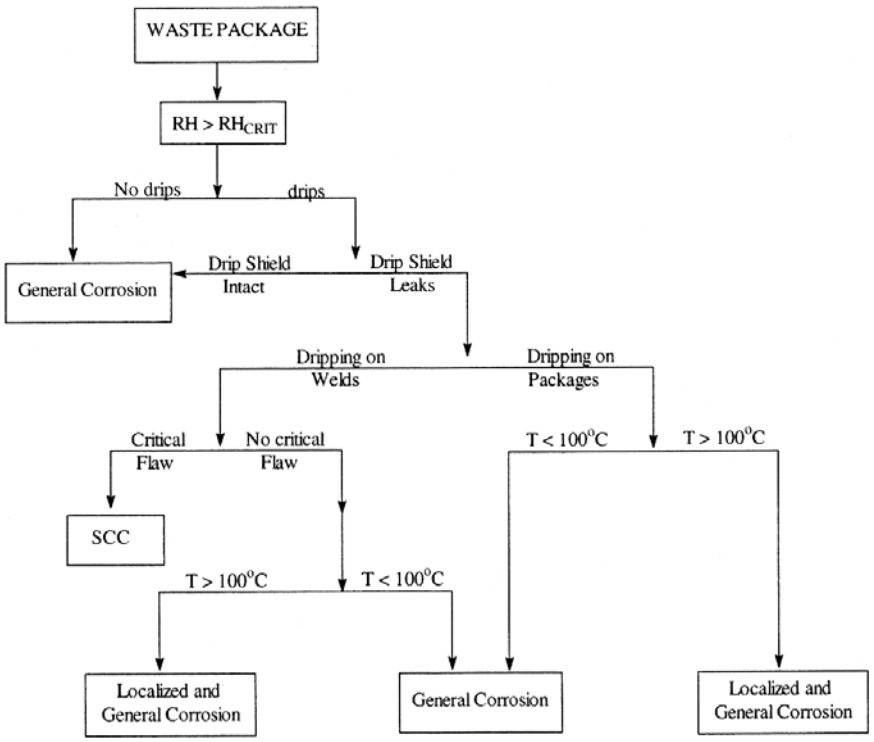

Figure A-25
Flowchart for corrosion modes of Alloy C-22 outer barrier of waste packages (EPRI, 2000).

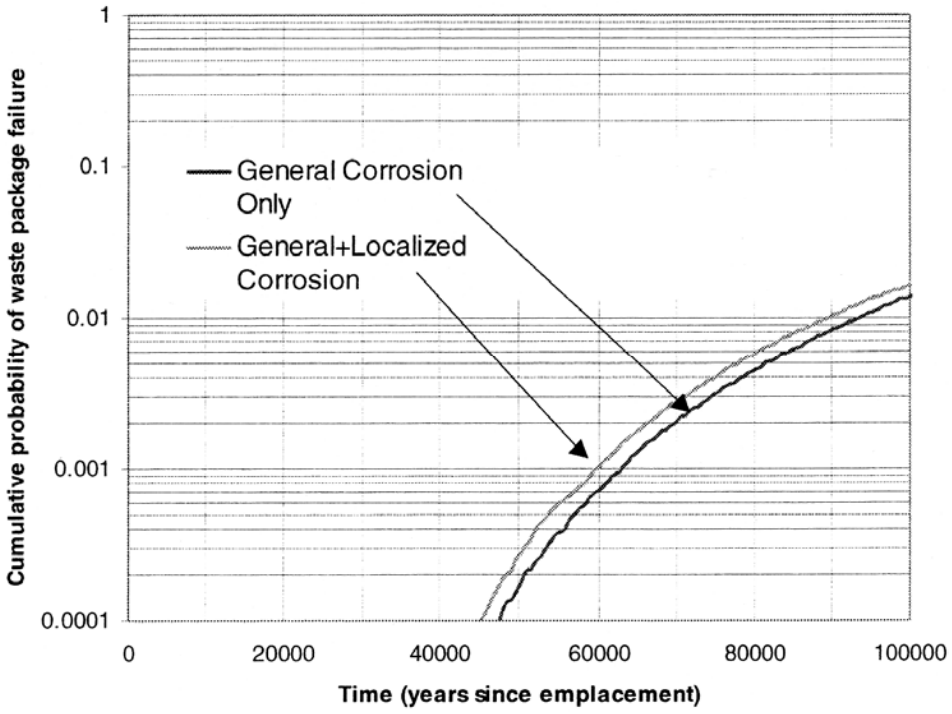

Figure A-26
Derived cumulative failure curves for Alloy C-22 (EPRI, 2000).

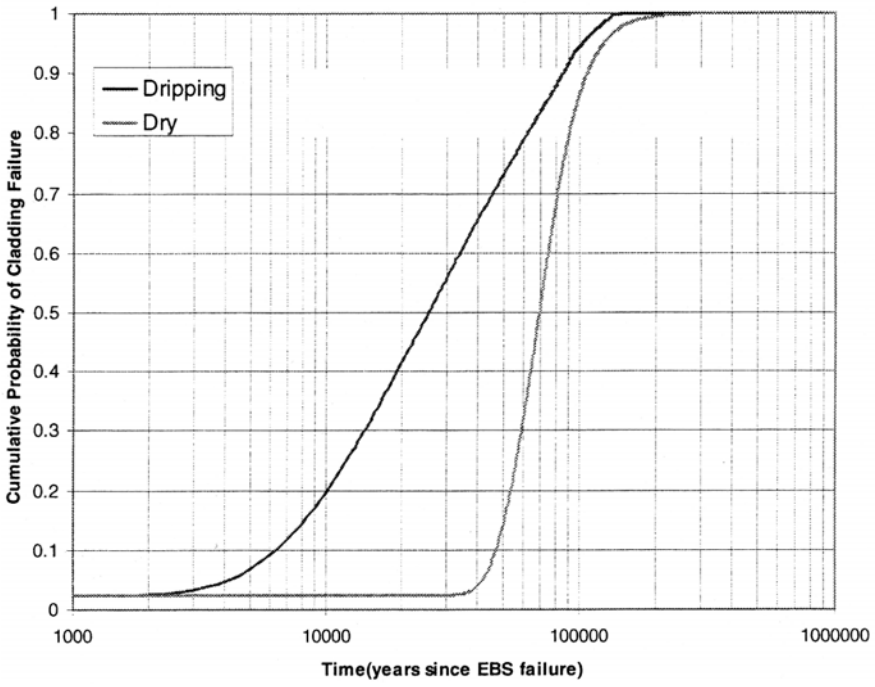

Figure A-27
Derived cumulative failure curves for zircaloy cladding (EPRI, 2000).

A.6.4 Source-term Model

The COMPASS source-term sub-model of IMARC was modified in accordance with the new dimensions for the SRCR design. Extensive review and updating of data inputs for radioelement solubilities (Table A-7) and sorption coefficients for possible corrosion products were also provided in the Phase 5 study (EPRI, 2000).

A.6.5 Flow and Transport Models

Revision of the SRCR design did not modify any significant aspect of previous unsaturated and saturated zone flow and transport modeling performed by EPRI (EPRI, 1998). Modifications to the saturated zone sub-model of IMARC5 code were necessary, however, because the draft EPA standard defined an 18-km saturated zone (SZ) from the edge of the repository to the accessible environment. The SZ domain as modeled in Phase 5 IMARC (EPRI, 2000) is shown in Figure A-28. A vertical thickness of 200 meters was assumed, smaller than values previously used (EPRI, 1996; 1998), based on evidence that open fractures in the SZ were restricted to a few hundred meters of the water table and were not as abundant deeper in the SZ. This modification restricted the ability of the migrating radionuclide plume to spread in the vertical direction, although the Phase 5 IMARC was judged to be sufficiently wide to permit transverse horizontal spreading to continue to reduce plume concentrations as a function of travel time. However, given the formulization specified in EPA's 40 CFR Part 197, the entire plume was assumed to be captured, albeit mixed in 3000 acre-feet of groundwater, during extraction in a well at the compliance boundary.

Table A-7
Radioelement solubility values adopted for IMARC 5 [Revised values from IMARC 4 are shown in *BOLD ITALICS*] (from EPRI, 2000).

Element	Solubility Values (moles/liter)			Comments/References
	Low (5% Probability)	Median (90% Probability)	High (5% Probability)	
Se	1E-03	1E-02	7E+00	No change; selenium expected to be highly soluble.
Tc	***1E-08***	1E-03	1E+01	Median and high values – no change; low value based on measurements by Eriksen et al. (1992); redox potential key variable.
Cs	9E-06	3E-03	1E-02	No change
I	3E+00	1E+01	2E+01	No change
Pb	***5E-09***	***5E-06***	***5E-05***	Median and high values based on measurements by Marani et al. (1995); low value based on data review by Marani et al. (1995).
Ra	1E-10	***1E-06***	***1E-05***	Median and high values based on calculations by Runde (2000) relevant to Yucca Mountain waters; low value no change.
Ac	1E-10	1E-09	3E-06	Am conservatively used as chemical homolog; Ac solubilities may be lower (x10) due to less radiation damage of solid phase.
Th	1E-10	3E-09	1E-06	No change.
Pa	6E-07	***3E-05***	***6.5E-04***	Np used as chemical homolog.
U	1E-05	***4E-05***	***5E-04***	Values based on measurements by Sandino and Bruno (1992); only slight changes to median and high values.
Np	6E-07	***3E-05***	***6.5E-04***	Median and high values based on measurements by Efurd et al. (1998); pH7 and pH6 respectively.
Pu	1E-10	***2E-08***	***1E-06***	Median based on measurements by Efurd et al. (1998), pH7; high value based on measurements by Nitsche et al. (1992), pH 8.5.
Am	1E-10	***1E-09***	***3E-06***	Median based on measurements by Nitsche et al. (1992); high based on measurements by Nitsche et al. (1992), for slightly higher carbonate water; low value arbitrarily set 10x lower.

A.6.6 Biosphere Model

The Phase 5 study (EPRI, 2000) was the last presentation of an alternative approach to biosphere pathway analysis. The promulgation of EPA's Yucca Mountain specific safety standard, 40 CFR Part 197, had basically superseded the need for different stakeholders to speculate on diverse approaches to biosphere analysis. The biosphere pathway analysis prescribed by the EPA and incorporated in 40 CFR Part 197 avoided possibly conflicting, alternative approaches and assumptions regarding uncertain human behavior and radiological impacts.

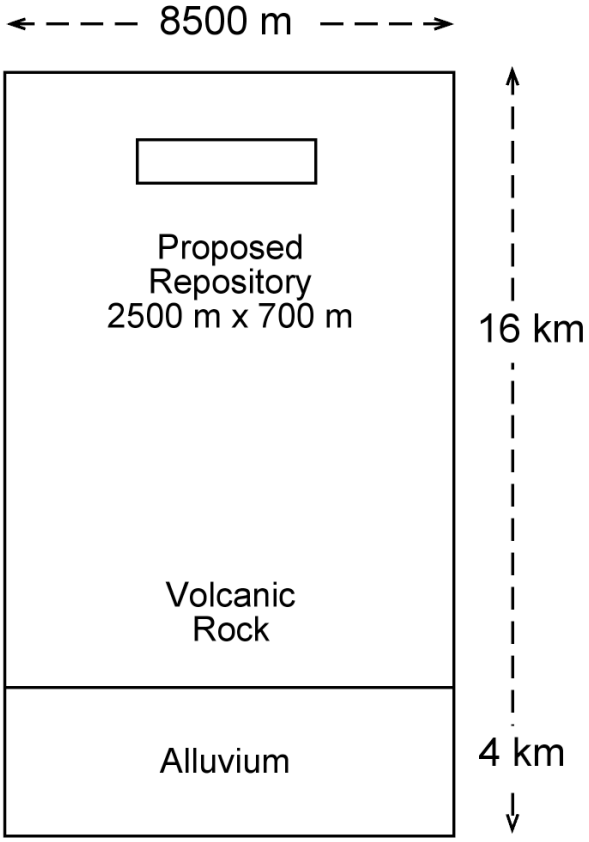

Figure A-28
Sketch of the simulation domain in the Saturated Zone (SZ) (EPRI, 2000).

A.6.7 Phase 5 Results

Numerous sensitivity analyses were conducted in the Phase 5 report (EPRI, 2000) to illustrate how different barriers, processes and assumptions affected repository performance. In addition, a series of "barrier neutralization" calculations were also made for the purpose of identifying which barriers, processes and assumptions were of highest significance to repository performance, as measured by (a) the magnitude of peak dose rate, and (b) the timing of peak dose rate. Results from the Phase 5 analyses re-confirmed the long-term safety of a HLW repository at Yucca Mountain.

A.7 Phase 6 (EPRI, 2002a)

The primary purpose of the Phase 6 study (EPRI, 2002a) was to provide an independent evaluation of whether the Yucca Mountain site and repository concept would be suitable as a permanent geological repository for U.S. HLW. At the time of the Phase 6 study in early 2002, a recommendation by the Secretary of Energy (and accepted by the President) had just been presented to the U.S. Congress to proceed with development of the Yucca Mountain system as a repository for U.S. HLW.

The Phase 6 IMARC code was modified to accommodate new data and information regarding the Yucca Mountain site and revisions to the EBS design. A series of sensitivity analyses were conducted to explore the key uncertainties and processes affecting long-term isolation of HLW at Yucca Mountain.

A.7.1 Net Infiltration Model

After an extensive review of then-recent data, it was decided that no changes were needed for the Phase 6 IMARC net infiltration sub model.

A.7.2 Thermal and Seepage Model

Sub-models for evaluating the fraction of waste packages contacted by seeping water (Figure A-29) and the seepage rate (Figure A-30) as a function of local percolation (infiltration) rate around emplacement drifts were updated in the Phase 6 study (EPRI, 2002a). In Figures 1-29 and 1-30, "*MAX*" refers to the maximum values derived in the modeling, "*MIN*" refers to the minimum values derived in the modeling, and "*PEAK*" refers to the intermediate values that are assigned the highest probabilities.

A.7.3 Containment Models

Based on data available in 2002, cumulative failure functions for the Ti-7 drip shield and alloy C-22 waste package were updated. Figure A-31 shows Phase 6 alternative failure curves for Ti-7 depending on whether the peak surface temperature would be 160ûC or 120ûC. With respect to the containment performance of the alloy C-22 waste package outer barrier, a series of possible alternative sensitivity cases were evaluated.

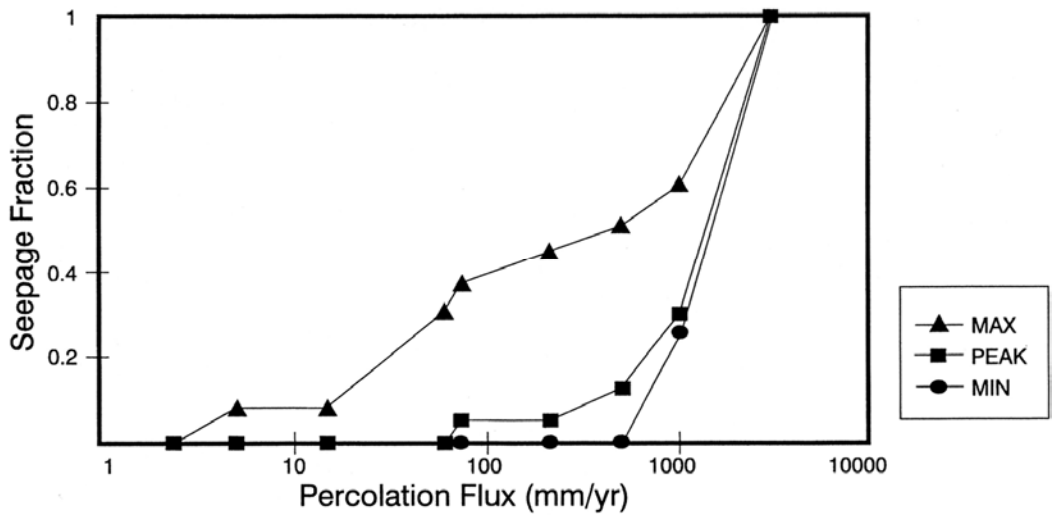

Figure A-29
Phase 6 fraction of waste packages experiencing seepage ("Seepage Fraction") as a function of local percolation flux (EPRI, 2002a).

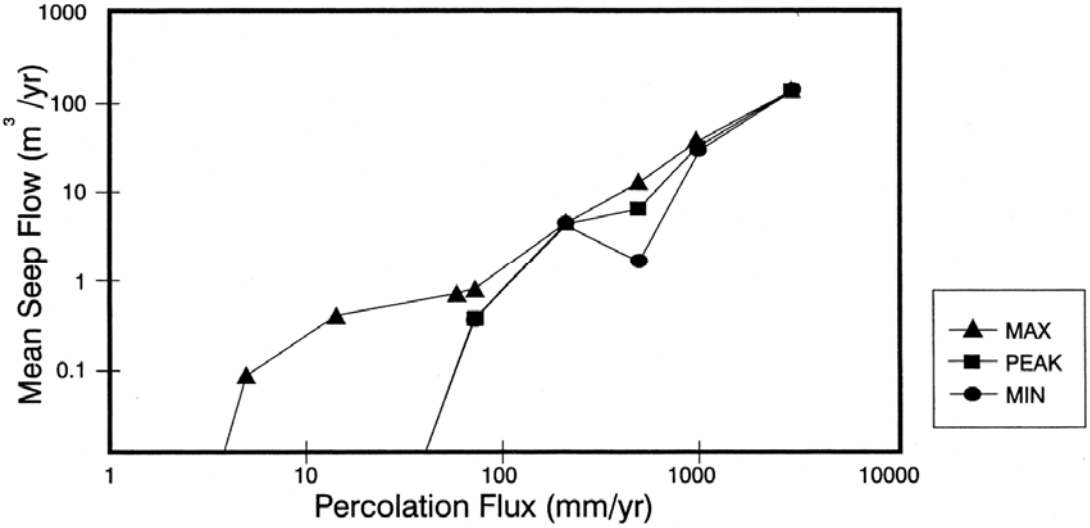

Figure A-30
Phase 6 mean seepage rate as a function of local percolation flux (EPRI, 2002a).

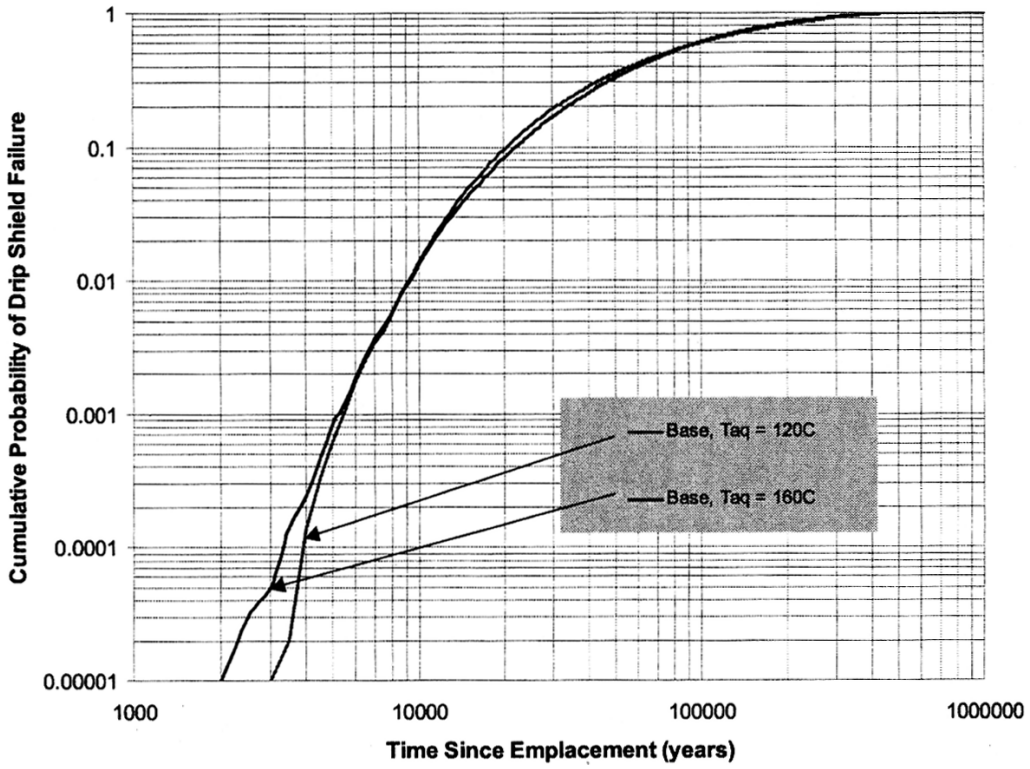

Figure A-31
Phase 6 cumulative failure function for titanium grade-7 drip shield as a function of peak temperature (EPRI, 2002a).

Figure A-32 shows one set of calculational cases in which the onset of aqueous corrosion was conservatively assumed to initiate at 160˚C and the lower temperature threshold for the initiation of crevice corrosion was assumed to be 85˚C. The four cases shown are:

- dripping (seeping) water, with emplacement of intact waste packages (WP) and drip shields (DS),
- no dripping water, with emplacement of intact waste packages (WP) and drip shields (DS),
- dripping (seeping) water, with emplacement of intact waste packages (WP) but immediate failure of drip shields (DS), and
- dripping (seeping) water, with emplacement of intact drip shields (DS), but immediate failure of waste packages (WP).

A range of other alternatives, including elevated concentrations of fluoride in seeping groundwater and uncertainties in activation energy for localized corrosion, were also evaluated.

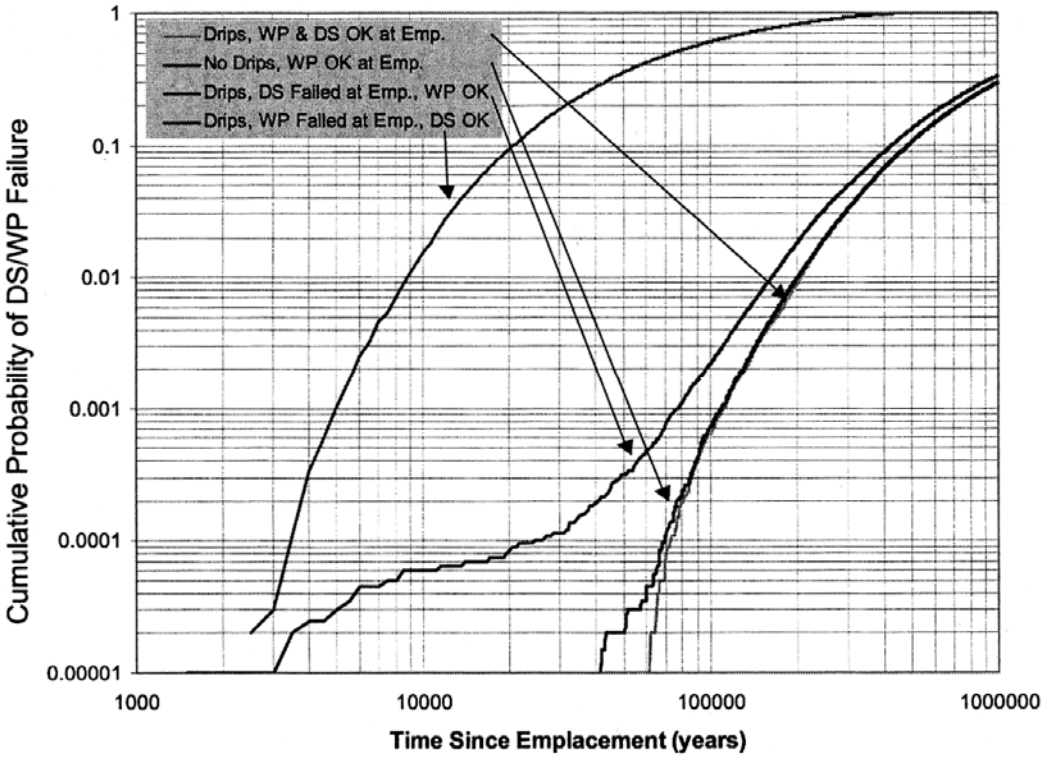

Figure A-32
Phase 6 cumulative failure curves of Alloy C-22 for alternative environments (EPRI, 2002a).

A.7.4 Source-term Model

Several new concepts were reviewed in the Phase 6 study (EPRI, 2002a) with respect to the source-term sub-model of IMARC. These concepts included the:

- amount of water inside a failed waste package,
- thickness (hence, transport properties) of thin water films connecting the inside and outside of failed waste packages,
- colloid formation, stability and potential radionuclide transport within the EBS,
- potential for formation of above-boiling deliquescent brines within the EBS, and
- use of chemical divide theory to establish bounds on the composition of groundwater impacted by reflux in boiling and condensation conditions of the initial thermal period.

With respect to data inputs, an extremely conservative range of UO_2 dissolution times (alteration times) based on the limited information at that time was established in the IMARC 6 logic tree as 1,000 years (with a probability of 5%), 3,000 years (with a probability of 90%) and 5,000 years (with a probability of 5%), based on available information as cited in the Phase 6 report. A comparison was also made (Figure A-33) between the range of radioelement solubility values used in the Phase 6 IMARC code and those values used by DOE/OCRWM in 2002.

Furthermore, a comparison was made between the Phase 6 IMARC code capabilities and conservatisms with those used in 2002 by DOE/OCRWM.

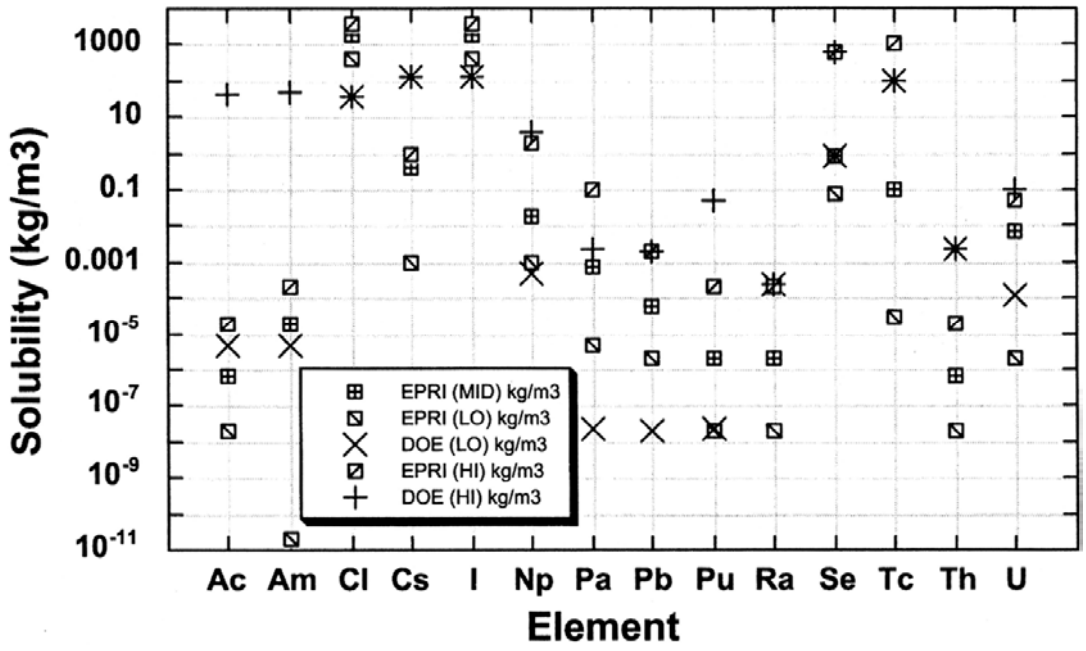

Figure A-33
Comparison of radioelement solubility values used in the EPRI Phase 6 study (EPRI, 2002a) and values used by the DOE/ OCRWM.

A.7.5 Flow and Transport Models

No modifications were made to the capabilities for the UZ and SZ flow and transport models for the Phase 6 IMARC code (EPRI, 2002a), although data inputs were updated based on data available at that time. Sensitivity analyses in the Phase 6 report supported the concept of sluggish flow in the Yucca Mountain region, and indicated that the 2002 DOE/ OCRWM conceptual flow and transport models (DOE/OCRWM, 2002) were likely to be conservative.

A.7.6 Phase 6 Results

In order to expand the number of radionuclides under consideration for TSPA analyses by the Phase 6 IMARC code, a reduced set of 54 logic-tree branches were evaluated (Figure A-34). It was possible to reduce the number of branches of the logic tree, because of improved understanding that some of the branches were not risk significant. Exceptionally low peak dose rates on the order of 0.1 mrem/year (compared to a compliance limit of 15 mrem/year for the draft EPA standard) were calculated (Figure A-35). ^{237}Np and its decay daughters, ^{233}U and ^{229}Th, were found to dominate the calculated peak dose rate. Among the many observations and conclusions in the Phase 6 study (EPRI, 2002a), it was specifically concluded that:

"EPRI shows in this report [EPRI, 2002a] that DOE has many engineered and natural features that are effective "barriers" within the Yucca Mountain system that contribute to overall safety. Thus, if the long-term behavior of one or more of those barriers turns out to be less favorable than currently projected, EPRI analyses suggest it is likely that overall repository performance from the remaining features would still protect public health and safety…In many instances in the DOE analyses for which there is uncertainty about future behavior, DOE introduces conservatisms in their analysis such that RMEI dose rates are likely to be overestimated. In this case, additional data collected in the future may allow for current dose estimates to be lowered."

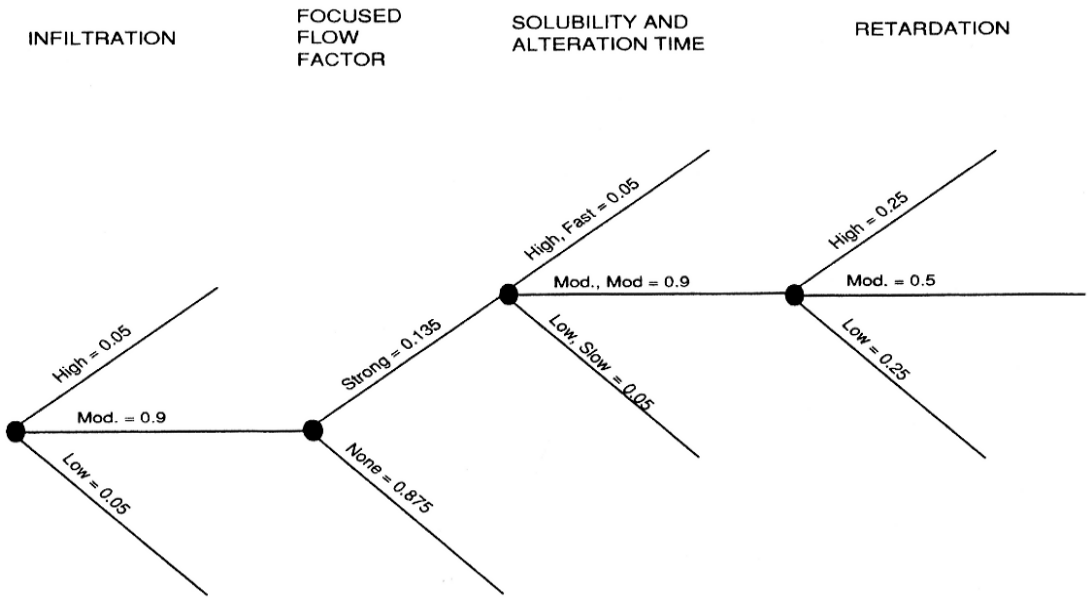

Figure A-34
Phase 6 logic tree for IMARC calculations (EPRI, 2002a).

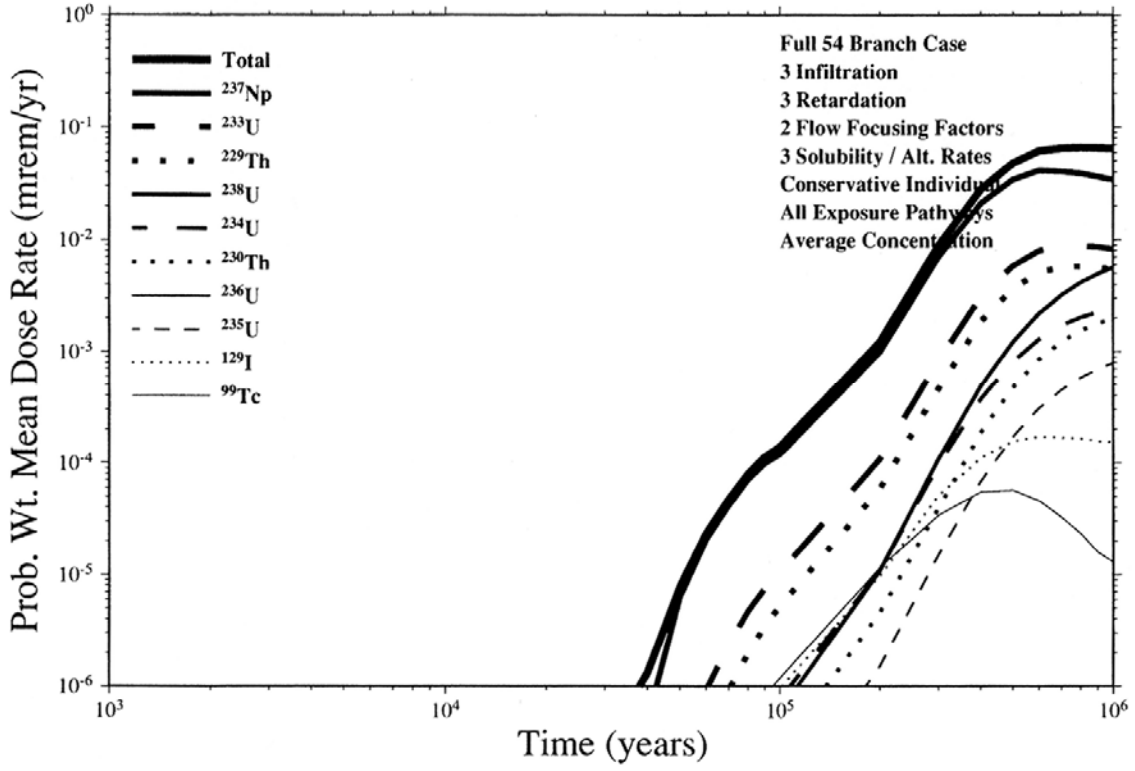

Figure A-35
Phase 6 calculated "Base Case" of time-dependent, probability-weighted dose rate from a repository at Yucca Mountain (EPRI, 2002a).

A.8 Phase 7 (EPRI, 2002b)

By the end of 2002, the US Congress had voted to override the State of Nevada veto (as permitted by the Nuclear Waste Policy Act of 1982, as revised), and accept the recommendation of Yucca Mountain as the candidate repository for HLW disposal. This Congressional action effectively moved the US program to the construction pre-license application phase with the NRC. A successful license application (LA) depended on a robust demonstration of long-term safety, as well as focusing and prioritizing remaining research and design activities to resolve any remaining key technical issues (KTIs).

The purpose of EPRI's Phase 7 study (EPRI, 2002b) was to evaluate the performance and safety of the proposed repository concept at Yucca Mountain on the basis of "reasonable expectation/ reasonable assurance," per the then-draft EPA safety standard 40 CFR Part 197 and draft NRC 10 CFR Part 63 regulation. In addition, specific analyses were conducted with respect to key technical issues affecting long-term repository performance.

Given the short period between the Phase 6 and Phase 7 reports (less than 12 months), no fundamental changes were made to the Phase 7 IMARC code, and only minor data updates were made. The conceptual model for the UZ portion of the repository system, which includes transport through unsaturated tuff and unsaturated alluvium, is shown in Figure A-36.

The logic tree for the Phase 7 analyses was expanded to 108 branches (Figure A-37) (EPRI, 2002b) compared to the 54 branches of the Phase 6 (EPRI, 2002a) analyses. The increased logic tree was implemented to introduce the seepage fraction branches. The Phase 7 probability-weighted dose rate analysis is shown in Figure A-38. The peak dose rate calculated out to 10^6 years in the Phase 7 analysis was 0.03 mrem/year, well below the 15 mrem/year compliance limit in the draft EPA standard for Yucca Mountain for the first 10,000 years following repository closure.

A.9 Phase 8 (EPRI, 2005b)

IMARC Phase 8 (EPRI, 2005b) was the same as IMARC Phase 7, although it was at this time that substantial testing and verification activities were undertaken, and the code was placed under formal change control and configuration management systems. As discussed in EPRI (2005b), the component modules of IMARC were subjected to testing to ensure that the code was properly implemented, and that it produces reliable results consistent with the intended conceptual model implementation. IMARC 8, therefore, represents a significant baseline from which later IMARC versions may be compared (Kessler *et al.,* 2006).

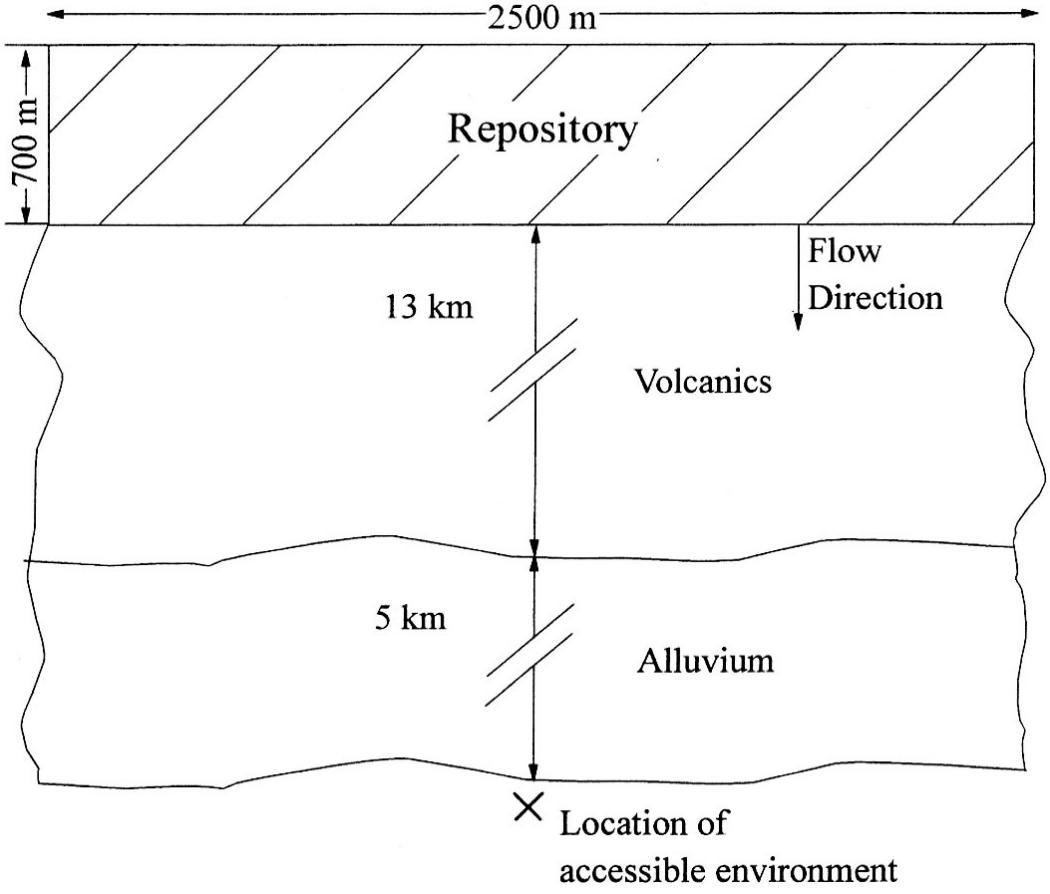

Figure A-36
Graphical representation of unsaturated zone (UZ) portion of the Phase 7 IMARC code (EPRI, 2002b).

A.10 Phase 9 (Kessler *et al.*, 2006)

IMARC Phase 9 represented an update of parameters and understanding to bring it current with contemporary DOE and NRC analyses. In Phase 9, analyses were conducted to evaluate the consequences of seismicity (EPRI, 2005c) and igneous intrusion (EPRI, 2005a). In addition, EPRI commissioned an independent review team (IRT) comprising individuals with broad experience in TSPA (Garisto *et al.*, 2008; EPRI, 2009). The IRT reviewed an interim draft IMARC report with full descriptions of the models and parameters used in the code.

Garisto *et al.* (2008) provided a summary of the IRT findings. The complete IRT report has been published in EPRI (2009). Generally, it was found that IMARC 9 captured the main processes in TSPA and their interactions. The IRT stated its belief that IMARC 9 was "fit for purpose" in the sense that it provided a risk-based methodology for integration of information from various disciplines affecting long-term repository performance and focused on reasonable expectation of the dose consequence to the RMEI. The IRT also stated its belief that IMARC 9 was a very well integrated model, which focuses on those processes that could affect the long-term performance of the repository.

The IRT also provided recommendations on moving some parameters to a less conservative basis by conducting ancillary analyses to support the improved parameter values. Specifically, the IRT suggested re-evaluation of the alteration rate of spent nuclear fuel. These analyses were subsequently completed and parameters in IMARC 10 have been updated in this report to reflect the improved, longer alteration rates indicated by the new analyses.

Many of the IRT comments related to improving the IMARC 9 documentation. Other comments provided suggestions for sensitivity analysis to identify which parameters contributed most to the uncertainty in the estimated dose rates, and sensitivity analyses to provide improved understanding of the modeled system.

The IRT review was completed in the months immediately prior to the issuance of the Yucca Mountain License Application Safety Analysis Report (DOE/OCRWM, 2008). The IRT review and the review of the DOE LA provided a significant new basis for re-evaluation of the IMARC code, parameter values used in it, and its documentation. To address this new basis, significant updates were necessary. The result of those updates is IMARC 10, as documented in this report.

A.11 Evolution of the Inventory

A.11.1 Radionuclides and Inventory Modeled

In line with EPRI's focus on the commercial electric power industry, IMARC analyses to date have examined the 63,000 MTHM commercial SNF inventory of the full 70,000 MTHM legal capacity for the proposed repository at Yucca Mountain. Accordingly, the current IMARC inventory considers nuclides only from commercial spent nuclear fuel (CSNF). This is not an intrinsic limitation of the code, but rather reflects EPRI's research focus. The CSNF contains the majority of the long-lived activity in the repository. In the current statuary limit of waste capacity 70,000 MTHM for the Yucca Mountain repository, 63,000 MTHM is from CSNF, comprising 7,796 waste packages (TSPA-LA Table 6.3.7-1) including PWR and BWR spent-fuel with various burnups. DOE analysis identified "all of the radionuclides of major importance to dose and virtually all of the marginally important radionuclides." (BSC, 2004a). These nuclides are listed in Table A.1 along with reasons for their inclusion in the DOE's analysis (BSC, 2004a).

In Table A.8, a total of 32 nuclides are listed. The "Dose" column lists the radionuclides that contribute to 95% of the dose for the 10,000-yr period, including both major and minor dose contributors. The "Precursor" column lists nuclides that are included because of their major dose contributing progeny nuclides. The "EPA" column lists the radionuclides that are included for the sake of evaluation of groundwater protection issues based on U.S. Environmental Protection Agency (EPA) regulations (40 CFR 197.30 and 10 CFR 63.331). The "FEIS" column lists the additional radionuclides that were included for the million-year calculation in the Final Environmental Impact Statement (FEIS). The last column, "IMARC 10", lists nuclides that are included in the current IMARC inventory.

Table A-8
Included Radionuclides and Screened-in Reasons

Nuclide	Half Life [yrs]	Dose	Precursor	EPA	TSPA-LA	IMARC 10
Ac-227	21.773	Ac-227			Ac-227	
Am-241	432.2	Am-241			Am-241	(1)
Am-243	7,370	Am-243			Am-243	
C-14	5,730	C-14			C-14	
Cl-36	3.01×10^{5}				Cl-36	Cl-36
Cm-245	8,500		Cm-245		Cm-245	(1)
Cs-135	2.3×10^{6}	Cs-135			Cs-135	
Cs-137	30.07	Cs-137			Cs-137	
I-129	1.59×10^{7}	I-129			I-129	I-129
Np-237	2.14×10^{6}	Np-237			Np-237	Np-237
Pa-231	32,760	Pa-231			Pa-231	
Pb-210	22.6				Pb-210	
Pu-238	87.7	Pu-238			Pu-238	
Pu-239	2.44×10^{4}	Pu-239			Pu-239	Pu-239
Pu-240	6,580	Pu-240			Pu-240	
Pu-241	14.35		Pu-241		Pu-241	(1)
Pu-242	3.73×10^{5}	U-238	Pu-242		Pu-242	Pu-242 (2)
Ra-226	1,600	Ra-226		Ra-226	Ra-226	Ra-226
Ra-228	5.75			Ra-228	Ra-228	
Se-79	2.95×10^{5}				Se-79	Se-79
Sn-126	2.5×10^{5}				Sn-126	
Sr-90	28.84	Sr-90			Sr-90	
Tc-99	2.15×10^{5}	Tc-99			Tc-99	Tc-99
Th-229	7,340	Th-229			Th-229	Th-229
Th-230	7.7×10^{4}		Th-230		Th-230	Th-230
Th-232	1.41×10^{10}		Th-232		Th-232	
U-232	68.9	U-232			U-232	
U-233	1.59×10^{5}	U-233			U-233	U-233
U-234	2.47×10^{5}	U-234			U-234	U-234
U-235	7.1×10^{8}		U-235		U-235	U-235
U-236	2.34×10^{7}		U-236		U-236	
U-238	4.51×10^{9}	U-238			U-238	U-238
Total		20	7	2	4	12

1. Radionuclide included by adding the inventory to the inventory of Np-237, providing an overestimate of Np-237 inventory
2. Pu-242 decays to produce U-238. However, the contribution of Pu-242 to U-238 is negligible, and Pu-242 is a significant dose contributor by itself. Therefore in IMARC Pu-242 is modeled as a simply decaying radionuclide.

Early IMARC calculations only included a few nuclides. In Phase 3 (EPRI, 1996), the number of nuclides considered in IMARC increased to about 22. Beginning with Phase 7 (EPRI, 2002b), and for all subsequent versions, a decision was made to only include the top 12 dose contributors, since the remaining radionuclides produced inconsequential doses. In IMARC 10 the radionuclides Se-79 and Cl-36 have been added back in at the request of the IRT. In addition, through IMARC 9 Pu-240 was included in the IMARC inventory, and this has been replaced in IMARC 10 by Pu-242, owing to its greater importance in the TSPA-LA. Similarly, Ra-226 was not included as a decay product in earlier versions of IMARC, but it has been added back in because of its relative importance in the TSPA-LA.

Specific reasons for the exclusion of each radionuclide are as follows:

- Ac-227: short-lived, in secular equilibrium with Pa-231, excluded for low dose consequence.
- Am-241: short-lived and low dose consequence, as a precursor to the major dose contributor, its initial inventory is added to Np-237.
- Am-243: short-lived and low dose consequence.
- C-14: was included in Phase 1 and 2 IMARC calculations (EPRI, 1990, 1992) as a gas release, but was later excluded in Phase 3 (EPRI, 1996) and thereafter due to low dose consequences.
- Cl-36: was added in IMARC Phase 6 (EPRI, 2000a) but was dropped in Phase 7 (EPRI, 2002b) because of low dose consequence. It has been added back in to IMARC 10 at the request of the IRT.
- Cm-245: as a precursor to major dose contributor (Am-241 and Pu-241); its inventory is added to Np-237.
- Cs-135: excluded for low dose consequences.
- Cs-137: excluded for short half life.
- Pa-231: excluded for low dose consequences.
- Pb-210: short-lived, in secular equilibrium with Ra-226, excluded for low dose consequence.
- Pu-241: short-lived precursor of Np-237; its inventory is added to Np-237.
- Pu-242: Added in to IMARC 10 owing to its importance in the TSPA-LA.
- Ra-226: Added in to IMARC 10 owing to its importance in the TSPA-LA.
- Ra-228: excluded for low dose consequence.
- Se-79: Excluded for low dose consequence in prior versions of IMARC. Included in IMARC 10 at the request of the IRT.
- Sn-126: excluded for low dose consequence.
- Sr-90: excluded short half life.
- Th-232: excluded for low dose consequence.
- U-232: excluded for short half life.

Table A-9 lists the latest inventory data for the 14 nuclides included in IMARC calculation. The fraction of inventory for nuclides in the gap and grain boundary is also listed. Note that the inventories are calculated for 2030 years – the time for the proposed waste acceptance of the Yucca Mountain repository.

Table A-9
Initial Inventory per CSNF Package

Nuclide	Daughter	Initial Inventory [mol][a]	Gap Fraction [%]
Cl-36		8.7×10^{-2}	6.0
I-129		13.4	11.24[b]
Np-237	U-233	64.3	0.0
Pu-239	U-235	181.0	0.0
Pu-242		21.8	0.0
Ra-226		0.0	0.0
Se-79		0.531	3.0
Tc-99		76.3	0.1[b]
Th-229		0.0	0.0
Th-230	Ra-226	6.61×10^{-4}	0.0
U-233	Th-229	2.47×10^{-4}	0.0
U-234	Th-230	7.48	0.0
U-235		266.	0.0
U-238	U-234	3.29×10^{4}	0.0

[a]: based on TSPA-LA Table 6.3.7-3.

[b]: mean value based on BSC (2004b).

The IMARC inventory contains only CSNF, in keeping with its focus on waste from nuclear power generation. Omission of the co-disposal waste does not significantly affect peak dose estimates, for several reasons. First, total activity in co-disposal waste packages is about two orders of magnitude below that in CSNF waste packages. Furthermore, in DOE's TSPA (DOE/OCRWM, 2008) the co-disposal waste packages are projected to fail at much earlier times than the CSNF waste packages. As a result, co-disposal packages contribute to a modest increase in projected doses at intermediate times, but do not contribute significantly to peak dose. Consequently, while the co-disposal waste packages have been omitted from the IMARC inventory, estimates of peak dose are not significantly affected by this assumption.

A.12 Summary

Table A-10 presents a summary of the key developments in capabilities of the IMARC code for each of the EPRI studies from Phase 1 to Phase 10. Review and updates of input parameters were made during each Phase report, although such specific data revisions are not cited in Table A-10. Also noted in Table A-10 are important contemporaneous events in the US repository program that affected the development and application of the IMARC code.

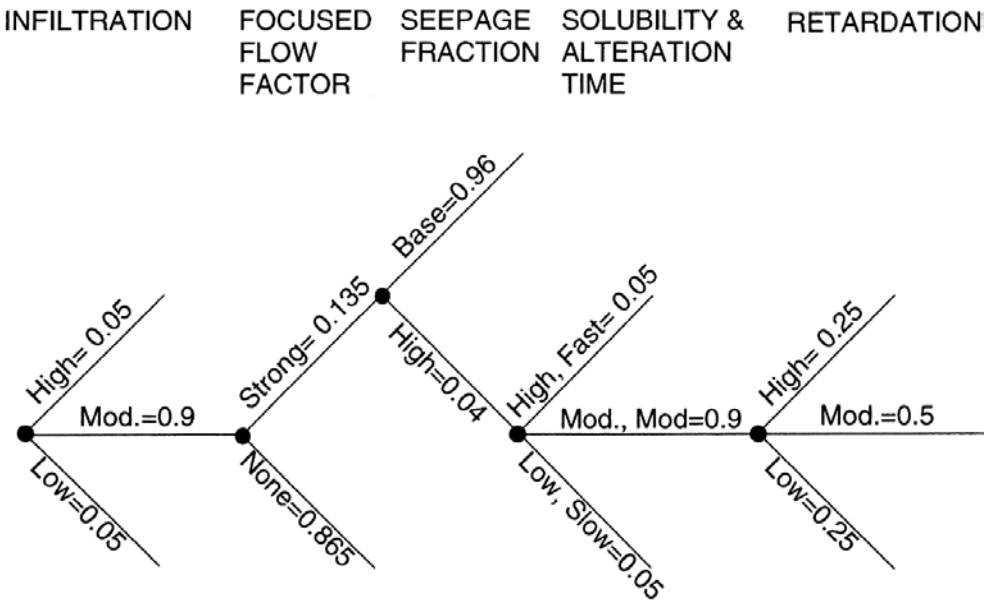

Figure A-37
Phase 7 Logic Tree for IMARC Calculations (EPRI, 2002b).

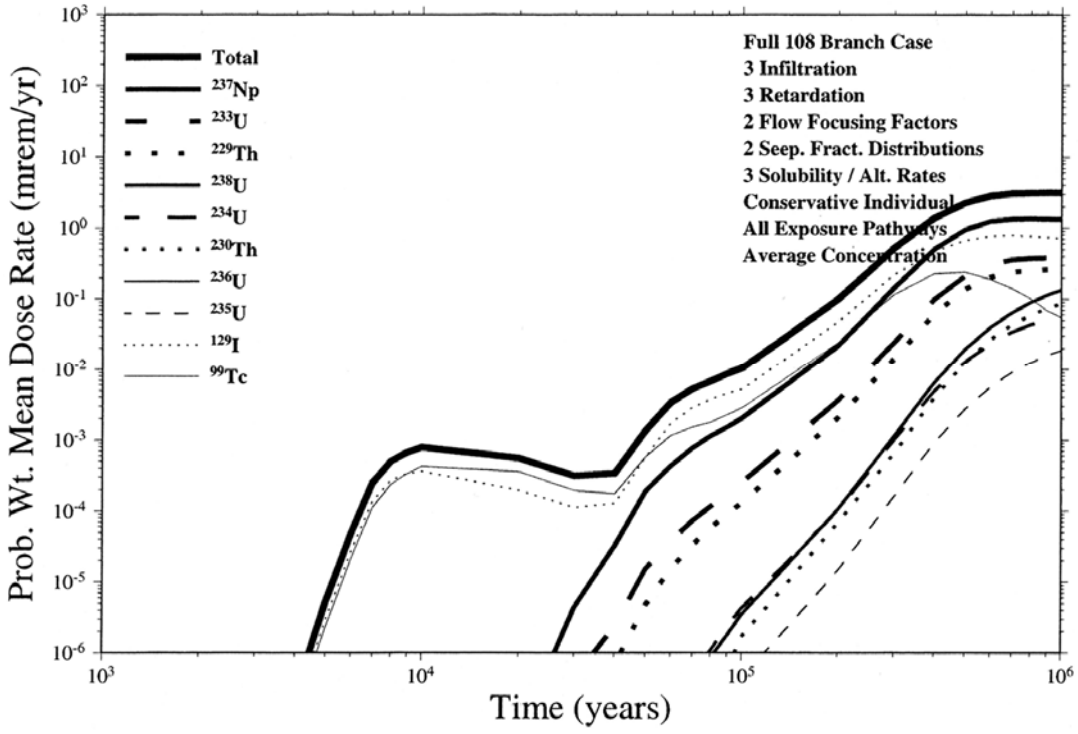

Figure A-38
Phase 7 calculated "Base Case" of time-dependent, probability-weighted dose rate from a repository at Yucca Mountain (EPRI, 2002b).

Table A-10
Summary of the phased development of the IMARC code.

IMARC models	Phase 1 (EPRI, 1990)	Phase 2 (EPRI, 1992)	Phase 3 (EPRI, 1996)	Phase 4 (EPRI, 1998)	Phase 5 (EPRI, 2000)	Phase 6 (EPRI, 2002a)	Phase 7 (EPRI, 2002b)	Phase 8 (EPRI, 2005c)	Phase 9-10 (current report)
Climate Change	Not considered	10^6-yr climate-change model added	• 10^6-yr climate-change model added • 3 alternative climate-change scenarios	Review of fossil data on climate	No change	No change	No change	No change	Constant climate
Infiltration	Simple precipitation vs. infiltration model	• Added plant, soil, topography properties • Added time and spatial variations	Formalized different precipitation vs. net infiltration/ percolation relations	Added improved rain run-off model	Comparision of different infiltration models for YM	No change	No change	No change	No change
Thermal/ Seepage	Not considered	Derived temperature vs. time curves for three different regions of repository	Fraction of waste packages (WPs) wetted and seepage rate as a function of heat load, heat transfer and rock	Fraction of WPs wetted and seepage rate as function of percolation rate	Update fraction of SRCR WPs wetted and seepage rate per percolation rate	Revise fraction of SRCR WPs wetted and seepage rate per percolation rate	No change	No change	No change
Containment	Simple containment time model	• Weibull statistical approach • 304 SS and alloy-825 considered	Alloy-825, alloy C-22 and zircaloy cladding considered	Physically-based approach (relative humidity, temperature, critical threshold)	Alloy C-22, Ti-7 and zircaloy cladding considered out to 10^6 years	Added stress corrosion cracking as a possible failure mode	No change	No change	EBSCOM model
Source-term	Only Np-237 Dissolution rate only, no solubility constraint	• Analytical ST models • Multiple SNF sources • Alternative water-contact modes	• Compartment model (COMPASS) • Revised water-contact modes	Corrosion-product sorption added	Revised SRCR WP dimensions	• Colloids evaluated • Coupled THC effects on water chemistry	No change	No change	No change

Table A-10 (continued)
Summary of the phased development of the IMARC code.

IMARC models	Phase 1 (EPRI, 1990)	Phase 2 (EPRI, 1992)	Phase 3 (EPRI, 1996)	Phase 4 (EPRI, 1998)	Phase 5 (EPRI, 2000)	Phase 6 (EPRI, 2002a)	Phase 7 (EPRI, 2002b)	Phase 8 (EPRI, 2005c)	Phase 9-10 (current report)
Flow and Transport	Simple flow and transport model	• Separate models for unsaturated zone (UZ), saturated zone (SZ) • Change in water table	Integrated UZ and SZ model	No change	SZ model revised to conform to draft EPA 40 CFR 197	No change	Revised well model	Change to 2-D SZ model	No change
Biosphere	Applied draft EPA 40 CFR 191 standard (cumulative release)	Evaluated human intrusion scenario	Developed Yucca Mountain-specific biosphere pathways and dose factors	Examined alternative approaches to biosphere modeling	Biosphere model revised to conform to draft EPA 40 CFR 197	No change	No change	Updated parameters	Updated model and uncertainty analyses
Seismic/ Rockfall	• Evaluated borehole stability • Evaluated seismic damage to containers	• Estimated probability of earthquakes • Evaluated thermal spalling of rock	Developed rockfall analysis for diverse rock properties	No change	No change	No change	No change	No change	EPRI analyses of seismicity, rockfall, and effects on EBS
Igneous Event	Evaluated volcano effects on water table	Evaluated igneous event probability	Input to Probabilistic Volcanic Hazard Analysis (PVHA)	No change	Evaluated event (dike) characteristics	No change	No change	EPRI analyses of extrusive event	EPRI analyses of intrusive event
Program Context	Site Characterization Plan design	• EPA to make a Yucca Mountain standard • Concerns about C-14 and water table rise	• NAS report • Revised ACD design • 10^4 vs 10^6 -year compliance period	• 1st draft of EPA 40 CFR 197 standard • Viability assessment	• New SRCR design (wth drip sheld) • Probability-weighted peak dose over 10^4 yr.	Recommendation of Yucca Mountain site by President	• Nevada veto • Congress overrides veto to accept Yucca Mountain site	Monitor Scientific takes over responsibility for IMARC	DOE submits License Application

A.13 References

Apted, M.J., W.J. O'Connell, K.H. Lee, A.T. MacIntrye, T.-S. Ueng, T. H. Pigford, and W.-L. Lee, 1991. "Preliminary calculations of release rates from spent fuel in a tuff repository," in *Proceedings of the 2nd International Conference on High Level Radioactive Waste Management*, American Nuclear Society, La Grange Park, IL, Vol 2, pp. 1080-1090.

CRWMS M&O, 1994. Generic Subsurface Layouts for Various Repository Thermal Loadings. CRWMS M&O Doc. No. BC0000000-01717-5705-00002, Rev. 00.

CRWMS M&O, 2000a. Drift Scale Coupled Processes (DST and THC Seepage) Models, MDL-NBS-HS-000001 REV 00.

CRWMS M&O, 2000b. General corrosion and localized corrosion of the drip shield. ANL-EBS-MD-00000 4 REV 00.

DOE/OCRWM, 1988. *Site Characterization Plan, Yucca Mountain Site, Nevada Research and Development Area, Nevada,* US Department of Energy, Office of Civilian Radioactive Waste Management, Washington DC (9 volumes.

DOE/OCRWM, 1995. *Total System Performance Assessment-1995: An Evaluation of the Potential Yucca Mountain Repository*, B00000000-01717-2200-00136, REV 1, US Department of Energy, Office of Civilian Radioactive Waste Management, Washington, DC.

DOE/OCRWM, 2002. *Yucca Mountain Science and Engineering Report*, Technical Information Supporting Site Recommendation Consideration Revision 1, DOE/RW-0539-1, U.S. Department of Energy, Office of Civilian Radioactive Waste Management, February 2002.

DOE, 2008. Probabilistic Volcanic Hazard Analysis Update (PVHA-U) For Yucca Mountain, Nevada, TDR-MGR-PO-000001 REV 01, U.S. Department of Energy, Office of Civilian Radioactive Waste Management, September 2008.

DOE, 2008a. Total System Performance Assessment Model/Analysis for the License Application, MDL-WIS-PA-000005 Rev. 0 January 2008 Office of Civilian Radioactive Waste Management, Las Vegas, NV.

DOE, 2008b, Yucca Yucca Mountain Repository License Application: Safety Analysis Report, DOE/RW-0573, Rev 0., Office of Civilian Radioactive Waste Management, Las Vegas, NV.

Dudley, A., R.R. Peters, J.H. Gauthier, M.L. Wilson, M.S. Tierney and E.A. Klavetter, 1985. *Total System performance Assessment Code (TOPSAC), Volume 1: Physical and Mathematical Bases,* SAND850002, Sandia National Laboratories, Albuquerque, NM.

EPRI, 1990. Demonstration of a risk-based approach to high-level waste repository evaluation, EPRI NP-7057, Electric Power Research Institute, Palo Alto, CA.

EPRI, 1992. Demonstration of a Risk-Based Approach to High-Level Waste Repository Evaluation: Phase 2, EPRI TR-100384, Electric Power Research Institute, Palo Alto, CA.

EPRI, 1996. *Yucca Mountain Total System Performance Assessment, Phase 3*, EPRI TR-107191, Electric Power Research Institute, Palo Alto, CA.

EPRI, 1998. Alternative Approaches to Assessing the Performance and Suitability of Yucca Mountain for Spent Fuel Disposal, EPRI TR-108732, Electric Power Research Institute, Palo Alto CA, CA.

EPRI, 2000. Evaluation of the Candidate High-Level Radioactive Waste Repository at Yucca Mountain Using Total System Performance Assessment: Phase 5, Report number 1000802, EPRI, Palo Alto, CA.

EPRI, 2002a. Evaluation of the Proposed High-Level Radioactive Waste Repository at Yucca Mountain Using Total System Performance Assessment: Phase 6, Report number 1003031, Electric Power Research Institute, Palo Alto, CA.

EPRI, 2002b. Integrated Yucca Mountain Safety Case and Supporting Analysis: EPRI's Phase 7 Performance Assessment, Report number 1003334, Electric Power Research Institute, Palo Alto, CA.

EPRI, 2005a. Program on Technology Innovation: Potential Igneous Processes Relevant to the Yucca Mountain Repository: Intrusive-Release Scenario, Analysis and Implications. EPRI Report 1011165, Electric Power Research Institute, Palo Alto, CA.

EPRI, 2005b. Potential Igneous Processes Relevant to the Yucca Mountain Repository: Intrusive-Release Scenario. EPRI Report 1011165, Electric Power Research Institute, Palo Alto, CA.

EPRI, 2005c. Effects of Seismicity and Rockfall on Long-Term Performance of the Yucca Mountain Repository: 2005 Progress Report. EPRI Report 1011812. Electric Power Research Institute, Palo Alto, CA.

EPRI, 2009. International Review Team Report: A Peer Review of the Yucca Mountain IMARC Total System Performance Assessment EPRI Model. EPRI Report 1018711. Electric Power Research Institute, Palo Alto, CA.

Garisto, N.C., D.G. Bennet and J. Andersson, 2008. "A peer review of the Yucca Mountain IMARC total system performance assessment EPRI model," in Proc. 2008 International High-level Radioactive Waste Management Conference, American Nuclear Society (La Grange Park, IL).

Geomatrix, 1996. *Probabilistic Volcanic Hazard Analysis for Yucca Mountain, Nevada*, BA0000000-01717-2200-00082, US Department of Energy, Office of Civilian Radioactive Waste Management, Las Vegas, NV.

Goodess, C.M and J.P. Palutikof, 1993. *Studies of climate transition periods following the present temperature climate state,* published by Climate Research Unit, School of Environmental Sciences, University of East Anglia, Norwich, NR4 7TJ, NIREX, NSS/R316, 64 pages.

Kessler, J., M.W. Kozak, M. Apted, W. Zhou, and G. Mungov, 2006. "EPRI's Total System Performance Assessment of Yucca Mountain using IMARC 9," *Proc. International High-Level Waste Management Conference.* Las Vegas.

Kool, J., P. Huyakorn, E. Sudicky and Z. Saleem, 1994. "A composite modeling approach for subsurface transport of degrading contaminant from land-disposal sites," *Jour. Contam. Hydrol*., Vol. 17, pp. 69-90.

NAS, 1992. *Groundwater at Yucca Mountain; How High Can It Rise?,* National Research Council, National Academy Press, Washington, DC.

NAS, 1995. *Technical Bases for Yucca Mountain Standards*, National Research Council, National Academy Press, Washington, DC.

NWTRB, 2000. January to December 2000 Report to the US Congress and the Secretary of Energy, US Nuclear Waste Technical Review Board, Washington, DC.

O'Connell, W.J. and R.S. Drach, 1986. *Waste Package Performance Assessment: Deterministic System Model Program Scope and Specifications*, UCRL-53761, Lawrence Livermore National Laboratory, Livermore, CA.

Pigford, T. and P. Chambré, 1988. "Near-field mass transfer in geologic disposal systems: A review," in *Scientific Basis for Nuclear Waste Management XI*, Pittsburgh PA, Vol. 112, pp 125-141.

Romero, L., L. Moreno and I. Neretnieks, 1991. *A Compartment Model for Solute Transport in the Near-field of a Repository for Radioactive Waste*, SKB-TR-91-48, Swedish Nuclear Fuel and Waste Management Co. (SKB), Stockholm, Sweden.

Wilson, M., J. Gauthier, R. Barnard, G. Barr, H. Dockery, E. Dunn, R. Eaton, D. Guerin, N. Lu, M. Martinez, R. Nilson, C. Rautman, T. Robey, B. Ross, E. Ryder, A. Schenker, S. Shannon, L. Skinner, W. Halsey, J. Gansemer, L. Lewis, A. Lamont, I. Triary, A. Meijer and D. Morris, 1993. *Total System Performance Assessment for Yucca Mountain- SNL Second Iteration* (TSPA-1993), SAND93-2675, Sandia National Laboratories, Albuquerque, NM.

Worgan, K. and P.C. Robinson, 1992. *The CALIBRE Source-term Code: Technical Documentation for Project-90,* SKI-TR-91:18, Swedish Nuclear Power Inspectorate, SKI), Stockholm, Sweden.

B
APPENDIX B: COMPASS PARAMETER VALUES

COMPASS requires input parameters that can be categorized as follows:

- Nuclide-dependent,
- Element-dependent,
- Containment,
- Geometry,
- Physical, and
- Transport.

Each category of parameter values will be discussed in details in this section.

B.1 Nuclide-dependent Parameters

The current IMARC inventory considers nuclides only from commercial spent nuclear fuel (CSNF). This is not an intrinsic limitation of the code, but rather reflects EPRI's focus on CSNF. In the current statuary limit of waste capacity 70,000 MTHM for the Yucca Mountain repository, 63,000 MTHM is from CSNF, comprising 7,796 waste packages (TSPA-LA Table 6.3.7-1) including PWR and BWR spent-fuel with various burnups. DOE analysis identified "all of the radionuclides of major importance to dose and virtually all of the marginally important radionuclides." (BSC, 2004a). These nuclides are listed in Table B.1 along with reasons for their inclusion in the DOE's analysis (BSC, 2004a).

In Table B.1, a total of 32 nuclides are listed. The "Dose" column lists the radionuclides that contribute to 95% of the dose for the 10,000-yr period, including both major and minor dose contributors. The "Precursor" column lists nuclides that are included because of their major dose contributing progeny nuclides. The "EPA" column lists the radionuclides that are included for the sake of evaluation of groundwater protection issues based on U.S. Environmental Protection Agency (EPA) regulations (40 CFR 197.30 and 10 CFR 63.331). The "FEIS" column lists the additional radionuclides that were included for the million-year calculation in the Final Environmental Impact Statement (FEIS). The last column, "IMARC 10", lists nuclides that are included in the current IMARC inventory.

Table B-1
Included Radionuclides and Screened-in Reasons

Nuclide	Half Life [yrs]	Dose	Precursor	EPA	TSPA-LA	IMARC 10
Ac-227	21.773	Ac-227			Ac-227	
Am-241	432.2	Am-241			Am-241	(1)
Am-243	7,370	Am-243			Am-243	
C-14	5,730	C-14			C-14	
Cl-36	3.01×10^{5}				Cl-36	Cl-36
Cm-245	8,500		Cm-245		Cm-245	(1)
Cs-135	2.3×10^{6}	Cs-135			Cs-135	
Cs-137	30.07	Cs-137			Cs-137	
I-129	1.59×10^{7}	I-129			I-129	I-129
Np-237	2.14×10^{6}	Np-237			Np-237	Np-237
Pa-231	32,760	Pa-231			Pa-231	
Pb-210	22.6				Pb-210	
Pu-238	87.7	Pu-238			Pu-238	
Pu-239	2.44×10^{4}	Pu-239			Pu-239	Pu-239
Pu-240	6,580	Pu-240			Pu-240	
Pu-241	14.35		Pu-241		Pu-241	(1)
Pu-242	3.73×10^{5}	U-238	Pu-242		Pu-242	Pu-242 (2)
Ra-226	1,600	Ra-226		Ra-226	Ra-226	Ra-226
Ra-228	5.75			Ra-228	Ra-228	
Se-79	2.95×10^{5}				Se-79	Se-79
Sn-126	2.5×10^{5}				Sn-126	
Sr-90	28.84	Sr-90			Sr-90	
Tc-99	2.15×10^{5}	Tc-99			Tc-99	Tc-99
Th-229	7,340	Th-229			Th-229	Th-229
Th-230	7.7×10^{4}		Th-230		Th-230	Th-230
Th-232	1.41×10^{10}		Th-232		Th-232	
U-232	68.9	U-232			U-232	
U-233	1.59×10^{5}	U-233			U-233	U-233
U-234	2.47×10^{5}	U-234			U-234	U-234
U-235	7.1×10^{8}		U-235		U-235	U-235
U-236	2.34×10^{7}		U-236		U-236	
U-238	4.51×10^{9}	U-238			U-238	U-238
Total		20	7	2	4	12

1. Radionuclide included by adding the inventory to the inventory of Np-237 due to the relatively short half-life of Am-241.
2. Pu-242 decays to produce U-238. However, the contribution of Pu-242 to U-238 is negligible, where as the dose contribution from Pu-242 is of direct interest. Therefore, Pu-242 modeling in IMARC accounts for simple decay only and does not track the relatively insignificant ingrowth of U-238.

Early IMARC calculations only included a few nuclides. In Phase 3 (EPRI, 1996), the number of nuclides considered in IMARC increased to about 22. Beginning with Phase 7 (EPRI, 2002b), and for all subsequent versions, a decision was made to only include the top 12 dose contributors, since the remaining radionuclides represented inconsequential dose contributions and did not significantly influence repository performance. In IMARC 10 the radionuclides Se-79 and Cl-36 have been added back in at the recommendation of the IMARC International Review Team (IRT, EPRI, 2009), and owing to their prominence in the TSPA-LA. In addition, through IMARC 9 Pu-240 was included in the IMARC inventory, and this has been replaced in IMARC 10 by Pu-242, owing to its greater importance in the TSPA-LA. Similarly, Ra-226 was not included as a decay product in earlier versions of IMARC, but it has been added back in because of its relative importance in the TSPA-LA.

Specific radionuclides were excluded from IMARC based on consideration of source term composition, half-life, relationship to decay series, and contribution to dose. Notable examples and rationales for their exclusion include:

- Ac-227: short-lived, in secular equilibrium with Pa-231, excluded for low dose consequence.[15]
- Am-241: short-lived and low dose consequence, as a precursor to the major dose contributor, its initial inventory is added to Np-237.
- Am-243: short-lived and low dose consequence.
- C-14: was included in Phase 1 and 2 IMARC calculations (EPRI, 1990, 1992) as a gas release, but was later excluded in Phase 3 (EPRI, 1996) and thereafter due to low dose consequences.
- Cl-36: was added in IMARC Phase 6 (EPRI, 2000a) but was dropped in Phase 7 (EPRI, 2002b) because of low dose consequence. It has been added back in to IMARC 10 per the recommendation of the IRT and its prominence in the TSPA-LA.
- Cm-245: as a relatively short-lived precursor to major dose contributor (Am-241 and Pu-241); its inventory is added to Np-237.
- Cs-135: excluded for low dose consequences.
- Cs-137: excluded for short half life.
- Pa-231: excluded for low dose consequences. However, the contribution to dose from short-lived progeny is included in the biosphere model.
- Pb-210: short-lived, in secular equilibrium with Ra-226, excluded for low dose consequence.
- Pu-241: short-lived precursor of Np-237; its inventory is added to Np-237.
- Pu-242: Added in to IMARC 10 due to its importance in the TSPA-LA.
- Ra-226: Added in to IMARC 10 due to its importance in the TSPA-LA.

[15] Short-lived radionuclides are omitted owing to the longevity of the EBS. In the analysis of the ingneous extrusive scenario (EPRI, 2004b) these short-lived radionuclides were not screened, and a full set of radionulides in the inventory was used.

- Ra-228: excluded for low dose consequence.
- Se-79: Excluded for low dose consequence in prior versions of IMARC. Included in IMARC 10 per the recommendation of the IRT and in light of its prominence in the DOE TSPA-LA.
- Sn-126: excluded for low dose consequence.
- Sr-90: excluded for short half life.
- Th-232: excluded for low dose consequence.
- U-232: excluded for short half life.

Throughout the development of the IMARC code, the list of radionuclides included in EPRI's performance assessment has been revisited and revised as needed to reflect changes in understanding as well as evolution of DOE's approach to and results from TSPA.

Table B.2 lists the latest inventory data for the 14 nuclides included in IMARC calculation. The fraction of inventory for nuclides in the gap and grain boundary is also listed. Note that the inventories are calculated for the year 2030 – a date that has been proposed for initiation of waste acceptance at the Yucca Mountain repository (DOE/OCRWM,2008).

Table B-2
Initial Inventory per CSNF Package for IMARC 10

Nuclide	Daughter	Initial Inventory [mol][a]	Gap Fraction [%]
Cl-36		8.7×10^{-2}	6.0
I-129		13.4	11.24[b]
Np-237	U-233	64.3	0.0
Pu-239	U-235	181.0	0.0
Pu-242		21.8	0.0
Ra-226		0.0	0.0
Se-79		0.531	3.0
Tc-99		76.3	0.1[b]
Th-229		0.0	0.0
Th-230	Ra-226	6.61×10^{-4}	0.0
U-233	Th-229	2.47×10^{-4}	0.0
U-234	Th-230	7.48	0.0
U-235		266.	0.0
U-238	U-234	3.29×10^{4}	0.0

[a]: based on TSPA-LA Table 6.3.7-3.

[b]: mean value based on BSC (2004b).

B.2 Element-dependent Parameter

Element-dependent parameters required by COMPASS include elemental solubility and sorption coefficients. The later also depend on materials, or compartments. Solubility is treated as uncertain parameter and the values are listed in Table B.3. Additional discussion of solubility is provided in Appendix D.

Table B-3
Elemental Solubility Values [mol/l] Used in COMPASS/ IMARC

Element	Low	Medium	High	Source
I	0.78	0.78	0.78	EPRI (2003)
Np	4.2×10^{-10}	4.2×10^{-9}	4.2×10^{-8}	Langmuir (2006)
Pu	8.3×10^{-11}	8.3×10^{-9}	8.3×10^{-7}	EPRI (2003)
Tc, Se, Ra, Cl	1.0	1.0	1.0	EPRI (2003)
Th	8.7×10^{-11}	3×10^{-9}	8.7×10^{-8}	EPRI (2003)
U	4.2×10^{-7}	2.9×10^{-5}	2.1×10^{-4}	EPRI (2003)

Sorption coefficients in the near field are treated as fixed parameters. Their values are shown in Table B.4. Note that the tuff gravel invert and near-field rock have the same sorption coefficients, listed as "Tuff" in Table B.4.

Table B-4
Elemental Sorption Coefficients K_d [m^3/kg]

Element	Corrosion Product	Tuff	Source
I	0.0	0.0	EPRI (2002a)
Np	9.7×10^{-4}	0.001	EPRI (2002a)
Pu	0.099	10	EPRI (2002a)
Tc	0.0	0.0	EPRI (2002a)
Th	11	10	EPRI (2002a)
U	0.002	1.0	EPRI (2002a)
Ra	0.03	0.5	EPRI (2002a)
Cl	0.0	0.0	Mobile contaminant
Se	0.0	0.0	Conservative values selected

B.3 Containment Parameters

Specifically, four input parameters are required:

- "Inventory starting time" is the time when the initial inventories shown in Table B.2 are determined. For example, if the repository will open on 2033, the starting time for the inventories listed in Table B.2 would be equal to zero. If the repository will open on 2038, the starting time for the inventories listed in Table B.2 would be 5 years. Alternatively, the inventories will be adjusted so that the starting time is zero and always the same as the emplacement. Since these radionuclides are all very long lived differences in assumed starting dates are negligible.
- "Canister failure time" is the time when the COMPASS computation starts. In IMARC, this parameter is predicted as time-dependent to take into account of non-uniform spatial and temporal water contact across the repository. COMPASS is run for each time step with the fraction of waste packages failed during that time step, to account for the instant release fraction released during that time, and to account for the delay in releases from the UO_2 matrix up to that time step. The failure function for the components of the EBS is presented in Chapter 4.
- "Alteration time" is the time elapsed between the onset of water contact of spent-fuel UO_2 matrix to the completion of matrix alteration. This parameter depends on the near-field environment. The inverse of alteration time is assumed to be the constant dissolution rate for the spent-fuel matrix in COMPASS.
- "Cladding failure fraction vs. time" is the cumulative fraction of claddings that are breached as a function of time. This parameter is also predicted by the corrosion sub-model of IMARC and depends on the near-field environment. Once the cladding has failed, COMPASS also takes no credit for the cladding potentially providing an additional transport barrier.

The relationship between these times is illustrated in Figure B.1. It can be seen that the inventory starting time is earlier than the canister failure time. The alteration time is used after waste canister fails. The distributed cladding failure is dependent on time since canister failure. Note that a small fraction of claddings fails before canister failure.

The alteration time is treated as an uncertain parameter that is bound in one node in the "event tree" with solubility data. The alteration times in IMARC 10 are based on updated information developed by EPRI during 2008 (EPRI, 2008); values are shown in Table B.5.

Table B-5
Spent-fuel Alteration Times [yrs] (EPRI [2008])

Low	Medium	High
3000	30,000	300,000

Figure B.2 shows the cumulative cladding failure as a function of time for "dry" (i.e., no dripping water into the drift) and "wet" (dripping water into the drift) conditions. As discussed in EPRI (1998), the failure of cladding is assumed to proceed by reaction of zirconium with fluoride introduced in seepage drips into the failed waste package. The wet and dry failure functions reflect differing rates of ingress of fluoride into the waste package.

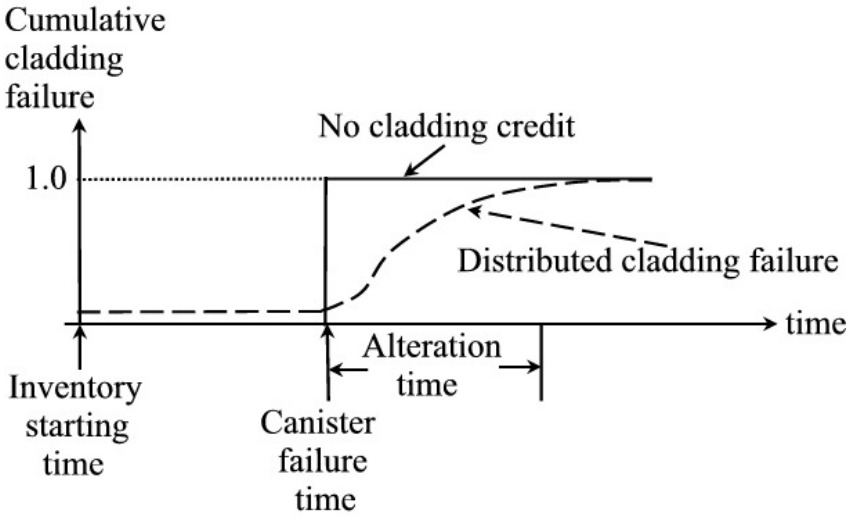

Figure B-1
Illustration of relationships of different containment parameters (times).

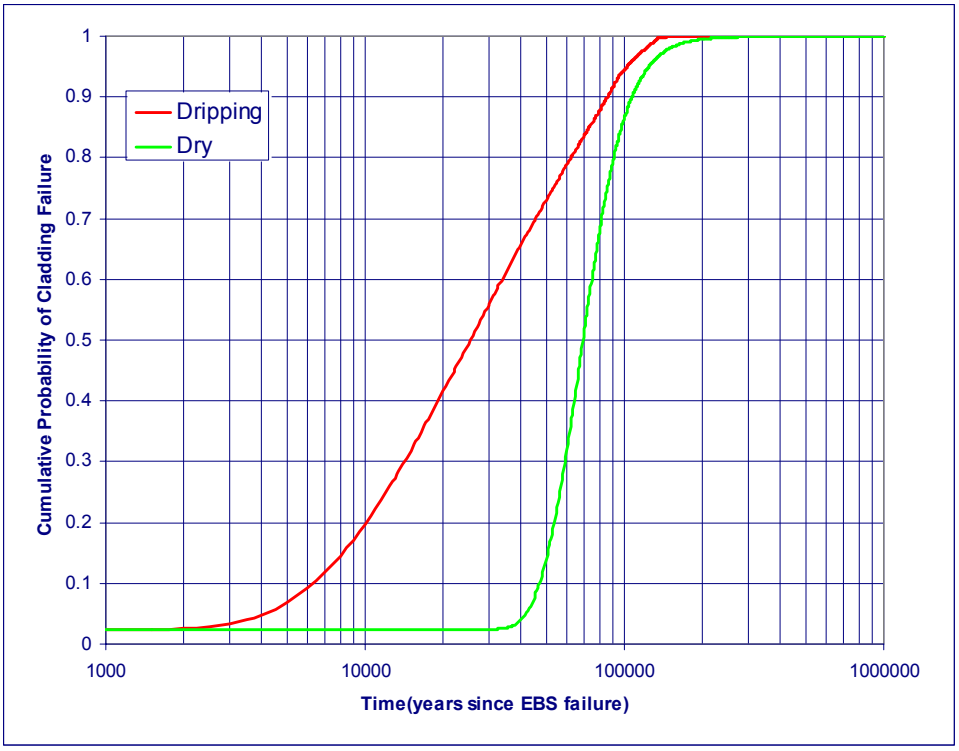

Figure B-2
Cladding failure distribution with time.

B.4 Geometry Parameters

Geometry parameters include the following parameters for all the compartments considered:

- Internal volume is needed for evaluating concentrations.
- Interface area is used for evaluating diffusive mass transfer rate.
- Diffusion distance is also used for evaluation diffusive mass transfer rate.

For the waste-form compartment, the 21-PWR fuel assembly waste package is assumed to be the representative package. Although the initial cylindrical waste package configuration cannot be maintained after the canister loses mechanical integrity due to general corrosion, the cylindrical configuration is used as the reference configuration for deriving reference geometry parameters for the waste-form compartment. This treatment is illustrated in Figure B.3. The UO_2 waste-form volume is assumed to be the total volume of the 5544 spent-fuel rods contained in a 21-PWR waste package. Given fuel rod diameter 0.823 cm (excluding cladding) and length 3.85 m (BSC, 2004c), the total volume can be calculated and listed in Table B.6. The diffusive length from the waste-form to the corrosion-product compartments is assumed to be the radius of the reference cylinder shown in Figure B.3. Given the volume in Table B.6 and fuel rod length, the reference cylinder radius can be calculated, also shown in Table B.6. The interface area between the waste form and corrosion product compartments is assumed to be the reference cylindrical outer surface area that can be calculated using the reference radius and the fuel-rod length (Table B.6).

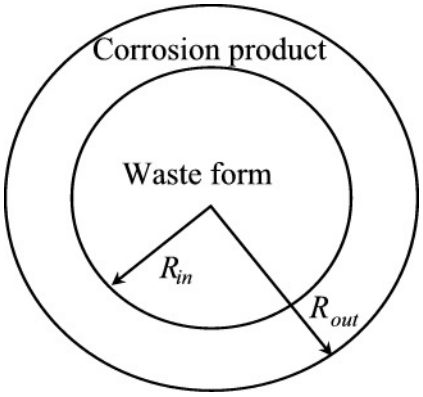

Figure B-3
Reference configuration for the waste-form and corrosion-product compartments.

The reference configuration of corrosion-product compartment is also shown in Figure B.3 as the annulus surrounding the waste form. The corrosion product volume is those of all metal materials within a 21-PWR waste package. The numerical value is given by BSC (2004c) and listed in Table B.6. Assuming that this volume is the reference annulus volume, the annulus outer radius can be determined as 0.55m using the known waste-form reference radius and spent-fuel rod length. The corrosion-product annulus inner and outer radii are used to determine the perimeter of the annulus. Because diffusive transport is directed to the invert located at the bottom of the waste package, the diffusive length from the corrosion-product to the invert compartments should be on the order of magnitude of the annulus average perimeter. In the

current IMARC calculation, half of the perimeter, shown in Table B.6, item No .6, is assumed for the diffusive length of corrosion-product compartment. The interface area between the corrosion-product and invert compartments is assumed to be the projection area of the original waste canister that is equal to the waste canister outer diameter 1.644m (BSC, 2004c) multiplied by the canister length 5.165m (BSC, 2004c).

The invert geometry is shown in Figure B.4 where R = 2.75 m and h = 0.60 m (US DOE, 2001). This gives:

$$\theta = \arccos\left(\frac{R-h}{R}\right) = 38.77 \text{ deg} = 0.678 \text{ rad} \qquad \textbf{eq. B-1}$$

$$A_{inv} = \frac{1}{2}R^2\left[2\theta - \sin(2\theta)\right] = 1.44 \text{ m}^2 \qquad \textbf{eq. B-2}$$

where θ in (2) is in rad

$$b = R\sin\theta = 1.72 \text{ m} \qquad \textbf{eq. B-3}$$

$$l = 2R\theta = 4.61 \text{ m} \qquad \textbf{eq. B-4}$$

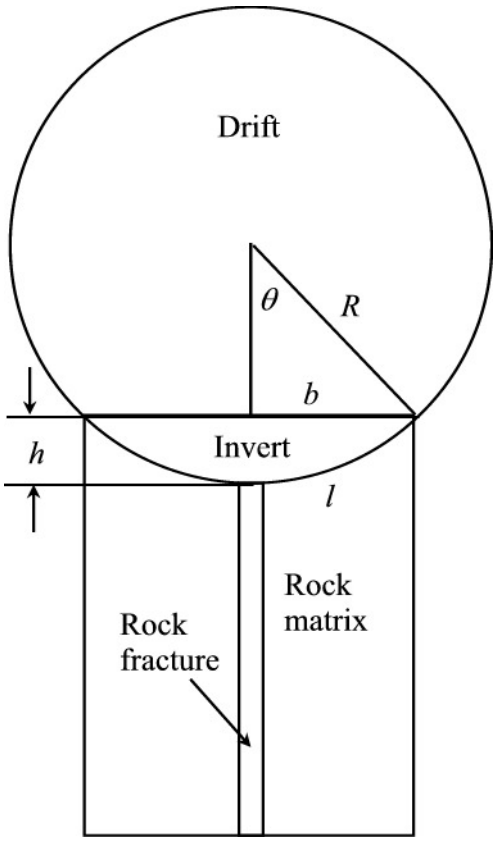

Figure B-4
Geometry for invert and near-field rock compartments where *R* = 2.75m and *h* = 0.6m.

The invert volume is determined by the invert vertical cross section area (Equation B.2) multiplied by the canister length. The invert diffusive length is assumed to be half of the invert central thickness. The invert-rock interface area is equal to the invert bottom area that is the arc *l* (Figure B.4 and Equation B.4) multiplying the canister length.

The total near-field rock volume is assumed to be the volume of the rock below the invert shown in Figure B.4 and depends on the "shadow zone" length. The rock volume is partitioned into matrix and fracture volumes according to fracture aperture and spacing (values shown in Table B.6 reported in EPRI, 2002a). For matrix diffusion, the interface area for the matrix and fracture is needed. This area is simply equal to the rock length (5m is assumed) multiplied by the canister length. Table B.6 also lists sorption depth for rock fractures. This value is used for modeling fracture sorption and is taken from SKI (1996).

These parameters are listed in Table B.6.

Table B-6
Geometry Parameters

No.	Parameter	Value
1	Waste-form volume [m^3]	1.135
2	Waste-form diffusion length [m]	0.153
3	Interface area between waste-form and corrosion-product [m^2]	7.4
4	Corrosion-product volume [m^3]	2.477
5	Corrosion-product diffusion length [m]	0.733
6	Interface area between corrosion-product and invert [m^2]	6.302
7	Invert volume [m^3]	11.16
8	Invert diffusion length [m]	0.403
9	Interface area between invert and near-field rock [m^2]	22.31
10	Near-field rock volume [m^3]	89.30
11	Near-field rock diffusion length [m]	2.5
12	NF rock fracture spacing [m]	0.31
13	NF rock fracture aperture [m]	1.8×10^{-4}
14	NF fracture-matrix interface area [m^2]	51.65
15	NF fracture sorption depth [m]	0.01
16	Interface area between NF rock and FF rock [m^2]	20.1

B.5 Physical Parameters

For each compartment outside the intact waste form, COMPASS requires input of:

- Density (for sorption calculation),
- Porosity, and
- Water saturation

Uncertainty exists for porosity and water saturation values. In COMPASS, the "best estimate" is selected for these parameters.

The waste-form compartment is assumed to consisting of spent-fuel pellets. Furthermore, the property of schoepite is assumed for degrading spent fuel pellets (BSC, 2004d). In the COMPASS model, only porosity is needed and assumed to be the same of that of schoepite. No sorption is considered within the waste-form compartment, which means the density for this compartment is not needed (zero value is assigned). Because of uncertainty in determining water saturation within the schoepite pores, an assumption is made that the waste-form void space is fully saturated with water in light of tight pores and hence, high capillary pressure. This assumption will tend to overestimate the amount of solubility-limited radionuclides that can be released, and to maximize the diffusion rate through this compartment, so it is arguably conservative.

Corrosion products are mainly hydrated iron oxide (Fe_2O_3). Its porosity value is taken as the "best estimate" (EPRI, 2002a; BSC, 2004b). In failed waste packages through which water is moving by advection, the corrosion-product water saturation is assumed to be 1.0. In dry waste packages, the water saturation is determined from water adsorption mechanism given by Equations 6.5.1.2-27 in BSC (2004c) or Equation I-10 in BSC (2006) assuming a relative humidity of 95%.

The invert solid density is the same as tuff solid density. Its porosity is determined by the typical gravel size (BSC, 2006). Water saturation in the invert is estimated by equilibrium of hydrological system involving gravel and the host rock under various infiltration rates (BSC, 2006).

Near-field rock properties are taken from a detailed analysis on drift-scale radionuclide transport (BSC, 2004e). Because the fractures are assumed to be open, the fracture compartment porosity is unity.

Table B-7
Physical Parameter Values

Compartment	Density [kg/m^3]	Porosity	Saturation
Waste form	0.0	0.17	1.0
Corrosion product (dry)	5240.0	0.4	1.0
Corrosion product (wet)	5240.0	0.4	2×10^{-5}
Invert	2540.0	0.45	0.11
NF rock matrix	2540.0	0.131	0.88
NF rock fracture	2540.0	1.0	0.015

These include seepage rates for the waste packages on which seepage occurs and diffusion coefficients for all compartments. The time-dependent seepage rate is determined by the seepage sub-model of IMARC that integrates information concerning climate, infiltration rate, flow focusing, etc. Seepage diversion (the flow rate going around the outside of the WP as opposed to the flow rate passing through the canister) to the invert is implemented in the model but is not currently considered in calculation.

The effective diffusion coefficients for all the compartments are determined from experimental data on diffusion in unsaturated porous media in Conca and Wright (1992) for a given moisture content determined by:

$$\theta = \phi S \qquad \textbf{eq. B-5}$$

where ϕ is porosity and S is water saturation. Using the numerical values for compartments' porosity and saturation in Table B.7, the effective diffusion coefficients are determined and listed in Table B.8. Note that the water saturation for the dry corrosion product is too low for Conca and Wright's experimental results. In this case, the effective diffusion coefficient is determined using Archie's law (BSC, 2004c):

$$D_{eff} = D_0 \phi^{1.3} S^2 \qquad \textbf{eq. B-6}$$

where D_0 is free-water diffusion coefficient assumed to be 0.0316 m^2/yr (10^{-9} m^2/s).

It can be shown that for other compartments, the effective diffusion coefficients determined from Conca and Wright (1992) fit quite well with those calculated using Archie's law.

Table B-8
Effective Diffusion Coefficients

Compartment	Diffusion Coefficient [m^2/yr]
Waste form	2.46×10^{-3}
"Wet" corrosion product	2.47×10^{-5}
"Dry" corrosion product	3.84×10^{-12}
Invert	2.63×10^{-4}
NF rock matrix	1.41×10^{-3}
NF rock fracture	3.46×10^{-5}

B.6 References

BSC, 2001. *FY01 Supplemental Sciences and Performance Analyses*, TDR-MGR-MG-000007, Bechtel SAIC Company, Las Vegas, Nevada.

BSC, 2004a. *Initial Radionuclide Inventories*, ANL-WIS-MD-000020 Rev 01, September 2004, Bechtel SAIC Company, Las Vegas, Nevada.

BSC, 2004b. *CSNF Waste Form Degradation: Summary and Abstraction*, ANL-EBS-MD-000015 Rev 02, Bechtel SAIC Company, Las Vegas, Nevada.

BSC, 2004c. *EBS Radionuclide Transport Abstraction*, ANL-WIS-PA-000001 Rev 01, November 2004, Bechtel SAIC Company, Las Vegas, Nevada.

BSC, 2004d. *Technical Basis Document No.7: In-Package Environment and Waste Form Degradation and Solubility*, Rev.1, July 2004, Bechtel SAIC Company, Las Vegas, Nevada.

BSC, 2004e. *Drift-Scale Radionuclide Transport*, Rev.1, MDL-NBS-HS-000016, September 2004, Bechtel SAIC Company, Las Vegas, Nevada.

BSC, 2006. *EBS Radionuclide Transport Abstraction*, ANL-WIS-PA-000001 Rev 02, July 2006, Bechtel SAIC Company, Las Vegas, Nevada.

Conca J.L. and J. Wright, 1992. "Diffusion and Flow in Gravel, Soil, and Whole Rock", *Applied Hydrogeology*, Vol.1., No.1., 1992, pp.5-24.

EPRI, 1990. *Demonstration of a Risk-Based Approach to High-Level Waste Repository Evaluation*, NP-7057, Electric Power Research Institute, Palo Alto, California.

EPRI, 1992. *Demonstration of a Risk-Based Approach to High-Level Waste Repository Evaluation: Phase 2*, TR-100384, Electric Power Research Institute, Palo Alto, California.

EPRI, 1996. *Yucca Mountain Total System Performance Analysis, Phase 3,* TR-107191, Electric Power Research Institute, Palo Alto, California.

EPRI, 1998. *Alternative Approaches to Assessing the Performance and Suitability of Yucca Mountain for Spent Fuel Disposal*, TR-108732, Electric Power Research Institute, Palo Alto, California.

EPRI, 2000. *Evaluation of the Candidate High-Level Radioactive Waste Repository at Yucca Mountain Using Total System Performance Assessment*, *Phase 5*, TR-1000801, Electric Power Research Institute, Palo Alto, California.

EPRI, 2002a. *Evaluation of the Proposed High-Level Radioactive Waste Repository at Yucca Mountain Using Total System Performance Assessment*, *Phase 6*, TR-1003031, Electric Power Research Institute, Palo Alto, California.

EPRI, 2002b.*Integrated Yucca Mountain Safety Case and Supporting Analysis, EPRI's Phase 7 Performance Assessment*, TR-1003334, Electric Power Research Institute, Palo Alto, California.

EPRI, 2003. Scientific and Technical Priorities at Yucca Mountain, TR-1003335, Electric Power Research Institute, Palo Alto, California.

EPRI, 2004b. Potential Igneous Processes Relevant to the Yucca Mountain Repository: Extrusive-Release Scenario Analysis and Implications, Report number 1008169, Electric Power Research Institute, Palo Alto, CA.

EPRI, 2006. *Program on Technology Innovation: EPRI Yucca Mountain Spent Fuel Repository Evaluation*, 2006 Progress Report, EPRI TR-1013445, Electric Power Research Institute, Palo Alto, California.

EPRI, 2008. *Evaluation of a Spent Fuel Repository at Yucca Mountain, Nevada: 2008 Progress Report*. EPRI, Palo Alto, CA: 2008. 1016631.

EPRI, 2009. International Review Team Report: A Peer Review of the Yucca Mountain IMARC Total System Performance Assessment EPRI Model. EPRI Report 1018711. Electric Power Research Institute, Palo Alto, CA.

Langmuir, D., 2006. "Maximum Neptunium Concentrations at the Proposed Yucca Mountain Repository," 11th IHLRWM, Apr 30th - May 4th 2006, Las Vegas, Nevada.

SKI, 1996. *SITE-94: Deep Repository Performance Assessment Project*, Volume II, Swedish Nuclear Inspectorate, SKI Report 96:36.

US DOE, 2001. *Yucca Mountain Science and Engineering Report*, U.S. Department of Energy, Office of Civilian Radioactive Waste Management, DOE/RW-0539, May 2001.

C
APPENDIX C: IMARC 10 BIOSPHERE DOSE CONVERSION FACTORS FOR GROUNDWATER RELEASE: INPUT PARAMETERS

C.1 Data for Deterministic BDCF assessment

Element independent data are provided in Table C.1; element specific data are provided in Tables C.2 to C.11 and radionuclide specific data are in Table C.12. Single values of parameters to be used in calculations are provided, with references. This approach relies upon justifying the selection of parameters from previous modeling experience, notably IAEA (2003). Given the dependence of the overall dose estimate on the relative combination of radionuclides in the water, it is difficult to identify critical but uncertain parameters until a real source term is applied. However, several examples of potentially important data deficiencies were identified in IAEA (2003).

The data used were substantially taken from the BIOMASS Example 2A (IAEA, 2003). Where the data in this model were clearly not suitable for this Yucca Mountain-specific assessment, data were found in alternative literature, e.g. with more relevant parameter values for the arid climate of Yucca Mountain. For example, where available, sorption coefficients in soil were used for low organic content, sandy soils likely to be prevalent in Amargosa Valley. Note however, that soil modification by farming practice and in back yard cultivation does not make a definitively better assumption.

Table C-1
Element-independent data

Parameter	Value	Units	Comments and References
Irrigation rate, V_{irr}	0.8E0	$m^3m^{-2}y^{-1}$	Irrigation rates will vary from crop to crop. The value adopted is an assumed average of irrigation rates applied by commercial growers in the Amargosa Valley and by those involved in back yard cultivation.
Concentration in well water, C_w	1.0E0	mol m^{-3}	
Infiltration rate, I	6.0E-1	m y^{-1}	
Wet soil porosity, θ	2.0E-1	-	
Total soil porosity, θ_t	5.0E-1	-	
Cultivated soil thickness, d	3.0E-1	m	Typical plowing/tilling depths
Soil grain density,	2.65E3	kg m^{-3}	
Water ingestion rate humans, ING_w	7.305E-1	m^3 y^{-1}	Regulatory specification
Crop ingestion rate human, ING_{crop}		kg y^{-1}	
- Root veg	4.73E0		Consumption rates are for locally produced crops, which may be dominated by gardeners or small producers in Amargosa Valley (i.e. not the total consumption rates). Values used previously (Wasiolek, 2001) have been updated (Wasiolek and Rautenstrauch, 2003).
- Green veg	3.78E0		
- Grain	2.3E-1		
- Fruit	1.268E1		
Crop soil contamination, S_{crop}		kg / kg	kg dw soil per kg fw crop
- Root veg	2.0E-4		Chosen from consideration of data in (BIOMOVS, 1990), (Müller and Prohl, 1993), (Ashton and Sumerling, 1988), (EPRI, 2002) and (Brown and Simmonds, 1995)
- Green veg	2.0E-4		
- Grain	2.0E-4		
- Pasture	2.0E-3		
- Fruit	2.0E-4		
Crop annual yield, Y		kg fw y^{-1}	Values are all per m^2 of soil area
- Root veg	3.0E0		Chosen from consideration of data in (BIOMOVS, 1990), (Müller and Prohl, 1993), (Ashton and Sumerling, 1988), (EPRI, 2002) and (Brown and Simmonds, 1995)
- Green veg	3.0E0		
- Grain	4.0E-1		
- Pasture, Y_{past}	5.0E0		
- Fruit	7E-1		
Standing yield of fodder, SB_{past}	8.3E-1	kg	Assumes the annual yield is grazed six times (EPRI, 1996)

Table C-1 (continued)
Element-independent data

Parameter	Value	Units	Comments and References
Consumption rate, ING_{prod}		$kg\ y^{-1}$	Refers to locally produced animal products
- Cow meat	2.85E0		Values used previously (Wasiolek, 2001) have been updated (Wasiolek and Rautenstrauch, 2003).
- Cow liver	0E0		
- Milk	4.66E0		
- Chicken meat	4.2E-1		
- Chicken eggs	5.3E0		
Animal consumption rate, fodder ING_{fodd}		$kg\ d^{-1}$	Fresh weight. All animal feed is assumed to be produced locally, from crops produced with contaminated irrigation water.
- Cow	6E1		(EPRI, 2002)
- Chicken	3E-1		
Animal groundwater consumption rate, ING_{wa}		$m^3\ d^{-1}$	All animal water is assumed to be from contaminated well
- Cow	6E-2		(EPRI, 2002)
- Chicken	5E-4		
Animal soil consumption rate, ING_{sa}		$kg\ d^{-1}$	Wet soil, assumed to be irrigated soil
- Cow	6E-1		(EPRI, 2002)
- Chicken	2E-2		
Water density, ρ_w	1.0E3	$kg\ m^{-3}$	
Animal breathing rate, BR_a		$m^3\ h^{-1}$	Animals assumed to reside on irrigated soil
-cow	5.4E0		(Brown and Simmonds, 1995)
-chicken	1E-2		(EPRI, 2002)
Animal occupancy, O_{an}	2.4E1	$h\ d^{-1}$	
Dust in air, $dust_s$		$kg\ m^{-3}$	(IAEA, 2003)
- normal activity	1.0E-7		
- physical working including plowing in dry soil conditions	5.0E-6		
Enhancement factor for concentration of contaminants on dust compared with soil, E_f	3	-	Based on consideration of Wasiolek (2008) and Raitenstrauch et al., (2003)

Table C-1 (continued)
Element-independent data

Parameter	Value	Units	Comments and References
Number of animals in area of interest, SD		m^{-2}	
- Cow	4.3E-4		(EPRI, 2002)
- Chicken	3.0E0		
Inadvertent soil consumption, human, ING_{soil} (adults)	1.825E-2	kg y^{-1}	Fresh weight, (Wasiolek and Rautenstrauch, 2003).
Soil occupancy, human O_s	3.387E3	h y^{-1}	(Wasiolek and Rautenstrauch, 2003).
Inhalation occupancy, human O_{inh} - normal activity - hard physical activity in dry soil conditions	 5.459E3 6.14E2	h y^{-1}	(Wasiolek and Rautenstrauch, 2003) for total, but ratio between the two activities as per IAEA (2003)
Bathing occupancy, O_{wout}	3.65E2	h y^{-1}	(IAEA, 2003)
Human Adult Breathing rate, BR - normal activity - physical working in dry soil conditions	 1.2E0 1.7E0	m^3h^{-1}	(IAEA, 2003)
Time from irrigation to harvest, T		y	
- Root veg	4.0E-2		Typical farming practice as suggested by personal communications to G Smith from G Prohl and P Coughtrey.
- Green veg	2.0E-2		
- Grain	7.5E-2		
- Pasture	2.0E-2		
- Fruit	2.0E-2		

C.1.1 Quantitative description of exposure groups and exposure assumptions

Assumptions are required for consumption of the following foods and water, assumed to be consumed:

- root vegetables;
- green vegetables;
- grain;
- fruit;
- cow meat;
- chicken meat;
- eggs; and
- water.

These foods are chosen because of their correspondence to the system description and to habit survey data for Amargosa Valley residents. In addition, inadvertent ingestion of soil is included. Consumption data for these relevant to Amargosa Valley were taken from Wasiolek and Rautenstrauch (2003). These are mean values allowing for the proportion of food derived from uncontaminated sources. Of the small proportion which is produced locally, it is not known how much of that is produced in back yards or commercially. This could affect the assumption for irrigation rate. All water for humans and animals is assumed to come from contaminated wells. All animal feed is assumed to be produced locally from ground irrigated with contaminated water.

Occupancy times and breathing rates are also required for inhalation and external irradiation pathways. Data are taken from (Wasiolek and Rautenstrauch, 2003); however, the occupancy for inhalation of dust from soil is split into two values, one at low dust level for most of the year and low breathing rate and the other at a raised dust level (associated with working/recreation with the soil itself) and high breathing rate, but only for a small proportion of the year. That is, it is assumed here that the critical group member spends some time doing activities which involve creation of dust, but most of the time not doing so (IAEA, 2003).

No consideration has been given to exposure from radon. Other radioactive progeny of radionuclides for which groundwater concentrations are evaluated in the geosphere part of the TSPA are assumed to be in secular equilibrium with their parents in the groundwater at the point of abstraction, and thereafter, their behavior and contribution to dose is assessed dynamically. However, if the half-life is less than 25 days, then they are assumed to be in secular equilibrium with the parent in the biosphere, and their contributions to dose are included by adding the relevant dose coefficient to that of the parent.

C.1.2 Element specific data

Table C-2
Sorption Coefficients in Soil

Element	Kd, m3/kg	Range	Reference
Ac	0.45		(EPRI, 2002)
Cl	0.0008		(EPRI, 2002)
I	0.007	0 to 0.44	(BIOPROTA, 2006)
Np	0.005	0.0005 to 0.39	(BIOPROTA, 2006)
Pa	0.54		(EPRI, 2002), (Ashton and Sumerling, 1988)
Pb	9.7	0.8 to 5.5	(BIOPROTA, 2006)
Po	0.15	0.009 to 7	(BIOPROTA, 2006)
Pu	0.54		(EPRI, 2002)
Ra	0.49	0.003 to 20	(BIOPROTA, 2006)
Se	0.003	0.001 to 0.03	(Fuhrmann and Schwartzman, 2008), (BIOPROTA, 2006)
Tc	0.0001	0 to 0.001	(BIOPROTA, 2006)
Th	3	0.2 to 150	(BIOPROTA, 2006)
U	0.015	0.002 to 4.5	(BIOPROTA, 2006)

Table C-3
Crop Concentration Factors (CFcrop)

Element	Fruit	Grain	Green veg	Pasture	Root veg	Reference
	Bq kg-1 fw per Bq kg-1 dw					
Ac	0.0005	0.001	0.001	0.001	0.001	(EPRI, 2002)
Cl	50	50	50	5 75	50	(EPRI, 2002), (Smith et al., 1988) (Coughtrey et al., 1983-85), (BIOPROTA, 2006)
Range	1 - 400	1 - 1000	1 - 400	10 - 450	1 - 500	
I	0.05	0.025	0.1	0.1	0.1	(EPRI, 2002), (Smith et al., 1988), (Coughtrey et al., 1983-85), (Ashton and Sumerling, 1988) (Klos et al., 1989) (IAEA, 1995) (Simmonds and Crick, 1982) (IAEA, 2003) (BIOPROTA, 2006)
Range	0.01 – 5					
Np	0.01	0.002	0.01	0.01	0.01	(EPRI, 2002), (Smith et al., 1988), (Coughtrey et al., 1983-85), (Ashton and Sumerling, 1988) (Klos et al., 1989) (IAEA, 1995) (Simmonds and Crick, 1982) (IAEA, 2003) (BIOPROTA, 2006)
Range	1E-4 – 1	1E-4 – 0.1	2E-4 – 0.3	1E-4 - 1	2E-4 – 0.3	
Pa	0.04	0.04	0.04	0.04	0.04	(EPRI, 2002)
Pb	0.015	0.015	0.015	0.015	0.015	(EPRI, 2002)
Range	3E-4 - 1	3E-4 - 1	3E-4 - 1	3E-4 - 1	3E-4 - 1	(BIOPROTA, 2006)
Po	0.0002	0.01	0.01	0.0002	0.05	(EPRI, 2002) (BIOPROTA, 2006)
Pu	0.0001	3.0E-05	0.0001	0.001	0.001	(EPRI, 2002)
Ra	0.04	0.04	0.04	0.04	0.04	(EPRI, 2002) (BIOPROTA, 2006)
Range	0.01 – 1					
Se	1	1	1	1	1	(EPRI, 2002) (Klos et al., 1989) (BIOPROTA, 2006)
Range	0.1 – 30					

Table C-3 (Continued)
Crop Concentration Factors (CFcrop)

Element	Fruit	Grain	Green veg	Pasture	Root veg	Reference
	Bq kg-1 fw per Bq kg-1 dw					
Tc	5	2	50	10	10	(EPRI, 2002), (Smith et al., 1988), (Coughtrey et al., 1983-85), (Ashton and Sumerling, 1988) (Klos et al., 1989) (IAEA, 1995) (Simmonds and Crick, 1982) (IAEA, 2003) (BIOPROTA, 2006)
Range	0.1 - 200	0.1 - 10	3 - 500	1 - 100	1 - 100	
Th	0.001	0.0003	0.001	0.001	0.001	(BIOPROTA, 2006)
Range	0.0001 – 0.01					
U	0.001	0.001	0.001	0.001	0.001	(BIOPROTA, 2006)
Range	1E-4 – 0.02					

Table C-4
Crop Interception Factor (Icrop)

Element	Icrop	Reference
Ac	0.3	(EPRI, 2002)
Cl	0.3	(EPRI, 2002)
I	0.3	(EPRI, 2002), (IAEA, 2003), (Ashton and Sumerling, 1988)
Np	0.5	(EPRI, 2002), (IAEA, 2003), (Ashton and Sumerling, 1988)
Pa	0.3	(Ashton and Sumerling, 1988)
Pb	0.3	(EPRI, 2002)
Po	0.3	(EPRI, 2002)
Pu	0.3	(EPRI, 2002)
Ra	0.3	(EPRI, 2002)
Se	0.5	(Ashton and Sumerling, 1988)
Tc	0.1	(EPRI, 2002), (IAEA, 2003), (Ashton and Sumerling, 1988)
Th	0.3	(EPRI, 2002)
U	0.3	(EPRI, 2002)

Table C-5
External Interception Fraction Retained after Food Processing (Fp3), Internal Food Processing Retained Fraction (Fp2) and External Contamination Due to Soil, Food Processing Retained Fraction (Fp1)

	Fp3				Fp2	Fp1	
Element	Fruit	Grain	Green veg	Root veg	All	All	Reference
Ac	1	0.01	0.1	0	1	0.1	(EPRI, 2002), (IAEA, 2003)
Cl	1	0.01	0.1	0	1	0.1	(EPRI, 2002), (IAEA, 2003)
I	1	0.01	0.1	0	1	0.1	(EPRI, 2002), (IAEA, 2003)
Np	1	0.01	0.1	0	1	0.1	(EPRI, 2002), (IAEA, 2003)
Pa	1	0.01	0.1	0	1	0.1	(EPRI, 2002), (IAEA, 2003)
Pb	1	0.01	0.1	0	1	0.1	(EPRI, 2002), (IAEA, 2003)
Po	1	0.01	0.1	0	1	0.1	(EPRI, 2002), (IAEA, 2003)
Pu	1	0.01	0.1	0	1	0.1	(EPRI, 2002), (IAEA, 2003)
Ra	1	0.01	0.1	0	1	0.1	(EPRI, 2002), (IAEA, 2003)
Se	1	0.01	0.1	0	1	0.1	(EPRI, 2002), (IAEA, 2003)
Tc	1	0.01	0.1	0	1	0.1	(EPRI, 2002), (IAEA, 2003)
Th	1	0.01	0.1	0	1	0.1	(EPRI, 2002), (IAEA, 2003)
U	1	0.01	0.1	0	1	0.1	(EPRI, 2002), (IAEA, 2003)

Table C-6
Absorbed Fraction, External to Internal (Fabs)

Element	Fruit	Grain	Green veg	Pasture	Root veg	Reference
Ac	0.48	0.5	0.5	0.5	0.5	(EPRI, 2002), (IAEA, 2003)
Cl	0.48	0.5	0.5	0.5	0.5	(EPRI, 2002), (IAEA, 2003)
I	0.48	0.5	0.5	0.5	0.5	(EPRI, 2002), (IAEA, 2003)
Np	0.48	0.5	0.5	0.5	0.5	(EPRI, 2002), (IAEA, 2003)
Pa	0.48	0.5	0.5	0.5	0.5	(EPRI, 2002), (IAEA, 2003)
Pb	0.48	0.5	0.5	0.5	0.5	(EPRI, 2002), (IAEA, 2003)
Po	0.48	0.5	0.5	0.5	0.5	(EPRI, 2002), (IAEA, 2003)
Pu	0.48	0.5	0.5	0.5	0.5	(EPRI, 2002), (IAEA, 2003)
Ra	0.48	0.5	0.5	0.5	0.5	(EPRI, 2002), (IAEA, 2003)
Se	0.48	0.5	0.5	0.5	0.5	(EPRI, 2002), (IAEA, 2003)
Tc	0.48	0.5	0.5	0.5	0.5	(EPRI, 2002), (IAEA, 2003)
Th	0.48	0.5	0.5	0.5	0.5	(EPRI, 2002), (IAEA, 2003)
U	0.48	0.5	0.5	0.5	0.5	(EPRI, 2002), (IAEA, 2003)

Table C-7
Translocation Factor (Ftrans)

Element	Fruit	Grain	Green veg	Pasture	Root veg	Reference
Ac	1	0.2	0.45	0	0.29	(EPRI, 2002)
Cl	1	0.1	1	0	0.1	(EPRI, 2002)
I	1	0.1	1	0	0.1	(EPRI, 2002), (IAEA, 2003)
Np	1	0.01	1	0	0.21	(EPRI, 2002), (IAEA, 2003)
Pa	1	0.2	0.45	0	0.29	(EPRI, 2002), (IAEA, 2003)
Pb	1	0.1	0.22	0	0.22	(EPRI, 2002)
Po	1	0.1	0.22	0	0.22	(EPRI, 2002)
Pu	0.19	0.16	0.36	0	0.043	(EPRI, 2002)
Ra	1	0.08	0.18	0	0.099	(EPRI, 2002)
Se	1	0.13	0.3	0	0.068	(EPRI, 2002), (IAEA, 2003), (Ashton and Sumerling, 1988), (Simmonds and Crick, 1982), (Coughtrey et al., 1983-85)
Tc	1	0.1	1	0	0.1	(EPRI, 2002), (IAEA, 2003)
Th	0.13	0.13	0.038	0	0.29	(EPRI, 2002)
U	0.19	0.16	0.36	0	0.043	(EPRI, 2002)

Table C-8
Weathering Rate (W)

Element	Fruit	Grain	Green veg.	Pasture	Root veg	Reference
	(/y)					
Ac	18	8.4	18	18	18	(EPRI, 2002)
Cl	32	18	18	18	18	(EPRI, 2002)
I	32	8.4	18	18	18	(EPRI, 2002), (IAEA, 2003)
Np	32	18	18	18	18	(EPRI, 2002)
Pa	18	8.4	18	18	18	(EPRI, 2002)
Pb	18	8.4	18	18	18	(EPRI, 2002)
Po	18	8.4	18	18	18	(EPRI, 2002)
Pu	18	51	51	18	18	(EPRI, 2002)
Ra	18	8.4	18	18	18	(EPRI, 2002)
Se	32	8.4	18	18	18	(EPRI, 2002), (IAEA, 2003)
Tc	32	8.4	18	18	18	(EPRI, 2002), (IAEA, 2003)
Th	18	8.4	18	18	18	(EPRI, 2002)
U	18	8.4	18	18	18	(EPRI, 2002)

Table C-9
Animal Product Transfer Factor (TFproding)

Element	Chicken egg	Chicken meat	Cow liver	Cow meat	Cow milk	Reference
	(day/kg)				(day/l)	
Ac	0.016	0.0066	0.014	0.0016	4.00E-07	(EPRI, 2002)
Cl	8.7	8.7	0.043	0.043	0.017	(EPRI, 2002) (Coughtrey et al., 1983-85) (Dickson J M (1993)
I	1.6	0.2	0.002	0.003	0.003	(EPRI, 2002) (Coughtrayt et al., 1983-85) (Dickson J M (1993) (Smith et al., 1988) (Simmonds and Crick, 1982) (IAEA, 2003) (Bishop et al., 1989) (Ng et al., 1982) (Ng, 1982) (IAEA, 1994) (Ashton and Sumerling, 1988)
Np	0.017	0.0017	0.02	0.00012	5.00E-06	(EPRI, 2002)
Pa	0.0041	0.0041	0.0011	5.00E-05	5.00E-06	(EPRI, 2002)
Pb	1.2	1.2	1.3	0.01	0.0003	(EPRI, 2002)
Po	1.2	1.2	0.004	0.004	0.0003	(EPRI, 2002)
Pu	0.008	0.1	0.068	0.0002	5.00E-06	(EPRI, 2002)
Ra	0.25	0.48	0.019	0.0013	0.0013	(EPRI, 2002)
Se	8.3	8.3	1	0.54	0.004	(EPRI, 2002) (Coughtrey et al., 1983-85) (Dickson J M (1993) (Smith et al., 1988) (Simmonds and Crick, 1982) (Ng et al., 1982) (Ng, 1982) (IAEA, 1994) (Ashton and Sumerling, 1988)
Tc	1.2	1.2	0.021	0.006	0.0075	(EPRI, 2002) (Dickson J M (1993) (Smith et al., 1988) (Simmonds and Crick, 1982) (IAEA, 2003) (Bishop et al., 1989) (Ng, 1982) (IAEA, 1994) (Ashton and Sumerling, 1988)
Th	0.18	0.18	0.063	0.0027	5.00E-06	(EPRI, 2002)
U	0.1	0.1	0.00069	0.00069	0.0004	(EPRI, 2002)

Table C-10
Animal Product Transfer Factor From Inhalation (TFprodinh)

Element	Chicken egg	Chicken meat	Cow liver	Cow meat	Cow milk
	(day/kg)				(day/l)
Ac	4.8E+00	2.0E+00	4.8E-01	1.2E-04	4.2E+00
Cl	6.1E+00	6.1E+00	3.0E-02	1.2E-02	3.0E-02
I	1.1E+00	1.3E-01	2.0E-03	2.0E-03	1.3E-03
Np	5.1E+00	5.1E-01	3.6E-02	1.5E-03	6.0E+00
Pa	1.2E+00	1.2E+00	1.5E-02	1.5E-03	3.3E-01
Pb	1.2E+00	1.2E+00	1.0E-02	3.1E-04	1.3E+00
Po	4.9E-01	4.9E-01	1.6E-03	1.2E-04	1.6E-03
Pu	2.4E+00	3.0E+01	6.0E-02	1.5E-03	2.0E+01
Ra	2.6E-01	4.9E-01	1.3E-03	1.3E-03	1.9E-02
Se	6.5E+00	6.5E+00	4.2E-01	3.1E-03	7.9E-01
Tc	4.9E-01	4.9E-01	2.5E-03	3.1E-03	8.6E-03
Th	1.5E+01	1.5E+01	2.2E-01	4.0E-04	5.1E+00
U	8.1E-01	8.1E-01	5.6E-03	3.2E-03	5.6E-03

Table C-11
Inhalation and Ingestion Fractions in Humans

Element	f1_ing	f1_inh	f_C	f_L	Reference
Ac	0.0005	0.0005	0.55	0.15	(ICRP, 1996) (Coughtrey et al., 1983-85)
Cl	1	1	0.55	0.15	(ICRP, 1996) (Coughtrey et al., 1983-85)
I	1	1	0.16	0.5	(ICRP, 1996) (Coughtrey et al., 1983-85)
Np	0.0005	0.0005	0.55	0.15	(ICRP, 1996) (Coughtrey et al., 1983-85)
Pa	0.0005	0.0005	0.55	0.15	(ICRP, 1996) (Coughtrey et al., 1983-85)
Pb	0.2	0.1	0.55	0.15	(ICRP, 1996) (Coughtrey et al., 1983-85)
Po	0.5	0.1	0.55	0.15	(ICRP, 1996) (Coughtrey et al., 1983-85)
Pu	0.0005	0.0005	0.55	0.15	(ICRP, 1996) (Coughtrey et al., 1983-85)
Ra	0.2	0.1	0.55	0.15	(ICRP, 1996) (Coughtrey et al., 1983-85)
Se	0.8	0.8	0.16	0.5	(ICRP, 1996) (Coughtrey et al., 1983-85)
Tc	0.5	0.1	0.55	0.15	(ICRP, 1996) (Coughtrey et al., 1983-85)
Th	0.0005	0.0005	0.6	0.04	(ICRP, 1996) (Coughtrey et al., 1983-85)
U	0.02	0.02	0.55	0.15	(ICRP, 1996) (Coughtrey et al., 1983-85)

Table C-12
Half life and Dose Coefficient Data

Radionuclide	Half lifea	Ingestion Dosec coefficient†		Inhalation Dosec Coefficient†		External Irradiation from soild	External Irradiation from Waterd
	Years	Sv/Bq	mrem/mol	Sv/Bq	mrem/mol	(mrem/h)/ (mol/kg)	(mrem/h)/ (mol/m3)
Cl-36	3.01E+05	9.30E-10	4.1E+06	7.30E-09	3.2E+07	3.5E-2	0.0E+00
Se-79b	1.13E+06	2.90E-09	3.4E+06	6.80E-09	8.0E+06	0.0E+00	1.9E-01
Tc-99	2.13E+05	6.40E-10	4.0E+06	1.30E-08	8.1E+07	0.0E+00	1.5E+00
I-129	1.57E+07	1.10E-07	9.3E+06	3.60E-08	3.0E+06	4.1E+01	3.1E-01
Pb-210	2.23E+01	6.90E-07	4.1E+13	5.60E-06	3.3E+14	4.5E+06	4.2E+04
Po-210	3.79E-01	1.20E-06	4.2E+15	4.30E-06	1.5E+16	6.0E+06	1.2E+04
Ra-226	1.60E+03	2.80E-07	2.3E+11	9.50E-06	7.9E+12	2.0E+08	5.6E+05
Ac-227	2.18E+01	1.10E-06	6.7E+13	5.50E-04	3.3E+16	2.3E+09	9.1E+06
Ra-228	5.75E+00	6.90E-07	1.6E+14	1.60E-05	3.7E+15	3.0E+10	7.8E+07
Th-228	1.91E+00	1.40E-07	9.7E+13	4.00E-05	2.8E+16	6.3E+10	3.9E+08
Th-229	7.34E+03	4.90E-07	8.8E+10	2.40E-04	4.3E+13	5.2E+06	2.3E+04
Th-230	7.70E+04	2.10E-07	3.7E+09	1.00E-04	1.7E+12	1.0E+02	3.2E+00
Pa-231	3.27E+04	7.10E-07	2.9E+10	1.40E-04	5.7E+12	6.9E+04	4.4E+02
Th-232	1.41E+10	2.30E-07	2.2E+04	1.10E-04	1.0E+07	2.9E-04	9.3E-06
Pa-233	7.39E-02	8.70E-10	1.6E+13	3.90E-09	7.0E+13	5.6E+11	1.3E+09
U-233	1.59E+05	5.10E-08	4.2E+08	9.60E-06	8.0E+10	4.2E+01	2.1E-01
U-234	2.45E+05	4.90E-08	2.6E+08	9.40E-06	5.1E+10	2.1E+01	4.7E-01
U-235	7.04E+08	4.70E-08	8.8E+04	8.50E-06	1.6E+07	1.9E+01	1.2E-01
U-236	2.34E+07	4.70E-08	2.7E+06	8.70E-06	4.9E+08	1.8E-01	3.2E-03
Np-237	2.14E+06	1.10E-07	6.8E+07	5.00E-05	3.1E+10	8.7E+03	5.0E+01
U-238	4.47E+09	4.50E-08	1.3E+04	8.00E-06	2.4E+06	7.7E-01	3.9E-03
Pu-239	2.41E+04	2.50E-07	1.4E+10	1.20E-04	6.6E+12	9.3E+01	2.4E+00
Pu-240	6.54E+03	2.50E-07	5.1E+10	1.20E-04	2.4E+13	9.7E+02	1.1E+01
Pu-242	3.76E+05	2.40E-07	8.4E+08	4.80E-05	1.7E+11	1.3E+01	1.5E-01
Am-243	7.38E+03	2.00E-07	3.6E+10	9.60E-05	1.7E+13	7.9E+05	3.2E+03

†The mrem/mol values were obtained by converting Sv/Bq to moles according to the half life of the radionuclide

[a]ICRP Publication 38 ICRP, 1983)

[b](Songsheng et al., 1997)

[c]ICRP Publication 72 (ICRP, 1996)

[d](Ashton and Sumerling, 1988)

Data presented in Table C.12 include those for radioactive progeny of half-life less than 25 days. These are not dynamically modelled, and are assumed to be in equilibrium with the parent isotope and contributing to the resulting parent doses.

C.2 Data for Probabilistic Assessment

The radionuclides to be included in the probabilistic assessment are: Cl-36, Se-79, Tc-99, I-129, Ra-226, U-235 and Np-237.

C.2.1 Identifying Significantly Uncertain Parameters

The approach taken here was first to identify for each radionuclide the exposure pathways that contribute to more than 10% of the total deterministic BDCF. Then a Normalised Dose Distribution (NDD) was calculated, according to the description of (Yu et al., 2000):

$$NDD = (D_{high} - D_{low}) / D_{base} * 100\%$$

where D_{high} and D_{low} are the maximum and minimum doses corresponding to maximum and minimum values for a given parameter and D_{base} is the normalisation factor, here, the deterministic BDCF. From this additional sensitivity analysis, the original list of parameters identified because of their association with the main exposure pathways, was reduced to only those parameters with a high NDD.

The parameters thus selected for probabilistic consideration were as follows:

- irrigation rate, m/y per m^2,
- infiltration rate, m/y per m^2,
- soil-water distribution coefficients, m^3/kg (dw),
- interception factor, the fraction of irrigation water directly affecting crops,
- the rate of weathering of contamination from plant surfaces,
- annual yields per unit area of eggs, meat and fruit,
- transfer factors relating animal intake of a radionuclide to concentration levels in animal products, for eggs and meat,
- concentration factors relating radionuclide concentrations in soil to concentrations in crops,
- fodder consumption rate by cows, kg/y, but assumed to be 100% produced locally,
- dust level in air, mg/m^3,
- dust enhancement factor, the degree to which dust is assumed to contain higher levels of activity than soil from which it is derived,
- RMEI occupancy of contaminated soil areas, h/y,
- RMEI consumption rate for locally produced meat, eggs and fruit, kg/y.

C.2.2 Selection of PDFs

The selection of appropriate PDFs for all these parameters, some of which are radionuclide specific, presents similar problems to those arising when choosing sets of appropriately cautious deterministic values. However, relevant guidance and radio-ecology data were taken from (BIOPROTA, 2006) and (Yu et al., 2000), as well as the ranges given in the tables in Section 4.1. This was used to identify physically credible ranges and to choose the type of distribution function. In cases where there was very little information beyond a reasonable upper and lower bound, a uniform distribution was adopted. Data on consumption rate distributions in Amargosa Valley were taken from (Wasiolek and Rautenstrauch, 2003). However, since the water consumption rate is fixed at 2 l/d, this parameter was not sampled for.

The resulting selection of PDFs is described in the following tables.

Table C-13
PDFs for Radionuclide Independent Parameters Selected for Probabilistic Approach

Parameter	Units	Distribution type	Min value	Max value	Mean, mode or average	SD
Ingestion of crops INGcrop	kg/y					
Root veg		lognormal			4.73	0.67
Green veg		lognormal			3.78	0.88
Grain		lognormal			0.23	0.11
Fruit		lognormal			12.68	1.36
Volume of irrigation Virr	m3/y	Triangular	0.2	1.2	0.8	
Yield of fruit Y (fruit)	kg(fw)/y	Cumulative	0.73	0%	2.75E+00	
			1.51	5%		
			2.67	28%		
			2.92	51%		
			3	72%		
			3.63	95%		
			6.89	100%		
Infiltration rate I	m/y	Cumulative	0.009	0%	7.90E-02	
			0.03	19%		
			0.045	38%		
			0.076	57%		
			0.128	76%		
			0.233	95%		
			0.275	100%		
Consumption of animal products INGprod	kg/y					
Cow meat		Lognormal			2.85	0.65
Cow liver		Lognormal			0	0
Milk		Lognormal			4.66	1.68
Chicken meat		Lognormal			0.42	0.13
Chicken eggs		Lognormal			5.3	0.83
Consumption of Fodder by Cows INGfodd	kg(fw)/d	Uniform	29	68		
High soil occupancy Oinh_high	h/y	Truncated lognormal		6073.5	5458.9	545.9
Dust level (low loading) dusts	mg/m3	Triangular	0.06	0.175	0.1	
Dust enhancement factor, Ef	-	Triangular	1	5	3	

Table C-14
PDFs for Radionuclide Dependent Parameters Selected for Probabilistic Approach

Parameter	Unit	Distribution type	Min value	Max value	Mean, mode or average	SD	Radionuclide
Interception factor Icrop	-	Triangular	0.05	0.75	0.10		Tc-99
			0.03	0.75	0.30		I-129
			0.03	0.75	0.30		Cl-36
			0.05	0.75	0.50		Se-79
			0	1	0.30		U-235
			0.05	0.75	0.50		Np-237
Sorption Coefficient Kd	m3/kg(dw)	Truncated lognormal	0	0.001	1.40E-04	6 E-03	Tc-99
		Truncated lognormal	0	0.44	4.5E-03	7.4E-3	I-129
		Truncated lognormal	0.002	4.5	3.30E-02	2.5E-02	U-235
		Truncated lognormal	0.0005	0.39	2.5E-02	3.3E-3	Np-237
		Lognormal			1.40E-04	6 E-03	Cl-36
		Logtriangular	0.001	0.03	0.003		Se-79
		Logtriangular	0.8	55	9.7		Pb-210
		Logtriangular	0.009	7	0.15		Po-210
Animal Product Transfer Factor (meat) TFproding	d/kg	Lognormal			8.80E-02	5.8	Se-79
Concentration Factor	Bq/kg(fw) per Bq/kg(dw)						
Fruit CFfruit		Truncated lognormal	1	400	50	2	Cl-36
		Truncated lognormal	0.0002	1	0.057	2.8	I-129
		Truncated lognormal	0.0001	1	0.034	6.9	Np-237
		Logtriangular	3.00E-04	1	0.015		Pb-210
		Logtriangular	0.01	1	0.04		Ra-226
		Truncated lognormal	0.1	30	0.046	3.8	Se-79
		Truncated lognormal	0.1	200	4.3	4.6	Tc-99
		Truncated lognormal	1.00E-04	0.02	0.0063	2.9	U-235
Grain CFgrain		Logtriangular	1	1000	50		Cl-36
		Logtriangular	1.00E-04	0.1	0.002		Np-237
		Logtriangular	3.00E-04	1	0.015		Pb-210
		Logtriangular	0.01	1	0.04		Ra-226
		Logtriangular	0.1	30	1		Se-79
		Logtriangular	0.1	10	2		Tc-99
		Logtriangular	1.00E-04	0.02	0.001		U-235
Green veg. CFgreen		Logtriangular	1	400	50		Cl-36
		Logtriangular	0.01	5	0.1		I-129
		Logtriangular	2.00E-04	0.3	0.01		Np-237
		Logtriangular	3.00E-04	1	0.015		Pb-210
		Logtriangular	0.01	1	0.04		Ra-226
		Logtriangular	0.1	30	1		Se-79
		Logtriangular	3	500	50		Tc-99
		Logtriangular	1.00E-04	0.02	0.001		U-235

Table C-14 (Continued)
PDFs for Radionuclide Dependent Parameters Selected for Probabilistic Approach

Parameter	Unit	Distribution type	Min value	Max value	Mean, mode or average	SD	Radionuclide
Pasture CFpast		Logtriangular	10	450	75		Cl-36
		Logtriangular	1.00E-04	1	0.01		Np-237
		Logtriangular	3.00E-04	1	0.015		Pb-210
		Logtriangular	0.01	1	0.04		Ra-226
		Truncated lognormal	0.1	3.00E+01	0.15	5.5	Se-79
		Logtriangular	1	100	10		Tc-99
		Logtriangular	1.00E-04	0.02	0.001		U-235
Root veg. CFroot		Logtriangular	1	500	50		Cl-36
		Logtriangular	2.00E-04	0.3	0.01		Np-237
		Logtriangular	3.00E-04	1	0.015		Pb-210
		Logtriangular	0.01	1	0.04		Ra-226
		Logtriangular	0.1	30	1		Se-79
		Logtriangular	1	100	10		Tc-99
		Logtriangular	1.00E-04	0.02	0.001		U-235
Weathering W (fruit)	y-1	Triangular	5.1	84	18		All

C.2.3 Addressing Correlations in PDFs

It is clear that some parameters are correlated, and in order not to sample meaningless combinations of parameter values, the issue must be addressed. There are two main approaches to dealing with parameter correlation, a derived approach and a statistical approach. A derived approach implies finding an analytical or empirical relationship between the two parameters of interest, and then making one of them dependent on the other. This way only the independent parameter would have to be sampled. A statistical approach requires knowledge of the degree of correlation between the two parameters (in terms of a correlation coefficient) and a sampling method capable of dealing with correlated distributions. The derived approach is in principle simpler; however, it has the drawback of requiring detailed knowledge of the appropriate relationships that are not always available or fully representative of the underlying correlation.

In this work we have followed the derived approach in the soil occupancy factors, as it is straightforward to derive a relationship between the high occupancy factor (which is a sampled parameter with a defined PDF) and the low occupancy factor (the sum of both must be the numbers of hours in a year).

However, a statistical approach has been used, albeit only in a limited fashion, for one of the most important correlations in the current context: sorption coefficients (Kds) and biotic concentration factors. This is because, the more mobile a radionuclide is, the more likely it is to be available to plants for bioaccumulation, e.g. root uptake, resulting in a negative correlation between the root uptake factor and the soil-water distribution coefficient. Correlation coefficients between these parameters for different plants are given in (Jones et al., 2004) (correlation coefficient between Kd soil and root uptake factor for pasturage: -0.8; correlation coefficient between Kd soil and root uptake factor for vegetables: -0.7). These values were used here as representative for pasture and fruit respectively.

C.3 Results and Discussion

C.3.1 Deterministic Results

Table C-15 gives the calculated BDCF values (mrem·y^{-1} per mole·m^{-3}) to the RMEI via each pathway for each radionuclide selected by EPRI for inclusion in the study. The total summed over all pathways for each radionuclide is also given. These doses are those arising from a concentration of one mol·m^{-3}, of the specified radionuclide, in the abstracted groundwater. They include the effects of radioactive progeny which grow in after release into the biosphere. For example the Th-230 dose value includes contributions to dose from Ra-226 which grows in from decay of Th-230 accumulating in soil. Note that the BDCFs listed are the value eventually reached after radionuclide equilibrium concentrations arises in the local biosphere after continuing year on year irrigation with the same unit contaminant concentration in the abstracted groundwater. In some cases, for mobile radionuclides, equilibrium is reached within just a few years, but in other cases, continuing accumulation in soil continues over hundreds of years.

The results for each radionuclide assessed in the geosphere part of the TSPA are included. Thus the total dose summed over all radionuclides for a particular geosphere calculation are obtained by summing the products of the molar concentration for each radionuclide in the groundwater abstracted via the well (calculated within the geosphere model) and the corresponding BDCF in Table C.15.

Some relatively short lived radionuclides are not modelled explicitly in the geosphere part of the assessment. They are assumed to be in secular equilibrium with their parents in all parts of the geosphere. However, because of the relatively fast rate of biosphere processes in the biosphere, they do require explicit dynamic representation in the biosphere model. These radionuclides are Ac-227, Pa-233, Th-228, Ra-228, Pb-210 and Po-210. Since no geosphere calculation is made of their concentration in the groundwater, their contribution to BDCFs is added in with the respective parents, on the assumption that the daughters are in secular equilibrium with their parents at the well head. This may not be true, especially if the parents and daughters are differently mobile in that environment. The total BDCF including these daughter contributions is also provided in Table C-15 for the relevant radionuclides.

Finally, some even shorter lived radionuclides are not modeled dynamically even in the biosphere. Their radiation effects have been included in with their parents, assuming secular equilibrium in all parts of the environment.

Table C-15
Updated BDCFs (mrem·y^{-1} per mole m^{-3}).

Pathway	Cl-36	Se-79	Tc-99	I-129	Ra-226	Ac-227	Th-229	Th-230	U-233	U-234	U-235	U-238	Np-237	Pu-239	Pu-242
aerosol inhalation	1.41E-02	3.49E-03	3.53E-02	1.33E-03	3.44E+03	1.46E+07	1.90E+04	7.67E+02	3.50E+01	2.22E+01	7.01E-03	1.04E-03	1.35E+01	2.88E+03	7.40E+01
root vegetable	1.07E+06	1.40E+05	8.67E+04	2.17E+05	2.82E+10	3.68E+12	6.25E+09	2.70E+08	3.53E+06	2.17E+06	7.28E+02	1.10E+02	4.53E+06	1.63E+08	9.79E+06
green vegetable consumption	1.46E+06	3.70E+05	4.60E+05	1.53E+06	2.79E+10	5.26E+12	2.56E+09	1.14E+08	2.76E+07	1.72E+07	5.75E+03	8.65E+02	1.83E+07	8.25E+08	5.08E+07
grain	7.74E+04	5.62E+04	1.02E+04	6.79E+04	2.53E+09	9.47E+11	8.33E+08	3.48E+07	4.84E+06	3.01E+06	1.01E+03	1.52E+02	9.87E+04	1.52E+08	9.34E+06
fruit	1.61E+07	1.88E+07	4.42E+06	3.05E+07	9.14E+11	2.45E+14	1.67E+11	6.99E+09	8.37E+08	5.21E+08	1.74E+05	2.63E+04	3.72E+08	2.71E+10	1.67E+09
dust inhalation	4.90E+02	5.55E+02	1.86E+02	4.97E+02	7.53E+10	3.39E+13	2.52E+12	1.19E+11	5.63E+07	1.79E+07	5.71E+03	8.37E+02	3.63E+06	9.13E+10	2.14E+09
external soil	1.06E-01	0.00E+00	0.00E+00	1.16E+03	3.17E+11	3.92E+11	5.09E+10	1.18E+06	5.04E+03	1.25E+03	1.13E+03	4.58E+01	1.75E+05	2.16E+05	2.83E+04
chicken meat	3.57E+05	2.57E+04	3.12E+03	9.08E+02	7.96E+08	3.38E+08	4.14E+08	2.00E+07	2.58E+04	1.20E+04	4.02E+00	6.03E-01	4.86E+01	9.17E+06	5.17E+05
cow meat	2.65E+06	6.78E+06	3.08E+04	5.66E+04	1.98E+09	2.21E+11	2.37E+09	1.12E+08	5.67E+05	3.46E+05	1.16E+02	1.74E+01	2.46E+04	1.30E+07	7.57E+05
cow milk	1.71E+06	8.22E+04	6.30E+04	9.26E+04	3.24E+09	9.03E+07	7.17E+06	3.39E+05	5.37E+05	3.28E+05	1.10E+02	1.65E+01	1.68E+03	5.31E+05	3.09E+04
cow liver	0.00E+00	0.00E+00	0.00E+00	0.00E+00	0.00E+00	0.00E+00	0.00E+00	0.00E+00	0.00E+00	0.00E+00	0.00E+00	0.00E+00	0.00E+00	0.00E+00	0.00E+00
eggs	4.51E+06	3.24E+05	3.94E+04	9.16E+04	5.23E+09	1.03E+10	5.23E+09	2.53E+08	3.26E+05	1.51E+05	5.08E+01	7.61E+00	6.13E+03	9.26E+06	5.22E+05
soil	6.68E+01	2.24E+02	2.07E+01	1.40E+03	2.00E+09	6.10E+10	4.63E+09	2.24E+08	2.72E+05	8.46E+04	2.86E+01	4.26E+00	7.40E+03	1.71E+08	9.60E+06
external water	0.00E+00	6.83E+01	5.44E+02	1.14E+02	2.02E+08	3.33E+09	8.54E+06	1.15E+03	7.63E+01	1.74E+02	4.31E+01	1.41E+00	1.81E+04	8.61E+02	5.51E+01
water consumption	2.99E+06	2.48E+06	2.90E+06	6.77E+06	1.69E+11	4.88E+13	6.45E+10	2.69E+09	3.10E+08	1.93E+08	6.46E+04	9.72E+03	4.97E+07	1.00E+10	6.17E+08
Total	3.09E+07	2.90E+07	8.02E+06	3.93E+07	1.55E+12	3.38E+14	2.83E+12	1.29E+11	1.24E+09	7.55E+08	2.54E+05	3.80E+04	4.48E+08	1.30E+11	4.50E+09
Total *					8.62E+12 Pb-210 and Po-210								4.51E+08 Pa-233		

* including daughters not modelled in the geosphere, assuming secular equilibrium with their parents in well water.

C.3.2 Probabilistic Results

The AMBER 5.0 software (Enviros and Quintessa, 2006) has been used to calculate the BDCF probabilistically for the radionuclides and parameters discussed above. Unfortunately, AMBER 5.0 is not capable of sampling correlated distributions, and therefore the Excel add-in @RISK (Palisade, 2008) has been applied to carry out the sampling and then import the obtained data into AMBER[16]. 2000 samples were run using a random scheme for selecting parameters values from their distributions. The case file for the deterministic case was used as a base for the probabilistic run. All parameters remained the same except the sampled parameters set out in subsection 4.2 above.

The results of the probabilistic run for the BDCFs are shown in the following figures and in tabular form at the end of this section. The information included in the graphs is: cumulative distribution functions, the mean and the 95 % confidence interval, several percentiles (5%, 25%, 50%, 75% and 95%) and the value of the deterministic calculation as reported previously.

Cumulative distribution functions are given in Figures C.1 to C.9 and Table C.16 gives the precise numerical values which characterize the distributions. Separate results are given for Ra-226 and Np-237 with (indicated by a + sign) and without the contributions from radioactive progeny which are assumed to be present with the parent in the abstracted groundwater.

[16] AMBER Version 5.1, the most recent release, does allow the correlations to be accounted for as here, and can be used in future work.

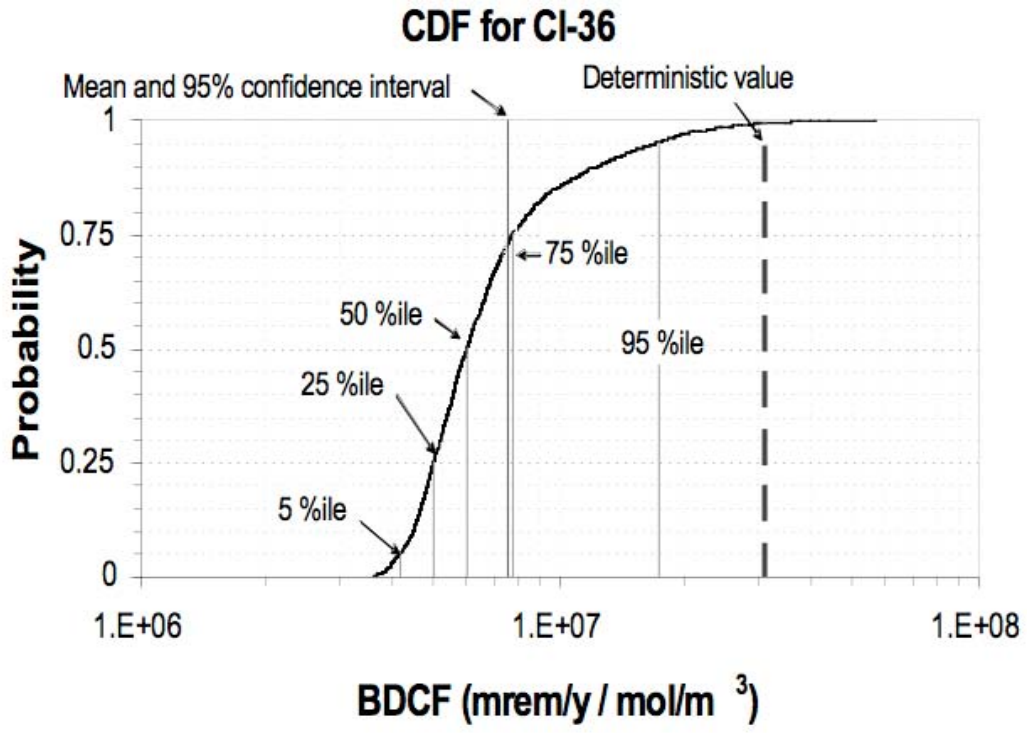

Figure C-1
CDF for Cl-36 showing the different quantities of interest.

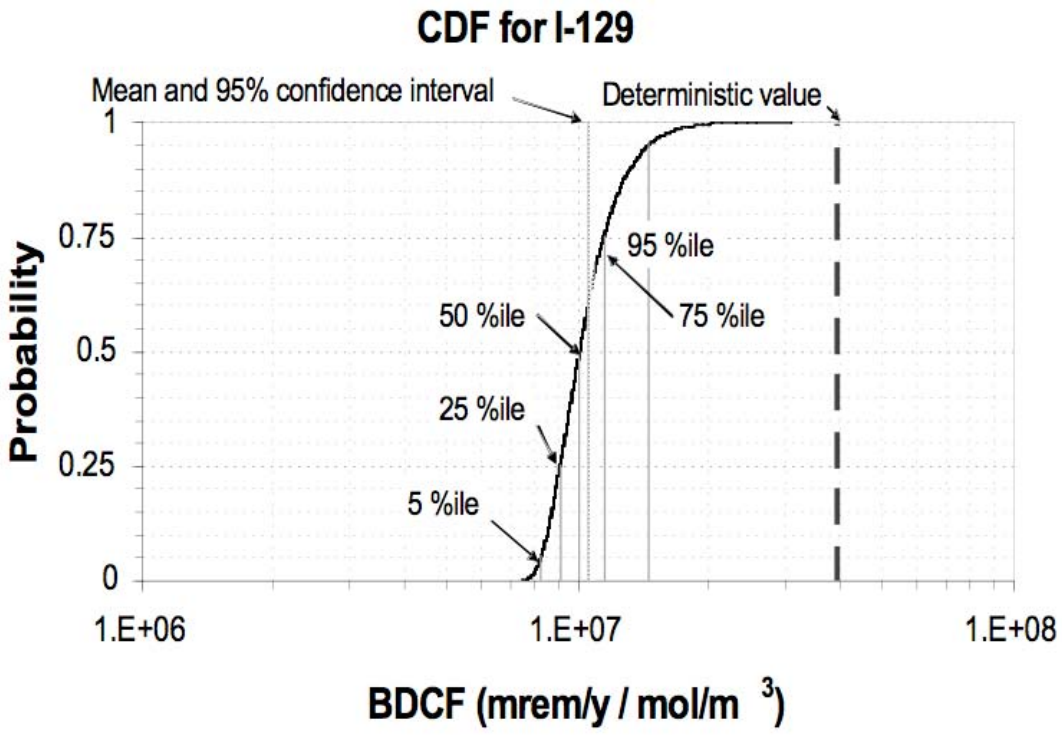

Figure C-2
CDF for I-129 showing the different quantities of interest.

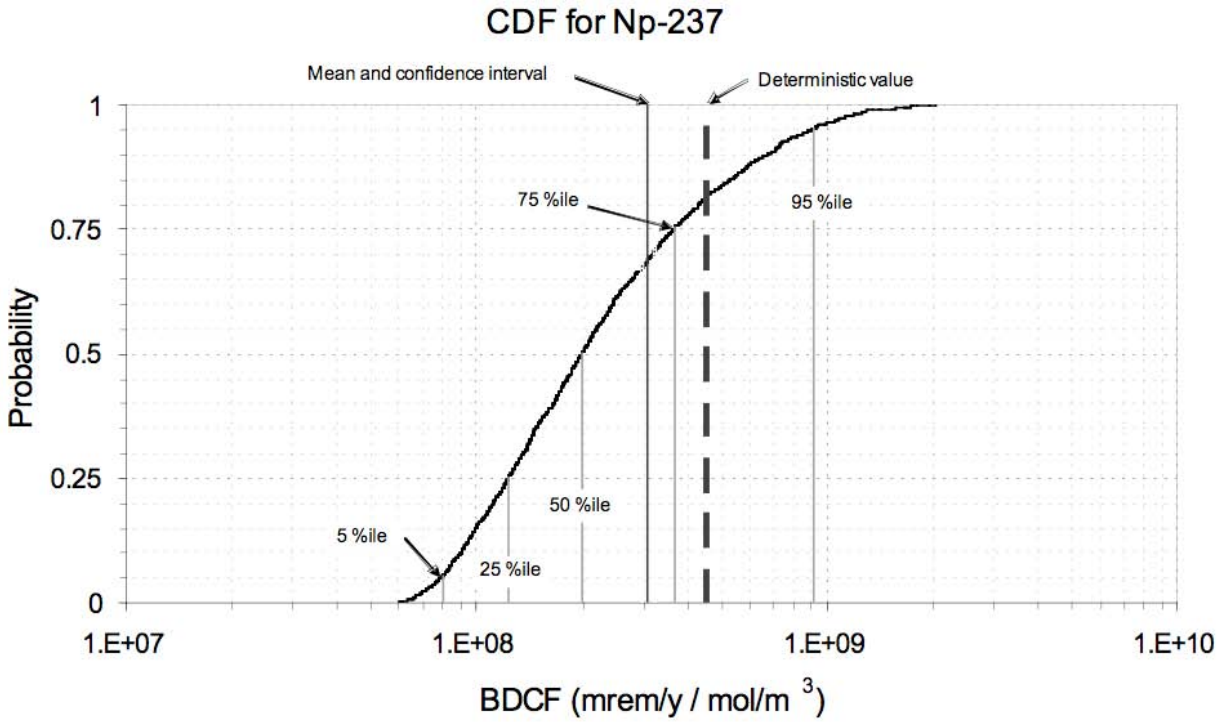

Figure C-3
CDF for Np-237 showing the different quantities of interest.

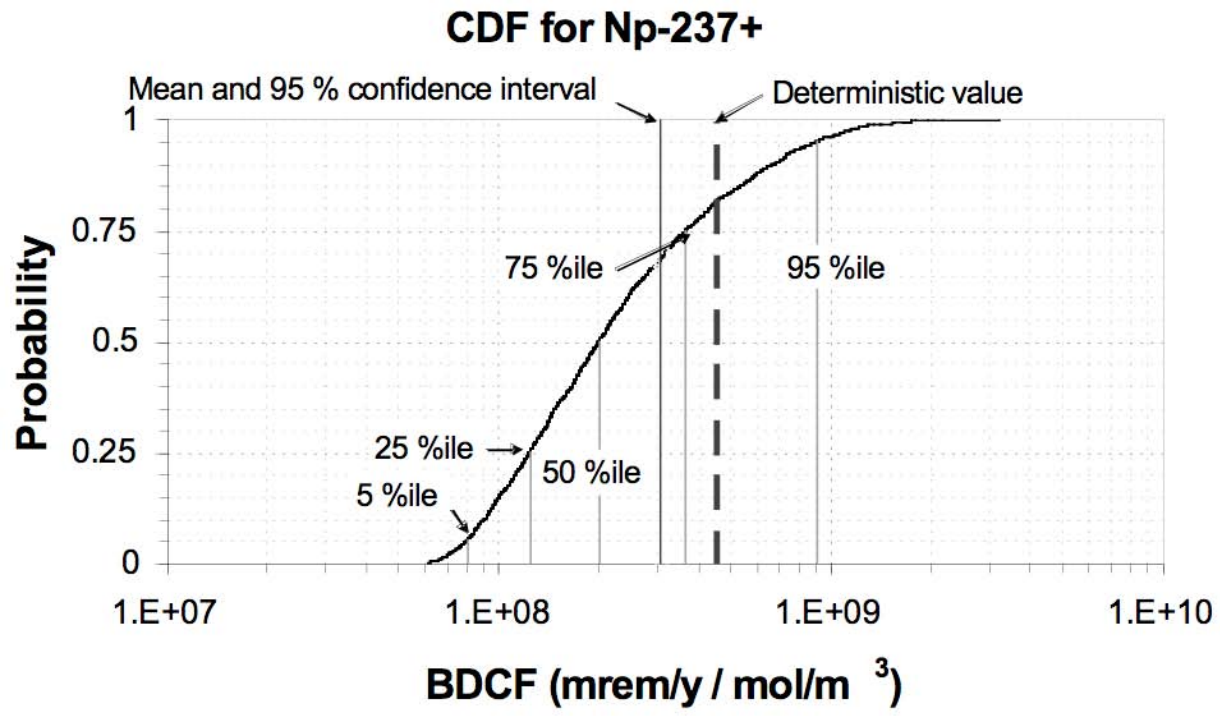

Figure C-4
CDF for Np-237 (including short-lived daughters) showing the different quantities of interest

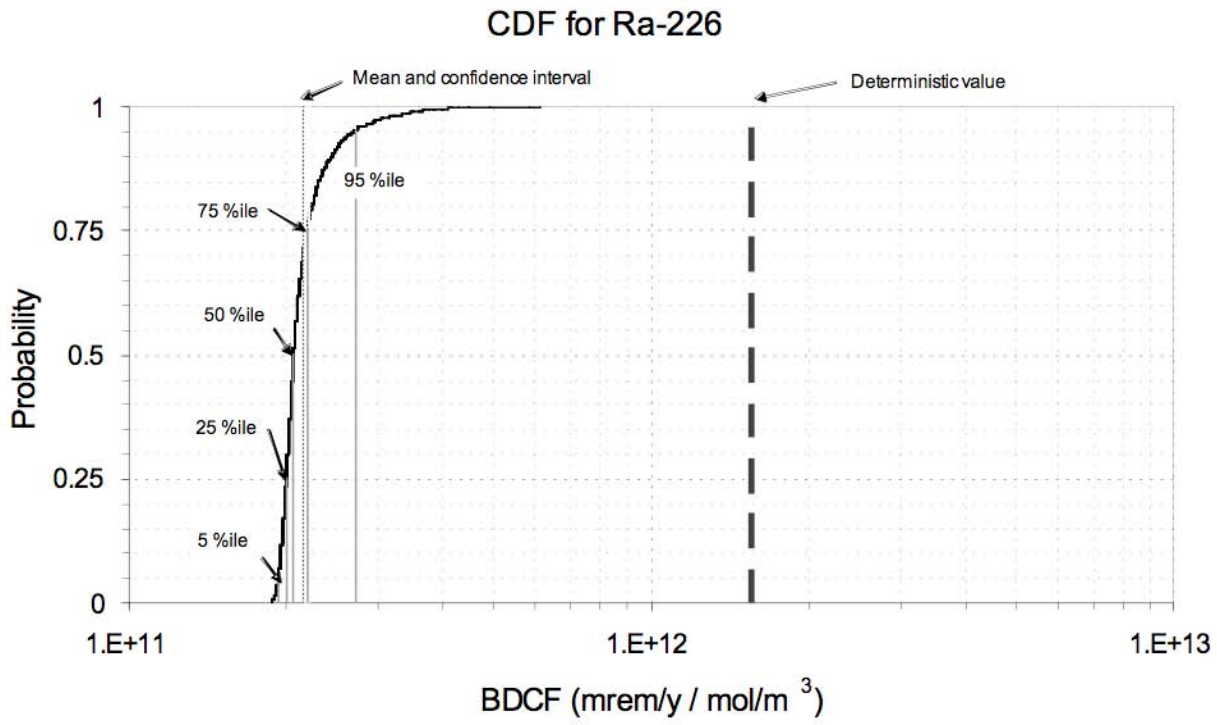

Figure C-5
CDF for Ra-226 showing the different quantities of interest

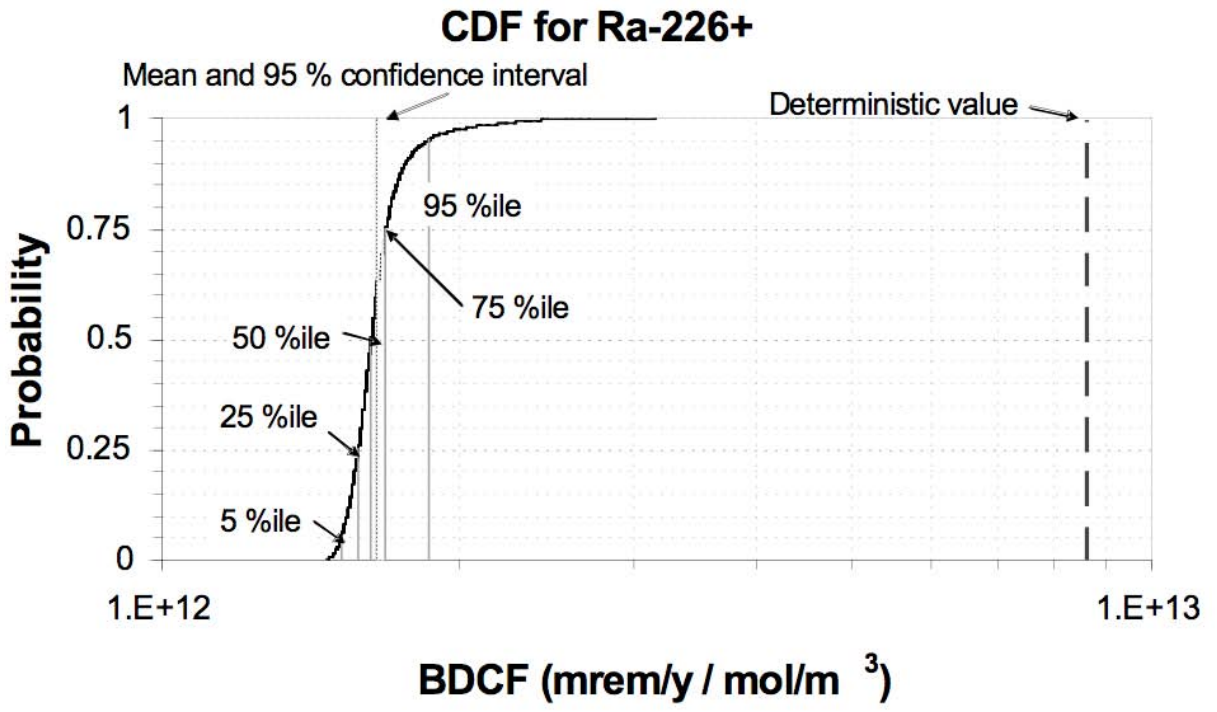

Figure C-6
CDF for Ra-226 (including short-lived daughters) showing the different quantities of interest.

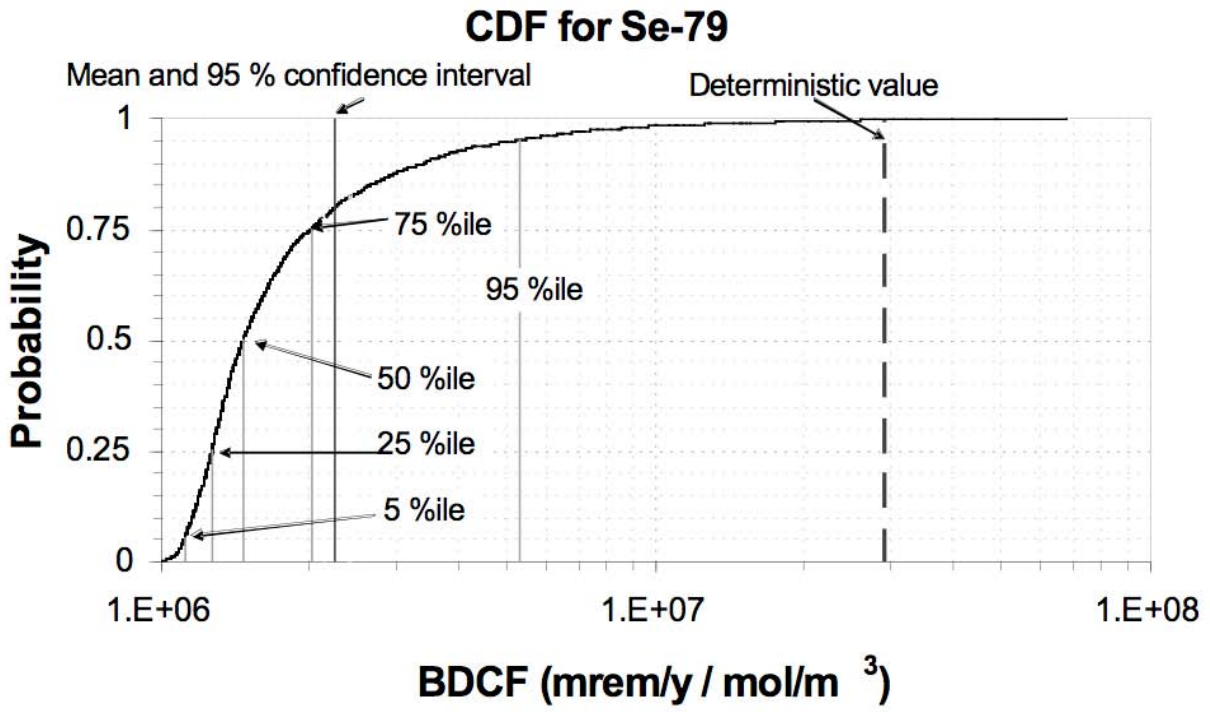

Figure C-7
CDF for Se-79 showing the different quantities of interest.

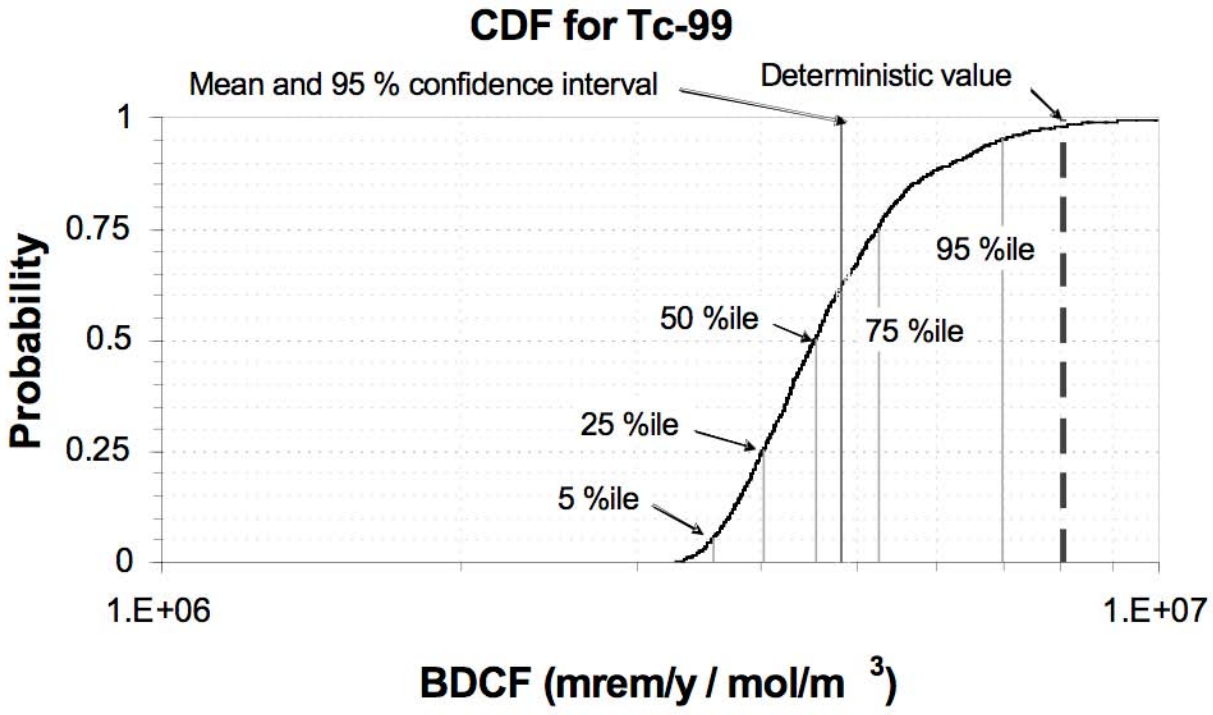

Figure C-8
CDF for Tc-99 showing the different quantities of interest.

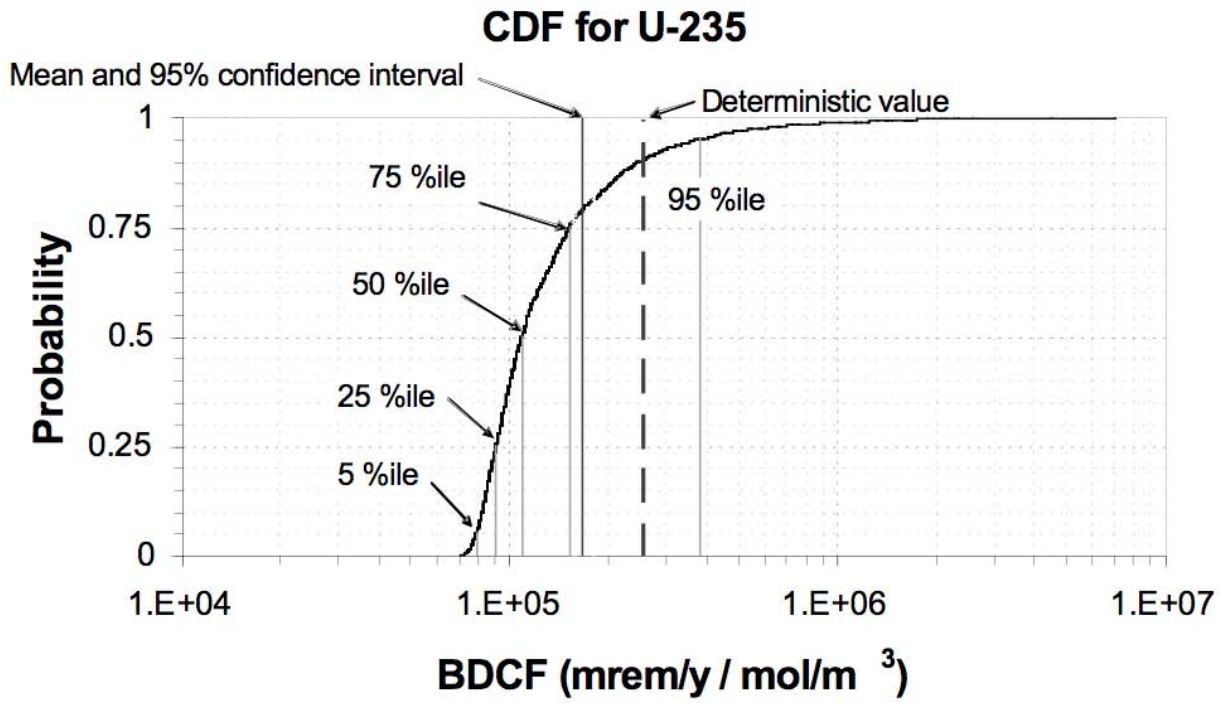

Figure C-9
CDF for U-235 showing the different quantities of interest.

Table C-16
Result of the probabilistic analysis of BDCF's for selected radionuclides

Radionuclide	Deterministic value	Mean	95%Confidence interval		Percentiles				
			Lower	Upper	5 %	25 %	50 %	75 %	95 %
Cl-36	3.09E+07	7.62E+06	7.40E+06	7.83E+06	4.22E+06	5.07E+06	6.09E+06	7.81E+06	1.74E+07
Se-79	2.90E+07	2.27E+06	2.12E+06	2.42E+06	1.12E+06	1.28E+06	1.48E+06	2.04E+06	5.37E+06
Tc-99	8.02E+06	4.82E+06	4.77E+06	4.87E+06	3.59E+06	4.03E+06	4.55E+06	5.26E+06	7.00E+06
I-129	3.93E+07	1.07E+07	1.06E+07	1.08E+07	8.31E+06	9.17E+06	1.02E+07	1.16E+07	1.47E+07
U-235	2.54E+05	1.68E+05	1.56E+05	1.80E+05	7.97E+04	9.17E+04	1.10E+05	1.54E+05	3.84E+05
Np-237	4.48E+08	3.08E+08	2.95E+08	3.21E+08	8.04E+07	1.24E+08	2.02E+08	3.69E+08	9.22E+08
Np-237+	4.51E+08	3.09E+08	2.96E+08	3.22E+08	8.09E+07	1.25E+08	2.02E+08	3.70E+08	9.22E+08
Ra-226	1.55E+12	2.18E+11	2.16E+11	2.19E+11	1.94E+11	2.01E+11	2.08E+11	2.20E+11	2.73E+11
Ra-226+	8.62E+12	1.66E+12	1.66E+12	1.67E+12	1.53E+12	1.59E+12	1.64E+12	1.69E+12	1.87E+12

The + value indicates the inclusion of short-lived daughters assumed to be in secular equilibrium with the parents: Np-237 and Ra-226

C.3.3 Discussion

The deterministic results are in all cases higher than the bulk of the distributions. This is to be expected given the cautious approach to parameter value selection for the deterministic calculations. However, in all cases these deterministic results are within one order of magnitude of the means of the probabilistic distributions. The worst agreement is for I-129, in which the deterministic result is a factor of 4 higher than the mean. In other words, the deterministic results do not appear grossly pessimistic. Nevertheless, it is clear, given the regulatory objective of assessing a reasonable expectation of dose, that the means of the probabilistic distributions are more appropriate for comparison with regulatory limits than the deterministic values used in previous EPRI TSPAs. This approach to assessing doses to representative persons is supported by discussion in ICRP Publication 101 (ICRP, 2006).

The confidence in the means is very narrow. Most simulations result in selection of a set of parameter values which in combination balance each other out in terms of enhancing or reducing the dose. The spread in results either side of the means is also of interest, particularly if one wishes to understand how likely a significantly different dose is to occur. Accordingly, it is interesting that in each case, the 95th percentile in the distribution is within an order of magnitude of the mean and the median. It is also the case that the medians are in all cases lower than the means. The most general observation of these probabilistic results is that the overall ranges of results are relatively narrow. Clearly, only the parametric uncertainty has been considered here, but, as noted in the Section 2, the conceptual model and process related assumptions have been subject to substantial peer review internationally (see BIOPROTA (2005a, b and c)).

It is however notable that the regulatory requirement is to calculate doses based on current habits in Amargosa Valley, so that the ranges of relevant parameters associated with human behaviour are limited compared with known past and possible future behavior at the RMEI location. Furthermore, since consumption of locally produced foods (i.e. contaminated foods) is small, but all consumed water is assumed to be taken from local (contaminated) wells, then drinking water tends to dominate compared with other deep repository assessments, which mostly assume that all foods consumed by the potential exposure group are from contaminated sources. In addition, since the consumption of drinking water is fixed at 2 l/d by regulatory prescription, then the doses in all simulations are at least as large as those from a fixed and significant drinking water pathway; the consequence is that there can be no simulations for which the doses are substantially lower than the mean, itself a strong function of the fixed drinking water dose.

While there may be significant uncertainties in concentrations of radionuclides in some environmental media, they have little impact on assessed doses and hence on the corresponding dose distributions, in part, because of the assumption that most food is imported from out of the area. For example, the uptake of Cl-36 into grain is assumed to vary by 3 orders of magnitude, but on average only 0.23 kg/y of locally produced grain is assumed to be consumed, and the standard deviation is 0.11 kg/y (Wasiolek and Rautenstrauch, 2003).

To the extent that different pathways contribute significantly to the values of BDCFs, then each of those contributions is itself not usually dependent upon a single parameter. For example, the dose from inhalation of suspended dust is dependent upon the amount of, say U-235, the

soil/water distribution coefficient, the dust loading in air, the enhancement factor and the occupancy. It would be a very unusual simulation where all four relevant parameters were selected at the upper end of their ranges.

Given the above, it could be interesting in future to present BDCFs results taking account of the distribution of consumption of locally derived drinking water. In addition, it seems unreasonable (and hence not consistent with a reasonable expectation) to assume that all animal feed is derived locally. Both these changes would have the effect of reducing inappropriate pessimism.

In addition, it is suggested that consideration should be given to inclusion of radon exposures and to chemical disequilibrium effects at the point in the ground where water is abstracted.

C.4 References

Ashton, J. and T.J. Sumerling, 1988. *Biosphere Database for Assessments of Radioactive Waste Disposals*, UK Department of the Environment Report DoE/RW/88/083.

BIOMASS, 2001a. *ERB2A revised mathematical model and results,* BIOMASS Theme 1, Task Group 6, Note version 2. February 2001. IAEA, Vienna.

BIOMOVS, 1990. *Scenario B6, Transport of Radionuclides to Root zone Soil from Contaminated Groundwater*, BIOMOVS Phase 1 Technical Report 9. Swedish Radiation Protection Institute, Stockholm.

BIOMOVS II, 1996. *Development of a Reference Biospheres Methodology for Radioactive Waste Disposal*, BIOMOVS II Technical Report No. 6, published on behalf of the BIOMOVS II Steering Committee. ISBN 91-972134-5-4, Swedish Radiation Protection Institute, Stockholm.

BIOPROTA, 2005a. *Model Intercomparison with Focus on Accumulation in Soil.* A report prepared within the international collaborative project BIOPROTA: Key Issues in Biosphere Aspects of Assessment of the Long-term Impact of Contaminant Releases Associated with Radioactive Waste Management, Main contributors: A. Albrecht, C. Damois, E. Kerrigan, R. Klos, G.M. Smith, M.C. Thorne, S.M. Willans and H. Yoshida. Published on behalf of the BIOPROTA Steering Committee by ANDRA (Agence nationale pour la gestion des dechets radioactifs), Chatenay-Malabry, France.

BIOPROTA,2005b. *Modelling the Inhalation Exposure Pathway*. A report prepared within the international collaborative project BIOPROTA: Key Issues in Biosphere Aspects of Assessment of the Long-term Impact of Contaminant Releases Associated with Radioactive Waste Management. Main Contributors: M. Wasiolek (Task Leader), A. Aguero, A. Albrecht, U. Bergstrom, H. Grogan, G.M. Smith, M.C. Thorne, S.M. Willans and H. Yoshida. Published on behalf of the BIOPROTA Steering Committee by Nexia Solutions Ltd, UK.

BIOPROTA, 2005c. *Model Review and Comparison for the Spray Irrigation Pathway*. A report prepared within the international collaborative project BIOPROTA: Key Issues in Biosphere Aspects of Assessment of the Long-term Impact of Contaminant Releases Associated with Radioactive Waste Management. Main Contributors: U. Bergstrom (Task Leader), A. Albrecht,

B. Kanyar, G. Smith, M.C. Thorne, H. Yoshida and M. Wasiolek. Published on behalf of the BIOPROTA Steering Committee by the Swedish Nuclear Fuel and Waste Management Company, Stockholm.

BIOPROTA, 2006. *BIOPROTA DATABASE*. Version 2. Available from the BIOPROTA Technical Secretariat, see www.bioprota.com

Bishop, G.P., C.J. Beetham and Y.S. Cuff, 1989. *Review of Literature Data for Chlorine, Technetium, Iodine and Neptunium*. Nirex Report NSS/R193.

Brown, J. and J.R. Simmonds, 1995. *FARMLAND, A Dynamic Model for the Transfer of Radionuclides through Terrestrial Foodchains*, NRPB R273.

Coughtrey, P.J., D. Jackson and M.C. Thorne, 1983-85. *Radionuclide Distribution and Transport in Terrestrial and Aquatic Ecosystems*. Volumes 1-6. AA Balkema, Rotterdam.

Dickson, J.M., 1993. *Derivation of a Quality Assured Database for BIOS*. Nirex Report NSS/B106.

Enviros & Quintessa, 2006. *AMBER 5 Reference Guide*. Version 1, September 2006, Enviros, Culham, UK. (see www.enviros.com/amber or www.quintessa.org/amber)

EPRI (1996). Biosphere Modelling and Dose Assessment for Yucca Mountain, TR-107190, Final Report, Prepared by QuantiSci Inc, UK. Electric Power Research Institute, Palo Alto.

EPRI (1998). Alternative Approaches to Assessing the Performance and Suitability of Yucca Mountain for Spent Fuel Disposal, EPRI TR-108732. Electric Power Research Institute, Palo Alto.

EPRI (2002). Evaluation of the Proposed High-Level Radioactive Waste Repository at Yucca Mountain Using Total System Performance Assessment, Phase 6, Technical Report 1003031.

FGR11 (1988). Federal Guidance Report No. 11, Limiting values of Radionulide Intake and Air concentration and dose conversion factors for inhalation, submersion and ingestion, 1988 EPA-5201/1-88-020 U.S. Environmental Protection Agency, Washington, D.C.

Fuhrmann M. and Schwartzman A. (2008). Letter to Health Physics. February 2008, Volume 94, Issue 2, p. 192.

IAEA (1994). Handbook of Parameter Values for the Prediction of Radionuclide Transfer in Temperate Environments. IAEA Technical Report Series No. 364. International Atomic Energy Agency, Vienna.

IAEA (1995). Generic Models and Parameters for Assessing the Environmental Transfer of Radionuclides from Routine Release. IAEA Safety Series No 57. International Atomic Energy Agency, Vienna.

IAEA (2003). "Reference Biospheres" for soild radioactive waste disposal. Report of BIOMASS Theme 1 of the BIOsphere Modelling and ASSessment (BIOMASS) Programme. Part of the IAEA Co-ordinated Research Project on Biosphere Modelling and Assessment (BIOMASS) IAEA-BIOMASS-6, International Atomic Energy Agency, Vienna.

ICRP (1983). ICRP Publication 38, Radionuclide Transformations: Energy and Intensity of Emissions, Annals of ICRP 11 13. International Commission on Radiological Protection, Pergamon Press.

ICRP (1996). ICRP Publication 72, Age-dependent Doses to members of the Public from Intake of Radionuclides: Part 5. International Commission on Radiological Protection, Pergamon Press.

ICRP (2006). Assessing Doses to the Representative Person for the Purpose of Radiation Protection of the Public. ICRP Publication 101. Annals of ICRP volume 36 No.3. International Commission on Radiological Protection, Elsevier.

Jones J, Vahlund F, and Kautsky U. (2004). Tensit – a novel probabilistic simulation tool for safety assessments. Tests and verifications using biosphere models. SKB Technical Report TR-04-07.

Klos R A, Smith K R, and Smith G M (1989). Calculations of the Radiological Impact of Unit Releases of Radionuclides to the Biosphere from Solid Waste Disposal Facilities. National Radiological Protection Board, NRPB-M150, Chilton, UK.

Müller H and Prohl G (1993). ECOSYS.87: A Dynamic Model for Assessing Radiological Consequences of Nuclear Accidents, Health Physics, Vol 64, No 3.

Ng Y C (1982). A review of Transfer Factors for Assessing the Dose from Radionuclides in Agricultural Products. Nuclear Safety, Vol 23, No 1, pp57.

Ng Y C, Colsher C S and Thompson S E (1982). Transfer Coefficients for Assessing the Dose from Radionuclides in Meat and Eggs. NUREG/CR 2976.

Palisade (2008). @RISK Risk Analysis and Simulation Add-In for Microsoft® Excel. Version 5.0. May, 2008. Palisade Corporation (www.palisade.com).

Rautenstrauch K.R., J. Smith A.J., and Andrews R. (2003). Technical Basis Document No. 12: Biosphere Transport. Revision 1. BECHTEL Report.

Simmonds JR and Crick MJ (1982). Transfer parameters for use in terrestrial foodchain models. NRPB report No M63.

Smith GM, Fearn HS, Smith KR, Davis JP and Klos R (1988). Assessment of the radiological impact of disposal of solid radioactive waste at Drigg. National Radiological Protection Board, NRPB-M148, Chilton, UK.

Songsheng J., Jingru G., Shan J., Chunsheng L., Anzhi C., Ming H., Shaoyong W., Shilin L. (1997). Determination of the half-life of 79Se with the accelerator mass spectrometry technique. Nuclear Instruments and Methods in Physics Research Section B: Beam Interactions with Materials and Atoms, Volume 123, Issues 1-4, 2 March 1997, Pages 405-409.

Walter H (1985). Vegetation of the Earth and Ecological Systems of the Geo-Biosphere. Springer-Verlag, New York, 318 pp.

Wasiolek M (2001). Data supplied as personal communication by the Yucca Mountain Project Biosphere Assessment team.

Wasiolek M (2008). Modelling the Inhalation Enhancement Factor in Prospective Radiological Risk Assessment. In Proc Int. Conf. Radioecology and Environmental Radioactivity. Bergen June 2008, Norwegian Radiation Protection Authority, Osteras.

Wasiolek MA and Rautenstrauch KR (2003). Characteristics of the Receptor for the Biosphere Model. Office of Civilian Radioactive Waste Management, Document ref. ANL-MGR-MD-000005 Rev 02, 27 June 2003.

Yu C, LePoire D, Gnanapragasam E, Arnish J, Kamboj S, Biwer B, Chang J, and Chen S (2000). Development Of Probabilistic Resrad 6.0 And Resrad-Build 3.0 Computer Codes NUREG/CR-6697.

D
APPENDIX D: VERIFICATION INPUT FILES

This appendix lists input files that were used to verify COMPASS model/ code. They also serve as an example of illustrating COMPASS input format.

D.1 Case 1. Transient Diffusion Problem

```
TITLE
'Verification 1: diffusional release'
END
POROSITY
 WASTE     1.00      # all data hypothetical
 CAN-CP    1.00
 PALLET    1.00  # used as basalt in igneous intrusion case and bypass otherwise
 INVERT    1.00
 FRACTURE  1.00
 MATRIX    1.00
END
DENSITY
 WASTE     2250.0
 CAN-CP    2250.0
 PALLET    2250.0
 INVERT    2250.0
 ROCK      2250.0
END
INFILTRATION
 DRIP-AREA  1.0
 NO-OF-DATA 2
 TIMES-AND-RATES
    0.0  0.0
    3.E7 0.0
 INVERT-FRACTION 0.0
 BASALT-FRACTION 0.0
END
SATURATION
 WASTE    1.0
 CAN-CP   1.0
 PALLET   1.0
 INVERT   1.0
 FRACTURE 1.0
 MATRIX   1.0
END
DIFFUSION
 WASTE    1.e-9 M2PSEC
 CAN-CP   1.e-9 M2PSEC
 PALLET   1.e-9 M2PSEC
 INVERT   1.e-9 M2PSEC
 FRACTURE 1.e-9 M2PSEC
 MATRIX   1.e-50 M2PSEC  # exclude matrix diffusion
END
GEOMETRY
 WASTE-VOL          1.0
```

```
 WASTE-LENGTH       0.5
 WST-CAN-AREA       1.0
 CAN-CP-VOL         1.0
 CAN-CP-LENGTH      0.5
 CAN-PALLET-AREA    1.0
 PALLET-VOL         1.0
 PALLET-LENGTH      0.5
 PALLET-INVERT-AREA 1.0
 INVERT-VOL         1.0
 INVERT-LENGTH      0.5
 INVERT-ROCK-AREA   1.0
 ROCK-VOL           1.0
 MAT-LENGTH         0.5
 FRAC-LENGTH        0.5
 FRACTURE-APERTURE  0.9999  # suppress matrix
 FRACTURE-SPACING   0.000001
 MAT-FRAC-AREA      1.e-10
 ZC-LENGTH          1.0
 SORB-DEPTH         0.0
END
DECAYS
 'Tc-99'  1e20  # hypothetical stable nuclide
END
INVENTORY
 'Tc-99'   1.0e+10  MOLES  M-FRAC 0.0 GAP-FRAC 1.00 # all inventory dissolved
instantly
END
SORPTION
 Tc  CORR-PROD  0.00  PALLET  0.0    TUFF 0.0e+0 # no sorption
END
SOLUBILITY
 UNITS MOLPM3
 Tc 1.e-6   # to cause solubility limit
END
CONTAINMENT
 FAIL-TIME 0.0
 INV-START-TIME 0.0
 ALTER-TIME 1.0
 NO-OF-DATA 1
 TIMES-AND-FRACTIONS
    0.0   1.0
END
OUTPUT-TIMES
 START-TIME 1.E1
 END-TIME   1.E6
 NO-PER-DECADE 20
END
FLUX-OUTPUT
 UNITS MOLPYR
 FLUX-FILE
# MASS-BALANCE     # logical for printing MASS_BALANCE.out at each output time
END
TIMESTEP-CONTROL
 ACCURACY-FACTOR 1.e-5
END
```

D.2 Case 2. Advective Release of Three-member Decay Chain

```
TITLE
'Verification 2: advection release for 3-member chain'
END
POROSITY
 WASTE     0.4      # all data hypothetical
 CAN-CP    0.4
 PALLET    0.4
 INVERT    0.4
 FRACTURE  0.4
 MATRIX    0.4
END
DENSITY
 WASTE     2250.0
 CAN-CP    2250.0
 PALLET    2250.0
 INVERT    2250.0
 ROCK      2250.0
END
INFILTRATION
 DRIP-AREA  1.0
 NO-OF-DATA 2
 TIMES-AND-RATES   # constant flow rate
   0.0000E+00  1.0000E2
   3.0000E+07  1.0000E2
 INVERT-FRACTION 0.0
 BASALT-FRACTION 0.0
END
SATURATION
 WASTE    0.8
 CAN-CP   0.8
 PALLET   0.8
 INVERT   0.8
 FRACTURE 0.8
 MATRIX   0.8
END
DIFFUSION  # exclude diffusion
 WASTE    1.e-19 M2PSEC
 CAN-CP   1.e-19 M2PSEC
 PALLET   1.e-19 M2PSEC
 INVERT   1.e-19 M2PSEC
 FRACTURE 1.e-19 M2PSEC
 MATRIX   1.e-50 M2PSEC
END
GEOMETRY
 WASTE-VOL          1e-5
 WASTE-LENGTH       0.001
 WST-CAN-AREA       1.0
 CAN-CP-VOL         1e-5
 CAN-CP-LENGTH      0.001
 CAN-PALLET-AREA    1.0
 PALLET-VOL         1e-5
 PALLET-LENGTH      0.001
 PALLET-INVERT-AREA 1.0
 INVERT-VOL         1e-5
 INVERT-LENGTH      0.001
 INVERT-ROCK-AREA   1.0
 ROCK-VOL           1.0
 MAT-LENGTH         0.001
 FRAC-LENGTH        0.001
```

```
 FRACTURE-APERTURE  0.9999
 FRACTURE-SPACING   0.0001
 MAT-FRAC-AREA      1.e-10
ZC-LENGTH          0.001
 SORB-DEPTH         0.0
END
DECAYS
 'Np-237' 2.14e+6 'U-233'
 'U-233'  1.59e+5 'Th-229'
 'Th-229' 7.34e+3
END
INVENTORY
 'Np-237'  1000. MOLES  M-FRAC 0.0  GAP-FRAC 1.0  # all inventory instantly dissolved
 'U-233'   100.  MOLES  M-FRAC 0.0  GAP-FRAC 1.0
 'Th-229'  10.   MOLES  M-FRAC 0.0  GAP-FRAC 1.0
END
SORPTION  # no sorption
 Np  CORR-PROD  0.00  PALLET  0.0    TUFF 0.0e+0
 U   CORR-PROD  0.00  PALLET  0.0    TUFF 0.0e+0
 Th  CORR-PROD  0.00  PALLET  0.0    TUFF 0.0e+0
END
SOLUBILITY
 UNITS MOLPM3
 Np 1.e6
 U 1.e6
 Th 1.e6
END
CONTAINMENT
 FAIL-TIME 0.0
 INV-START-TIME 0.0
 ALTER-TIME 1.0
 NO-OF-DATA 1
 TIMES-AND-FRACTIONS
   0.0   1.0
END
OUTPUT-TIMES
 START-TIME 1.E1
 END-TIME   1.E6
 NO-PER-DECADE 24
END
FLUX-OUTPUT
 UNITS MOLPYR
 FLUX-FILE
# MASS-BALANCE    #  logical for printing MASS_BALANCE.out
END
TIMESTEP-CONTROL
 ACCURACY-FACTOR 1.e-5
END
```

D.3 Case 3. Advective Release with Sorption

```
TITLE
'Verification 3: advection release with sorption'
END
POROSITY
 WASTE     0.40      # all data hypothetical
 CAN-CP    0.40
 PALLET    0.40
 INVERT    0.40
 FRACTURE  0.40
 MATRIX    0.40
END
DENSITY
 WASTE     2250.0
 CAN-CP    2250.0
 PALLET    2250.0
 INVERT    2250.0
 ROCK      2250.0
END
INFILTRATION
 DRIP-AREA  1.0
 NO-OF-DATA 2
 TIMES-AND-RATES
   0.0000E+00  1.0000E2
   3.0000E+07  1.0000E2
 INVERT-FRACTION 0.0
 BASALT-FRACTION 0.0
END
SATURATION
 WASTE    0.8
 CAN-CP   0.8
 PALLET   0.8
 INVERT   0.8
 FRACTURE 0.8
 MATRIX   0.8
END
DIFFUSION  # exclude diffusion
 WASTE    1.e-19 M2PSEC
 CAN-CP   1.e-19 M2PSEC
 PALLET   1.e-19 M2PSEC
 INVERT   1.e-19 M2PSEC
 FRACTURE 1.e-50 M2PSEC
 MATRIX   1.e-19 M2PSEC
END
GEOMETRY
 WASTE-VOL          1e-5
 WASTE-LENGTH       1e-5
 WST-CAN-AREA       1.0
 CAN-CP-VOL         5.0
 CAN-CP-LENGTH      1e-5
 CAN-PALLET-AREA    1.0
 PALLET-VOL         1e-5
 PALLET-LENGTH      1e-5
 PALLET-INVERT-AREA 1.0
 INVERT-VOL         1e-5
 INVERT-LENGTH      1e-5
 INVERT-ROCK-AREA   1.0
 ROCK-VOL           1e-5
 MAT-LENGTH         1e-5
 FRAC-LENGTH        1e-5
```

```
 FRACTURE-APERTURE  1.E-5
 FRACTURE-SPACING   0.99999  # suppress fracture
 MAT-FRAC-AREA      1.e-10
 ZC-LENGTH          1e-5
 SORB-DEPTH         0.0
END
DECAYS
 'Np-237' 2.14e+6
END
INVENTORY
 'Np-237'  1000.  MOLES  M-FRAC 0.0  GAP-FRAC 1.0
END
SORPTION
 Np  CORR-PROD  1.00  PALLET  1.0    TUFF 1.0
END
SOLUBILITY
 UNITS MOLPM3
 Np 1.e6
END
CONTAINMENT
 FAIL-TIME 0.0
 INV-START-TIME 0.0
 ALTER-TIME 1.0
 NO-OF-DATA 1
 TIMES-AND-FRACTIONS
    0.0   1.0
END
OUTPUT-TIMES
 START-TIME 1.E1
 END-TIME   1.E6
 NO-PER-DECADE 24
END
FLUX-OUTPUT
 UNITS MOLPYR
 FLUX-FILE
# MASS-BALANCE     #   logical for printing MASS_BALANCE.out
END
TIMESTEP-CONTROL
 ACCURACY-FACTOR 1.e-5
END
```

E
APPENDIX E: SORPTION COEFFICIENTS FOR SELECTED ACTINIDES IN THE NEAR-FIELD

Sorption coefficients are provided here for thorium, uranium, neptunium and plutonium in the form of recommended K_d values (m^3/kg) for sorption on corrosion products and tuff. These elements provide the key safety-relevant radionuclides in terms of contributions to dose, with the exception of iodine and technetium. K_d values for the latter two elements are zero (0 m^3/kg), indicating lack of sorption on all near-field substrates.

E.1 Corrosion Products

The recommended K_d values for the sorption of Th, U, Np and Pu on corrosion products are given in Table B-1. The rationale for the selected values in this table is given in EPRI (2000). It is worthwhile noting here that the recommended K_d value for Np is low relative to that for U, based on the results of an independent study (EdF, 2000) which indicated that the sorption of uranium will dominate sorption sites.

It is also noted that DOE no longer provides K_d values for sorption on corrosion products "*in order to avoid ambiguity in competition for adsorption sites"*. Thus, DOE's conceptual model "*precludes reversible sorption*" (BSC, 2005a; Page 6-46) with K_d values being set to zero (BSC, 2005b). Irreversible sorption of Pu (and Am) is now the focus of its modeling.

Table E-1
Recommended K_d values for the sorption of selected actinides on corrosion products.

Element	Recommended K_d Value (m^3/kg)
Th	10
U	1
Np	0.001
Pu	10

E.2 Tuff

The K_d values here refer to sorption on devitrified tuff and are applicable for the host rock as well as the invert, which is composed of tuff from the repository horizon. DOE (BSC, 2004c) provided K_d values for the sorption of different elements on devitrified tuff in the form of distributions, either cumulative (K_d value, probability) or uniform (K_d range) distributions. These distributions are shown in Table B-2 together with the recommended K_d values based on these distributions.

Table E-2
Recommended K_d values for sorption on devitrified tuff

Element	***K_d Distributions*** **(K_d m^3/kg* range) OR (K_d m^3/kg*, cumulative probability)**	**Recommended K_d Value (m^3/kg)**
Th	*Uniform*: 1 – 10	5
U	*Cumulative*: (0,0; 0.0002, 0.5; 0.004, 1.0)	0.0002
Np	*Cumulative*: (0,0; 0.0005, 0.5; 0.006, 1.0)	0.0005
Pu	*Cumulative*: (0.01,0; 0.07, 0.5; 0.2, 1.0)	0.07

*: Values in BSC (2004c) originally provided in ml/g but converted in the above table.

E.3 References

BSC (2004c): Engineered Barrier System: Radionuclide Transport Abstraction, AMR ANL-WIS-PA-000001, REV01, November 2004. Bechtel SAIC Company LLC, Las Vegas, Nevada.

BSC (2005a), *EBS Radionuclide Transport Abstraction*, ANL-WIS-PA-000001 Rev 02, August 2005, Bechtel SAIC Company, Las Vegas, Nevada.

BSC (2005b), *Technical Management Review Board (TMRB) Decision Proposal*, TMRB-2005-028, Bechtel SAIC Company, Las Vegas, Nevada.

EdF (2000), Report provided by Electricité de France, Paris, France.

EPRI (2000) *Evaluation of the Candidate High-Level Radioactive Waste Repository at Yucca Mountain Using Total System Performance Assessment*, *Phase 5*, TR-1000801, Electric Power Research Institute, Palo Alto, California.

F
APPENDIX F: NEPTUNIUM SOLUBILITY VALUES

Previous regulatory compliance calculations for the proposed Yucca Mountain geological repository indicate that for the period beyond about 10,000 years after permanent closure of the repository, neptunium-237 (Np-237 or ^{237}Np) and its decay products will be the largest contributors to RMEI dose rate by several orders of magnitude compared to other radionuclides contained in spent nuclear fuel (DOE/OCRWM, 2008; CNWRA, 2002). Because of its long half-life (2.14×10^{6} years), the peak dose rate at the compliance point (i.e., the point on the site boundary established by the regulations where compliance must be demonstrated) resulting from Np-237 will scale proportionally with the solubility limit for Np. Therefore, a realistic determination of Np solubility behavior is essential to a reasonable expectation assessment of the anticipated dose rate and determination of regulatory compliance. As a result, a significant effort was expended during the development of IMARC 9, to develop an improved technical basis for neptunium solubility.

The U.S. Department of Energy (DOE) has developed three conceptual models to define the maximum concentration of Np at the surface of dissolving spent nuclear fuel (Chen et al. 2002; DOE 2003; DOE 2005a). These are:

The *base-case conceptual model,* which makes the highly conservative assumption that maximum Np concentrations are limited by the solubility of Np_2O_5(cr). This Np(V) phase has a solubility of about 10^{-5} M (2.4 mg/L) Np in repository groundwaters (cf. Friese et al., 2004);

The *first alternative conceptual model,* which assumes that maximum Np concentrations are determined by the solubility of the Np(IV) solid phase NpO_2(cr) in the same oxidized groundwaters that was assumed for the base-case model (DOE 2003; DOE 2005a). There is evidence that NpO_2(cr) is thermodynamically more stable than Np_2O_5(cr) in the repository (Roberts et al., 2003). The DOE's modeled solubility of NpO_2(cr) is about 1.2 log units (a factor of 17) lower than that of Np_2O_5(cr) (DOE 2003; DOE 2005a); and

The *second alternative conceptual model*, also described as the *secondary phase neptunium solubility model* (DOE 2003; DOE 2005a), which assumes that maximum Np concentrations are determined by precipitation of the Np from spent fuel dissolution in solid solution with major secondary uranium minerals.

While there is experimental evidence to support each conceptual model, DOE has selected the most conservative (highest Np solubility) model as their reference (*base case*) for conducting LA-related regulatory compliance calculations (Chen et al. 2002; DOE 2003; DOE 2005a). Calculations using this base case model lead to peak ^{237}Np dose rates that are several orders of magnitude higher than if the more realistic *second alternative conceptual model* is used.

DOE did not adopt the second alternative conceptual model because it was not considered sufficiently supported by experimental evidence that was available in 2003 when the DOE performed its analyses. DOE did recognize, however, that Np concentrations predicted with this *secondary phase neptunium solubility model* are in excellent agreement with the concentration of Np released by dissolution of spent fuel, a value which is typically in the range of 10^{-8} to 10^{-10} M, whereas Np concentrations predicted using the *base case model* or *first alternative conceptual model* are 3 or more orders of magnitude higher than observed (DOE 2003; DOE 2005a).

Based on a review of presently available published studies, EPRI has concluded that DOE's *base case* assumption that Np_2O_5(cr) solubility defines maximum possible Np concentrations at Yucca Mountain is unrealistically conservative for the following reasons:

1. Pure Np phases have never been observed to precipitate in spent fuel leaching experiments (DOE, 2003). There is no evidence that Np concentrations from the leaching of spent fuel will ever be high enough to result in the precipitation of pure Np(V) phases such as Np_2O_5(cr);
2. Thermodynamic databases developed by the DOE (Kaszuba and Runde, 1999), and independently by international groups (Lemire et al., 2001; Guillaumont et al., 2003), indicate that NpO_2(cr) is probably more stable than Np_2O_5(cr) under all repository conditions; and
3. Laboratory experiments at 90°C and above in oxidized waters have precipitated NpO_2(cr) (DOE 2003; Roberts et al., 2003), suggesting that Np(V) phases such as Np_2O_5(cr) are metastable and, with time, will convert to more thermodynamically stable and less soluble NpO_2(cr) in the repository.

In experiments most closely simulating the heterogeneous conditions expected during the dissolution of spent fuel in the repository, the Np/U ratio of the leachates is the same as the Np/U ratio of the fuel, and Np concentrations do not increase with time relative to uranium concentrations as secondary uranyl minerals are formed (DOE, 2003). This confirms active uptake and incorporation (co-precipitation) of trace Np into secondary uranyl minerals at approximately the same Np/U ratio as was present in the spent fuel. Resultant Np(V) concentrations can be expected to be extremely low ($<10^{-7}$ to 10^{-9} M) and controlled by the solubility of secondary uranyl minerals and the mass fraction of Np incorporated in those minerals.

There are other reasons why Np releases from a repository at Yucca Mountain can be expected to be low, providing even more evidence of the conservatism of the *base case model*. The presence of major amounts of metallic iron (Fe[0]) in steel used to rib the drifts and to support waste packages on the floor of the drift, and the presence of ferrous iron (Fe[II)] in its corrosion products, should reduce sorbed Np(V) to relatively insoluble Np(IV) within the near-field region. Combined sorption and reduction of Np (V) to Np (IV) can also be expected in groundwater migrating beneath the repository via matrix flow through vitric layers in the tuffs of the Calico Hills Formation[17]. A number of researchers have shown the tendency for Np(V) to be adsorbed

[17] Assuming its composition is similar to that of the overlying Topopah Spring Tuff, the Calico Hills contains the Fe(II)- bearing minerals magnetite, ilmenite and pyrite at 0.19, 0.18 and 0.09 average weight percent, respectively.

by tuff minerals such as magnetite (and probably also ilmenite) that contain Fe(II), with reduction of Np(V) and its retention as less soluble Np(IV) species (Nakata et al., 2002; 2004).

Furthermore, EPRI's review determined that thermodynamic and kinetic analyses published by the DOE and outside international scientific peer reviews, support the use of the *first alternative conceptual model (*Np controlled by the solubility of NpO_2(cr)) over the *base case model* (Np controlled by the solubility of Np_2O_5(cr)). The solubility of NpO_2(cr) is about 17 times lower than that that of Np_2O_5(cr). Laboratory studies have precipitated NpO_2(cr) at and above 90°C but not at lower temperatures, suggesting that kinetic factors at low temperatures may prevent the precipitation of thermodynamically stable NpO_2(cr) instead of metastable Np_2O_5(cr). However, the ubiquitous presence of mineral and other surfaces in the repository drift, which were not available in the laboratory NpO_2(cr) precipitation experiments, should provide an abundance of sites for the ready nucleation and precipitation of NpO_2(cr) in the repository at temperatures below 90°C. Separately, there are considerable test data to show that in the presence of solids containing reduced forms of iron (Fe^0 and Fe^{2+}), dissolved Np(V) species are reduced to less soluble Np(IV) species. The abundance of reduced solids such as structural steel (Fe metal) in the drifts, and the far-field occurrence of ferrous-containing minerals such as ilmenite and magnetite in the matrix of the Calico Hills Formation, for example, indicate that Np(V) should not persist even if it forms in the repository.

Most importantly, *heterogeneous* tests conducted under conditions that most closely match anticipated repository conditions (drip tests and batch tests using actual spent fuel and, in some cases, crushed tuff at elevated temperatures) confirm that:

1. Np coprecipitates with U, forming a solid-solution within secondary uranium minerals;
2. Np concentrations predicted with the *secondary phase neptunium solubility model* (coprecipitation model) are in excellent agreement with the measured concentrations of Np released by dissolution of spent fuel.

These observed Np concentrations are 3 to 5 orders of magnitude lower than the *base case* solubility values. Furthermore, there are no credible processes or reactions by which the Np concentration in solutions from the dissolution of spent fuel could be increased to attain saturation with respect to pure Np oxides such as Np_2O_5(cr) or NpO_2(cr) under oxidizing conditions in a repository.

Based on these multiple lines of evidence and reasoning, EPRI has concluded that Np concentrations released from a repository at Yucca Mountain will be controlled at values below 10^{-7} M by co-precipitation in secondary uranyl minerals in the near field, and by reduction and sorption as Np(IV) in the repository and in underlying tuff formations. The adoption of an excessively conservative alternative conceptual model for Np solubility imposes an unwarranted perception of potentially higher dose levels resulting from a repository at Yucca Mountain than is reasonably supported by data from the DOE and independent international scientific peer groups.

In conclusion, EPRI considers that DOE's adoption of solubility constraints for the License Application based on either of the two conceptual models that assume formation of pure Np solids, is not only clearly conservative but also unrealistic. Of these two options, however, the assumption of control by Np_2O_5(cr), the present base case assumption, rather than control by the

lower solubility NpO_2(cr) is considered to be an unreasonable choice. It is EPRI's position that DOE's *secondary phase neptunium solubility model* (co-precipitation model) is the most prudent and defensible choice for predicting Np releases from Yucca Mountain and that this co-precipitation model should be adopted as the basis for any assessment of regulatory compliance.

EPRI further believes that if concerns regarding the selection of the second alternative model continue to exist, there will be ample opportunity to further evaluate the appropriateness of the Np co-precipitation model in the Performance Confirmation program to be conducted by DOE during the pre-closure period, the results of which will be submitted to the NRC staff for review.

F.1 References

Chen, Y., A.R. Loch, T.J. Wolery, T.L. Steinborn, P.V. Brady, and C.T. Stockman, 2002. "Solubility evaluation for Yucca Mountain TSPA-SR." Scientific Basis for Nuclear Waste Management XXV. Nov 26-29, 2001. McGrail, B.P., and Cragnolino, G.A., eds. *MRS. Symp. Proc.* 713, JJ10.4.1-8.

CNWRA, 2002. *System-level Performance Assessment of the Proposed Repository at Yucca Mountain, Nevada, Using the TPA Version 4.1 Code*. CNWRA-2002-05, Center for Nuclear Waste Regulatory Analysis, San Antonio, TX.

DOE/OCRWM, 2008. Total System Performance Assessment Model/Analysis for the License Application, MDL-WIS-PA-000005 Rev. 0 January 2008 Office of Civilian Radioactive Waste Management, Las Vegas, NV.

DOE, 2003, Dissolved Concentration Limits of Radioactive Elements. Report ANL-WIS-MD-000010 REV 02, June 2003. Office of Civilian Radioactive Waste Management, Las Vegas, NV.

DOE 2005a. Dissolved Concentration Limits of Radioactive Elements. ANL-WIS-MD-000010 Rev 05. July 2005. Office of Civilian Radioactive Waste Management, Las Vegas, NV.

Friese, J.I., M. Douglas, E.C. Buck, S.B. Clark, and B.D. Hanson, 2004. "Neptunium(V) incorporation/sorption with uranium(VI) alteration products." In *Materials Research Society Symp. Proc. 824*, CC9.2.1.

Guillaumont, R., Fanghanel, T., Fuger, J., Grenthe, I., Neck, V., Palmer, D.A., and Rand, M.H., Eds., F.J. Mompean, M. Illemassense, C. Domenech-Orti and K.Ben Said, 2003, Update on the Chemical Thermodynamics of Uranium, Neptunium, Plutonium, Americium and Technetium. Chem. Thermo., vol. 5. NEA OECD, Elsevier, New York, 919 pp.

Kaszuba, J.P. and W.H. Runde, 1999. "The aqueous geochemistry of neptunium: Dynamic control of soluble concentrations with applications to nuclear waste disposal." *Envir. Sci. & Technol.,* 33: 4427.

Kaszuba, J.P. and W.H. Runde, 1999. "The aqueous geochemistry of neptunium: Dynamic control of soluble concentrations with applications to nuclear waste disposal." *Envir. Sci. & Technol.,* 33: 4427.

Lemire, R.J., J. Fuger, H, Nitsche, P. Potter, M. H. Rand, J. Rydberg, K. Spahiu, J. C. Sulluvan,

W. J. Ullman, P. Vitorge and H. Wannter, 2001. "Chemical Thermodynamics of Neptunium and Plutonium." *Chem. Thermo*. 4, NEA OECD. Elsevier, New York. 843 pp.

Nakata, K., Nagasaki, S., Tanaka, S., Sakamoto, Y. Tanaka, T., and Ogawa, H., 2002, Sorption and reduction of neptunium(V) on the surface of iron oxides. Radiochim. Acta 90, 665-669.

Nakata, K., Nagasaki, S., Tanaka, S., Sakamoto, Y. Tanaka, T., and Ogawa, H., 2004, Reduction rate of neptunium(V) in heterogeneous solution with magnetite. Radiochim. Acta 92, 145-150.

Roberts, K.E., T. J. Wolery, C, E, Atkins-Duffin, T. G. Prussin, P. G. Allen, J. J. Bucher,D. K. Shuh, R. J. Finch and S. G. Prussin, S.G., 2003. "Precipitation of crystalline neptunium dioxide from near-neutral aqueous solution." *Radiochim. Acta* 91: 87.

G
APPENDIX G: EPRI RESPONSE TO INTERNATIONAL REVIEW TEAM (IRT) IMARC PEER-REVIEW FINDINGS AND RECOMMENDATIONS

Since 1989, EPRI has been conducting independent assessments of the proposed deep geologic repository for the disposal of spent nuclear fuel and high level radioactive waste at Yucca Mountain, Nevada. EPRI pioneered application of the total system performance assessment (TSPA) approach for evaluating performance of geologic repository systems on a probabilistic basis. Along the way, EPRI developed the Integrated Multiple Assumptions and Release Code (IMARC) as its primary analytical tool for TSPA-based evaluations. Over this two-decade time period, IMARC has been periodically revised to reflect the evolving state of knowledge and the changing programmatic and regulatory environment.

In 2007, EPRI commissioned an independent peer review of EPRI's most recent IMARC code version for TSPA.[18] An International Review Team (IRT) conducted its review during late 2007 and early 2008 following the guidelines and protocols of the International Atomic Energy Agency's Improvements on Safety Assessment Methodology (ISAM). This ISAM methodology was adopted as a framework to ensure a systematic review of the IMARC 9 draft report, as well as to conform to international standards.

This peer review was intended to provide an independent evaluation of EPRI's TSPA code, IMARC, in light of EPRI's role in providing an independent perspective on the key elements of and risk drivers for Yucca Mountain performance assessments. Specifically, the IRT was tasked with determining if IMARC is "fit for purpose" by

- Determining if the overall approach is reasonable, viable, and consistent with the goals of the EPRI Yucca Mountain research program
- Identifying areas, if any, where the code or its subcomponents would benefit from changes to better achieve the goals of the EPRI program
- Identifying assumptions and input data that warrant further review and possible revision
- Confirming the application of the reasonable/best estimate approach
- Evaluating the adequacy of IMARC code documentation in EPRI reports

[18] The IMARC code version reviewed by the IRT was interim version IMARC 9, which represented an incremental revision of IMARC 8 (EPRI report 1011813: *EPRI Yucca Mountain Total System Performance Assessment Code (IMARC) Version 8: Model Description*, 2005). The relatively minor revisions comprised changes in input data exclusively; no changes were made to the IMARC 8 conceptual or numerical models.

Drawing on more than 20 years of experience in the field of geologic repository performance assessment, EPRI and its principal research contractor, Monitor Scientific LLC, assembled a list of candidates based on the following areas of expertise required for the review:

- Climate/infiltration/seepage,
- Containment,
- Source-term release,
- Unsaturated and saturated zone flow and transport,
- Dose modeling, and
- QA of code development and performance assessment related modeling.

In addition, candidates were screened on the basis of independence with respect to the Yucca Mountain Project, direct experience in conducting performance assessments associated with geologic repositories, and availability with respect to the program schedule. A chairperson was selected jointly by Monitor Scientific and EPRI and served to assist Monitor Scientific with the selection of the remaining team members. Resource constraints, conflict of interest concerns, and logistical considerations limited the team to three members.

Monitor Scientific served as facilitator during the review for coordinating contact between the IRT and the EPRI research team (EPRI staff, Monitor staff, and other IMARC experts), organizing teleconference calls to enable the reviewers to ask questions and receive explanations directly from appropriate EPRI team experts, and providing additional supporting documentation as requested. Monitor Scientific developed and provided documentation of the current status of the IMARC code to the IRT. In addition, copies of all available historical documentation of the code and its development were made available to the review team. The review team members were also given the opportunity to examine the code in person at Monitor Scientific's Denver offices.

The review process was initiated with a kickoff meeting on September 6 - 7, 2007, among EPRI, the EPRI research team (Monitor Scientific and its subcontractors) and the IRT members during which an overview of the IMARC code and its history was given. The IRT also met separately at that time to establish review subject assignments and the process for the review (see Appendix B). Throughout the review, the IRT members communicated amongst themselves by teleconference as needed. A second face-to-face meeting was held on October 22 – 24, 2007, to permit the IRT to meet again with appropriate EPRI research team members and to receive further clarifications and input from IMARC experts.

After completion and documentation of initial reviews by IRT members, the peer review team chairperson compiled and integrated the review comments into an executive summary, checking the comments for relevance and consistency with respect to the established terms of reference (Appendix B, EPRI 2009a). Any disputes arising with regard to the disposition of comments by the chairperson resulted in written exceptions appended to the reviewer's comments. This integrated review document was then reviewed by all IRT members for accuracy and consistency. The chairperson made corrections as necessary and then distributed the initial draft review document to Monitor Scientific and EPRI in December 2007. A final face-to-face

meeting between the IRT, Monitor Scientific and EPRI was held on January 15, 2008, to resolve questions and comments requiring further clarification. A final consensus document was then prepared by the chairperson in consultation with the other IRT members and submitted to Monitor Scientific and EPRI in April 2008.

The IRT found that the IMARC code provides an integrated presentation of the total repository system and captures the main processes and their interactions for a repository located at Yucca Mountain, Nevada. The IRT concurred that IMARC is "fit for purpose" in that it provides a risk-based methodology for integrating information from various disciplines affecting long-term repository performance. The IRT found that the models and databases in the IMARC 9 code conformed to performance analyses that are consistent with a "reasonable expectation" approach per the EPA's Yucca Mountain standards. IMARC was also judged to be a well-integrated performance assessment tool, which focuses on those processes that could affect the long-term safety and regulatory compliance of a repository located at Yucca Mountain. Opportunities for expanding and refining the capabilities of the IMARC code were also identified in the IRT review. The IRT strongly supported verification and code inter-comparisons to gain additional insights into the various assumptions and modeling approaches and for enhancing the scientific credibility of the model. The IRT review called attention to a number of areas in which model documentation could be improved.

EPRI published the peer-review findings in April 2009 as received from the IRT (with minor formatting changes for publication) as report 1018711 (EPRI, 2009a). The IRT review represents an important independent technical assessment of the IMARC code, parameters, and implementation. This appendix is intended to document the EPRI research team response to the IRT findings and recommendations, principally by describing changes made to the IMARC code itself and the documentation provided herein. Table G-1 summarizes the IRT comments and the corresponding EPRI research team response along with explanations of those responses, as appropriate.

Table G-1
Disposition Table for International Review Team (IRT) Comments

	IRT Comment (from EPRI, 2009a)	EPRI Response
ES3 System Description	The IRT considers that the current IMARC 9 documentation could be improved by providing more detail on the disposal system and its (geometrical) conceptualization.	Substantial additional text has been added to the report to address this comment. In particular, Sections 1 and 2 have been substantially edited and reorganized to provide a better overall picture of IMARC.
ES4 Development and Justification of Scenarios	• The focus of the IRT's review has been on the nominal scenario. It is proposed that a future review will address EPRI's application of IMARC to alternative credible scenarios such as igneous events, rockfall and expanded capacity of the repository. • However, it is recommended that EPRI reviews the U.S. DOE FEPs documentation for comparison with its assessment models.	Review of FEPs is ongoing throughout the development of IMARC. Assumptions implemented in IMARC 10 represent the outcome of a critical review of FEPs implemented by DOE, and of FEPs screening conducted by DOE. An improved description of the role of the DOE FEPs approach in IMARC development has been added to Chapter 2. The incremental revision of IMARC to reflect the changing understanding of Yucca Mountain FEPs over the years has been documented in Appendix A.
ES5.1 Climate Change	The IRT recommends that EPRI incorporates a discussion of the potential effects of global warming into the document.	In IMARC 10, infiltration and percolation issues have been addressed by adopting the updated NRC deep percolation values specified in 10 CFR 63. However, elsewhere EPRI has evaluated the potential effects of global warming on Yucca Mountain (EPRI, 2009b)
ES5.2 Infiltration	Specific suggestions for improved documentation of the infiltration model include: • addition of a water balance diagram; • explanation of the coupling between infiltration, percolation and seepage in IMARC 9; • clarification of the effect (or lack thereof) of infiltration on EBS degradation rates; • addition of the model equations which use the infiltration rates (or reference to other sections where these may appear); • reference to the literature source(s) where the model and model parameters are derived.	In IMARC 10, infiltration and percolation issues have been addressed by adopting the updated NRC deep percolation values specified in 10 CFR 63. While the report retains a broad discussion of EPRI's position on net infiltration, IMARC 10 does not draw on this information in its current implementation. An expanded discussion has been added to Chapter 2 to clarify these issues and the interaction and justification of these FEPs.

Table G-1 (continued)
Disposition Table for International Review Team (IRT) Comments

	IRT Comment (from EPRI, 2009a)	EPRI Response
ES5.2 Infiltration	As IMARC is periodically updated to reflect scientific progress, the IRT suggests that it would be beneficial to use the IMARC 9 tool to evaluate the dose/risk implications of uncertainties related to selecting the (EPRI, 1998) range of net infiltration rates versus other recent work (e.g., Faybishenko, 2007) or other recent assessments. Since infiltration rates affect percolation through the Unsaturated Zone (UZ) and groundwater recharge, it would also be useful to carry out a sensitivity analysis to evaluate how sensitive the UZ and Saturated Zone (SZ) radionuclide transport are to uncertainty in the net infiltration rate over the first ten thousand years after disposal.	In IMARC 10, infiltration and percolation issues have been addressed by adopting the updated NRC deep percolation values specified in 10 CFR 63. Past experience with previous versions of IMARC has shown that infiltration analyses for the pre-10,000 year period are not risk significant (see Appendix A). Furthermore, the NRC percolation values are conservatively bounding compared to the sensitivities suggested by this comment. Accordingly, no action was taken to address this comment.
ES5.3 Seepage	• There is a need to expand the justification for omitting episodic flows. The fracture asperity argument presented in EPRI (2002a) is plausible, but does not provide sufficient evidence. The argument would be much enhanced if combined with observations from the existing drift at Yucca Mountain. • The handling of seepage during high sub-boiling temperatures would benefit from additional discussion. The IRT agrees that it is reasonable to omit this aspect from the model, because the containment model is not coupled to the seepage model, and because containment is generally long-term (*i.e.* it is functioning well into the temperate region when the IMARC seepage model becomes valid). However, should either of these conditions become invalid (e.g. by future updates of IMARC 9 or by new data on containment times), then it would be necessary to revisit the seepage model. The IRT, thus, recommends that this, as well as other critical assumptions, be clearly documented at an overview level.	The foundation for exclusion of episodic flows in IMARC is based on a critical review of the DOE FEP list, which also excludes episodic flow. An improved discussion of this issue has been added to Section 2.1 of the report. As the comment notes, treatment of the thermal period has not been found to be risk significant. The comment refers to a situation in which containment could be lost at an early time, when thermal effects would still be important to percolation and seepage. Such a situation could only be associated with a major redesign of the repository to omit the robust materials in the current design. Such a dramatic redesign of the repository is not envisioned at any time in the future. However, if it happened, it would require a fundamental re-evaluation of the basic assumptions in IMARC, and would require the revised assumptions to be carefully documented.

Table G-1 (continued)
Disposition Table for International Review Team (IRT) Comments

	IRT Comment (from EPRI, 2009a)	EPRI Response
ES5.4.1 Corrosion Aspects	The cladding failure model Furthermore, the IRT concurs with the argument that pitting corrosion is unlikely to lead to a major exposure of fuel for dissolution. However, the IRT recommends that EPRI adds a discussion providing rationale for this argument and showing that neglecting this process will not have a significant impact on the estimated dose. The waste package (WP) failure model The IRT suggests that EPRI carry out a Sensitivity Analysis to assess the risk importance of the stifling model. If this is important, the IRT recommends that EPRI provides further evidence to support the stifling model for the expected repository conditions.	Discussion of the technical basis for the cladding assumptions was expanded and enhanced and a sensitivity analysis was carried out to evaluate the importance of cladding to the results of the TSPA. That sensitivity analysis demonstrates that the presence of the cladding has a minor effect on TSPA results, and does not affect the peak dose. The current conceptualization of processes leading to failure of the waste packages is based on the dominance of general corrosion. As a result, a process that leads to a highly localized failure of the waste package outer barrier is not straightforward to implement. Sensitivity analyses to address this comment were based on an examination of a comprehensive failure of the waste package, rather than a localized failure. The revised report includes a number of sensitivity analyses to explore the relative importance of various aspects of the EBS. This approach identifies the relative risk importance of the components of the EBS from a total system perspective, rather than relying solely on mechanistic corrosion arguments.
ES5.4.2 Failures Caused by Initial Defects	Regarding documentation of the model in the IMARC 9 report, the IRT had difficulty understanding what specific probability was used for initial defects and what it was based on.	A revised discussion in the EBS failure section addresses this comment. The probability value has been adopted from DOE's work in this area, which indicates a probability less than 1e-4. That is, the expected number of initially defective waste packages is less than one. For IMARC, this information is reconceptualised to be represented by one failed waste package and one failed drip shield. The probability value is therefore the reciprocal of the total number of waste packages. This value is therefore higher (more conservative) than the number used by DOE.

Table G-1 (continued)
Disposition Table for International Review Team (IRT) Comments

	IRT Comment (from EPRI, 2009a)	EPRI Response
ES5.5.1 Screening	The IRT recommends that EPRI documents the radionuclide screening assessment within the IMARC 9 documentation	A discussion of the development of the radionuclide screening has been included in the revised report. The screening has been conducted over a period of several phases of IMARC development. New radionuclides have been added in for Phase 10, and the reasons for these additions has been documented.
ES5.5.2 Instant Release	The IRT recommends that EPRI includes a section on the selection of IRF parameter values, their justification and the mathematical implementation of instant release in the model.	The revised document has improved the discussion of the instant release fraction. The values themselves have been adopted from DOE estimates, since DOE's technical basis appears to be sound.
ES5.5.3 Wasteform Degradation	The IRT recommends that EPRI continues current efforts to evaluate the applicability of more mechanistic spent fuel alteration models.	IMARC 10 includes new estimates of spent fuel alteration, which are based on an independent model developed by EPRI. The new values for alteration time used in IMARC 10 are substantially longer than values used in past phases.
ES5.5.4 Element-Dependent Solubilities	The IRT notes that there is some uncertainty surrounding the precise nature of the solid precipitate and because of this the IRT recommends that EPRI carries out a sensitivity analysis to explore the effect of uncertainty in the value of Np solubility on the overall dose results.	A sensitivity analysis was undertaken to examine higher values of solubility on the TSPA. Older values of solubility (used in IMARC 8 and before) which were characteristic of a different assumption about the nature of the solid precipitate, were compared to the IMARC 10 results for the nominal case. The result showed that a 4 order of magnitude increase in solubility led to one order of magnitude increase in peak dose.
ES5.5.5 Mass Transport through the Engineered Barriers and UZ Interface	The IRT encourages the detailed documentation of COMPASS, recently undertaken by EPRI and recommends that it is included in the IMARC 9 document. It is also recommended that EPRI should provide an Assessment Model Flowchart (AMF) that gives an overview of IMARC 9 and its various sub-models.	The updated documentation includes an improved description of COMPASS. There is substantially more information on the flow of information through IMARC, including flowcharts to indicate how the models work together.
ES5.6 Unsaturated Zone Flow and Transport- UZ – SZ Interface	However, the IRT recommends that the IMARC document explicitly discusses this (single vertical column), and also generally remarks that the selection of a single vertical column is justified for current properties and boundary conditions.	Additional text has been added to the revised report to better describe the use of a single column. In addition, the section describing the historical development of IMARC includes past phases when multiple UZ columns were used.

Table G-1 (continued)
Disposition Table for International Review Team (IRT) Comments

	IRT Comment (from EPRI, 2009a)	EPRI Response
ES5.8.2 Exposure Pathways	The IRT notes that the U.S. DOE (2007) biosphere model includes a pathway that is not considered in the EPRI model, namely consumption of fish, farmed in radionuclide-contaminated water. The basis for the inclusion of this pathway in the US DOE biosphere model is that fish-farming is currently practiced in the Amargosa Valley. The IRT recommends that EPRI considers the potential significance of such a pathway.	The report contains the most recent biosphere model description. EPRI believes that inclusion of fish farming is not in accordance with reasonable expectation. Similarly, in IMARC 10, consumption of offal has been omitted from consumption rates, since it is not a significant component of US diets. Its inclusion would therefore not be consistent with reasonable expectation.
ES5.8.3 Biosphere Transfer Model	IMARC 9 uses a Kd for modelling radionuclide retardation in soil. This is commonly the approach used in safety assessments. It should be noted that for some radionuclides, such as Tc-99, this is a conservative approach because processes, such as chemical reduction and co-precipitation (e.g., Abdelouas *et al.* 2005; Zachara *et al.* 2007) may tend to further retard migration. The IRT notes that it would be useful to add a discussion on these processes in the report.	A discussion of these processes that was formerly in an appendix has been moved to the main report in Section 7.2.1. An elaboration has also been added to Section 7.3.2.1(b) to discuss this issue.
ES5.8.4 Data and Parameter Values	The IRT has found that the traceability of the data used in EPRI's biosphere modelling is very good. Nevertheless, it would be useful to improve the IMARC 9 documentation and explain the reasons for changes to the BDCFs that have occurred in IMARC 9 BDCFs as compared to IMARC 6 and 7. With regard to data selection and the use of up to date data, it is noted that the biosphere model cites Ashton and Sumerling (1988) as the source of dose coefficients for external irradiation from soil, whereas more recent data may be available (e.g., U.S. EPA, 2002). The IRT recommends therefore, that at an appropriate stage in its safety assessment process, EPRI reviews and updates its documentation and biosphere data.	The report contains the most recent biosphere model description which has additional justification. The current model continues to use the older external dose coefficients for external exposure. However, it is noted that external dose coefficients have not changed dramatically over the period in question. Furthermore, when used for TSPAs, external dose factors represent an approximation of soil densities, contamination depth, spatial extent of contamination etc. that are conservative compared to the real conditions. While the update to the newer coefficients is desirable from the standpoint of traceability, it will not substantively affect IMARC results.

Table G-1 (continued)
Disposition Table for International Review Team (IRT) Comments

	IRT Comment (from EPRI, 2009a)	EPRI Response
ES5.8.5 Parameter Uncertainty	IRT suggests that EPRI considers undertaking further analysis of the significance of uncertainties in the values of biosphere input parameters, and clarifies which BDCFs it is taking forward into TSPA (*i.e.*, best estimates, distributions, means, medians or other type of central value), and explains why the values used in TSPA are consistent with its assessment context.	The new version of the biosphere model has included an assessment of parameter uncertainty, and a discussion is provided of the implications of that uncertainty on the values selected for use in IMARC.
ES6 Integrated Model and Interpretation of the Results		
ES6.1 Conservatism and Realism	The IRT recommends that EPRI continues to study ways to move away from conservative assumptions (which are essential in the absence of sufficient data and full mechanistic understanding) towards more scientifically credible and realistic assumptions. This is important, particularly for risk-sensitive processes. For example, if a sensitivity analysis shows that the spent fuel dissolution rate in IMARC 9 is risk sensitive over the time-frame of interest, it would be useful to study the availability of data and the feasibility of developing a less conservative, and a more mechanistic fuel alteration model. The IRT supports an initiative being undertaken in this regard, by EPRI.	A significantly expanded set of sensitivity analyses are presented in the revised report. The specific example given in the comment of the spent fuel alteration assumption was indeed found to have a significant effect on model results, and the model outcomes have been implemented in IMARC 10. More generally, sensitivity analyses continue to be a key part of the use of IMARC to develop risk-informed insights into Yucca Mountain TSPA.
ES6.2 Treatment of Uncertainty	EPRI should consider carrying out sensitivity analyses to assess whether the approximation introduced by using discrete pdfs significantly affects calculated dose to the RMEI. Furthermore, it is recommended that EPRI justifies the selection of the various pdfs in IMARC. The focus of this documentation effort should be risk-informed.	To address this comment, a sensitivity analysis was specifically identified to determine the effect of the probability density function on IMARC results. The sensitivity analysis looks at varying the probabilities assigned to the high-medium-low categories of each parameter considered in IMARC. In this way, the potential range of results from any possible pdfs is spanned.

Table G-1 (continued)
Disposition Table for International Review Team (IRT) Comments

	IRT Comment (from EPRI, 2009a)	EPRI Response
ES6.3 Sensitivity Analysis	• The IRT recommends that the results of the IMARC 9 probabilistic assessment be subject to a systematic sensitivity analysis to identify which parameter uncertainties contribute most to the uncertainty in the calculated total dose rates. • The IRT recommends that model uncertainties be addressed in a systematic sensitivity analysis. This sensitivity analysis could be based on risk insight from existing assessments and detailed modelling work which could guide priorities towards risk-sensitive areas.	The revised report contains substantially more sensitivity analyses, which have the goal of addressing this comment. The sensitivity analyses have been selected to assist in drawing improved risk insights into the analyses, and to illustrate the risk importance of both model uncertainties and parameter uncertainties.
ES6.4 Code Inter-Comparison	The IRT recommends that significant benchmarking activities should be documented.	The revised report has improved the documentation of verification and benchmarking activities. Some verification activities that were carried out in past phases of IMARC, and which remain relevant, have been documented again in the IMARC 10 report.
ES6.5 System Understanding	The IRT understands that the system understanding and model selection are based on critical reviews of the U.S. DOE work by the EPRI team. Such reviews are documented in several of the IMARC reports. However, the IRT recommends that EPRI improves the overall documentation on the final judgements made based on these critical reviews. This would enhance traceability and credibility of the model.	The revised report contains improved documentation of the process of evaluating DOE's approaches. Where specific judgments have been made to deviate from DOE's approaches,
ES6.6 Information Quality and Management	To mitigate this potential problem the IRT recommends that EPRI should maintain a central record of the modelling assumptions made.	The IMARC 10 report contains a description of the AIMS information management system, which has been implemented to address this issue,

G.1 References

Abdelouas, A., B. Grambow, M. Fattahi, Y. Andres, and E. Leclerc-Cessac, 2005. Microbial Reduction of 99Tc in Organic Matter-Rich Soils, Science of the Total Environment, Volume 336, Issues 1-3, Pages 255-268.

Ashton, J. and T.J. Sumerling, 1988. Biosphere Database for Assessments of Radioactive Waste Disposals. UK DOE / RW / 88.083.

EPRI, 1998. Alternative Approaches to Assessing the Performance and Suitability of Yucca Mountain for Spent Fuel Disposal, EPRI TR-108732, Electric Power Research Institute, Palo Alto CA, CA.

EPRI, 2002. Evaluation of the Proposed High-Level Radioactive Waste Repository at Yucca Mountain Using Total System Performance Assessment: Phase 6. Report number 1003031, Electric Power Research Institute, Palo Alto, CA.

EPRI, 2009a. International Review Team Report: A Peer Review of the Yucca Mountain IMARC Total System Performance Assessment EPRI Model. Electric Power Research Institute, Palo Alto, CA: 2009. 1018711.

EPRI, 2009b. Long-Term Climate Modeling and Hydrological Response to Climate Cycles in the Yucca Mountain Region. EPRI Report 1018714 (*In Preparation*). Electric Power Research Institute, Palo Alto, CA.

Faybishenko, B., 2007. Climatic Forecasting of Net Infiltration at Yucca Mountain using Analogue Meteorological Data. *Vadose Zone Journal*. Vol. 6, pp.77-92.

USEPA, 2002. Federal Guidance Report 13, CD Supplement, Cancer Risk Coefficients for Environmental Exposure to Radionuclides, EPA-402-C-99-001, Rev. 1.

USDOE, 2007. Biosphere Model Report, DOC.2007.0830.0007, MDL MGR MD 000001, Rev. 02.

Zachara, J.M., S.M. Heald, B.H. Jeon, R.K. Kukkadapu, C. Liu, J.P. McKinley, A.C. Dohnalkova and D.A. Moore, 2007. Reduction of Pertechnetate [Tc(VII)] by Aqueous Fe(II) and the Nature of Solid Phase Redox Products, *Geochimica et Cosmochimica Acta*, Volume 71, Issue 9, 1 May 2007, pp. 2137-2157.

The Electric Power Research Institute, Inc. (EPRI, www.epri.com) conducts research and development relating to the generation, delivery and use of electricity for the benefit of the public. An independent, nonprofit organization, EPRI brings together its scientists and engineers as well as experts from academia and industry to help address challenges in electricity, including reliability, efficiency, health, safety and the environment. EPRI also provides technology, policy and economic analyses to drive long-range research and development planning, and supports research in emerging technologies. EPRI's members represent more than 90 percent of the electricity generated and delivered in the United States, and international participation extends to 40 countries. EPRI's principal offices and laboratories are located in Palo Alto, Calif.; Charlotte, N.C.; Knoxville, Tenn.; and Lenox, Mass.

Together…Shaping the Future of Electricity

Program:

Nuclear Power

Printed on recycled paper in the United States of America

1018712

Electric Power Research Institute
3420 Hillview Avenue, Palo Alto, California 94304-1338 • PO Box 10412, Palo Alto, California 94303-0813 USA
800.313.3774 • 650.855.2121 • askepri@epri.com • www.epri.com